NASA TECHNICAL NOTE

NASA TN D-4609

C. 1

NASA TN D-4609

HOT-GAS INGESTION INVESTIGATION OF LARGE-SCALE JET VTOL FIGHTER-TYPE MODELS

by H. Clyde McLemore and Charles C. Smith, Jr.

Langley Research Center
Langley Station, Hampton, Va.

NATIONAL AERONAUTICS AND SPACE ADMINISTRATION • WASHINGTON, D. C. • JUNE 1968

NASA TN D-4609

HOT-GAS INGESTION INVESTIGATION OF LARGE-SCALE JET VTOL FIGHTER-TYPE MODELS

By H. Clyde McLemore and Charles C. Smith, Jr.

Langley Research Center
Langley Station, Hampton, Va.

NATIONAL AERONAUTICS AND SPACE ADMINISTRATION

For sale by the Clearinghouse for Federal Scientific and Technical Information
Springfield, Virginia 22151 – CFSTI price $3.00

HOT-GAS INGESTION INVESTIGATION OF LARGE-SCALE JET VTOL FIGHTER-TYPE MODELS

By H. Clyde McLemore and Charles C. Smith, Jr.
Langley Research Center

SUMMARY

An investigation to study the problem of hot-gas ingestion has been conducted in the Langley full-scale tunnel and outdoors on large-scale jet VTOL fighter-type aircraft configurations. The investigation included several rectangular and in-line exhaust-nozzle arrangements, inlet positions, and wing positions for a range of forward and side-wind conditions. The exhaust-gas source was a turbojet engine operating at a nozzle pressure ratio of about 1.8 and a nozzle temperature of 1200° F (649° C).

The ingestion of hot-engine exhaust gases into the inlets was found to be very dependent upon the aircraft configuration and upon the wind speed. An in-line arrangement of engine exhaust nozzles resulted in virtually no hot-gas ingestion, whereas a rectangular arrangement of nozzles resulted in an inlet air temperature rise above ambient of 100° F to 200° F (56° C to 111° C) for many test conditions. The ingestion of hot exhaust gases was greatest at wind speeds from zero to 20 knots, and there was virtually no hot-gas ingestion at wind speeds greater than about 30 knots. Top inlets were, in general, less subject to hot-gas ingestion than the side inlets, and the low-wing configuration was found to result in lower inlet air temperatures than did the high-wing configuration. Deflecting the jet exhaust 25° rearward with the vectoring nozzles generally eliminated the ingestion of hot exhaust gases.

INTRODUCTION

There is, at the present time, an increasing interest in the problems associated with jet VTOL aircraft; one such problem is hot-gas ingestion, that is, ingestion into the engine inlet of hot exhaust gases or air heated by the hot exhaust. Hot-gas ingestion is a serious problem for jet VTOL aircraft because a thrust loss occurs as a result of the elevated temperature of the engine inlet air or an uneven inlet temperature distribution across the engine face.

Although hot-gas ingestion has for some time been recognized as a serious problem (see refs. 1 and 2), very little systematic research of a generalized nature has been done on it, and most of this generalized research has been on small-scale models. (See refs. 2

and 3.) A recent large-scale investigation of a relatively specific airplane configuration having in-line lift-engine arrangements with aft, side-by-side mounted lift/cruise engines is reported in references 4 and 5. Other research on specific configurations has been conducted by several investigators (refs. 6 to 8), but these investigations have not provided enough generalized information for confident application of the test results to configurations differing from the test vehicle. In order to provide additional generalized information at relatively large scale, the Langley Research Center has initiated an investigation to study the problem of hot-gas ingestion of jet VTOL fighter-type configurations with in-line, rectangular, and single engine arrangements. The present investigation was conducted in the Langley full-scale tunnel and outdoors (ref. 9), for purposes of comparison, with test variables of model height above the ground, wing height, engine-inlet position, and wind speed and direction.

SYMBOLS

The units for the physical quantities defined in this paper are given both in the U.S. Customary Units and in the International System of Units (SI).

D_e nozzle effective diameter (diameter of circle whose area is equal to the sum of the areas of all the individual nozzles), feet (meters)

h nozzle height above ground, feet (meters)

ΔT inlet air temperature rise (final inlet temperature minus initial ambient temperature), ^{o}F (^{o}C)

V wind speed, knots

δ exhaust-nozzle deflection (measured from the vertical), degrees

ψ model heading (azimuth), degrees

MODEL AND APPARATUS

The model used in the investigation was an approximately 1/3-scale jet VTOL fighter configuration. The principal dimensions of the model are given in figure 1. Not all of the many configurations investigated are presented in figure 1, but each of the inlet, exhaust, and wing arrangements is shown.

The model was powered by a turbojet engine (GE-YJ85-7) mounted horizontally in the fuselage, which could be fitted with the various inlet and exhaust arrangements to simulate several different jet VTOL configurations. One of the engine, inlet, and exhaust arrangements is shown schematically in figure 2. The turbojet engine was used in order to provide actual exit conditions of exhaust temperature and pressure that would occur for turbojet-powered fighter-type aircraft.

The inlet and exhaust arrangements were designed to simulate airplane configurations with inlets directly above the exhaust (lift engines mounted vertically) or configurations with forward-facing side inlets and deflected engine exhaust for VTOL operation.

The model is shown mounted for tests in the Langley full-scale tunnel in figure 3 and at the outdoor test facility in figure 4. The model was supported by three 2-inch-diameter (5.08-cm) pipes to minimize obstruction of the exhaust flow. The pipes were restrained from bending by steel guys of 3/8-inch (0.95-cm) diameter.

The model was constructed almost entirely of stainless steel to withstand the high exhaust temperatures and the weather conditions experienced during outdoor tests. The inlets were equipped with lips of 1.00-inch (2.54-cm) radius to assure unseparated flow into the inlets. (See fig. 5.) Each inlet was equipped with rakes of static- and total-pressure probes and with chromel-alumel temperature probes. The locations of the temperature and static-pressure probes are shown in the sketches of figures 6 and 7, respectively. The temperature probes were 24-gage welded, bare-bead thermocouples constructed from 1/8-inch-diameter (0.318-cm) swaged wire. (See fig. 6(c).) The ends of the temperature probes were approximately 30 diameters ahead of the 3/8-inch-diameter (0.95-cm) probe support structure.

The exhaust nozzles were equipped so that the engine exhaust flow could be directed 25° rearward (measured from the vertical) or straight downward by remote control. These nozzles had vanes, as shown in figure 8, to assure full turning of the exhaust stream. Tailpipe pressure measurements were obtained from total-pressure probes mounted just upstream of the nozzle vanes. These total-pressure probes were connected to sensitive dial gages for visual observation by the engine operators and connected to oscillograph recorders for a permanent record.

The size of the model was, in general, dictated by the size of the engine. The engine exhaust-nozzle area was 118 in^2 (761 cm^2), or about 1/9 the jet nozzle area of a 25 000-pound (111 200-newton) jet VTOL fighter. The fuselage was disproportionately wide because of the internal ducting and equipment, but this characteristic was believed to be relatively unimportant for the present investigation.

The wings were flat plates 2 inches (5.08 cm) thick with a rounded leading edge and a beveled trailing edge. The ratio of wing area to jet nozzle area was 42.7, which is

representative of current VTOL fighter designs. The alternate wings, which are shown in figure 1, had 60° delta and 42.5° sweptback planforms. These wings could be mounted in either a high or a low position on the fuselage.

For the top-inlet configurations, a survey rack was installed over and around the inlets, as shown in figures 3 and 4, with temperature probes attached to the rack to give the temperature variation of the air approaching the inlets. All of the temperature and pressure data were recorded in the form of time histories by using oscillograph recorders.

TESTS AND TEST TECHNIQUE

The tests were conducted both in the Langley full-scale tunnel and outdoors. The outdoor tests were conducted primarily to provide a basis for evaluating the wind-tunnel tests at zero and very low wind speeds. The wind tunnel has a ground board 42 feet wide by 52 feet long (12.8 meters by 15.8 meters), which was considered not large enough for the exhaust flow field to develop naturally under zero wind conditions before it reached the edge of the ground board. The edge of the ground board was 21 exhaust diameters to the side and 19 diameters forward of the model center reference.

Outdoor Tests

The outdoor tests were conducted first to check the model and equipment and to develop test techniques without utilizing tunnel test time. The outdoor tests were conducted for the wind conditions existing at the time of the tests as determined by propeller-type anemometers mounted at three heights in the vicinity of the model. The desired model heading relative to the wind could be obtained by lifting the model with a mobile crane and rotating it. Because of the dependence upon existing wind conditions, the outdoor tests did not result in large amounts of uniformly arranged data. For this reason, the only outdoor test data presented in this report will be those that aid in the discussion or interpretation of the wind-tunnel data. In most instances, the wing planform used in the outdoor tests was different from the one used in the wind-tunnel tests. The model configurations investigated during the outdoor tests are given in table I. Nozzle heights above the ground of 1.17, 2.00, 3.00, 4.00, and 5.00 nozzle effective diameters were investigated for a wind-speed range from zero to about 15 knots at azimuth angles from 0° to 90°.

For the outdoor tests the engine was started with the exhaust nozzles deflected 25° rearward. As soon as the engine stabilized at idle power (approximately 70 percent of maximum compressor speed) the throttle was rapidly advanced toward full power with the nozzles still deflected. Because deflection of the nozzle reduces the effective area, the tailpipe temperature would begin to rise above allowable limits before the engine reached

TABLE I.- CONFIGURATIONS INVESTIGATED IN OUTDOOR TESTS

Nozzle arrangement	Wing planform	Inlet position	Wing position
Rectangular	Swept	Top	High
		Side	
In-line	Swept	Top	High
		Side	
	Delta	Top	Low
		Side	
Single	Swept	Top	High
		Side	

maximum speed (100 percent); therefore, when the tailpipe temperature reached the maximum allowable value (≈1200° F (667° C)), which usually occurred at about 90 to 95 percent of maximum compressor speed, the nozzles were deflected to 0° (straight down) and the engine was quickly brought to full power. The test was continued for 5 to 10 seconds and then terminated by shutting off the engine.

For many test conditions, particularly with winds, the engine would stall prior to the attainment of full power. The inlet air temperature rise for these stalled conditions was considered to be the temperature rise that existed just prior to the stall.

The oscillograph recorders, which were used for all temperature- and pressure-data acquisition, were turned on at the time of engine ignition. Time zero for the oscillograph records is the time at which the nozzles were deflected downward. The inlet air temperature rise data were obtained by comparing the temperature existing at time zero with that existing for essentially stabilized inlet conditions some 10 to 12 seconds after nozzle deflection to 0°.

Wind-Tunnel Tests

The model configurations investigated during the wind-tunnel tests are given in table II. Nozzle heights investigated were 1.17, 3.00, and 5.00 nozzle effective diameters for azimuth angles of 0°, 45°, and 90°. For an azimuth angle ψ of 0°, wind speeds of 0, 5.92, 11.85, 17.78, 23.70, 29.63, and 35.55 knots were investigated, and at azimuth angles of 45° and 90° the wind speeds were 5.92 and 11.85 knots. The reason for testing over a larger range of airspeeds for $\psi = 0°$ than for $\psi = 45°$ or 90° was that it was considered that if there were high ground winds, an actual operational airplane should be turned

TABLE II.- CONFIGURATIONS INVESTIGATED IN WIND-TUNNEL TESTS

Nozzle arrangement	Wing planform	Inlet position	Wing position
Rectangular	Delta	Top	High
		Side	
		Top	Low
		Side	
In-line		Top	High
		Side	
		Top	Low
		Side	

to head into the wind. It was also considered desirable to represent the conditions of a rolling take-off, in which case higher forward speeds would be involved.

For the wind-tunnel tests a different procedure was decided upon after conversations with NASA test pilots who had jet VTOL experience. It was considered that a short pause should occur after nozzle deflection to 0° was accomplished at partial power, to allow time for the pilot to check the various equipment. For this reason, the wind-tunnel test procedure was as follows: (1) start the engine and bring the speed up to idle power with nozzles deflected 25°, (2) increase engine speed to about 80 percent of maximum, (3) deflect nozzles to 0°, (4) pause 3 to 4 seconds, (5) bring engine speed quickly to maximum, (6) run for 6 to 8 seconds at this condition, and (7) shut down. During several tests the engine stalled immediately after nozzle deflection. When this stall occurred the test was repeated with the engine being brought to the maximum allowable speed (tailpipe temperature limit) before the nozzles were deflected downward.

Because of the short duration of each of the wind-tunnel tests and the very large volume of the wind tunnel, the ambient temperature of the tunnel rarely increased more than 10° F (6° C) during a test, and from the time of downward nozzle deflection (time zero of the time histories) to the end of the test the ambient-temperature rise was estimated to be no more than 2° F (1° C). The inlet air temperature rise was considered to be the increase in inlet air temperature from the instant of downward nozzle deflection to the time when stabilized inlet air temperature conditions were reached some 10 to 12 seconds later. Ordinarily there was no inlet temperature rise prior to nozzle deflection to 0°. In the one or two instances of early ingestion, time zero was considered to be just prior to any increase in inlet temperature above the initial ambient condition.

RESULTS AND DISCUSSION

The data presented herein should be viewed in the light of the general discussions of the mechanism of hot-gas ingestion presented in references 2, 4, 5, and 9. These papers indicate that only small rises in the inlet air temperature result from recirculation of hot exhaust gases by convection or from recirculation of the far-field flow, but a very high inlet temperature rise (approximately 200° F (111° C)) can result from the flow of exhaust gas up around the fuselage for some multiple-nozzle configurations. These reference papers show that, near the ground, multiple exhaust-nozzle arrangements result in a jet efflux which tends to form a fountain of exhaust gas flowing back upward between the main jet streams. This fountain of hot exhaust gas spreads outward along the bottom of the aircraft, upward around the fuselage, and directly into the inlets with very little time for cooling by mixing with the surrounding air.

Presentation of Data

The data of the investigation are presented in the following figures:

Time histories of inlet air temperature (wind-tunnel data).-

Average inlet air temperature rise (wind-tunnel data).-

Comparison of wind-tunnel and outdoor tests.-

Time Histories

All the average inlet air temperature rise data presented in figures 33 to 42 were obtained from time-history information similar to that presented in figures 9 to 32. For purposes of clarity, the time histories for the side inlets present data from only five representative thermocouples of the 12 in each inlet; whereas, the average temperature-rise information was obtained by utilizing all 12 probes of each side inlet. The top-inlet time histories are complete in that data from all installed probes (five in each inlet) are represented. The time-history figures are presented to show the general characteristics of temperature buildup in the various inlets. Even though the temperature probes had relatively slow response (requiring about 500 milliseconds to reach 90 percent of the actual temperature), the time histories show the serious temperature distortions across the inlets, the rapid rise of inlet air temperatures, and the high overall level of inlet air temperature that can occur for some configurations and operating conditions. The variation of nozzle pressure with time is plotted at the bottom of each of the time-history figures (presented as gage pressure) to show the buildup of nozzle pressure as the engine is brought up to maximum speed.

Rectangular nozzle arrangement.- The variation of inlet air temperature rise ΔT with time for zero nozzle deflection (nozzles directed straight downward, $\delta = 0^{\circ}$) is shown in figures 9 to 20 for the top- and side-inlet arrangements with either a high or a low wing. The time histories are for a range of head-on and side-wind speeds for nozzle heights of 1.17, 3.00, and 5.00 nozzle effective diameters above the ground.

Top inlets: The time histories of figures 9 to 14 show that the two forward top inlets (inlets 1 and 2) in general experienced a greater inlet air temperature rise than the rear inlets for either the high- or low-wing configurations at low forward speeds. The reason for higher temperatures in the forward inlets is their proximity to the wing leading edge where they are not well shielded by the wing from the recirculating hot exhaust.

The inlet air temperature rise is also seen to be greater for the high-wing configuration. Smoke-flow studies made during the tests showed that the broad, flat wing of the low-wing configuration forced the fountain of hot exhaust gas flowing upward between the nozzles to spread outward away from the inlets.

For the headwind conditions at the lowest test height, the inlet temperatures increased with increasing speed to about 18 to 24 knots, after which the hot-gas ingestion was about eliminated. The highest temperature rise occurred for the rectangular nozzle configuration with top inlets and high wing at nozzle heights of 1.17 and 3.00 effective diameters. (See figs. 9 and 10.) For this configuration, the inlet temperature rise was as high as 150° F (83° C). The spread of the time-history traces also shows the inlet temperature distortion to be very large.

In general, increasing the model height to 5.00 diameters virtually eliminated hot-gas ingestion for all forward speed conditions including zero speed.

With side winds, high inlet temperatures and temperature distortions were experienced at all test conditions.

Side inlets: The time histories of the side-inlet air temperature rise for the rectangular nozzle arrangement (high and low wings) show, in figures 15 to 20, that these inlets experienced very large temperature rises (as large as 300° F (167° C)) at the lowest test height. The temperature distortion was very great for some operating conditions (temperature differences of approximately 50° F to 300° F (28° C to 167° C)) and the ingestion occurred very quickly after downward nozzle deflection.

For some of the tests, complete time histories could not be obtained because of engine compressor stall and flame-out before the desired operating condition was reached. (See fig. 15.) As stated previously, in such cases the test procedure was altered and the time histories presented are for repeat tests in which the engine was brought to full speed before downward nozzle deflection. It is not clear just why the engine stalled under some of these test conditions; however, after discussions with representatives of the engine manufacturer, it was learned that this particular model of the engine (the Y- or prototype model) was very sensitive to its environment and that small perturbations of inlet airflow and/or temperature could, under certain combinations of inlet air conditions, result in engine stall. It will be noted that engine stall occurred sometimes when the inlet air temperatures were relatively low (fig. 15(g)); therefore, the inlet air temperature rise is certainly not the sole cause of engine stall. Small perturbations of inlet pressure could not be measured during this investigation because of very long inlet pressure tubes which damped any rapid pressure changes. It is not known, therefore, whether inlet pressure perturbations contributed to engine stall. It should be noted here that very few engine stalls occurred with the top-inlet configuration. This fact can be attributed to some extent to the lower inlet temperatures of the top-inlet configuration as compared with the temperatures of the side-inlet configurations, but the lower number of stalls probably results primarily from the relatively long inlet ducting of the top-inlet configurations. The long ducting would allow for more mixing of the inlet air

and probably more uniformly distributed temperatures at the face of the engine. This surmise is substantiated by the fact that tests reported in references 4 and 5, which had engines standing upright in the fuselage with the actual engine inlet at the top of the fuselage, resulted in many engine stalls when the average inlet air temperature rise was relatively small. In any case, the fact that this particular engine stalled is not the important point of the present investigation. The important point is that very rapid inlet air temperature changes can occur and must be eliminated in the design of the aircraft or accommodated by the design of the engine.

It will be noted in figures 15(h) to 15(k) and figures 18(h) to 18(k) that side winds result in very high inlet air temperature rises and temperature distortions (distortions of about 75° F to 400° F (42° C to 222° C)) and that the inlet temperatures for the low-wing configuration are lower than those for the high-wing configuration. The low-wing configuration did, however, have a slight inlet temperature rise before downward nozzle deflection (figs. 18(j) and 18(k)), and the time histories for these conditions were begun before the nozzle was deflected downward.

The inlet air temperatures are seen to decrease with increasing nozzle height (figs. 16, 17, 19, and 20) and to decrease at the higher forward speeds. The side winds, in general, resulted in some inlet air temperature rise at all test heights.

In-line nozzle arrangement.- The time histories of the in-line nozzle arrangement are shown in figures 21 to 32 for the top- and side-inlet arrangements with either high or low wings. The test conditions are the same as those for the rectangular nozzle arrangement.

Top inlets: The in-line nozzle arrangement with top inlets resulted in very little inlet air temperature rise for any of the forward speeds or wing positions. However, there was a modest amount of ingestion for the side-wind conditions, and this ingestion occurred at all model heights tested with either wing installation. Where time histories are not presented for some of the wind speeds, hot-gas ingestion did not occur. Even though the model with four in-line nozzles and top inlets (inlets directly over the nozzles simulating vertically mounted lift engines) showed very little or no inlet air temperature rise, other investigators, particularly those of references 4 and 5, have found very large inlet air temperature rises (approximately 100° F (56° C)) for in-line engine arrangements with some combinations of model height and wing position.

Side inlets: The time histories of the side-inlet air temperature rise for the in-line nozzle arrangement (high and low wings) show, in figures 27 to 32, that the side inlets experience considerably more hot-gas ingestion than the top in-line inlets. The temperature level, however, is very much less than that for the rectangular nozzle arrangement. For this configuration, also, the ingestion problem is virtually eliminated by relatively low forward speeds and by increasing the nozzle height above the ground.

Average Inlet Air Temperature Rise

The average inlet air temperature rise data presented in figures 33 to 42 were obtained from time-history information similar to that presented in figures 9 to 32. Data from all the installed probes in each inlet were arithmetically averaged to determine the average inlet air temperature rise.

Rectangular nozzle arrangement.- The average inlet air temperature rise for the rectangular nozzle arrangement with top or side inlets and either high or low wing is presented in figures 33 to 36. All the data show the same general pattern of high inlet air temperature rise at low speeds, with the wind from any of the test directions, and little or no hot-gas ingestion at forward speeds above about 30 knots.

Top inlets: For the high-wing configuration with top inlets (fig. 33) the maximum average inlet air temperature rise for headwind conditions occurred at very low speeds and at the intermediate test height of 3 diameters. The inlet temperature rise was about 100° F (56° C) for the forward inlets and about 50° F (28° C) for the rear inlets. The thermocouple rack mounted above and around the top inlets showed high-temperature air near the wing leading edge which caused the higher temperatures for the forward inlets.

Replacing the high wing with a low wing resulted in lower inlet air temperatures. For example, comparison of the data of figures 33 and 34 for headwinds shows the inlet air temperature rise of the low-wing configuration to be about one-half as high as that of the high-wing configuration.

Side winds resulted in very high inlet air temperatures for the top-inlet configurations with either high or low wing.

Side inlets: The average inlet air temperature rise is very high for the rectangular nozzle configuration with side inlets and either high or low wing, as shown in figures 35 and 36. Inlet temperature rises of approximately 200° F (111° C) were experienced by the high-wing configuration at low forward speeds; the low-wing configurations had somewhat lower inlet temperatures. The inlet air temperatures increased with headwind speeds to about 20 knots, then decreased rapidly, and the hot-gas ingestion was virtually eliminated for speeds greater than 30 knots. Smoke-flow studies of the exhaust showed that at the higher forward speeds the hot gases were blown rearward and did not reach the inlets.

Side winds again resulted in very high inlet temperatures, and in some instances, at low values of h/D_e, increasing the speed of the side winds greatly increased the hot-gas ingestion. Because of the high inlet temperature conditions, side winds should definitely be avoided with this rectangular exhaust-nozzle arrangement.

In-line nozzle arrangement.- The average inlet air temperature rise for the in-line nozzle configuration with either top or side inlets and high or low wing is presented in figures 37 to 40.

Top inlets: The data of figures 37 and 38 show that very little inlet air temperature rise occurs for either wing configuration with headwinds or 45° side winds. However, for the 90° side-wind condition the two forward top inlets of the high-wing configuration experienced a temperature rise of approximately 30° F to 40° F (17° C to 22° C), and all four inlets of the low-wing configuration experienced a rise of approximately 15° F to 20° F (8° C to 11° C). Data for the 90° side-wind condition also indicated that increased ingestion could occur for side winds greater than the test maximum of 11.85 knots, and for this reason side winds should be avoided.

Side inlets: The average inlet air temperature rise of the in-line nozzle arrangement with side inlets for either the high or low wing is shown in figures 39 and 40. The hot-gas ingestion is quite low at zero airspeed, but at low forward speeds near the ground the ingestion becomes fairly large, with a temperature rise of approximately 60° F (33° C) at about 20 knots. For speeds greater than 20 knots the ingestion decreases very rapidly with increasing speed, and by the time a speed of about 30 knots is reached the ingestion is reduced to zero. The low-wing configuration has slightly lower values of inlet air temperature rise than the high-wing configuration.

For the in-line-nozzle side-inlet configurations, as for the other configurations, side winds result in appreciable inlet air temperature rises at the lowest test height (approximately 40° F (22° C)), and the variation of the inlet air temperature rise with increasing speed shows that even higher inlet temperatures would occur for speeds greater than the maximum side-wind test speed of 11.85 knots.

Outdoor tests.- Since the outdoor tests were of interest for comparison with the wind-tunnel tests to determine whether the low-speed wind-tunnel data might have been affected by wall constraint, the data that are comparable have been analyzed and presented in figures 41 and 42. No time histories are presented for the outdoor tests since the data-acquisition technique was different from that for the wind-tunnel tests. All the outdoor test data were analyzed, however, and the results were used as an aid in evaluating the wind-tunnel data.

The comparison of the left-hand inlet air temperature rise data for the rectangular nozzle configuration with side inlets and high wing is shown in figure 41. Different wing planforms were used in these wind-tunnel and outdoor tests, but this difference is believed to be of secondary importance. The right-hand inlet temperature acquisition system malfunctioned for these particular outdoor tests.

Figure 42 is a comparison of the inlet air temperatures in wind-tunnel and outdoor tests for the in-line nozzle arrangement with side inlets and a low delta wing. The bands indicating the outdoor test results represent the fluctuating nature of the wind speeds that existed during the tests. Since these outdoor test results are substantially the same as the wind-tunnel test results, the zero and very low forward speed conditions are believed to be adequately simulated by the wind-tunnel tests. The reason for this agreement appears to be that the inlet temperatures during the short time that an aircraft stays in the hot environment are a function of the near-field exhaust flow and that the far-field flow, which might be affected by the groundboard size or tunnel wall restraint, causes little if any inlet air temperature rise.

Another point of interest (although the data are not presented herein) is that the single-nozzle configuration with a high swept wing (fig. 1(c)) and with either top or side inlets experienced very little ingestion (approximately 10° F (6° C)) at zero wind speed. On striking the ground, the efflux from the single nozzle does not form a fountain of hot gas flowing up around the fuselage. It simply spreads outward along the ground and is carried far away where the temperature is dissipated. The inlet air temperature rise with forward speed or side winds for this configuration with side inlets was, however, appreciable. One test at 60° yaw with a nozzle height of 2 diameters and a 10-knot wind resulted in an inlet air temperature rise of approximately 60° F (33° C). Therefore, for this configuration as for the other configurations, wind is seen to be an important parameter causing hot-gas ingestion. Configurations with closely clustered multiple nozzles might be expected to have characteristics similar to those of the single-nozzle configuration.

Effect of Nozzle Deflection

Tests were made at the beginning of the investigation to determine the minimum nozzle deflection required to prevent hot-gas ingestion. These tests were made in relatively still air for the top inlet on the single-nozzle configuration at a nozzle height of 3 diameters. A 25° rearward deflection appeared to be satisfactory, and this deflection was used throughout the investigation as the condition for engine runup prior to deflecting the nozzles straight down (0° deflection). The records taken during engine runup with the nozzles deflected indicate that all the configurations were ingestion-free for all headwind test conditions (including $V = 0$) except for the single-nozzle configuration with side inlets and a nozzle height of about 1 diameter. It is not clear why hot-gas ingestion occurred for this configuration with 25° nozzle deflection; but in any case, the ingestion with 25° nozzle deflection was much lower than that with the nozzle undeflected.

The fact that inlet air temperatures rose little or not at all with nozzles deflected rearward 25° suggests that the problem of hot-gas ingestion during take-off might be

eliminated by leaving the nozzles deflected 25° and making rolling take-offs. For this type of take-off, called a rolling vertical take-off, the airplane is operated at a weight no greater than its VTOL take-off weight. The take-off speeds are so low that no significant wing lift is developed, and the take-off speeds and distances are much less than those associated with STOL operation. Rearward nozzle deflection cannot be used to avoid the problem of hot-gas ingestion during a vertical or very low-speed landing, however, since a near-vertical nozzle orientation would be required to support the aircraft in horizontal equilibrium. Small nozzle deflections would not eliminate the hot-gas environment near the ground, and even a small constant rearward nozzle deflection of 10° would result in a horizontal component of thrust sufficient to propel the aircraft at forward speeds of approximately 180 knots. Although a considerable loss in thrust might be tolerated for landing, since landings are generally made at weights considerably below the take-off weight, hot-gas ingestion that might cause the engine to stop operating could not be tolerated.

CONCLUDING REMARKS

Results of hot-gas ingestion tests conducted in the Langley full-scale tunnel and outdoors on large-scale VTOL jet fighter-type aircraft configurations have indicated the following conclusions:

1. Hot-gas ingestion is very configuration-dependent, the nozzle arrangement, inlet position, and wing location being important variables.

   (a) The rectangular nozzle arrangement resulted in, by far, the highest inlet air temperatures, the average temperature rise being as great as 200° F (111° C).

   (b) An in-line nozzle arrangement resulted in virtually no inlet air temperature rise except in side winds.

   (c) Side inlets generally had higher inlet air temperatures than top inlets.

   (d) In the low position the wing provided a fairly effective shield for the inlets by deflecting the recirculating hot exhaust gases away from the inlets and causing reduced inlet air temperatures at the critical conditions of zero and low forward speeds.

2. Wind speed and direction have a large effect on the magnitude of the inlet air temperatures.

   (a) Maximum inlet air temperatures were found to occur at wind speeds from zero to 20 knots for winds from any test direction.

   (b) With headwinds greater than about 30 knots the hot-gas ingestion was virtually eliminated.

3. Deflecting the exhaust rearward 25° with vectoring nozzles generally eliminated the ingestion of hot exhaust gases.

4. Although various large- and small-scale model investigations have produced much information of a general nature which can be used as design guidelines, the solution of hot-gas ingestion problems is still in an exploratory stage; thus, at present, tests should be conducted on each configuration at each operating condition that is expected to be encountered.

Langley Research Center,
National Aeronautics and Space Administration,
Langley Station, Hampton, Va., December 15, 1967,
721-03-00-03-23.

REFERENCES

1. McKinney, M. O., Jr.; Kuhn, R. E.; and Reeder, J. P.: Aerodynamics and Flying Qualities of Jet V/STOL Airplanes. [Preprint] 864A, Soc. Automotive Engrs., Apr. 1964.

2. Langfelder, Bodeneffekte bei Senkrechtstart-Flugzeugen: (Ground Effects of VTOL Aircraft). EWR-Nr. 37/62, Entwick lungsring Süd (München), Mar. 1963.

3. Speth, Robert F.; and Ryan, P. E.: A Generalized Experimental Study of Inlet Temperature Rise of Jet V/STOL Aircraft in Ground Effect. Rept. No. 2099-928003 (Contract No. N600 (19)63320), Bell Aerosyst. Co., Apr. 5, 1966. (Available from DDC as AD 641 610.)

4. Tolhurst, William H., Jr.; and Kelly, Mark W.: Characteristics of Two Large-Scale Jet-Lift Propulsion Systems. Conference on V/STOL and STOL Aircraft, NASA SP-116, 1966, pp. 205-228.

5. Lavi, Rahim: Parametric Investigation of VTOL Hot Gas Ingestion and Induced Jet Effects in Ground Proximity. Report NOR 67-32 (Contract NOw 66-0316-f), Northrop Corp., Feb. 14, 1967.

6. Rolls, L. Stewart: Operational Experiences With the X-14A Deflected-Jet VTOL Aircraft. Conference on Aircraft Operating Problems, NASA SP-83, 1965, pp. 299-307.

7. Mohne, E. A.: V/STOL Exhaust Gas Ingestion Test Hovering Test Facility. NA 64-1142, North Am. Aviation, Inc., Mar. 1964.

8. Smith, Fred: CL 757 Flight Test Results. Rept. No. LR 18781 (Contract AF 33(657)-10534), Lockheed-California Co., Apr. 28, 1965.

9. McLemore, H. Clyde: Considerations of Hot-Gas Ingestion for Jet V/STOL Aircraft. Conference on V/STOL and STOL Aircraft, NASA SP-116, 1966, pp. 191-204.

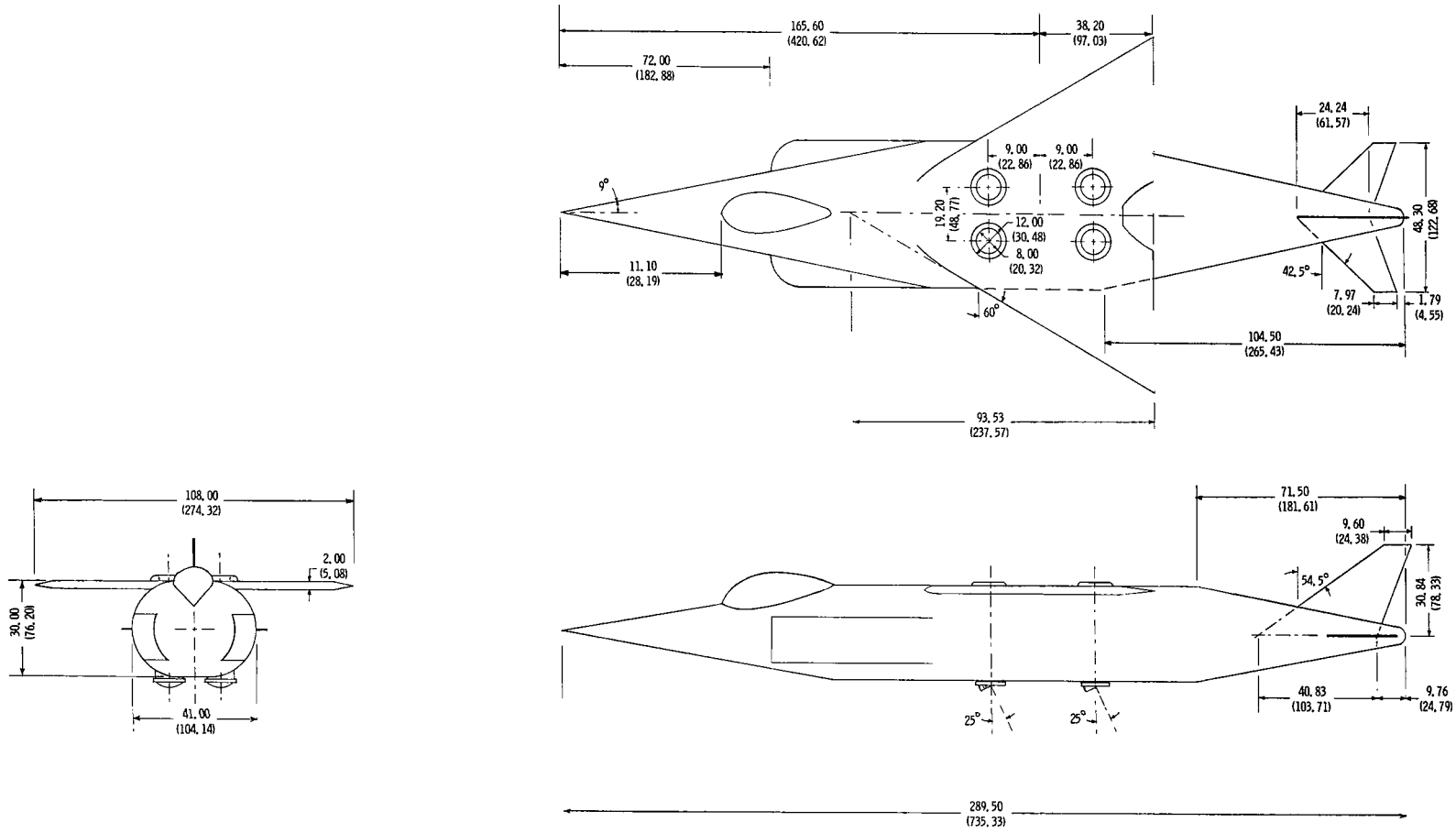

(a) Rectangular exhaust-nozzle arrangement with top inlets.

Figure 1.- General arrangement of model. All dimensions are in inches and parenthetically in centimeters.

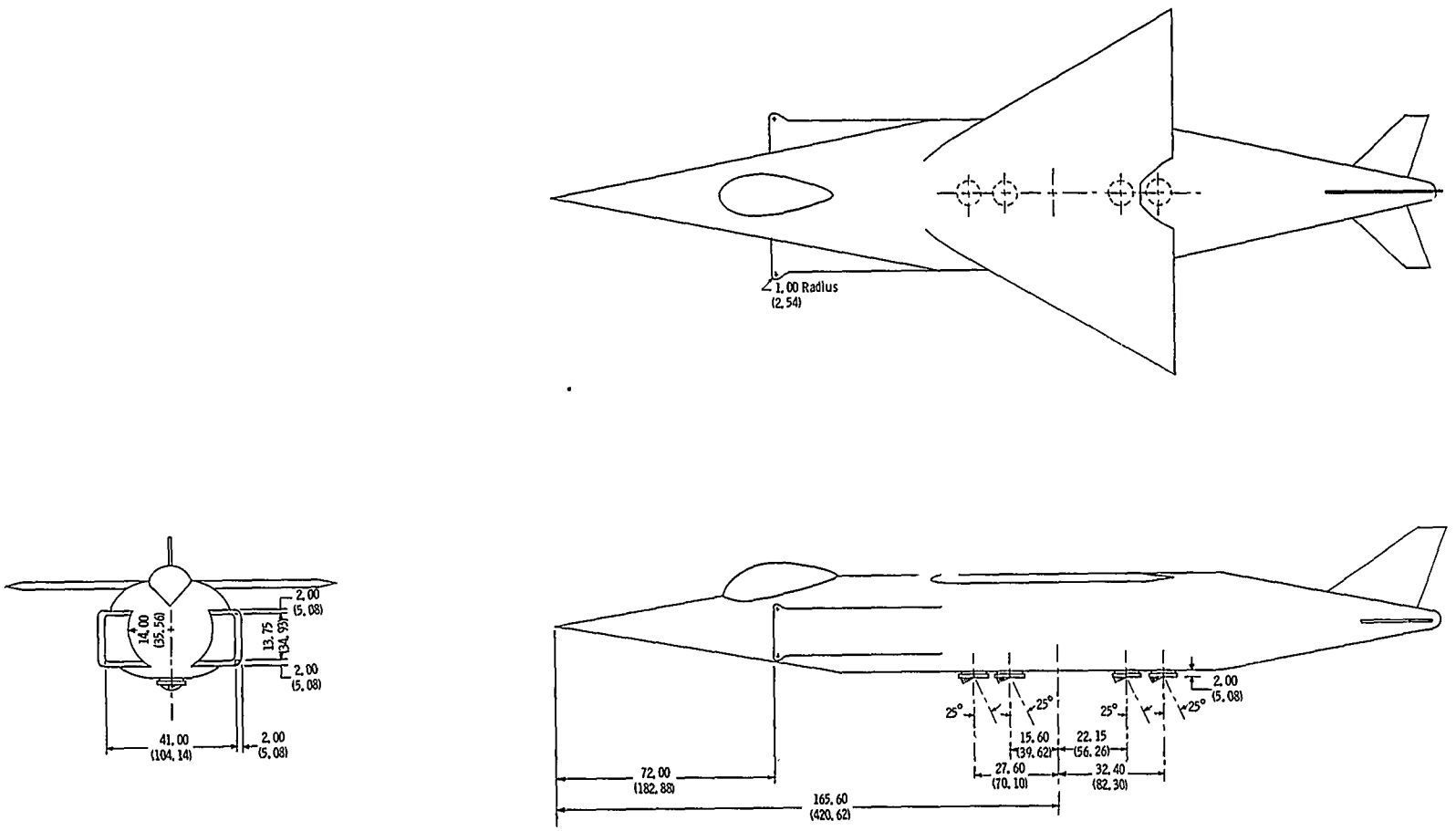

(b) In-line exhaust-nozzle arrangement with forward-facing side inlets.

Figure 1.- Continued.

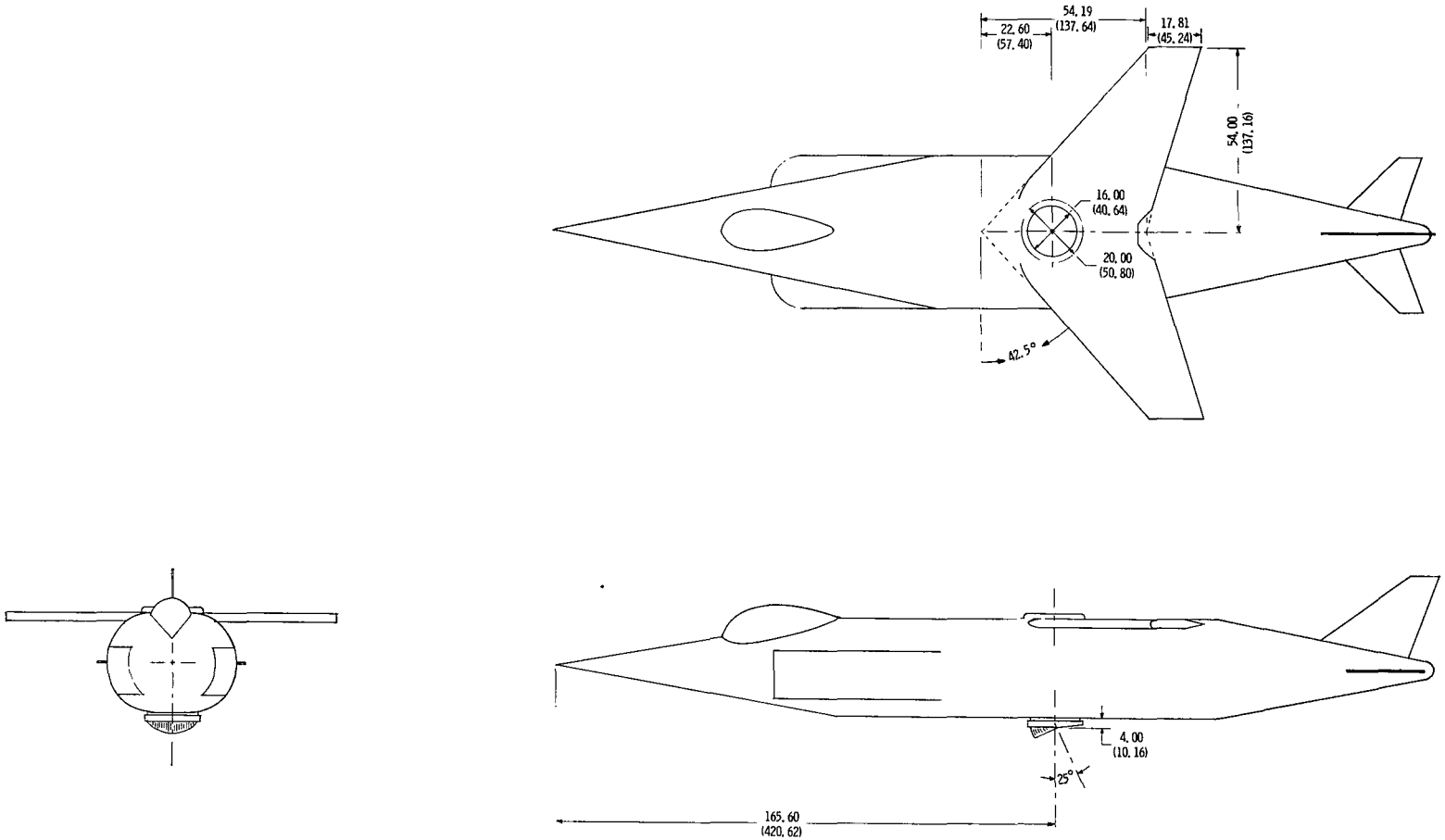

(c) Single exhaust-nozzle arrangement with top inlet and high swept wing.

Figure 1.- Concluded.

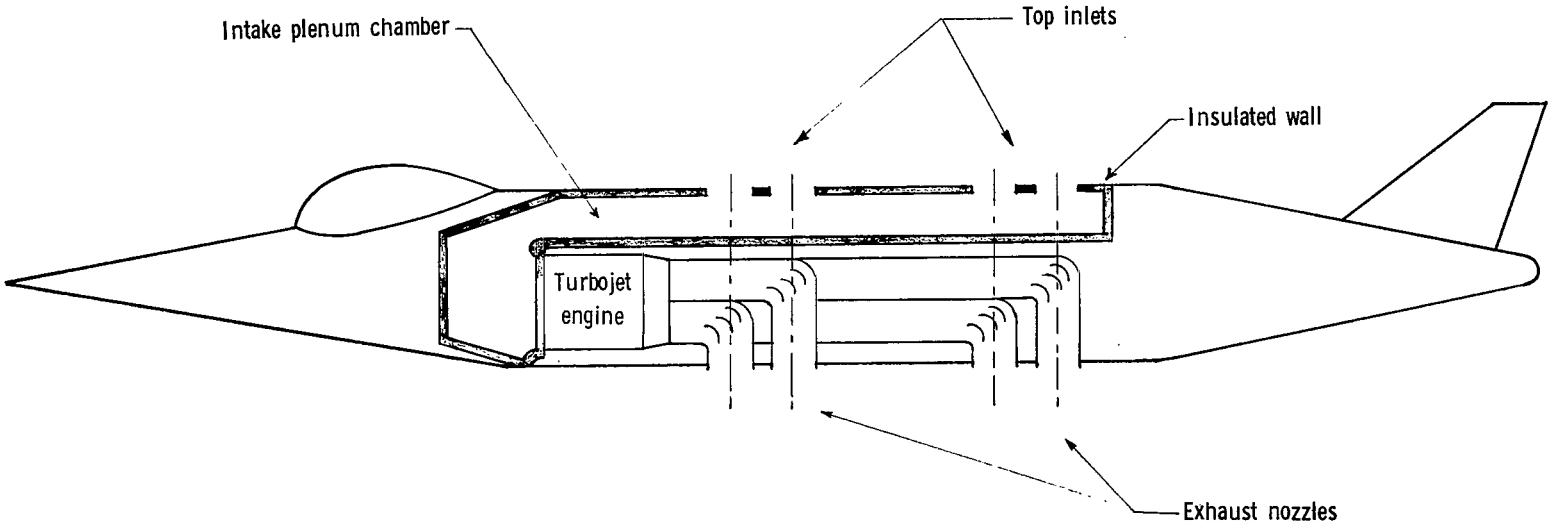

Figure 2.- Schematic arrangement of inlets, exhausts, and plenum chamber. (In-line lift-engine configuration illustrated.)

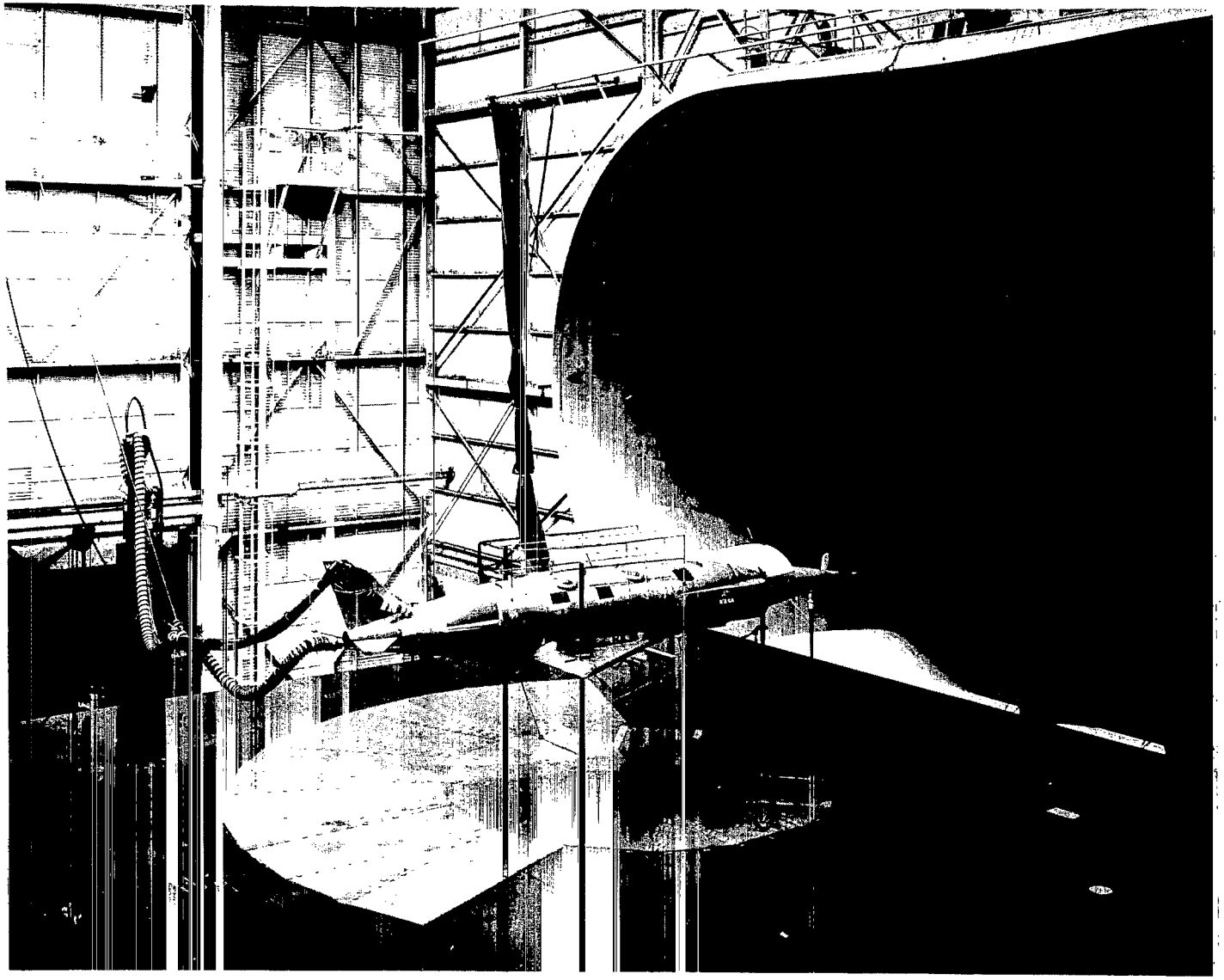

(a) Three-quarter rear view of model with top, rectangular arrangement of inlets. L-66-5802

Figure 3.- Model and test setup in the Langley full-scale tunnel.

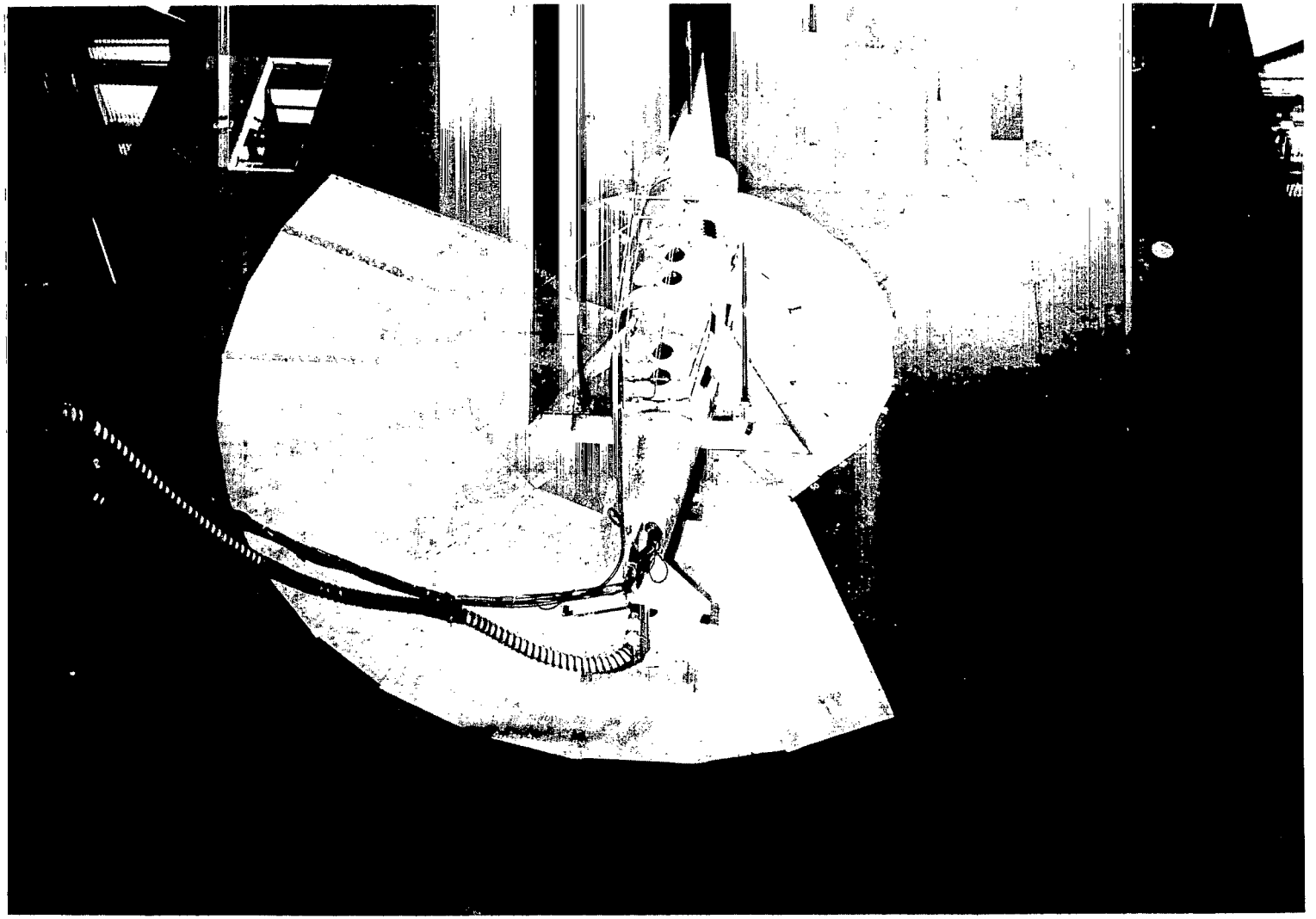

(b) Three-quarter top view of model with top, in-line arrangement of inlets. L-66-5088

Figure 3.- Concluded.

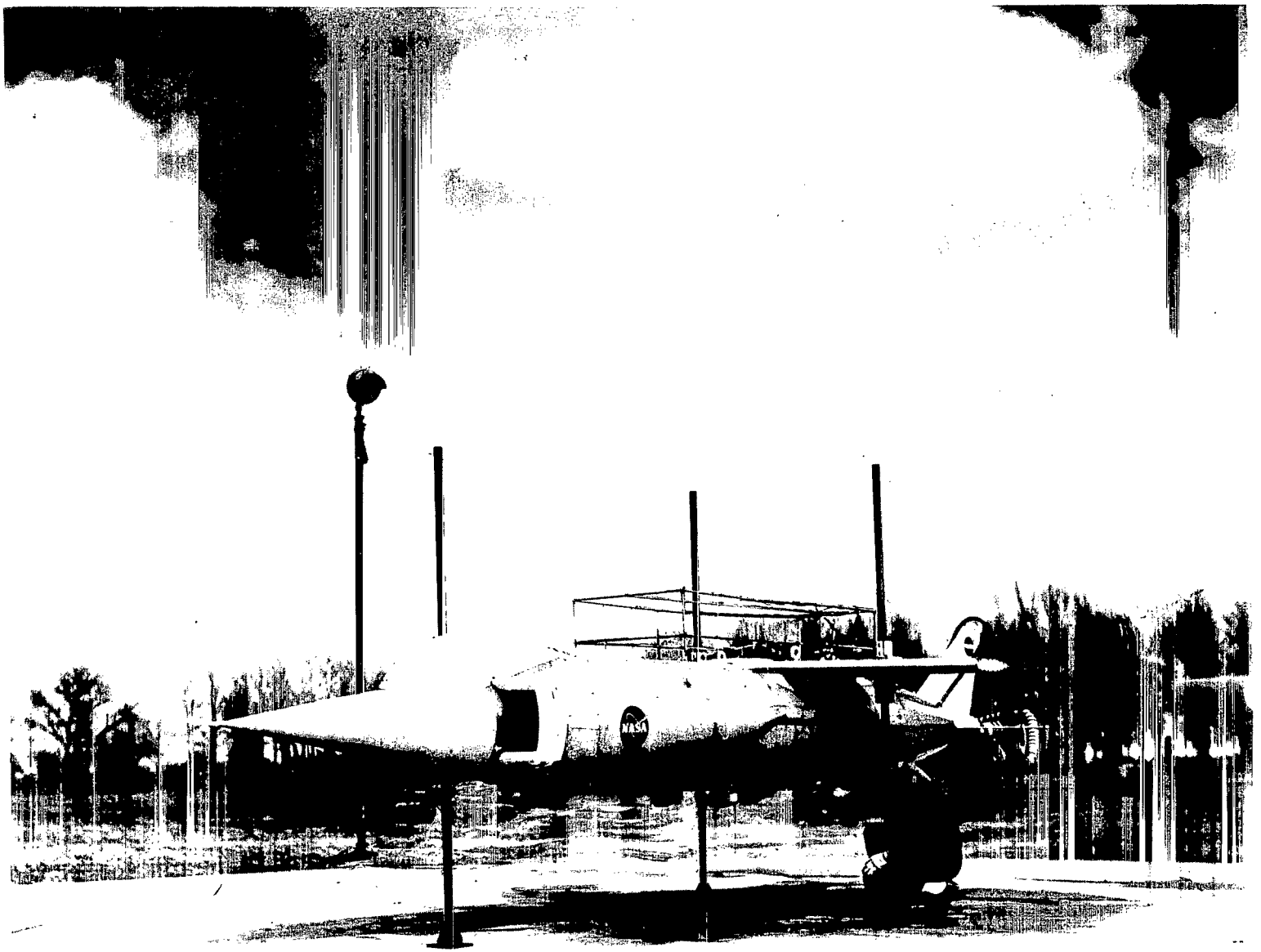

Figure 4.- Model mounted for outdoor tests. (Rectangular nozzle arrangement with side inlets.)

L-66-1973.1

Figure 5.- Typical temperature-pressure rake installation in top inlets. (Front inlets of in-line arrangement.) L-66-5086

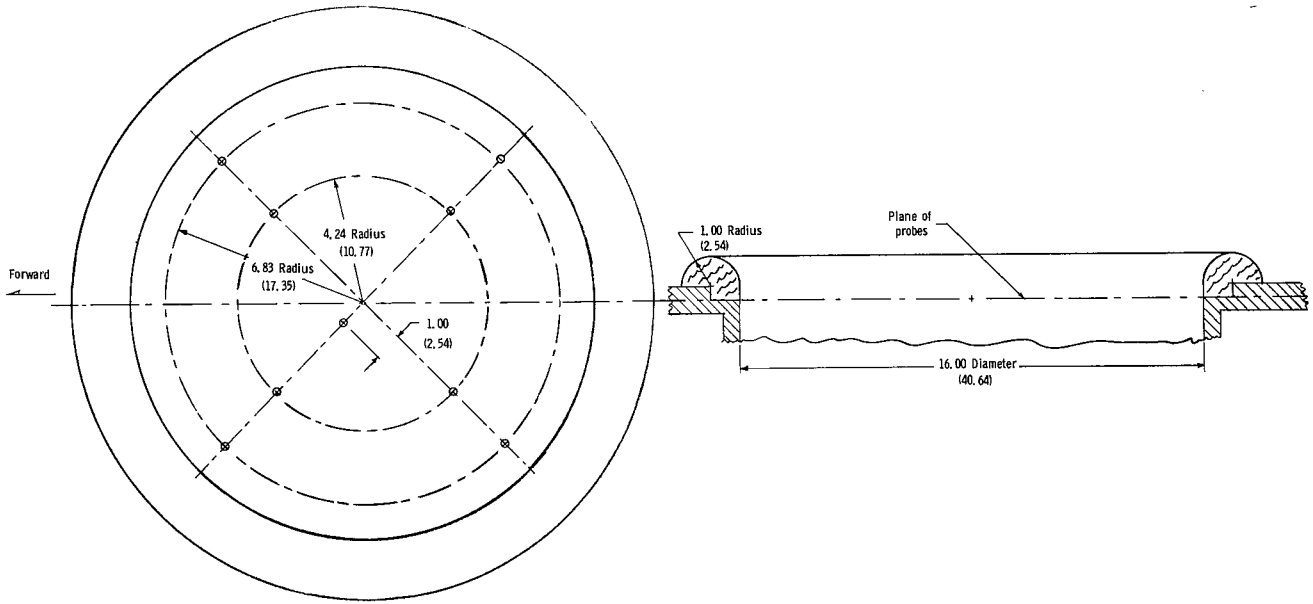

(a) Single top inlet. Symbols denote probe locations.

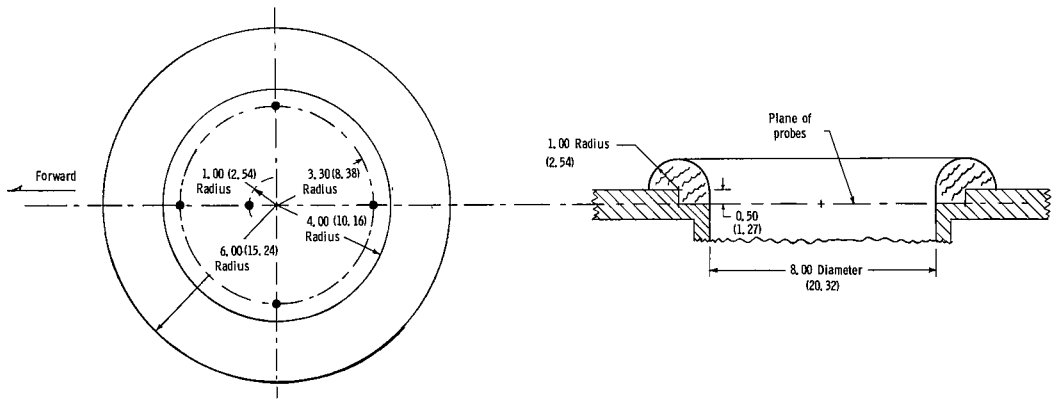

(b) Inlet 4 of in-line configuration. Symbols denote probe locations.

Figure 6.- Locations of temperature probes in inlet. All dimensions are in inches and parenthetically in centimeters.

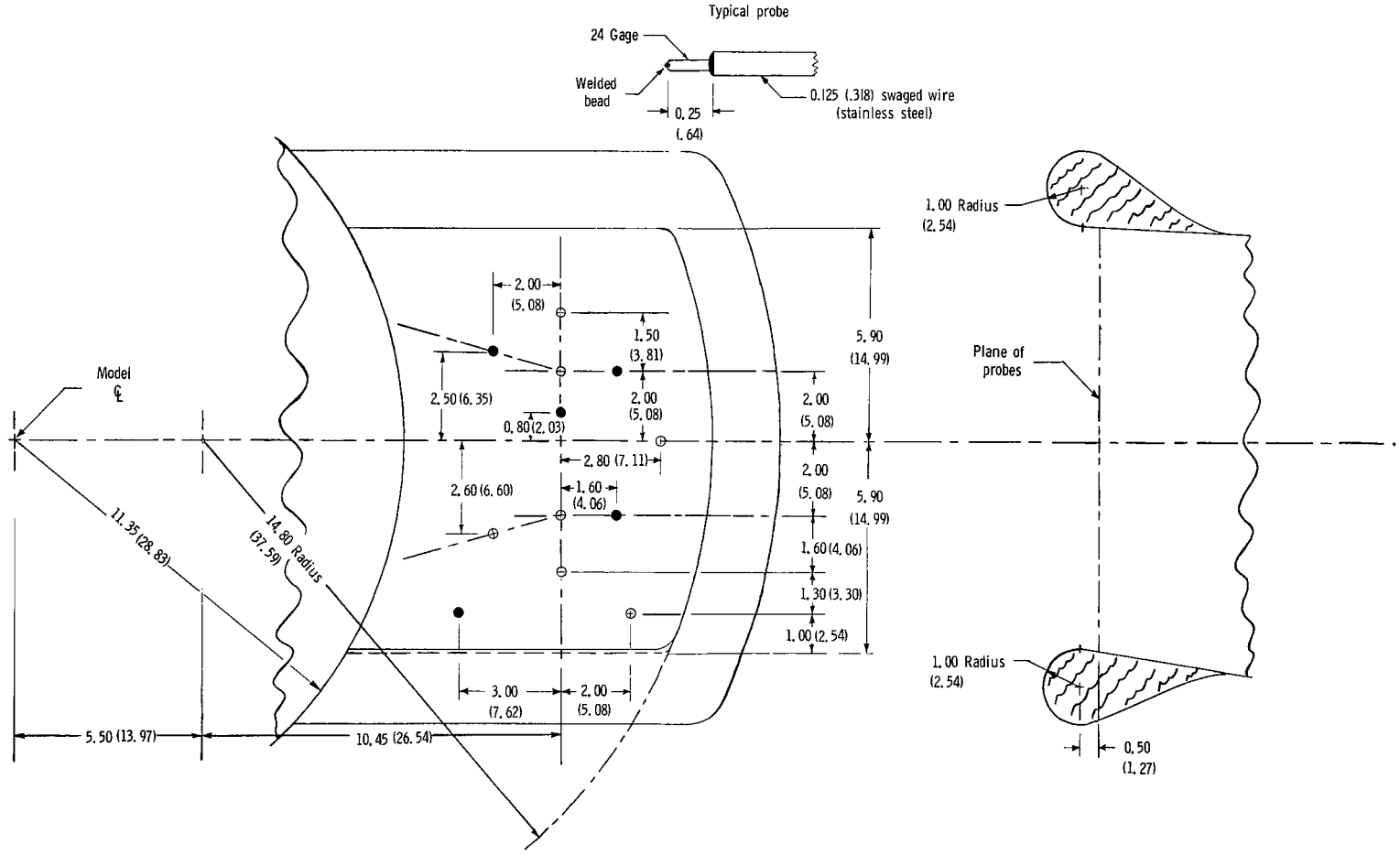

(c) Side inlet (inlet 1). Darkened symbols denote probe locations included in time histories.

Figure 6.- Concluded.

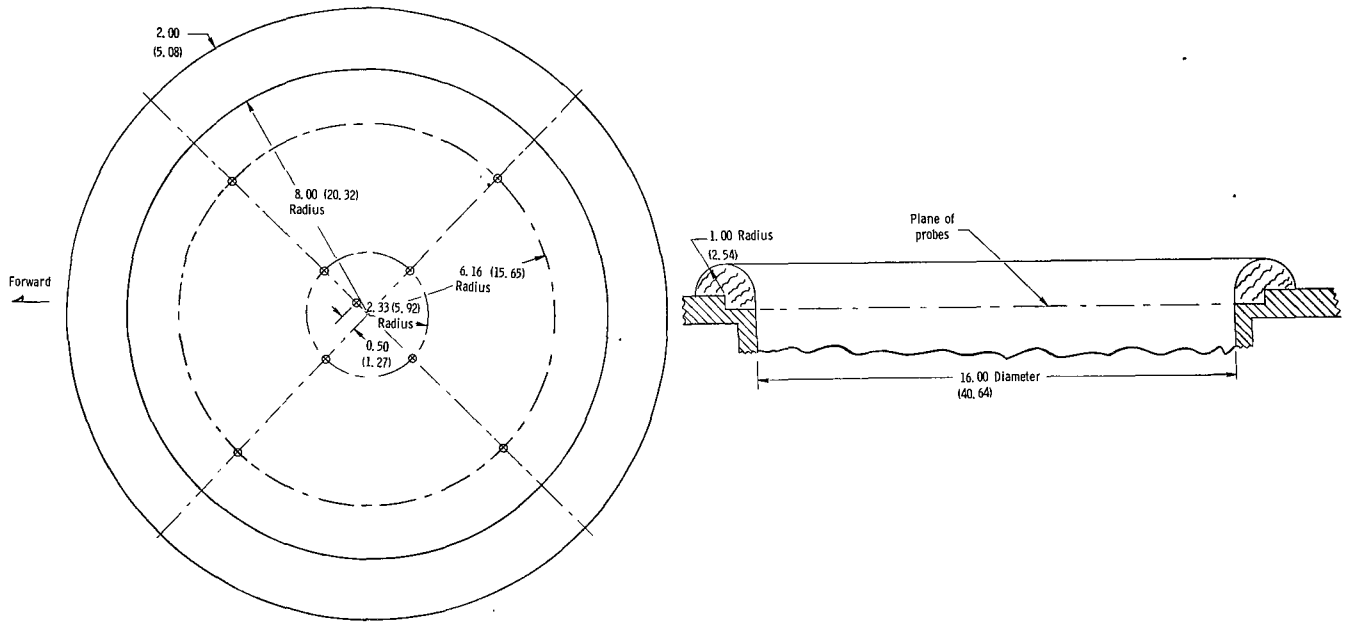

(a) Single top inlet. Symbols denote probe locations.

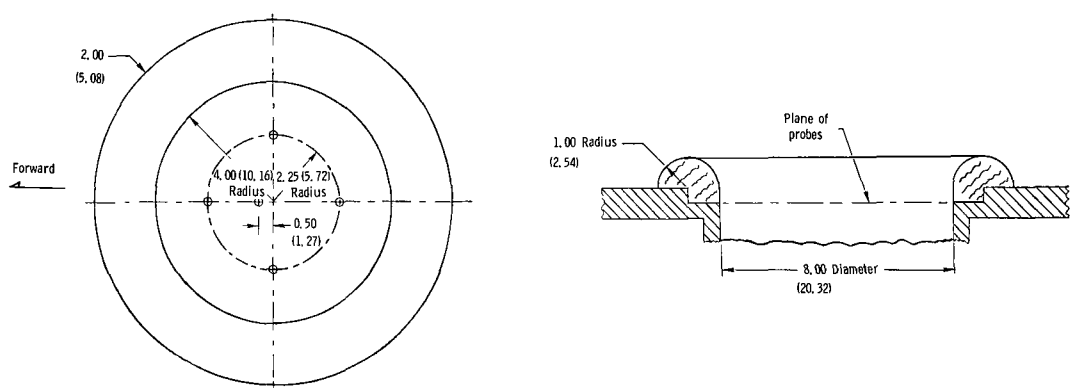

(b) Inlet 4 of in-line configuration. Symbols denote probe locations.

Figure 7.- Locations of static-pressure probes in inlet. All dimensions are in inches and parenthetically in centimeters.

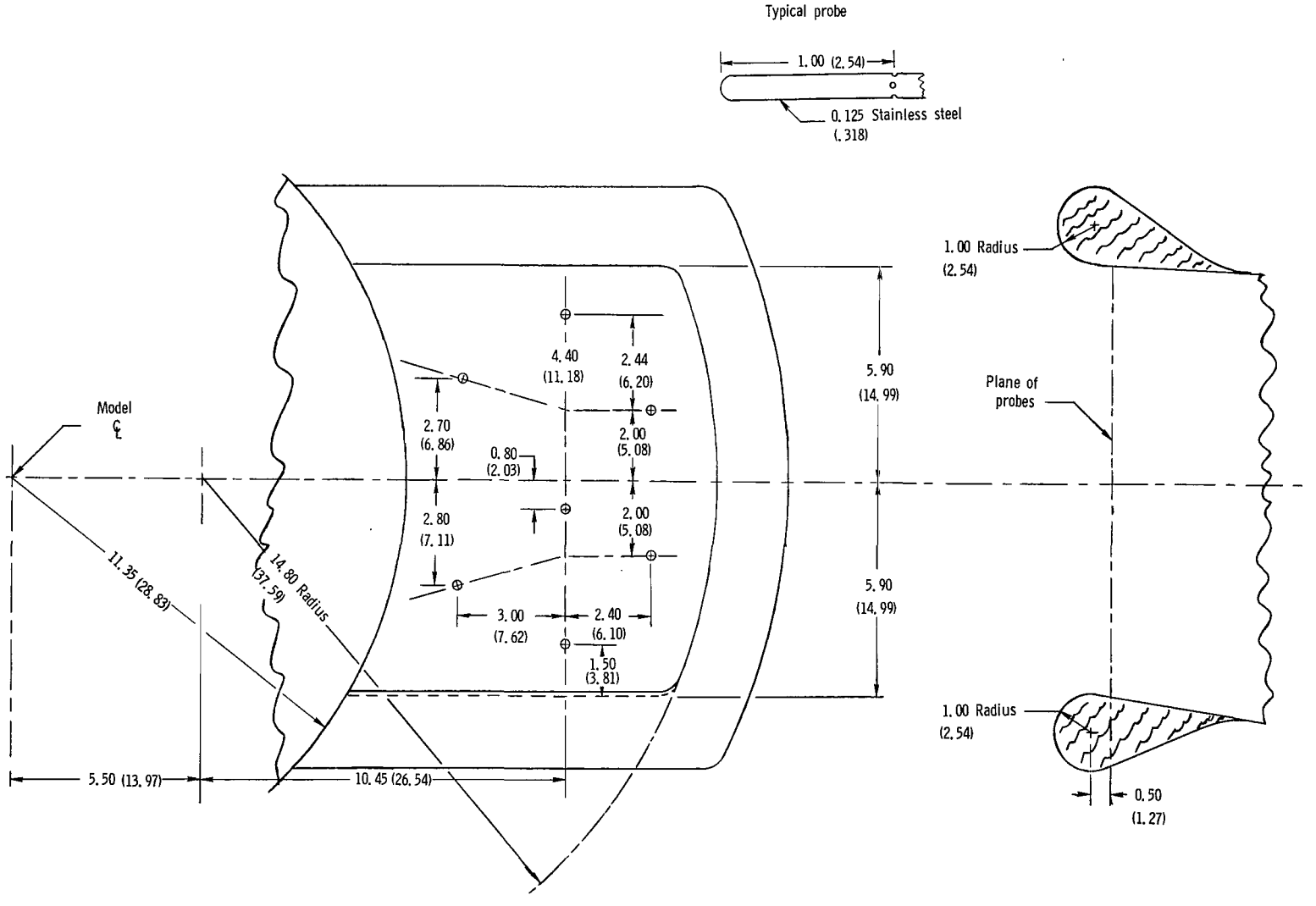

(c) Side inlet (inlet 1). Symbols denote probe locations.

Figure 7.- Concluded.

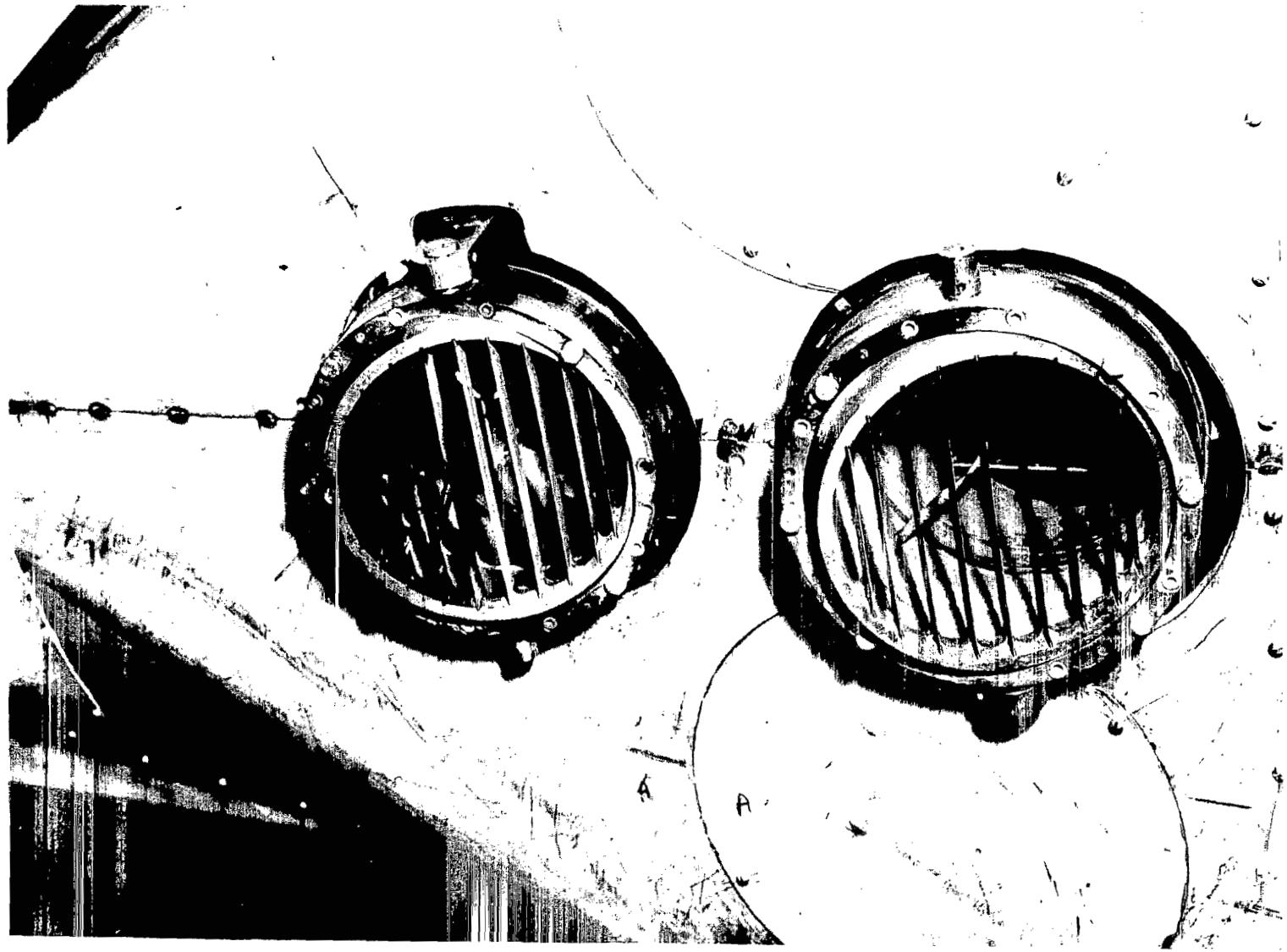

Figure 8.- Typical nozzles with vanes for deflecting the exhaust. (Front nozzles of in-line arrangement.)

L-66-5085

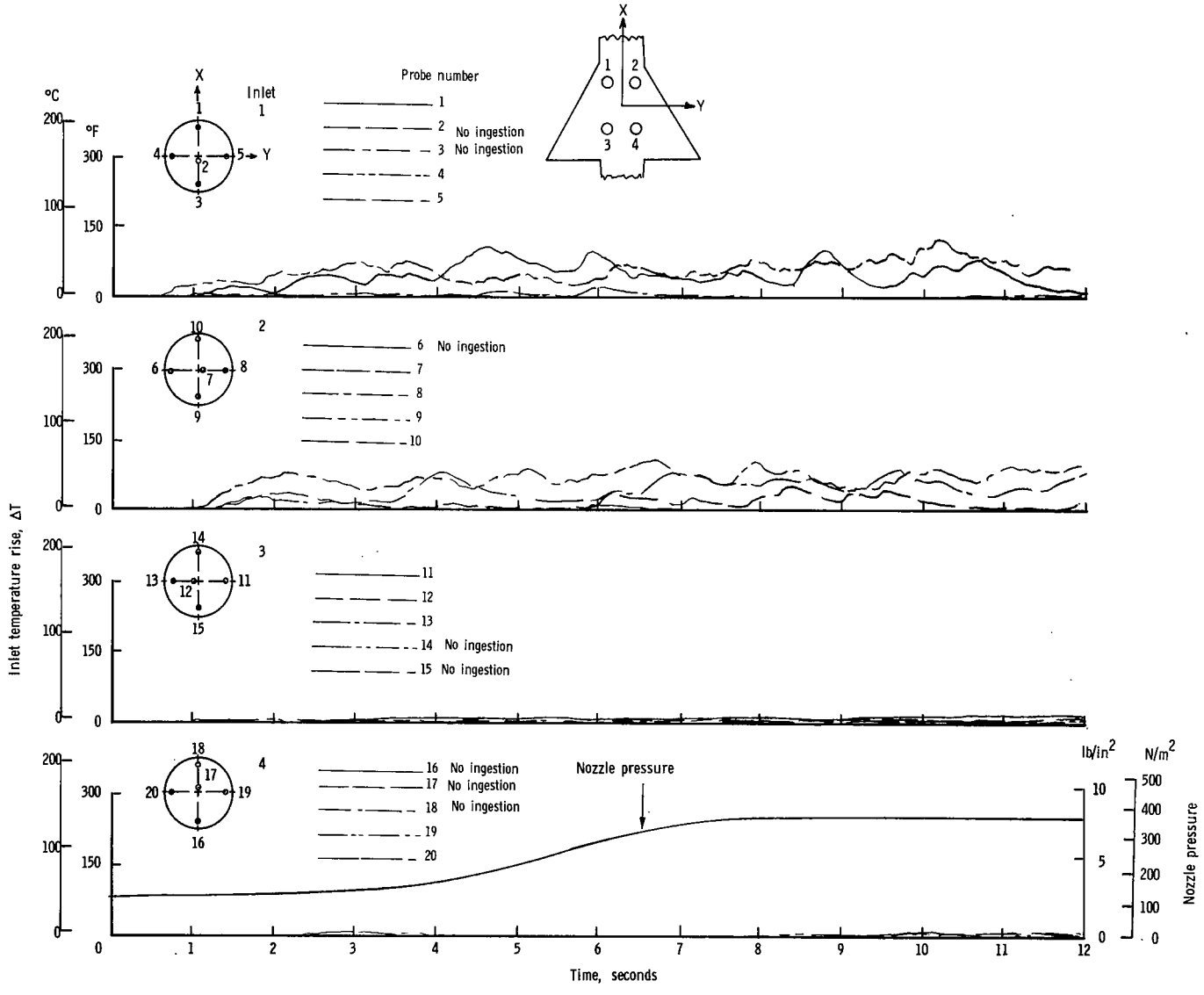

(a) $\psi = 0^0$; V = 0 knots.

Figure 9.- Variation of inlet air temperature rise with time for the rectangular nozzle arrangement with top inlets and high delta wing. $h/D_e = 1.17$.

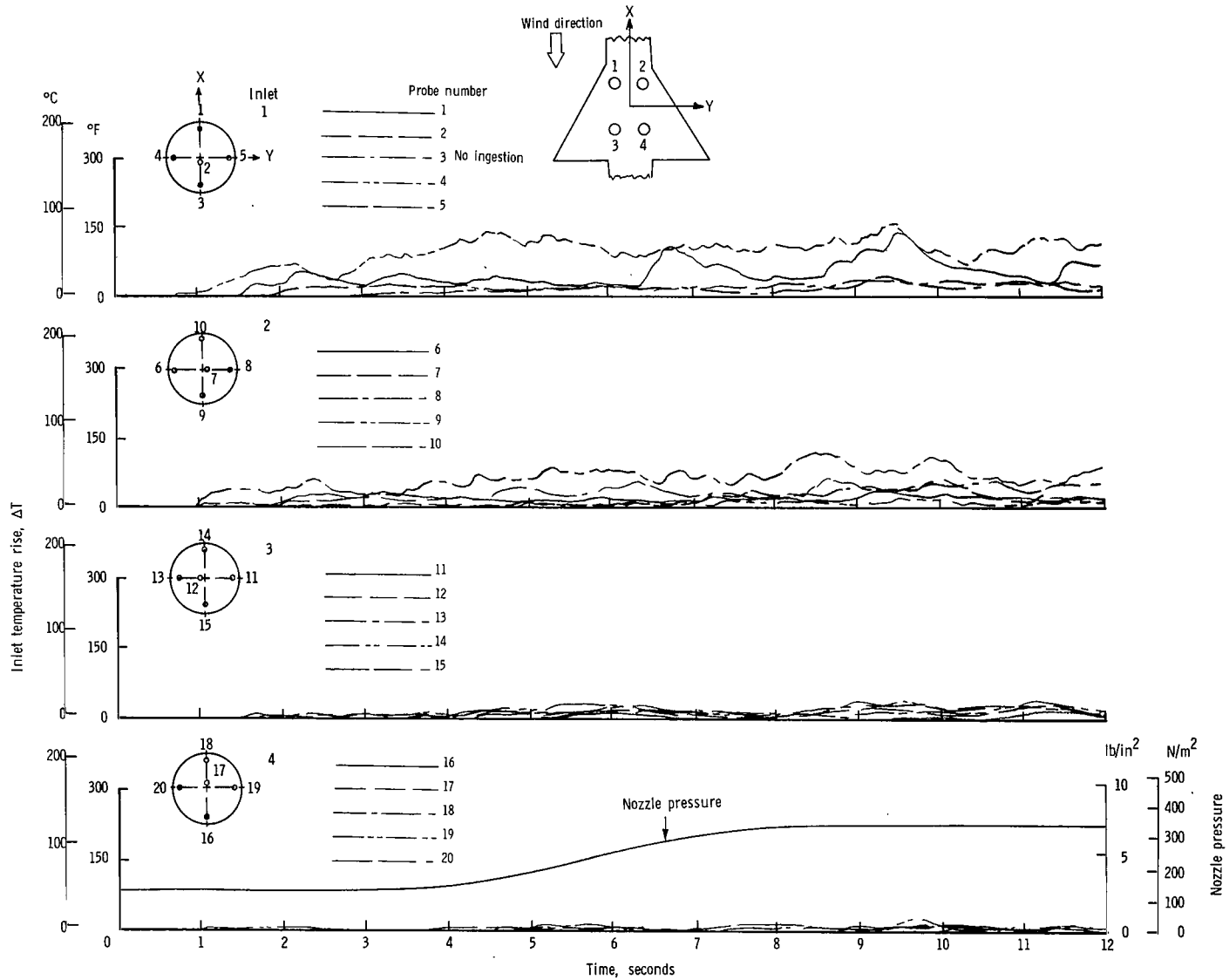

(b) $\psi = 0^0$; V = 5.92 knots.

Figure 9.- Continued.

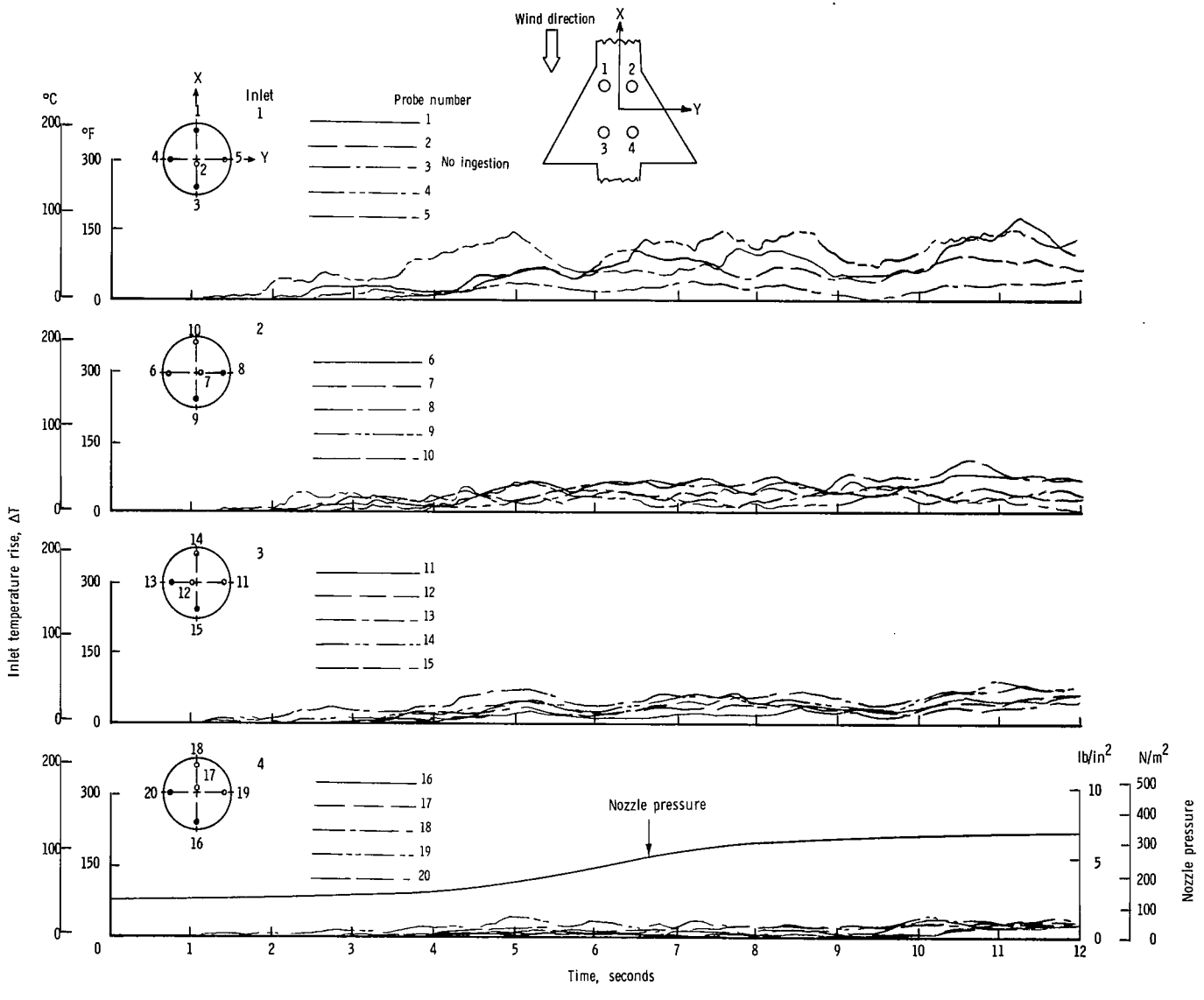

(c) $\psi = 0^0$; V = 11.85 knots.

Figure 9.- Continued.

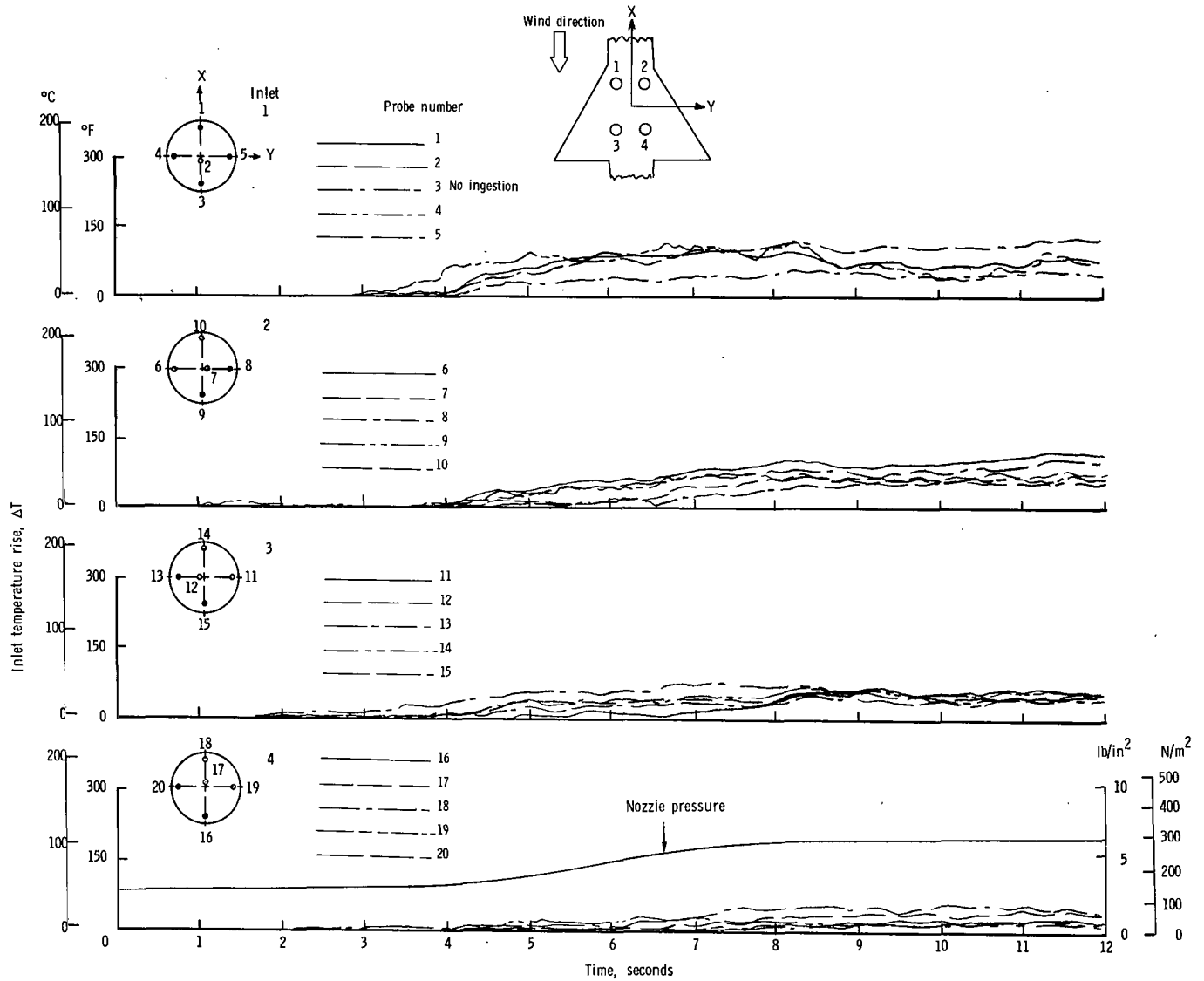

(d) $\psi = 0^{o}$; V = 17.78 knots.

Figure 9.- Continued.

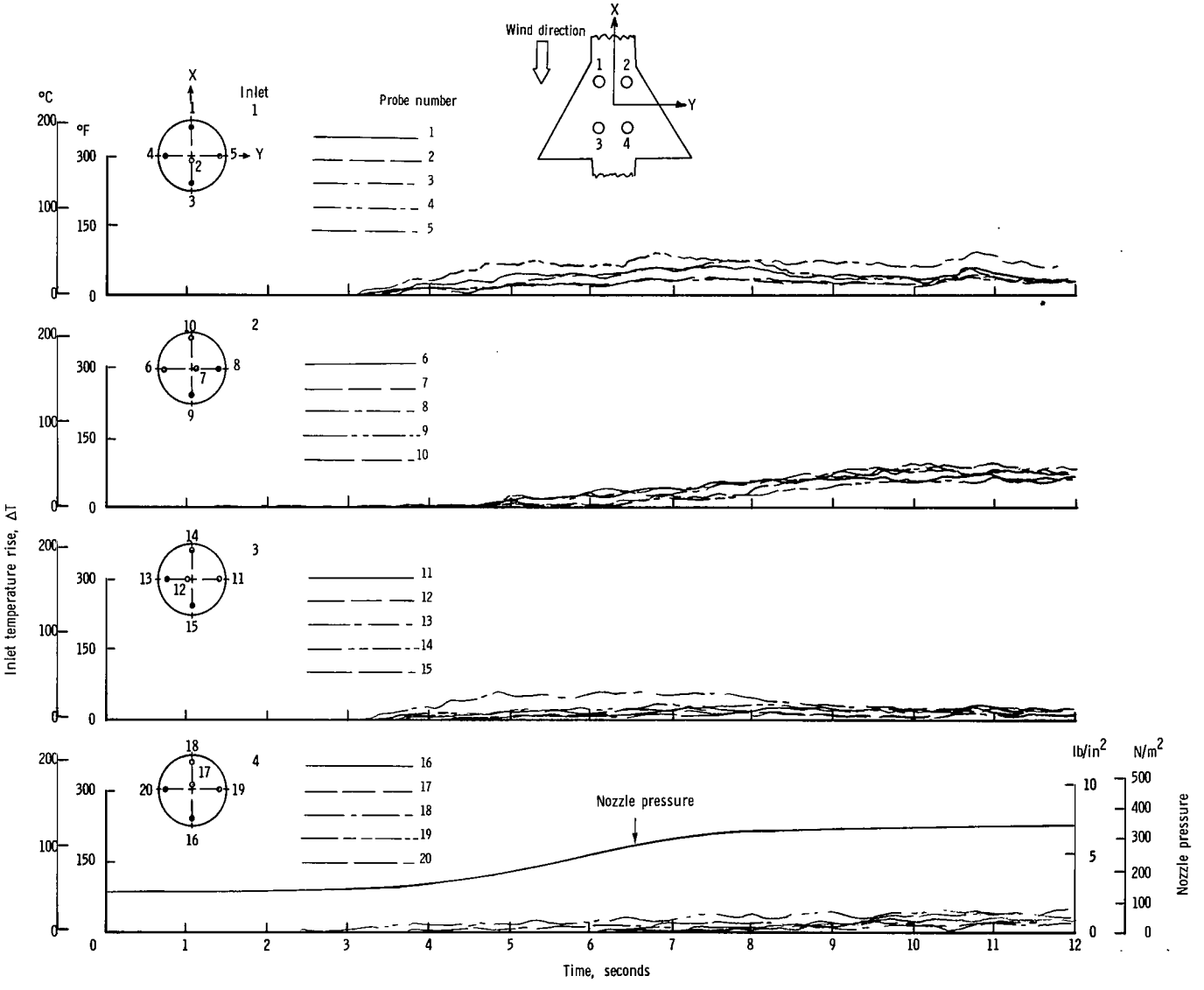

(e) $\psi = 0^{0}$; V = 23.70 knots.

Figure 9.- Continued.

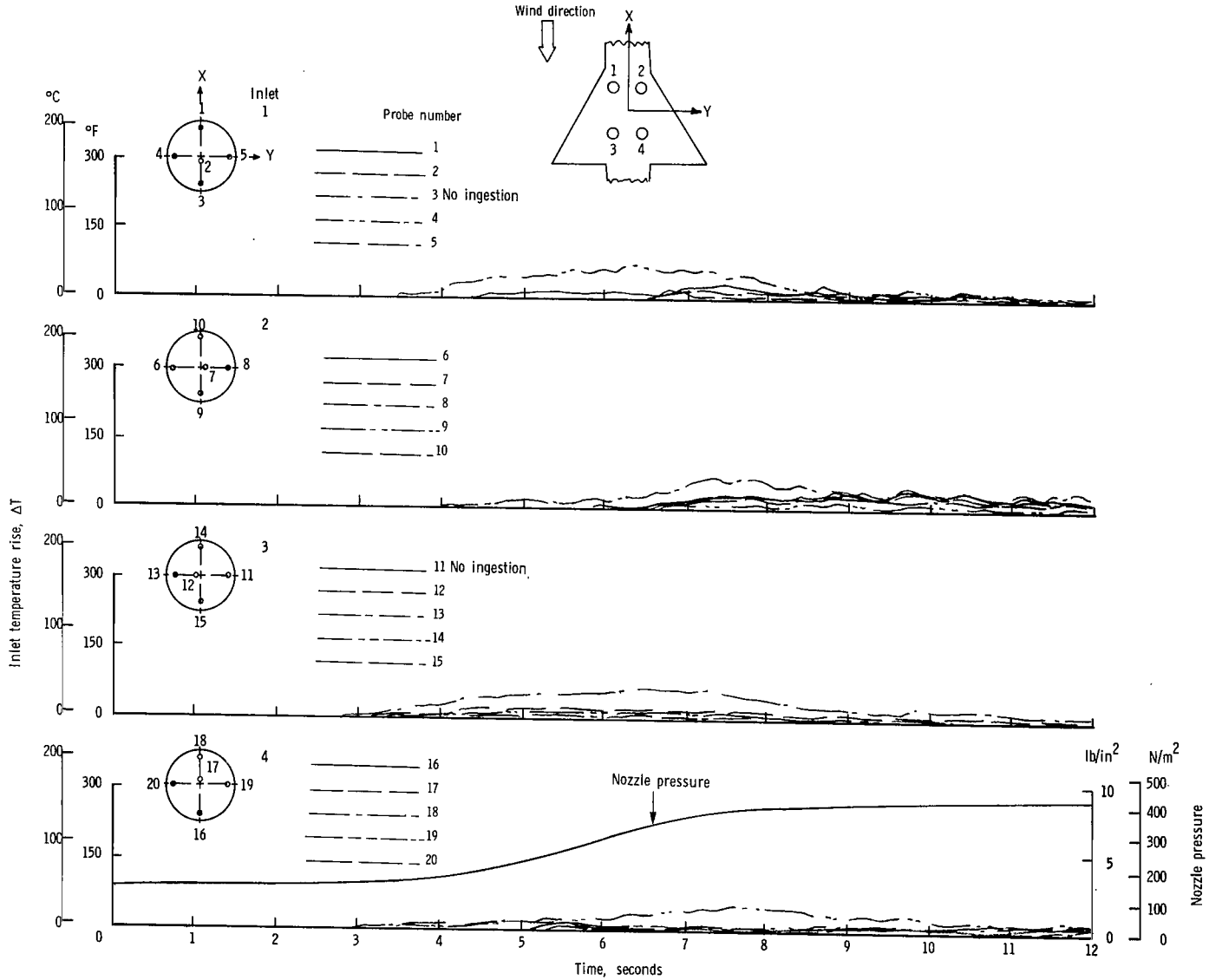

(f) $\psi = 0^0$; V = 29.63 knots.

Figure 9.- Continued.

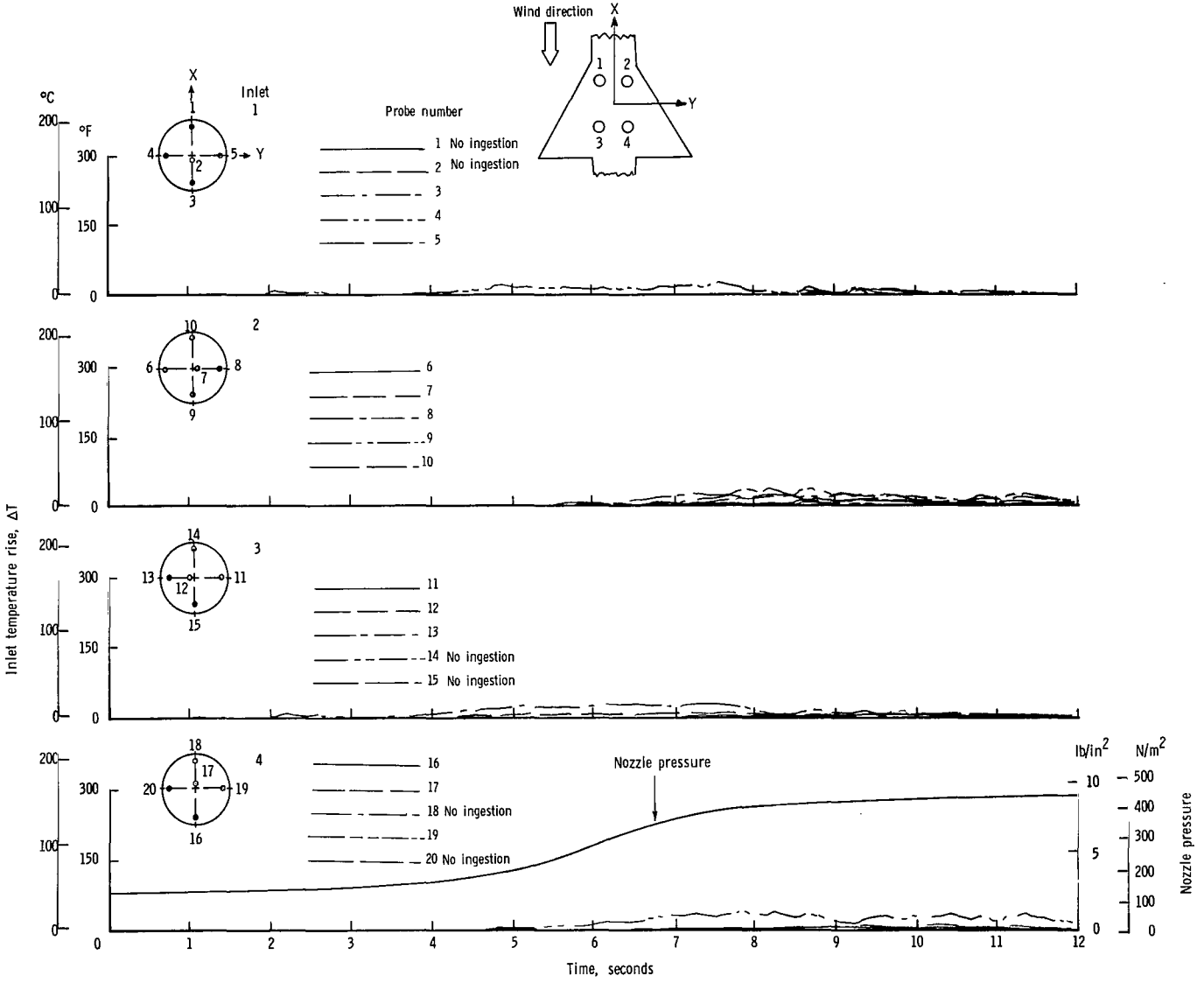

(g) $\psi = 0^0$; V = 35.55 knots.

Figure 9.- Continued.

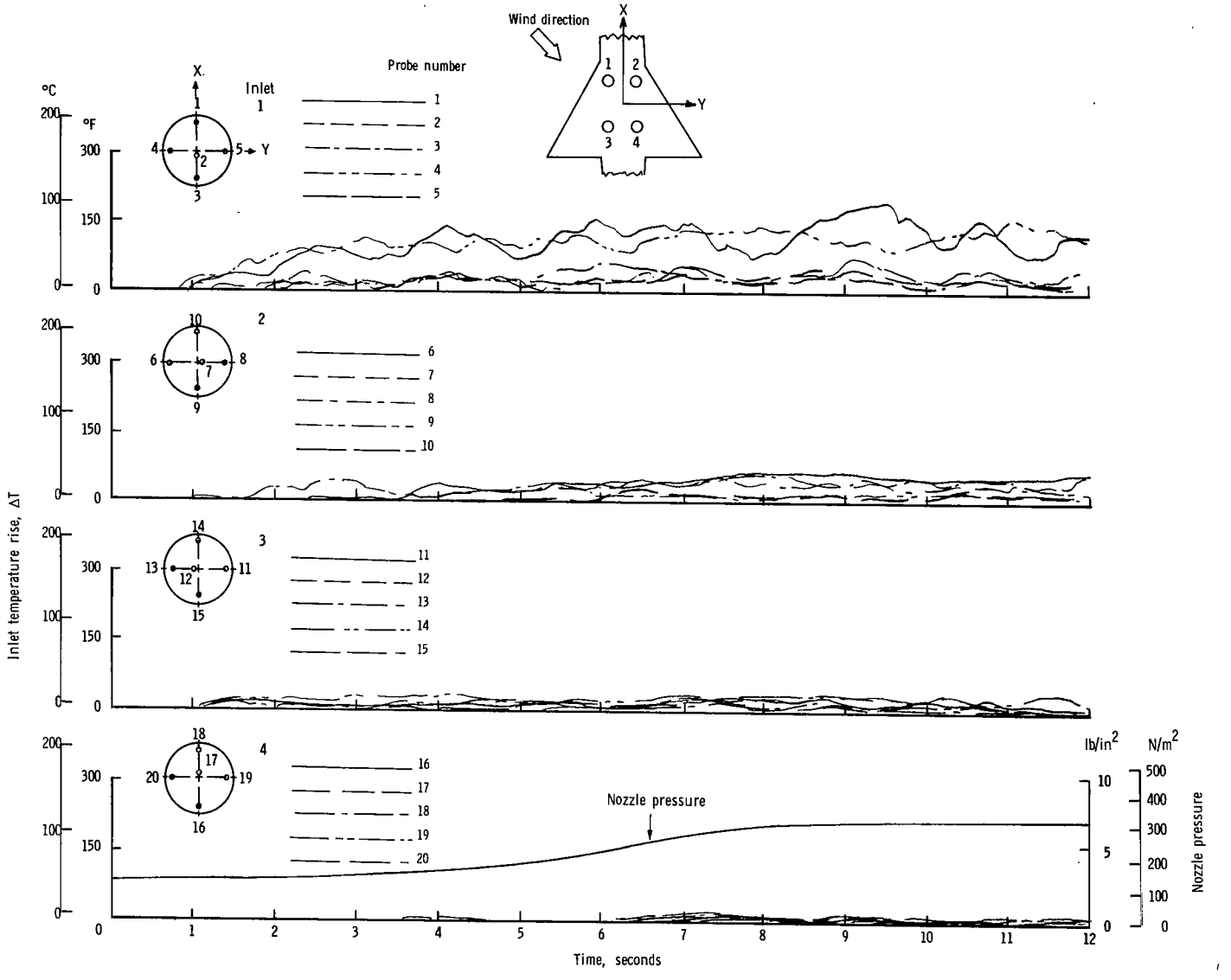

(h) $\psi = 45^0$; V = 5.92 knots.

Figure 9.- Continued.

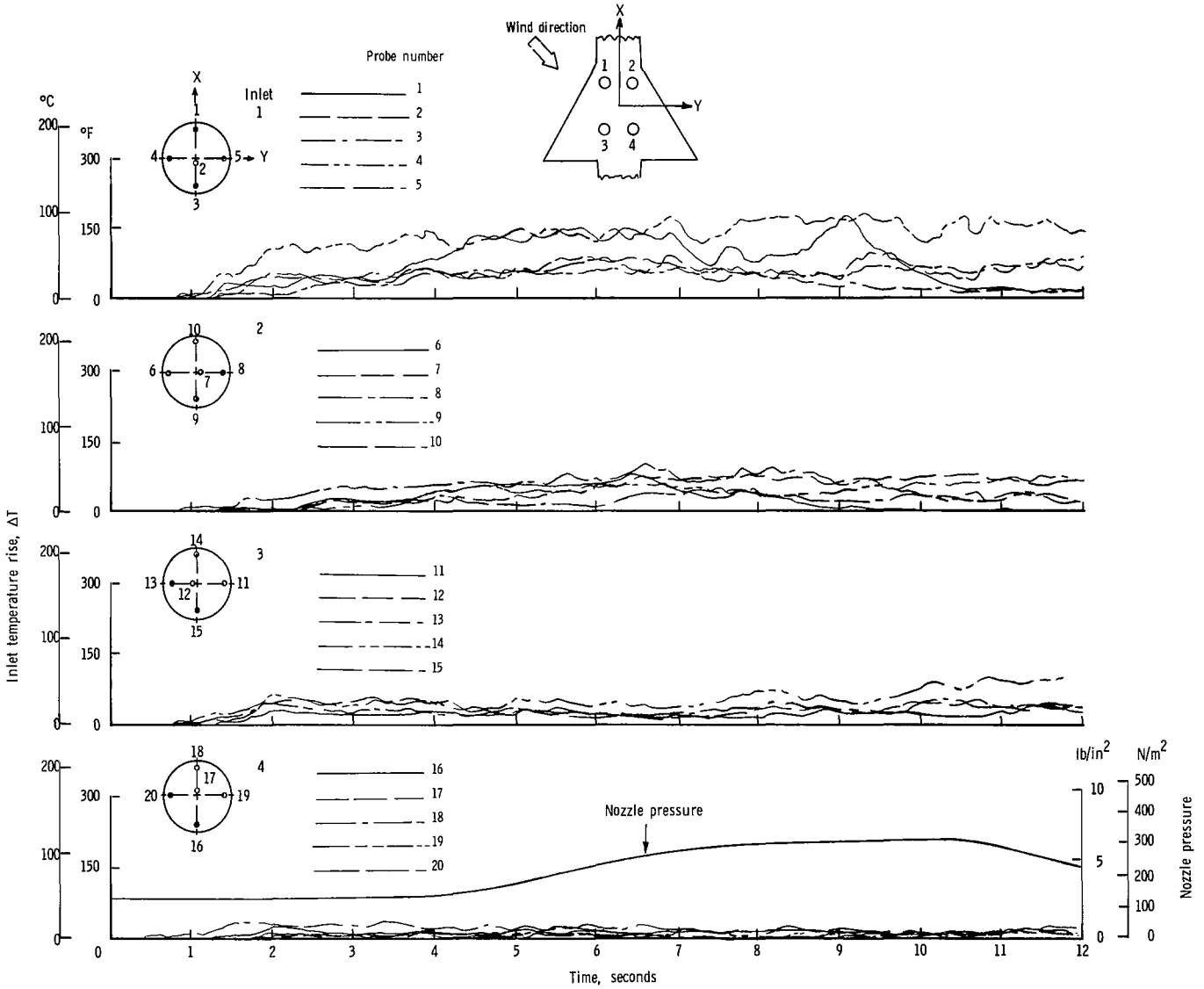

(i) $\psi = 45^{0}$; V = 11.85 knots.

Figure 9.- Continued.

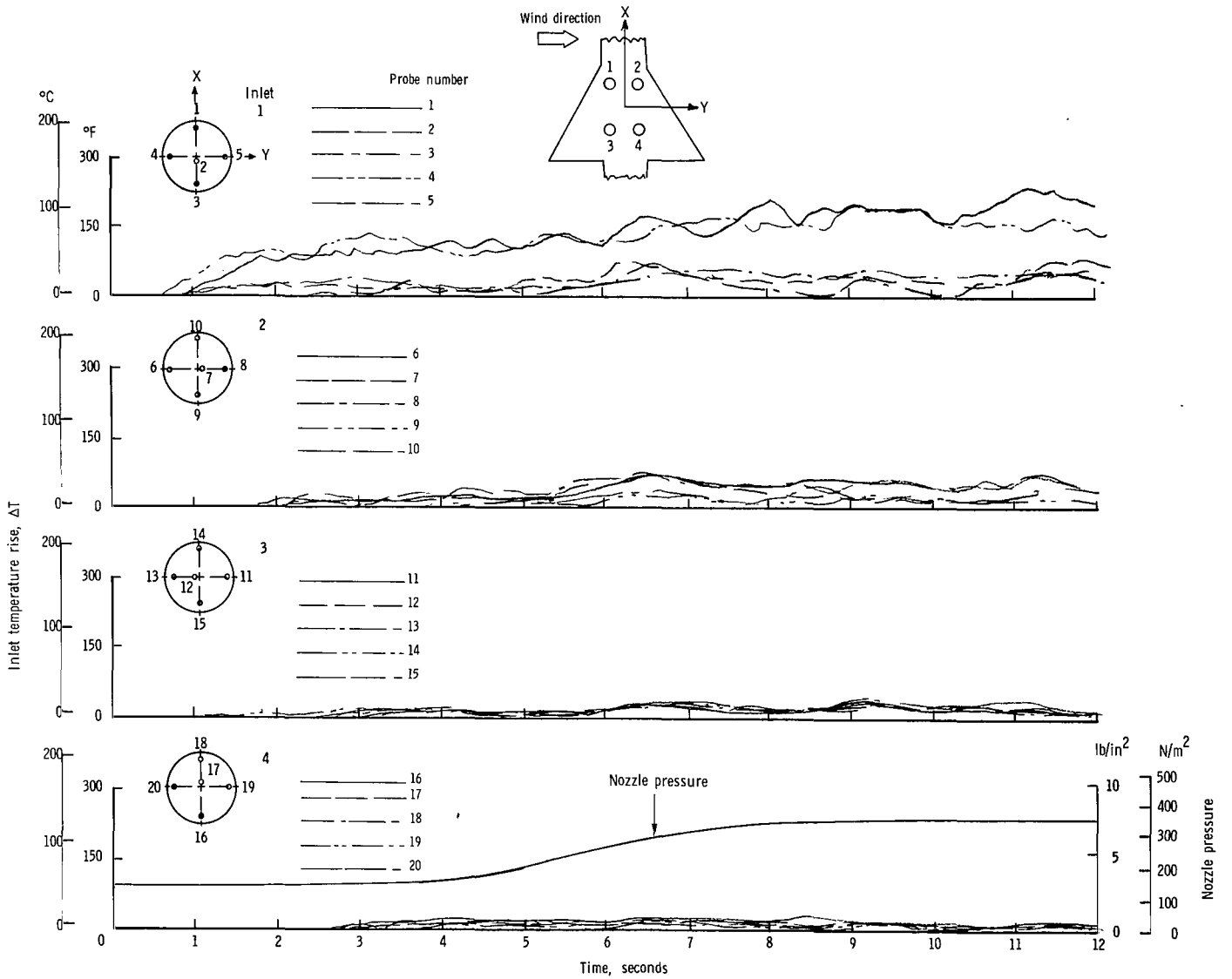

(j) $\psi = 90^{o}$; V = 5.92 knots.

Figure 9.- Continued.

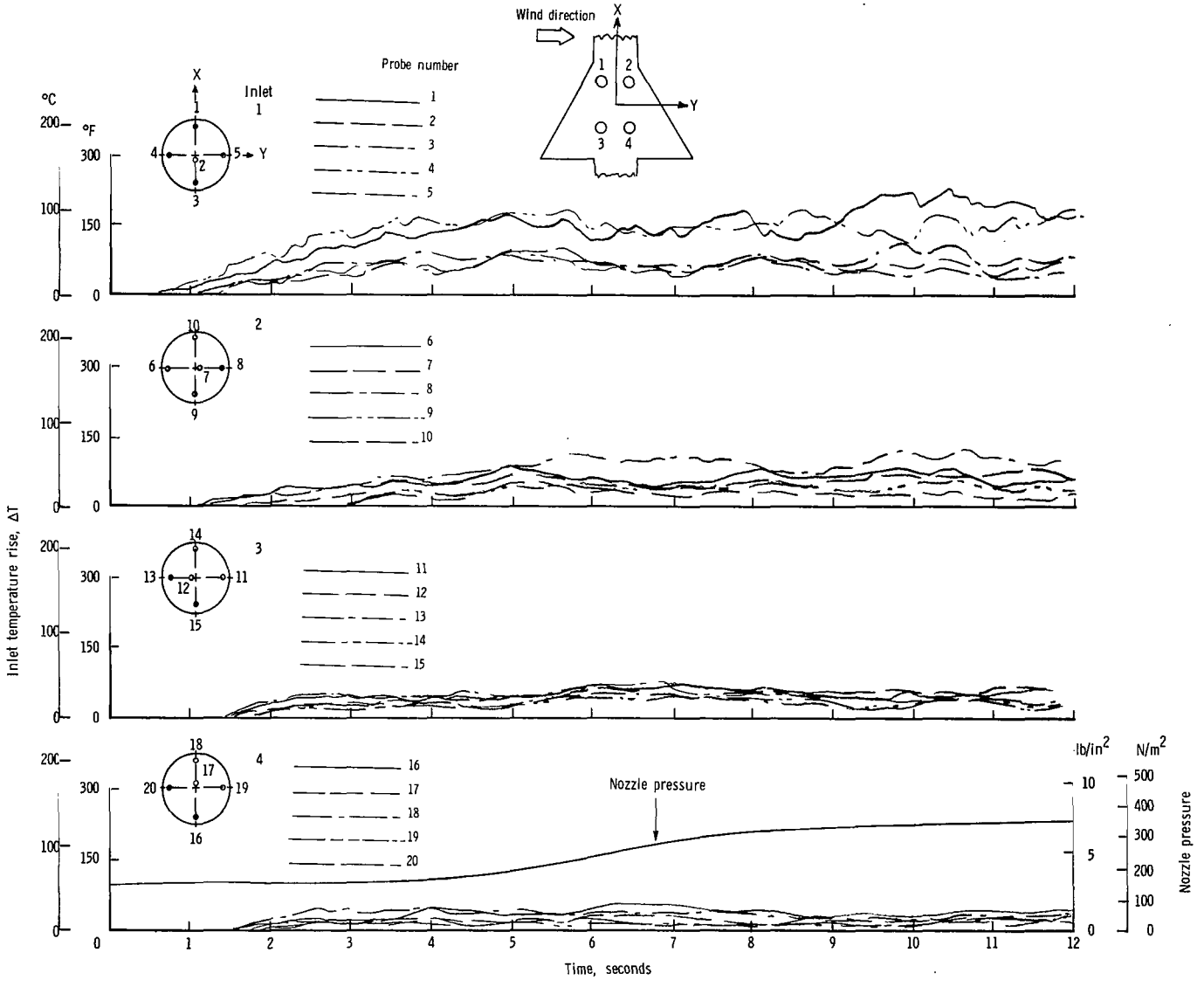

(k) $\psi = 90^{o}$; V = 11.85 knots.

Figure 9.- Concluded.

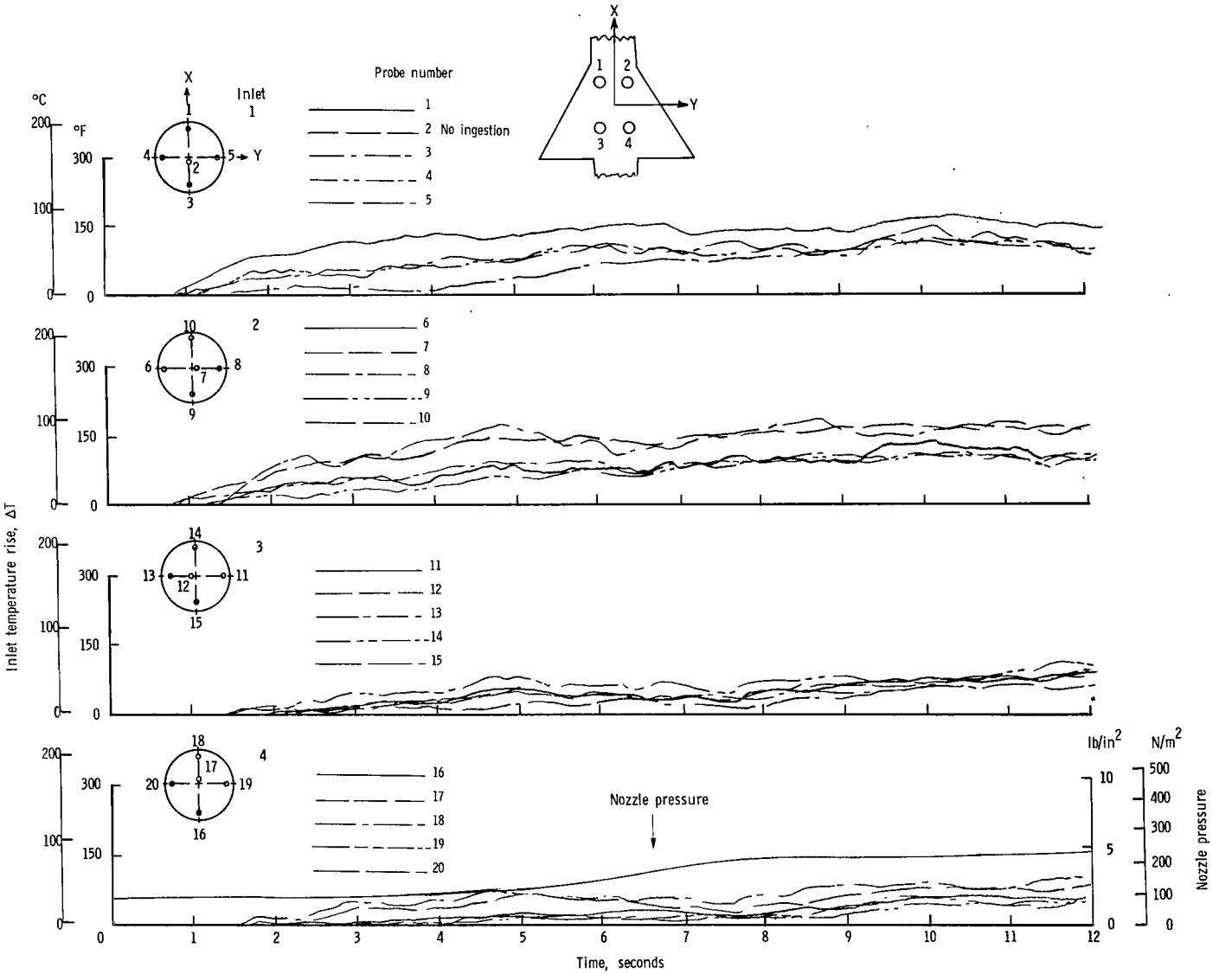

(a) $\psi = 0^{o}$; V = 0 knots.

Figure 10.- Variation of inlet air temperature rise with time for the rectangular nozzle arrangement with top inlets and high delta wing. $h/D_e = 3.0$.

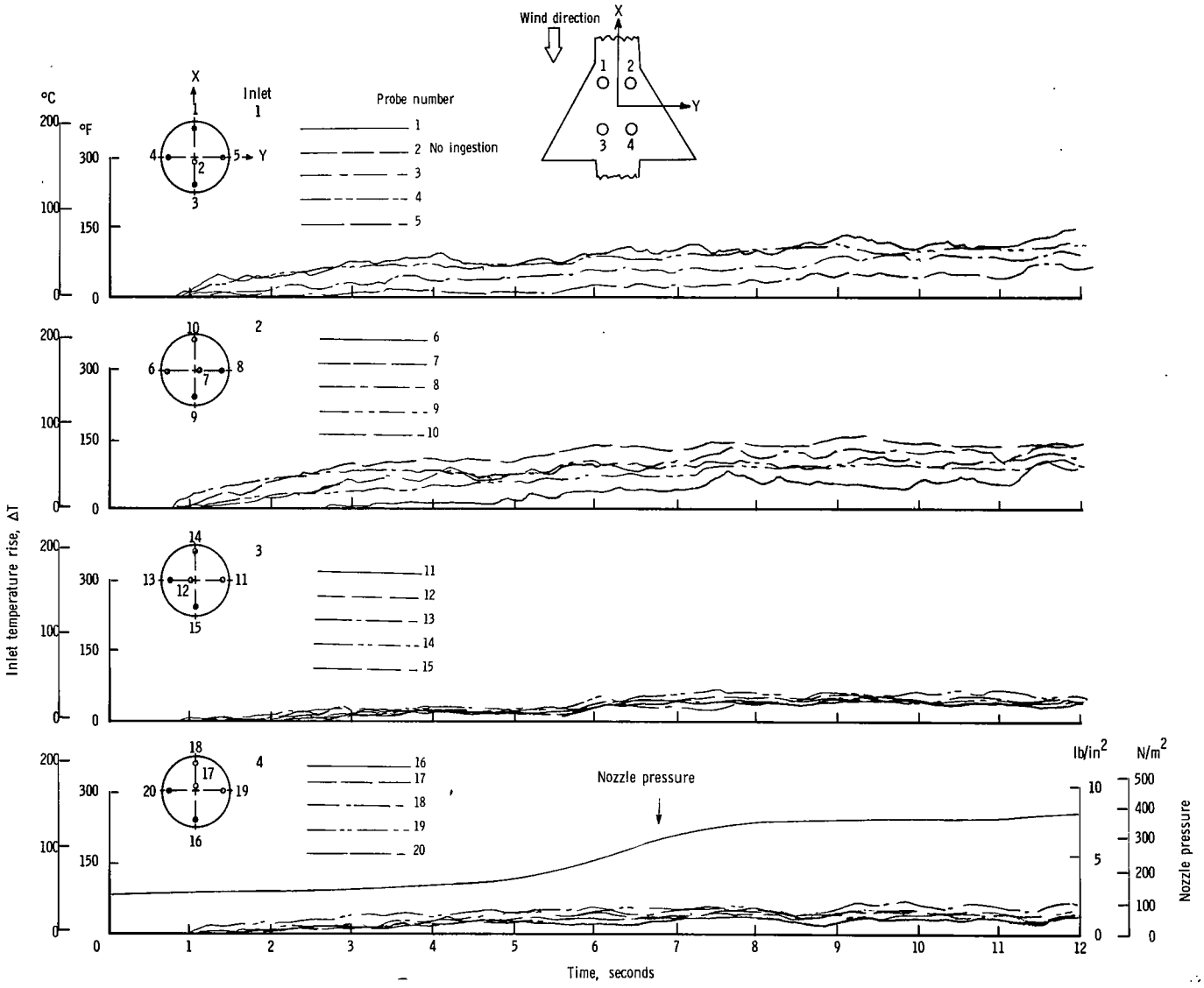

(b) $\psi = 0^{o}$; V = 5.92 knots.

Figure 10.- Continued.

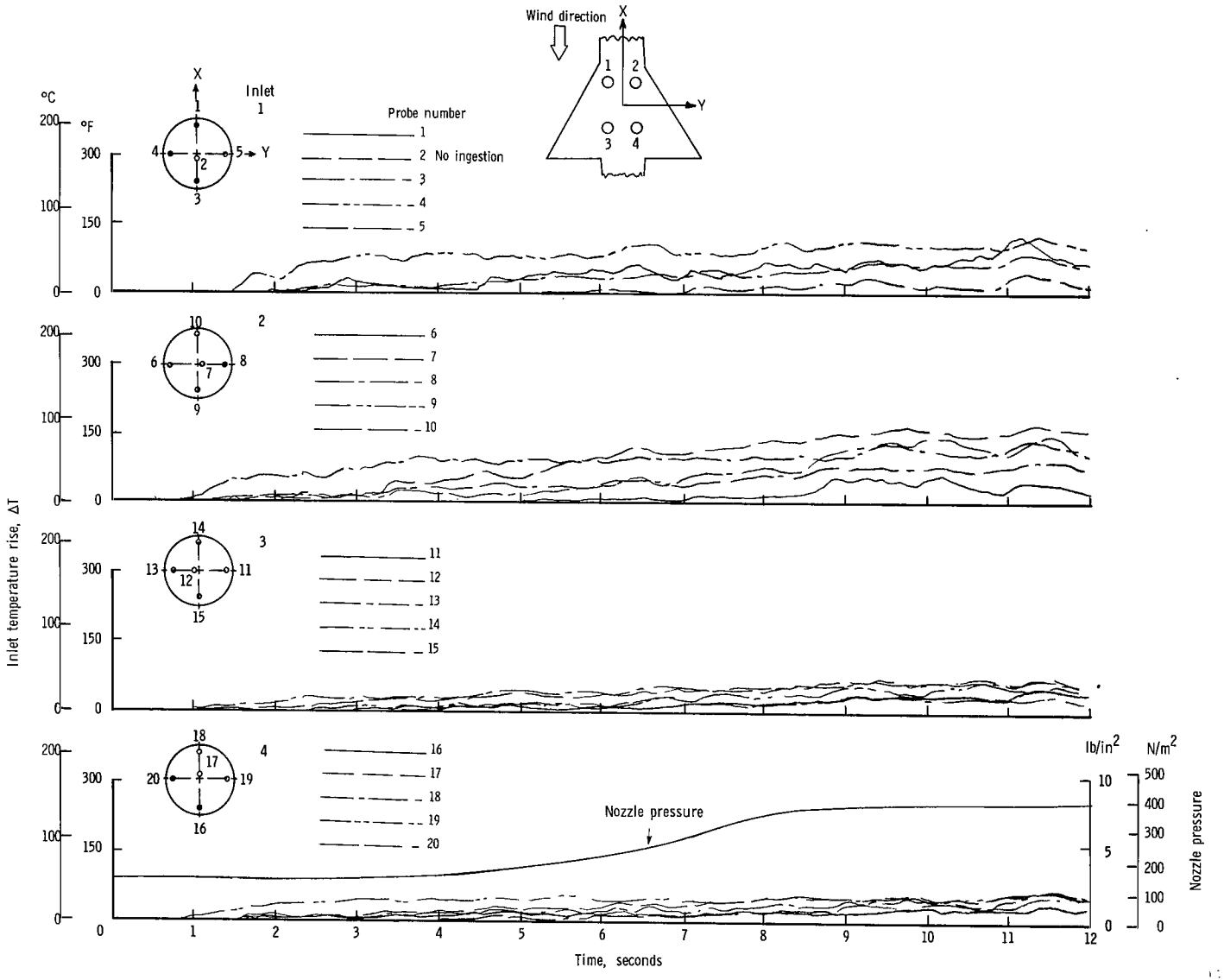

(c) $\psi = 0^0$; V = 11.85 knots.

Figure 10.- Continued.

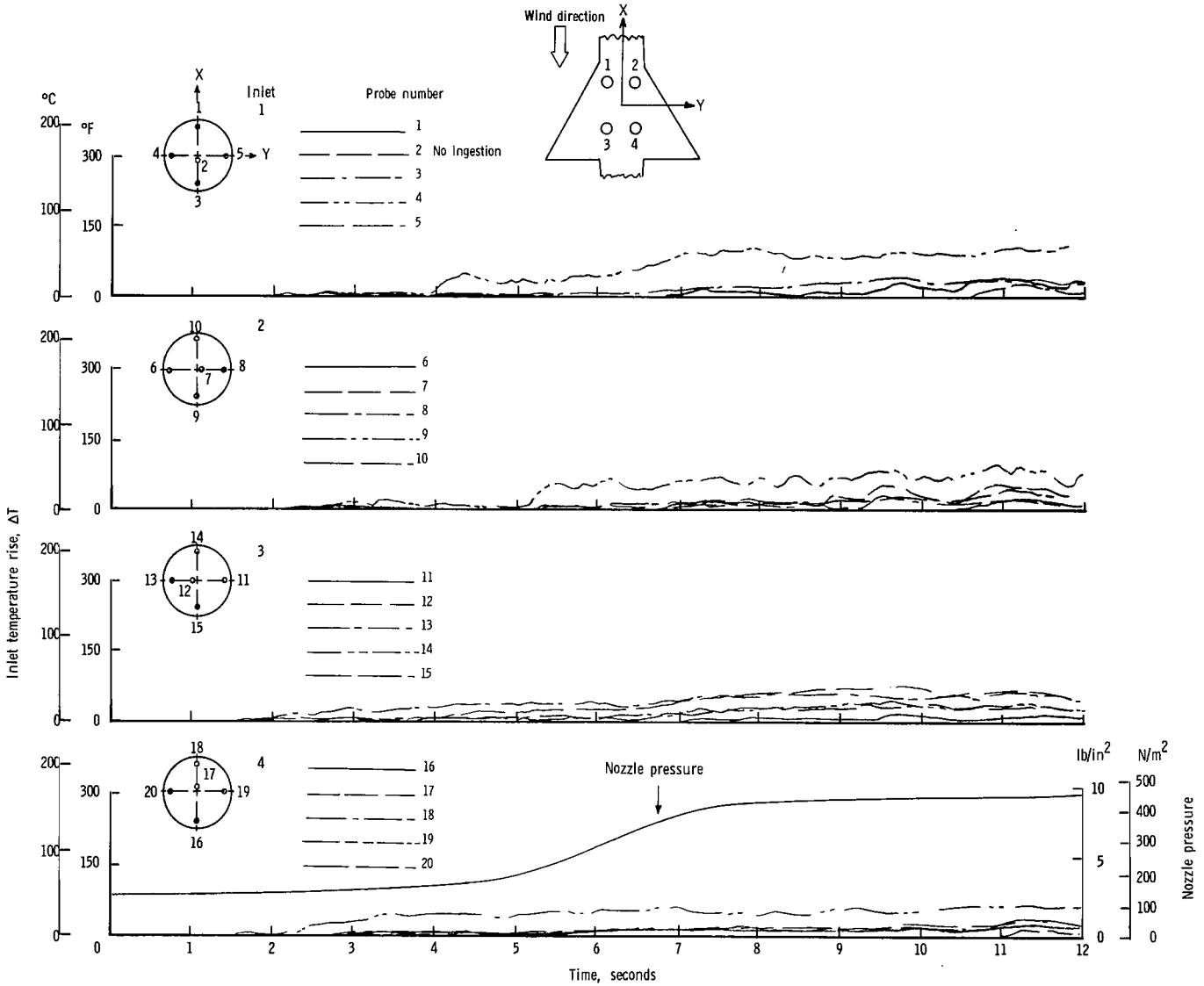

(d) $\psi = 0^{0}$; V = 17.78 knots.

Figure 10.- Continued.

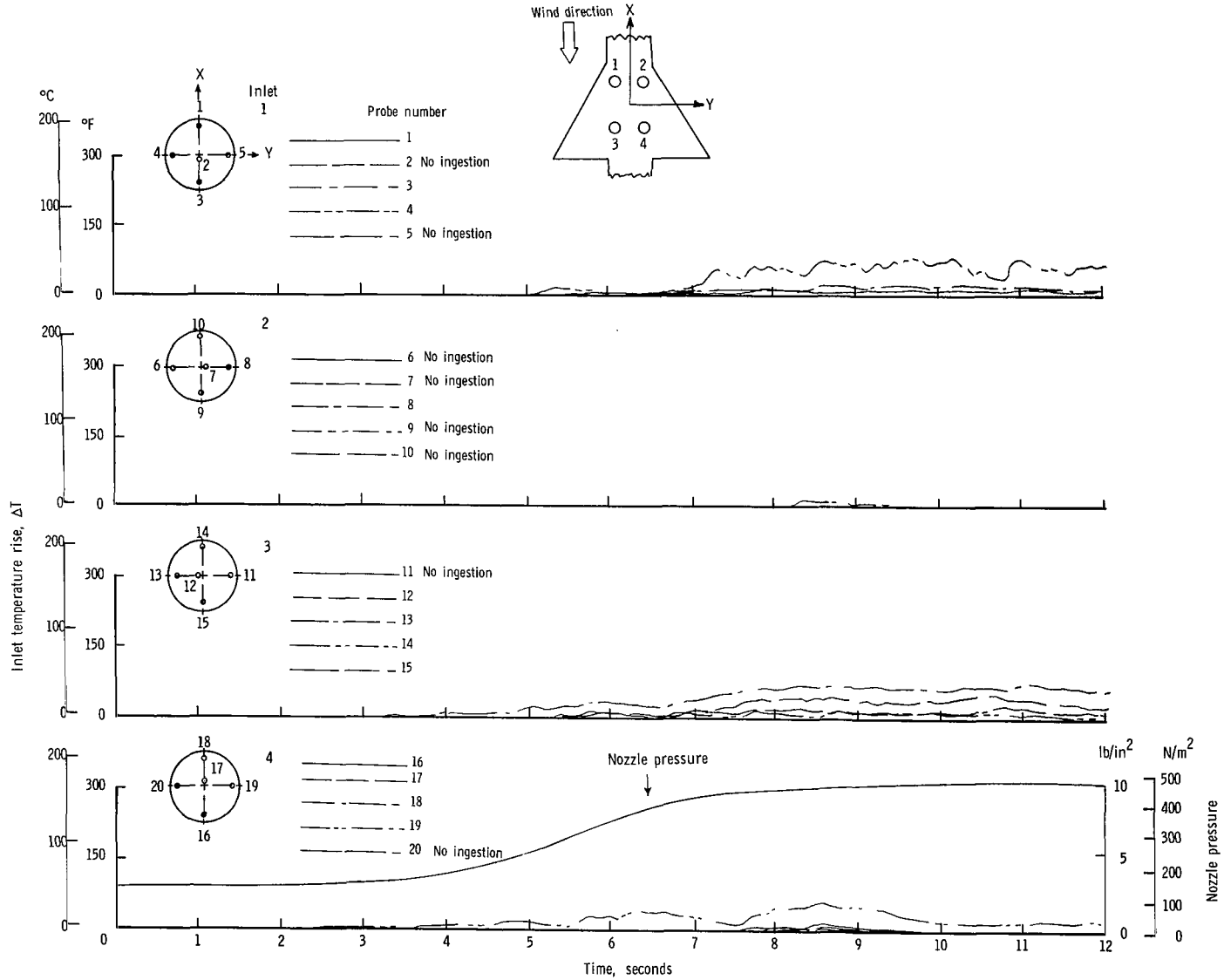

(e) $\psi = 0^0$; V = 23.70 knots.

Figure 10.- Continued.

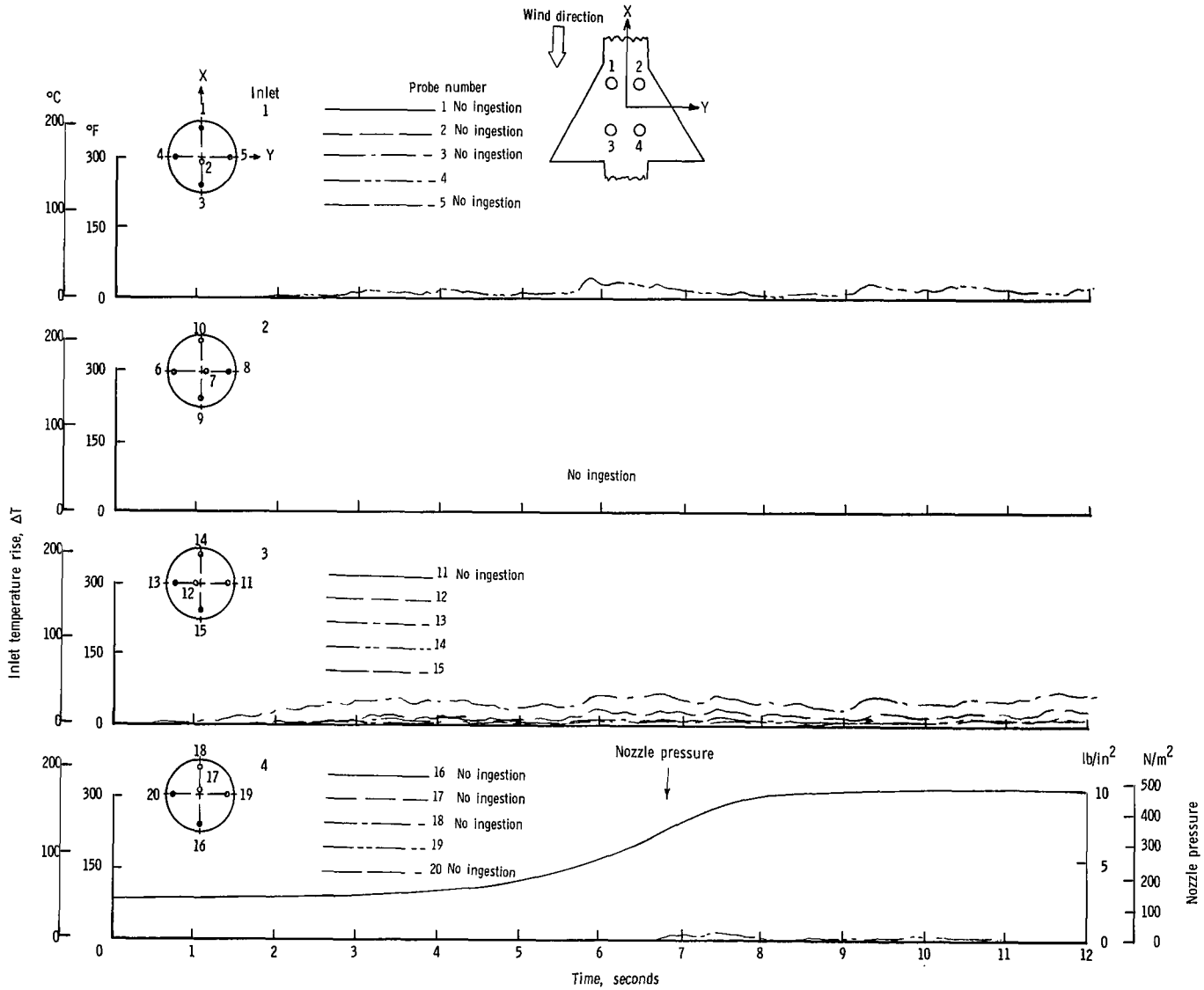

(f) $\psi = 0^0$; V = 29.63 knots.

Figure 10.- Continued.

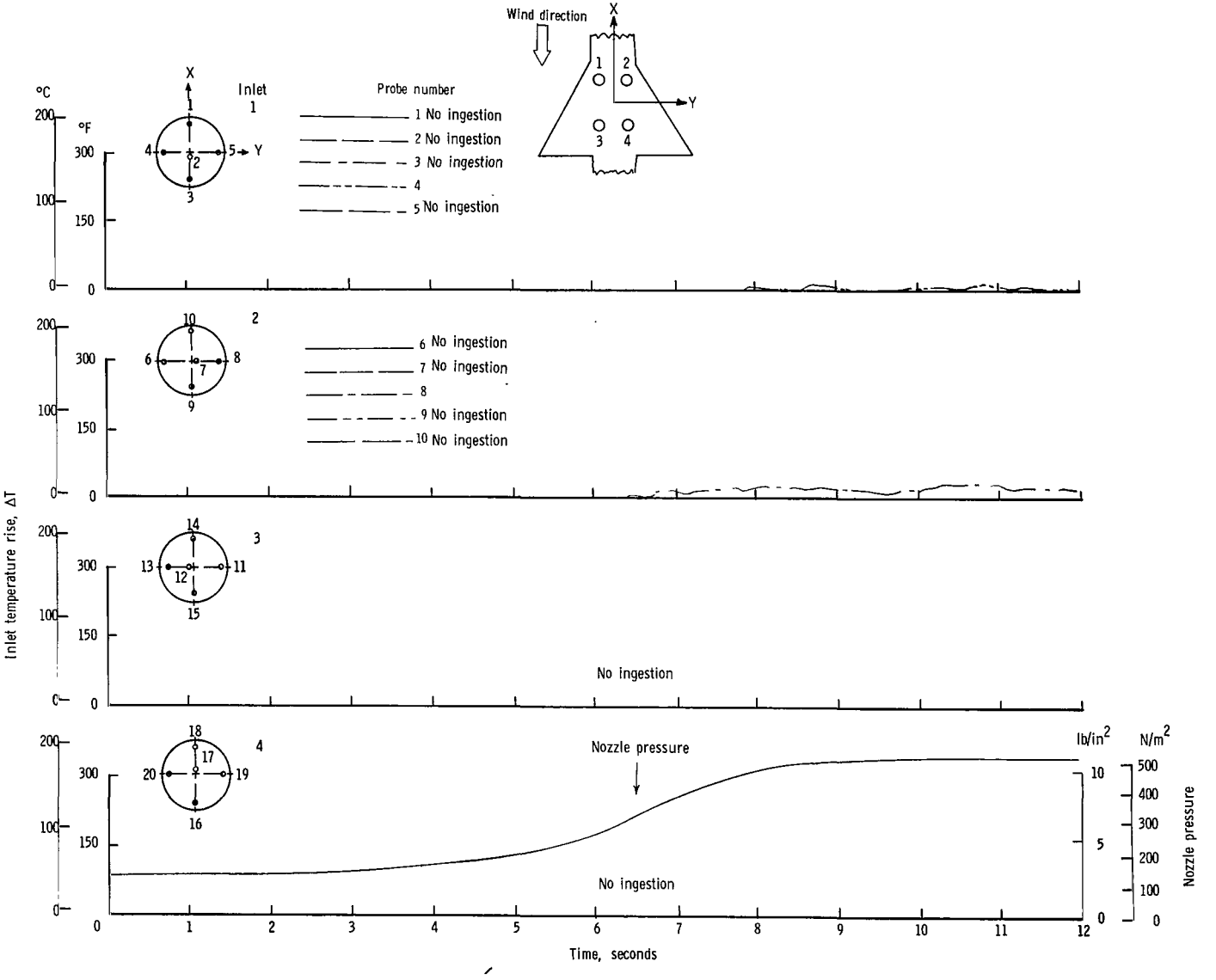

(g) $\psi = 0^{0}$; V = 35.55 knots.

Figure 10.- Continued.

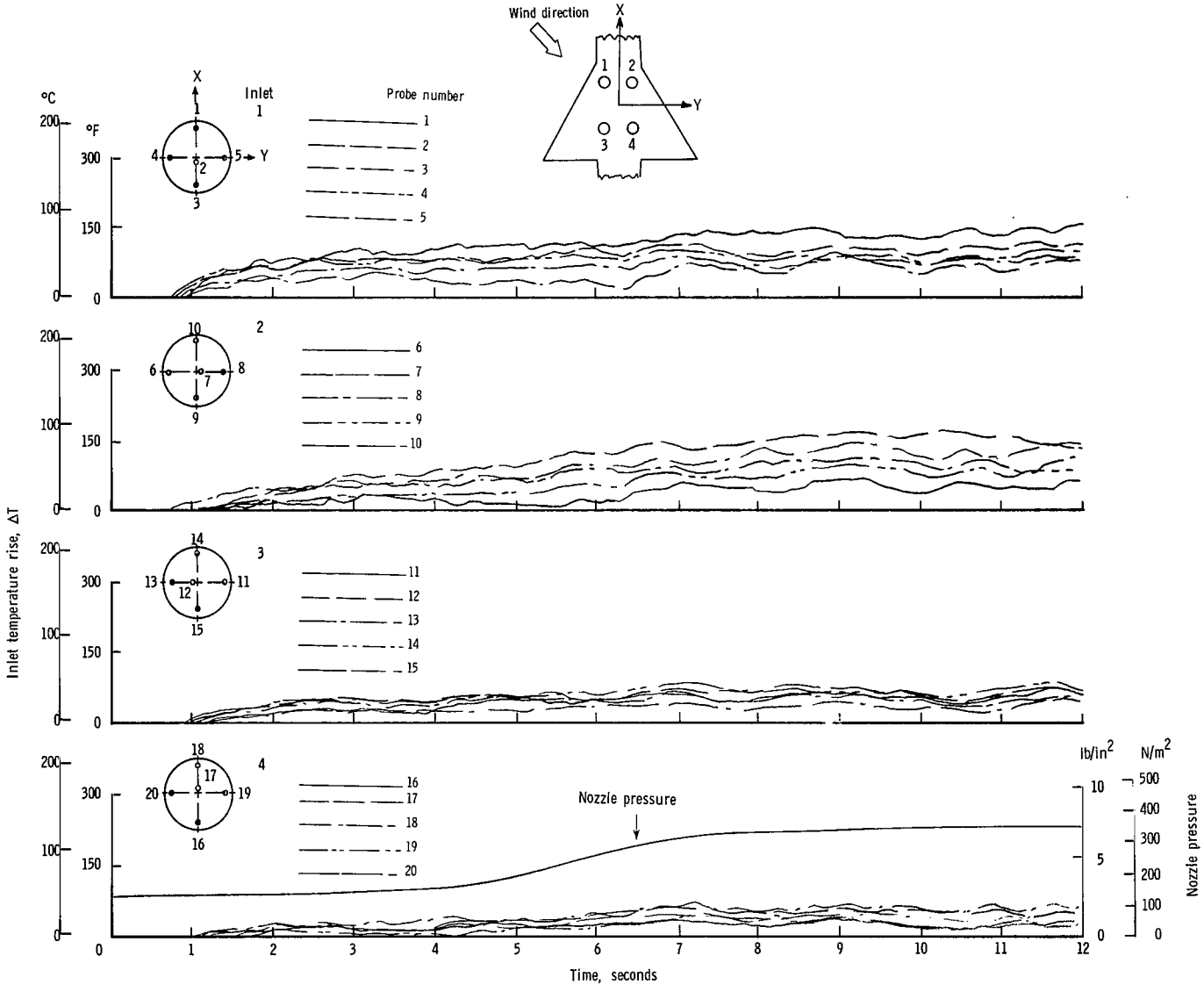

(h) $\psi = 45^0$; V = 5.92 knots.

Figure 10.- Continued.

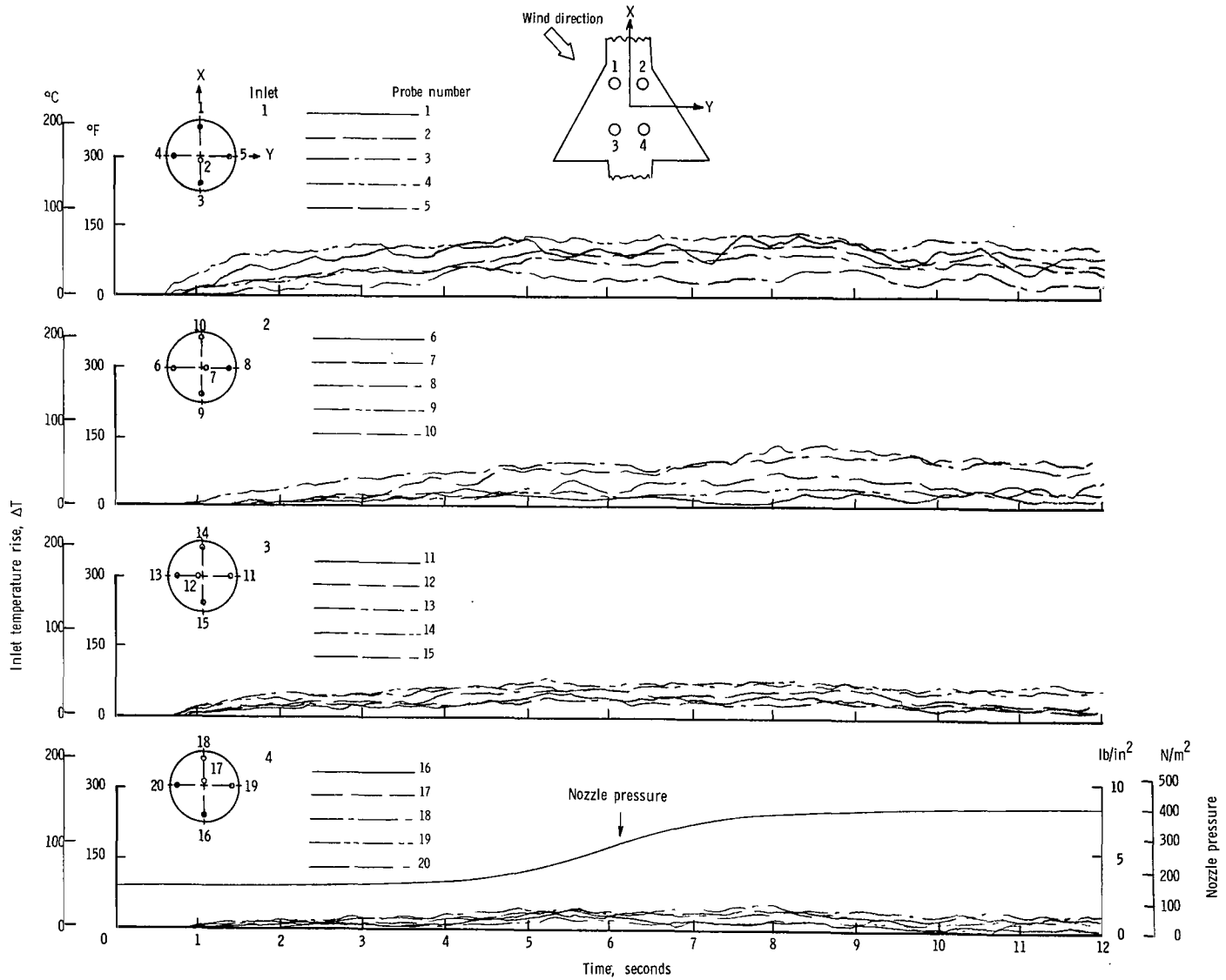

(i) $\psi = 45^{0}$; V = 11.85 knots.

Figure 10.- Continued.

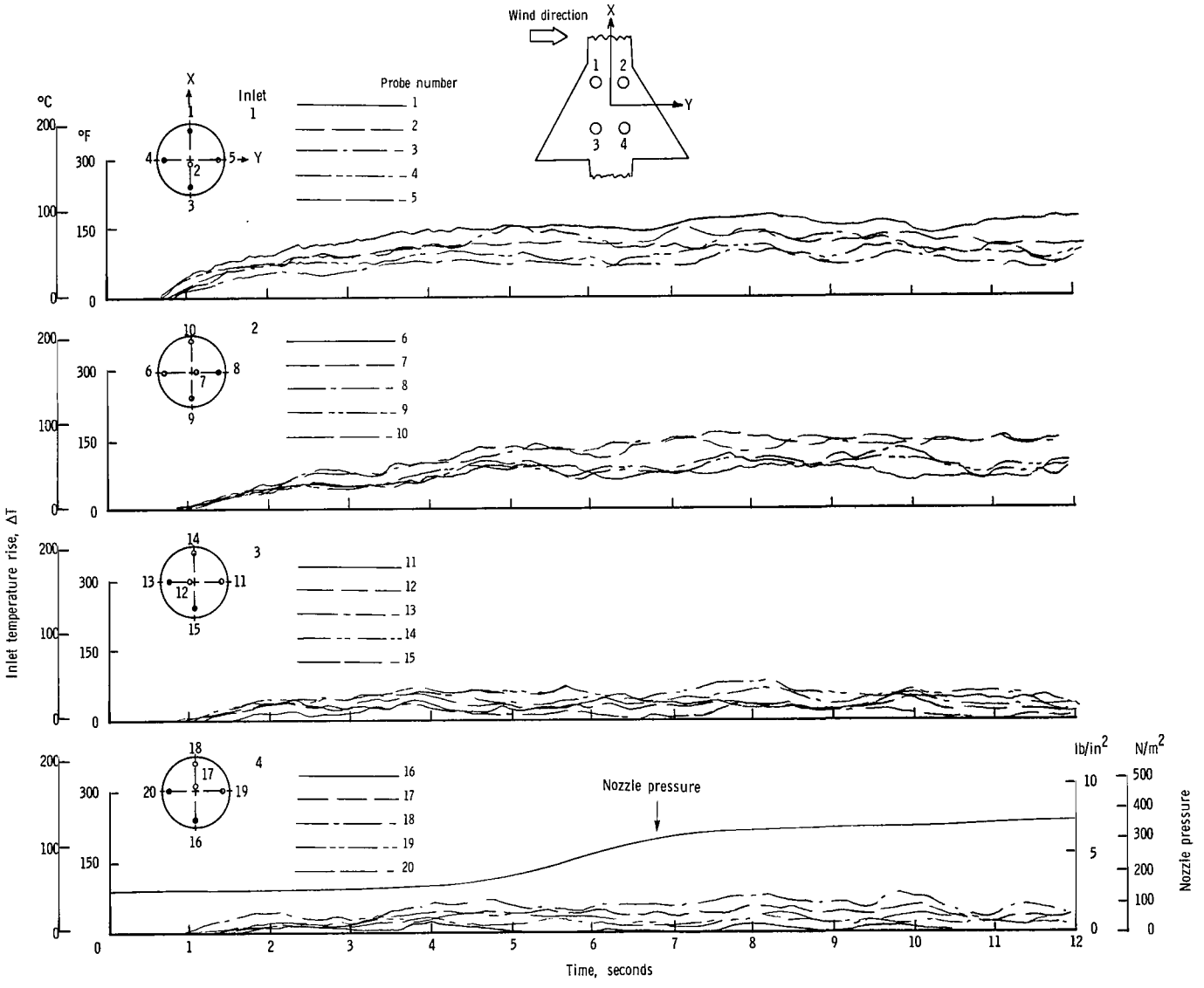

(j) $\psi = 90^{0}$; V = 5.92 knots.

Figure 10.- Continued.

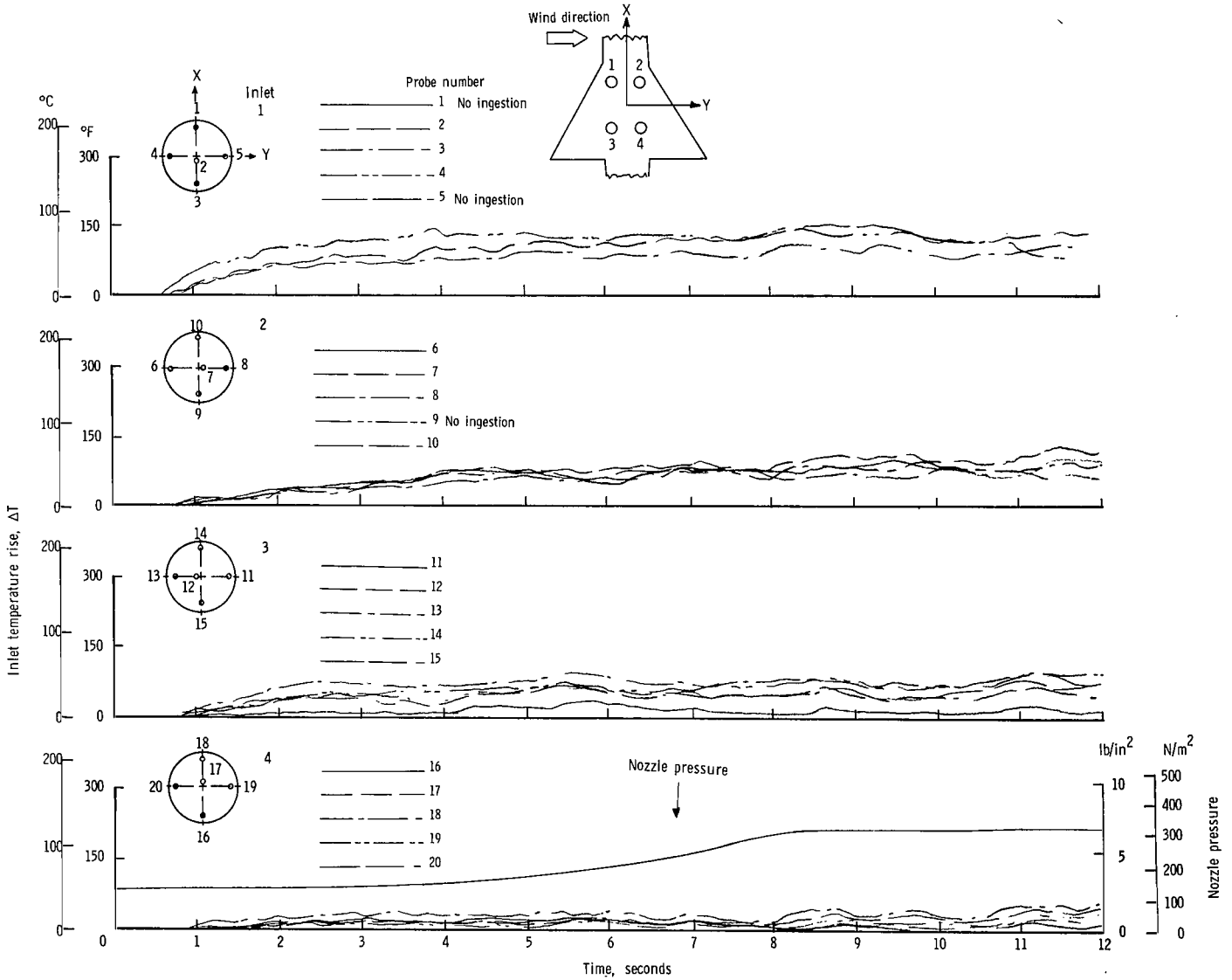

(k) $\psi = 90^{o}$; V = 11.85 knots.

Figure 10.- Concluded.

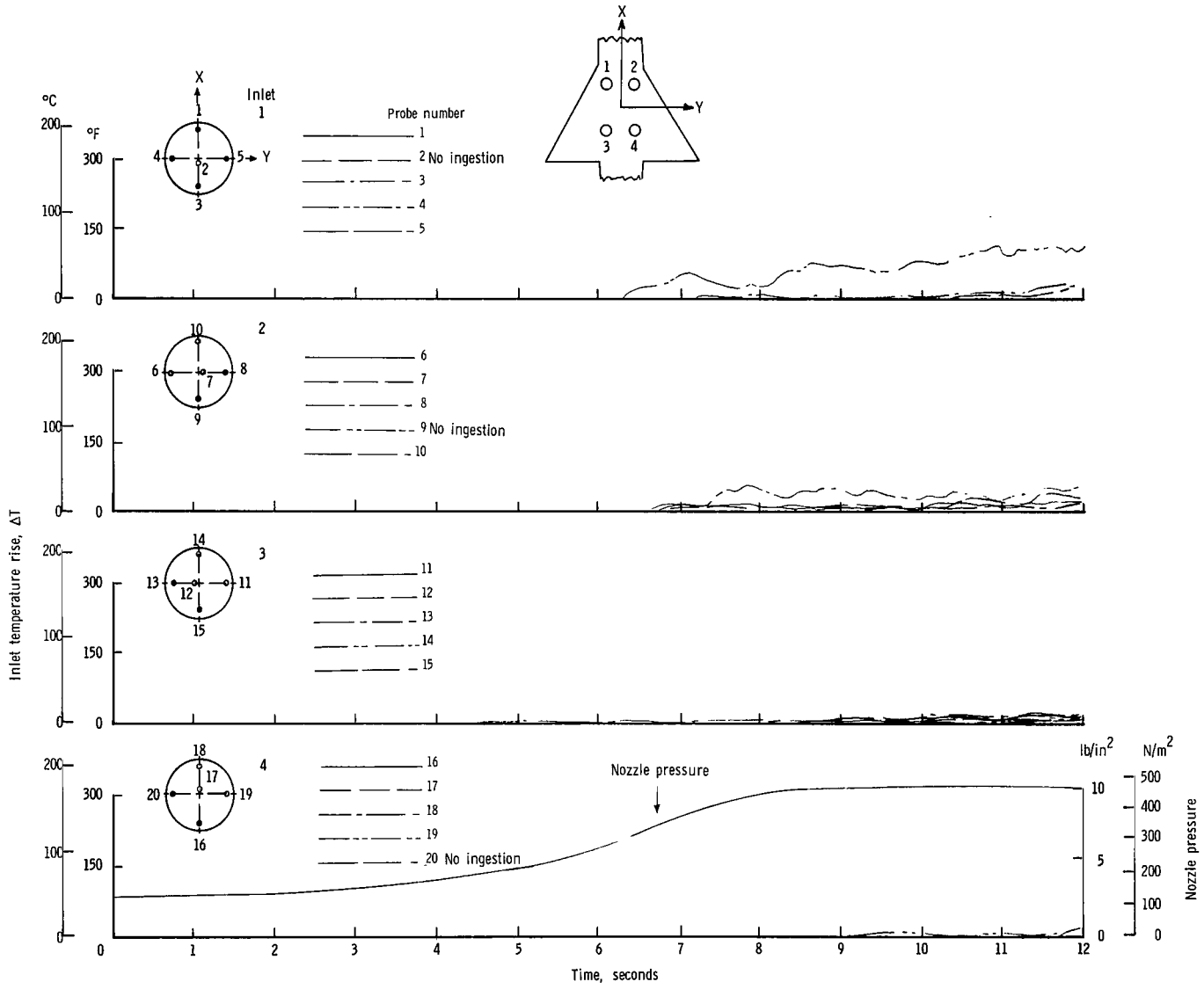

(a) $\psi = 0^{o}$; V = 0 knots.

Figure 11.- Variation of inlet air temperature rise with time for the rectangular nozzle arrangement with top inlets and high delta wing. $h/D_e = 5.0$.

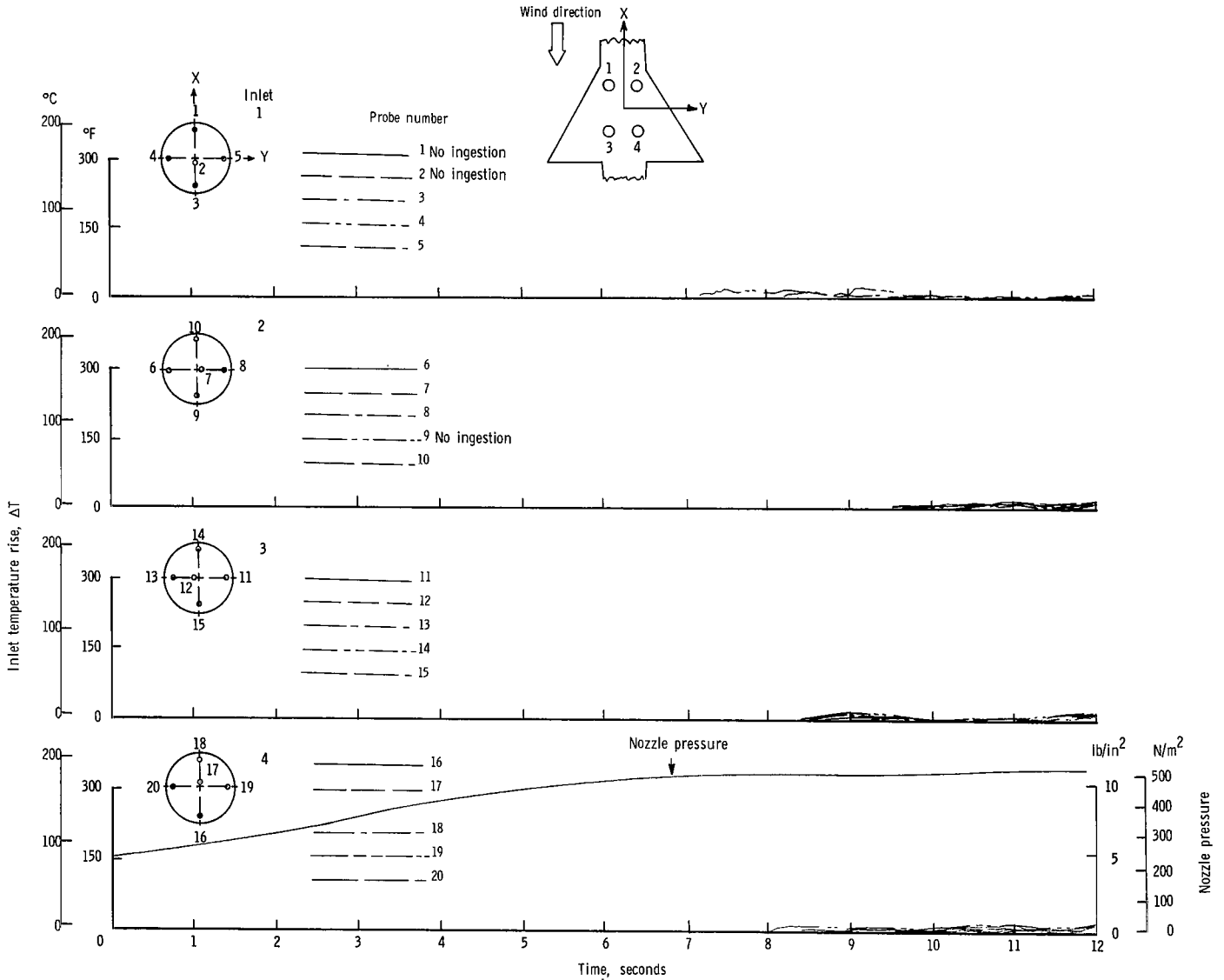

(b) $\psi = 0^{0}$; V = 5.92 knots.

Figure 11.- Continued.

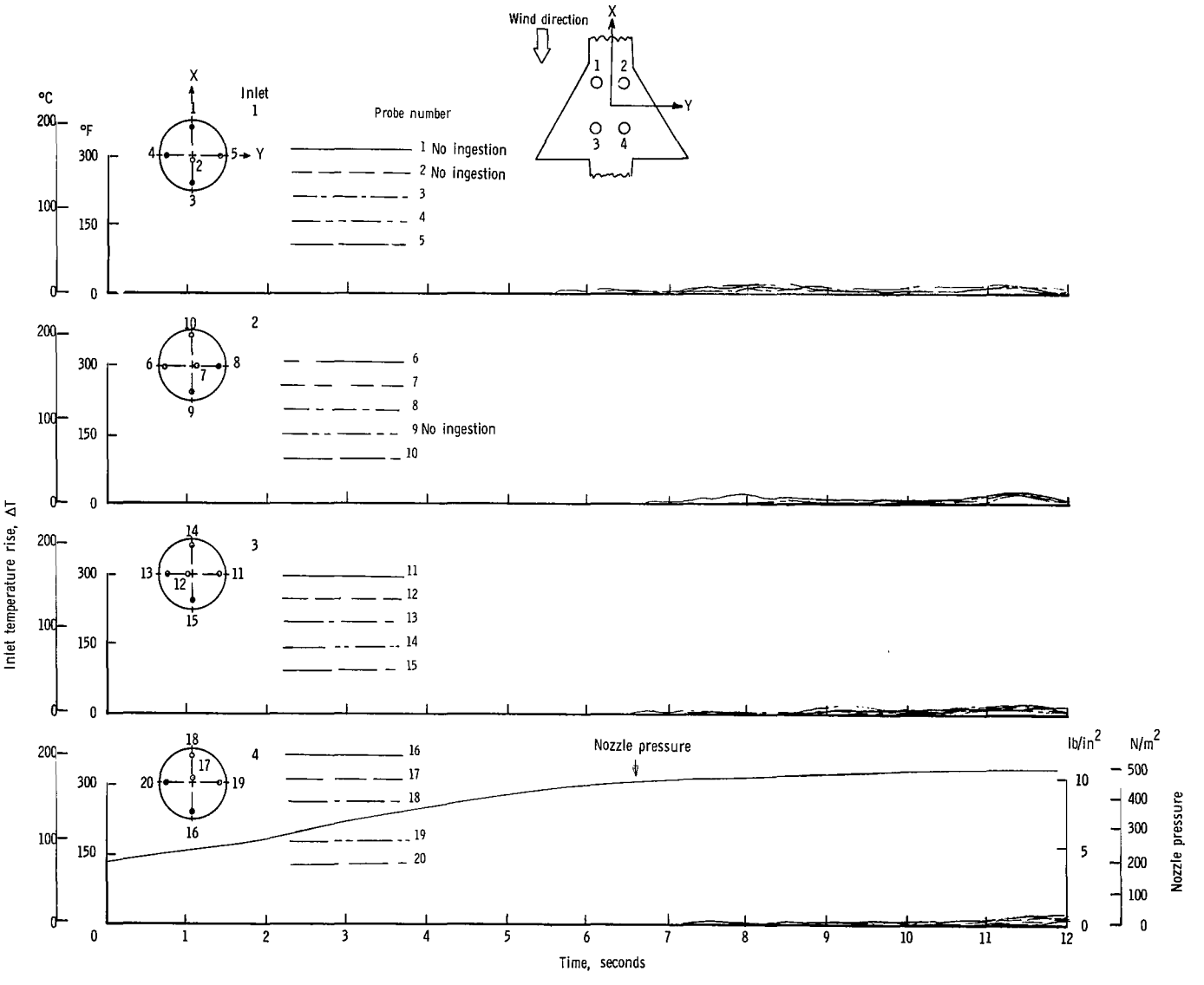

(c) $\psi = 0^0$; V = 11.85 knots.

Figure 11.- Continued.

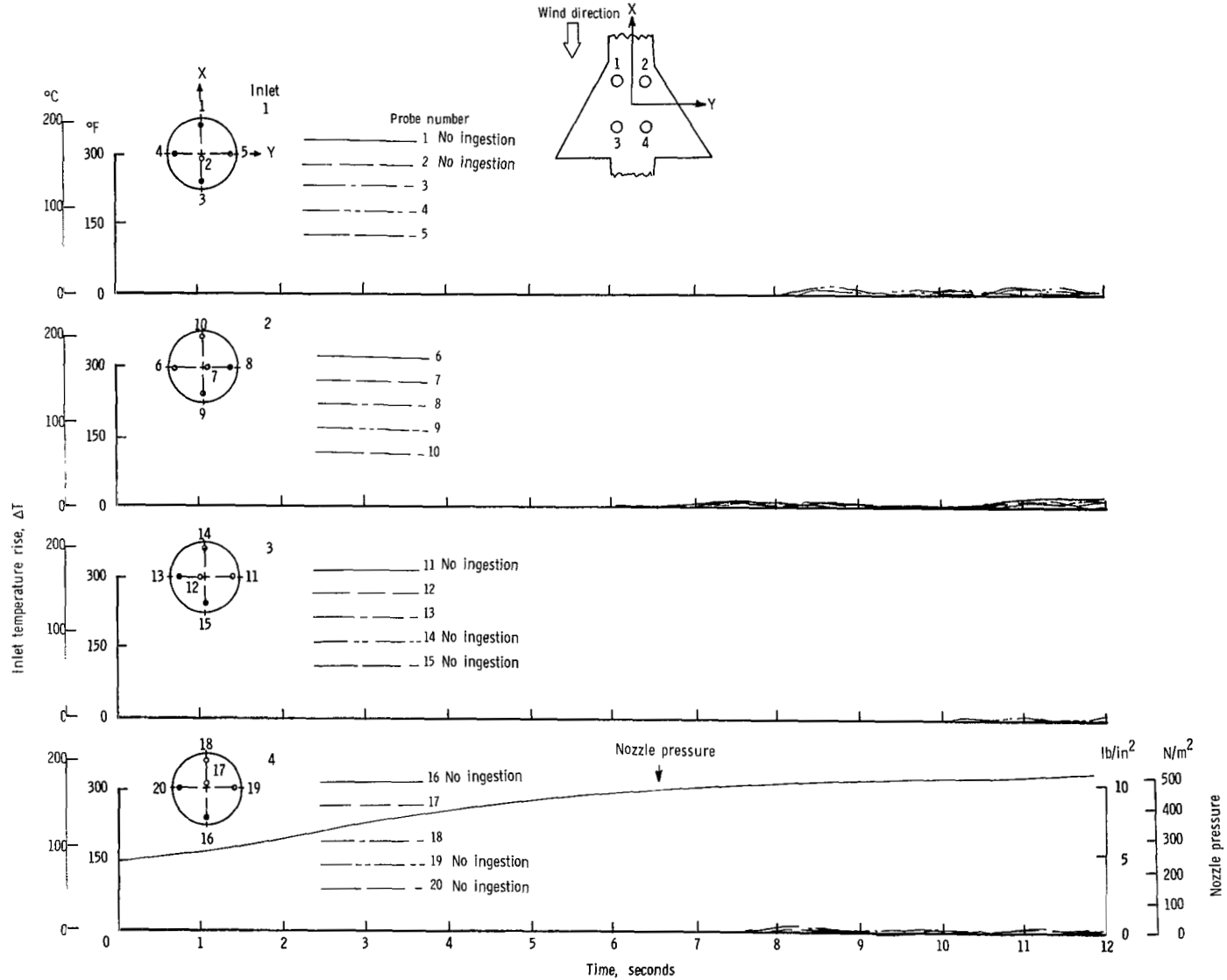

(d) $\psi = 0^0$; V = 17.78 knots.

Figure 11.- Continued.

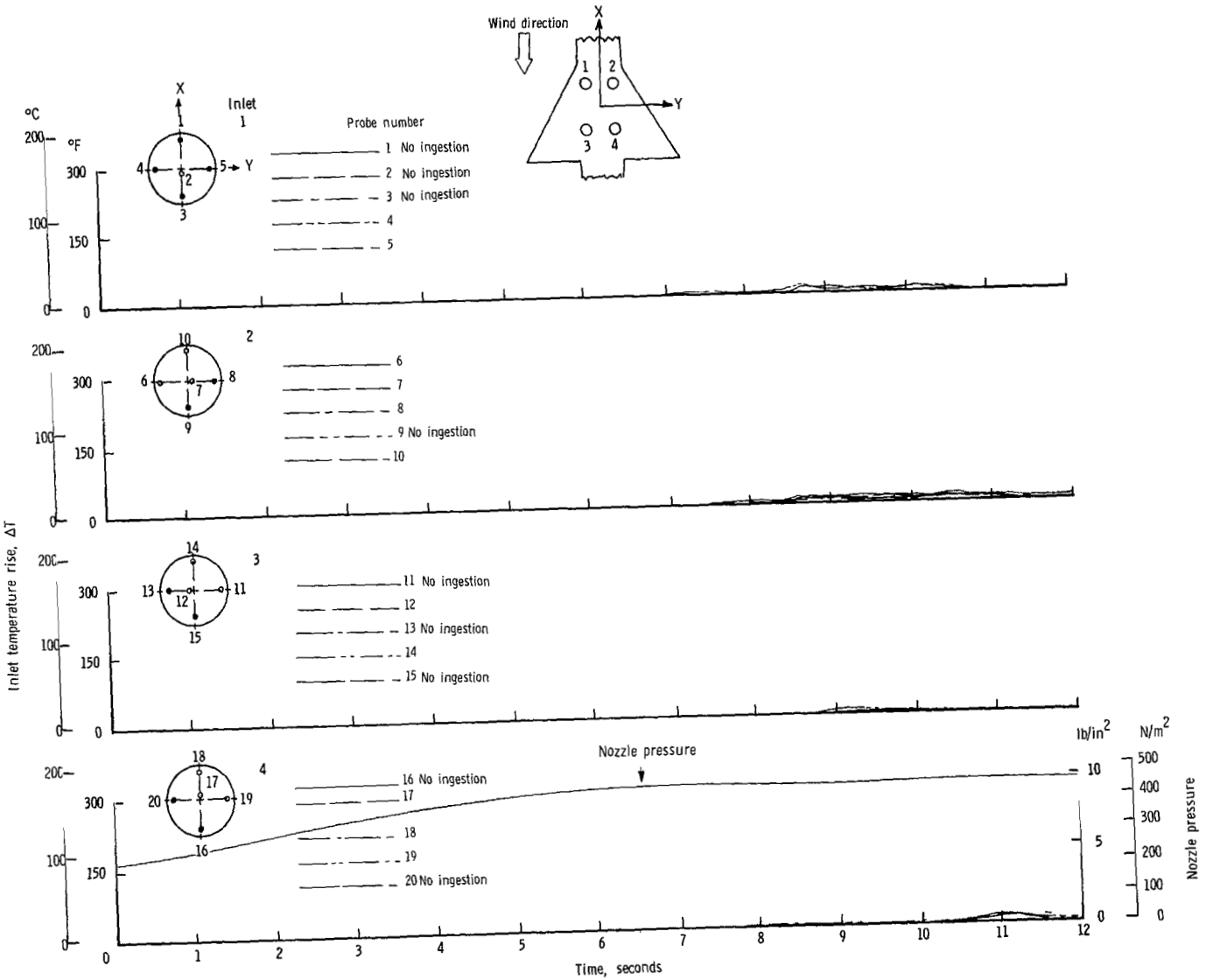

(e) $\psi = 0^0$; V = 23.70 knots.

Figure 11.- Continued.

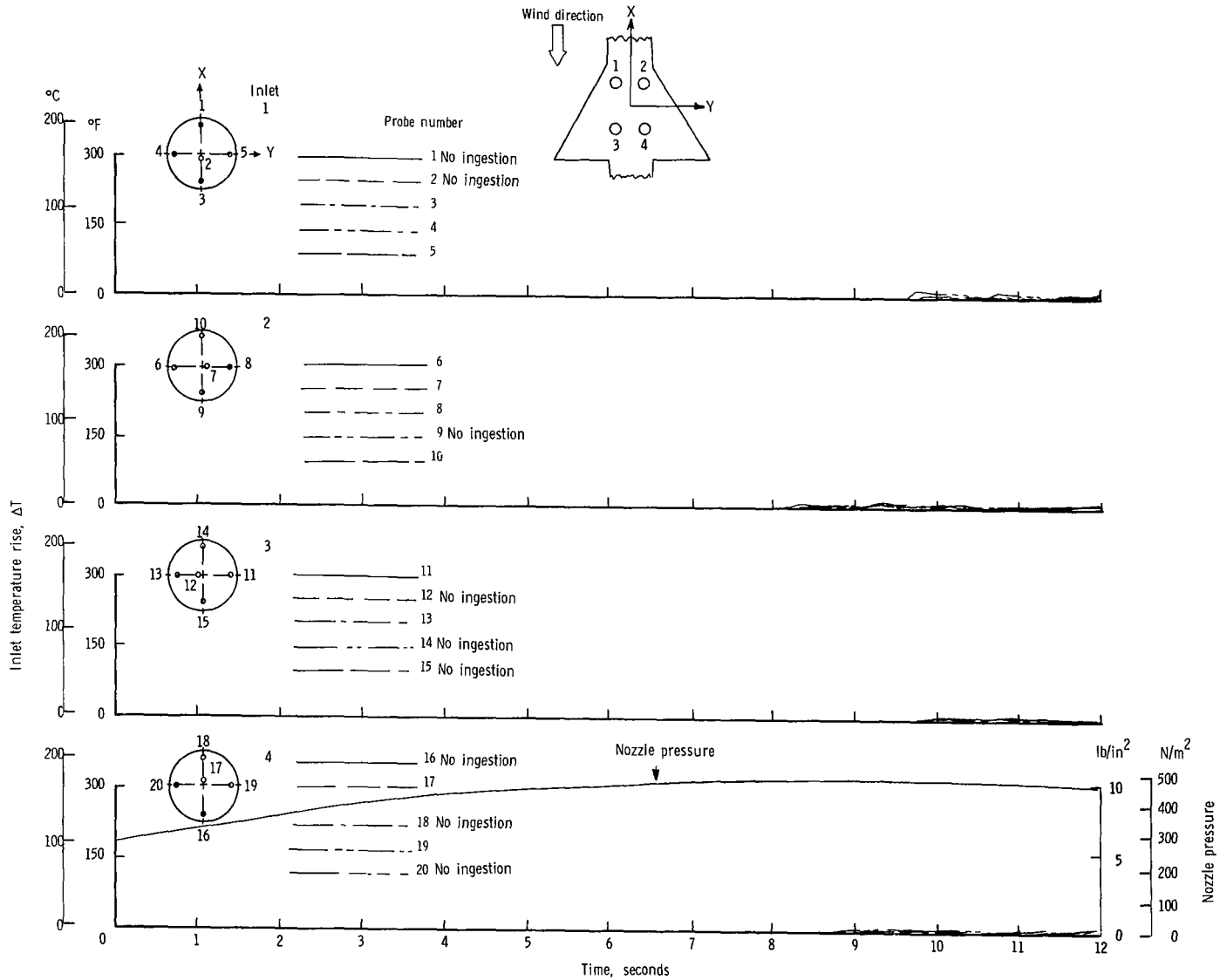

(f) $\psi = 0^0$; V = 29.63 knots.

Figure 11.- Continued.

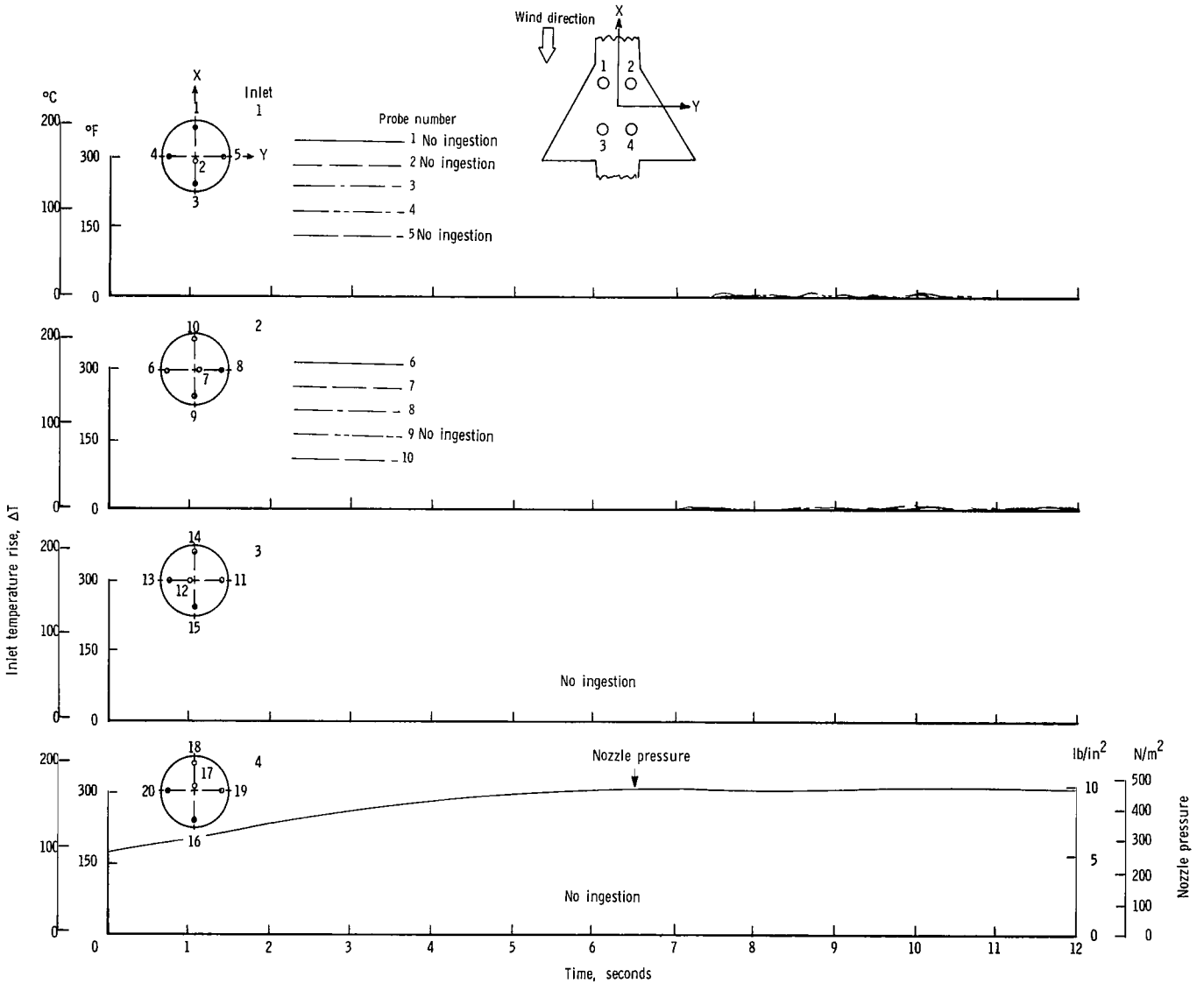

(g) $\psi = 0^0$; V = 35.55 knots.

Figure 11.- Continued.

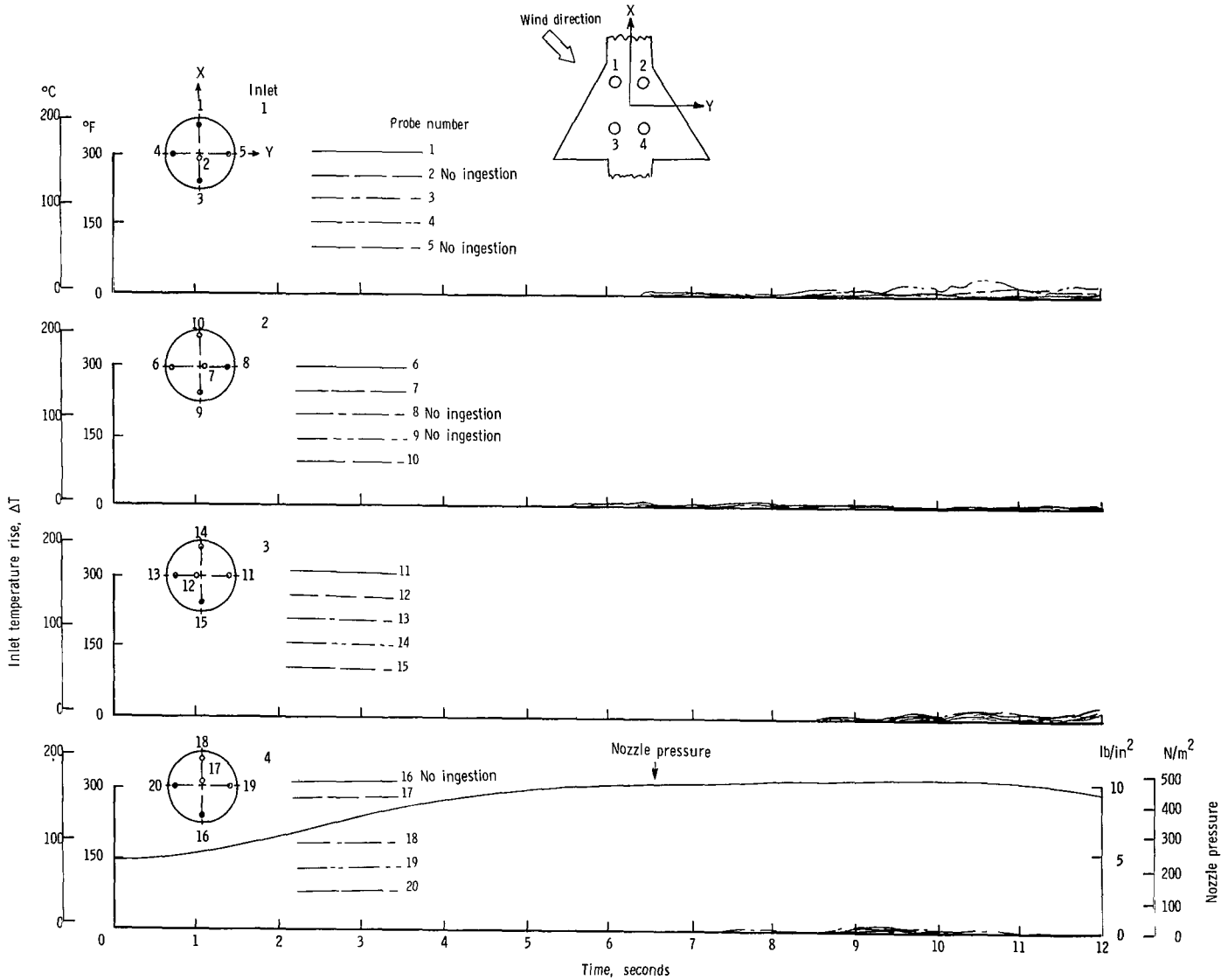

(h) $\psi = 45^0$; V = 5.92 knots.

Figure 11.- Continued.

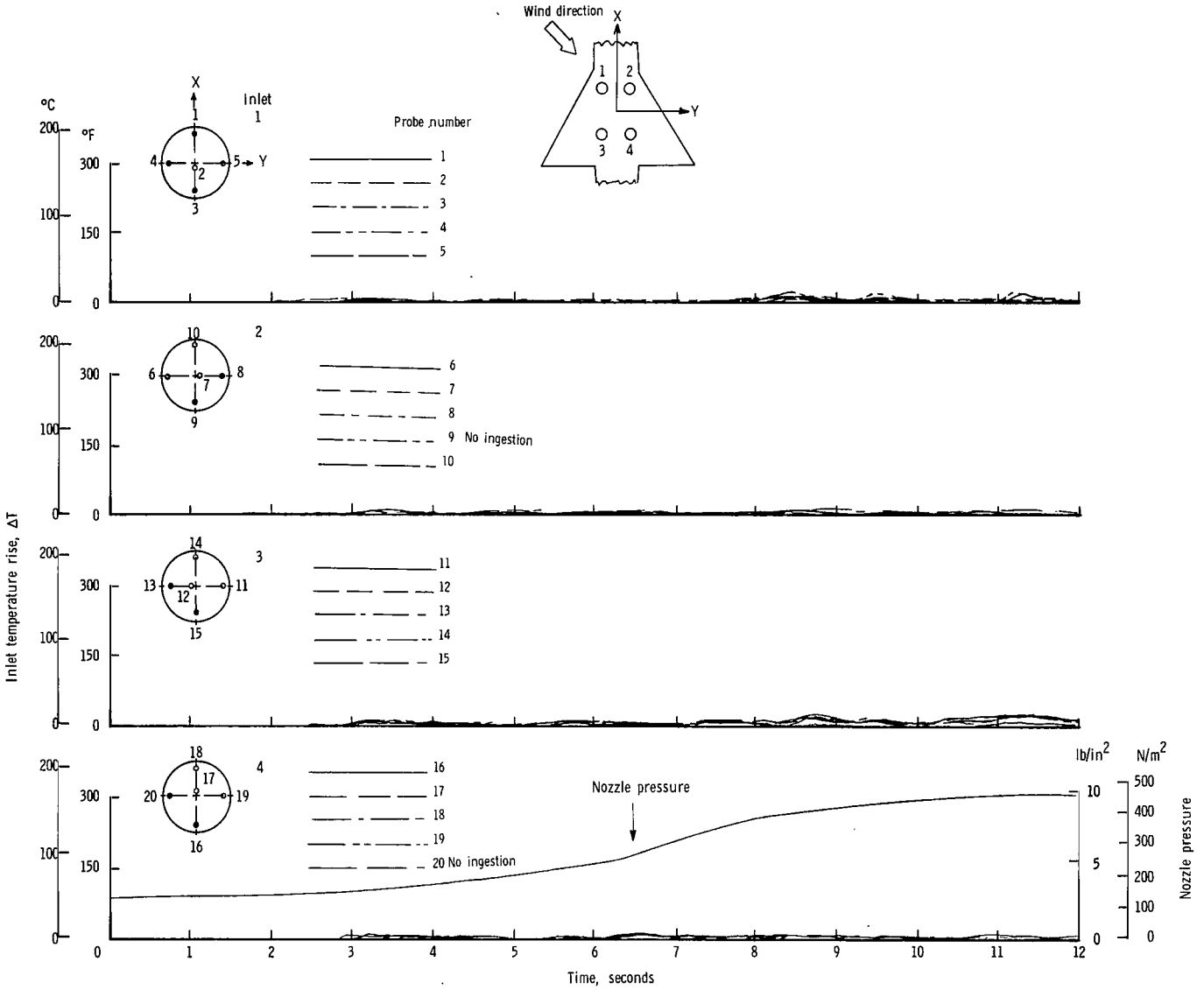

(i) $\psi = 45^{0}$; V = 11.85 knots.

Figure 11.- Continued.

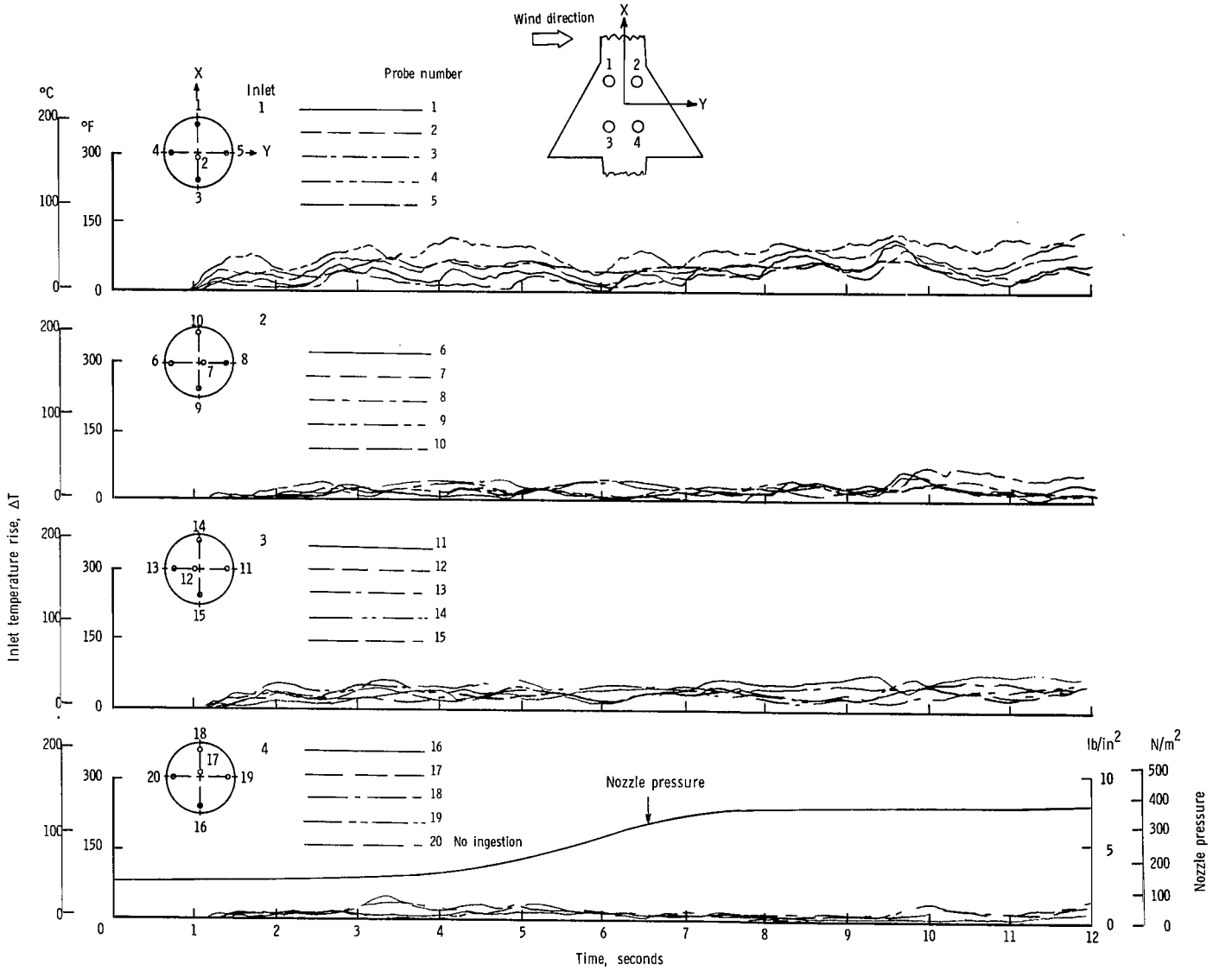

(j) $\psi = 90^0$; V = 5.92 knots.

Figure 11.- Continued.

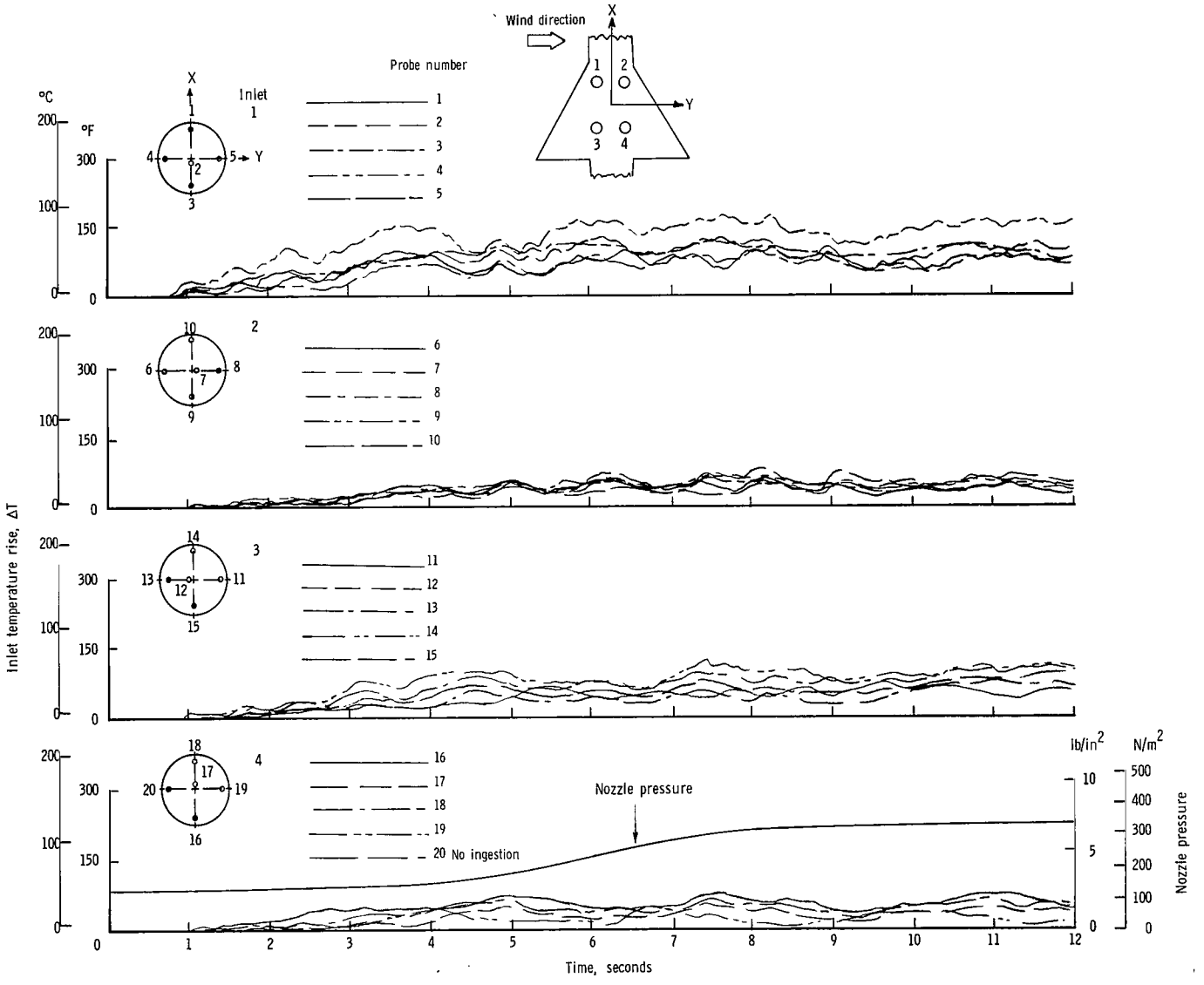

(k) $\psi = 90^{0}$; V = 11.85 knots.

Figure 11.- Concluded.

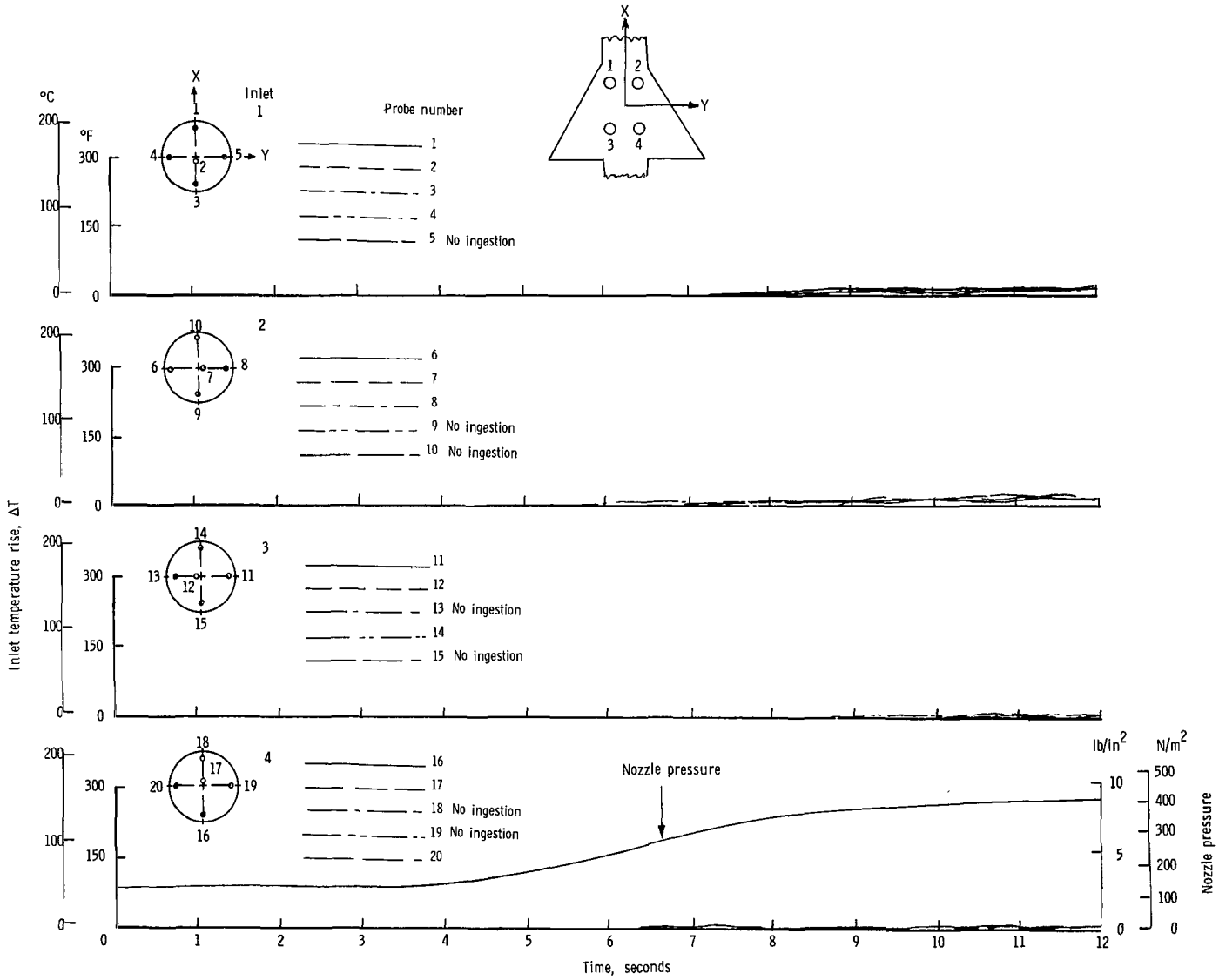

(a) $\psi = 0^0$; V = 0 knots.

Figure 12.- Variation of inlet air temperature rise with time for the rectangular nozzle arrangment with top inlets and low delta wing. $h/D_e = 1.17$.

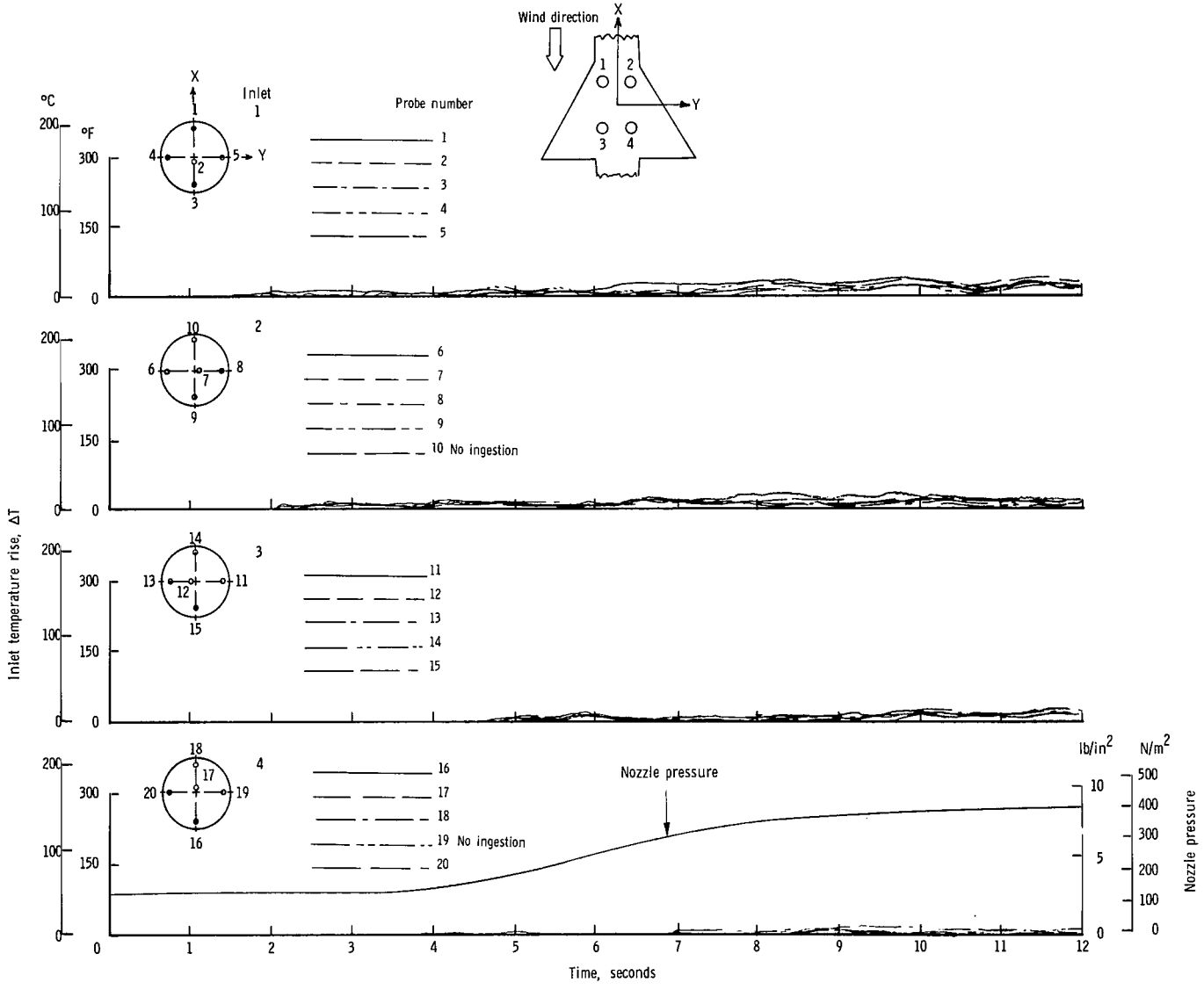

(b) $\psi = 0^{0}$; V = 5.92 knots.

Figure 12.- Continued.

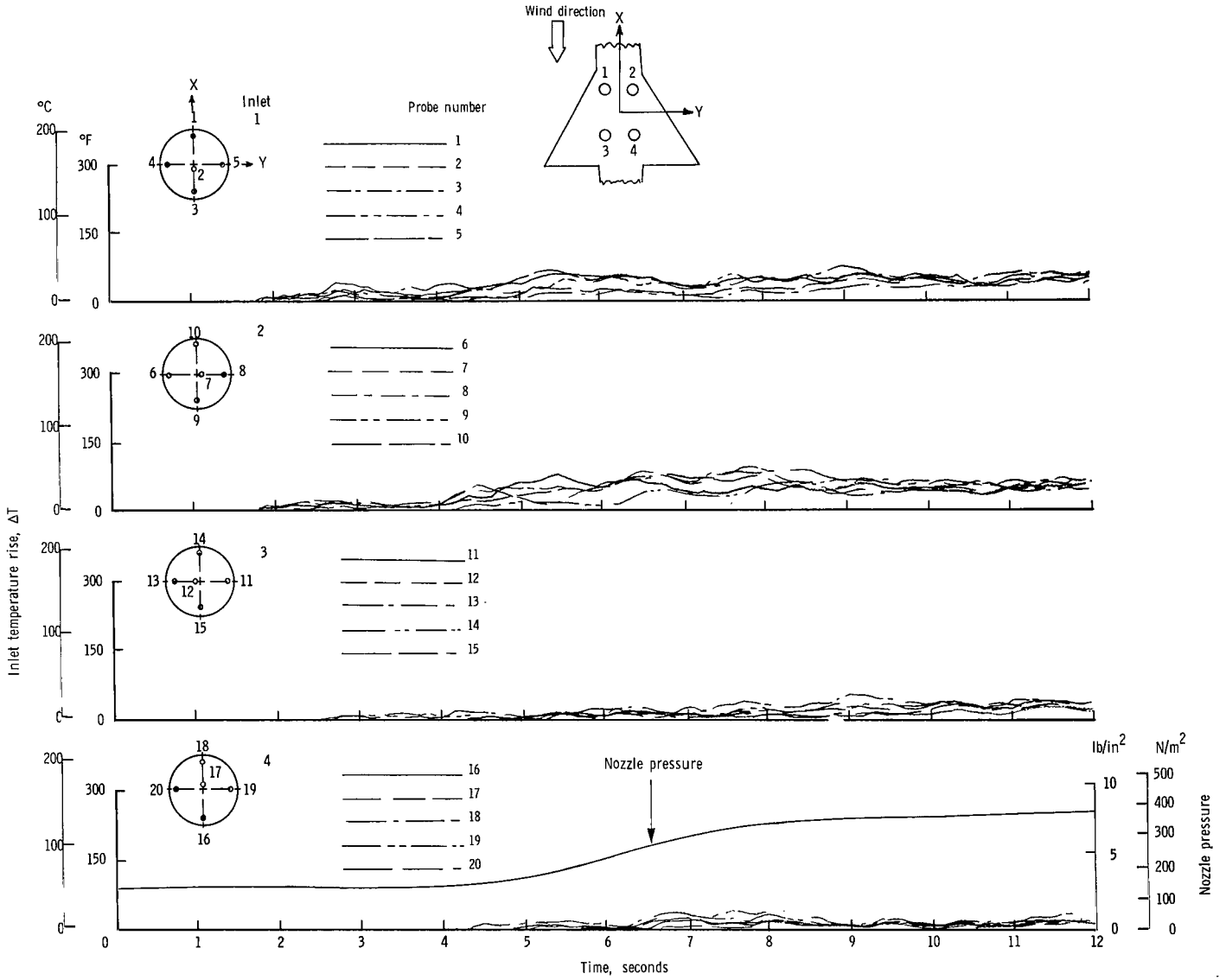

(c) $\psi = 0^0$; V = 11.85 knots.

Figure 12.- Continued.

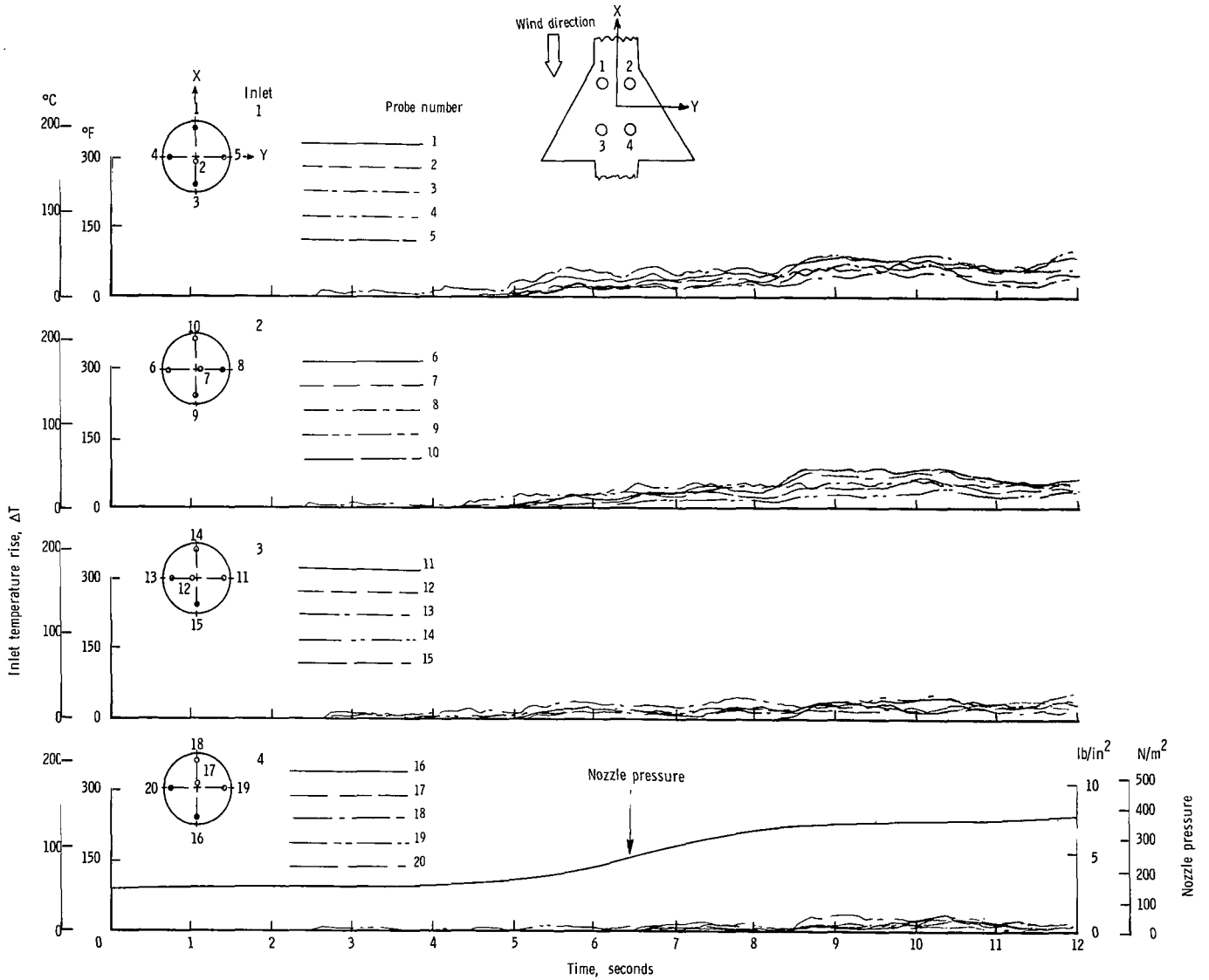

(d) $\psi = 0^0$; V = 17.78 knots.

Figure 12.- Continued.

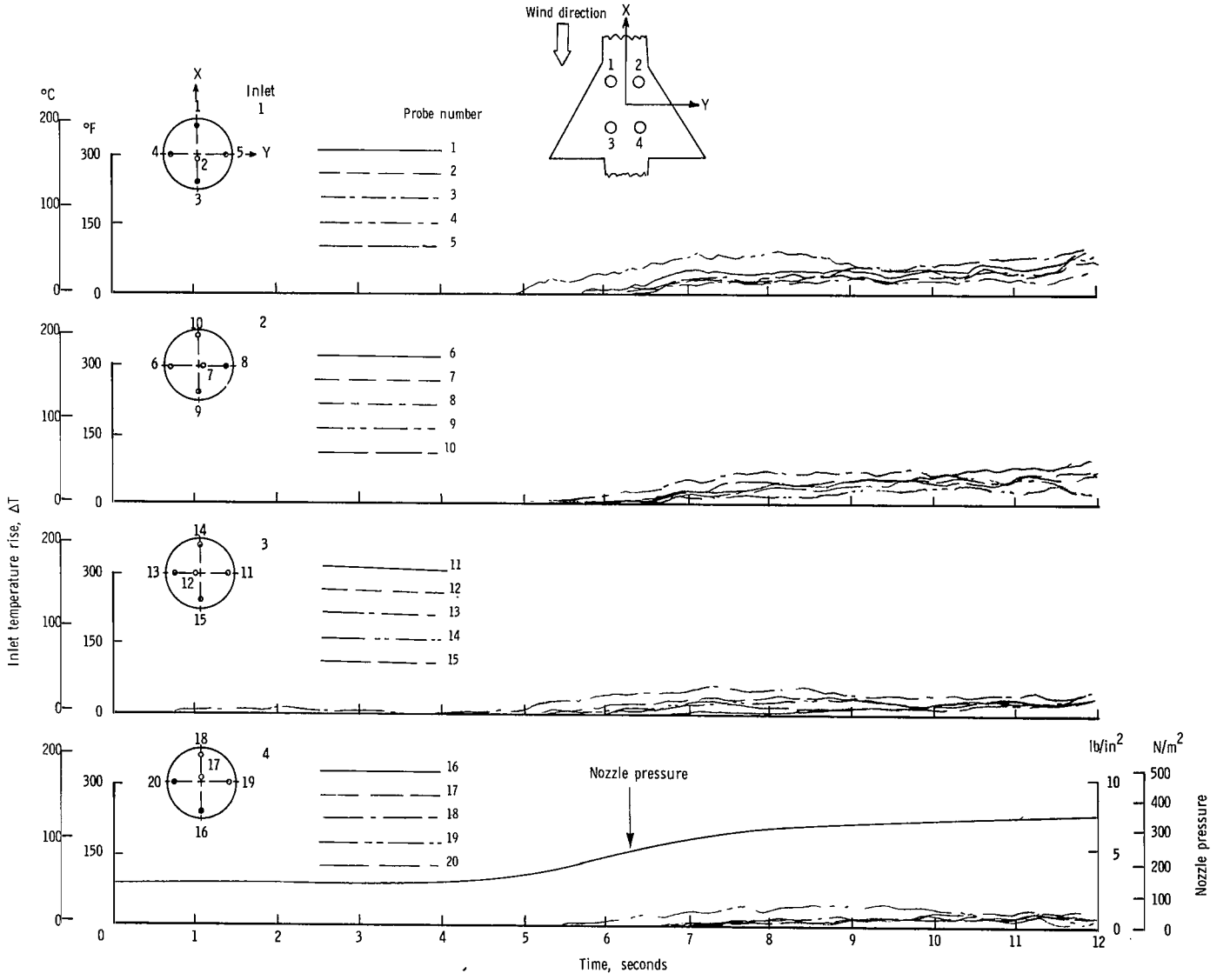

(e) $\psi = 0^0$; V = 23.70 knots.

Figure 12.- Continued.

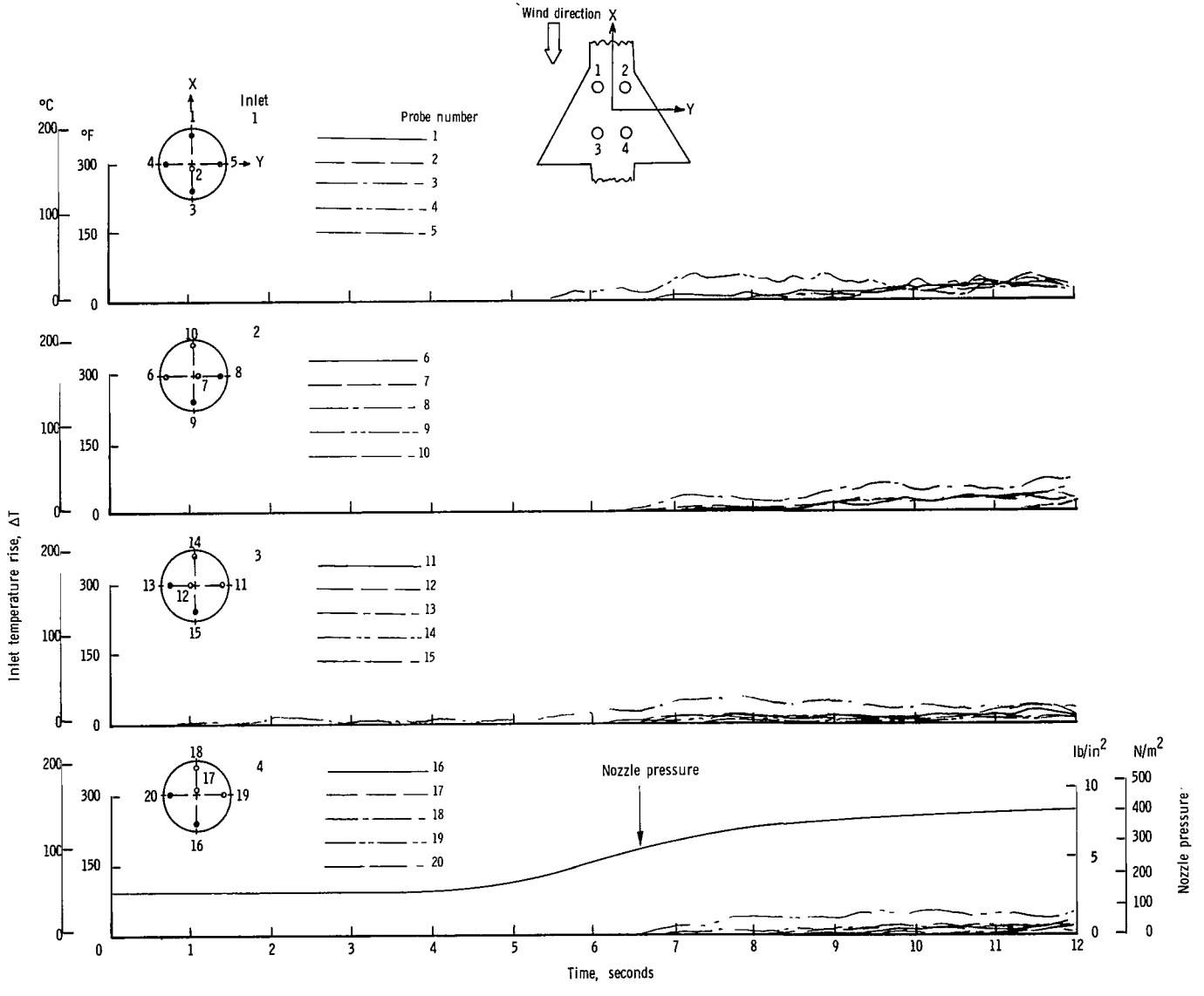

(f) $\psi = 0^{o}$; V = 29.63 knots.

Figure 12.- Continued.

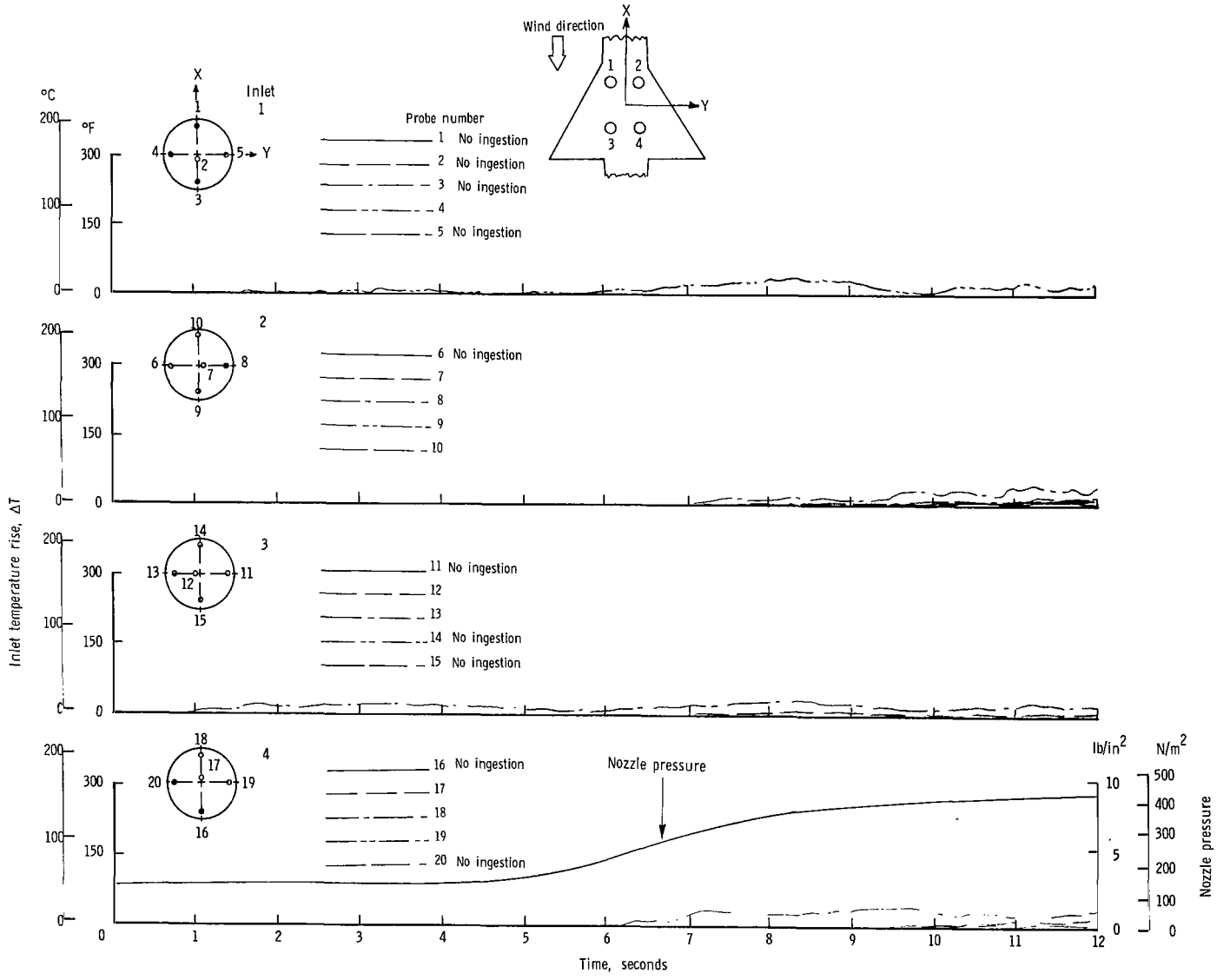

(g) $\psi = 0^0$; V = 35.55 knots.

Figure 12.- Continued.

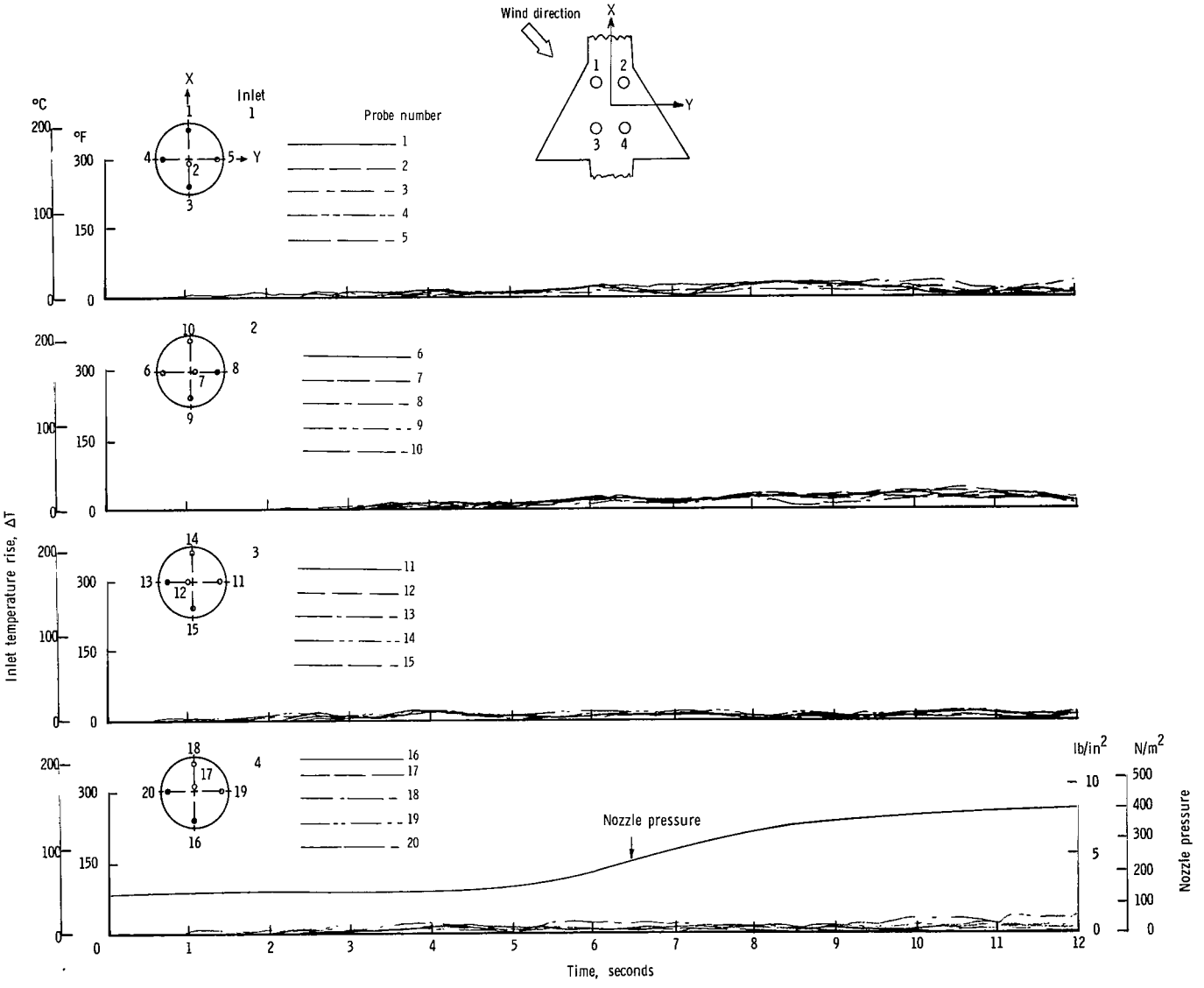

(h) $\psi = 45^{0}$; V = 5.92 knots.

Figure 12.- Continued.

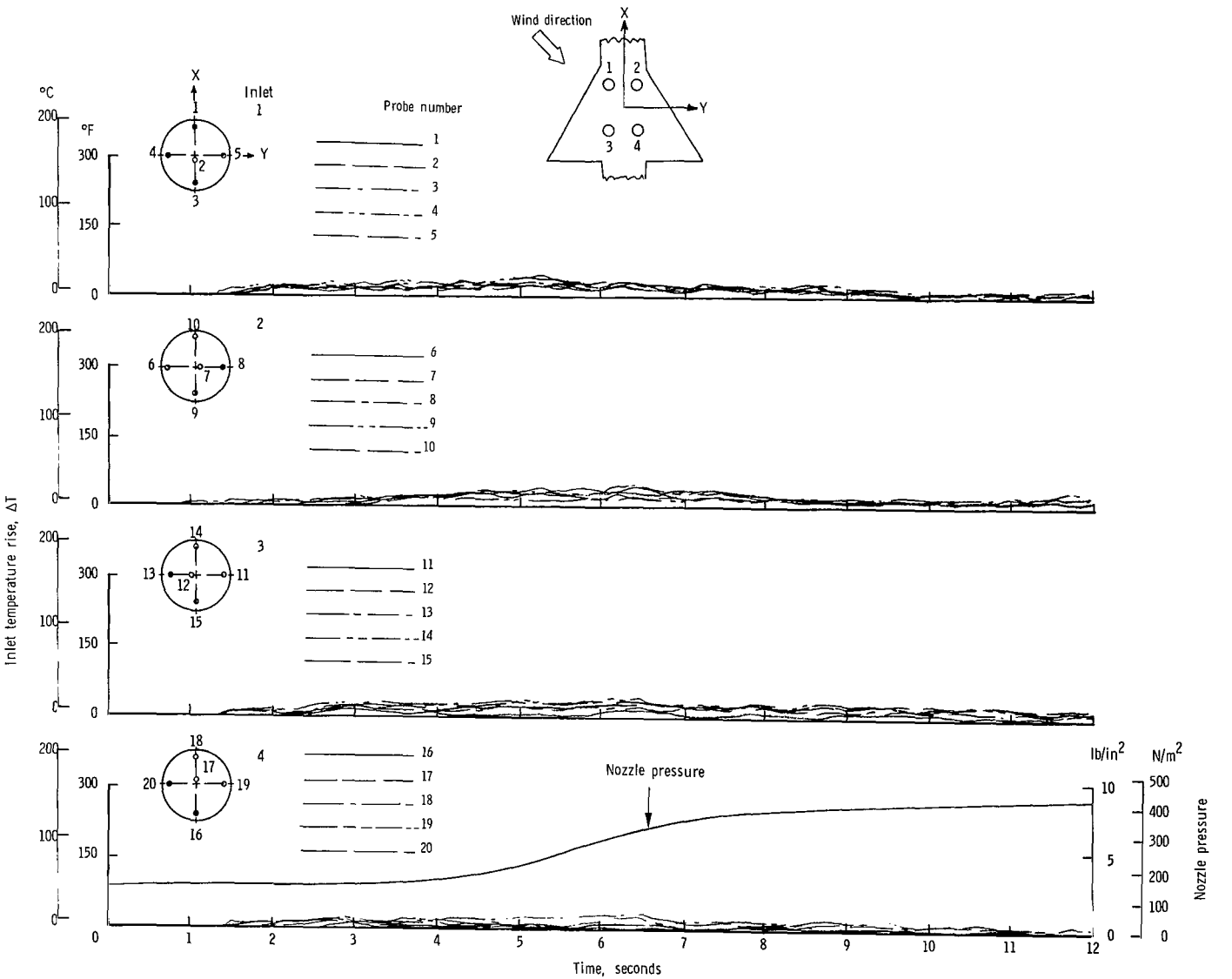

(i) $\psi = 45^{0}$; V = 11.85 knots.

Figure 12.- Continued.

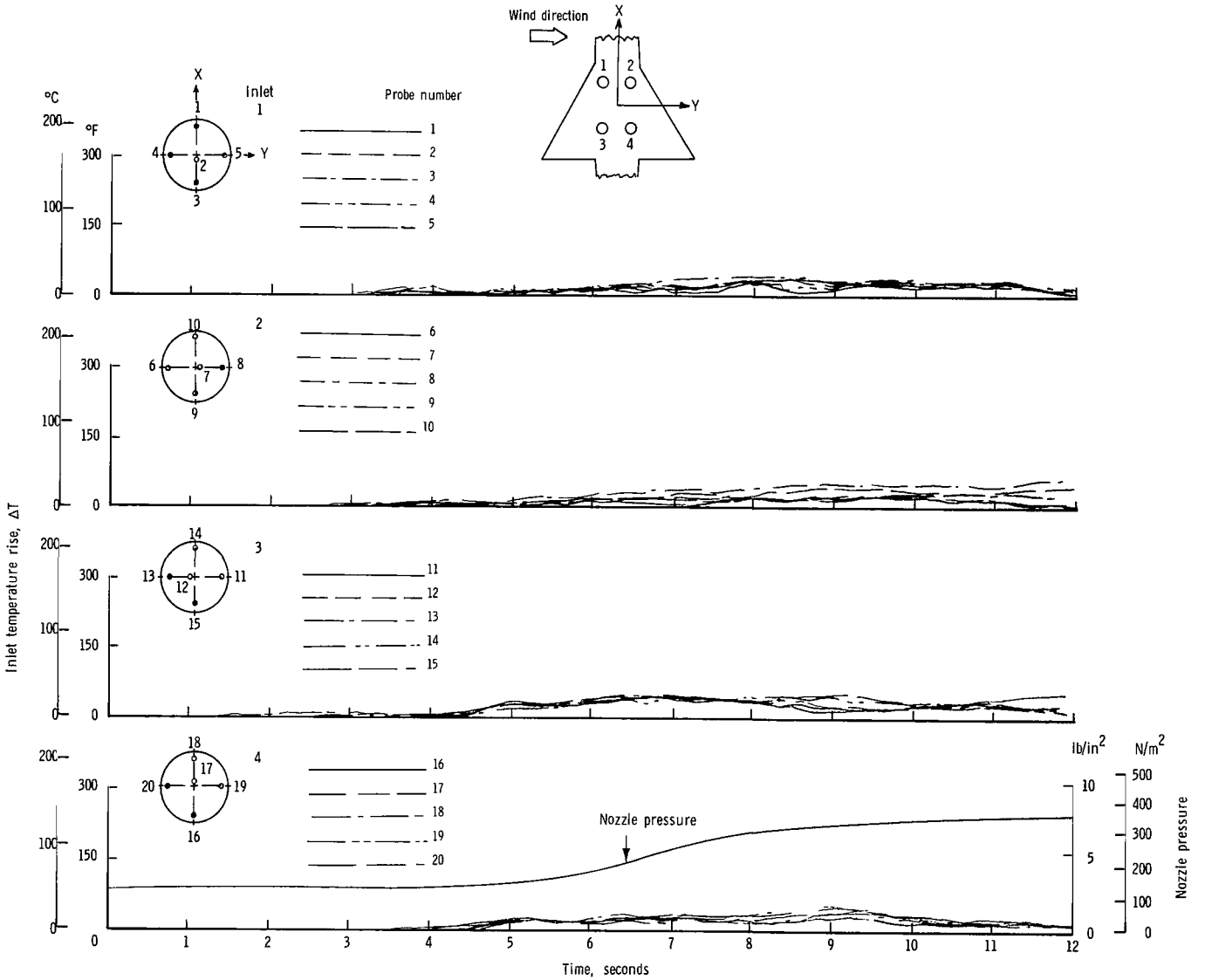

(j) $\psi = 90^{0}$; V = 5.92 knots.

Figure 12.- Continued.

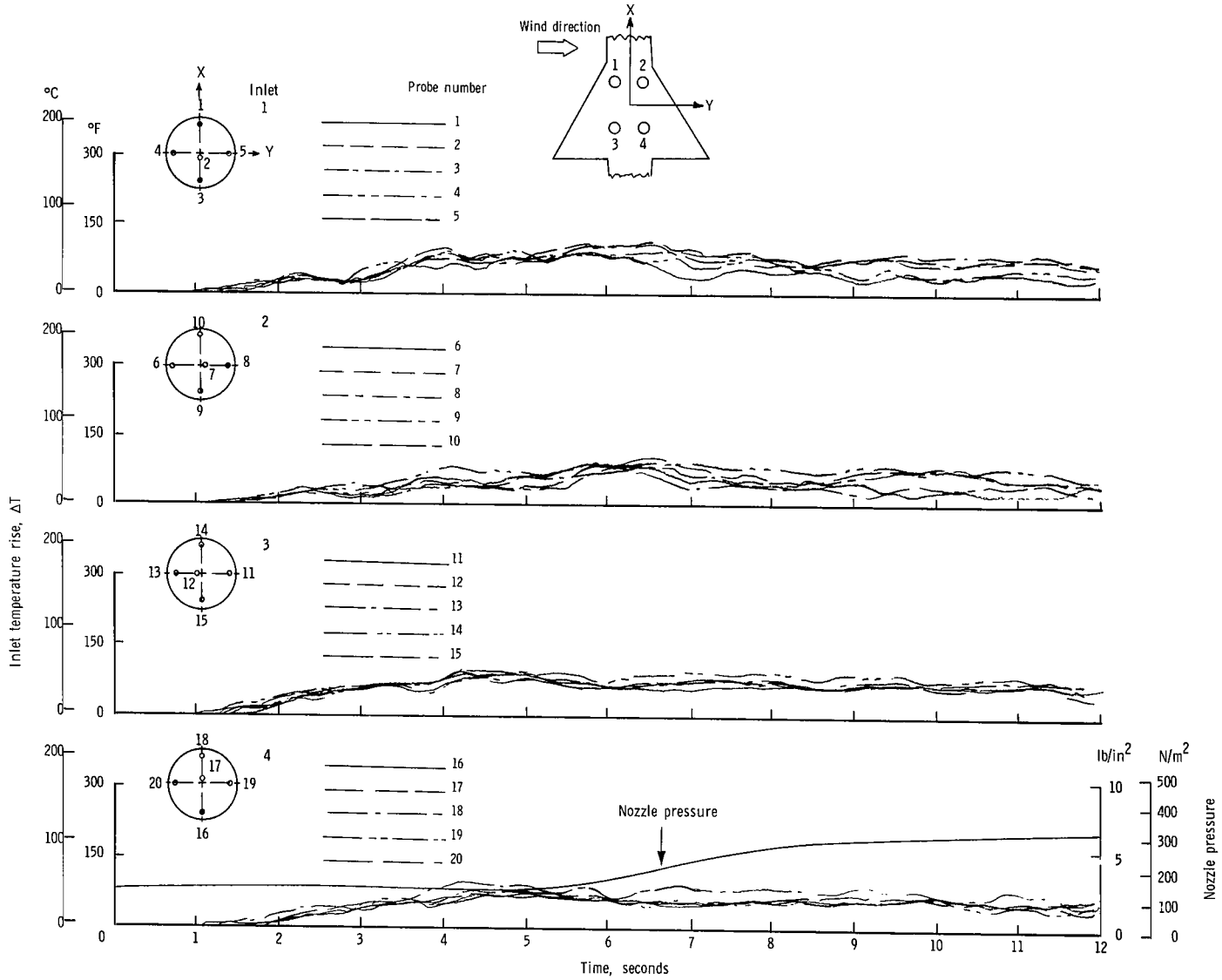

(k) $\psi = 90^{0}$; V = 11.85 knots.

Figure 12.- Concluded.

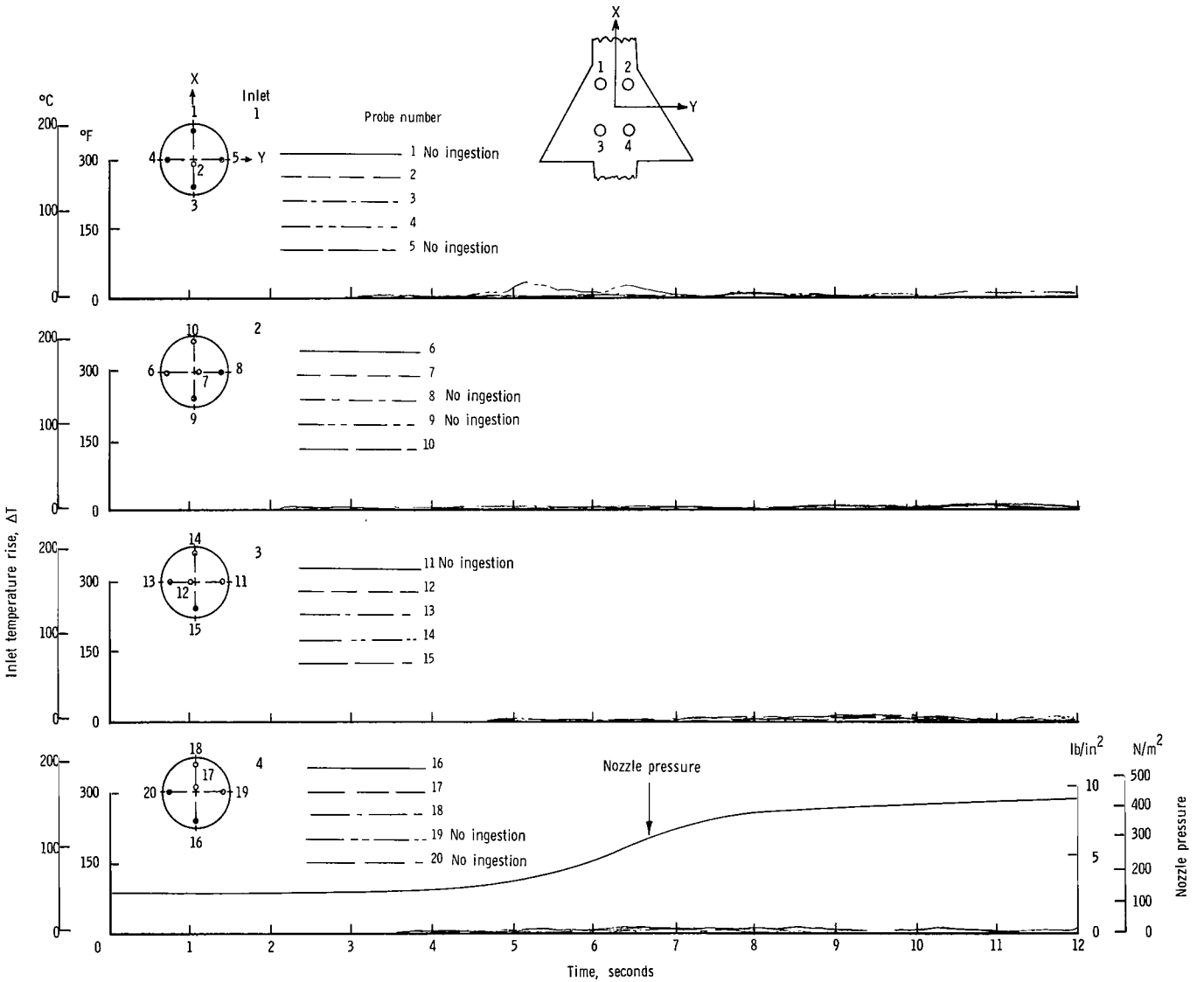

(a) $\psi = 0^{o}$; V = 0 knots.

Figure 13.- Variation of inlet air temperature rise with time for the rectangular nozzle arrangement with top inlets and low delta wing. $h/D_e = 3.0$.

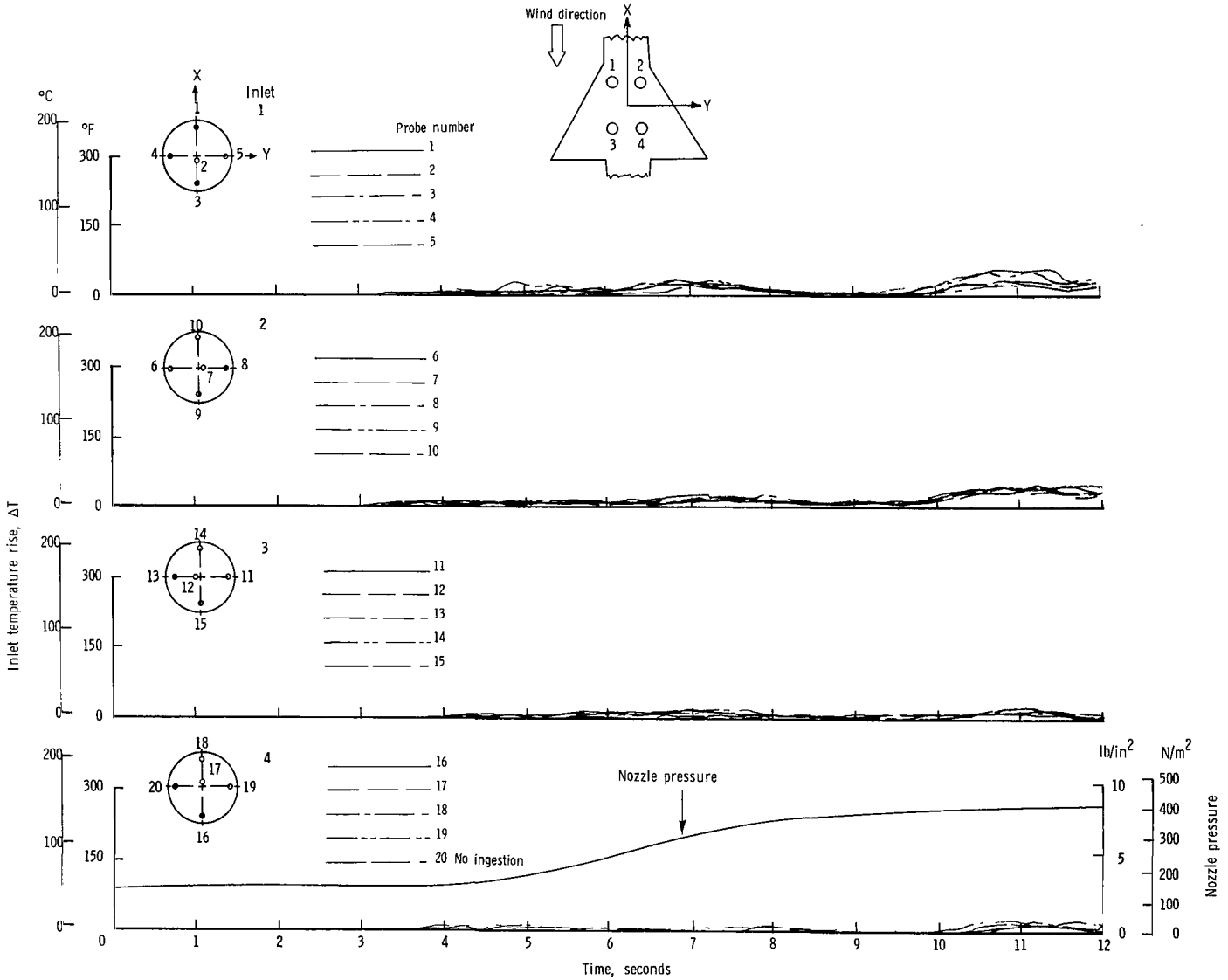

(b) $\psi = 0^{0}$; V = 5.92 knots.

Figure 13.- Continued.

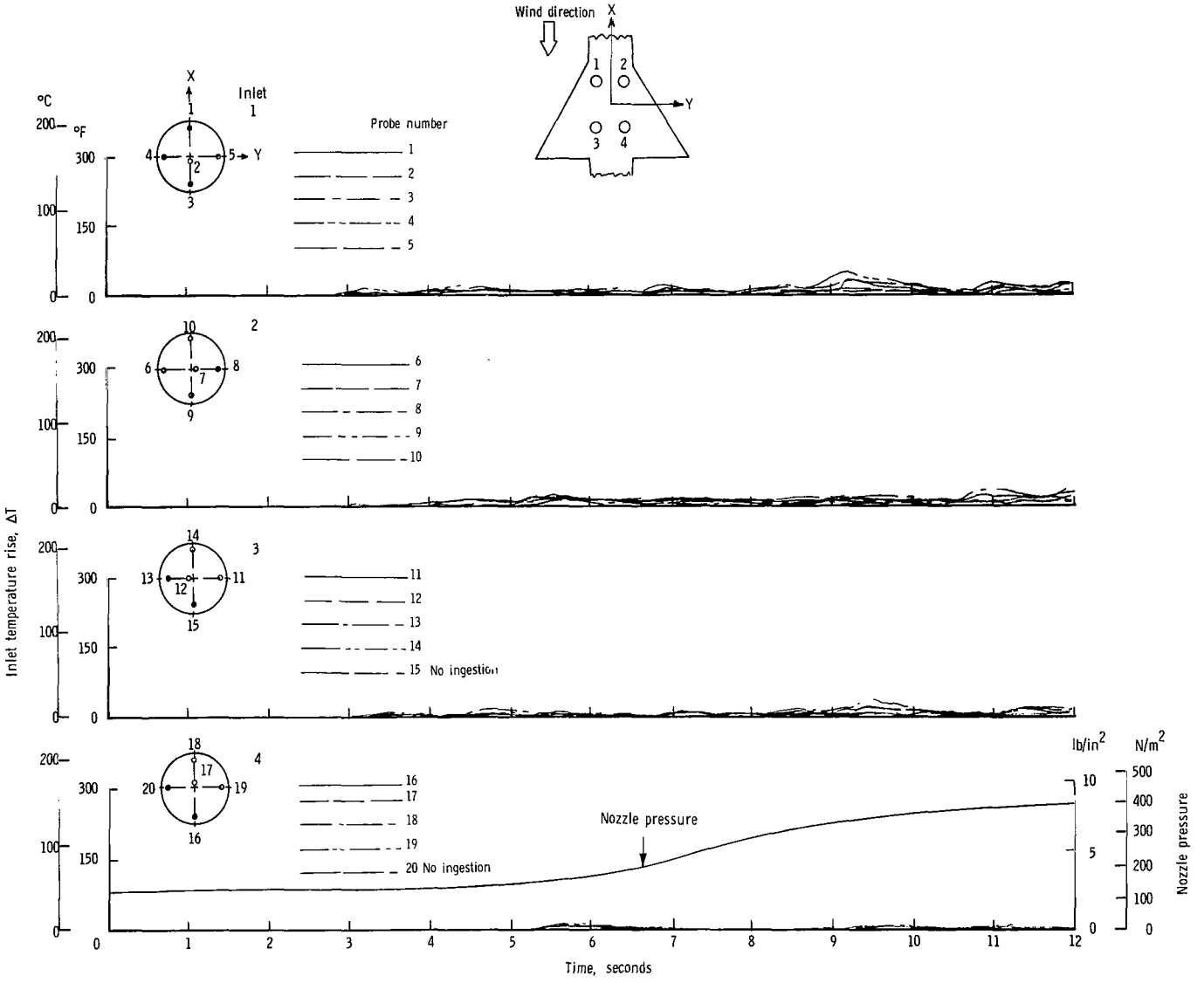

(c) $\psi = 0^0$; V = 11.85 knots.

Figure 13.- Continued.

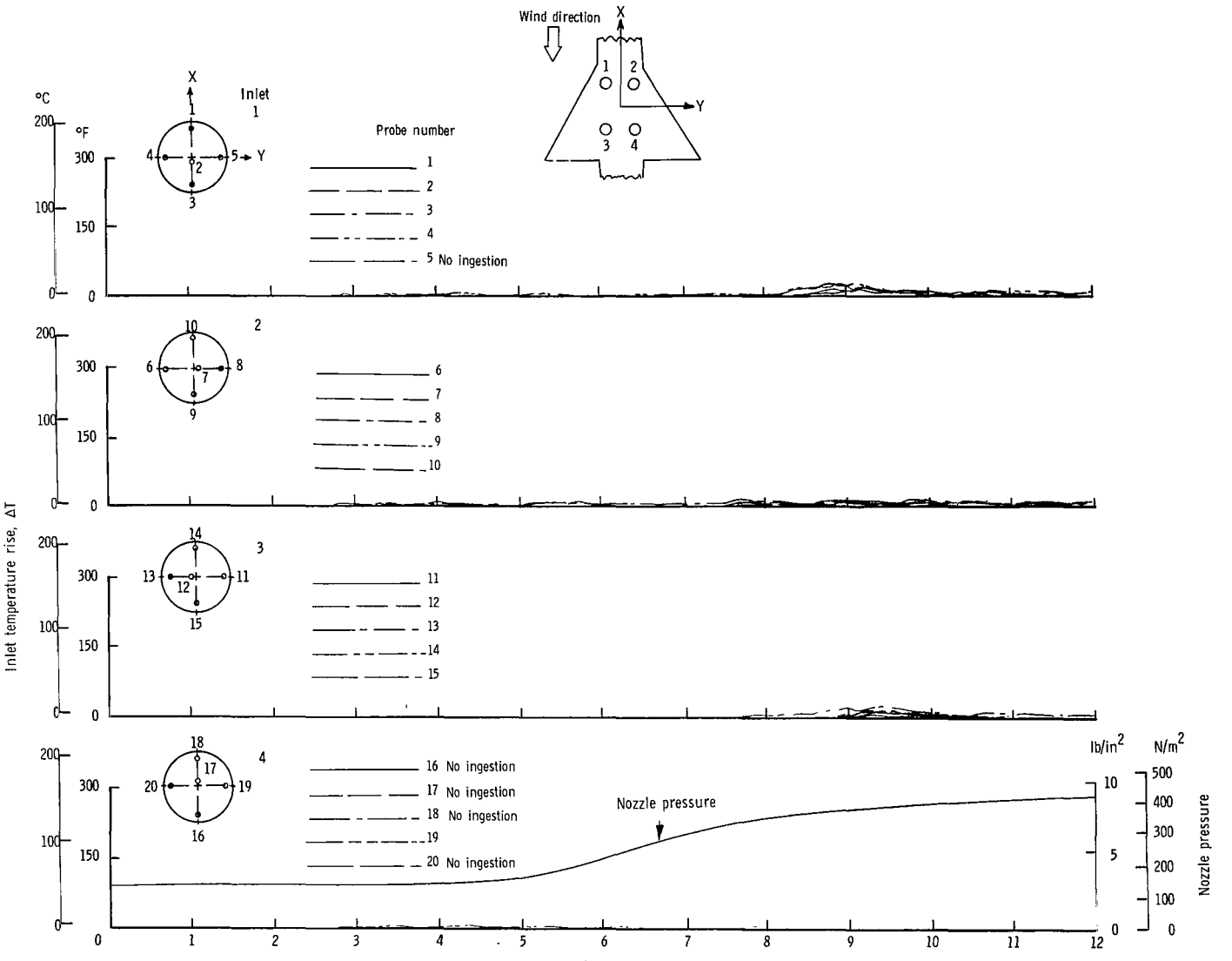

(d) $\psi = 0^{0}$; V = 17.78 knots.

Figure 13.- Continued.

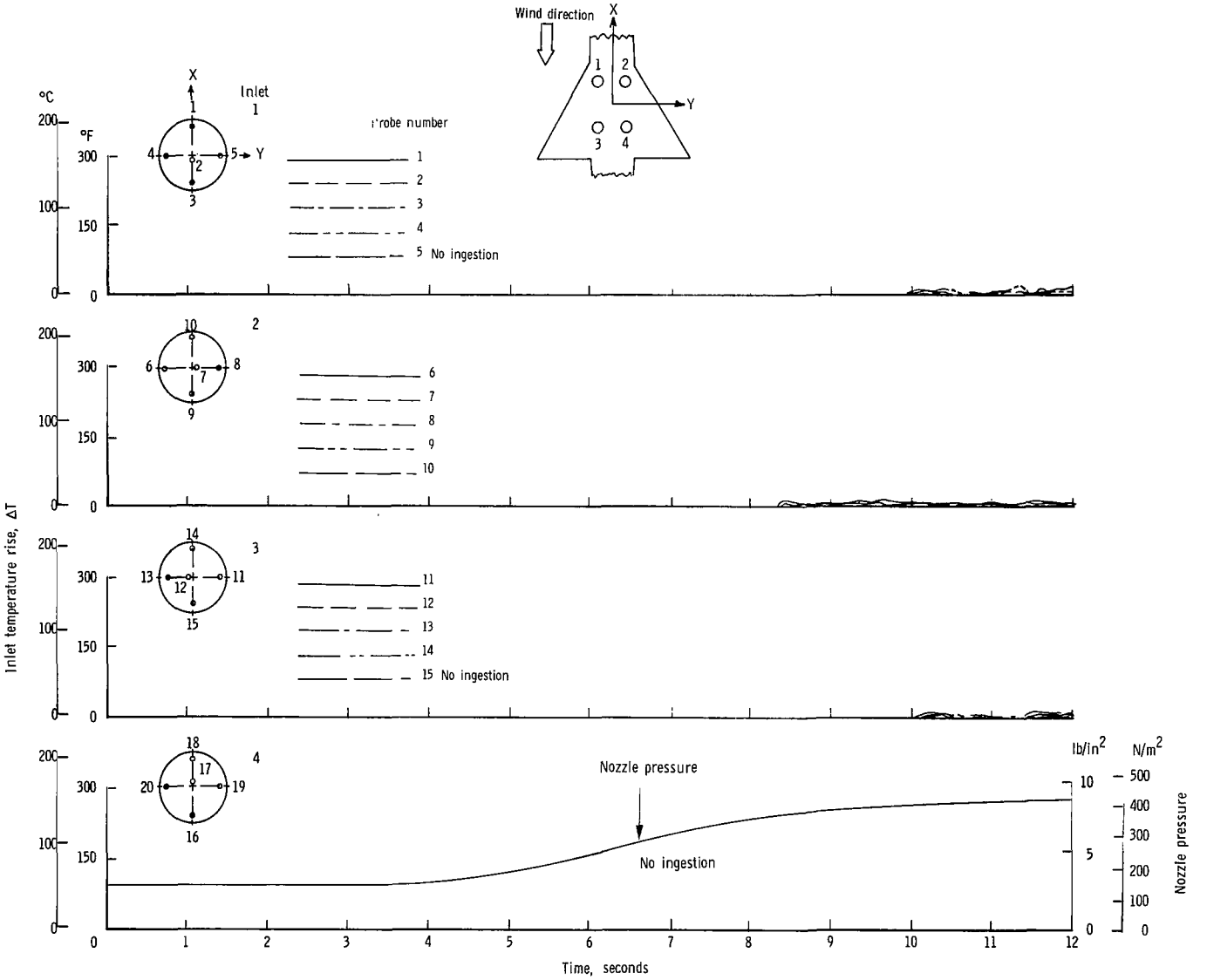

(e) $\psi = 0^0$; V = 23.70 knots.

Figure 13.- Continued.

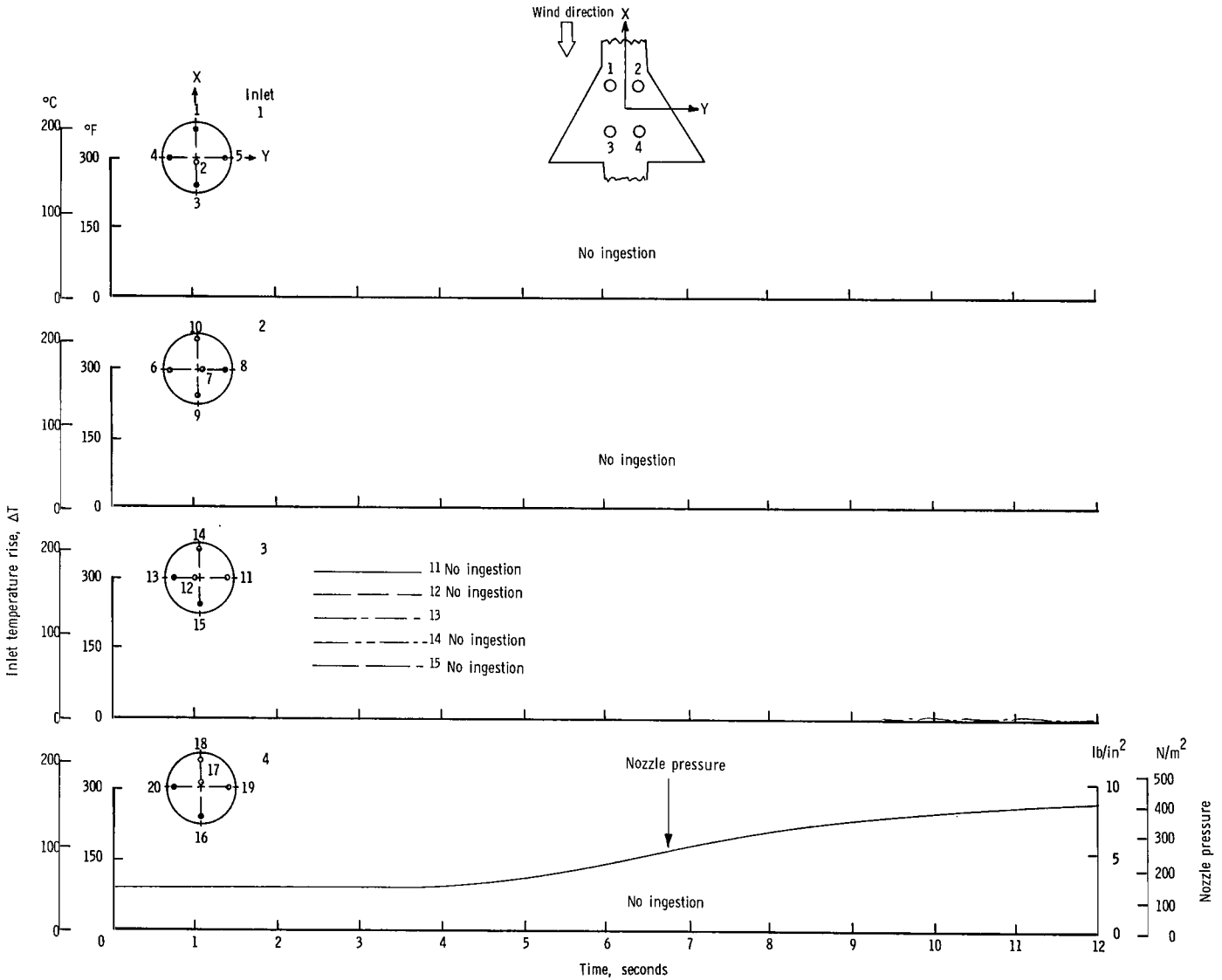

(f) $\psi = 0^0$; V = 29.63 knots.

Figure 13.- Continued.

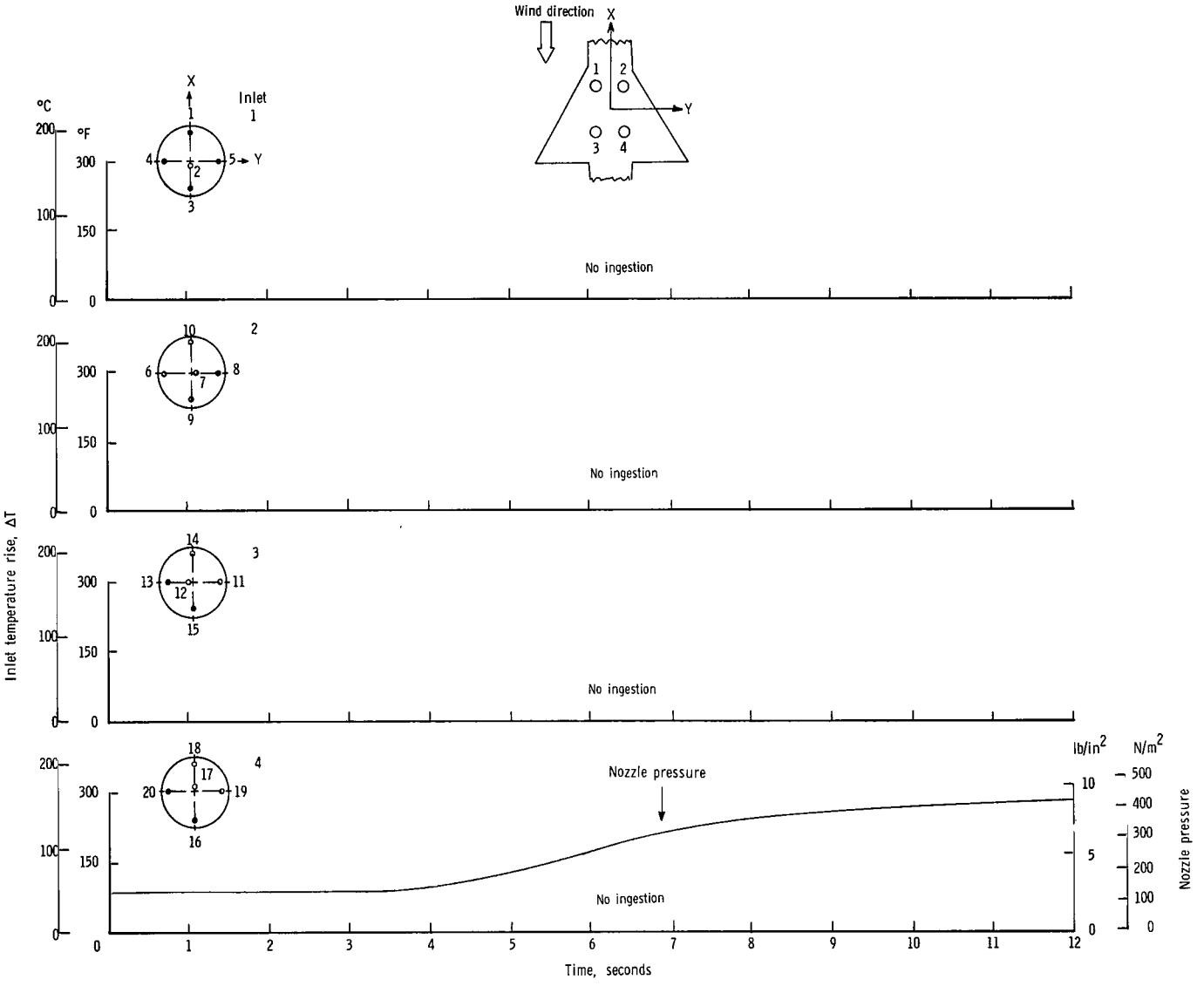

(g) $\psi = 0^{0}$; V = 35.55 knots.

Figure 13.- Continued.

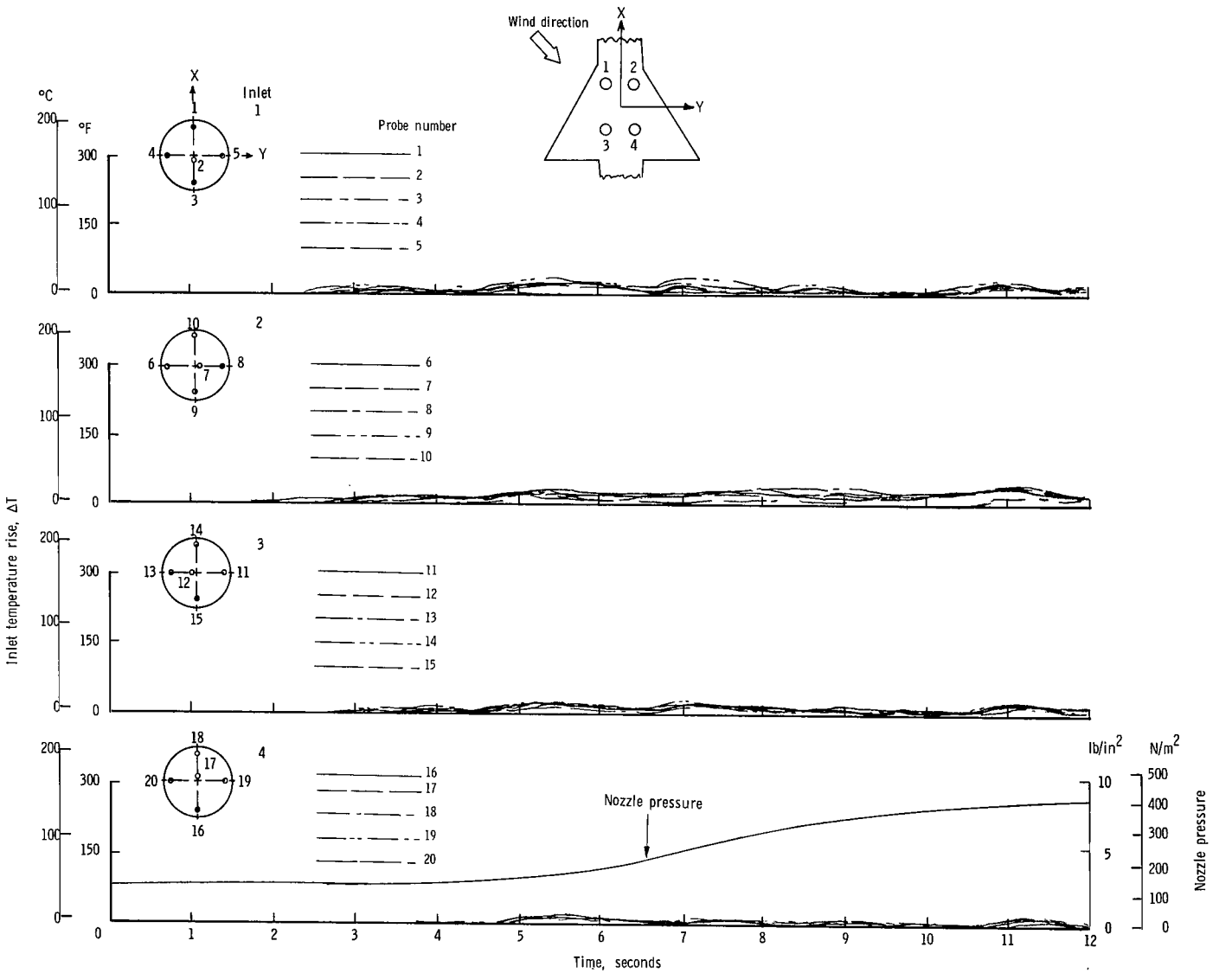

(h) $\psi = 45^{0}$; V = 5.92 knots.

Figure 13.- Continued.

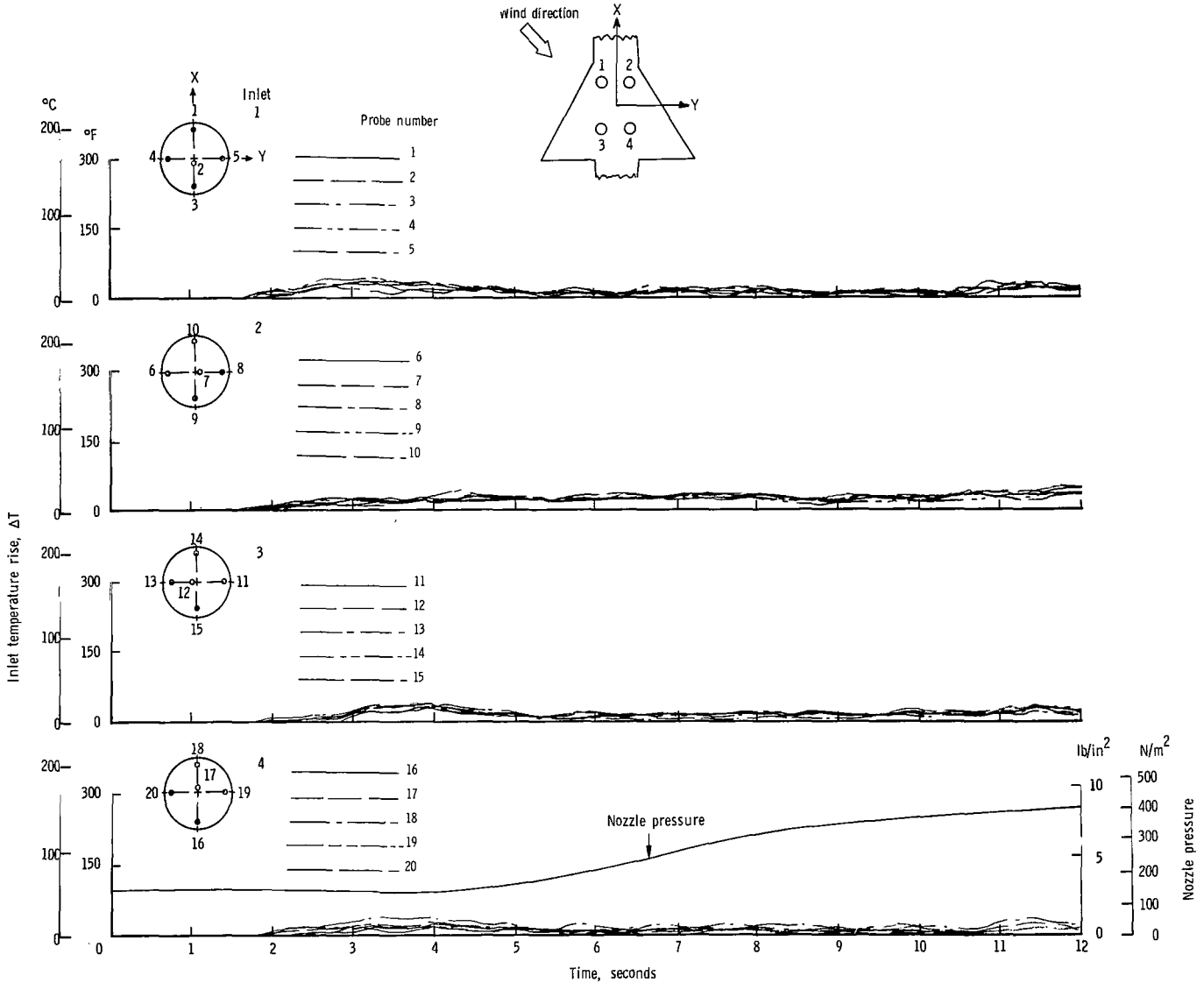

(i) $\psi = 45^0$; V = 11.85 knots.

Figure 13.- Continued.

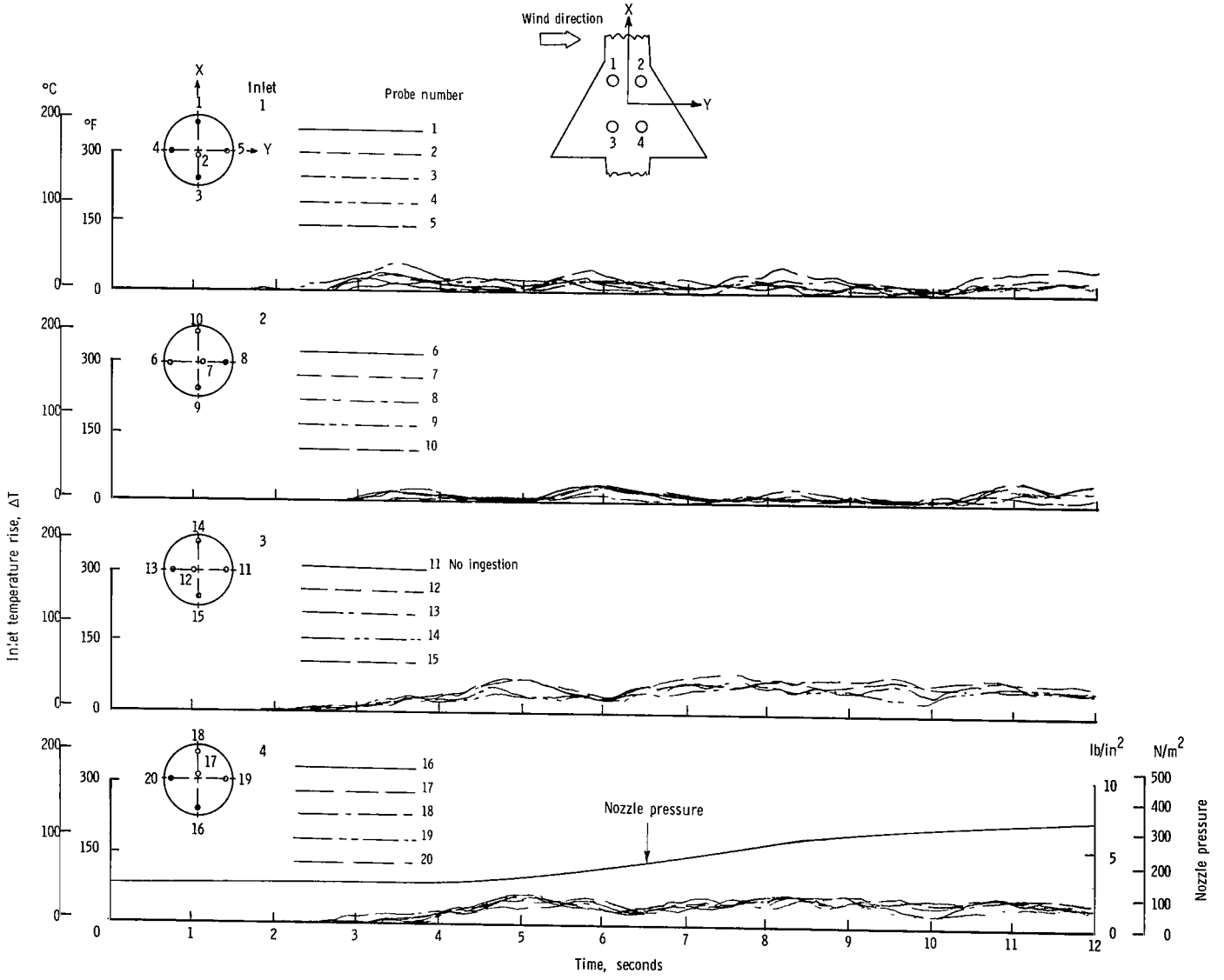

(j) $\psi = 90^{0}$; V = 5.92 knots.

Figure 13.- Continued.

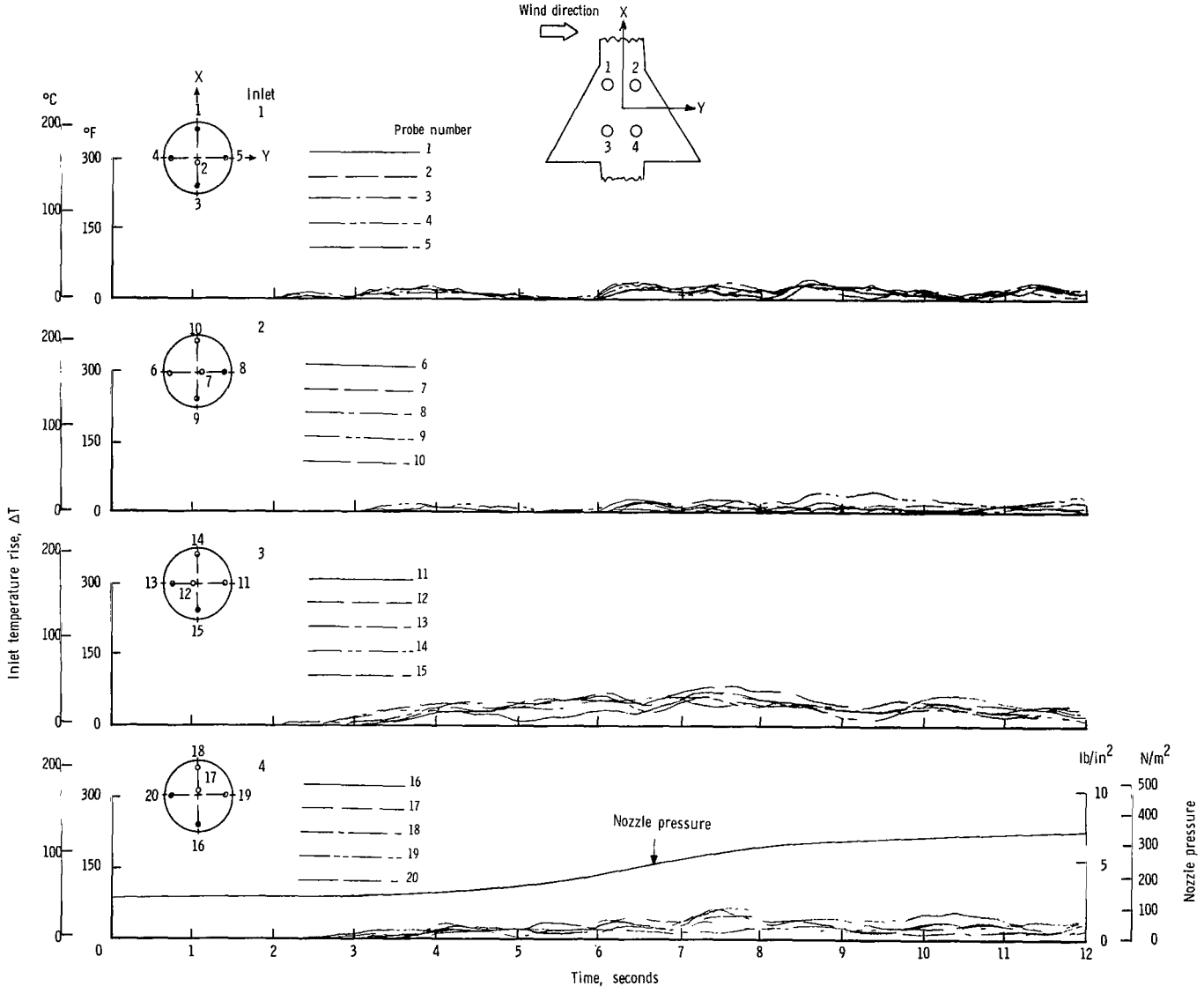

(k) $\psi = 90^{0}$; V = 11.85 knots.

Figure 13.- Concluded.

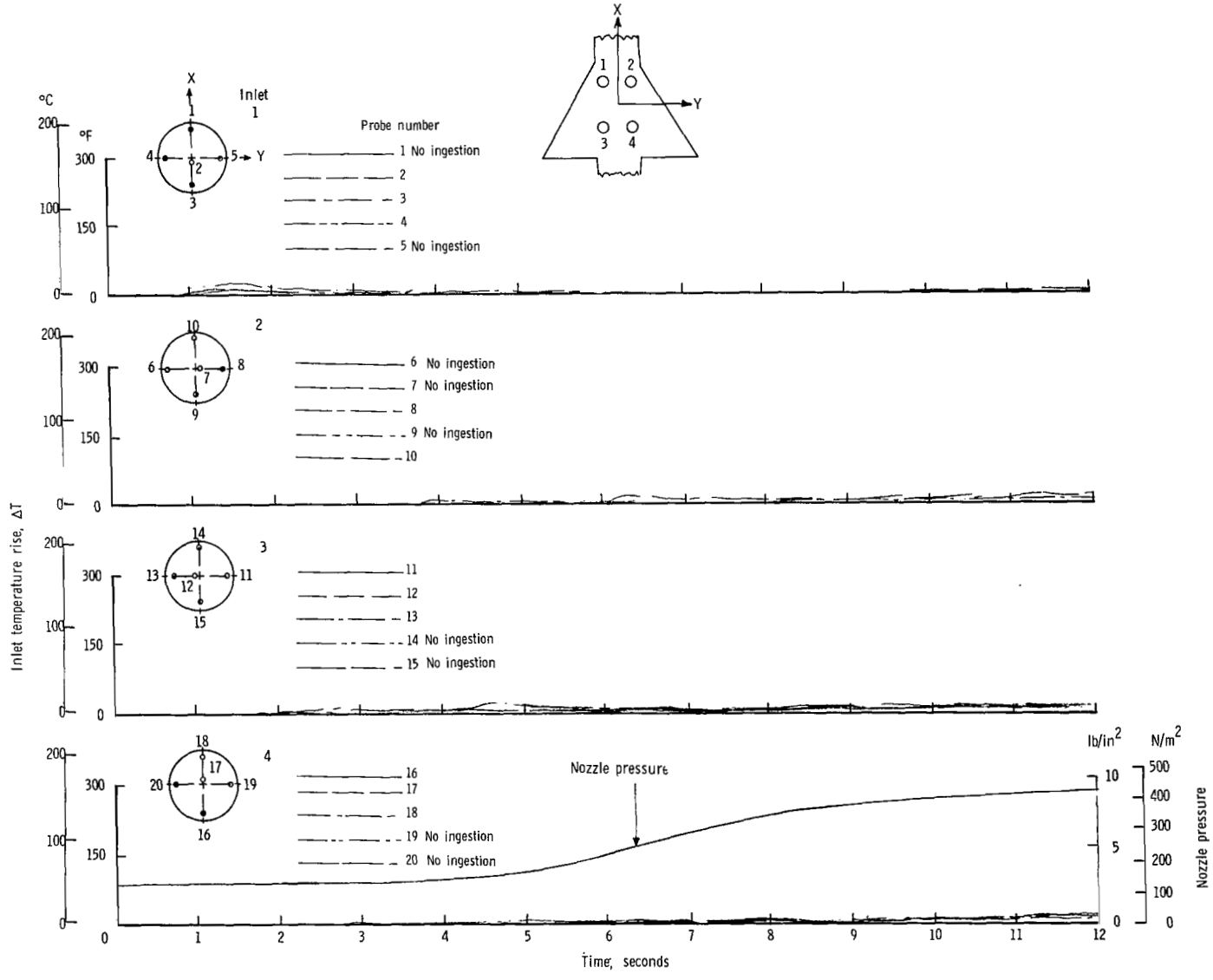

(a) ψ = 0°; V = 0 knots.

Figure 14.- Variation of inlet air temperature rise with time for the rectangular nozzle arrangement with top inlets and low delta wing. h/D_e = 5.0.

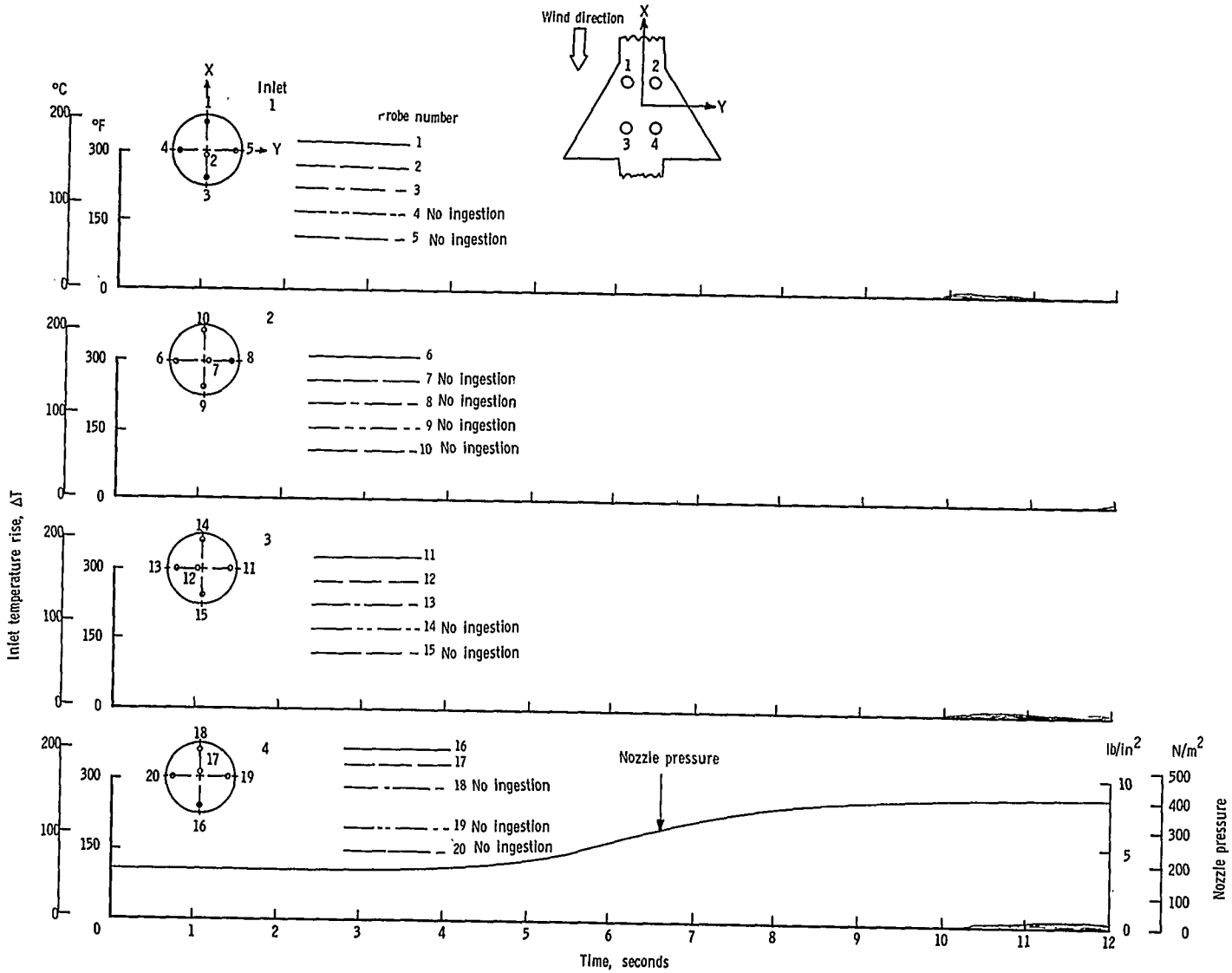

(b) $\psi = 0^0$; V = 5.92 knots.

Figure 14.- Continued.

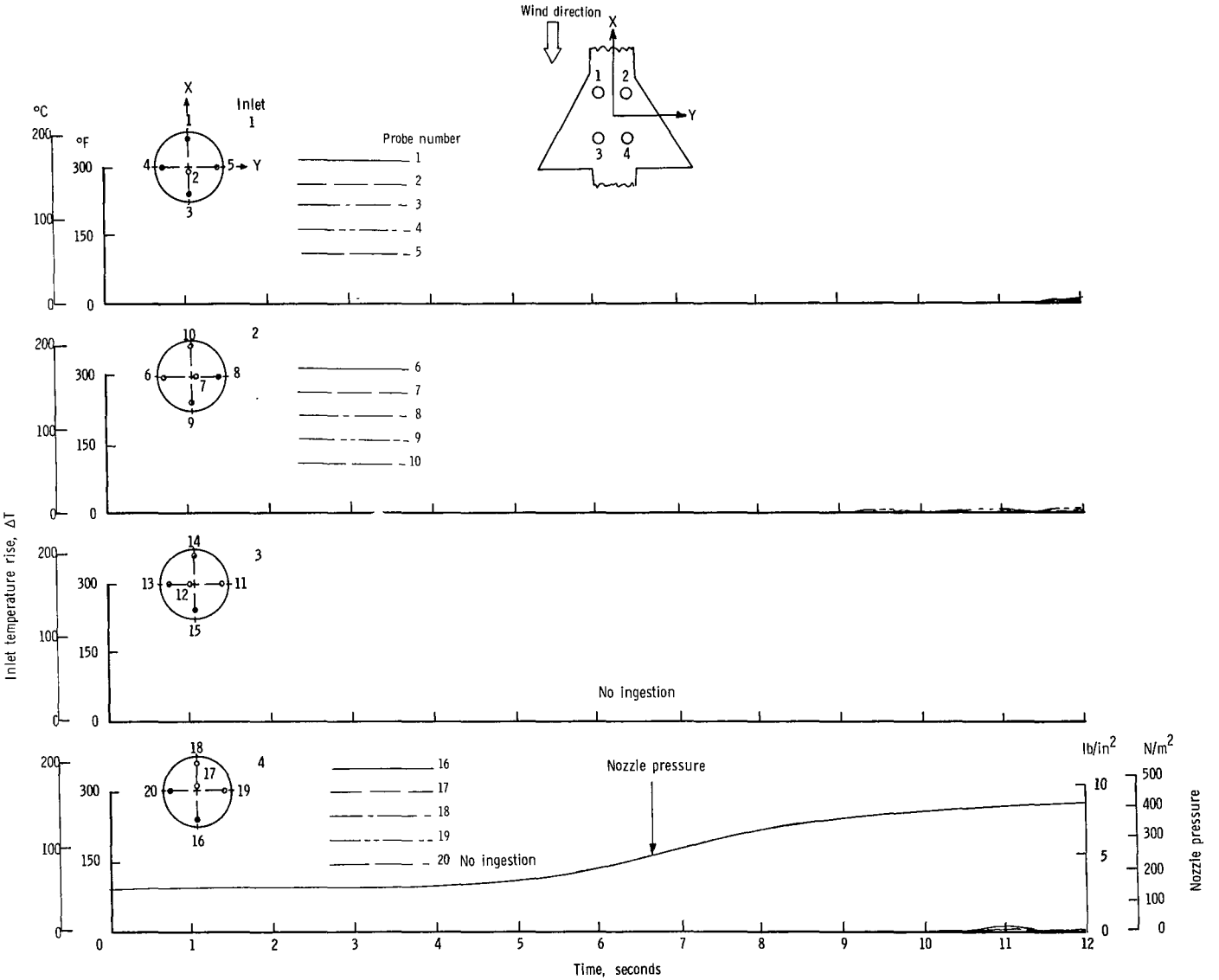

(c) $\psi = 0^0$; V = 11.85 knots.

Figure 14.- Continued.

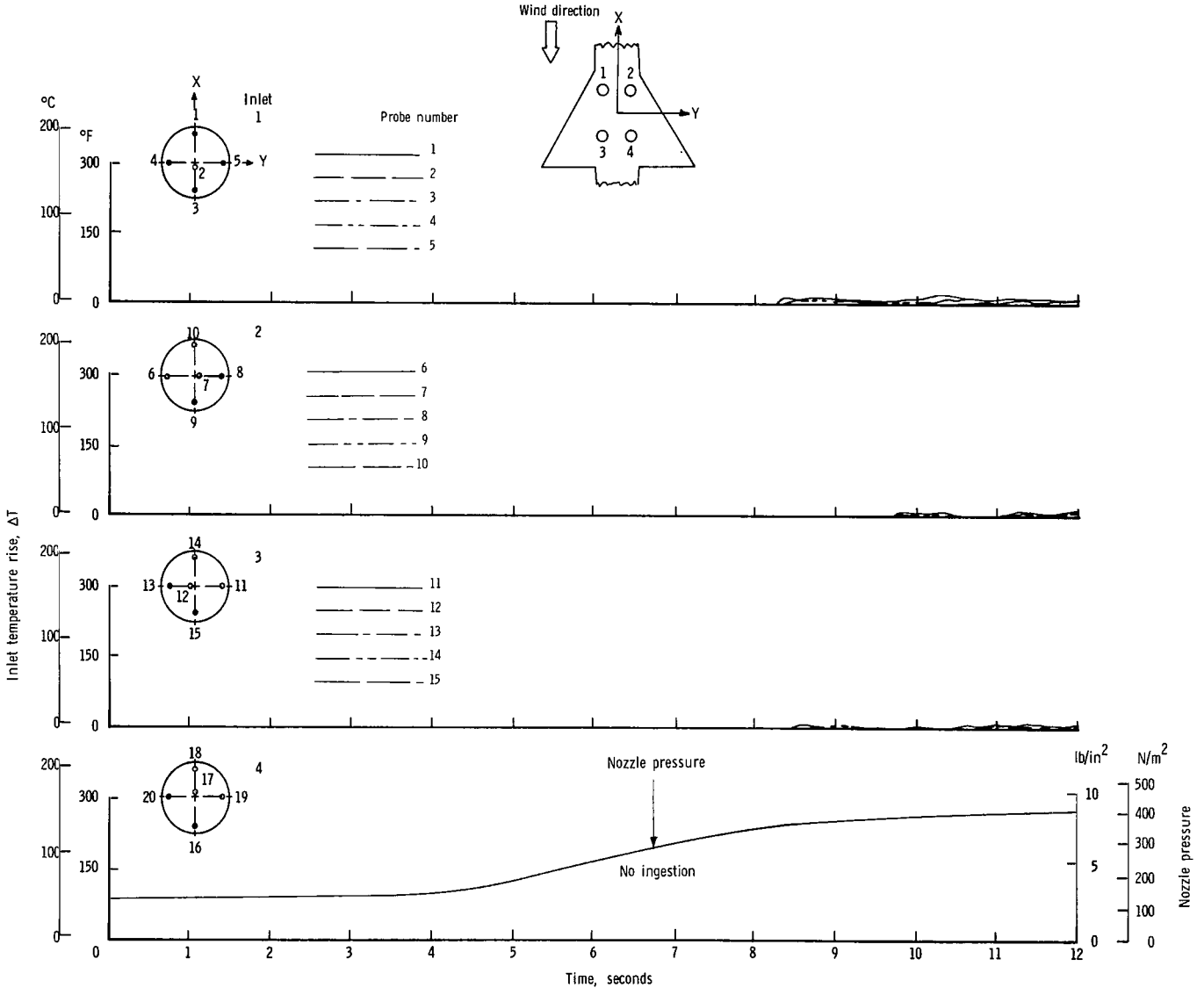

(d) $\psi = 0^{o}$; V = 17.78 knots.

Figure 14.- Continued.

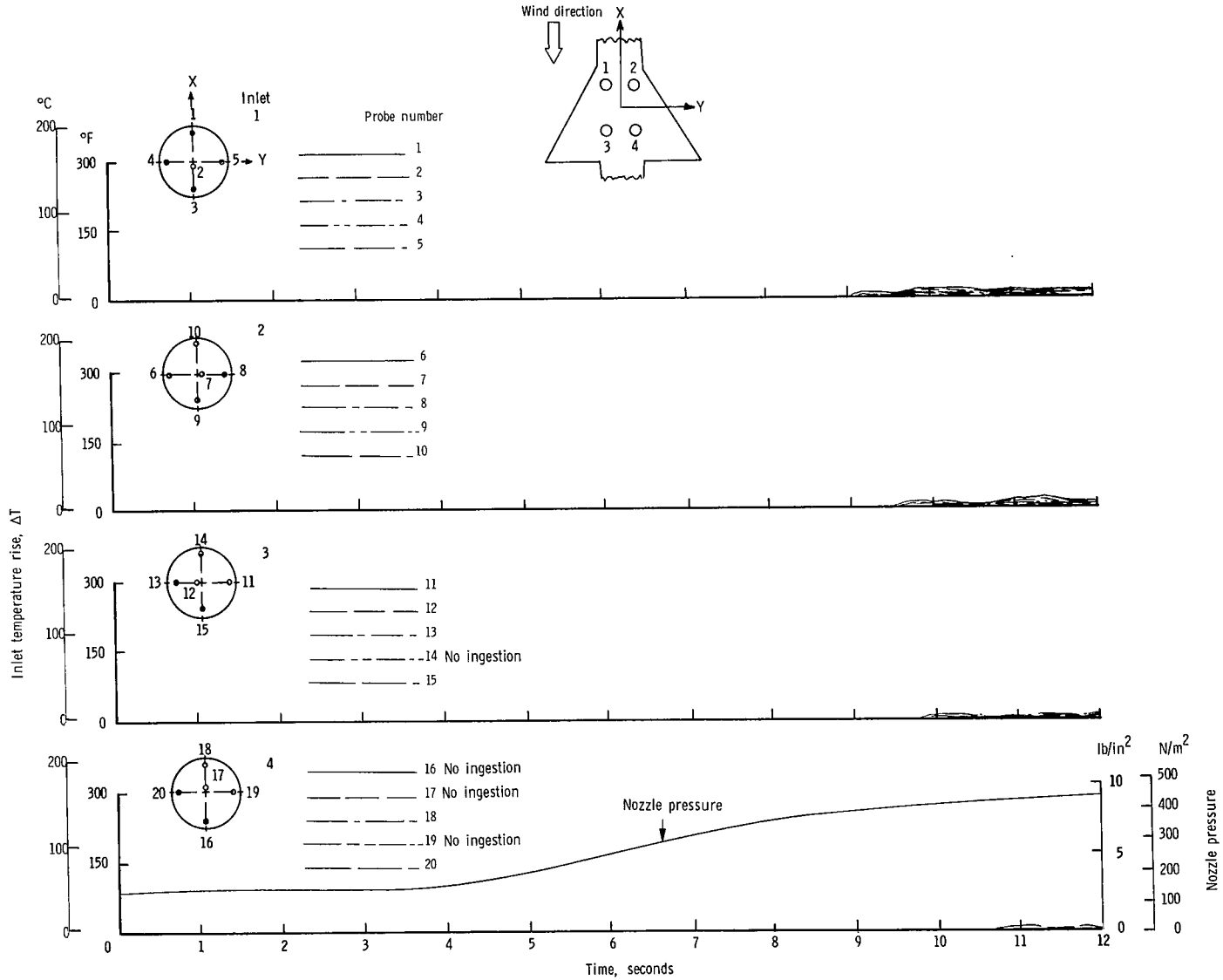

(e) $\psi = 0^0$; V = 23.70 knots.

Figure 14.- Continued.

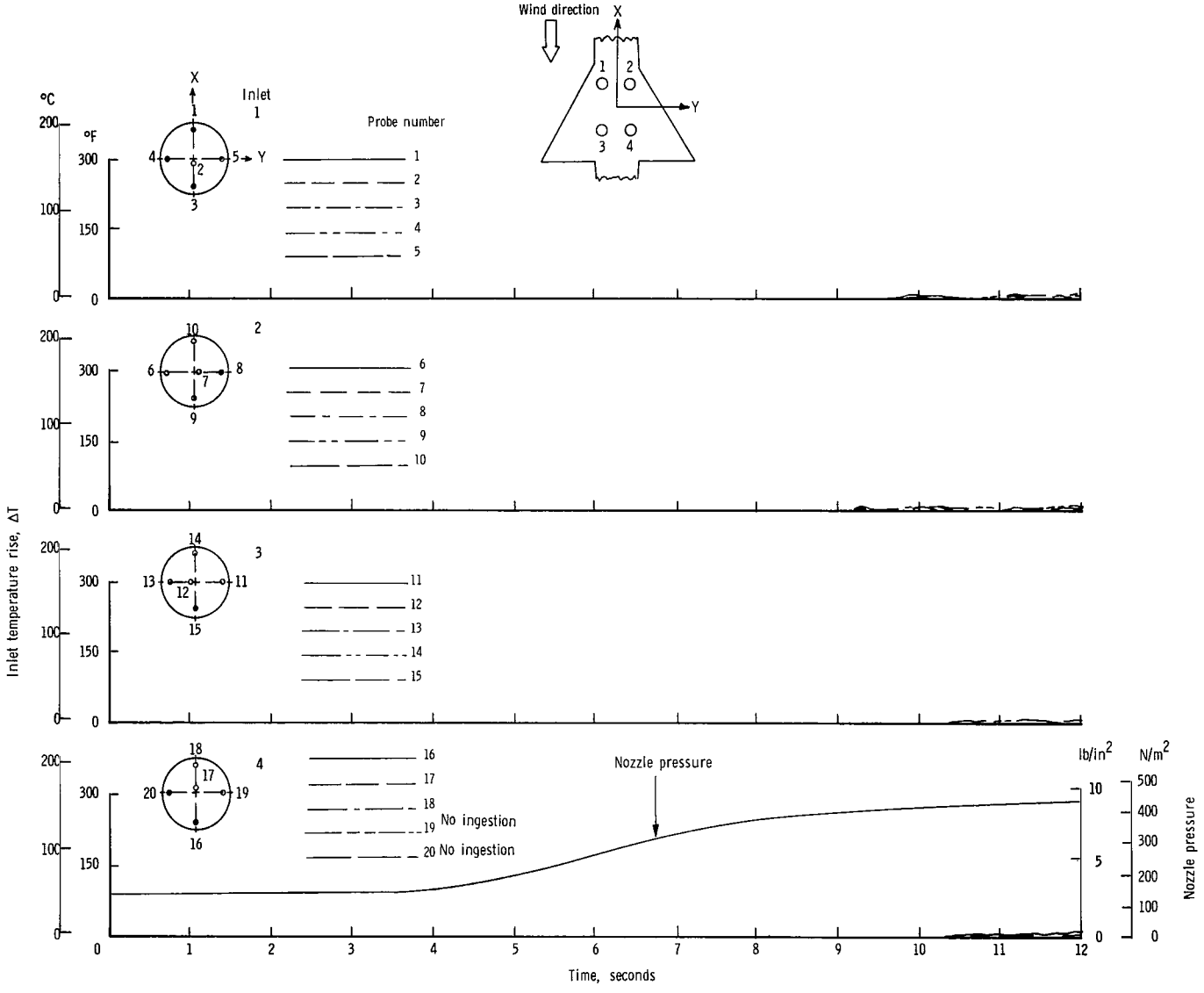

(f) $\psi = 0^0$; V = 29.63 knots.

Figure 14.- Continued.

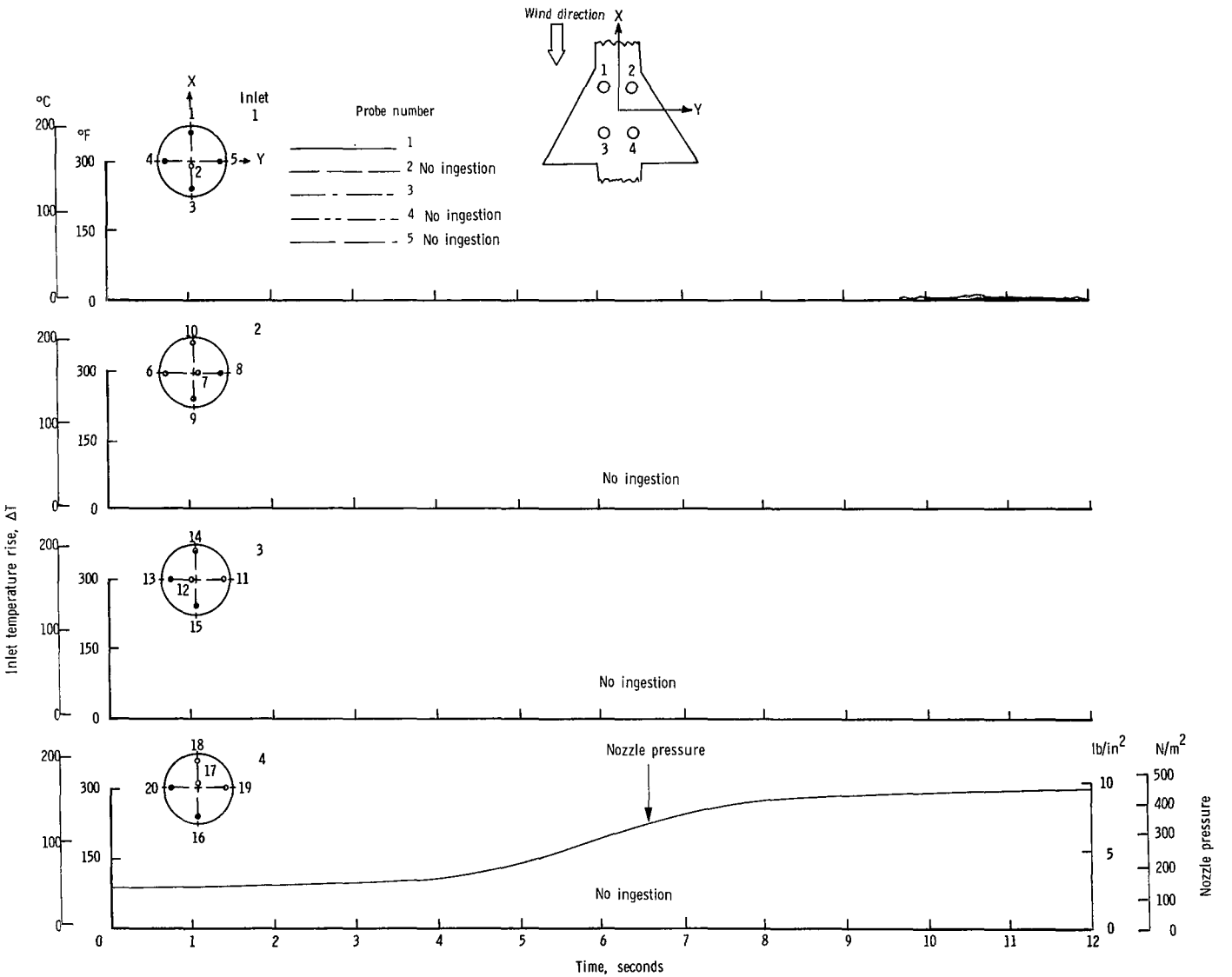

(g) $\psi = 0^0$; V = 35.55 knots.

Figure 14.- Continued.

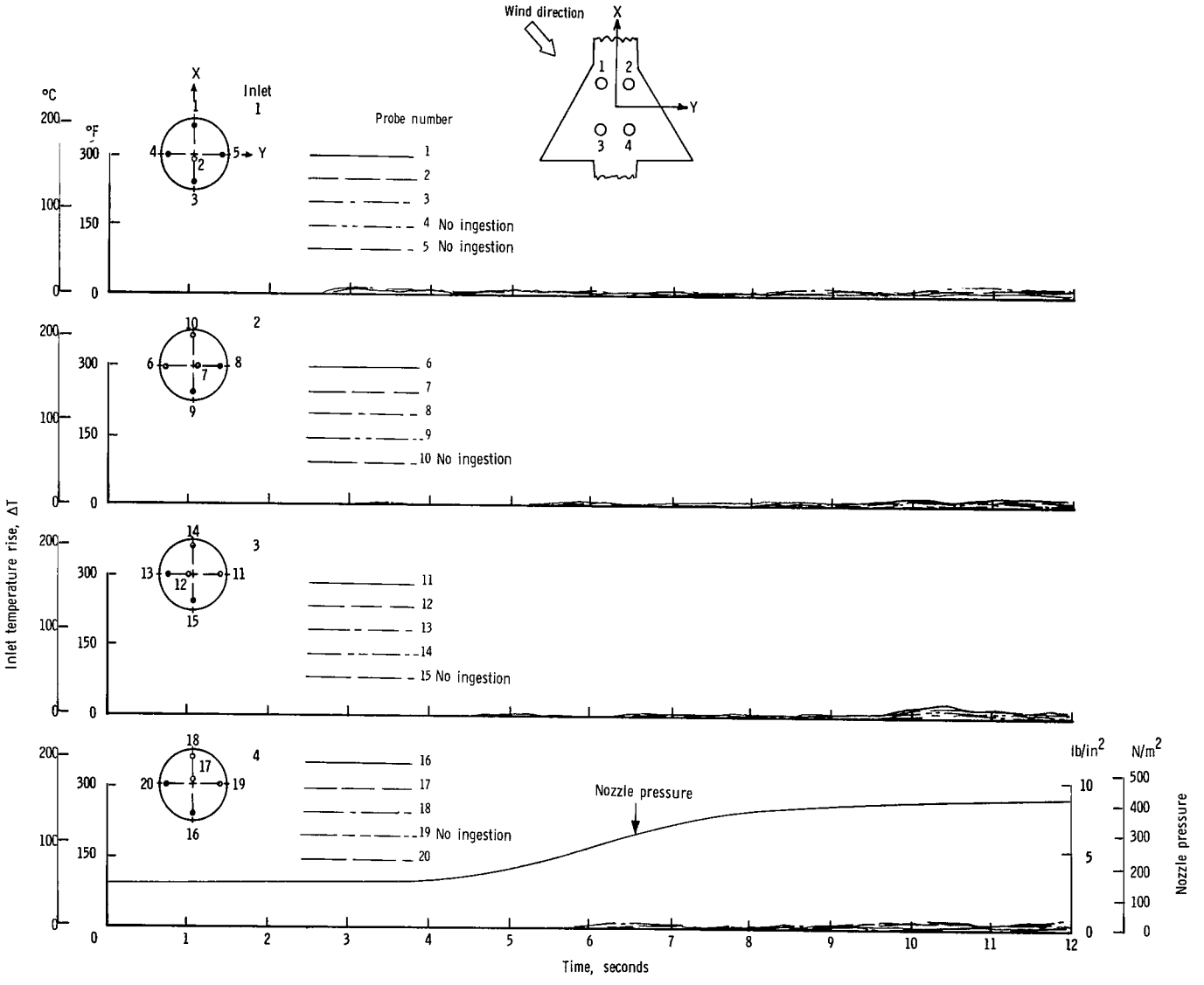

(h) $\psi = 45^{0}$; V = 5.92 knots.

Figure 14.- Continued.

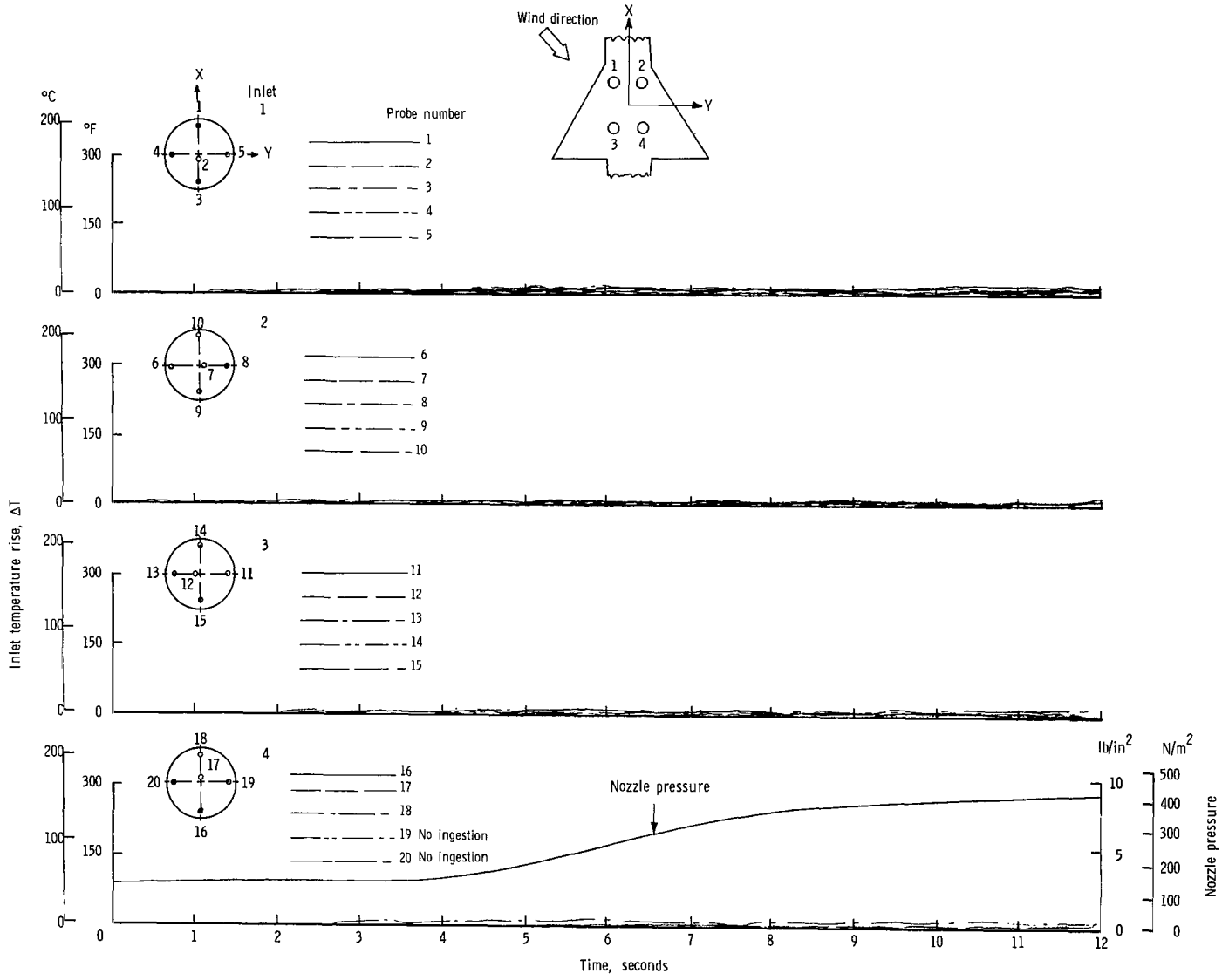

(i) $\psi = 45^{0}$; V = 11.85 knots.

Figure 14.- Continued.

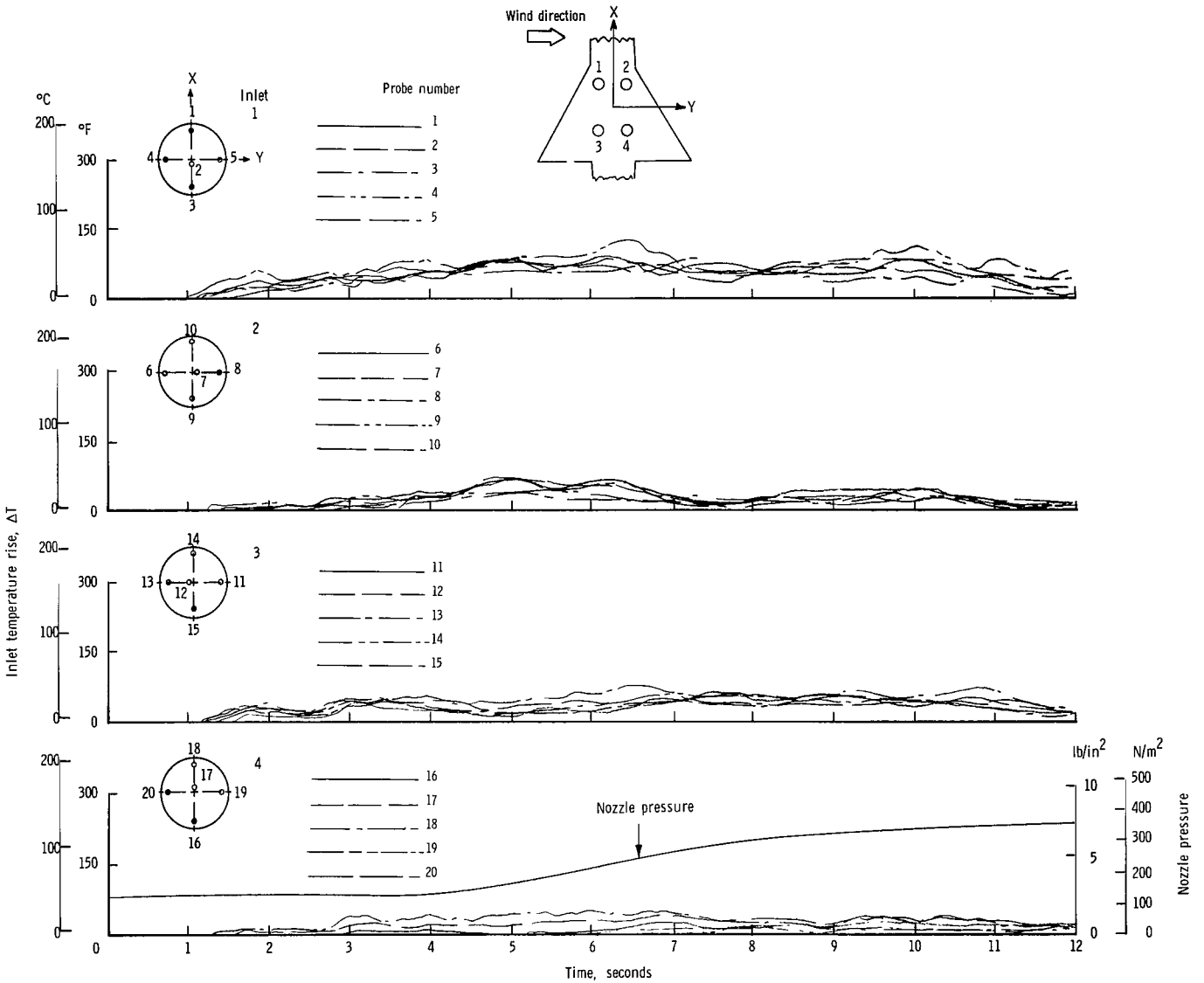

(j) $\psi = 90^0$; V = 5.92 knots.

Figure 14.- Continued.

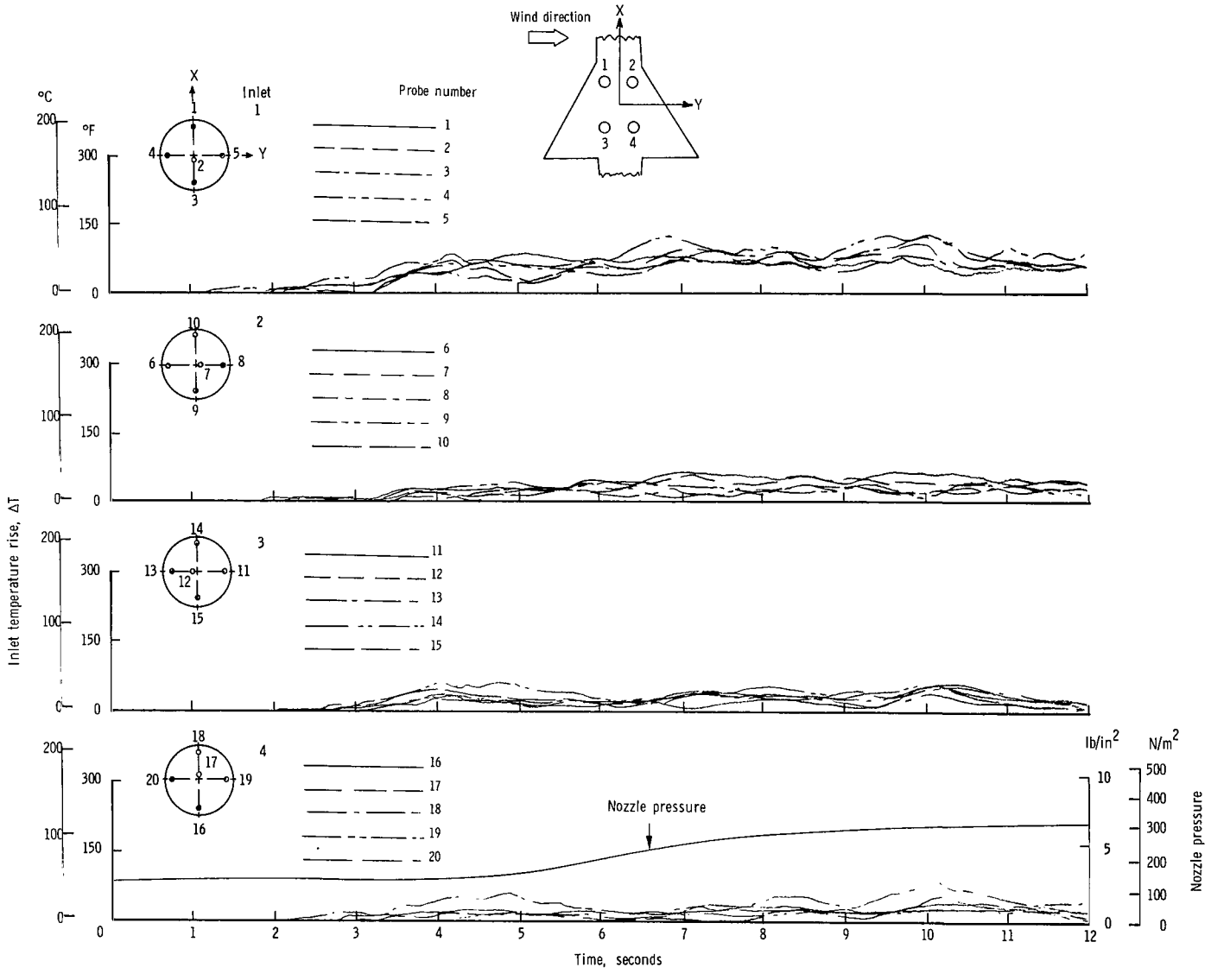

(k) $\psi = 90^{o}$; V = 11.85 knots.

Figure 14.- Concluded.

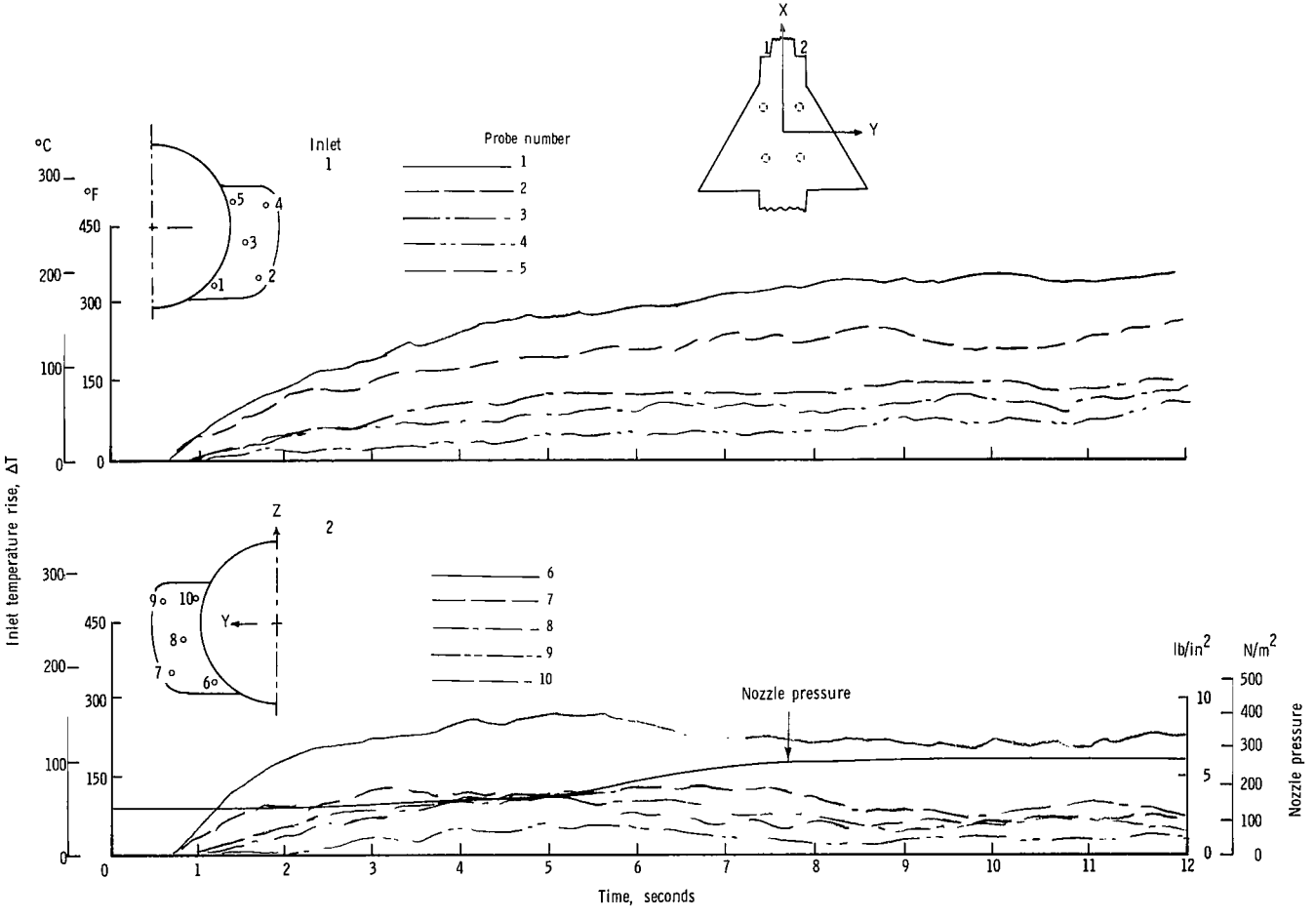

(a) $\psi = 0^0$; V = 0 knots.

Figure 15.- Variation of inlet air temperature rise with time for the rectangular nozzle arrangement with side inlets and high delta wing. $h/D_e = 1.17$.

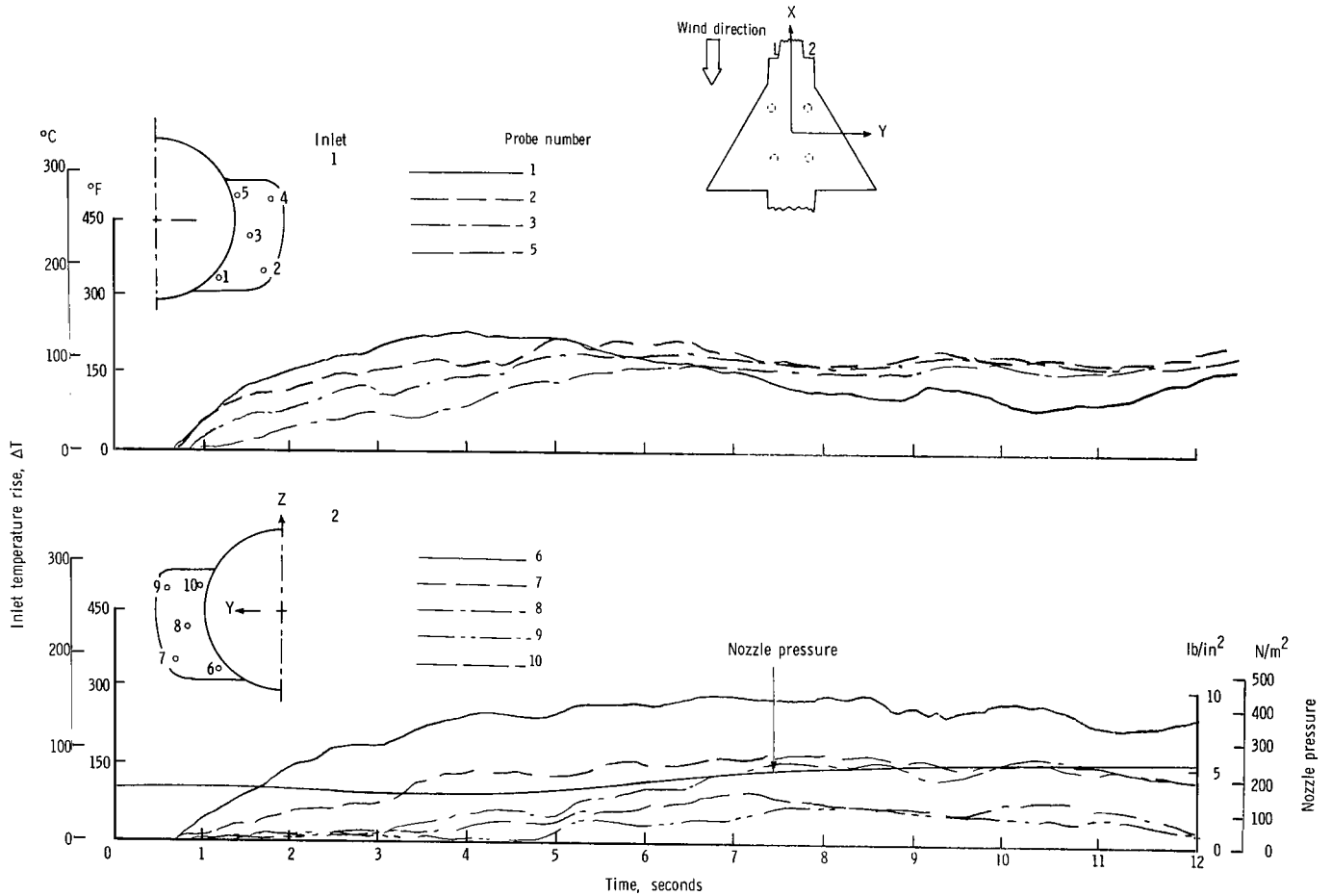

(b) $\psi = 0^0$; V = 5.92 knots.

Figure 15.- Continued.

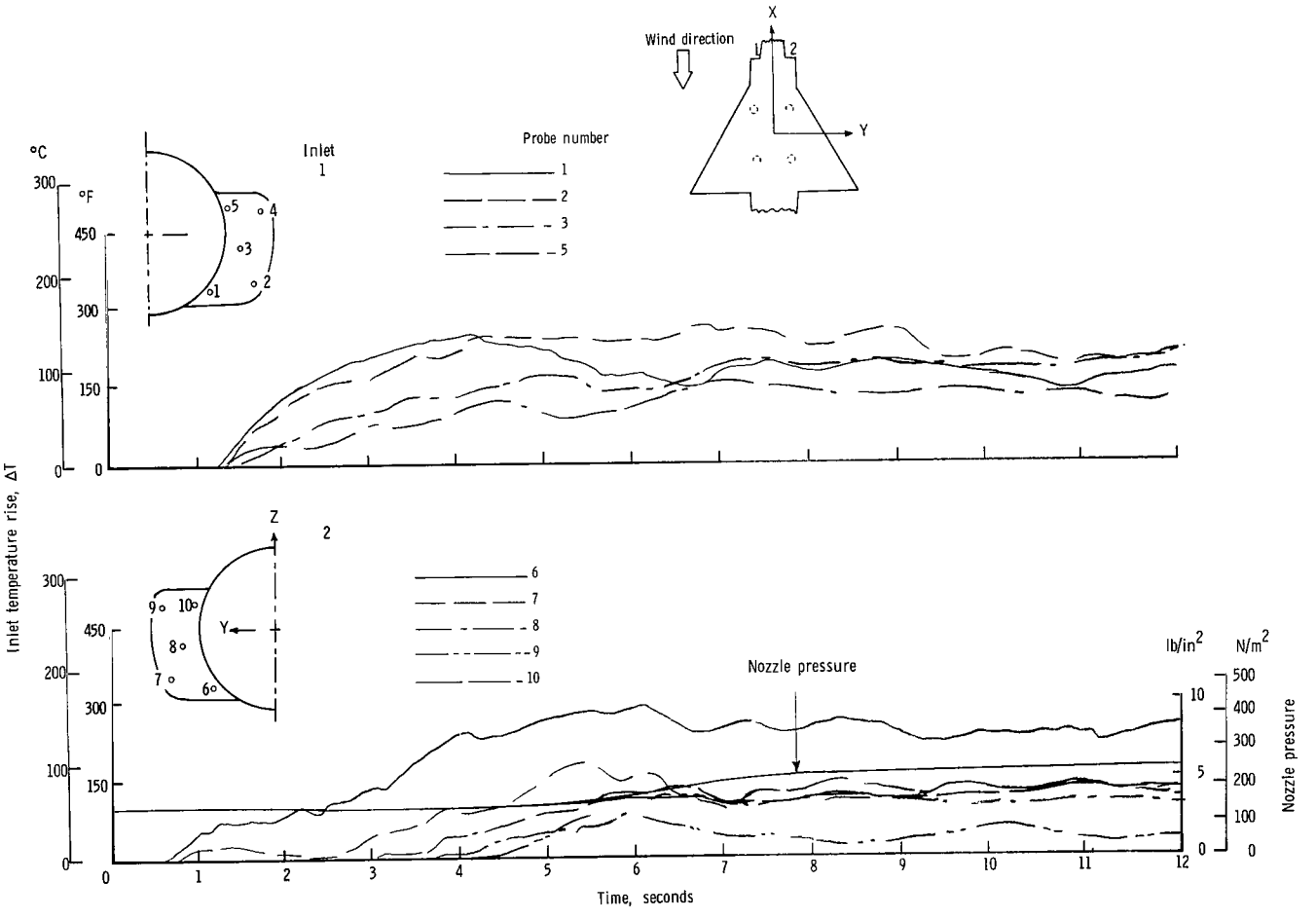

(c) $\psi = 0^0$; V = 11.85 knots.

Figure 15.- Continued.

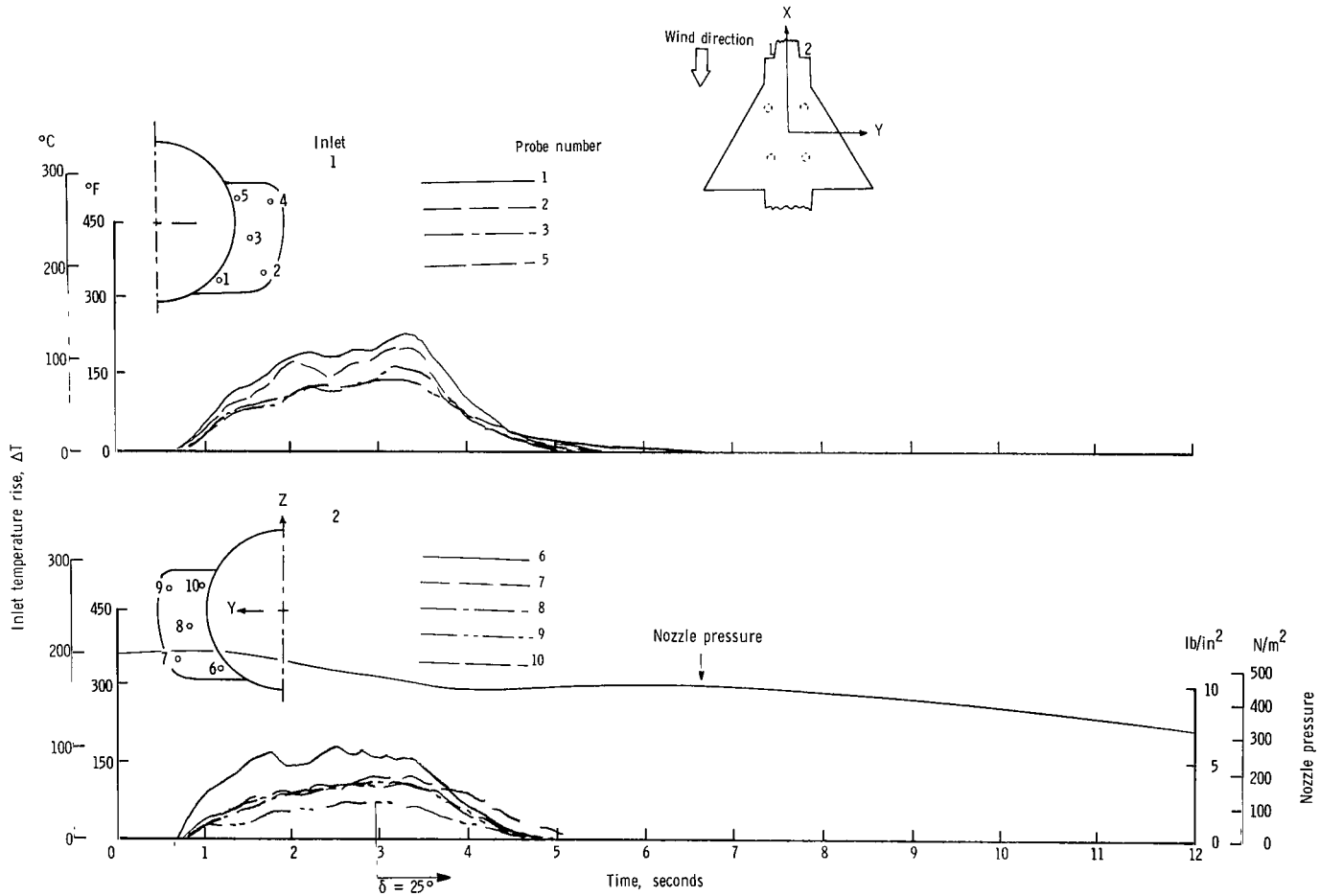

(d) $\psi = 0^{0}$; V = 17.78 knots.

Figure 15.- Continued.

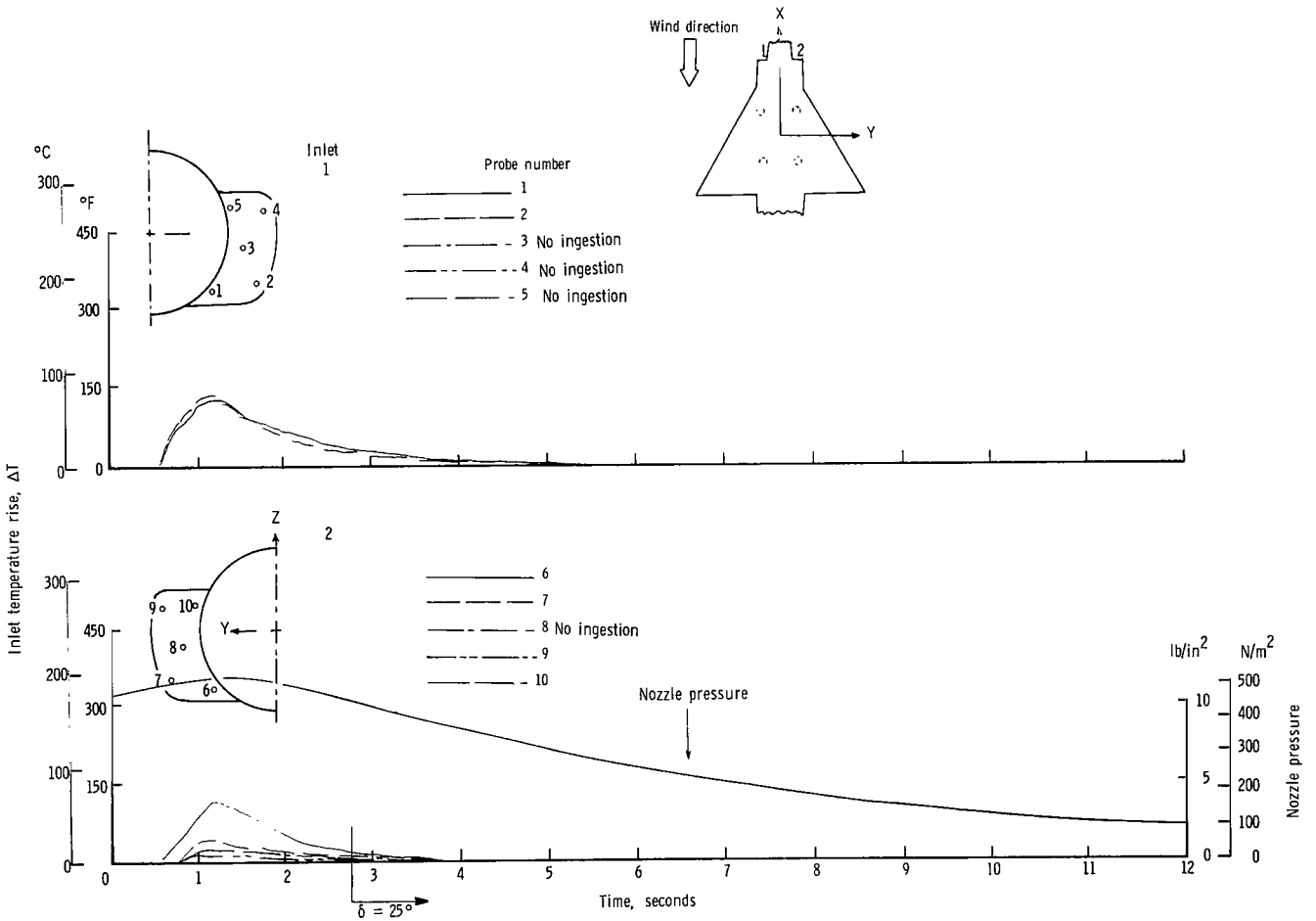

(e) $\psi = 0^{o}$; V = 23.70 knots.

Figure 15.- Continued.

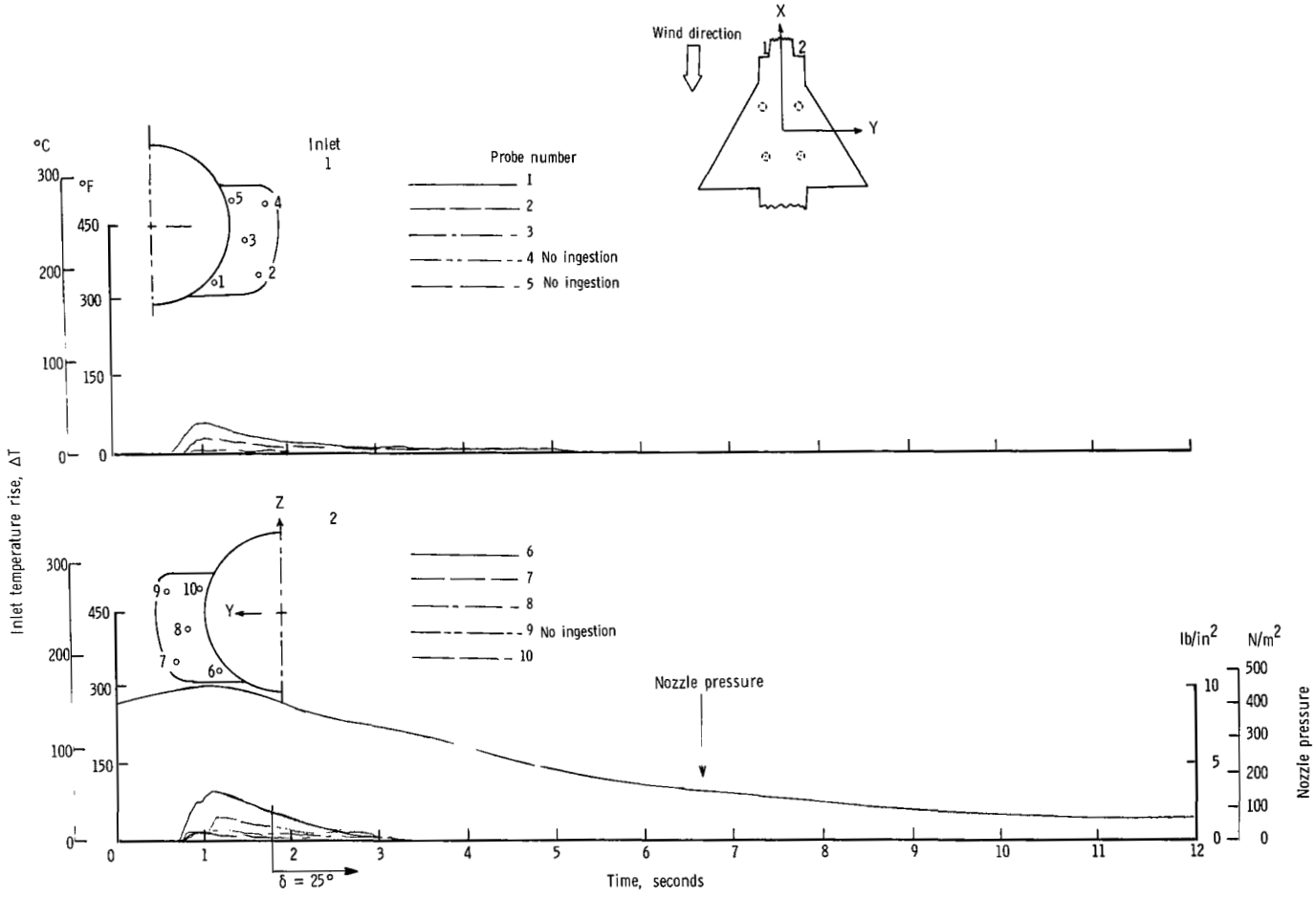

(f) $\psi = 0^0$; V = 29.63 knots.

Figure 15.- Continued.

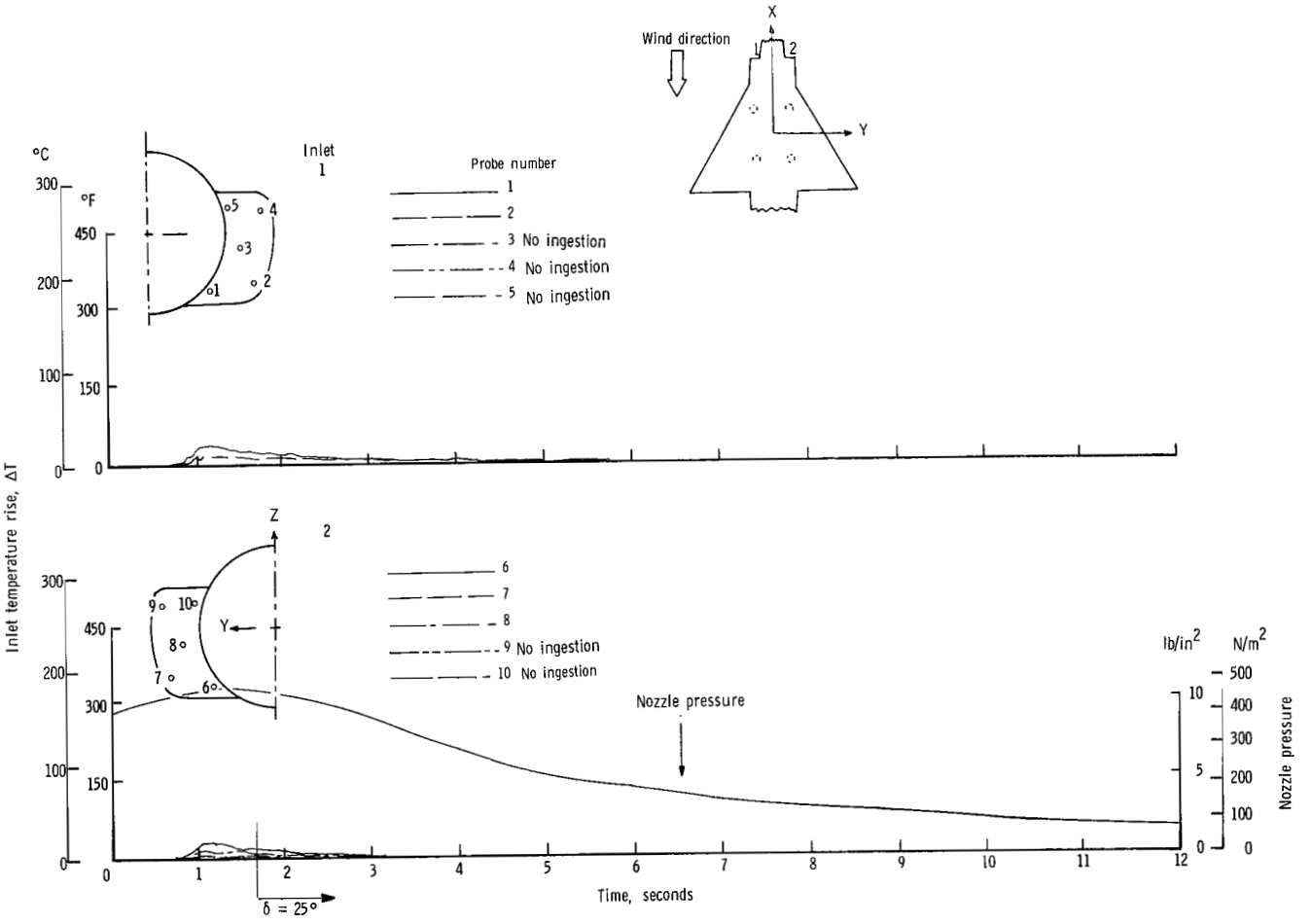

(g) $\psi = 0^{0}$; V = 35.55 knots.

Figure 15.- Continued.

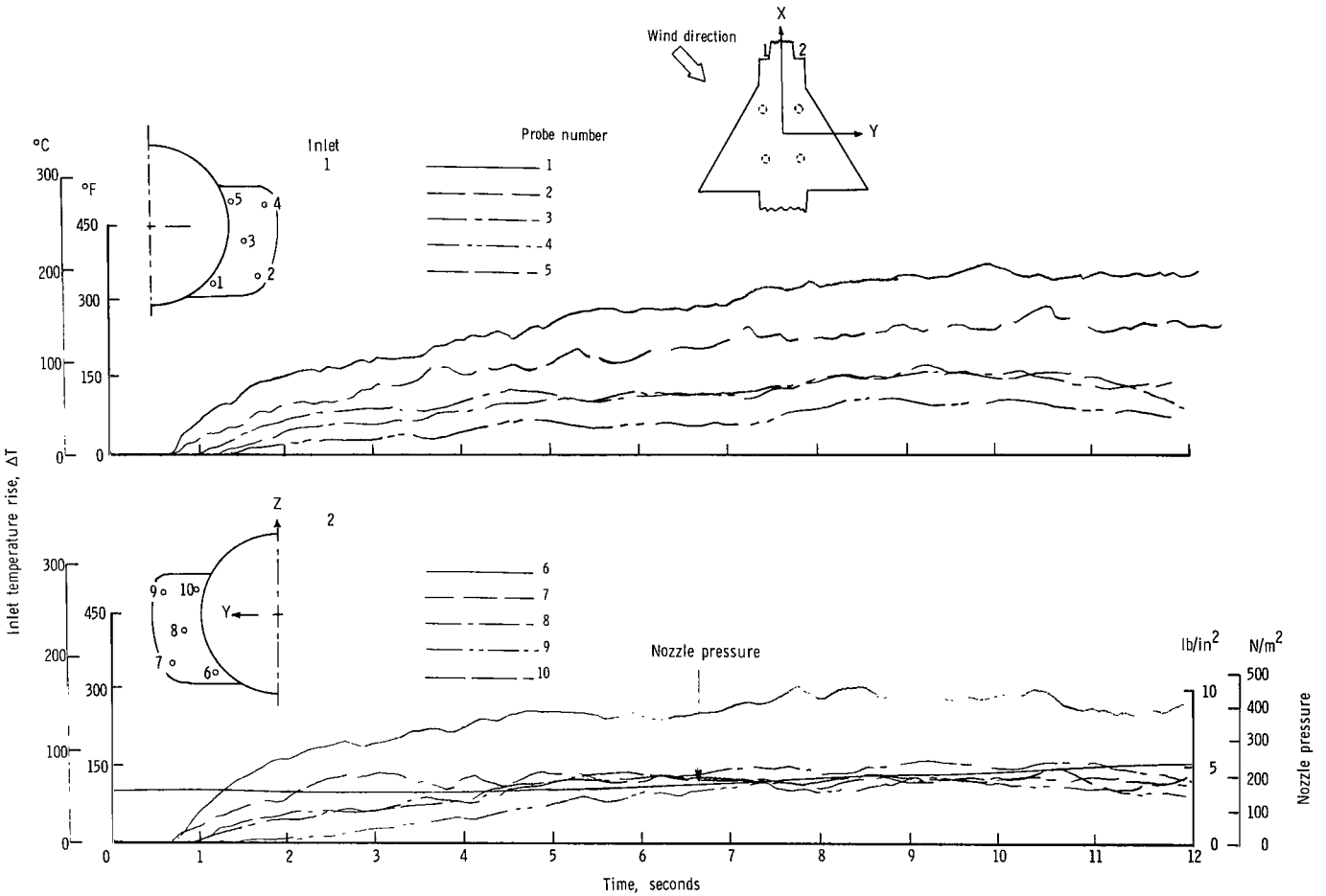

(h) $\psi = 45^{0}$; V = 5.92 knots.

Figure 15.- Continued.

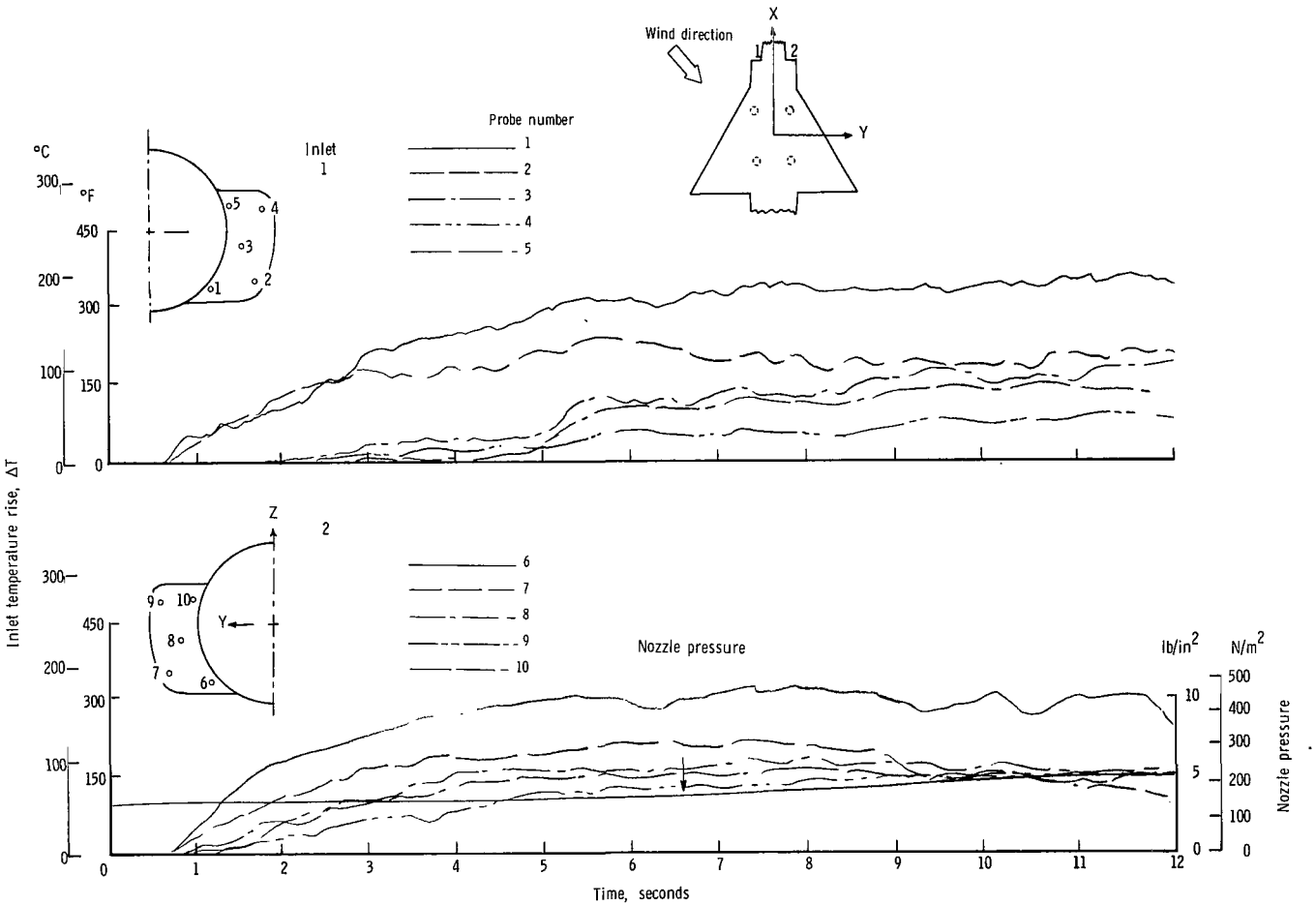

(i) $\psi = 45^0$; V = 11.85 knots.

Figure 15.- Continued.

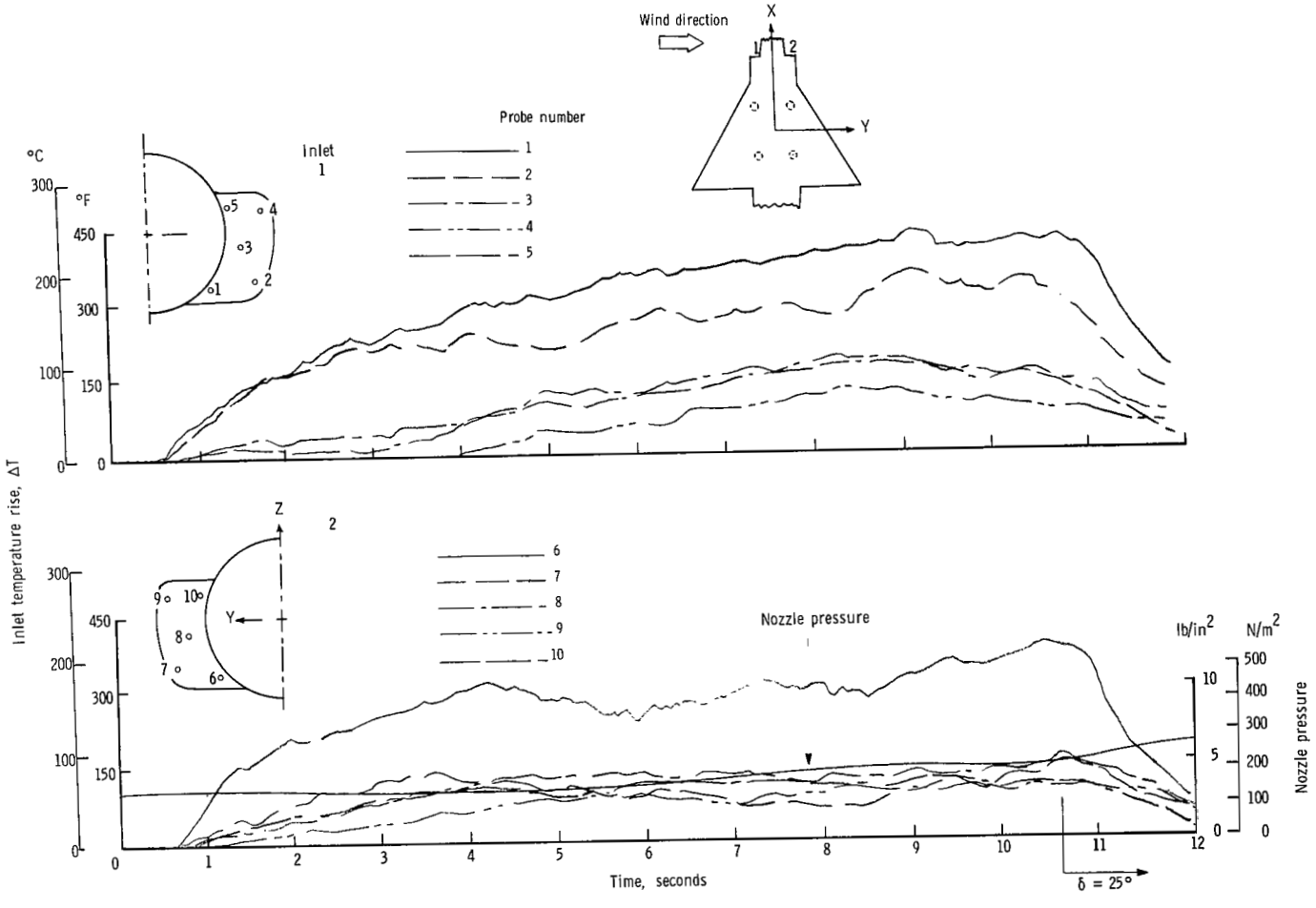

(j) $\psi = 90^{0}$; V = 5.92 knots.

Figure 15.- Continued.

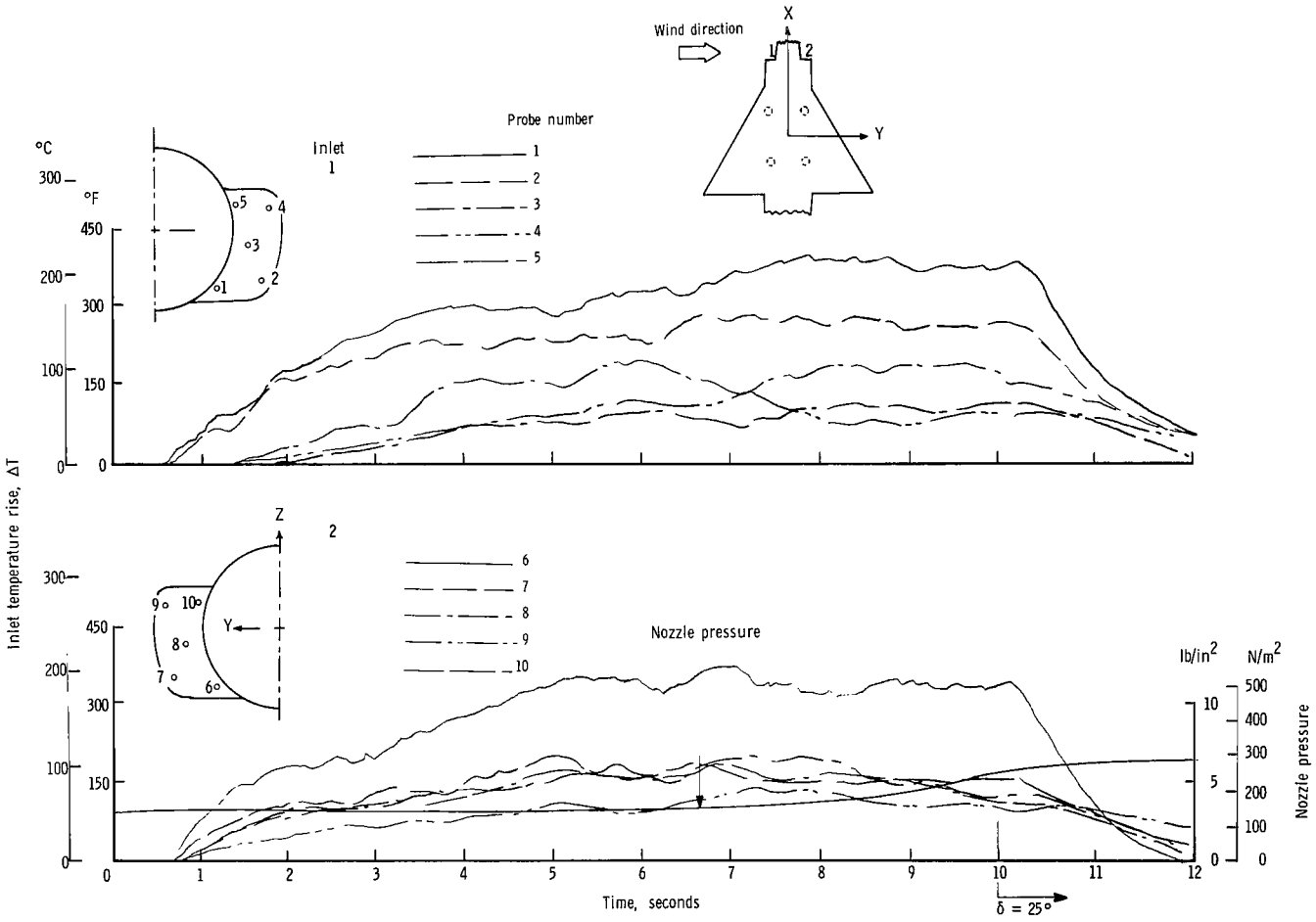

(k) $\psi = 90^0$; V = 11.85 knots.

Figure 15.- Concluded.

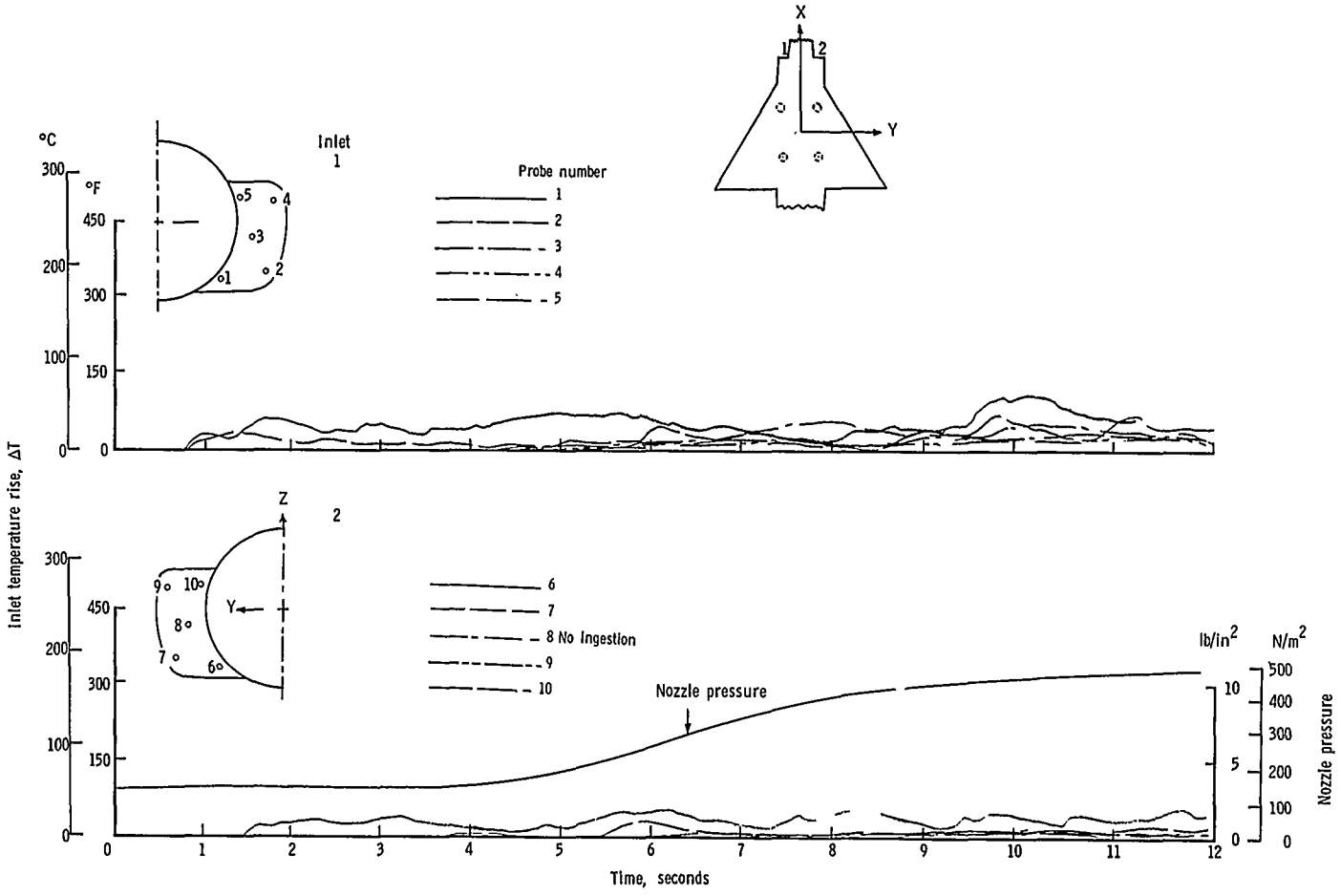

(a) $\psi = 0^0$; V = 0 knots.

Figure 16.- Variation of inlet air temperature rise with time for the rectangular nozzle arrangement with side inlets and high delta wing. $h/D_e = 3.0$.

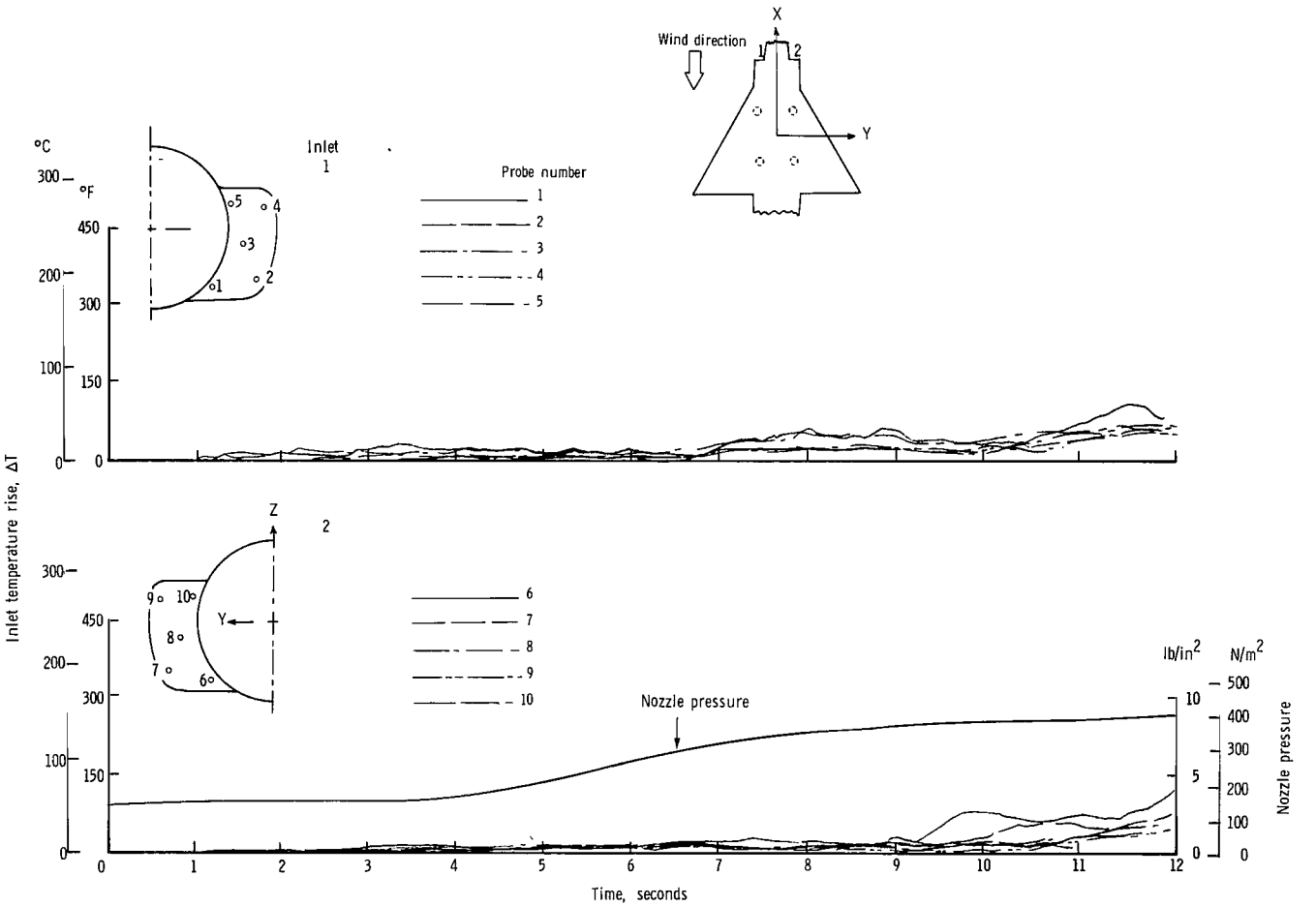

(b) $\psi = 0^{0}$; V = 5.92 knots.

Figure 16.- Continued.

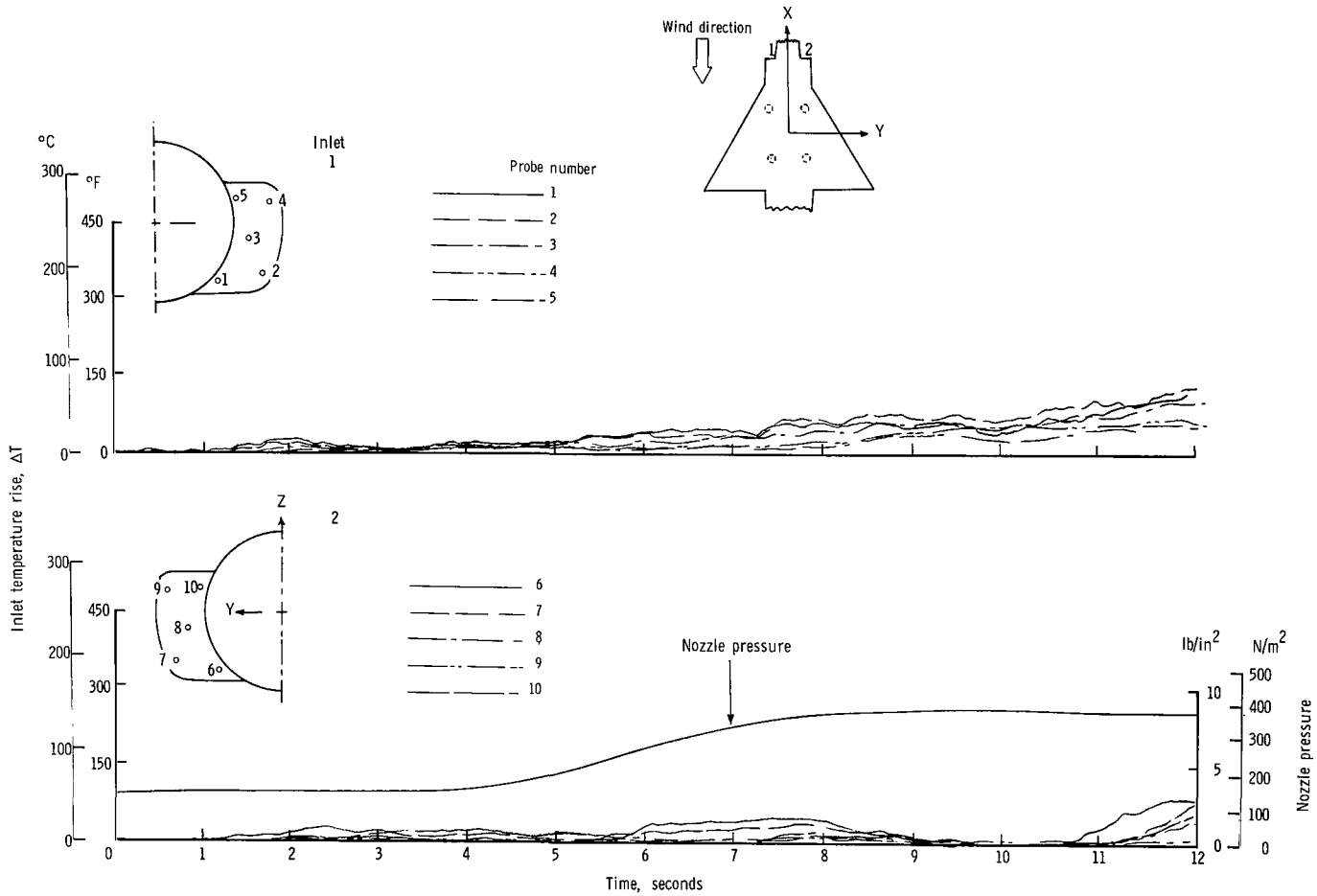

(c) $\psi = 0^{0}$; V = 11.85 knots.

Figure 16.- Continued.

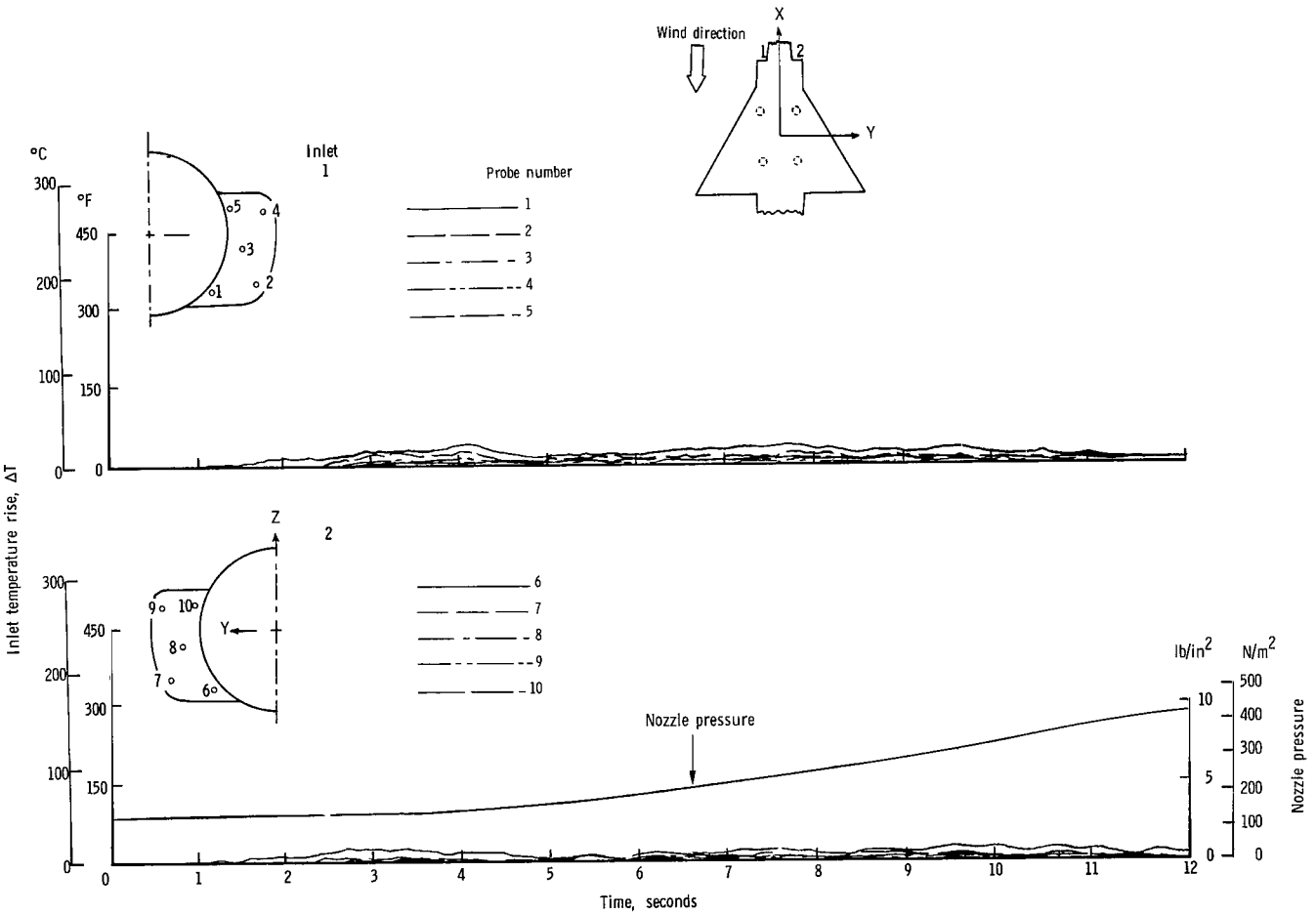

(d) $\psi = 0^0$; V = 17.78 knots.

Figure 16.- Continued.

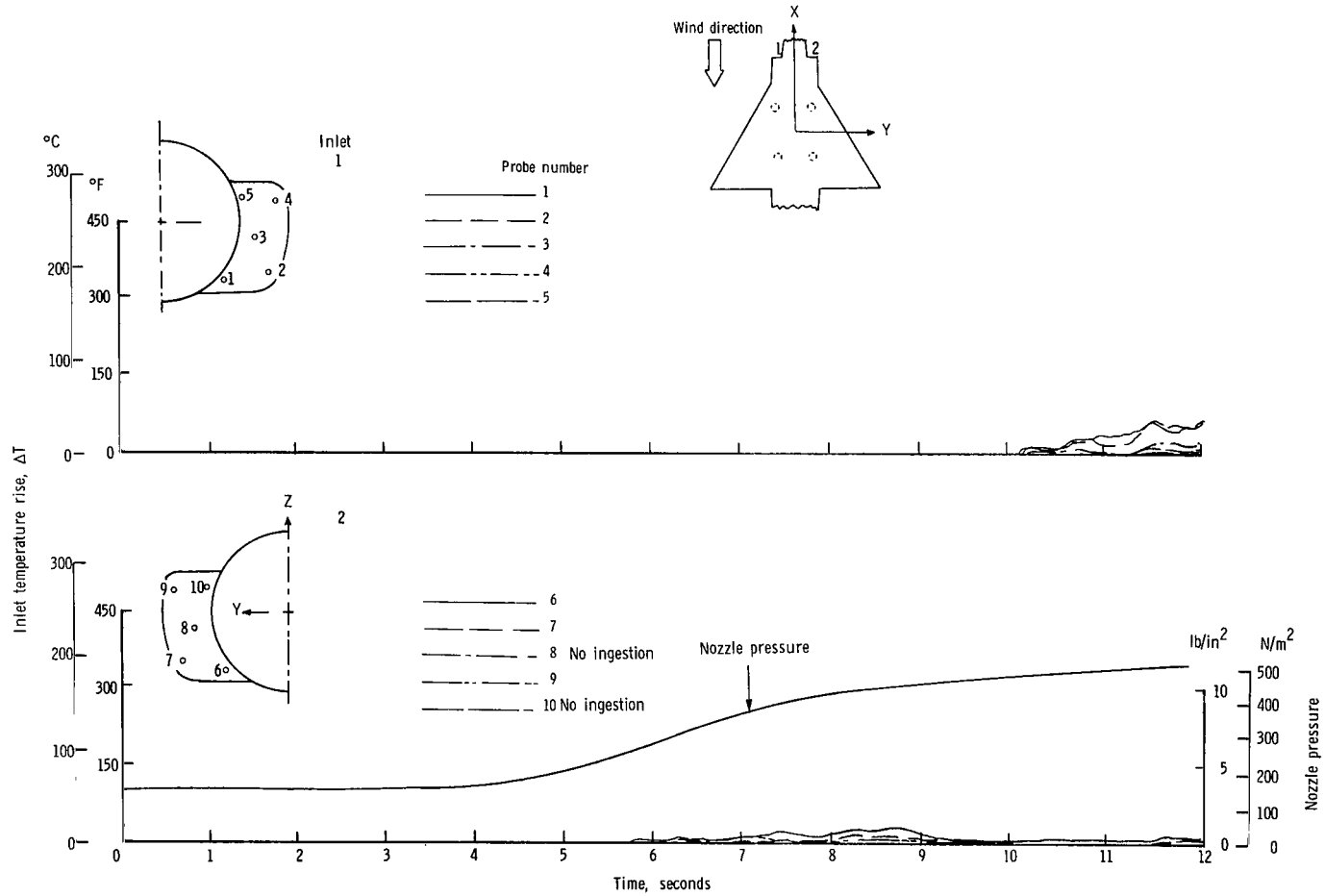

(e) $\psi = 0^0$; V = 23.70 knots.

Figure 16.- Continued.

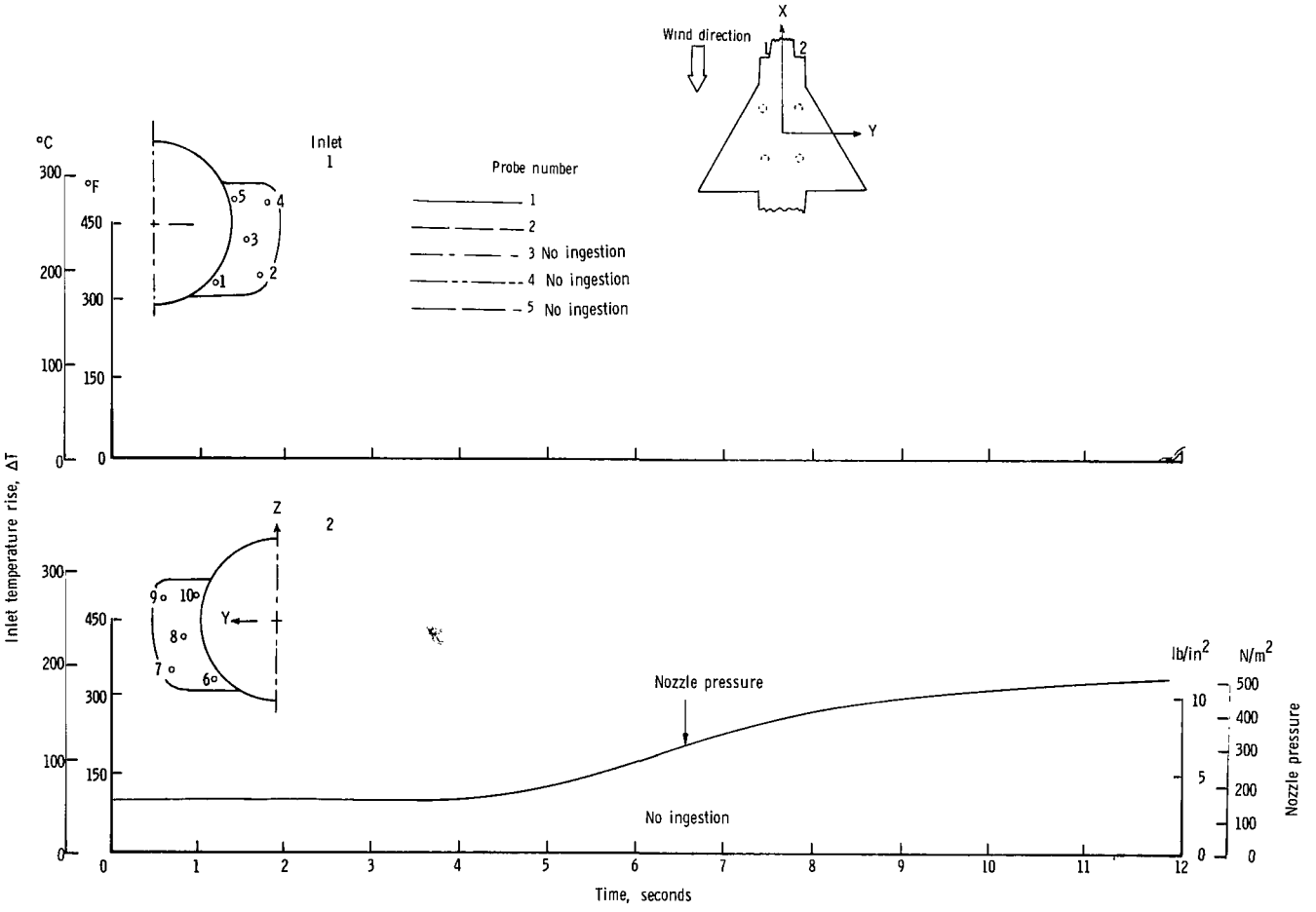

(f) $\psi = 0^0$; V = 29.63 knots.

Figure 16.- Continued.

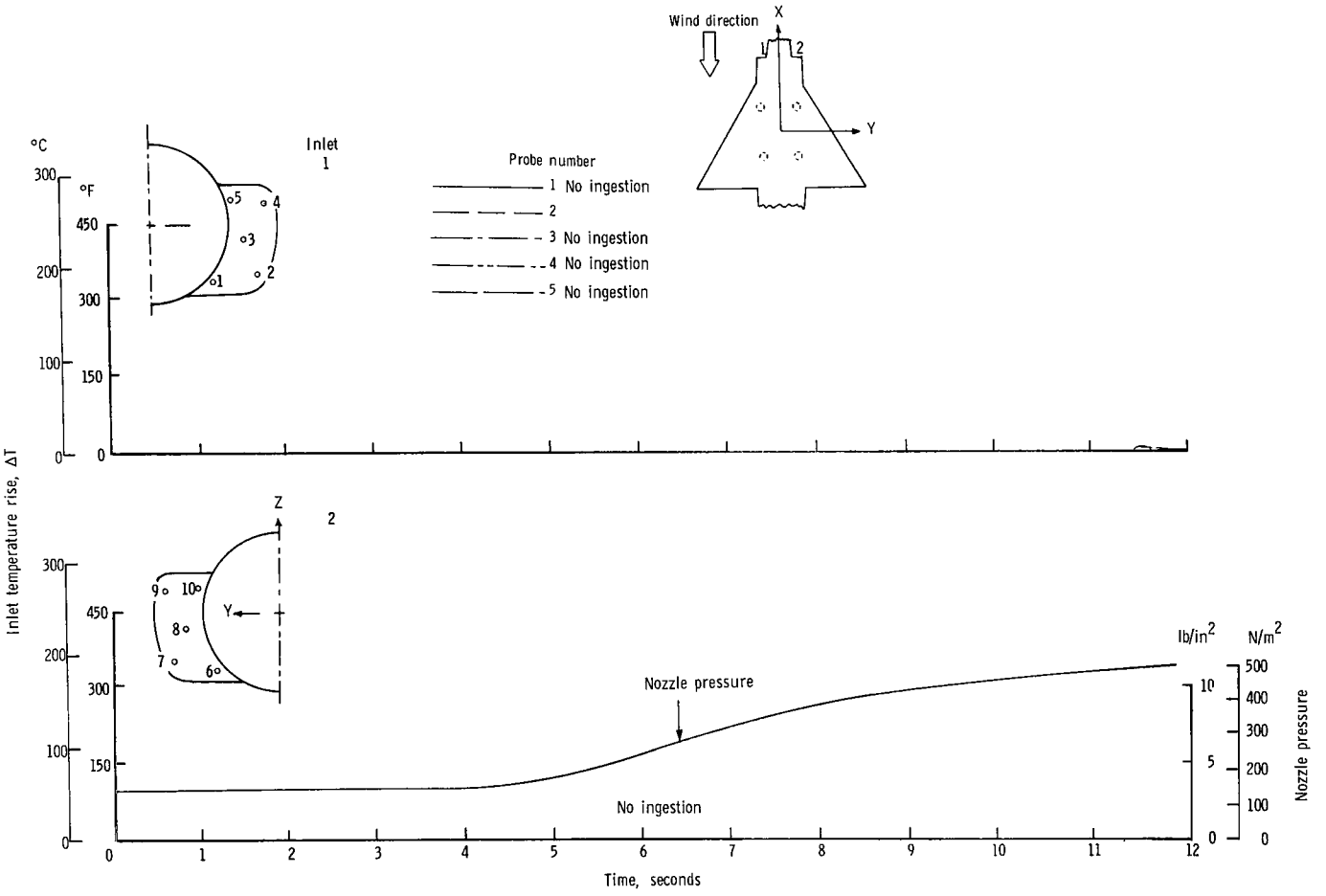

(g) $\psi = 0^{0}$; V = 35.55 knots.

Figure 16.- Continued.

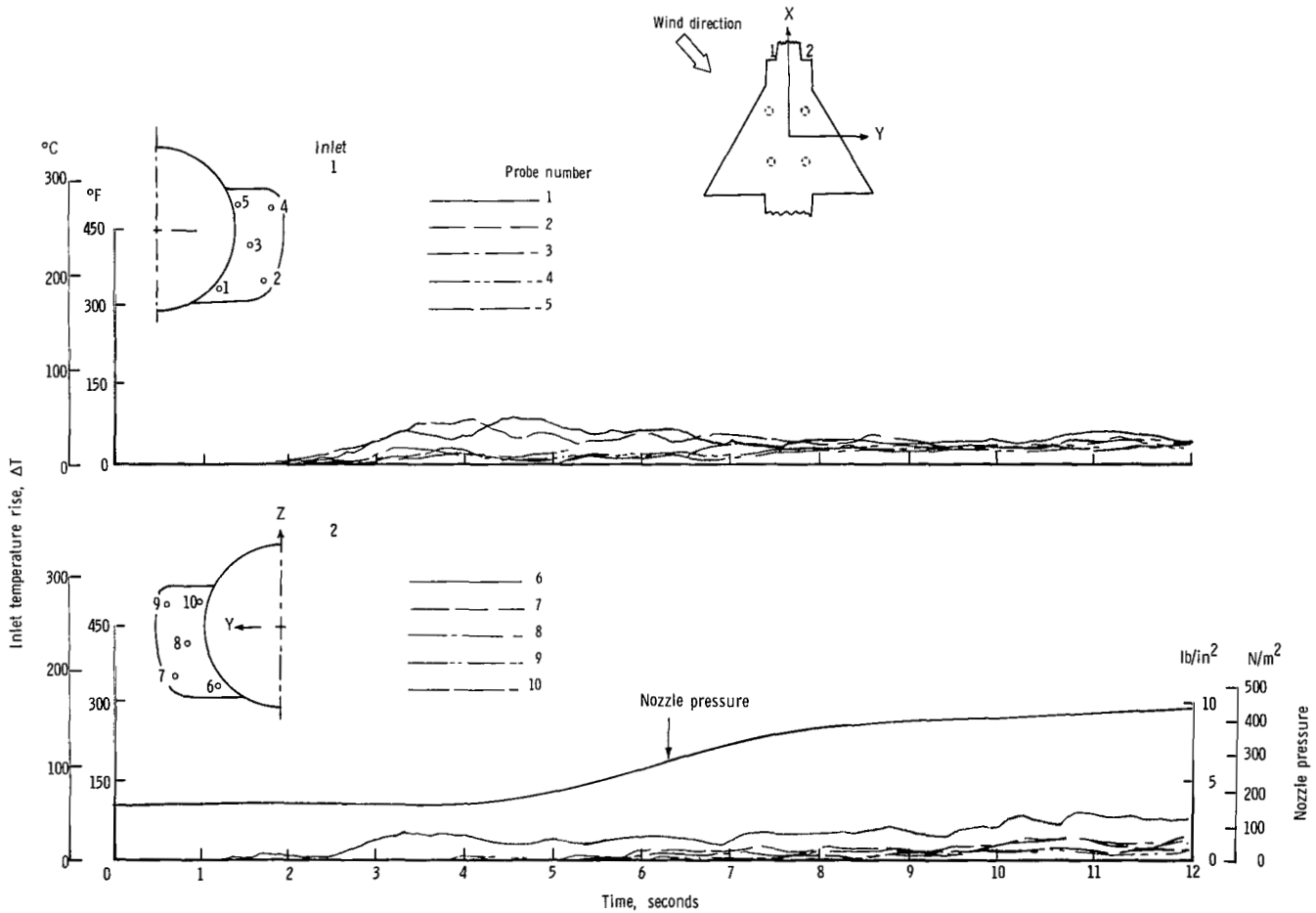

(h) $\psi = 45^0$; V = 5.92 knots.

Figure 16.- Continued.

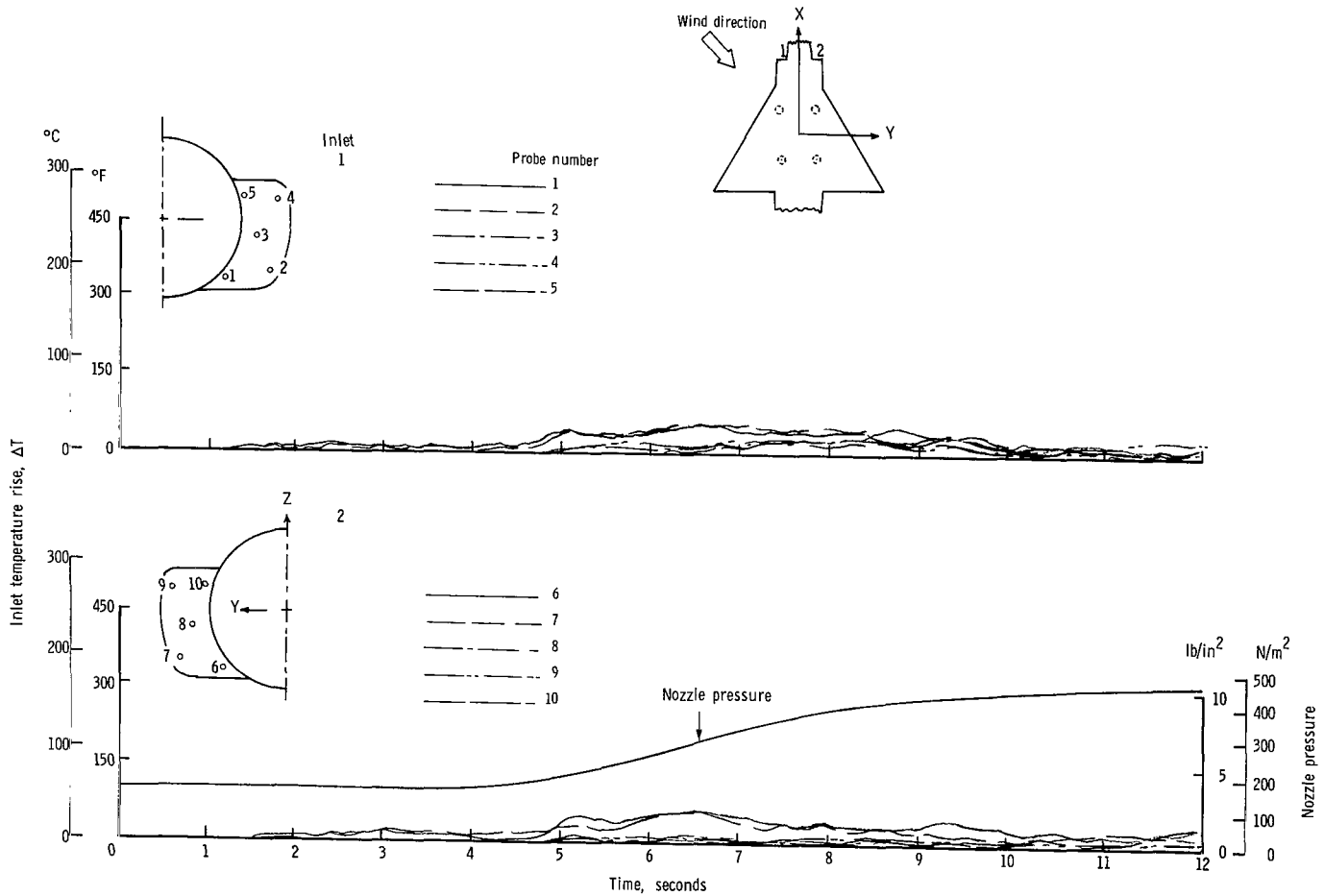

(i) $\psi = 45^{0}$; V = 11.85 knots.

Figure 16.- Continued.

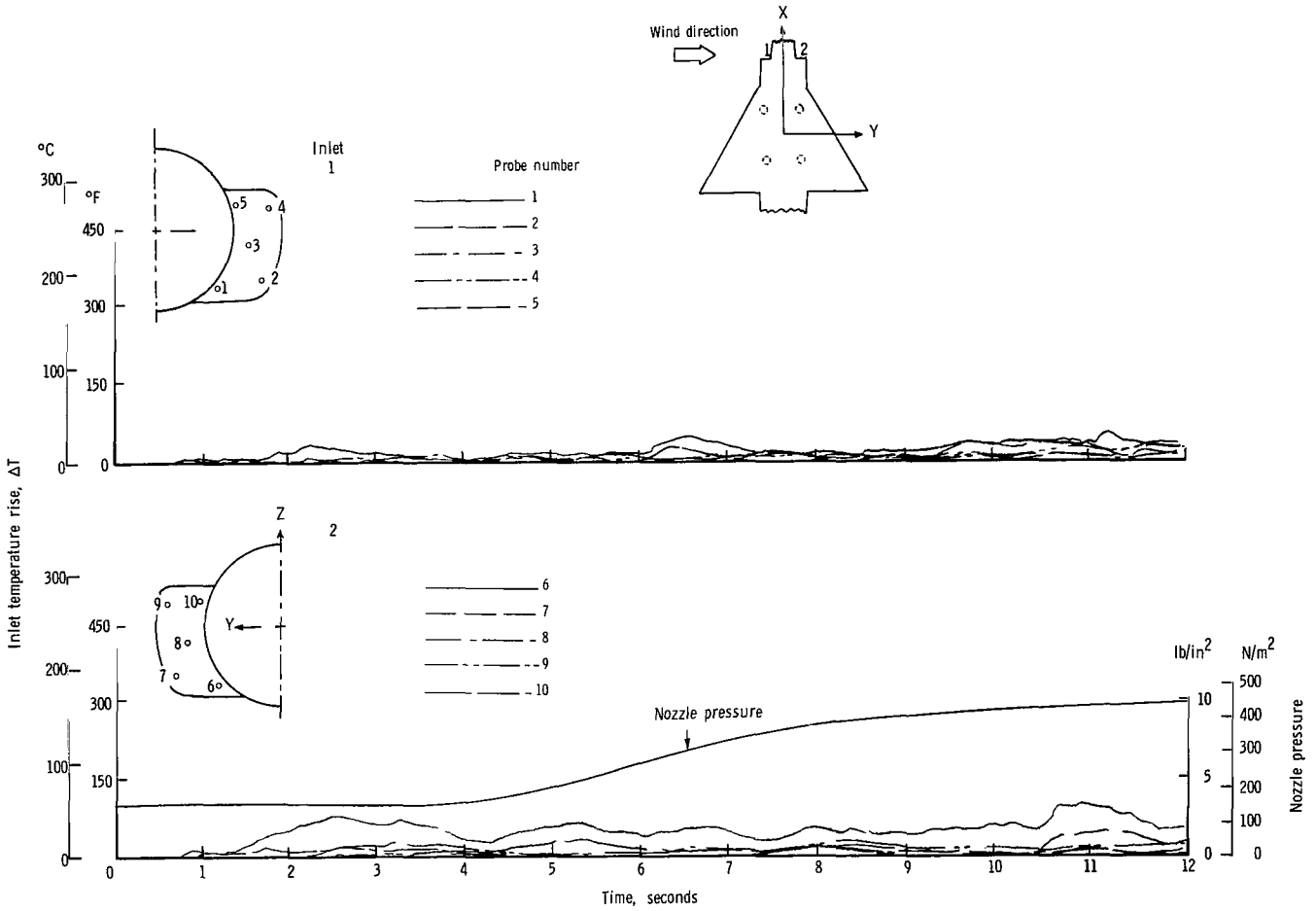

(j) $\psi = 90^0$; V = 5.92 knots.

Figure 16.- Continued.

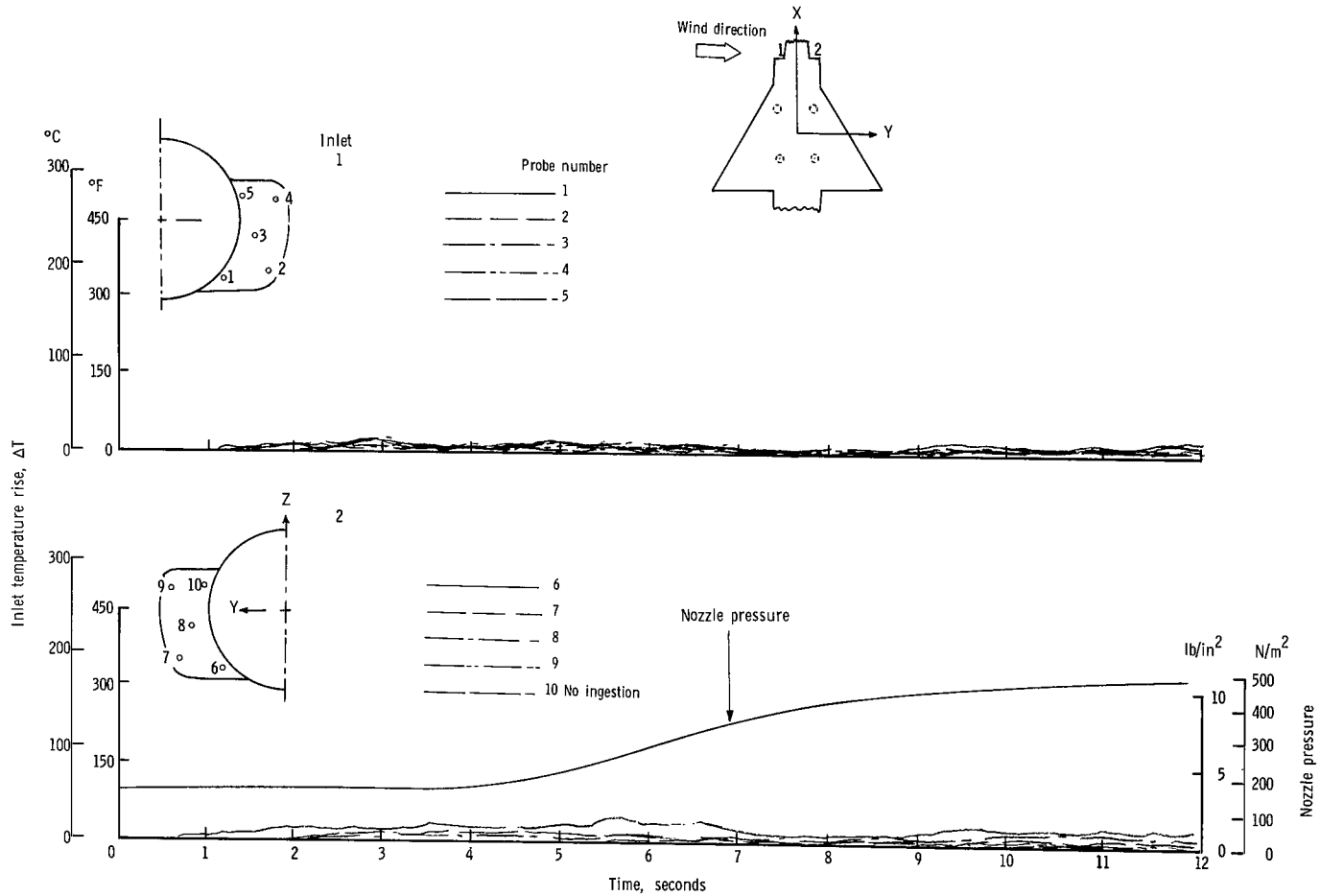

(k) $\psi = 90^0$; V = 11.85 knots.

Figure 16.- Concluded.

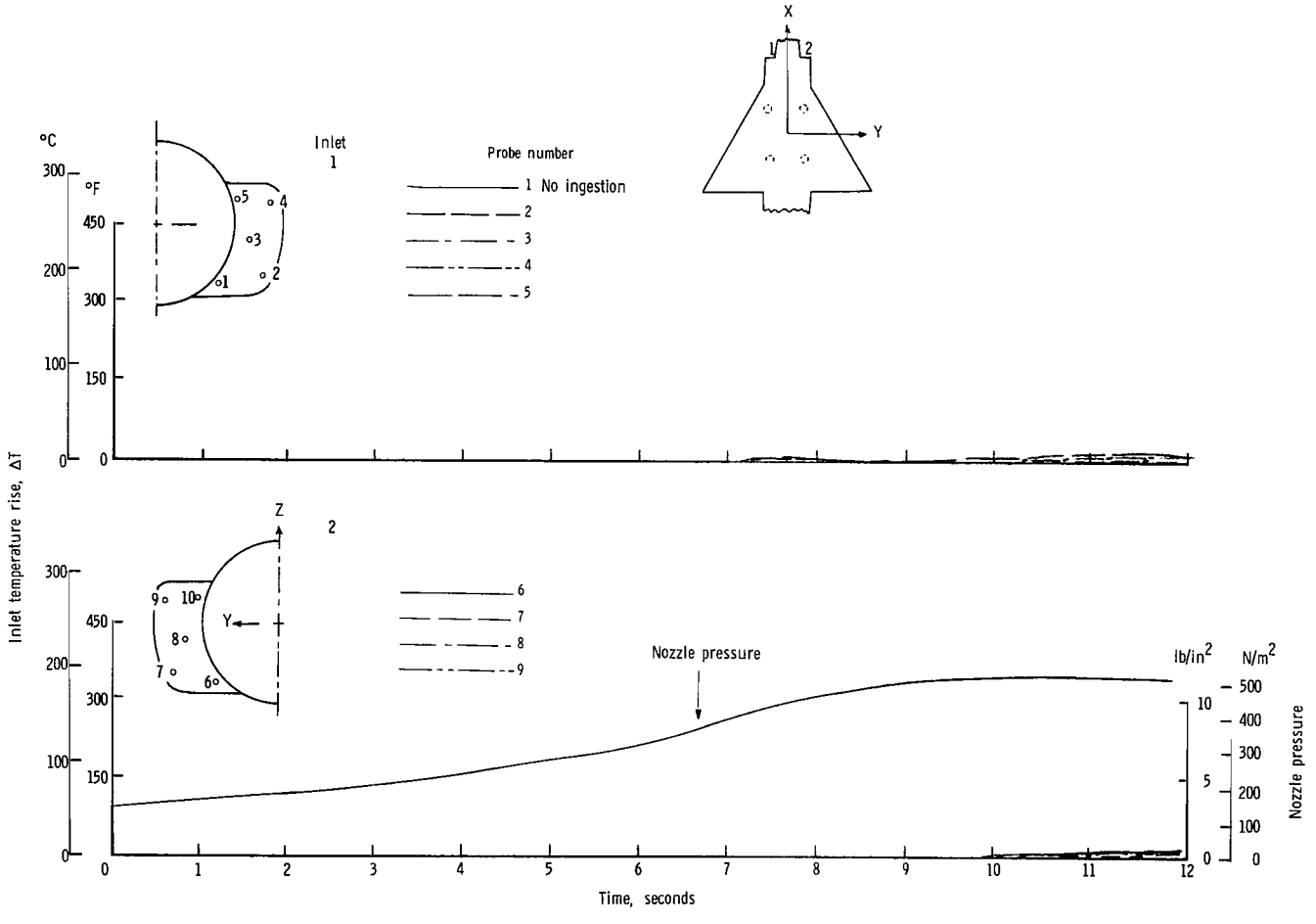

(a) $\psi = 0^0$; V = 0 knots.

Figure 17.- Variation of inlet air temperature rise with time for the rectangular nozzle arrangement with side inlets and high delta wing. $h/D_e = 5.0$.

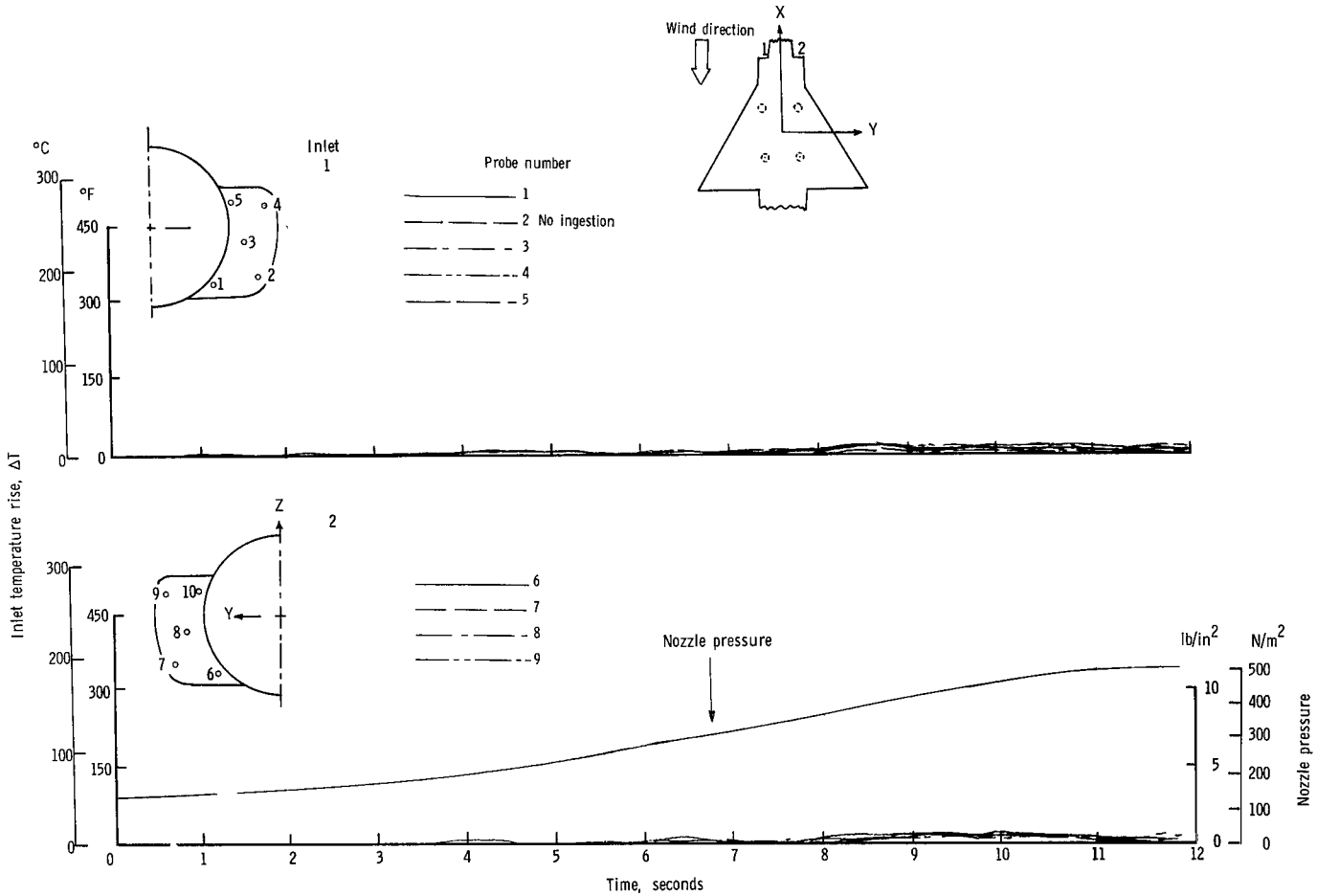

(b) $\psi = 0^0$; V = 5.92 knots.

Figure 17.- Continued.

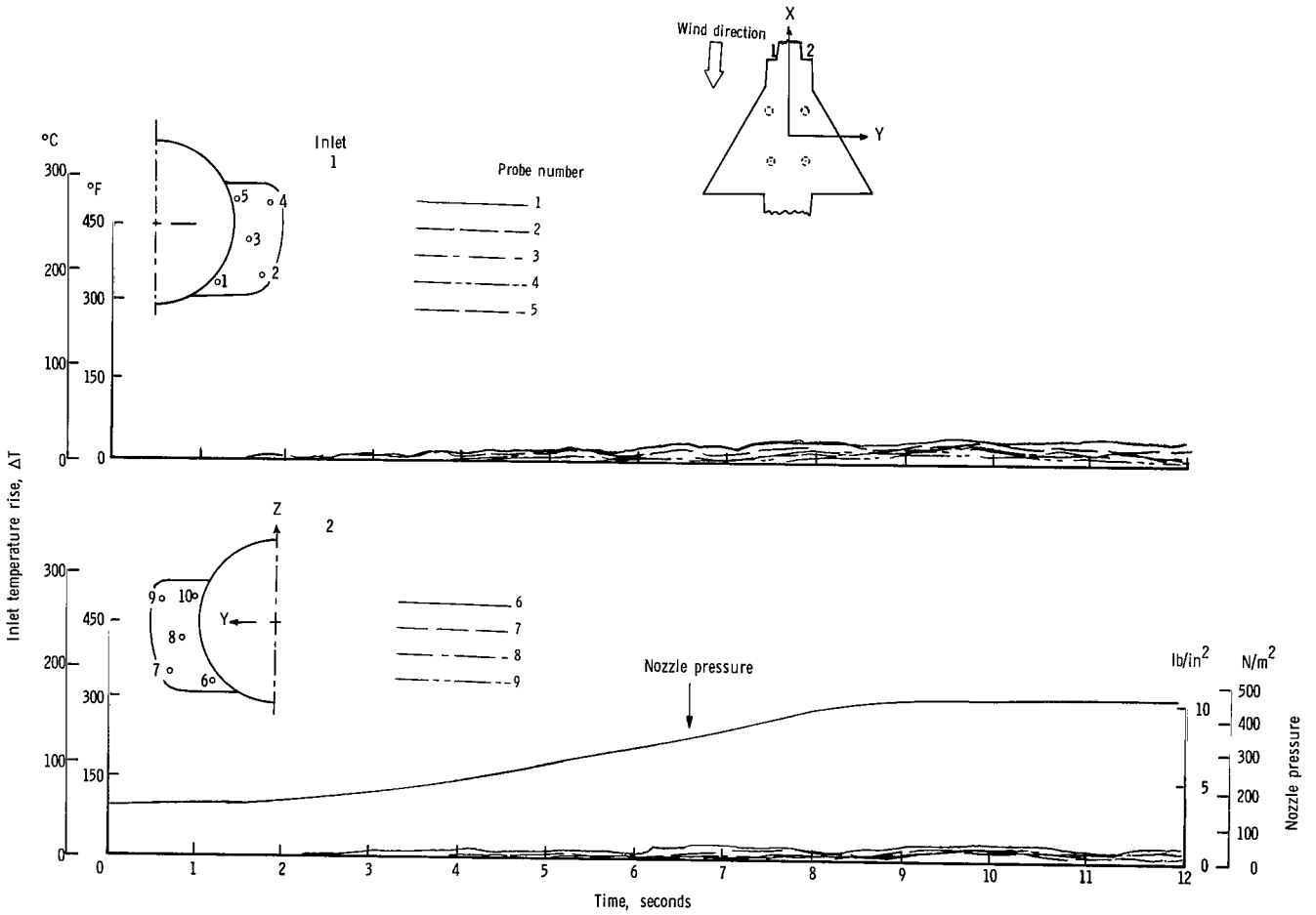

(c) $\psi = 0^0$; V = 11.85 knots.

Figure 17.- Continued.

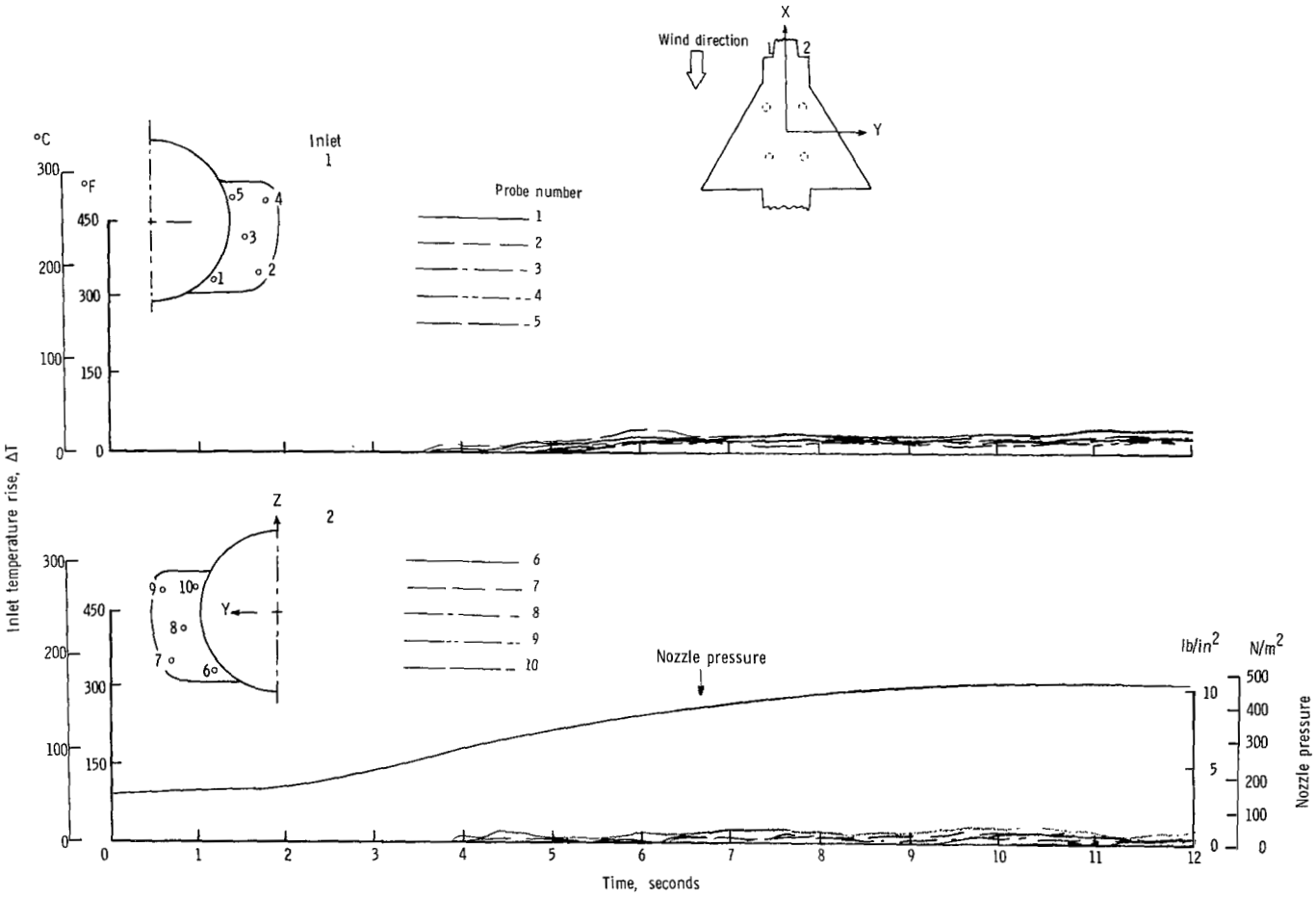

(d) $\psi = 0^0$; V = 17.78 knots.

Figure 17.- Continued.

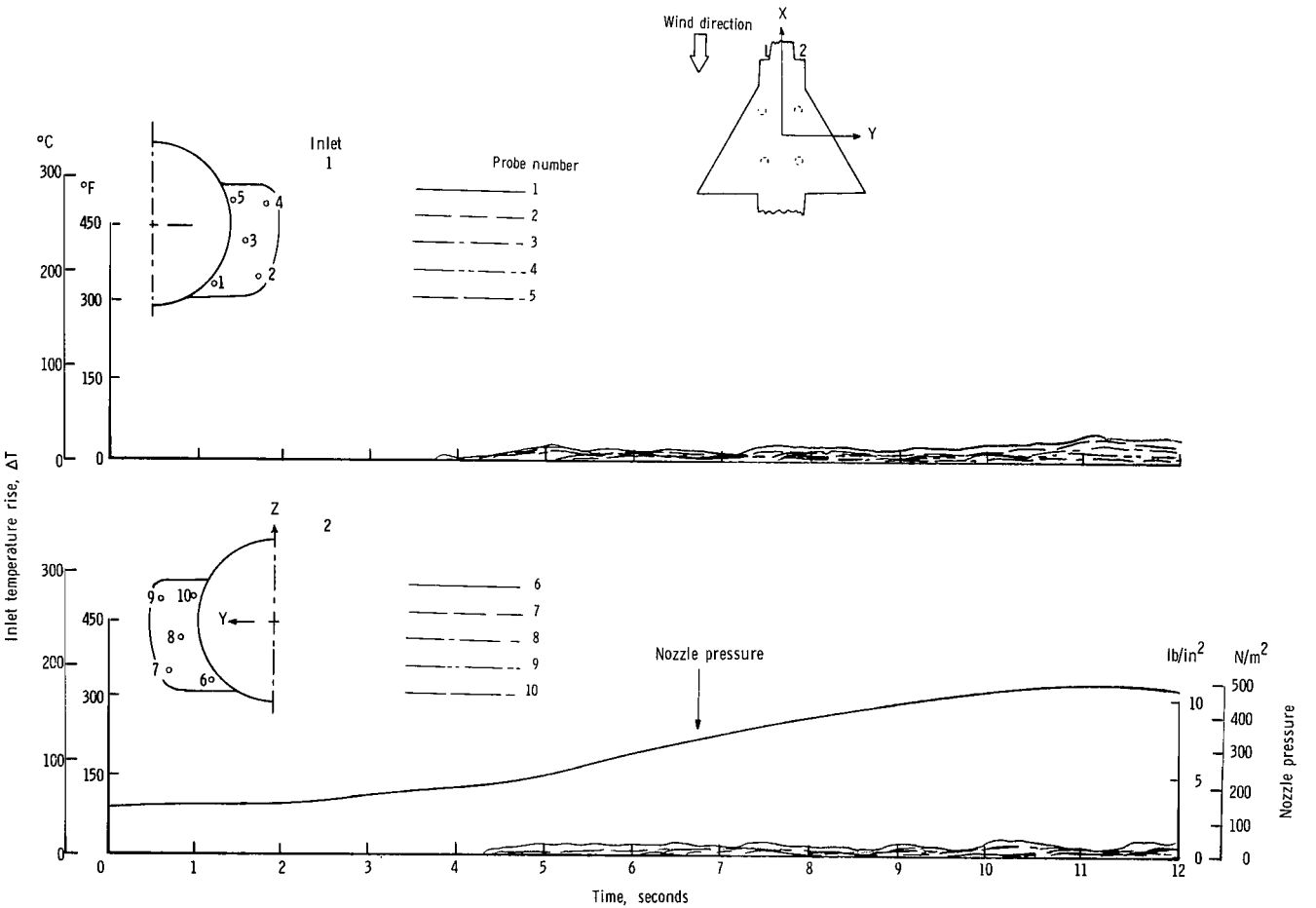

(e) $\psi = 0^0$; V = 23.70 knots.

Figure 17.- Continued.

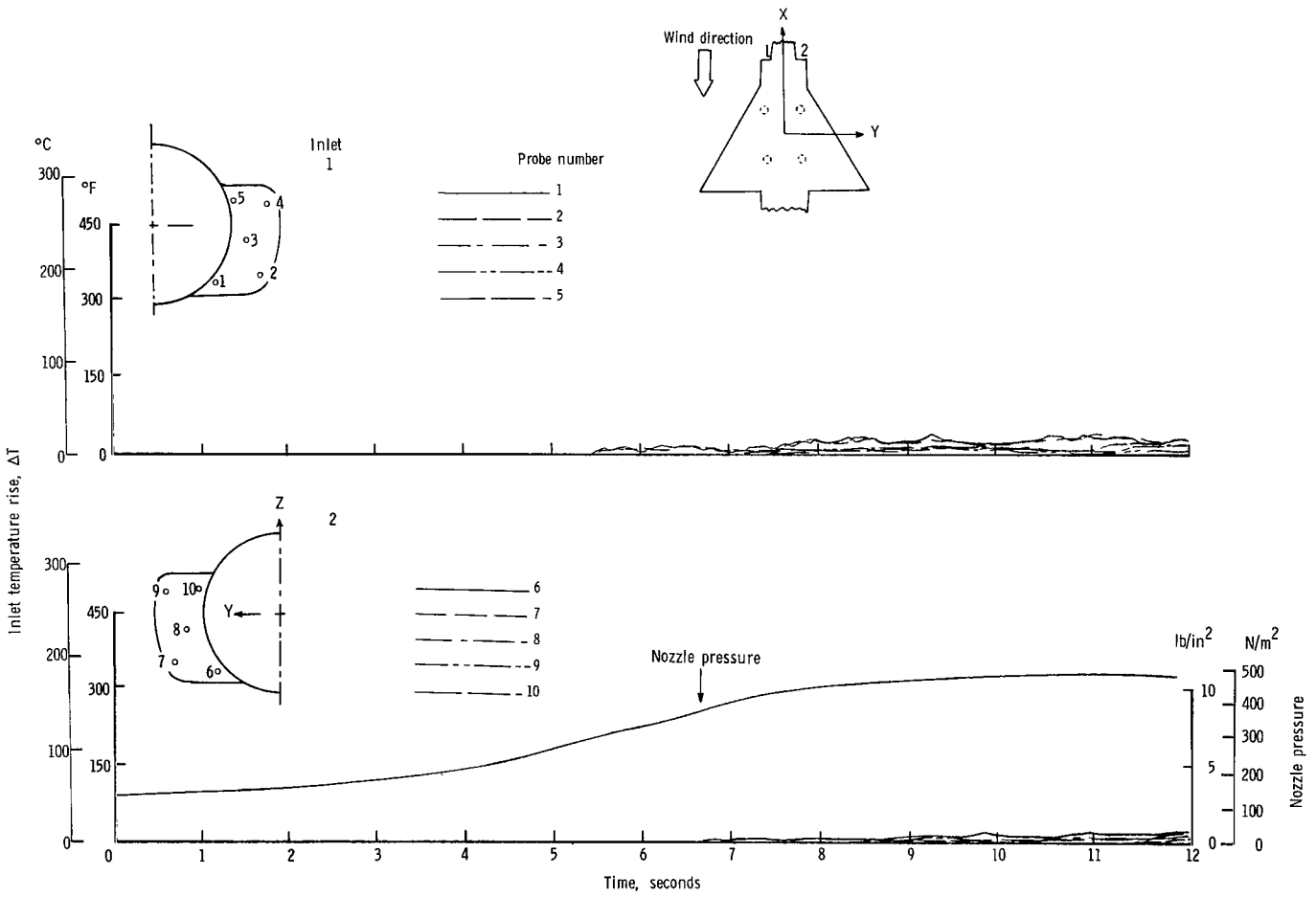

(f) $\psi = 0^0$; V = 29.63 knots.

Figure 17.- Continued.

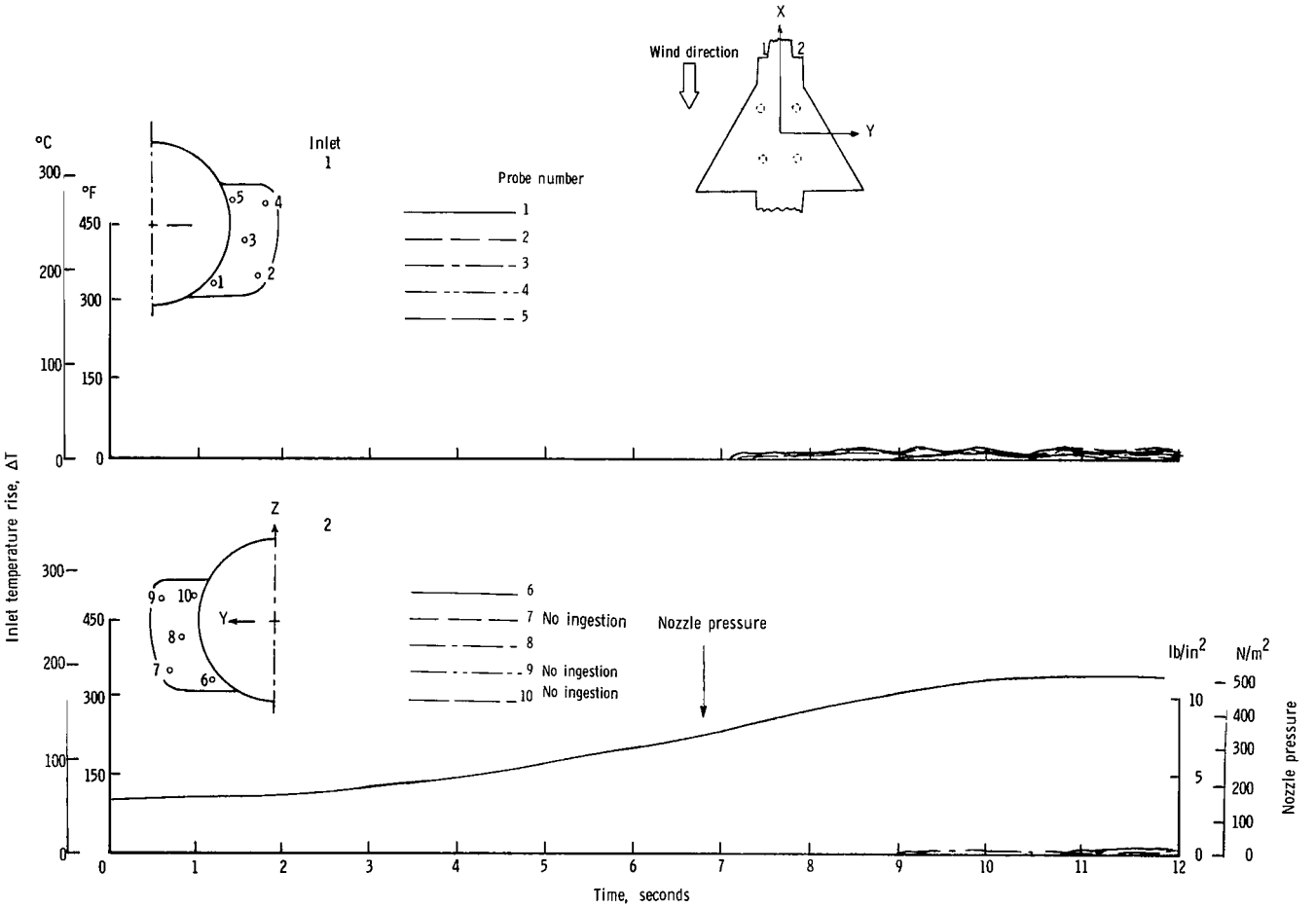

(g) $\psi = 0^0$; V = 35.55 knots.

Figure 17.- Continued.

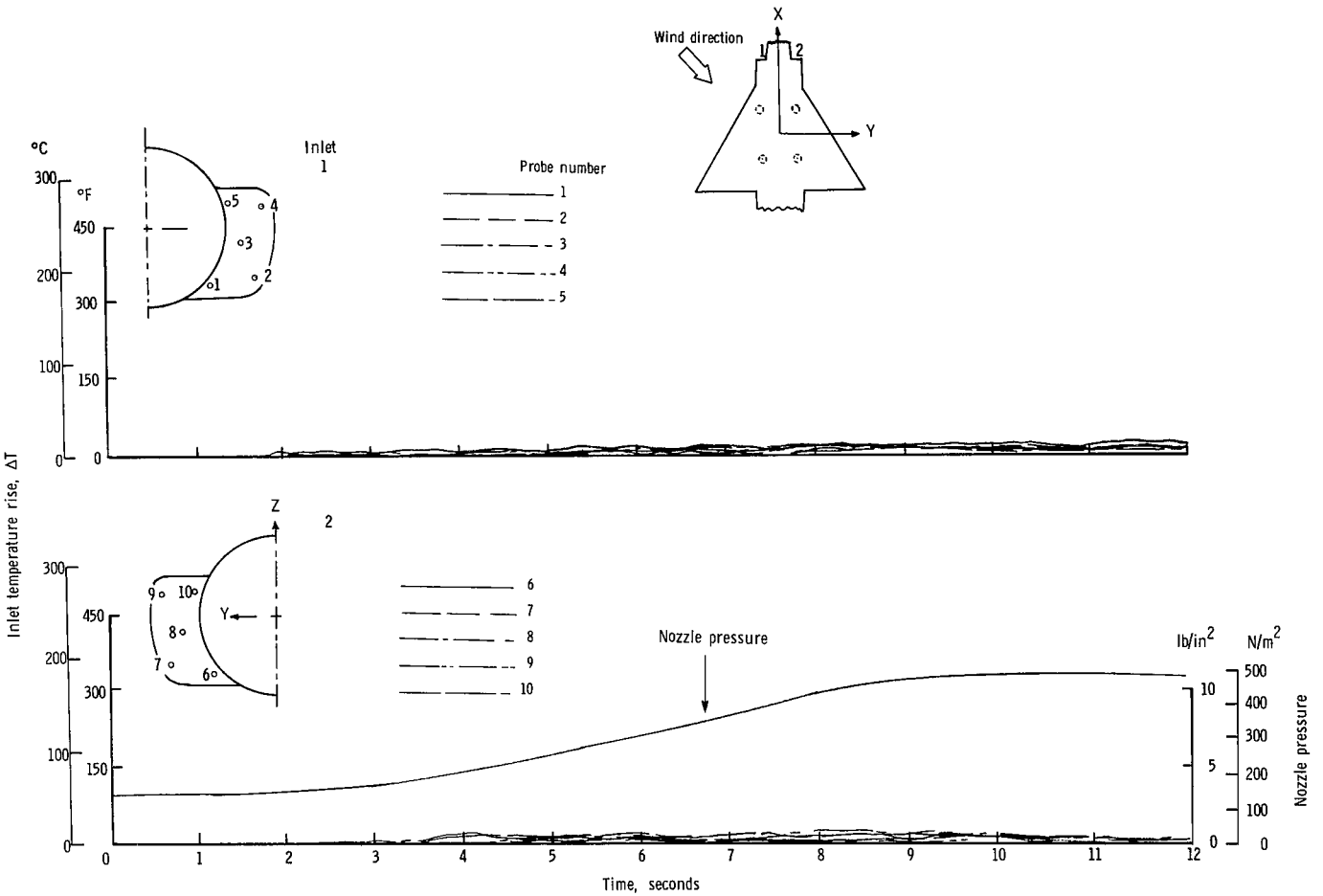

(h) $\psi = 45^0$; V = 5.92 knots.

Figure 17.- Continued.

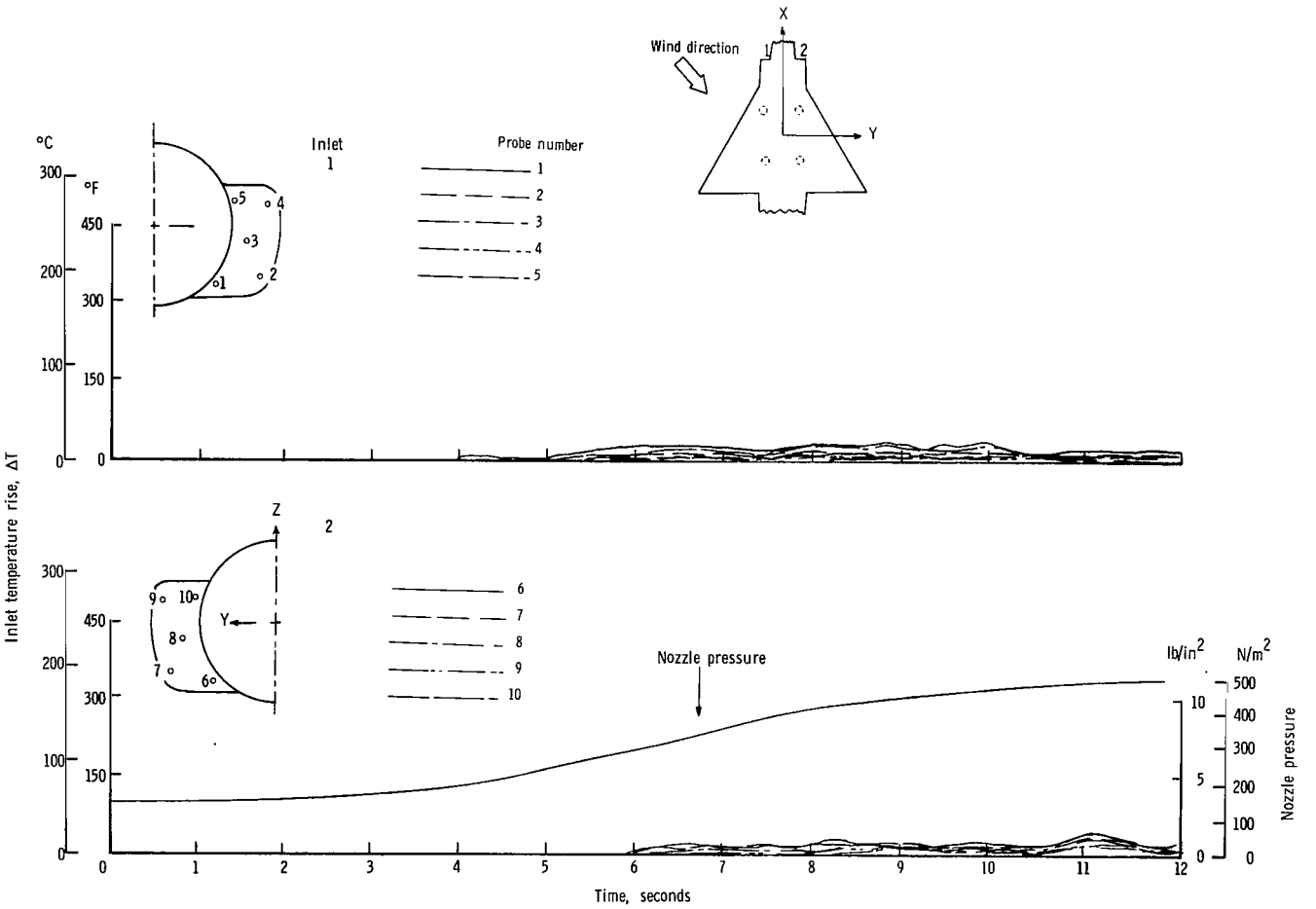

(i) $\psi = 45^0$; V = 11.85 knots.

Figure 17.- Continued.

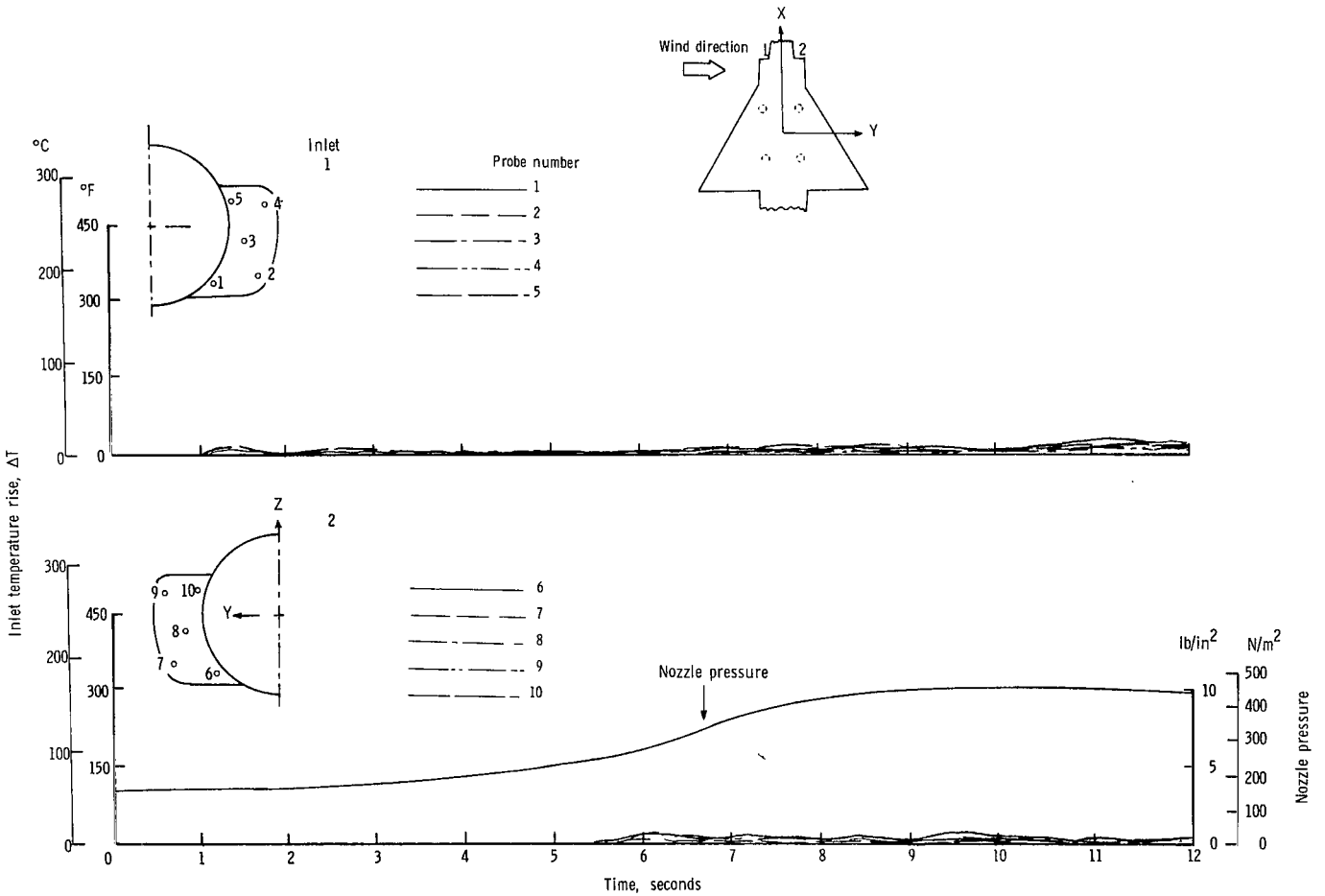

(j) $\psi = 90^{0}$; V = 5.92 knots.

Figure 17.- Continued.

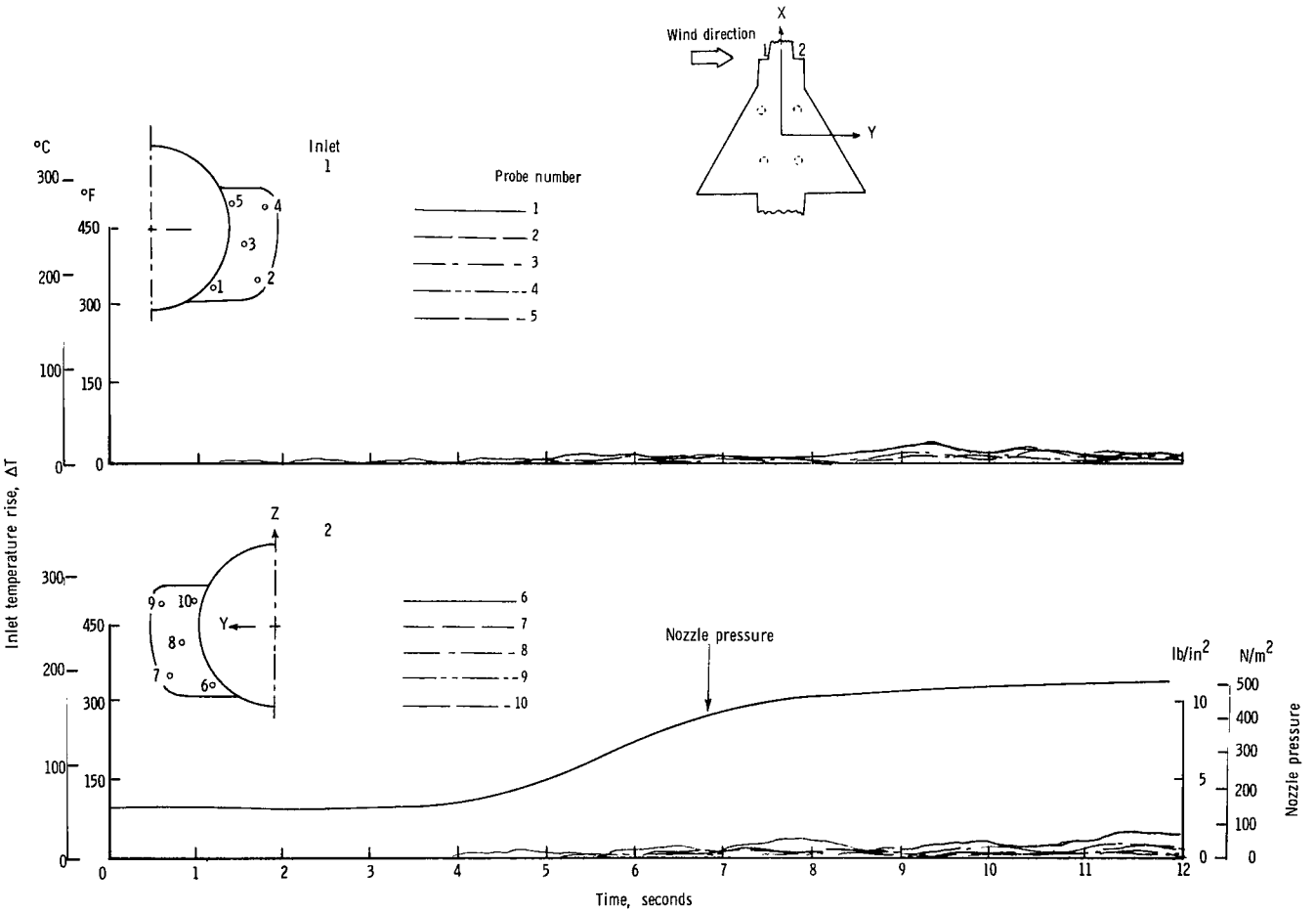

(k) $\psi = 90^0$; V = 11.85 knots.

Figure 17.- Concluded.

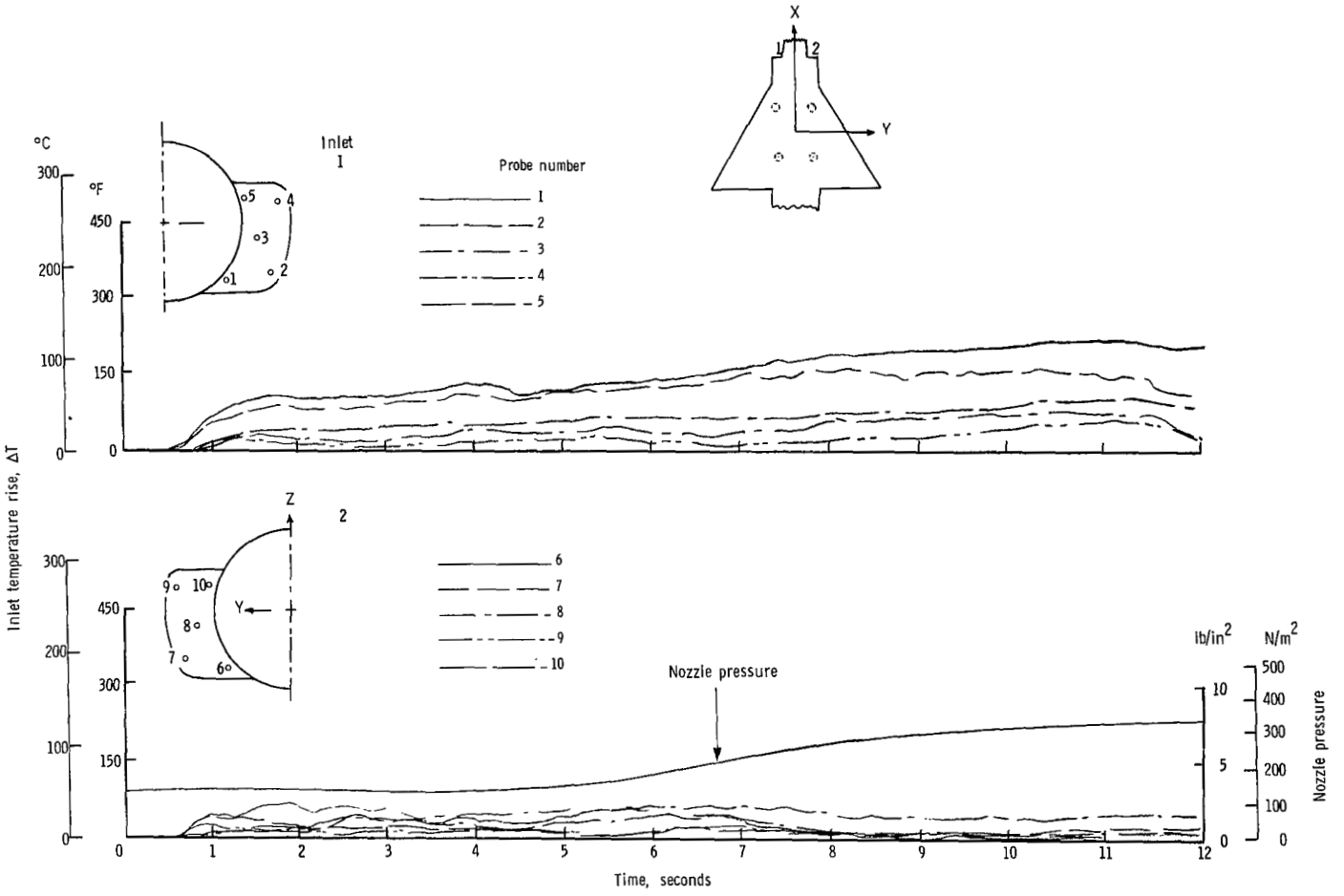

(a) $\psi = 0^0$; V = 0 knots.

Figure 18.- Variation of inlet air temperature rise with time for the rectangular nozzle arrangement with side inlets and low delta wing. $h/D_e = 1.17$.

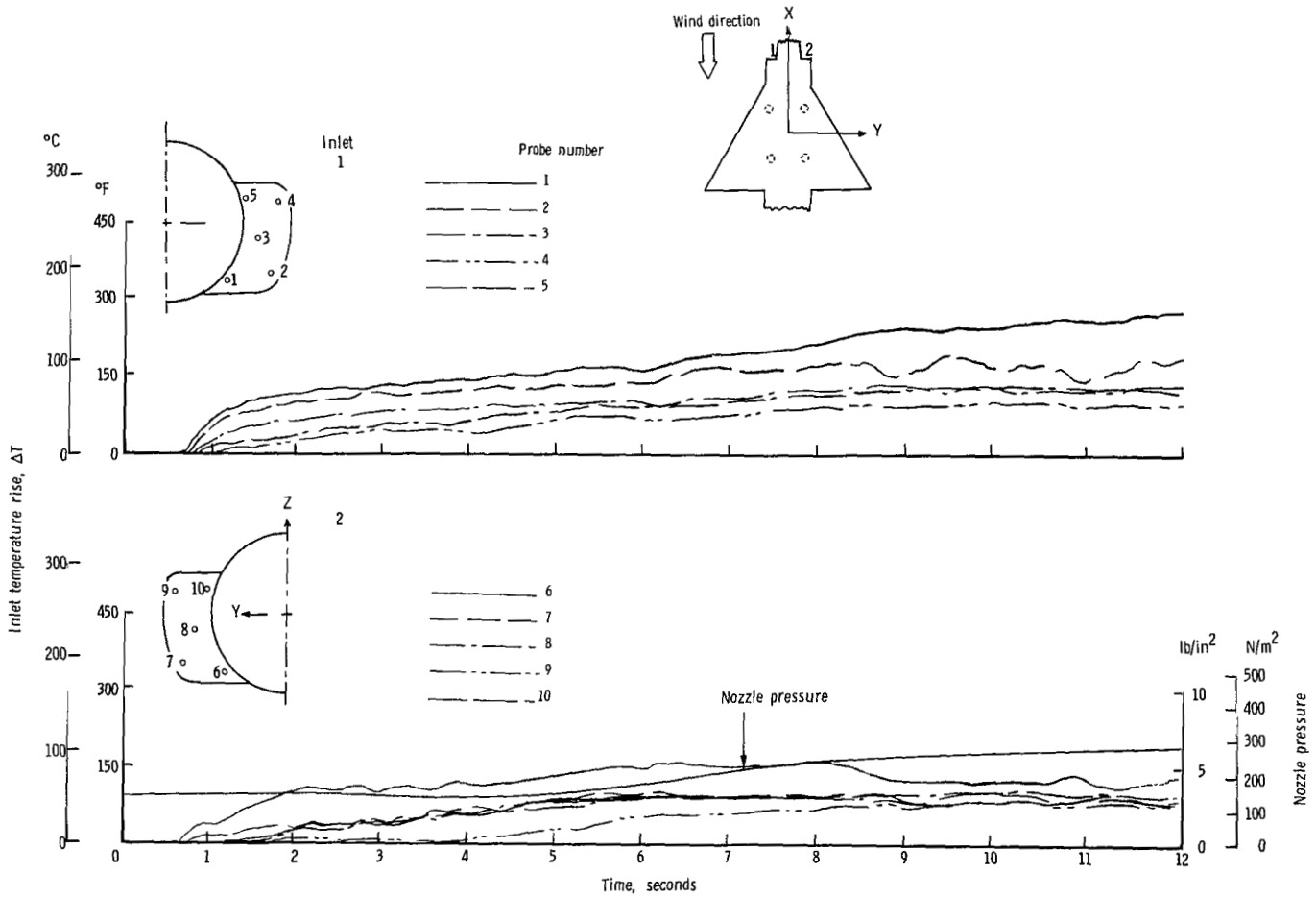

(b) $\psi = 0^0$; V = 5.92 knots.

Figure 18.- Continued.

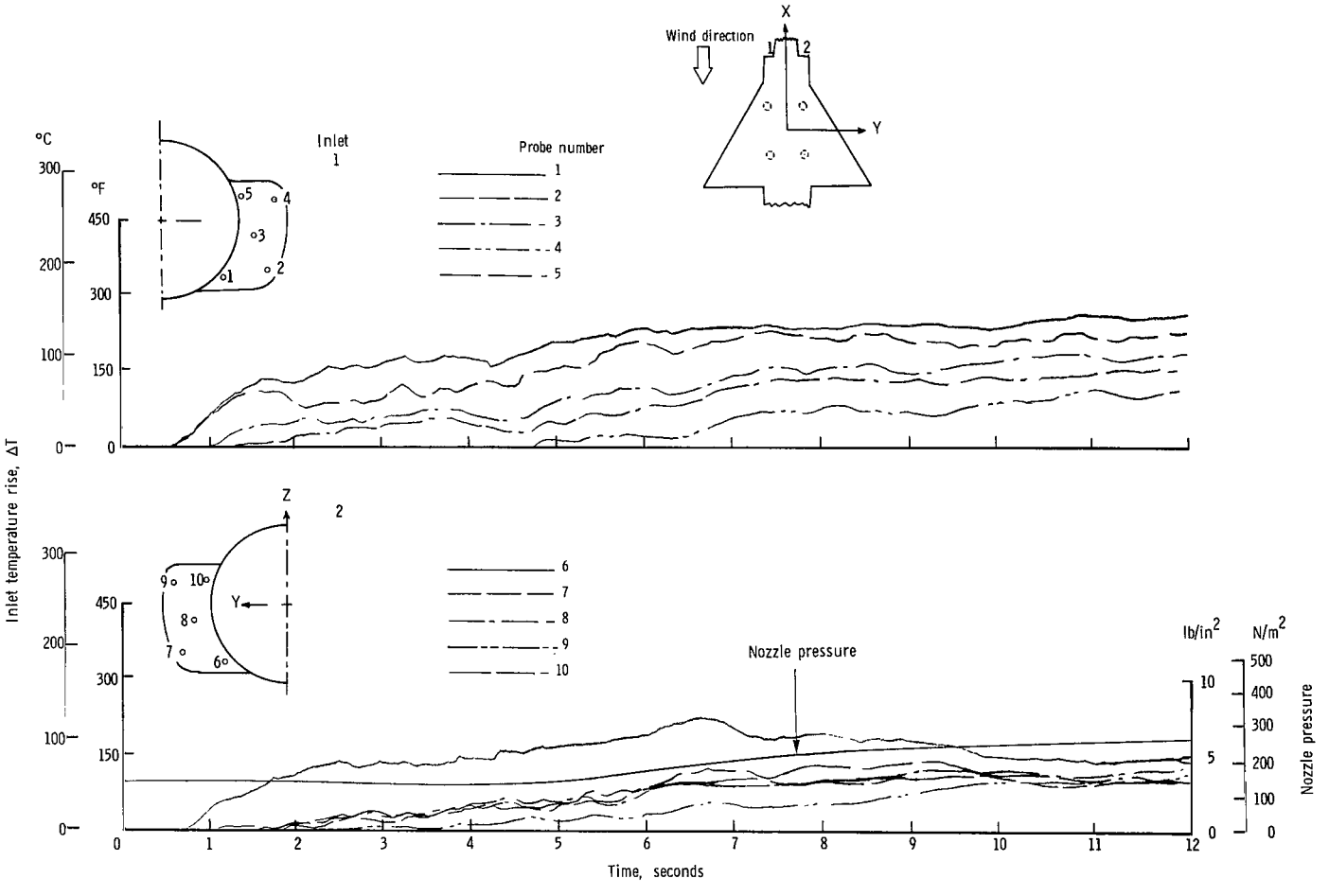

(c) $\psi = 0^0$; V = 11.85 knots.

Figure 18.- Continued.

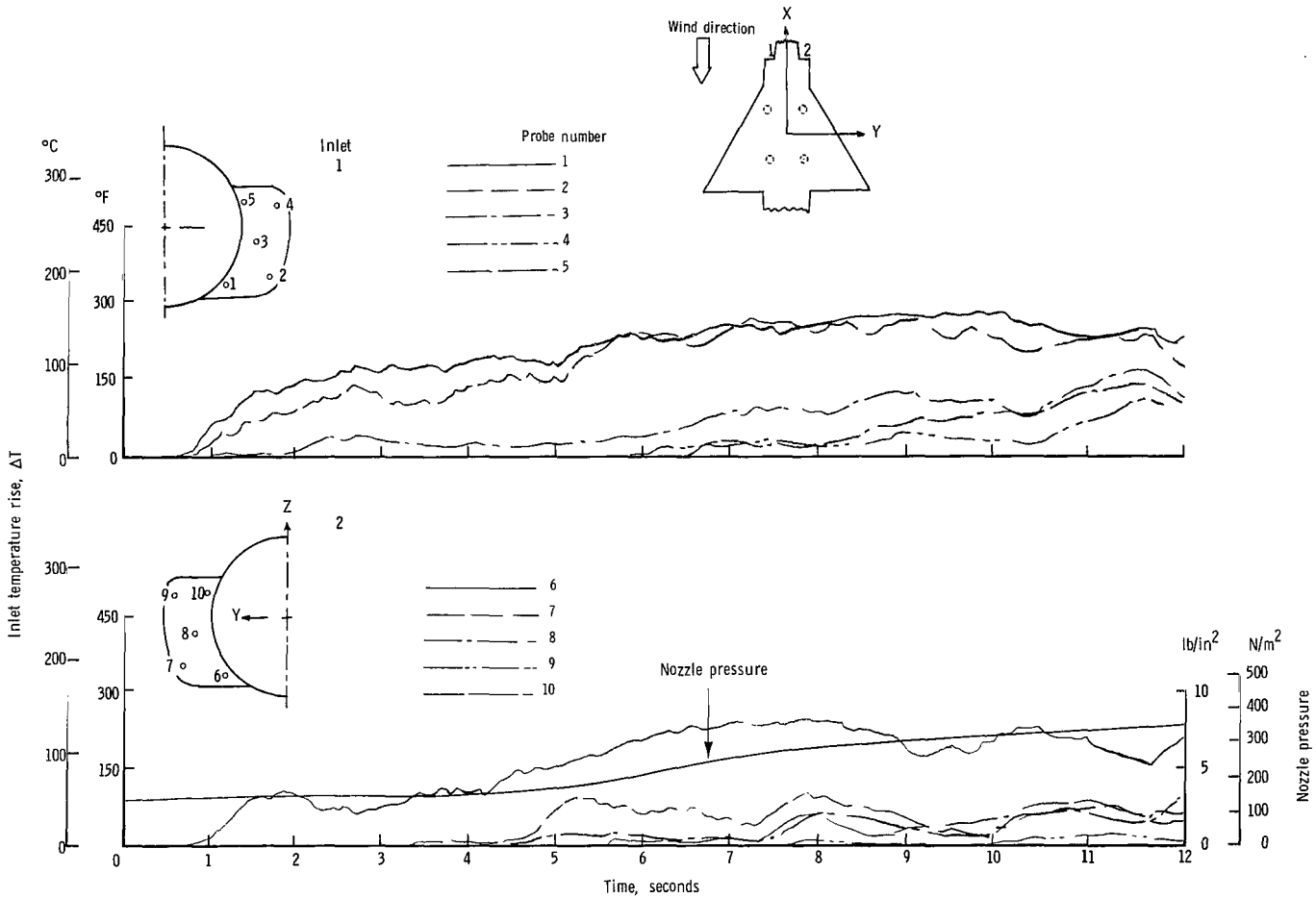

(d) $\psi = 0^0$; V = 17.78 knots.

Figure 18.- Continued.

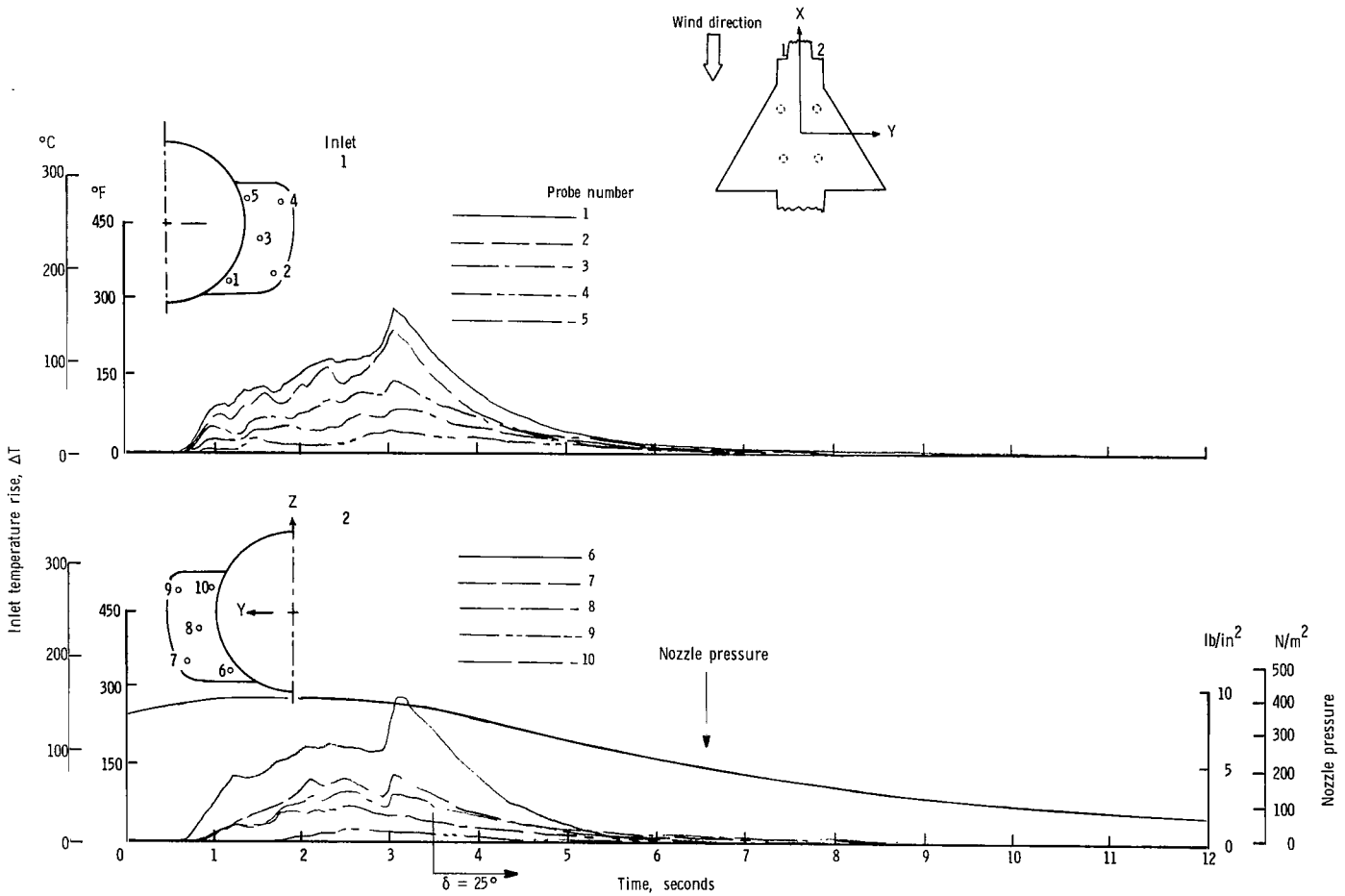

(e) $\psi = 0^0$; V = 23.70 knots.

Figure 18.- Continued.

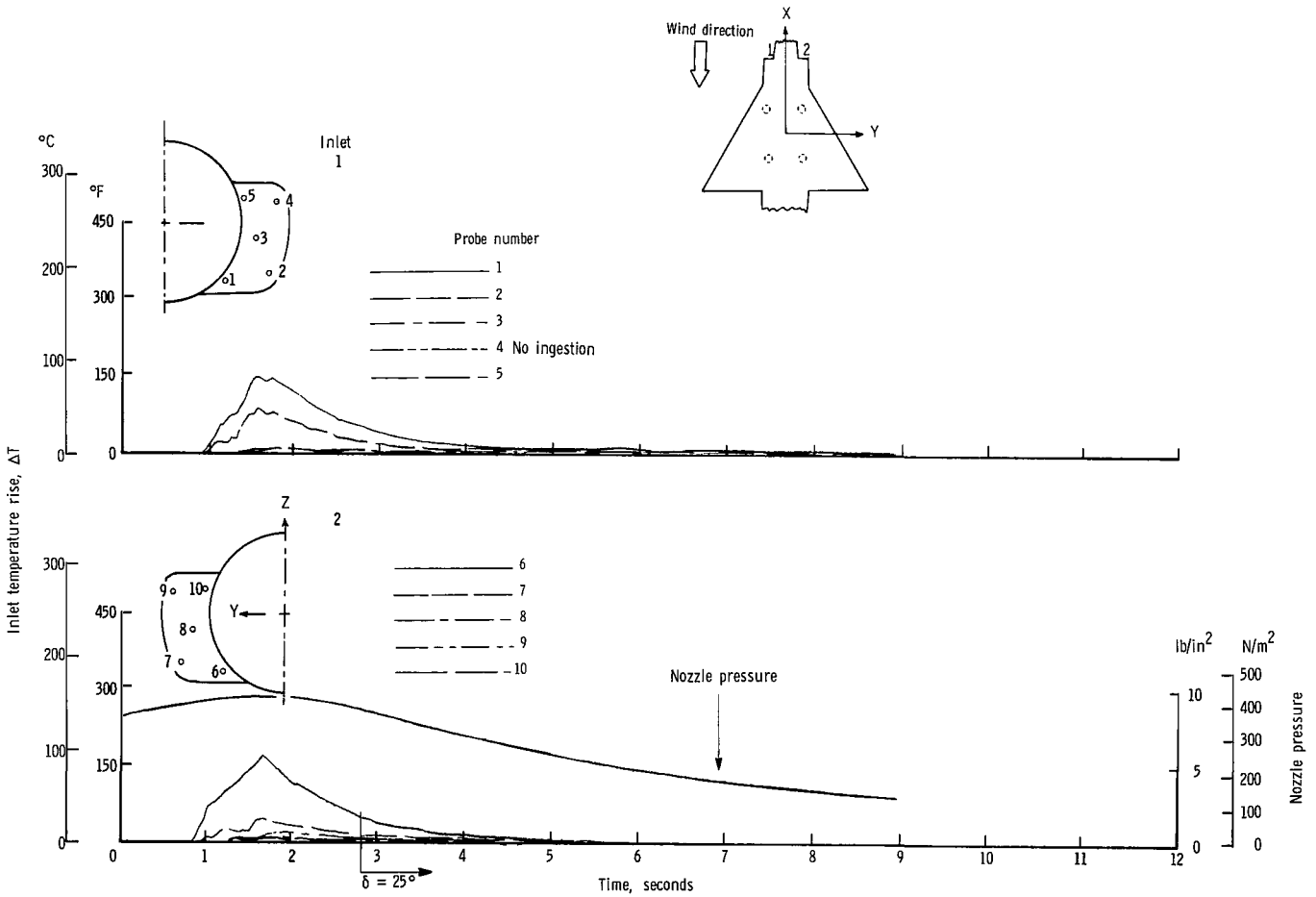

(f) $\psi = 0^0$; V = 29.63 knots.

Figure 18.- Continued.

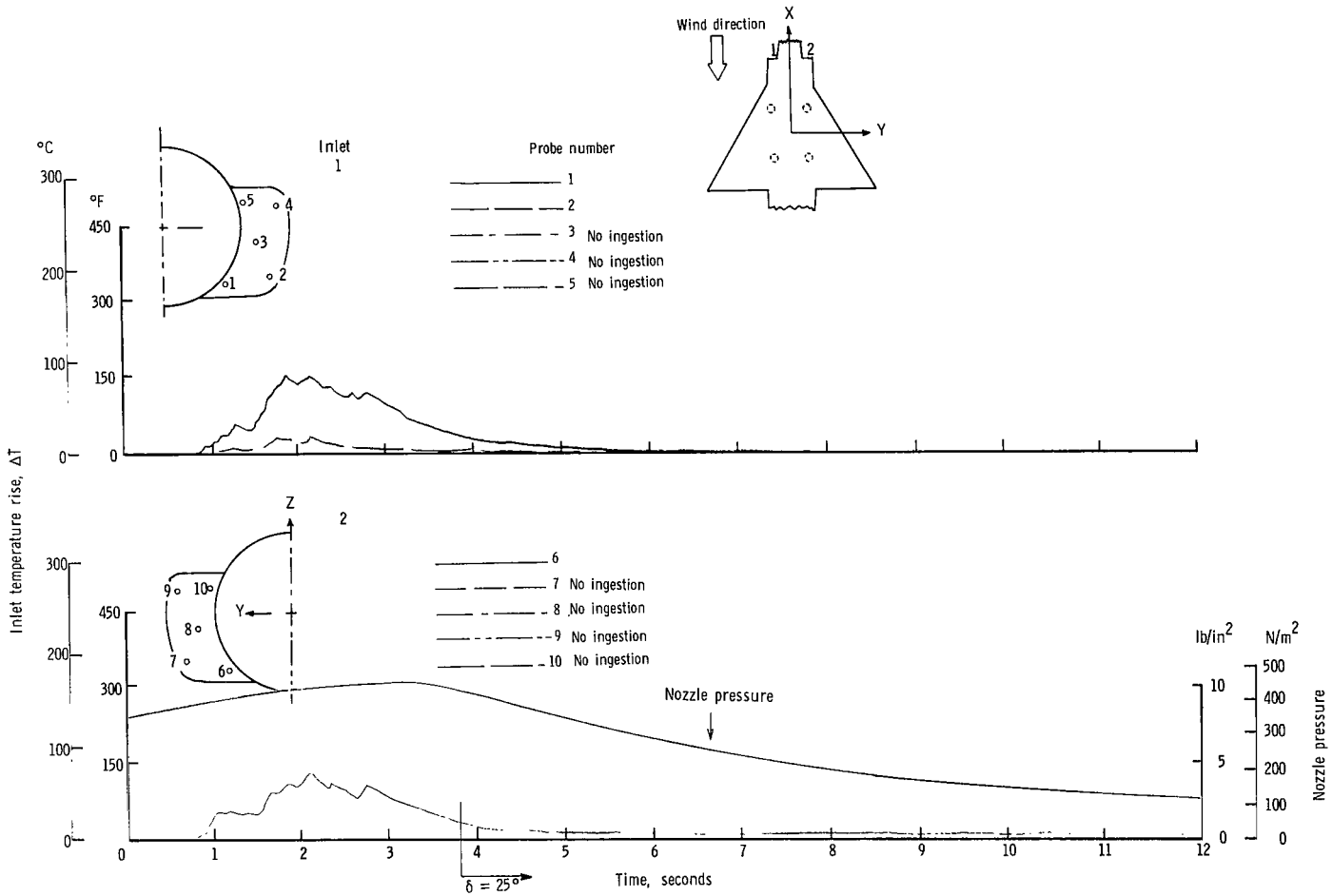

(g) $\psi = 0^{0}$; V = 35.55 knots.

Figure 18.- Continued.

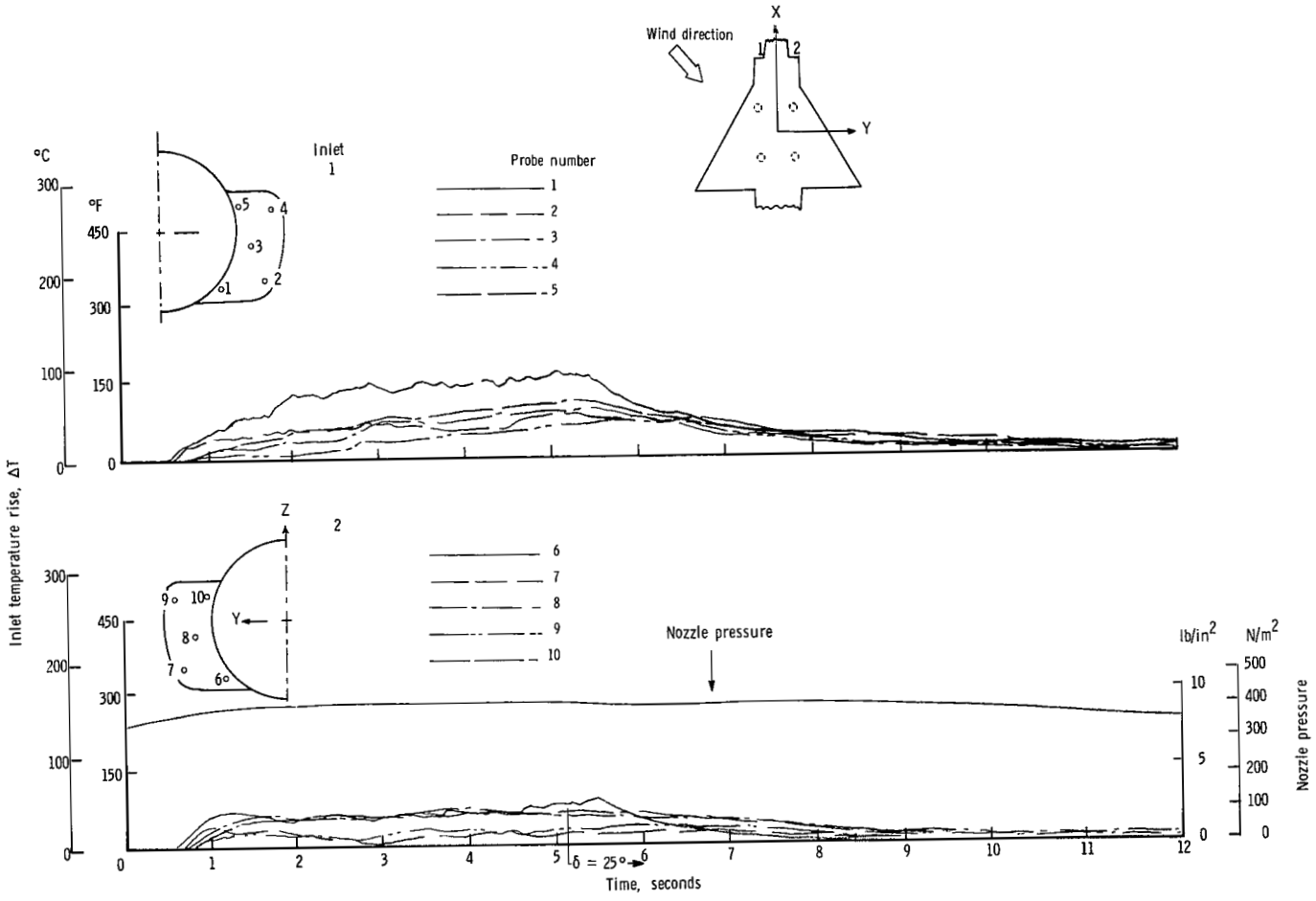

(h) $\psi = 45^{0}$; V = 5.92 knots.

Figure 18.- Continued.

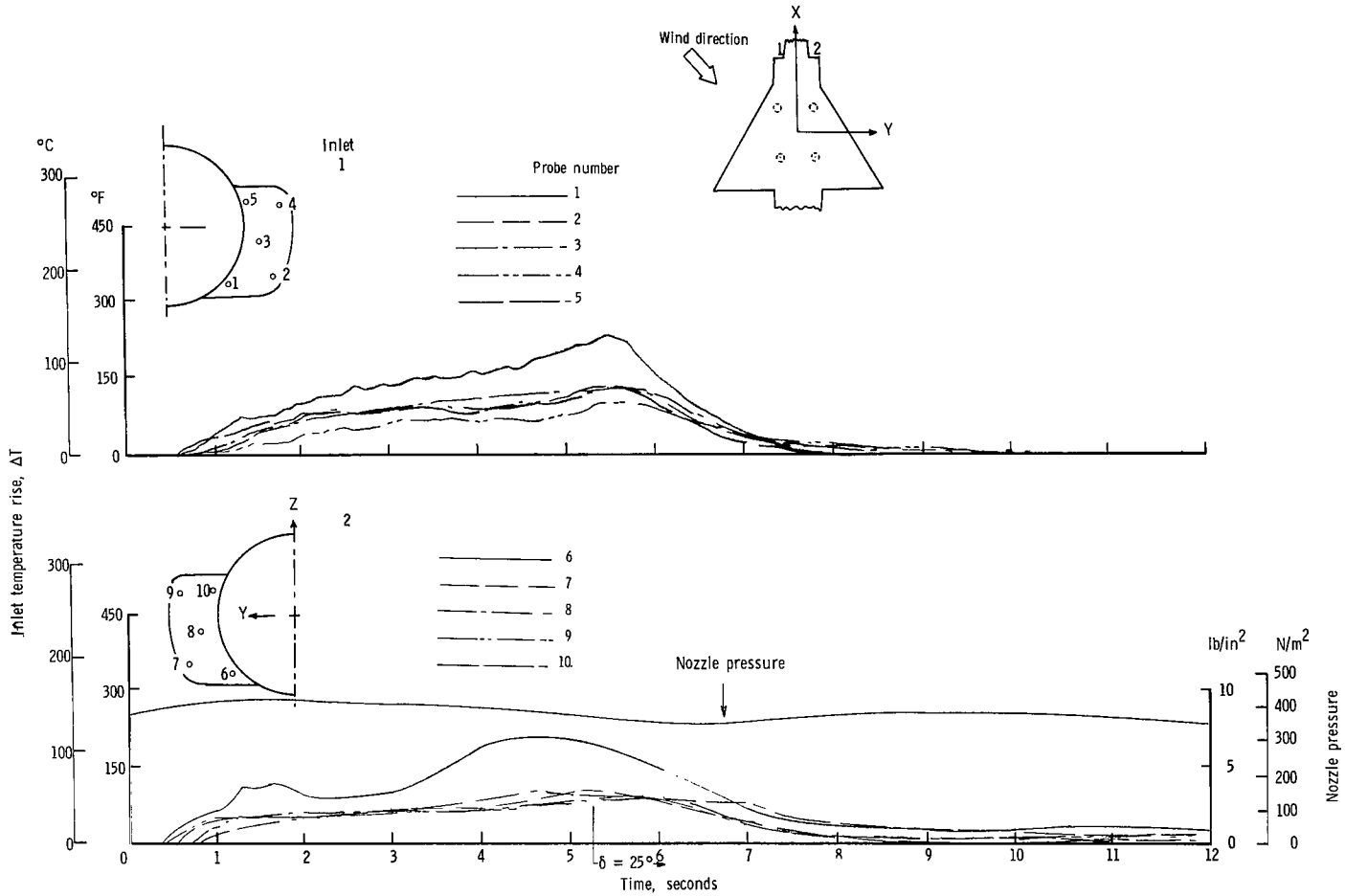

(i) $\psi = 45^{0}$; V = 11.85 knots.

Figure 18.- Continued.

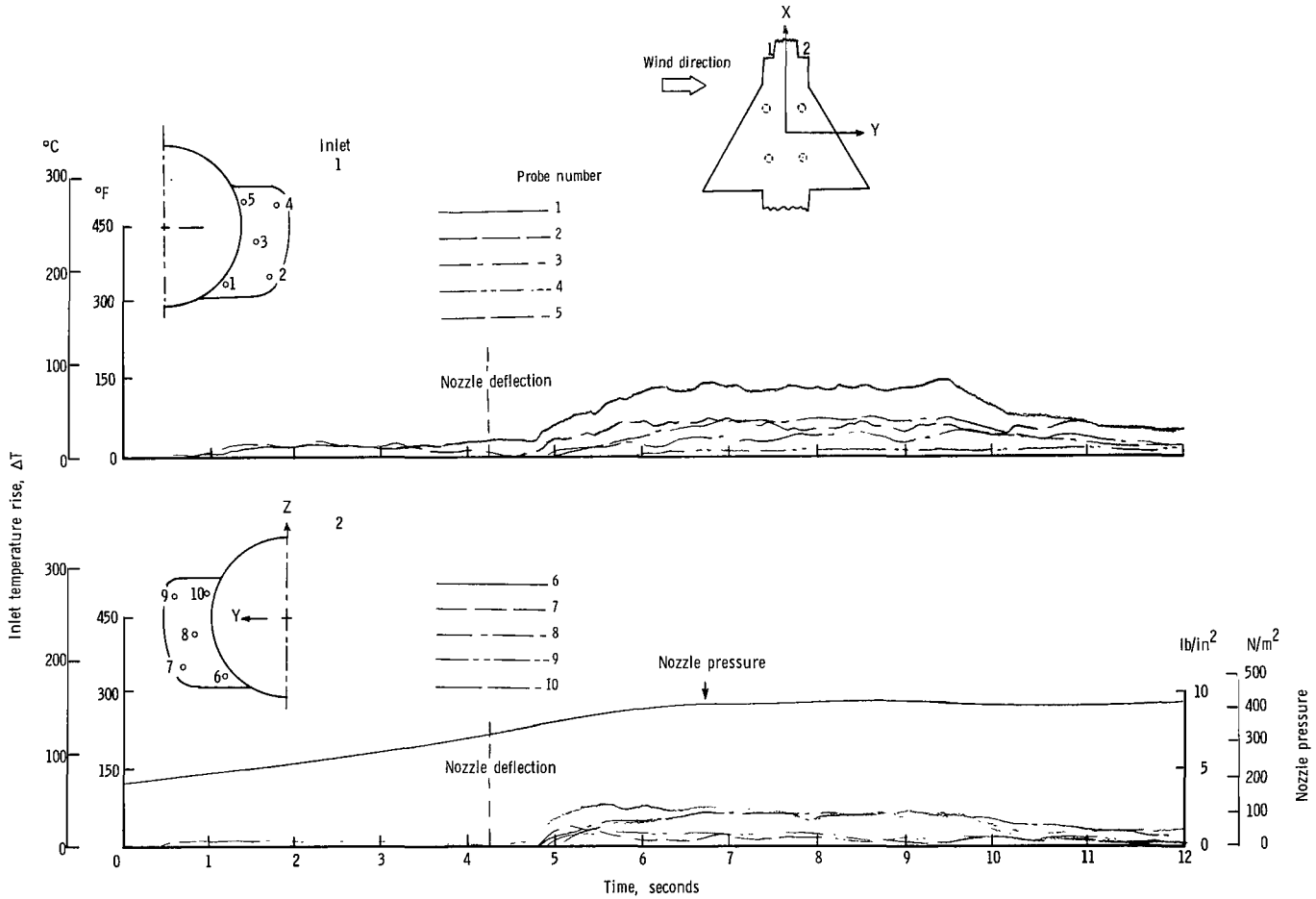

(j) $\psi = 90^0$; V = 5.92 knots.

Figure 18.- Continued.

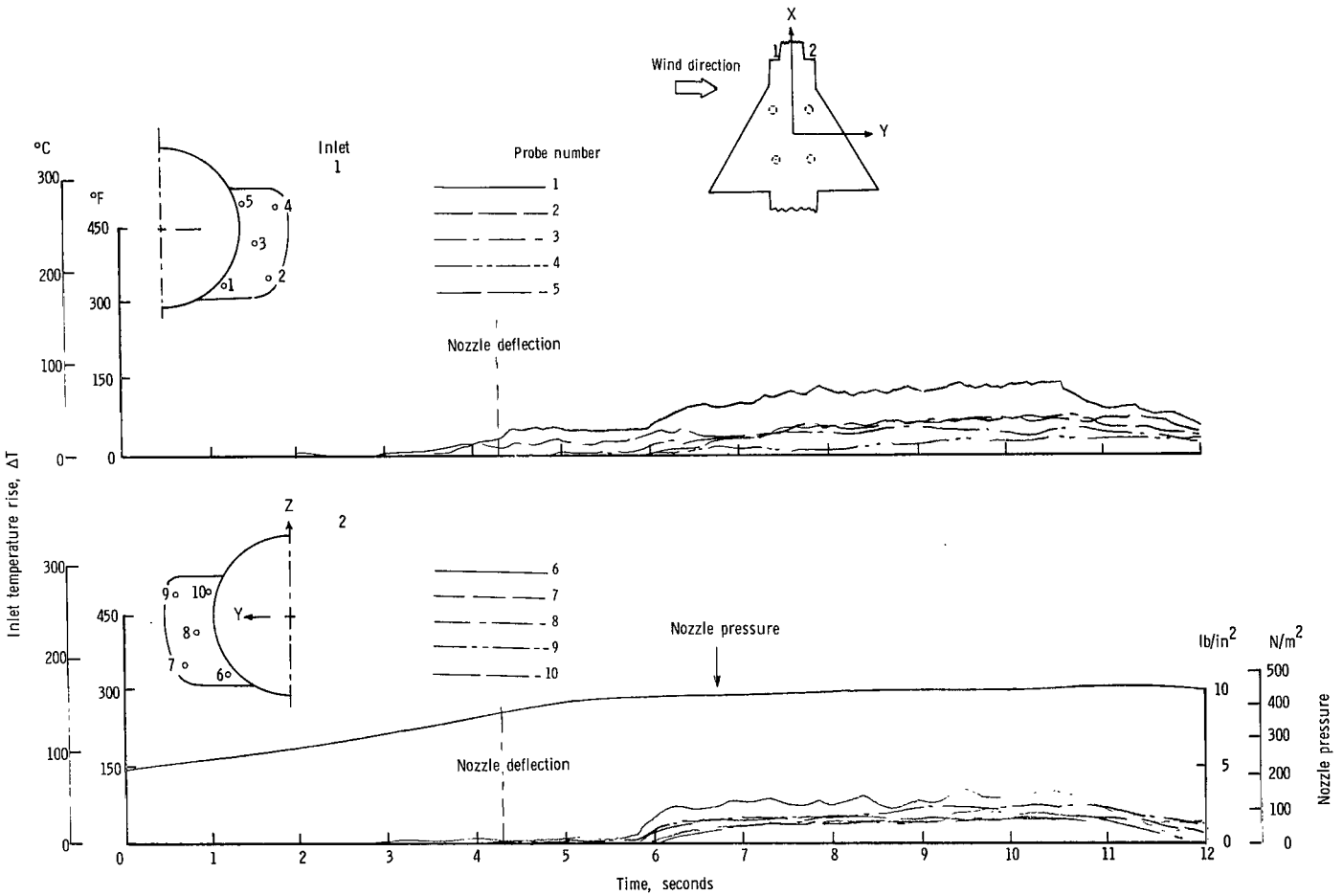

(k) $\psi = 90^{0}$; V = 11.85 knots.

Figure 18.- Concluded.

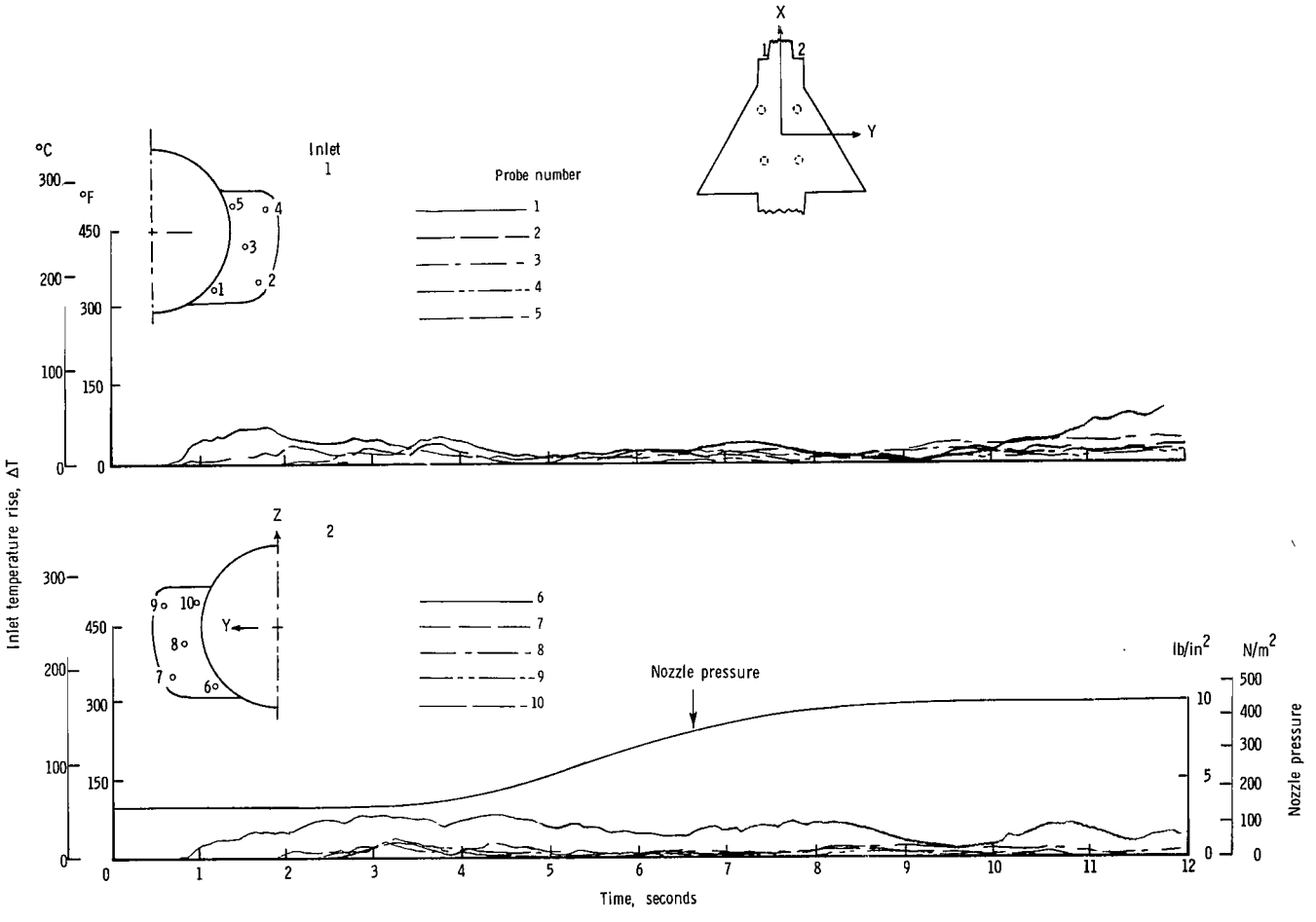

(a) $\psi = 0^{o}$; V = 0 knots.

Figure 19.- Variation of inlet air temperature rise with time for the rectangular nozzle arrangement with side inlets and low delta wing. $h/D_e = 3.0$.

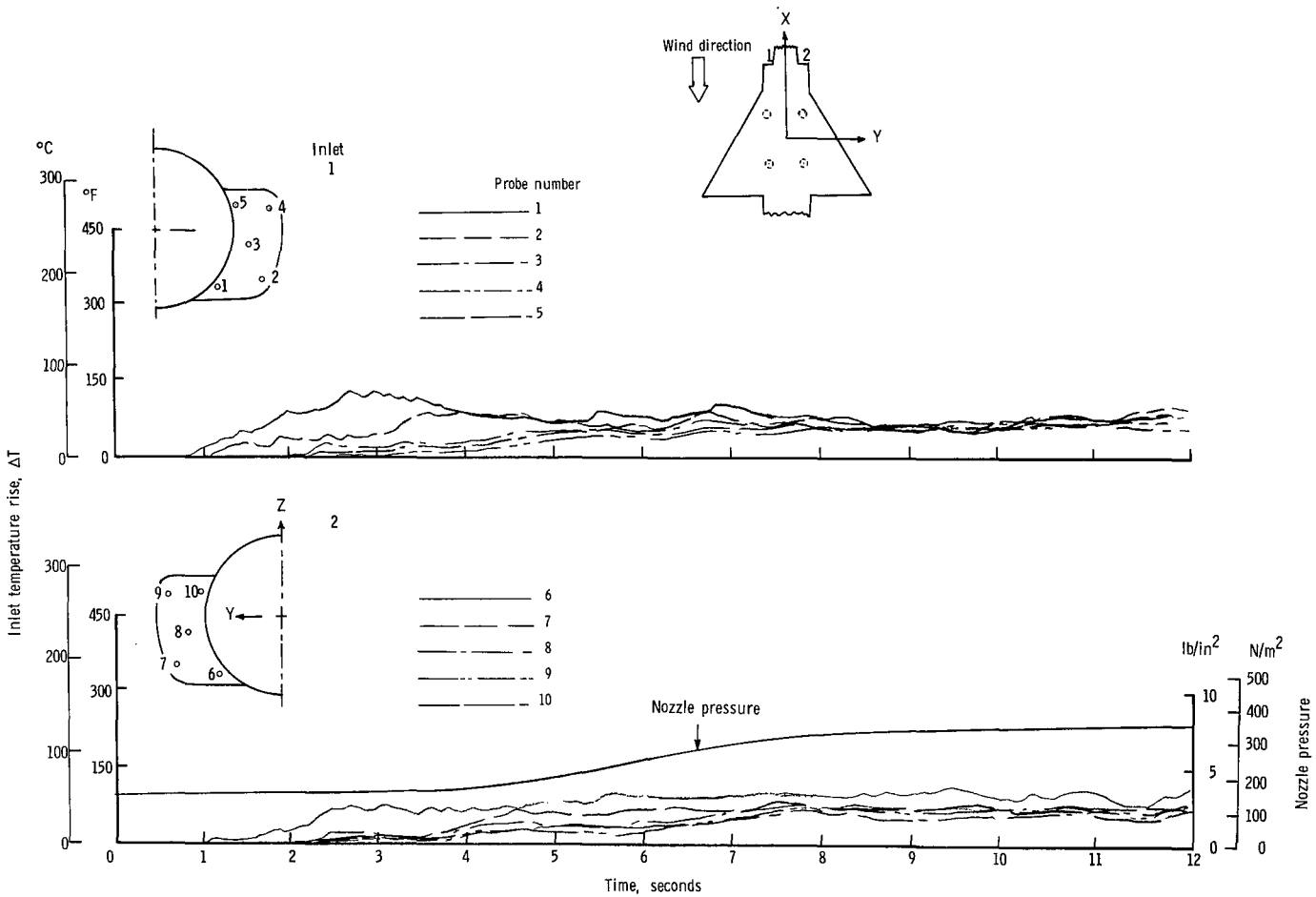

(b) $\psi = 0^{o}$; V = 5.92 knots.

Figure 19.- Continued.

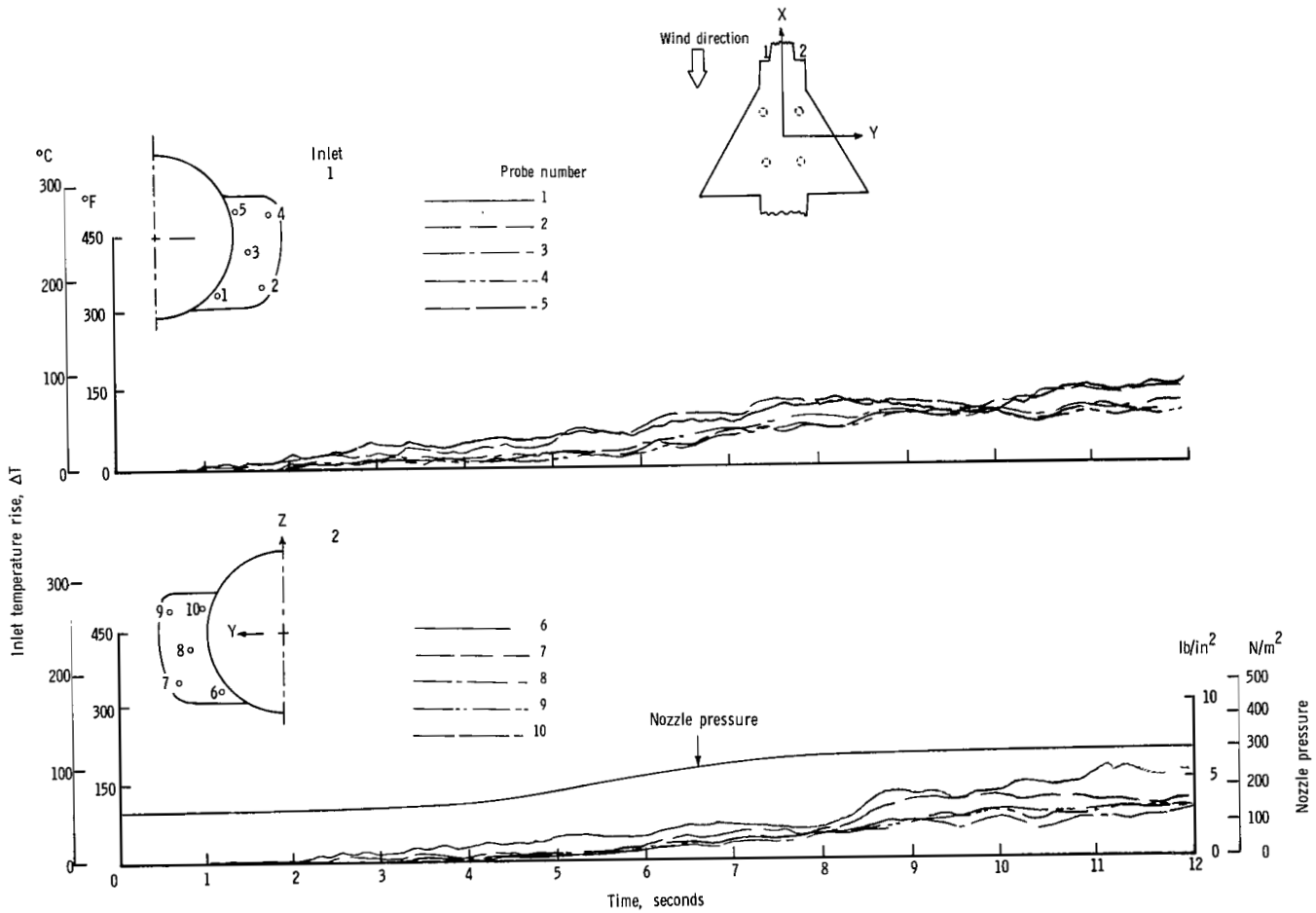

(c) $\psi = 0^0$; V = 11.85 knots.

Figure 19.- Continued.

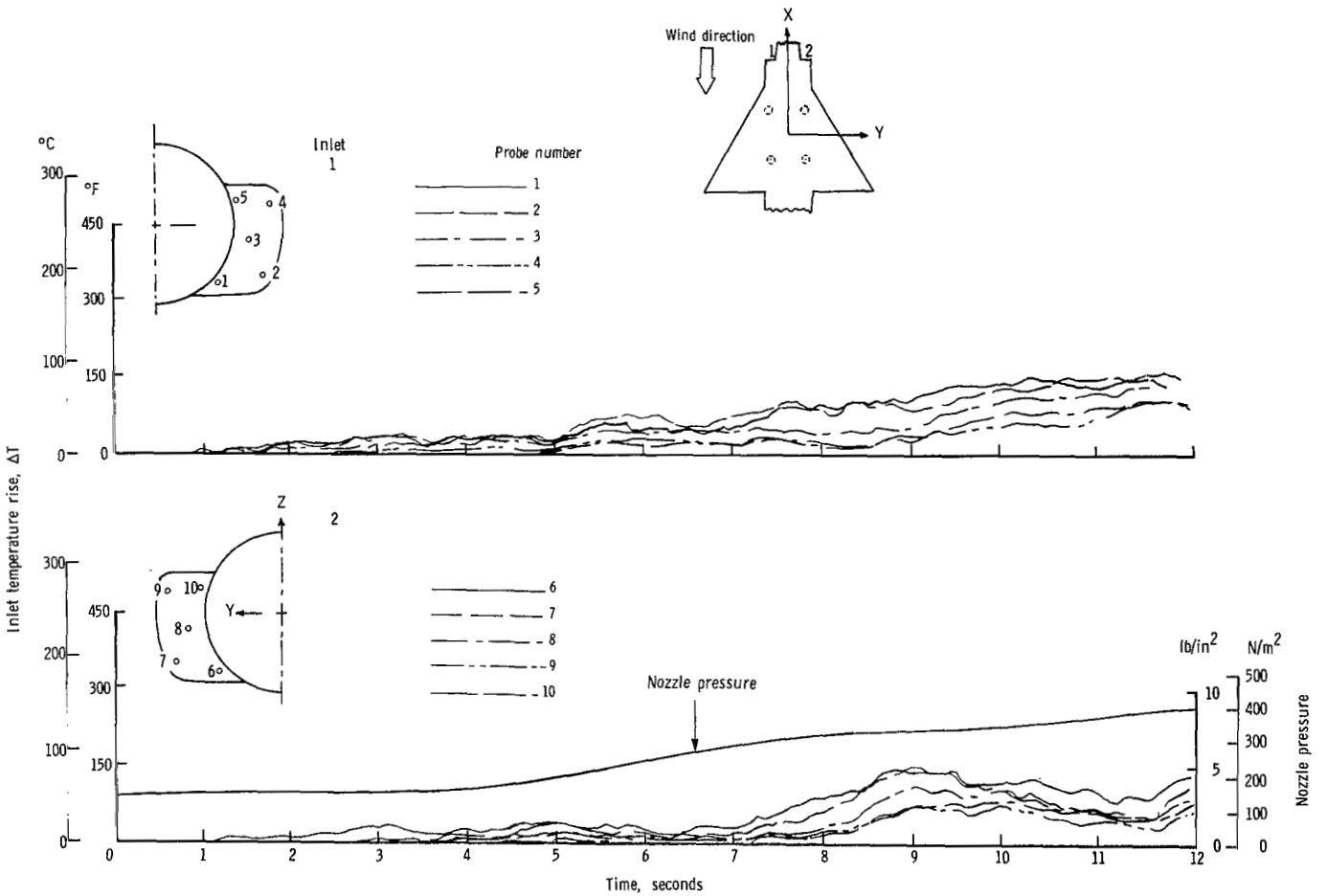

(d) $\psi = 0^{o}$; V = 17.78 knots.

Figure 19.- Continued.

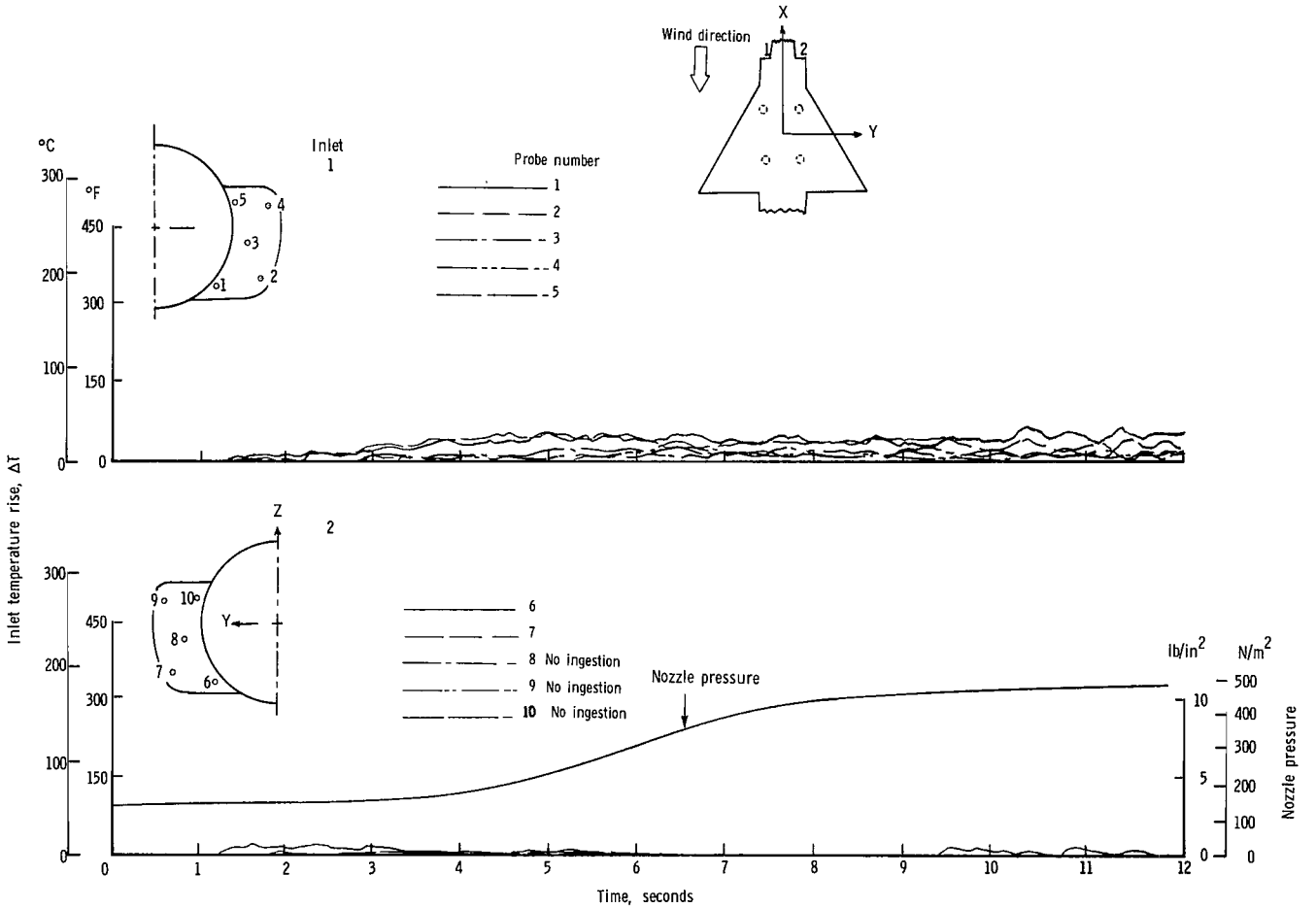

(e) $\psi = 0^0$; V = 23.70 knots.

Figure 19.- Continued.

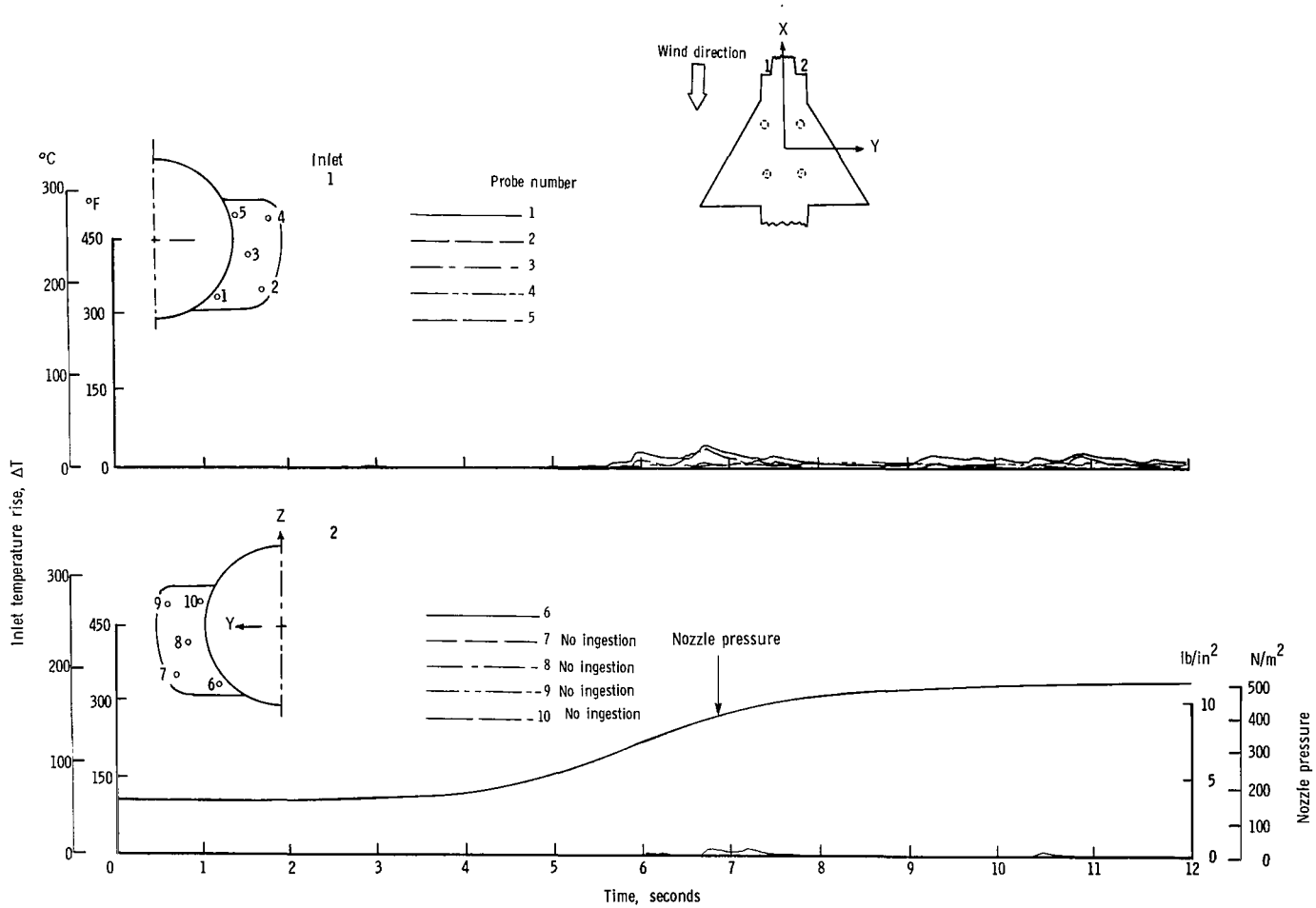

(f) $\psi = 0^0$; V = 29.63 knots.

Figure 19.- Continued.

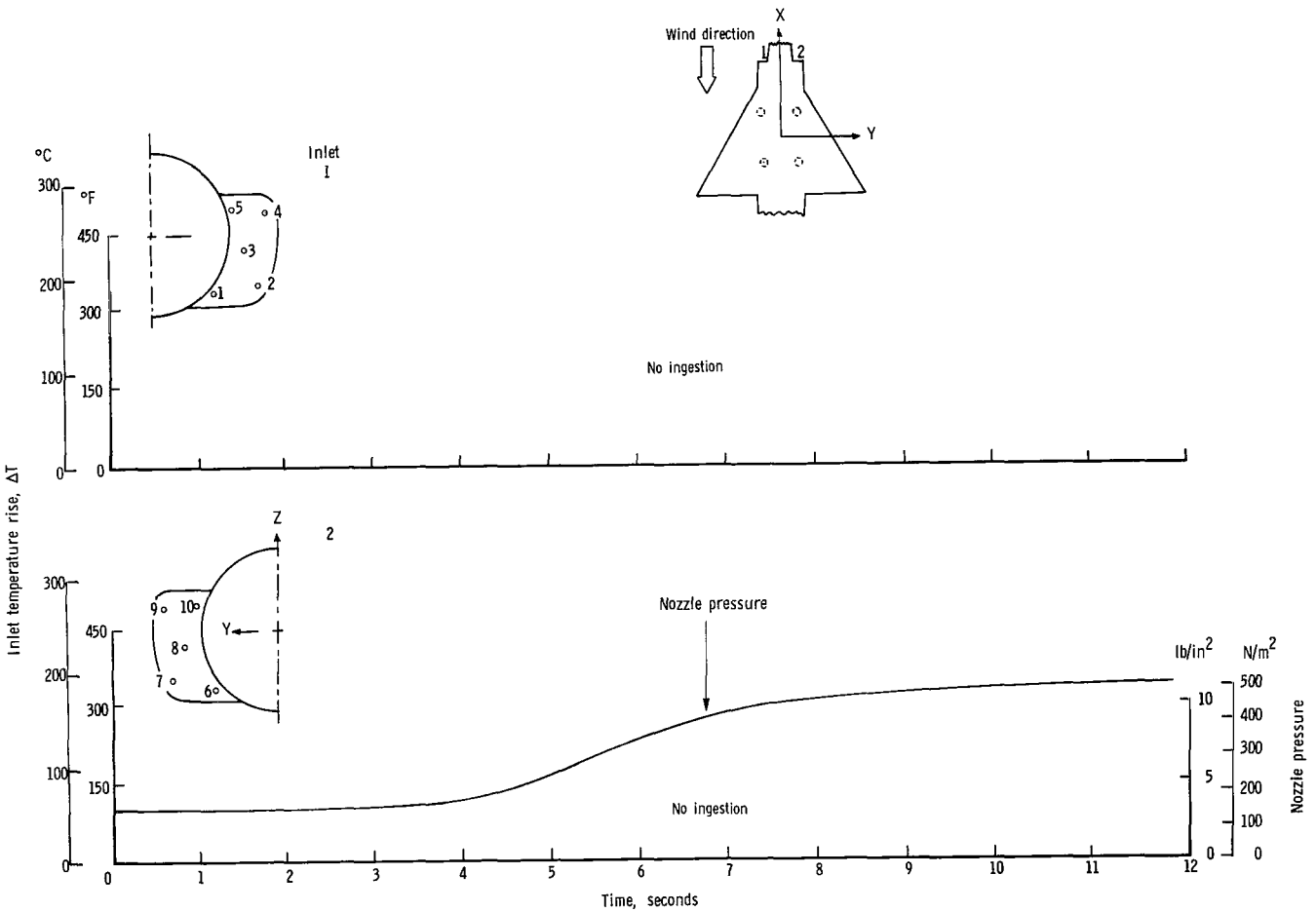

(g) $\psi = 0^0$; V = 35.55 knots.

Figure 19.- Continued.

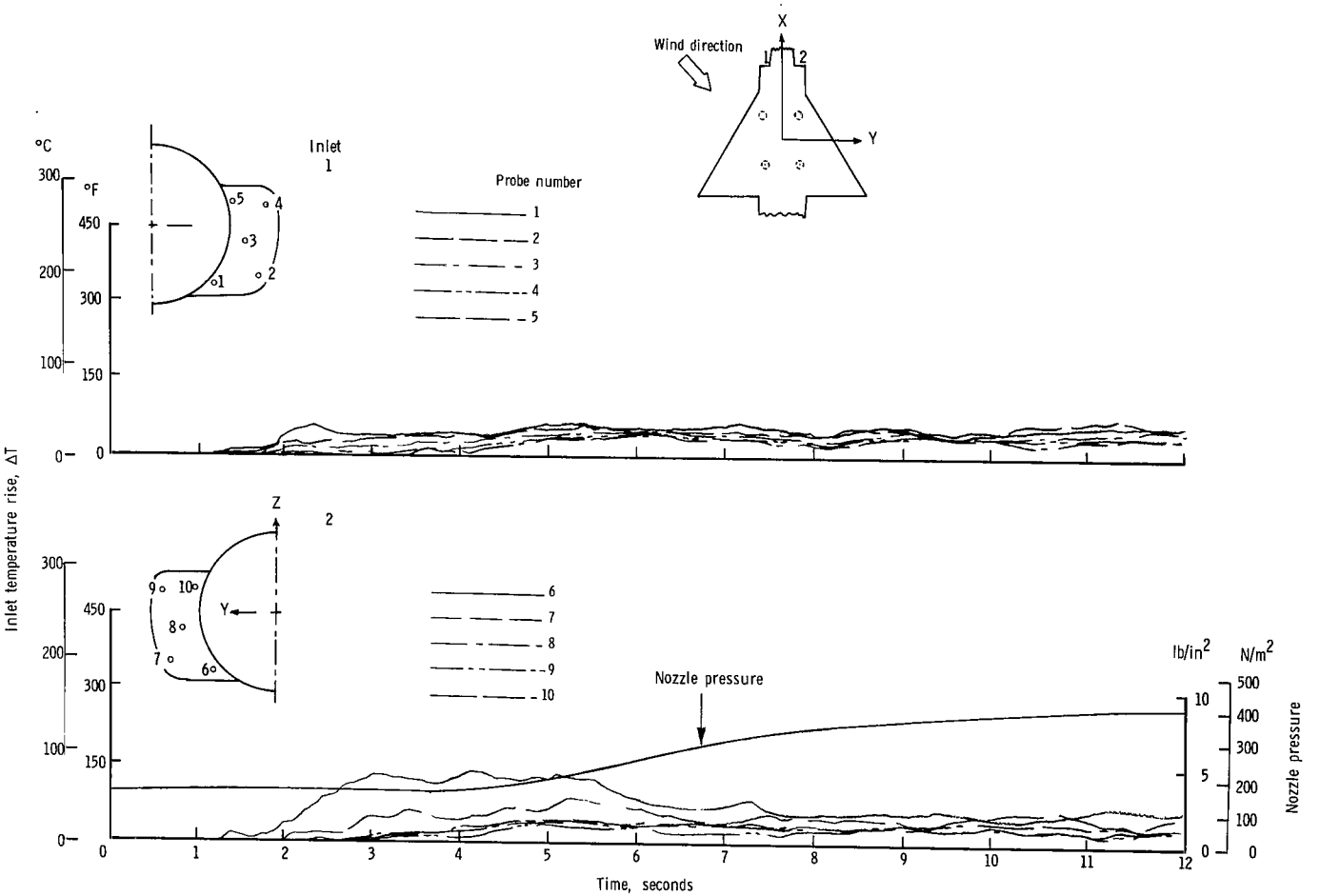

(h) $\psi = 45^0$; V = 5.92 knots.

Figure 19.- Continued.

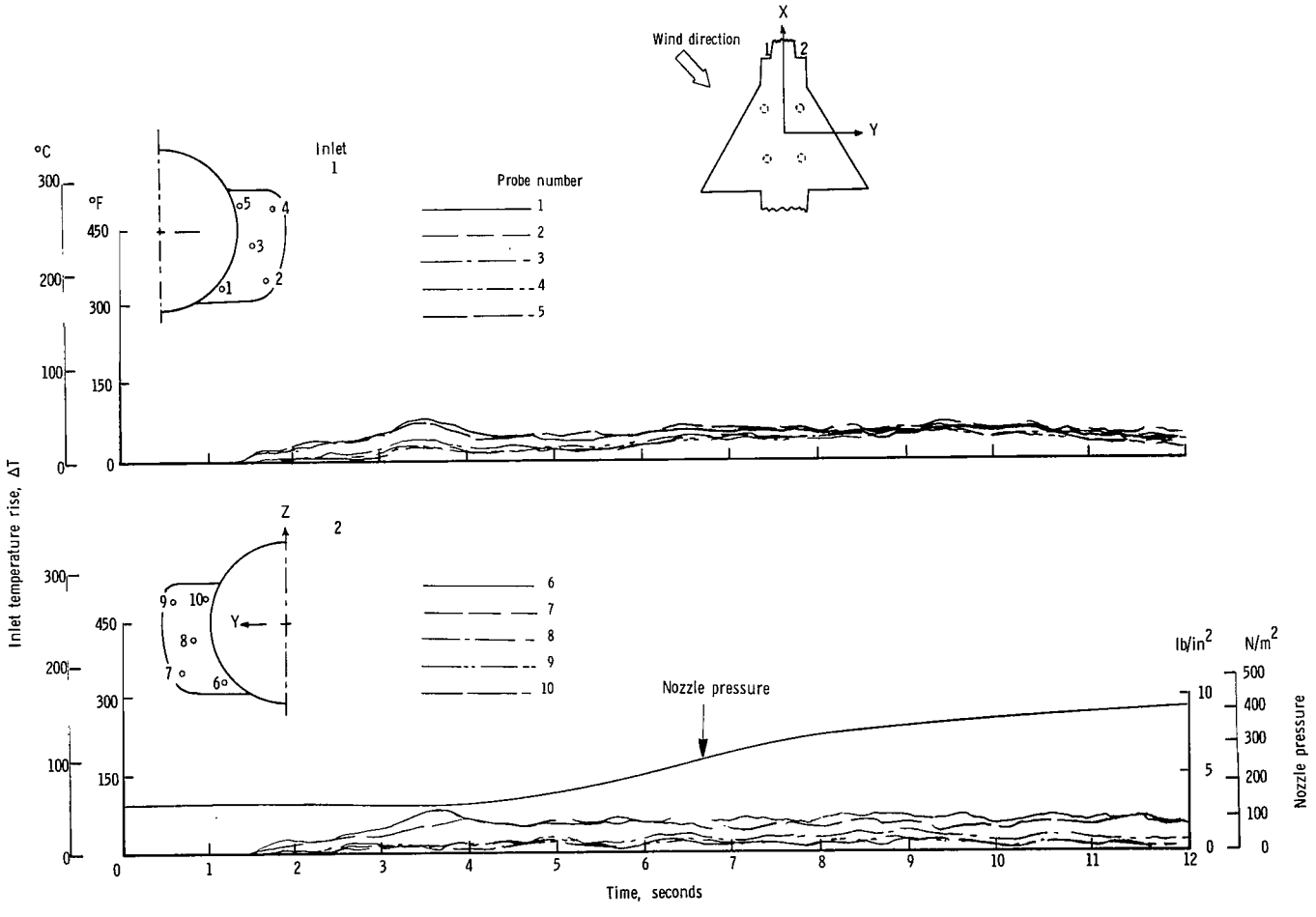

(i) $\psi = 45^0$; V = 11.85 knots.

Figure 19.- Continued.

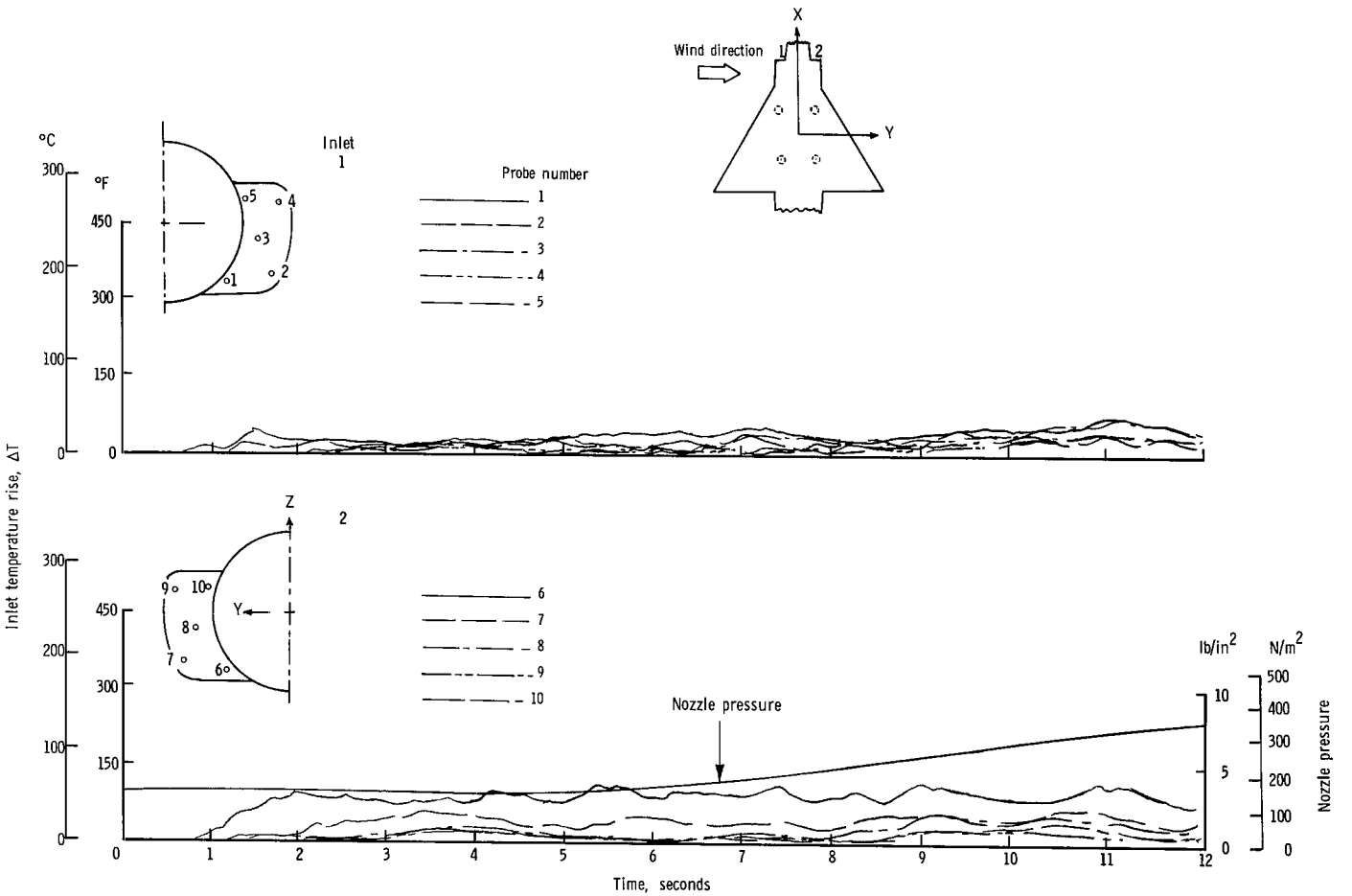

(j) $\psi = 90^0$; V = 5.92 knots.

Figure 19.- Continued.

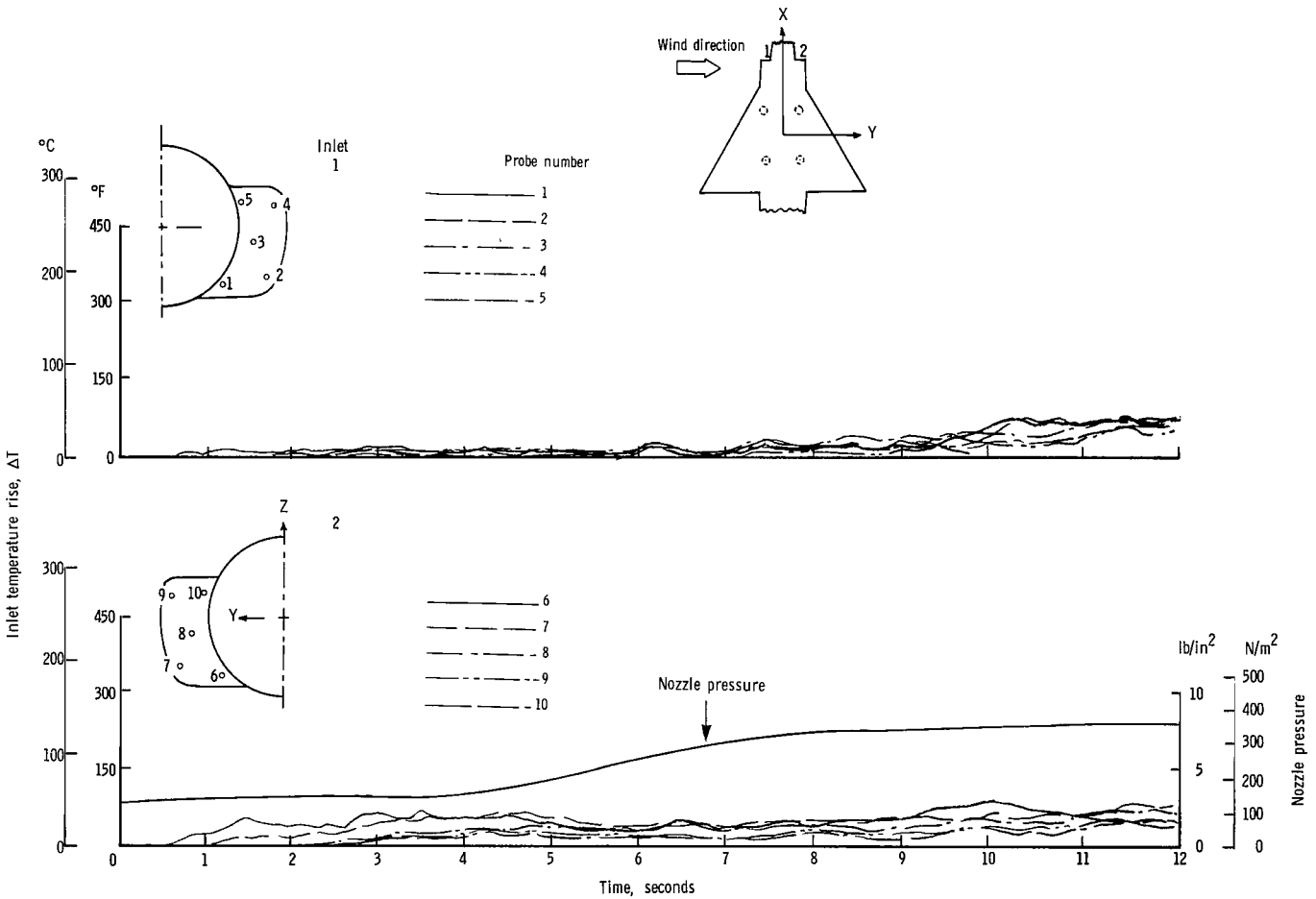

(k) $\psi = 90^{0}$; V = 11.85 knots.

Figure 19.- Concluded.

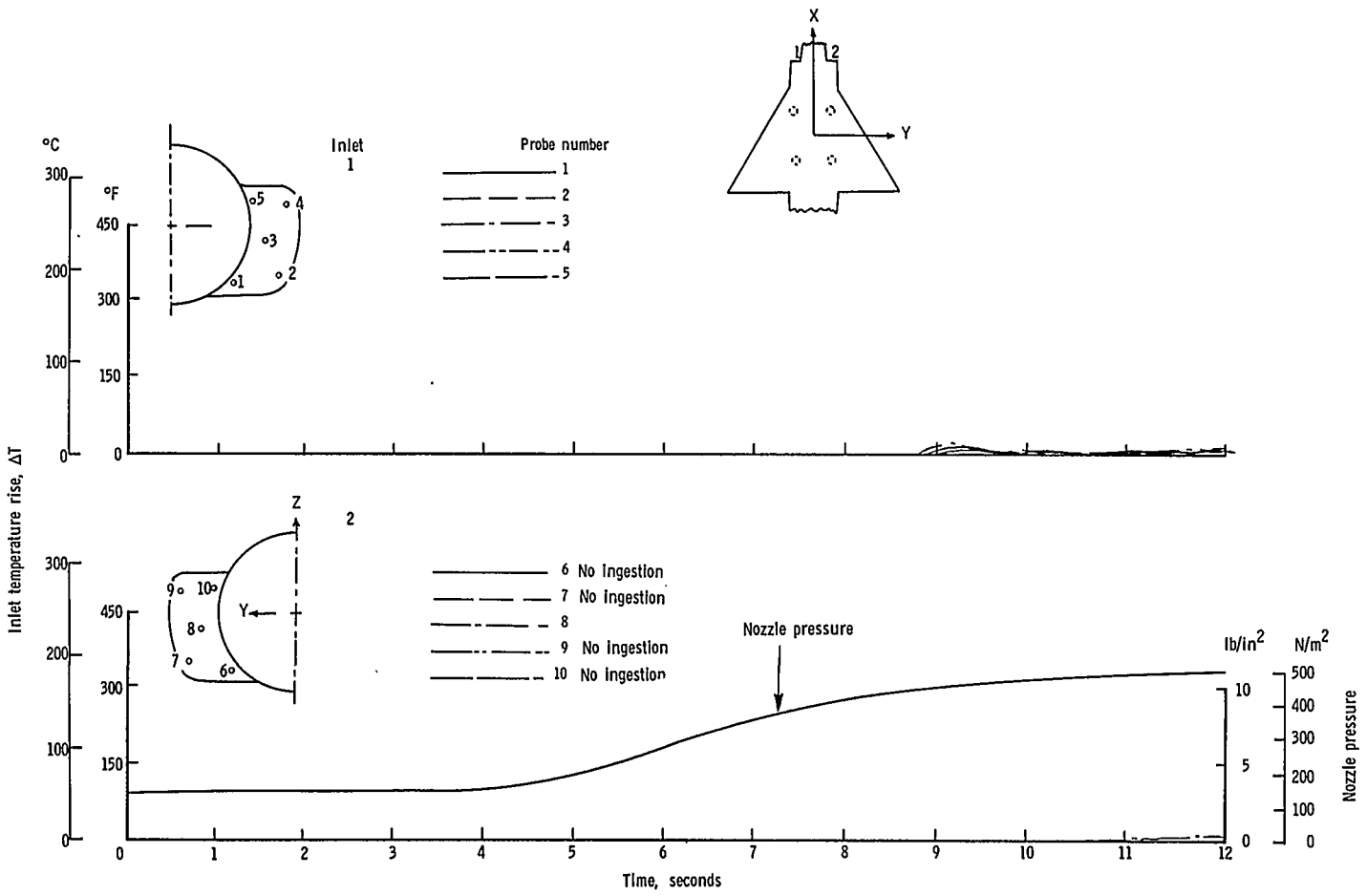

(a) $\psi = 0^0$; V = 0 knots.

Figure 20.- Variation of inlet air temperature rise with time for the rectangular nozzle arrangement with side inlets and low delta wing. $h/D_e = 5.0$.

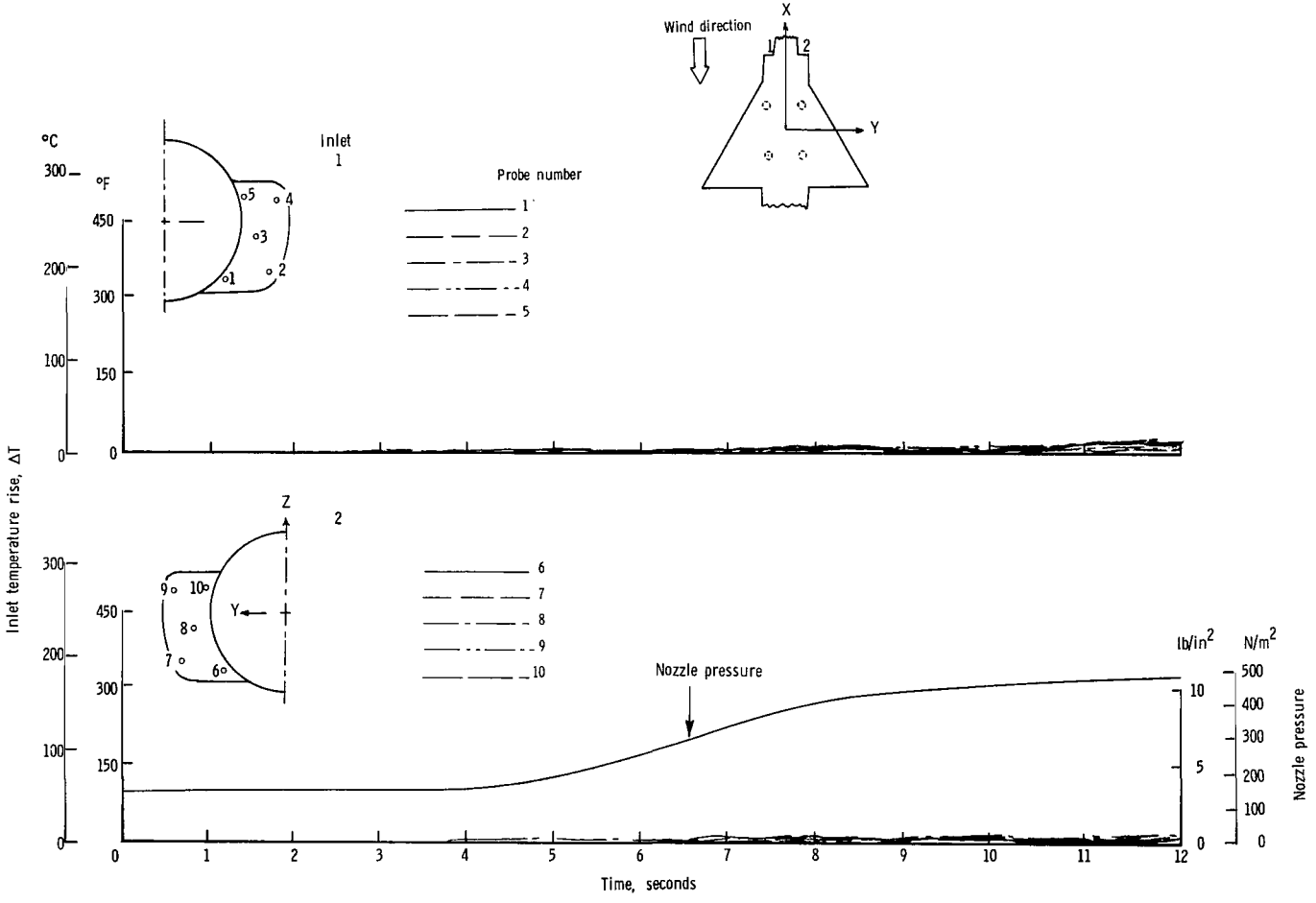

(b) $\psi = 0^0$; V = 5.92 knots.

Figure 20.- Continued.

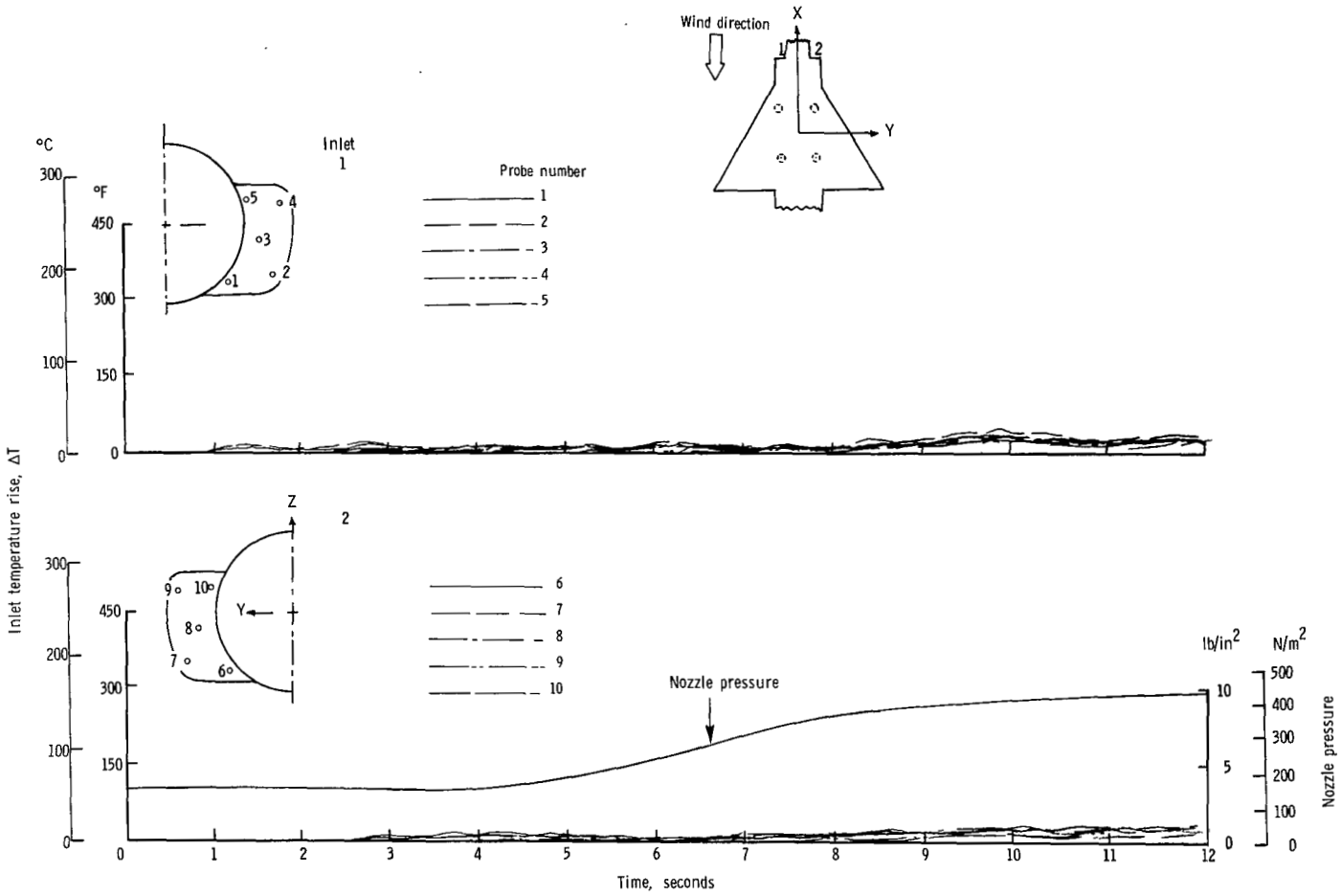

(c) $\psi = 0^0$; V = 11.85 knots.

Figure 20.- Continued.

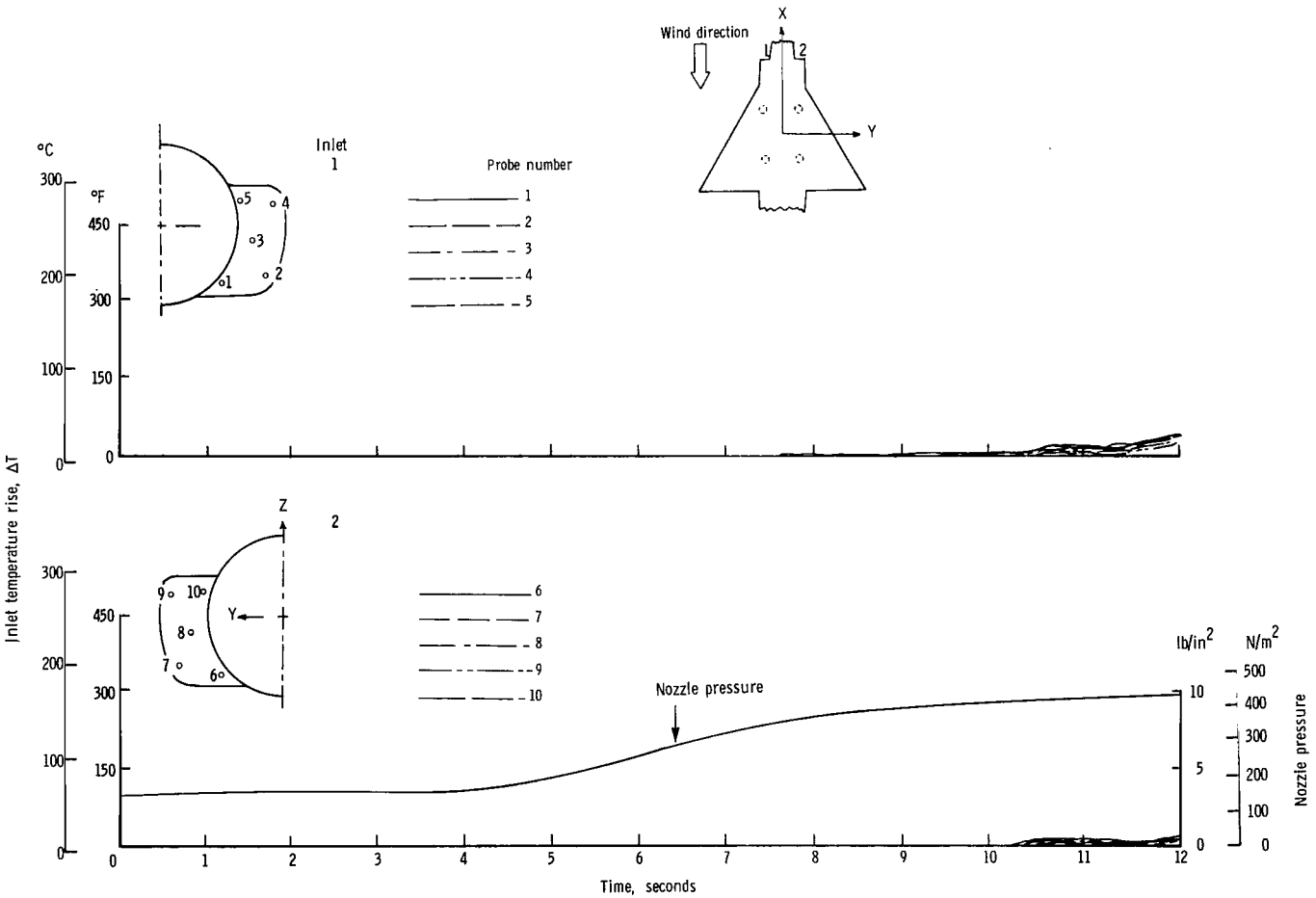

(d) $\psi = 0^0$; V = 17.78 knots.

Figure 20.- Continued.

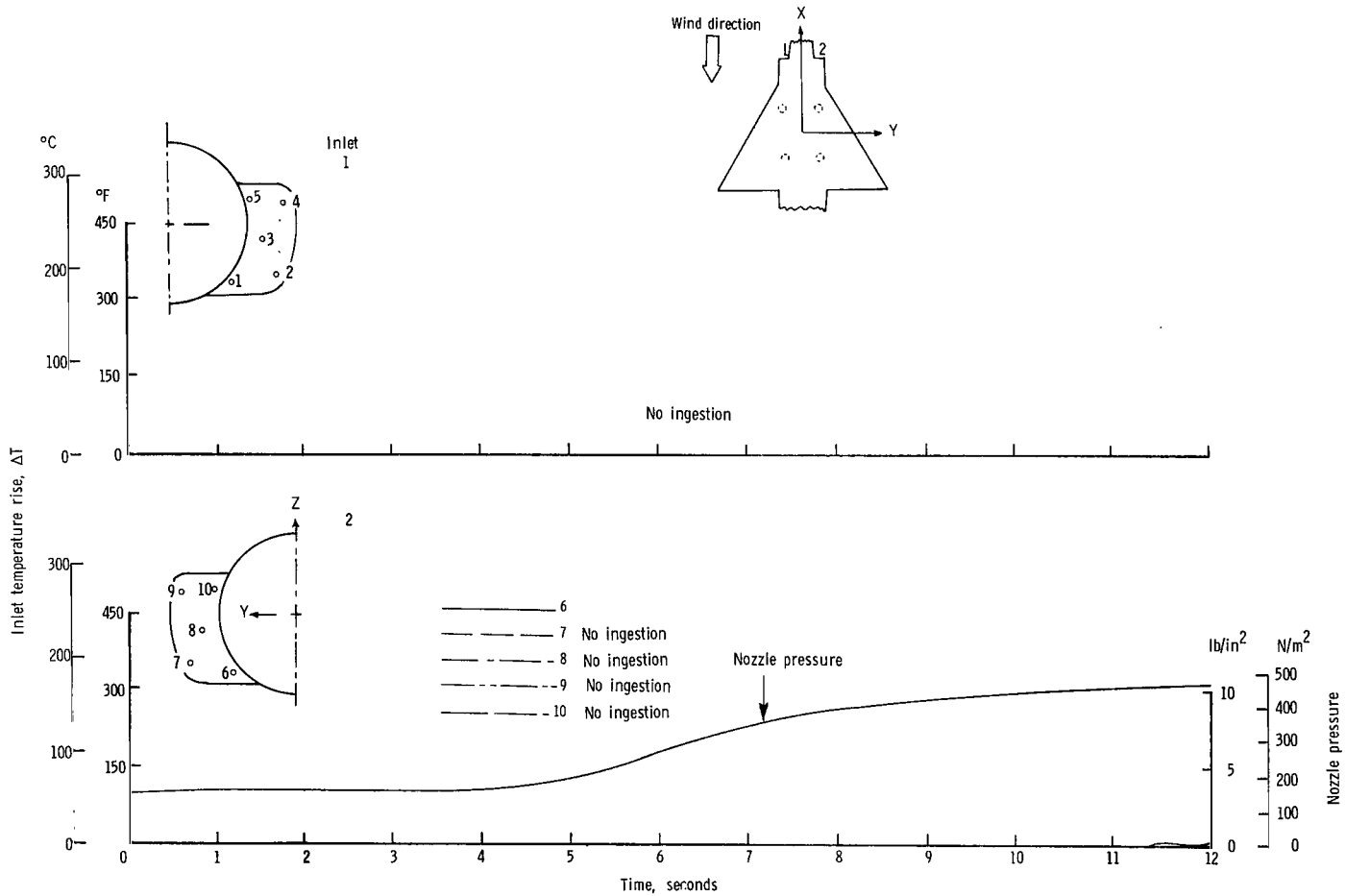

(e) $\psi = 0^0$; V = 23.70 knots.

Figure 20.- Continued.

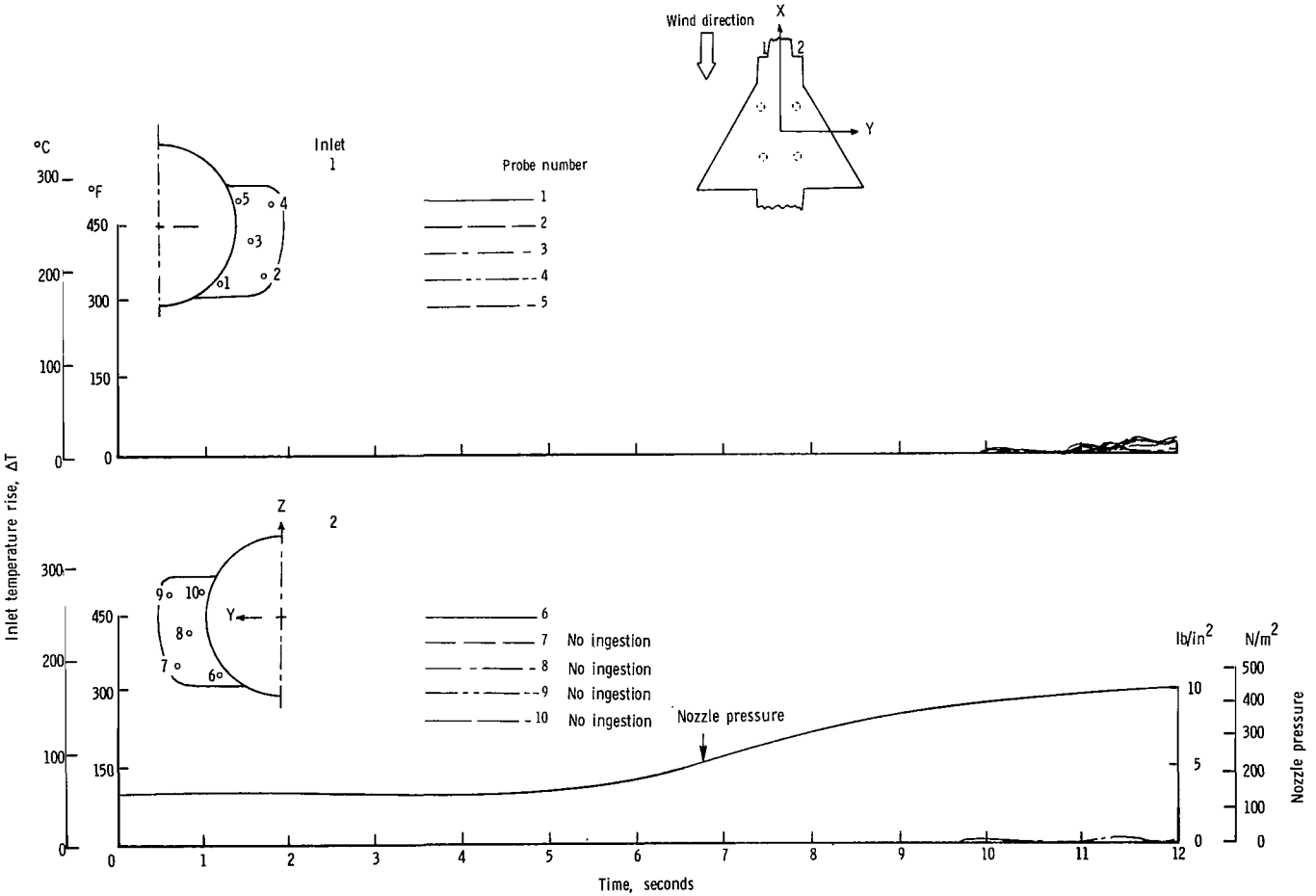

(f) $\psi = 0^0$; V = 29.63 knots.

Figure 20.- Continued.

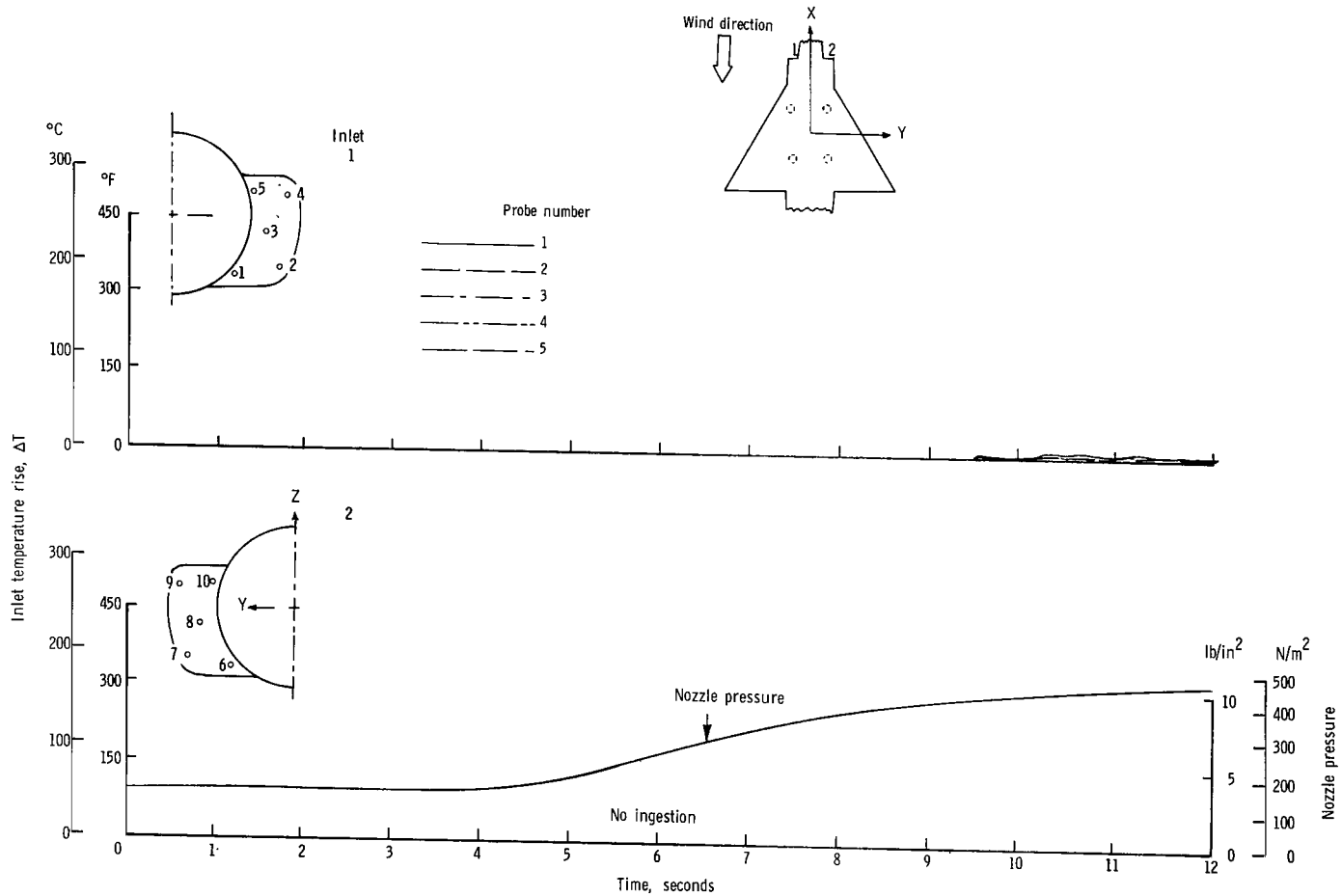

(g) $\psi = 0^0$; V = 35.55 knots.

Figure 20.- Continued.

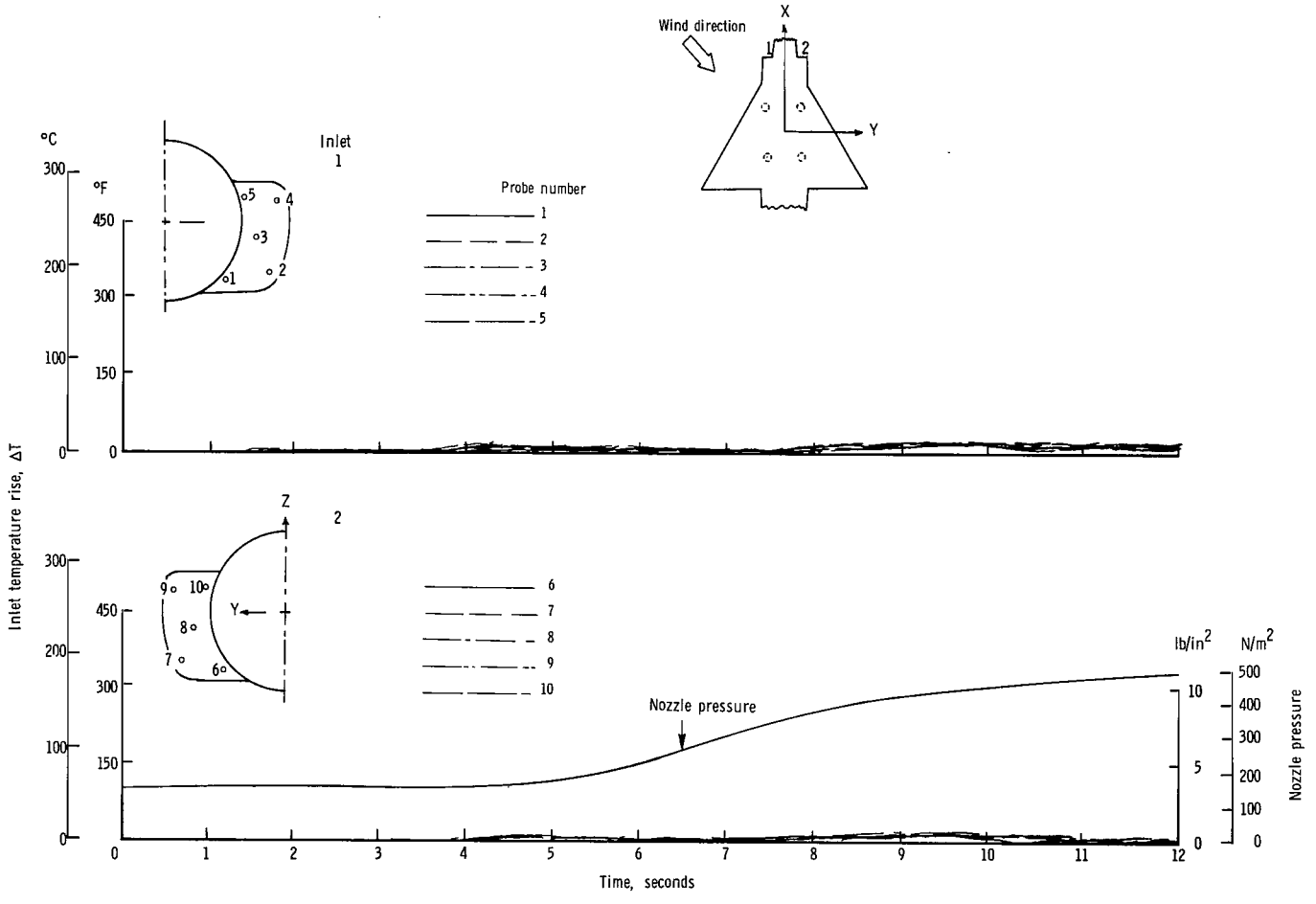

(h) $\psi = 45^0$; V = 5.92 knots.

Figure 20.- Continued.

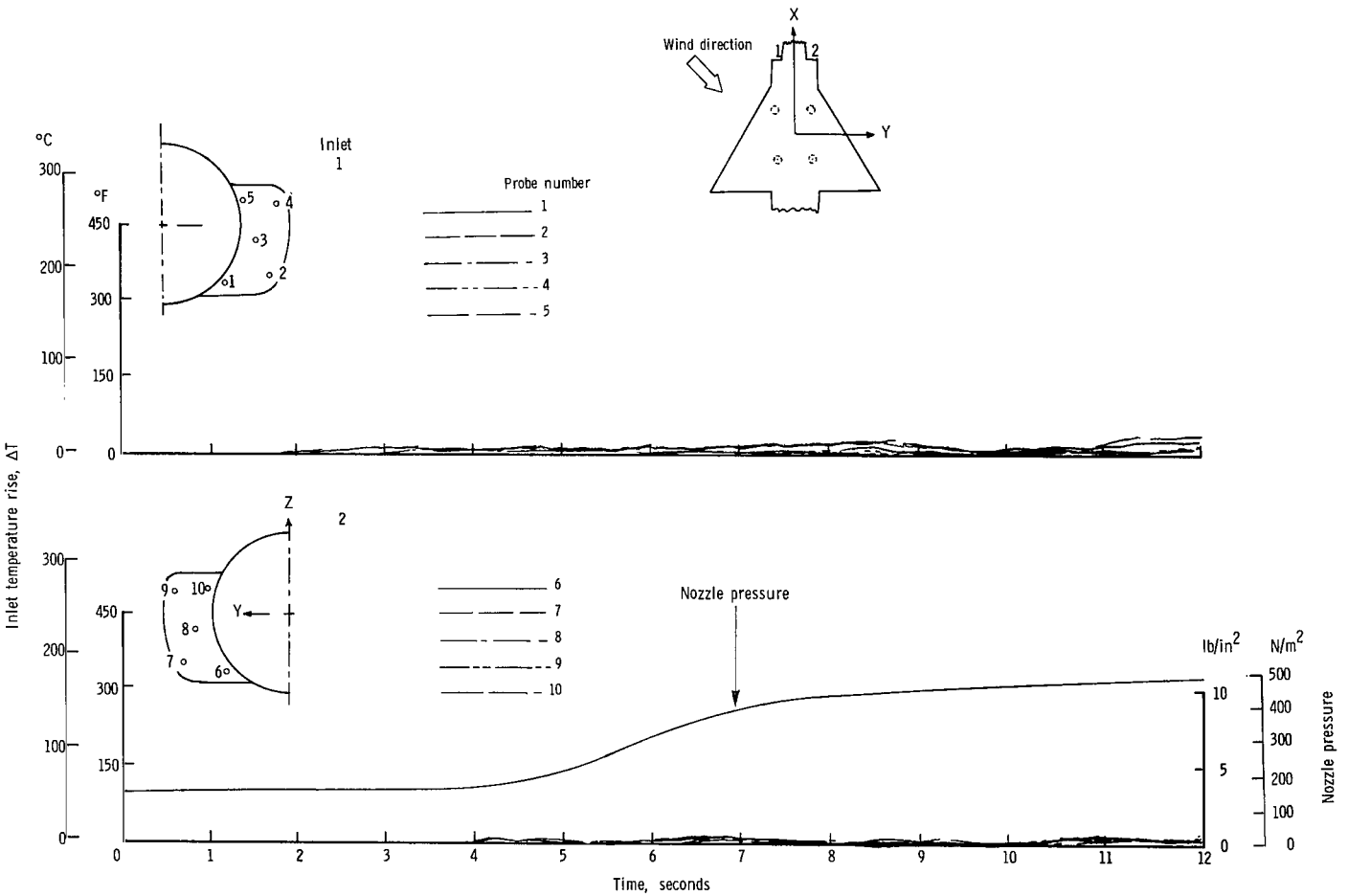

(i) $\psi = 45^0$; V = 11.85 knots.

Figure 20.- Continued.

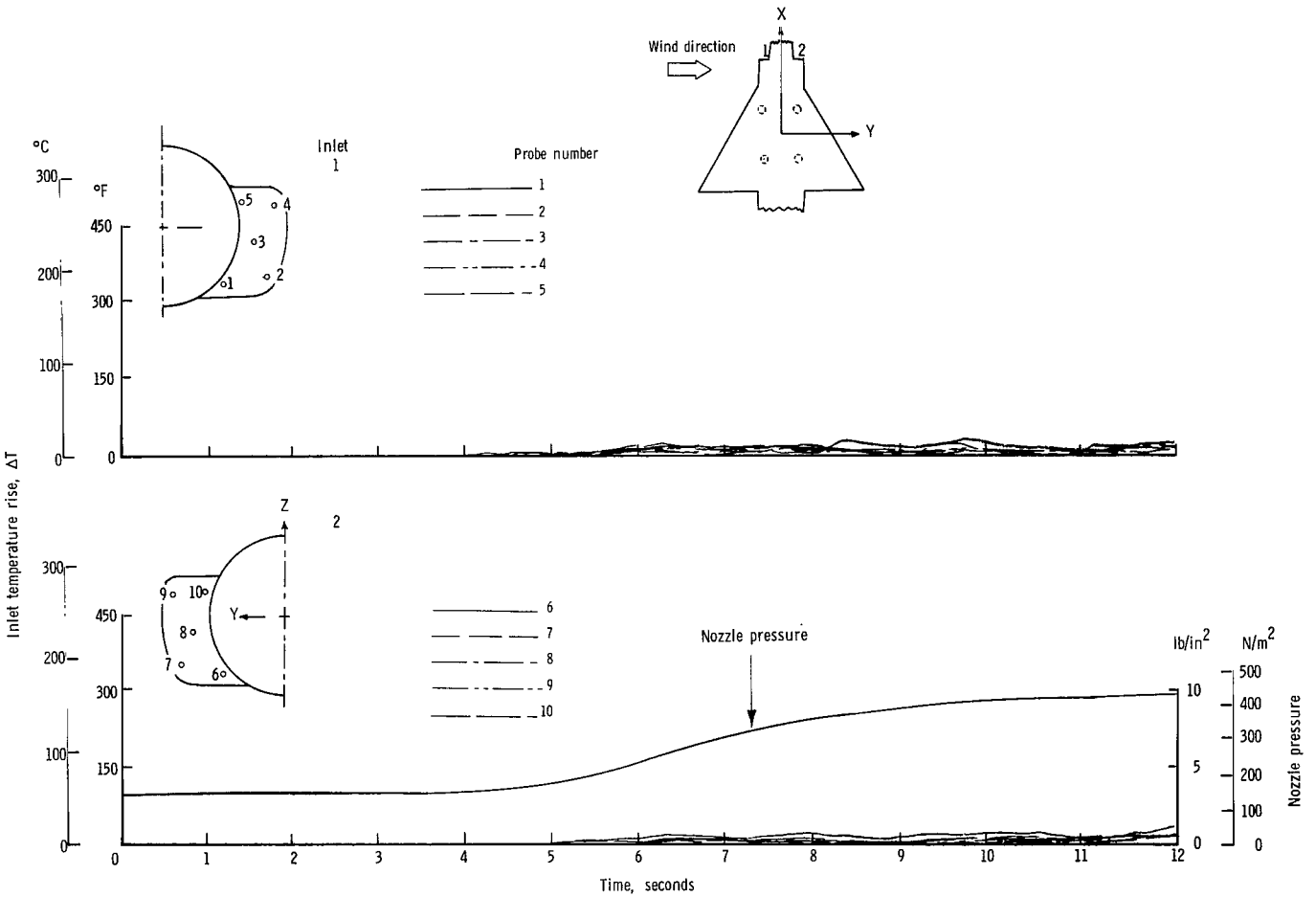

(j) $\psi = 90^0$; V = 5.92 knots.

Figure 20.- Continued.

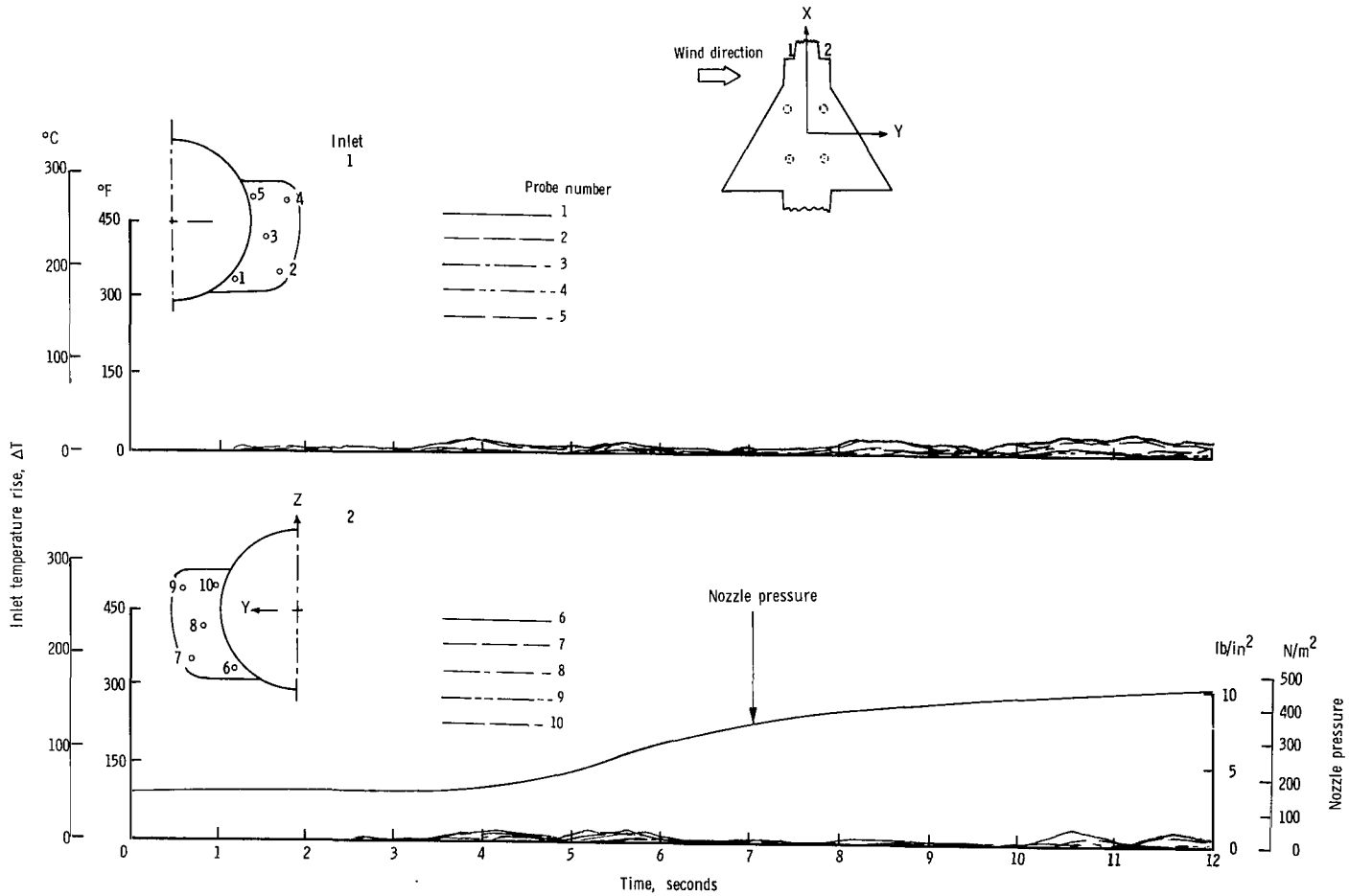

(k) $\psi = 90^{0}$; V = 11.85 knots.

Figure 20.- Concluded.

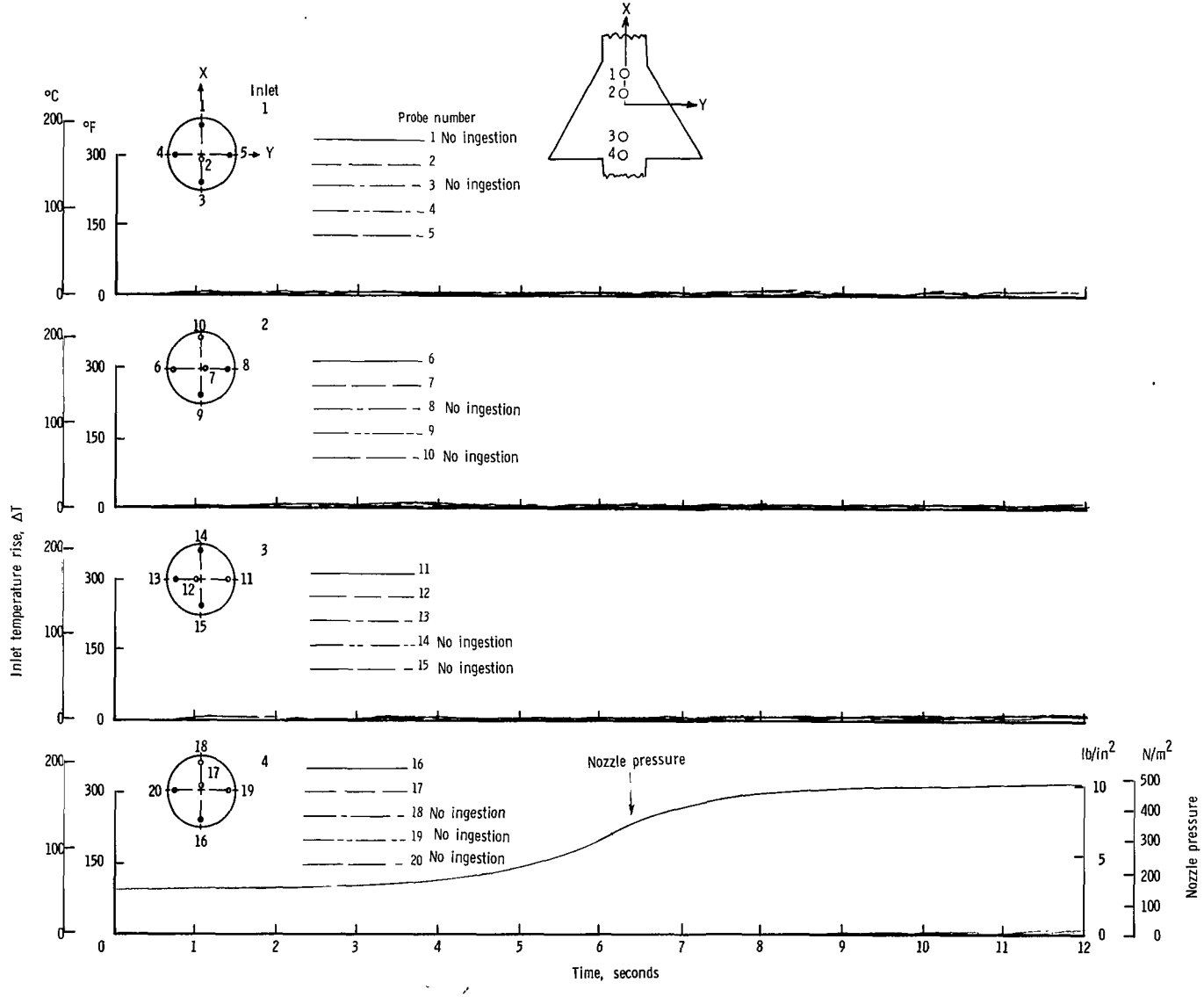

(a) $\psi = 0^{o}$; V = 0 knots.

Figure 21.- Variation of inlet air temperature rise with time for the in-line nozzle arrangement with top inlets and high delta wing. $h/D_e = 1.17$.

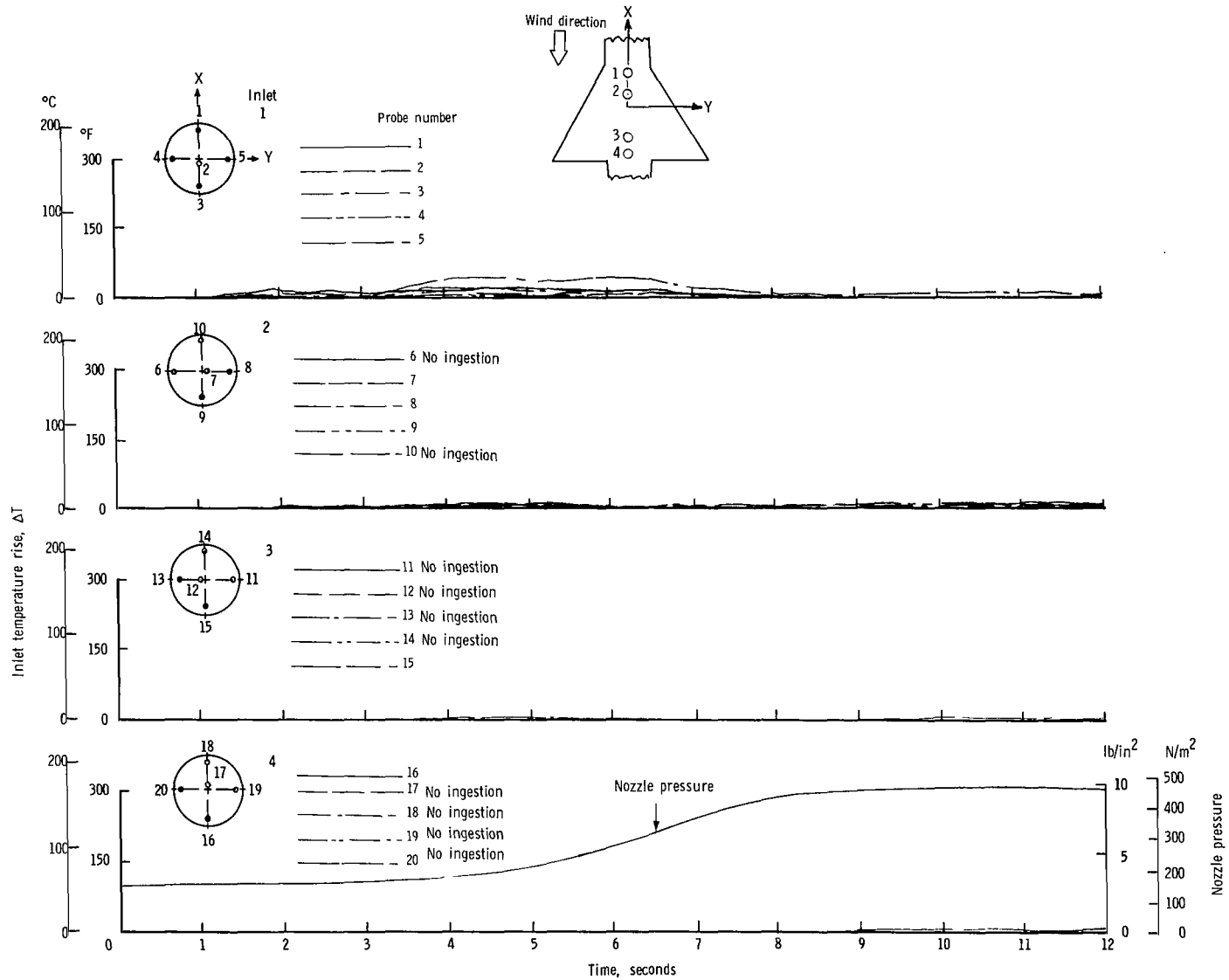

(b) $\psi = 0^{0}$; V = 5.92 knots.

Figure 21.- Continued.

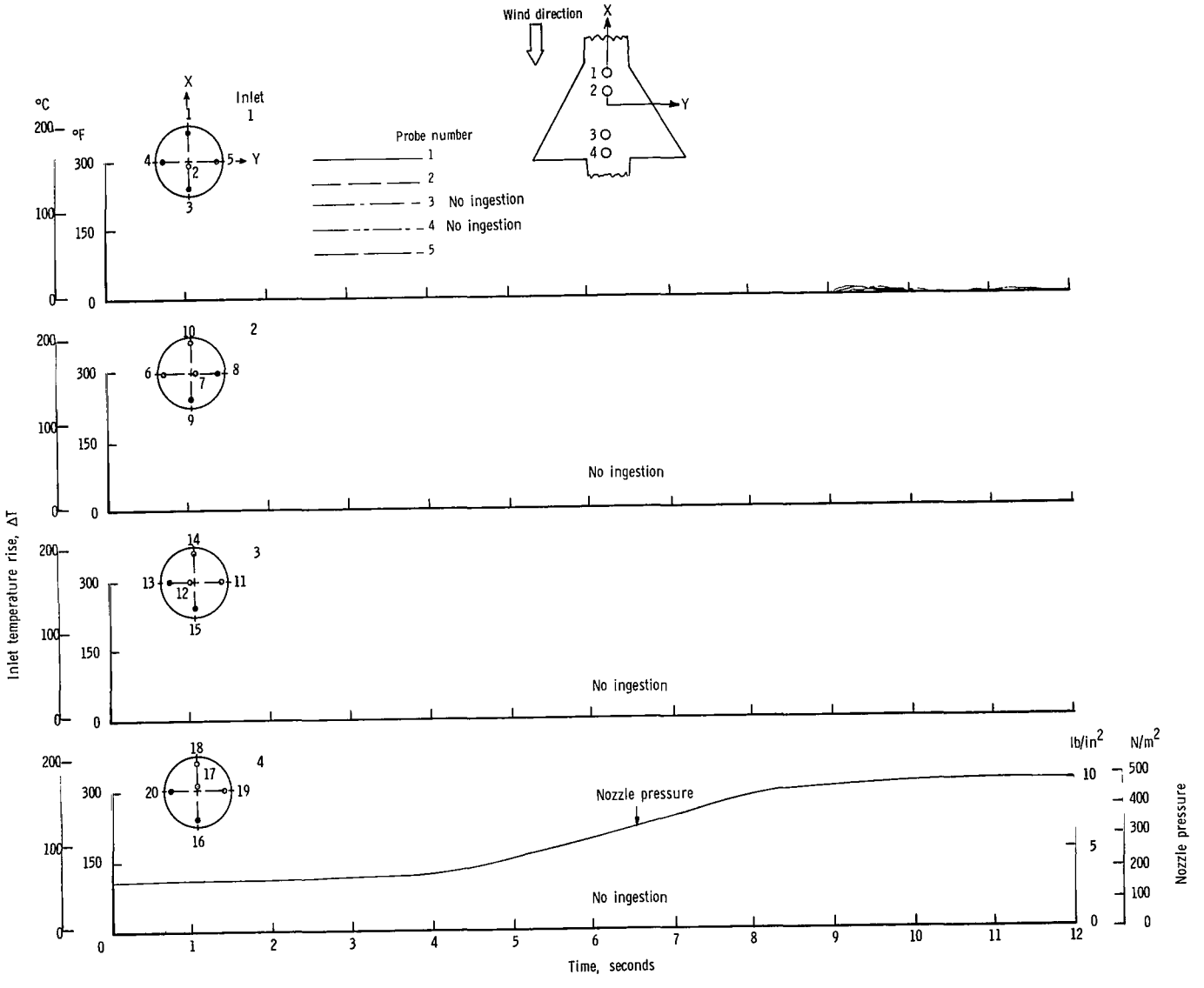

(c) $\psi = 0^0$; V = 11.85 knots.

Figure 21.- Continued.

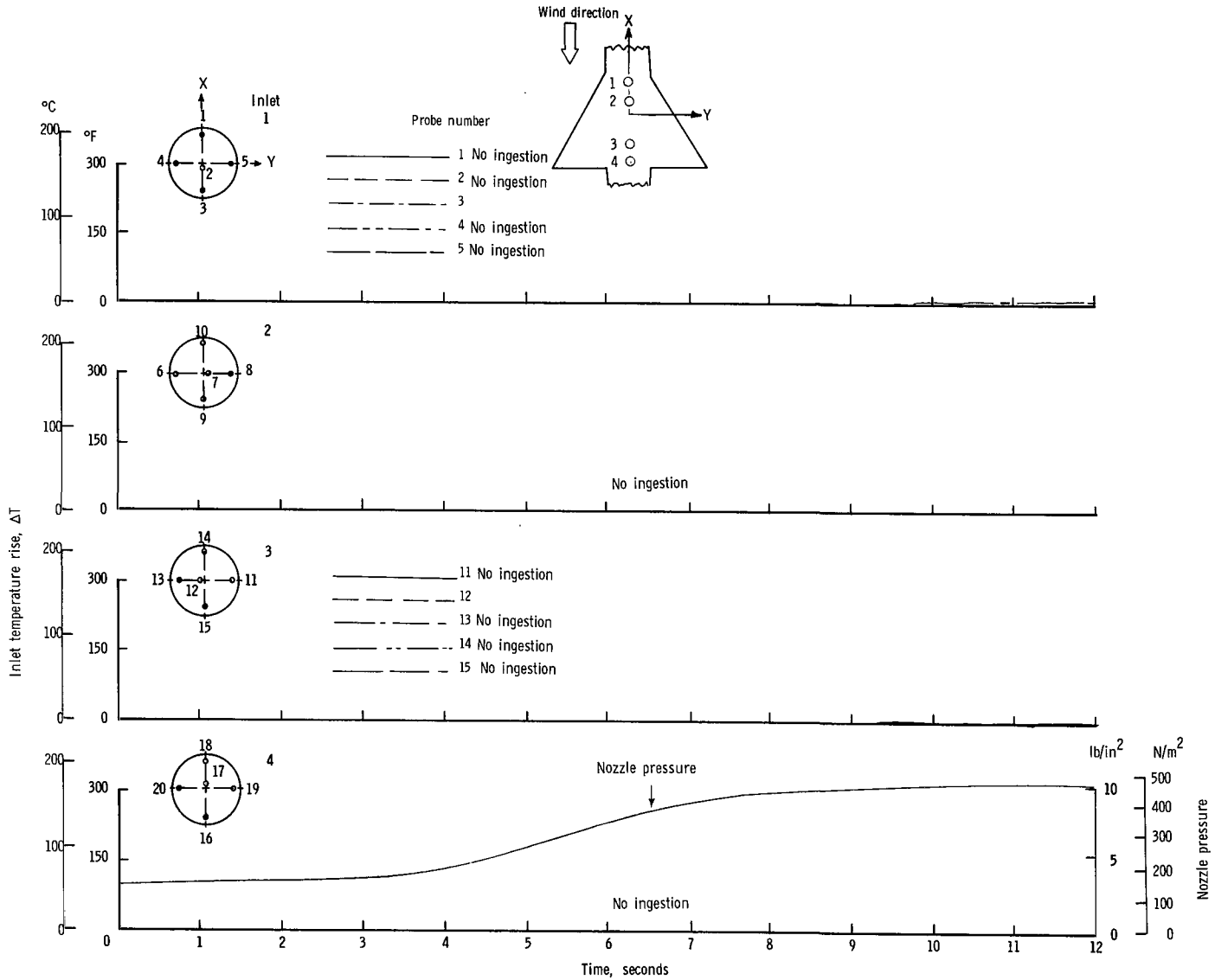

(d) $\psi = 0^0$; V = 17.78 knots.

Figure 21.- Continued.

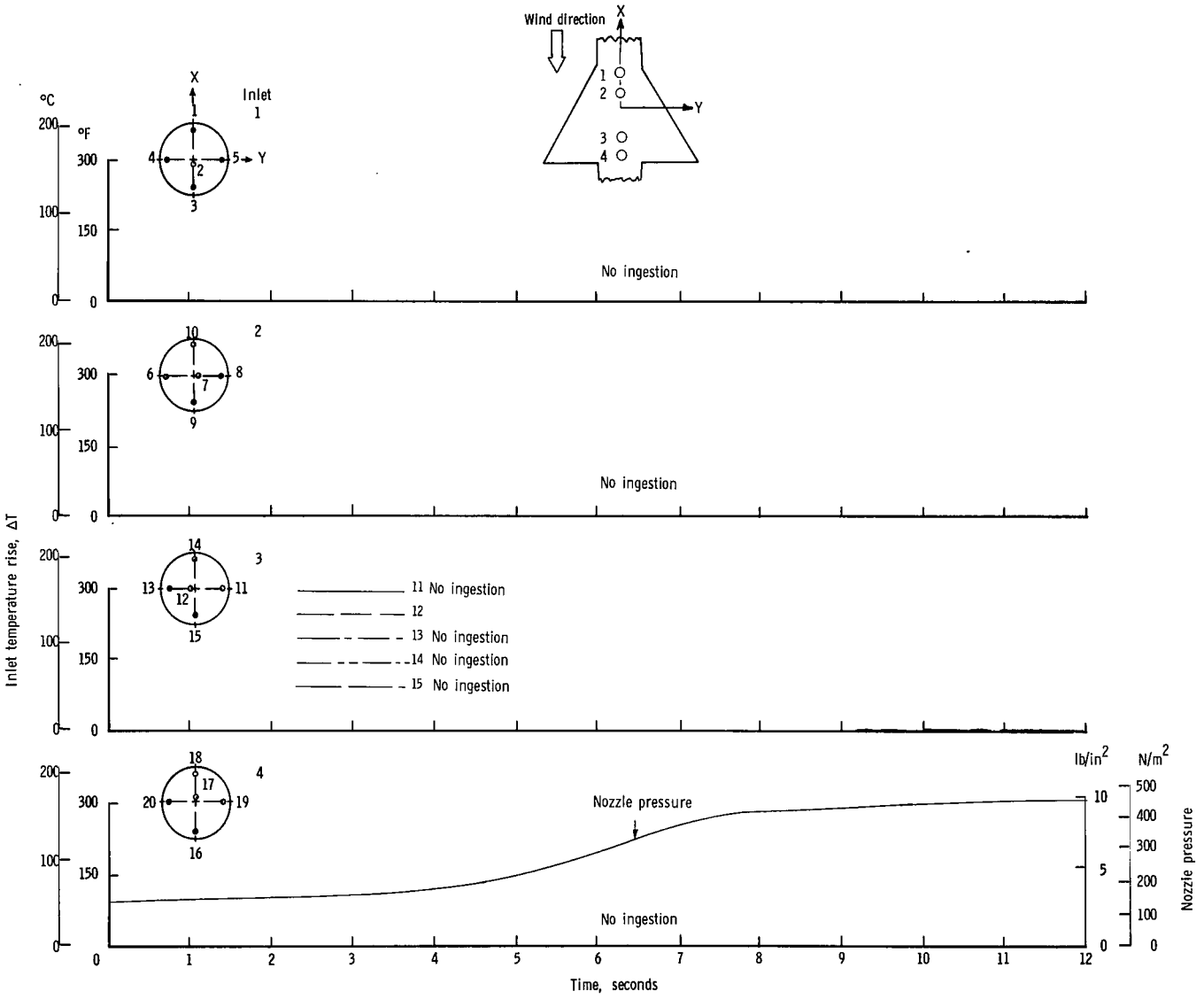

(e) $\psi = 0^0$; V = 23.70 knots.

Figure 21.- Continued.

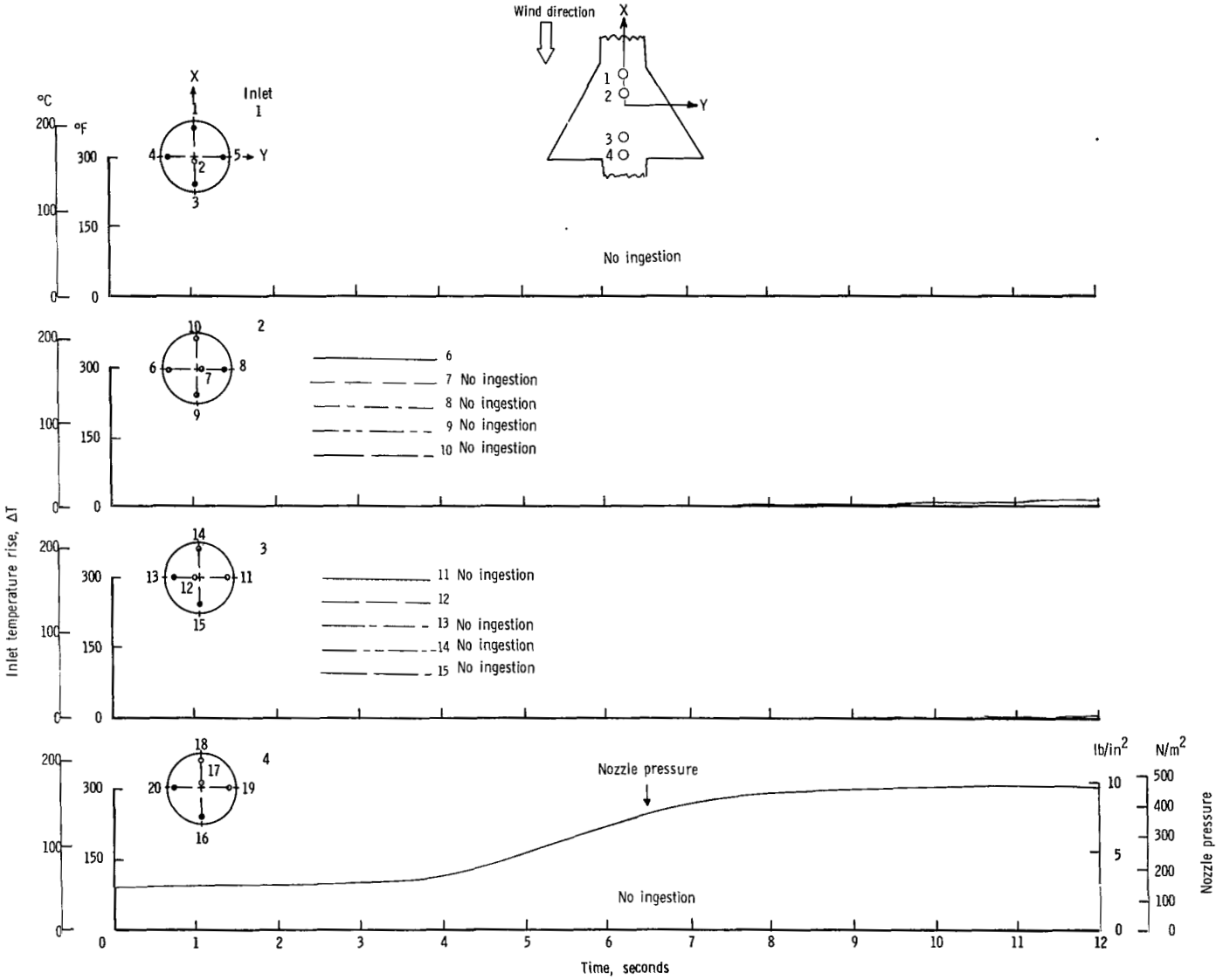

(f) $\psi = 0^0$; V = 29.63 knots.

Figure 21.- Continued.

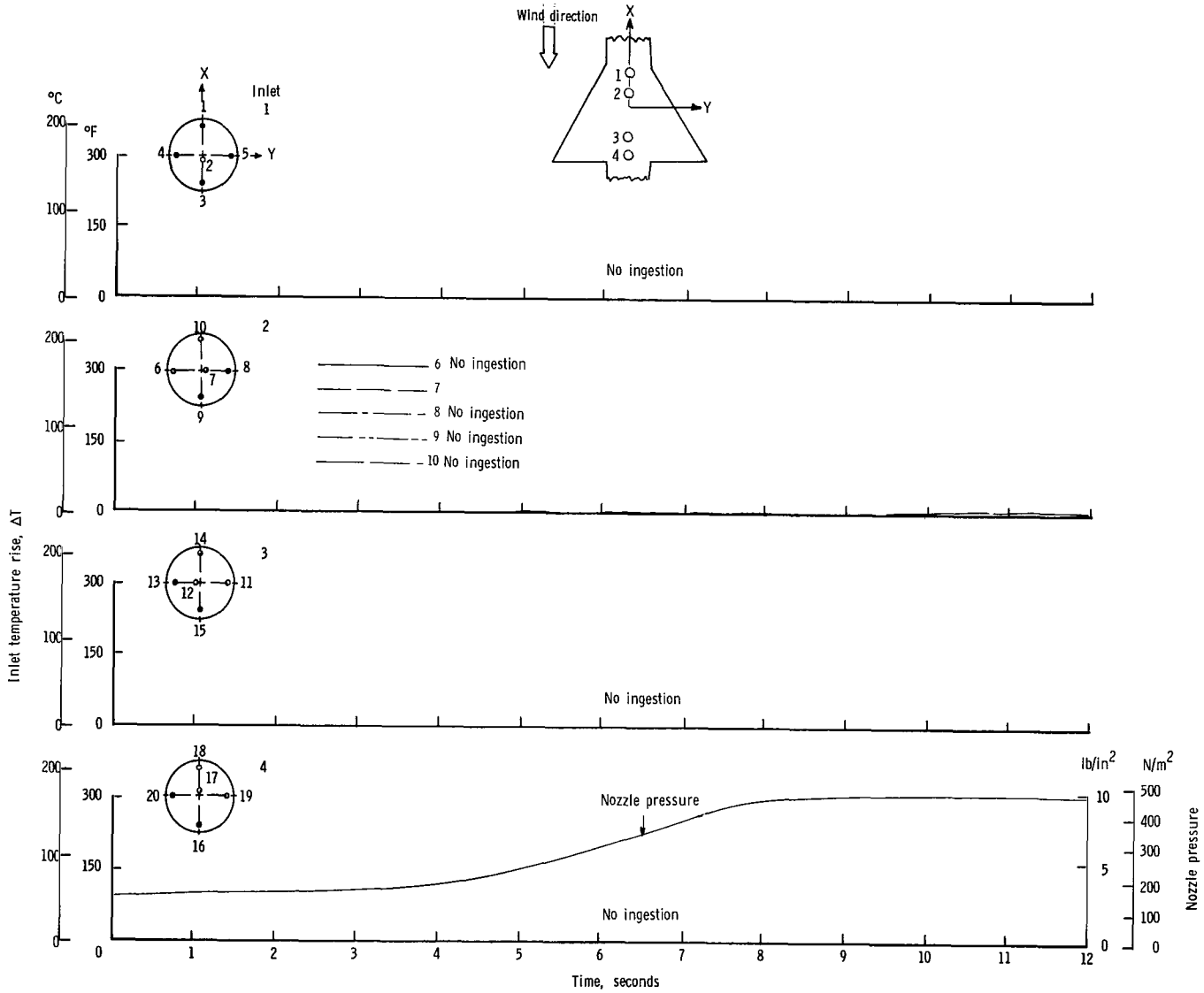

(g) $\psi = 0^0$; V = 35.55 knots.

Figure 21.- Continued.

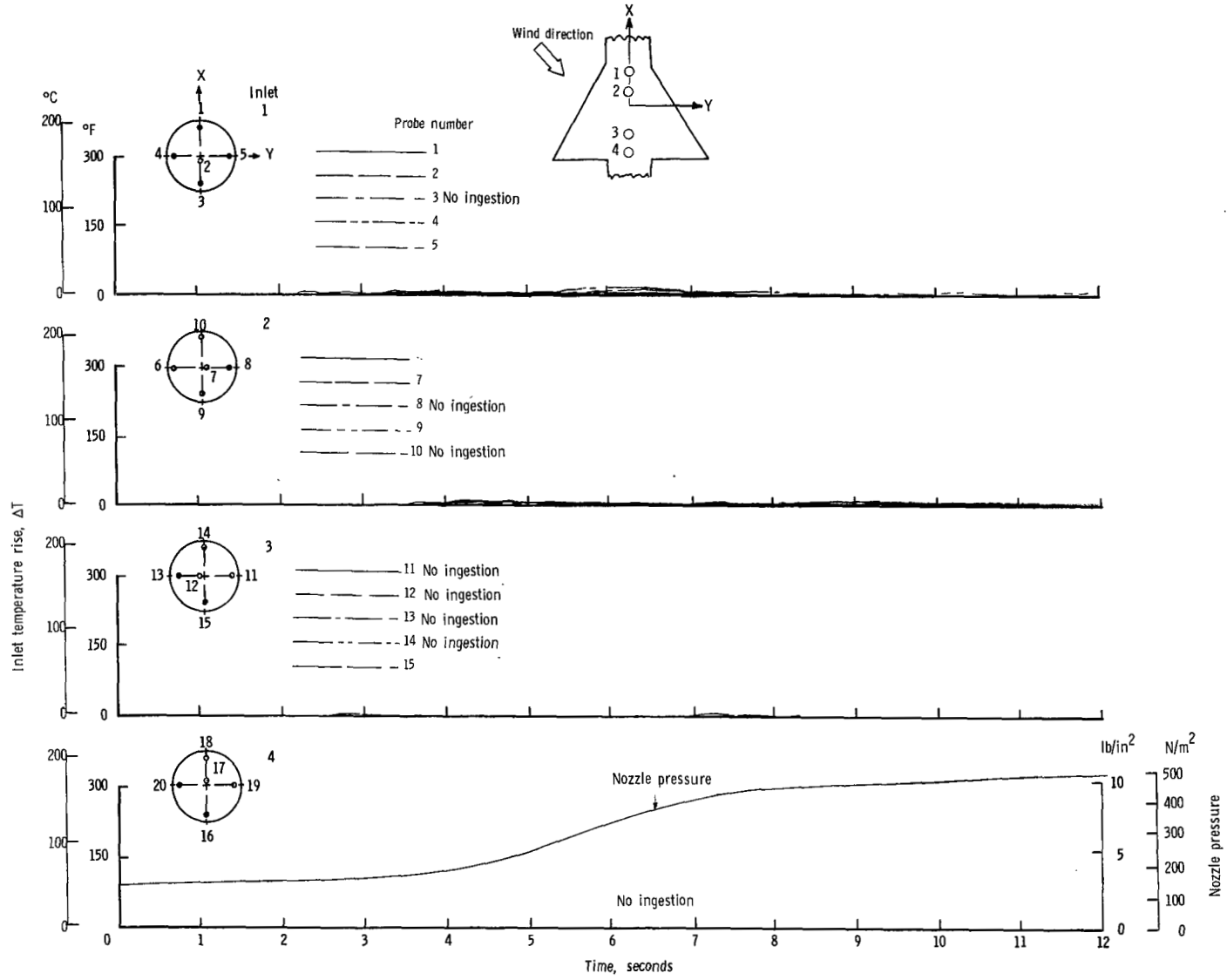

(h) $\psi = 45^{0}$; V = 5.92 knots.

Figure 21.- Continued.

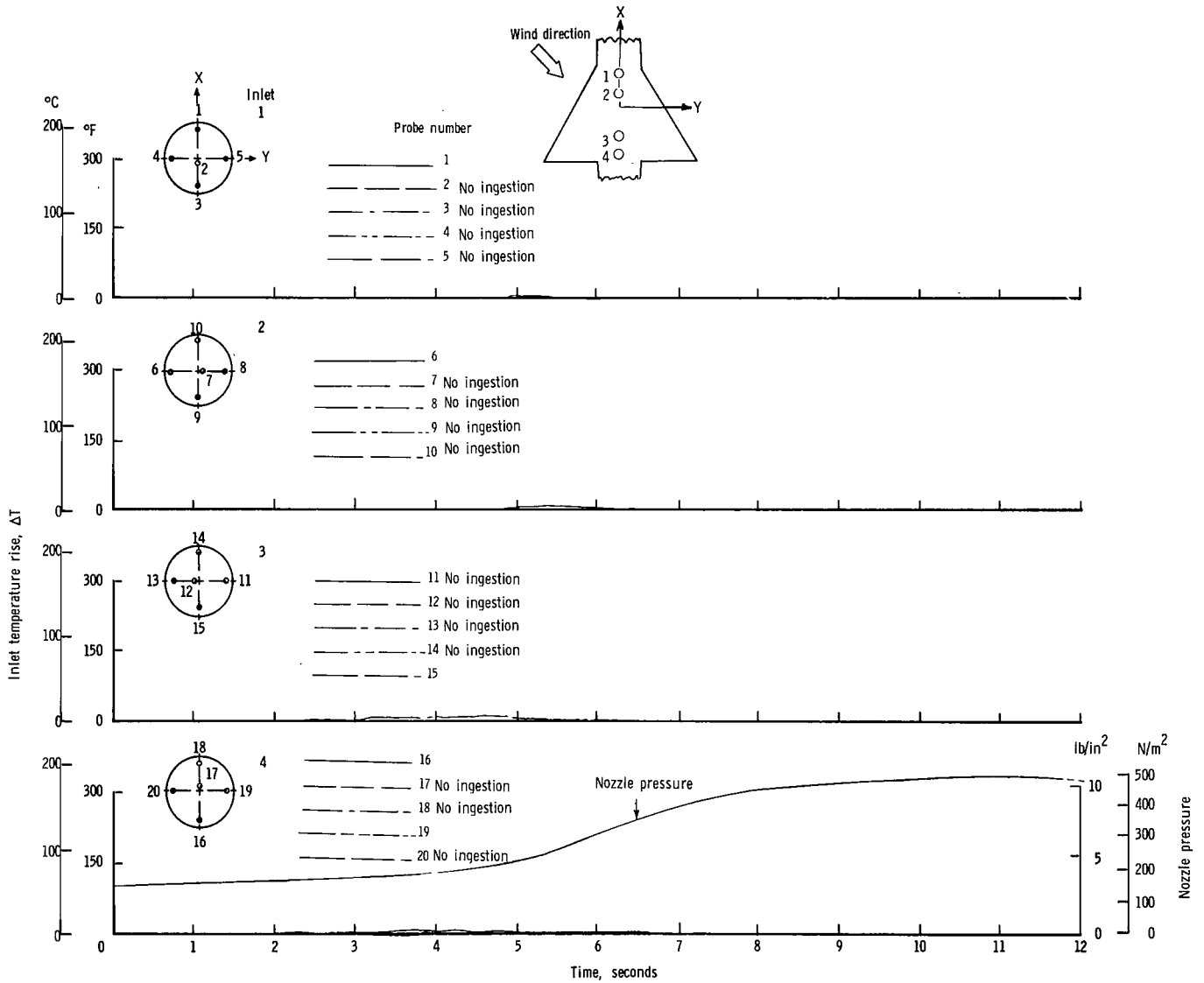

(i) $\psi = 45^0$; V = 11.85 knots.

Figure 21.- Continued.

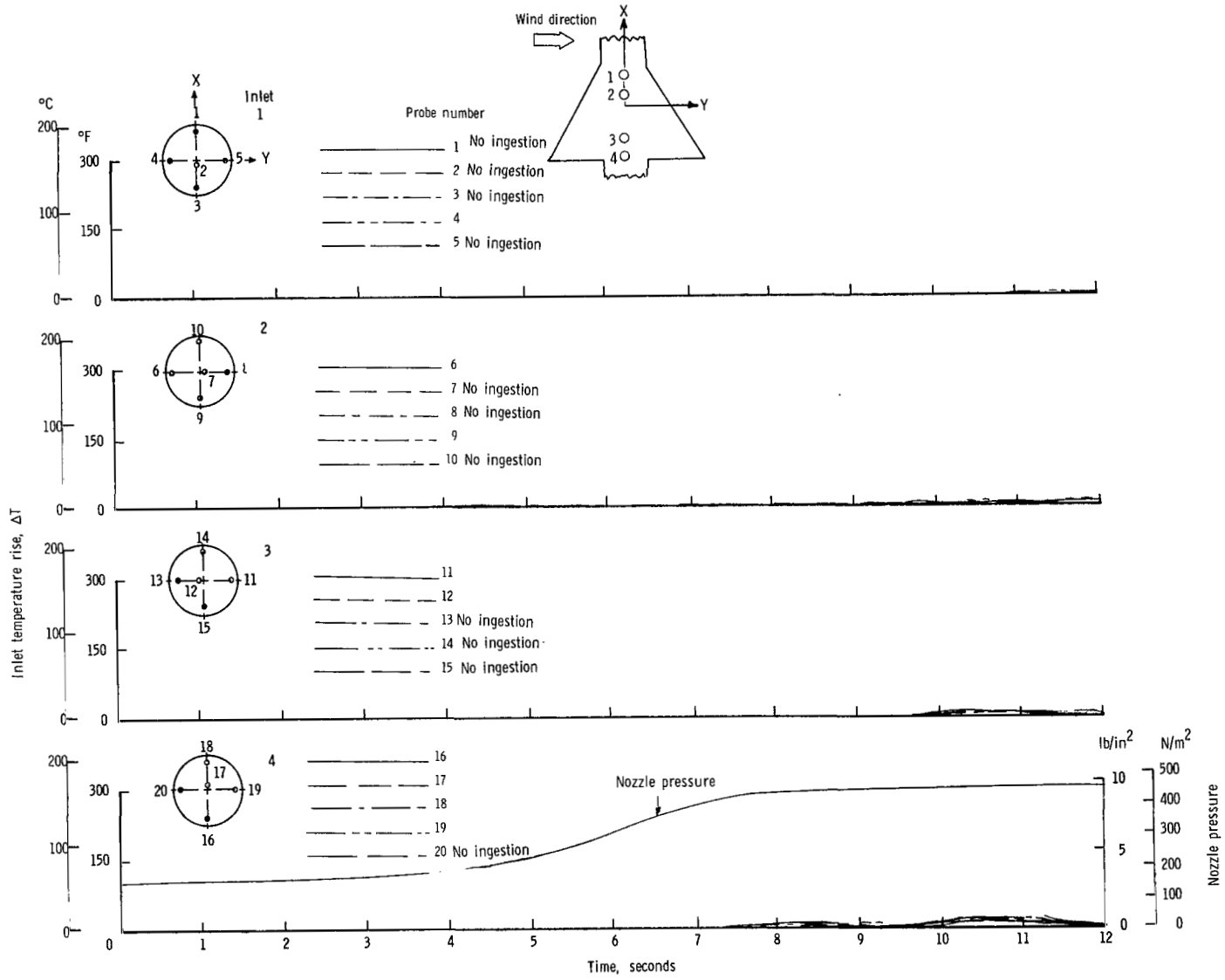

(j) $\psi = 90^0$; V = 5.92 knots.

Figure 21.- Continued.

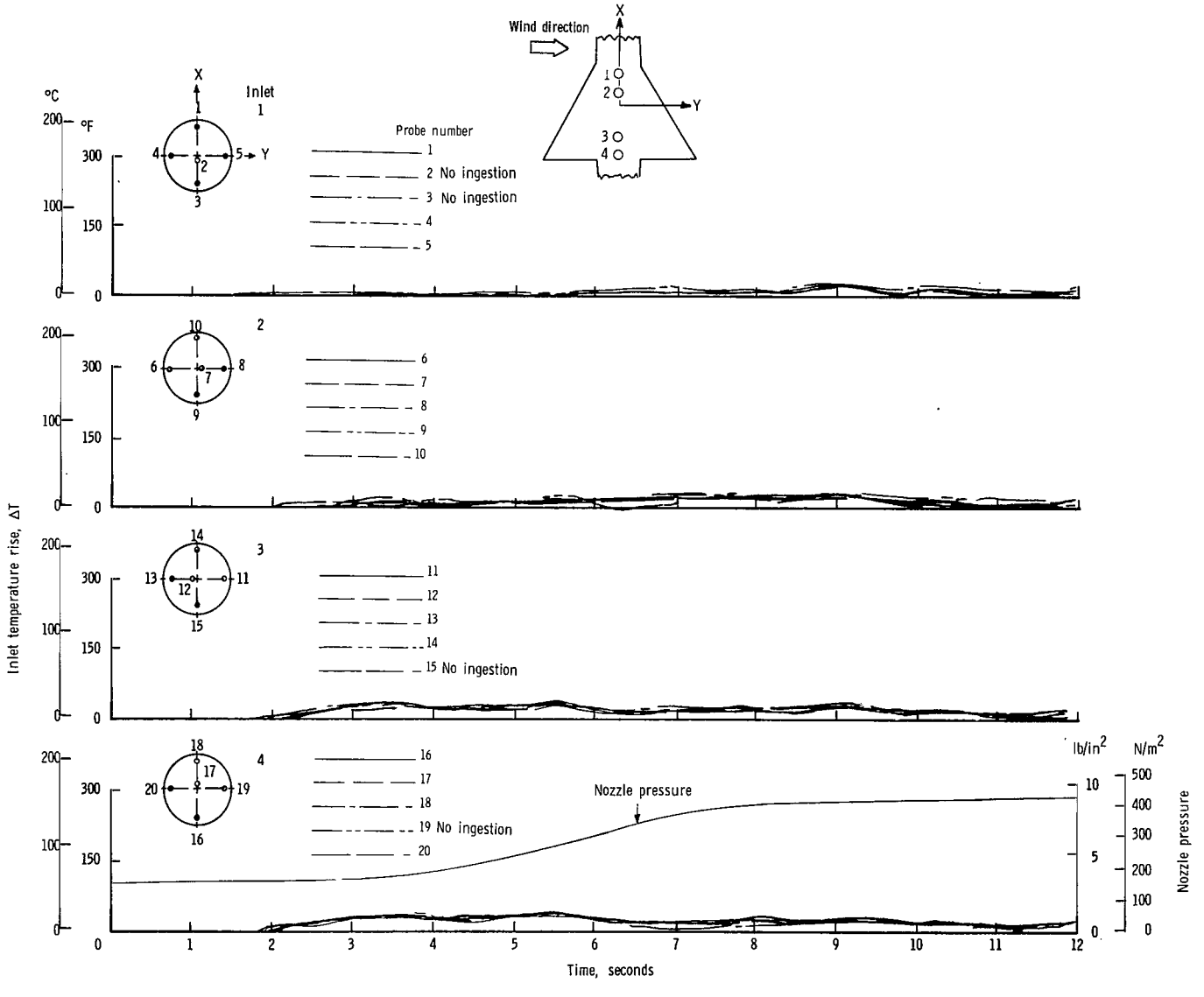

(k) $\psi = 90^{0}$; V = 11.85 knots.

Figure 21.- Concluded.

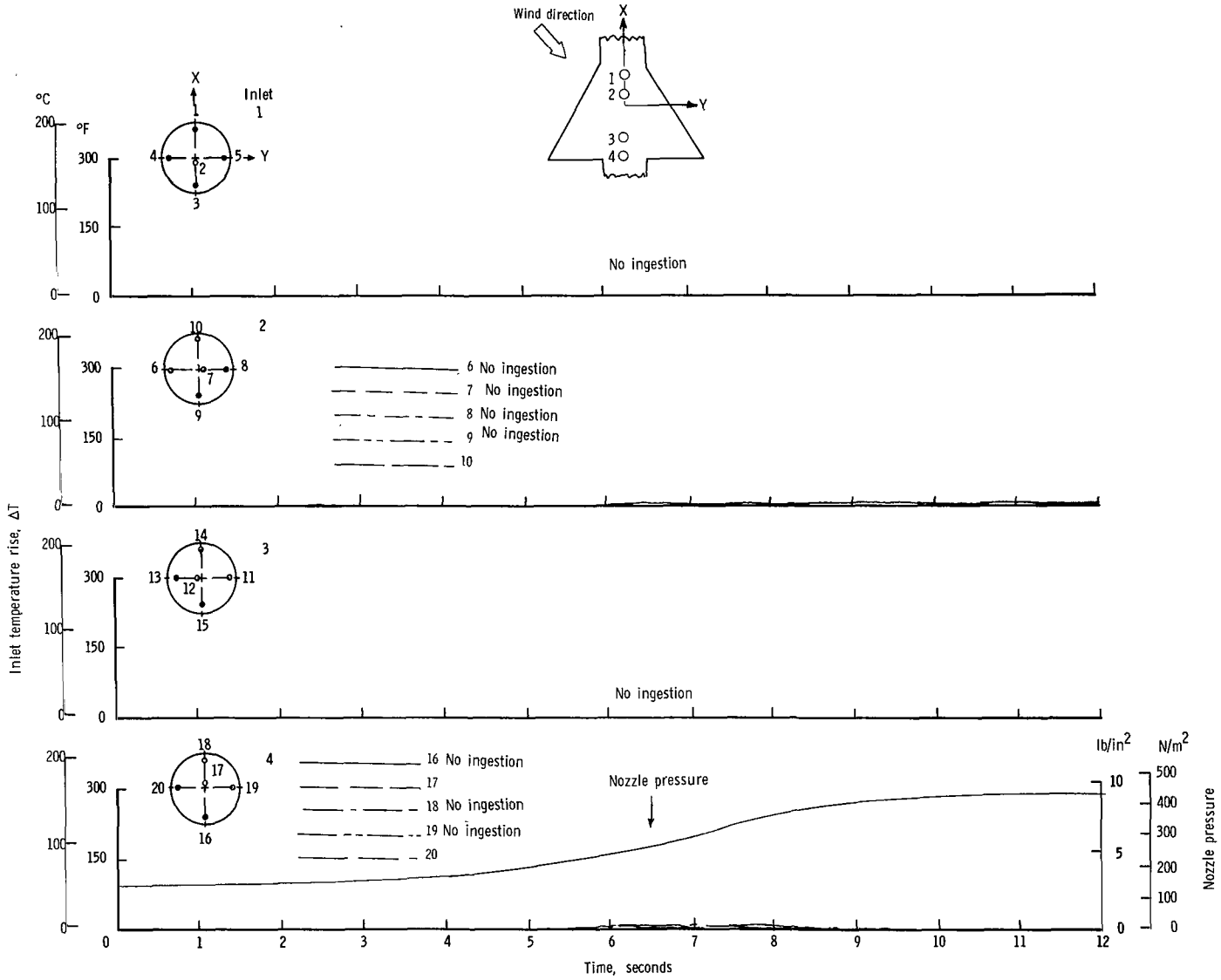

(a) $\psi = 45^{0}$; V = 5.92 knots.

Figure 22.- Variation of inlet air temperature rise with time for the in-line nozzle arrangement with top inlets and high delta wing. $h/D_e = 3.0$.

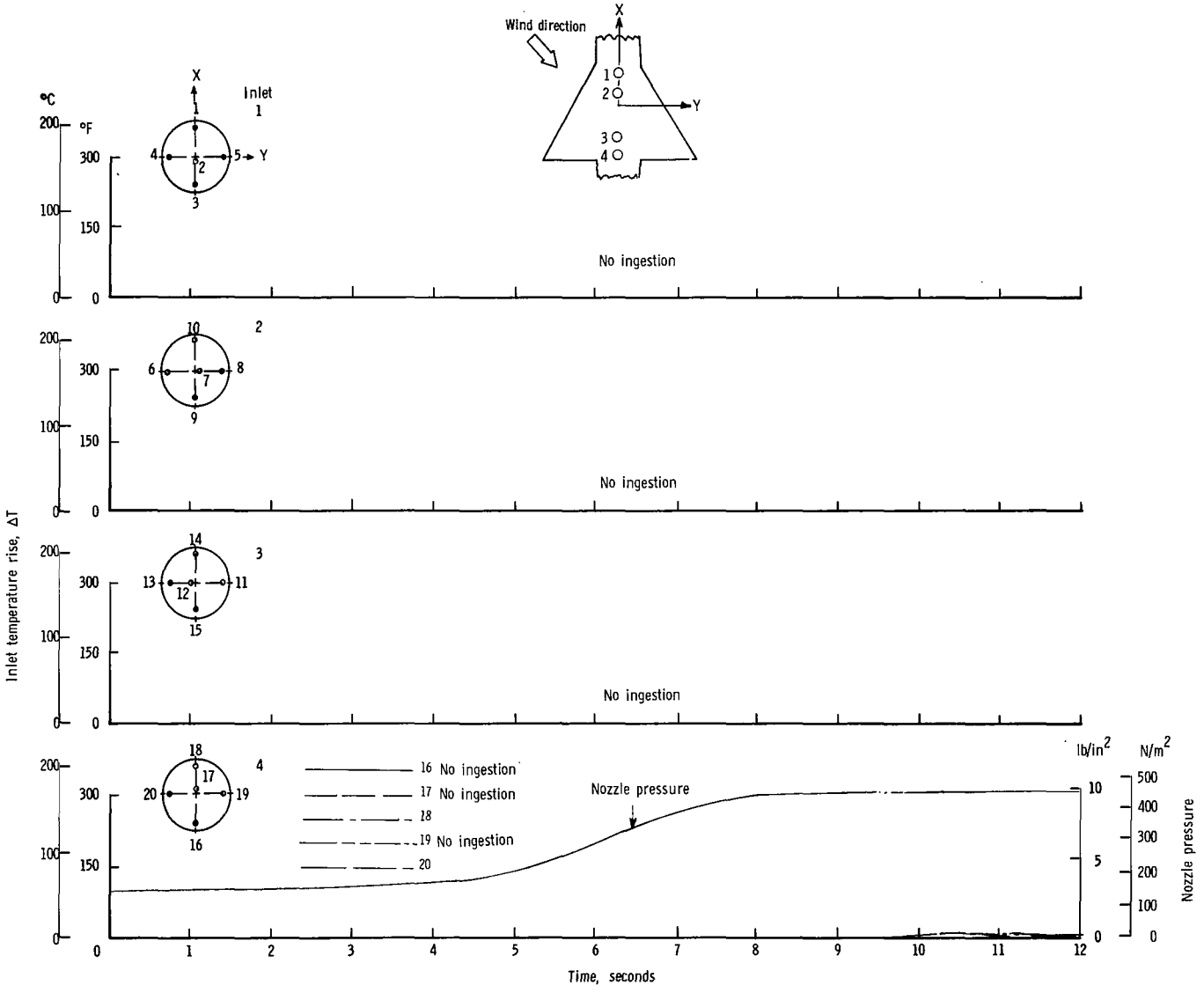

(b) $\psi = 45^{0}$; V = 11.85 knots.

Figure 22.- Continued.

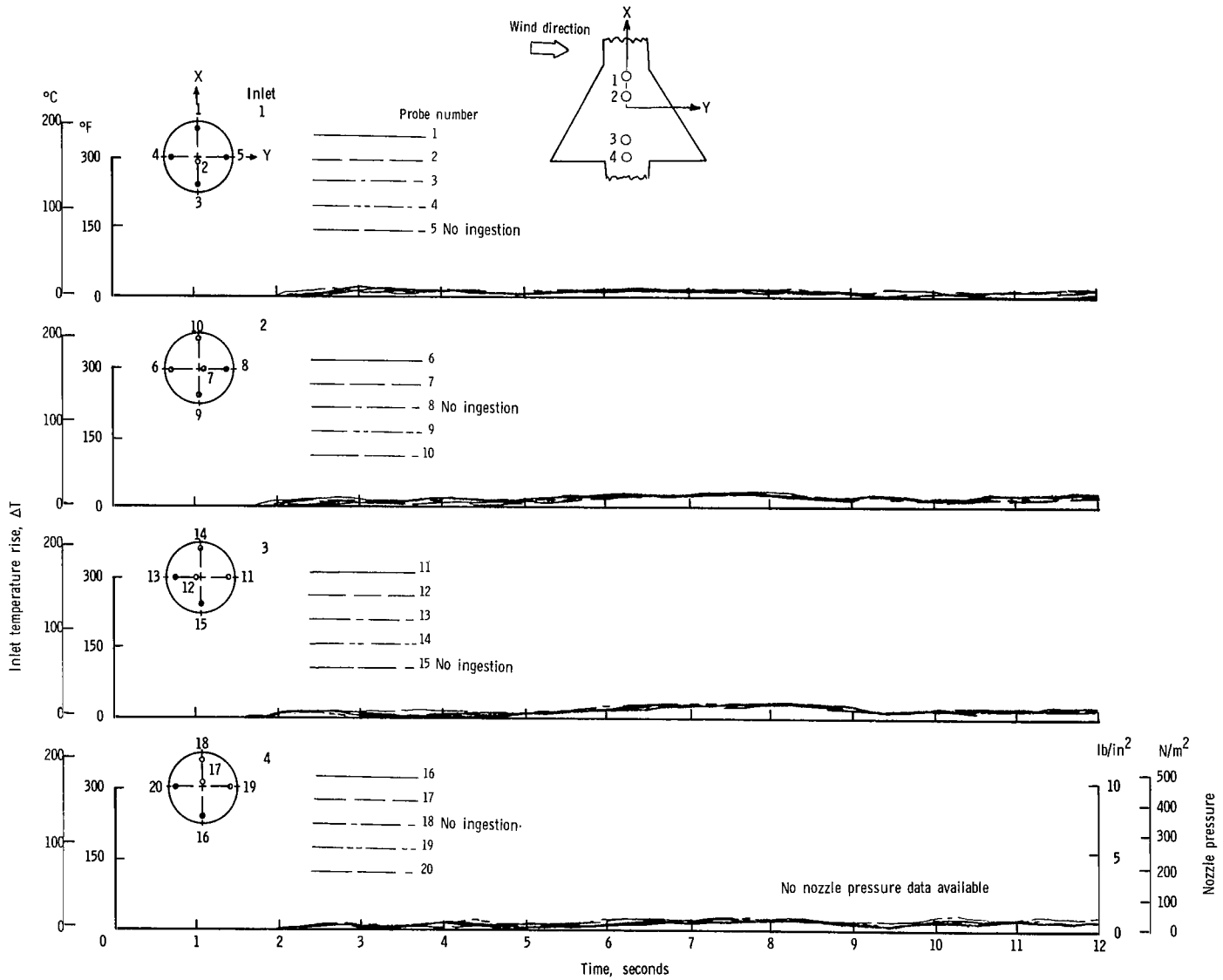

(c) $\psi = 90^0$; V = 5.92 knots.

Figure 22.- Continued.

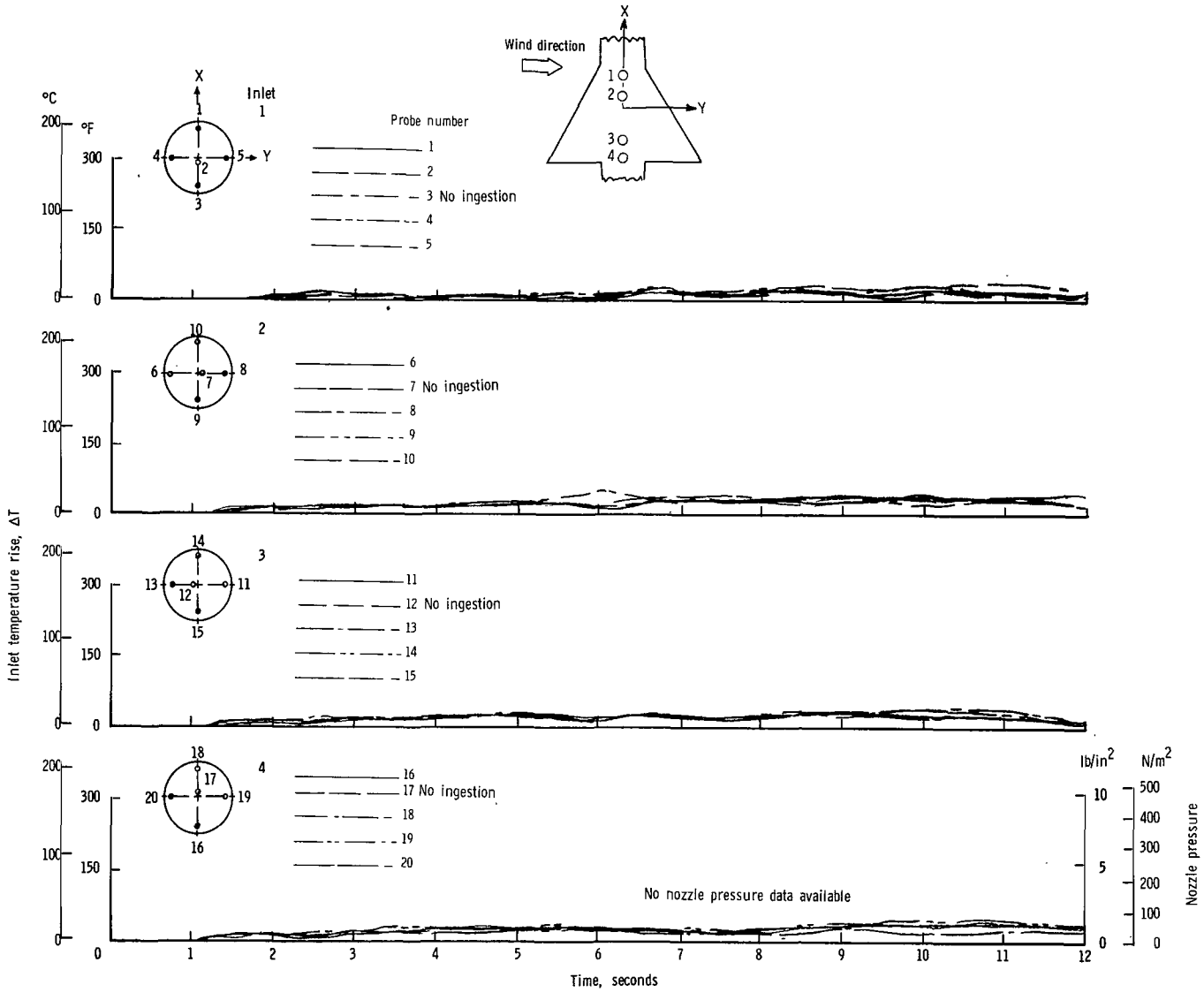

(d) $\psi = 90^{0}$; V = 11.85 knots.

Figure 22.- Concluded.

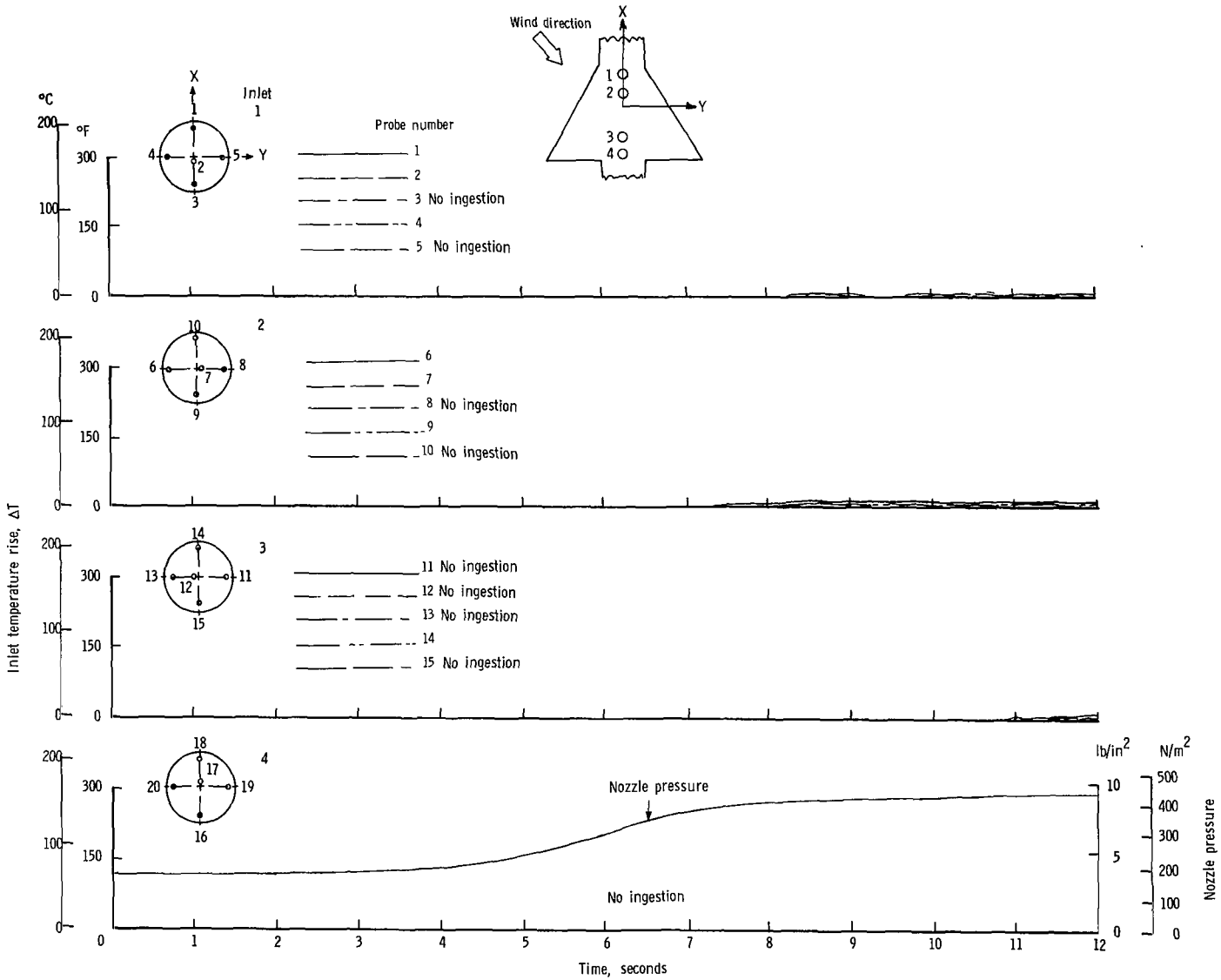

(a) $\psi = 45^0$; V = 5.92 knots.

Figure 23.- Variation of inlet air temperature rise with time for the in-line nozzle arrangement with top inlets and high delta wing. $h/D_e = 5.0$.

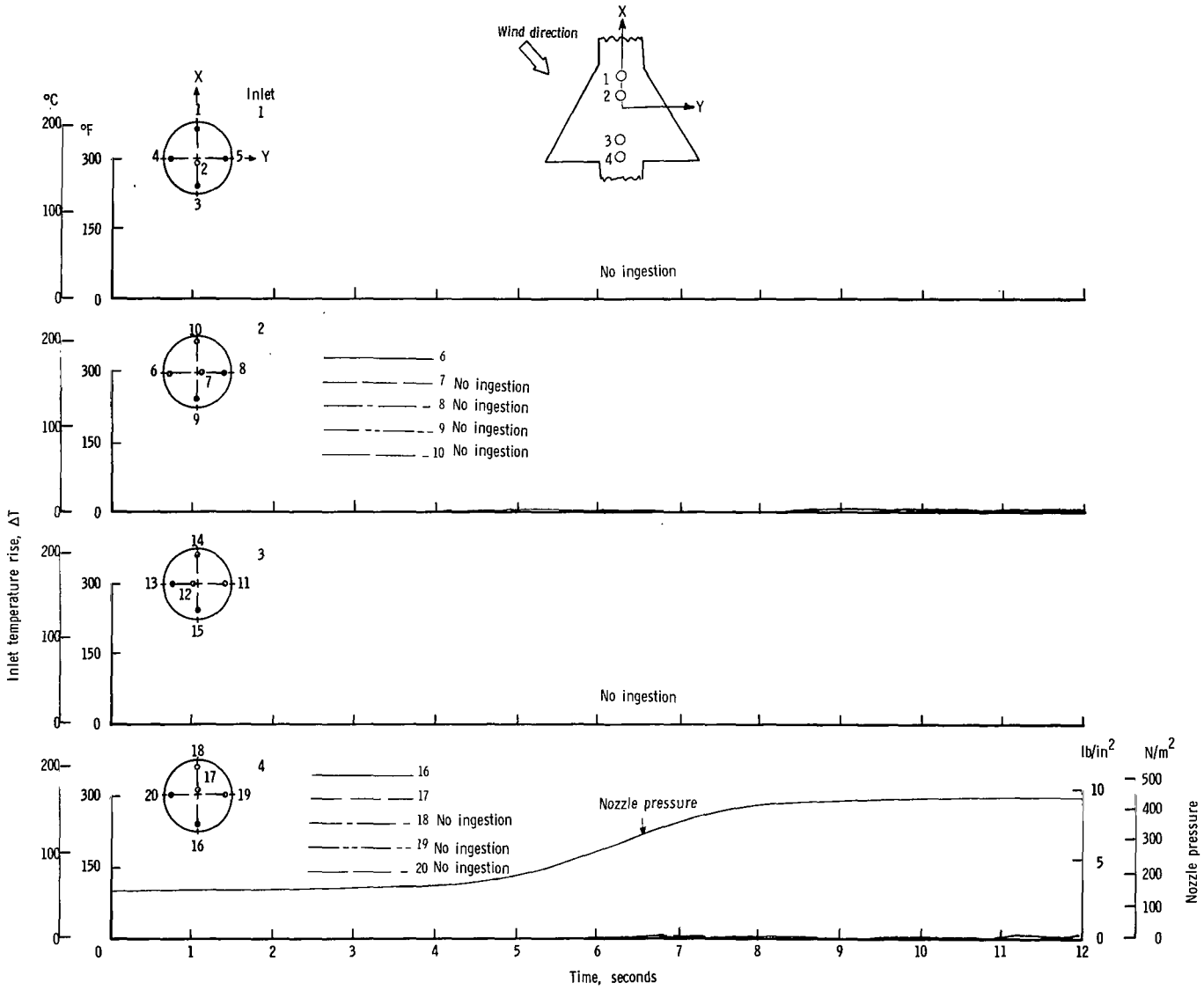

(b) $\psi = 45^0$; V = 11.85 knots.

Figure 23.- Continued.

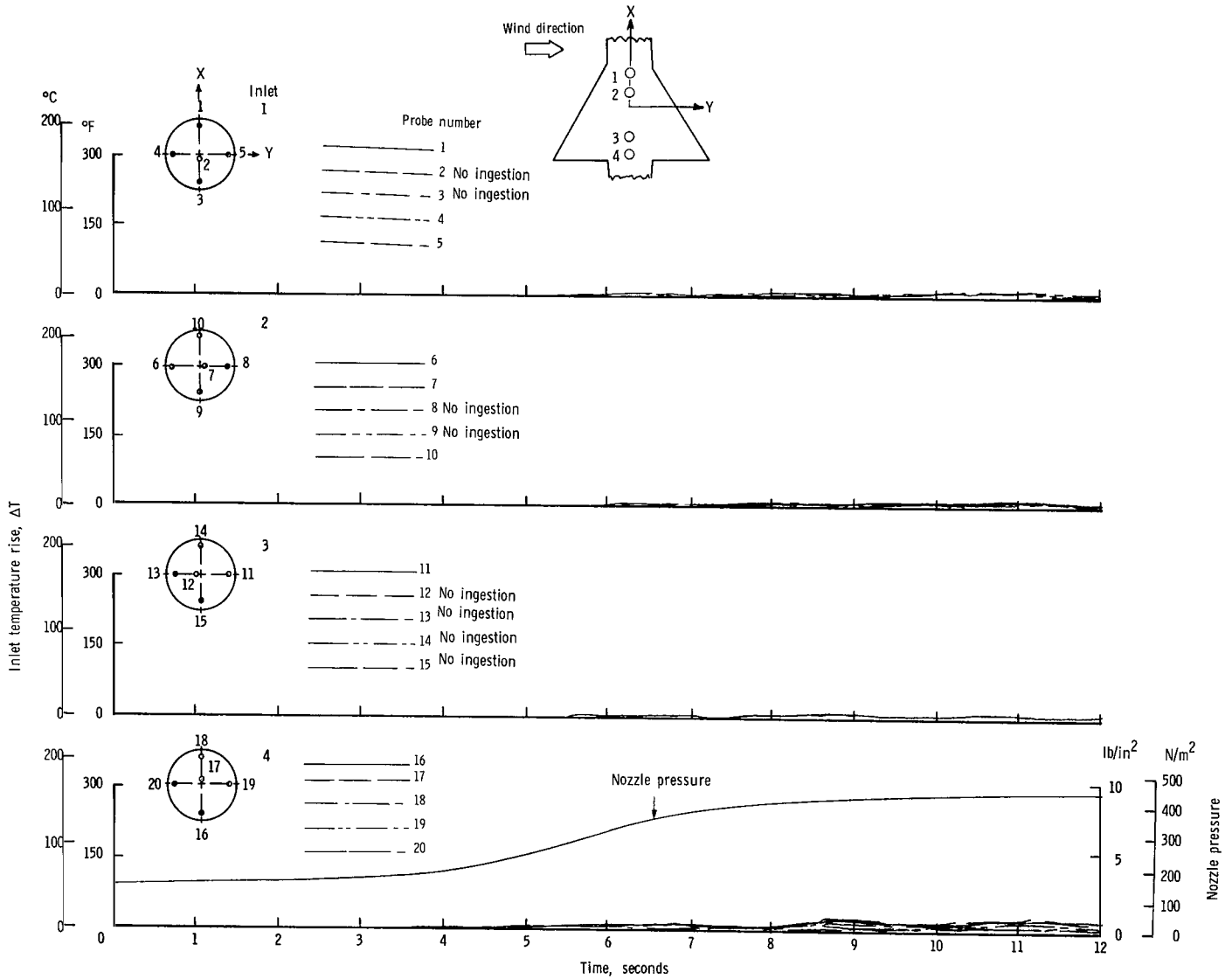

(c) $\psi = 90^0$; V = 5.92 knots.

Figure 23.- Continued.

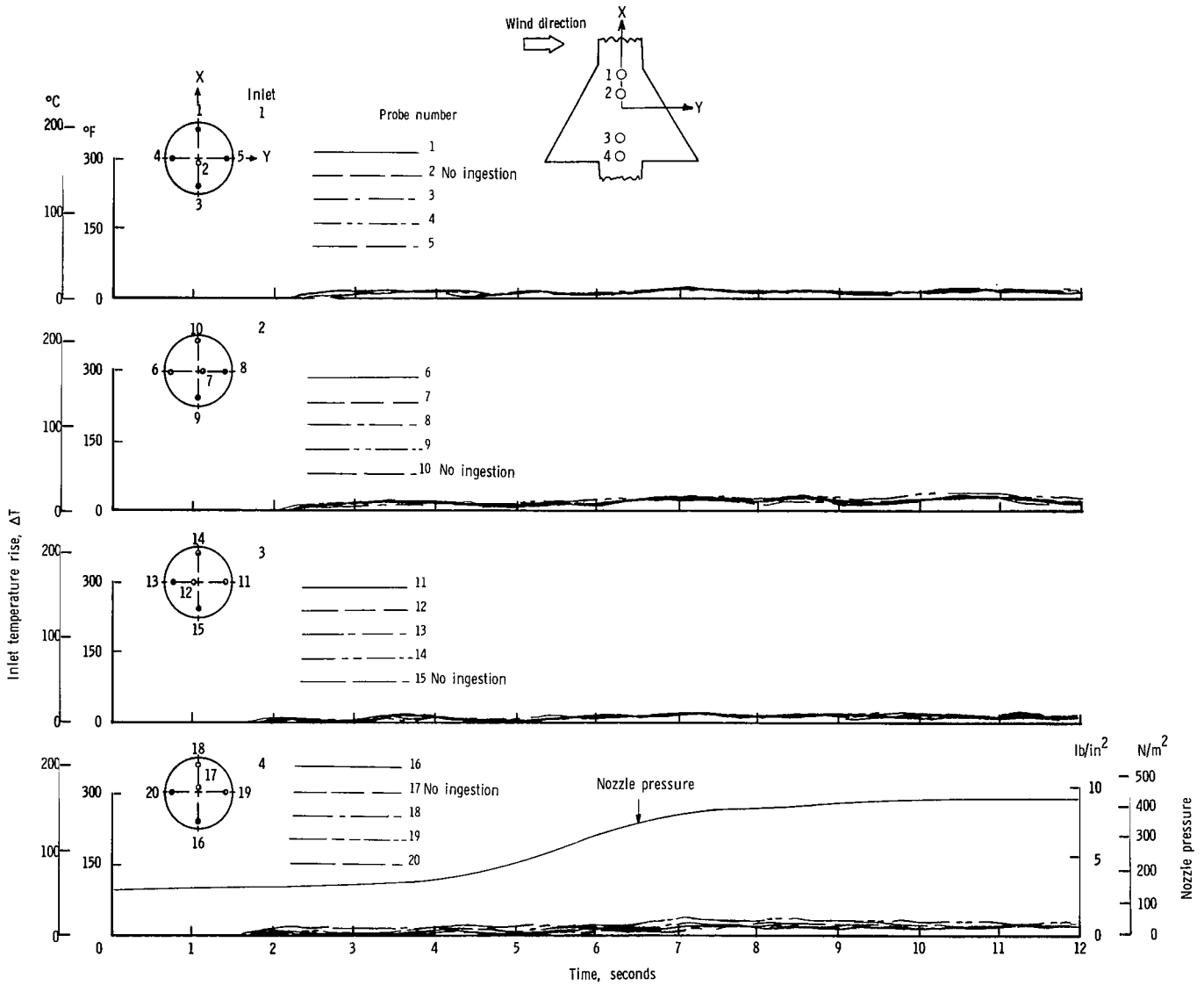

(d) $\psi = 90^0$; V = 11.85 knots.

Figure 23.- Concluded.

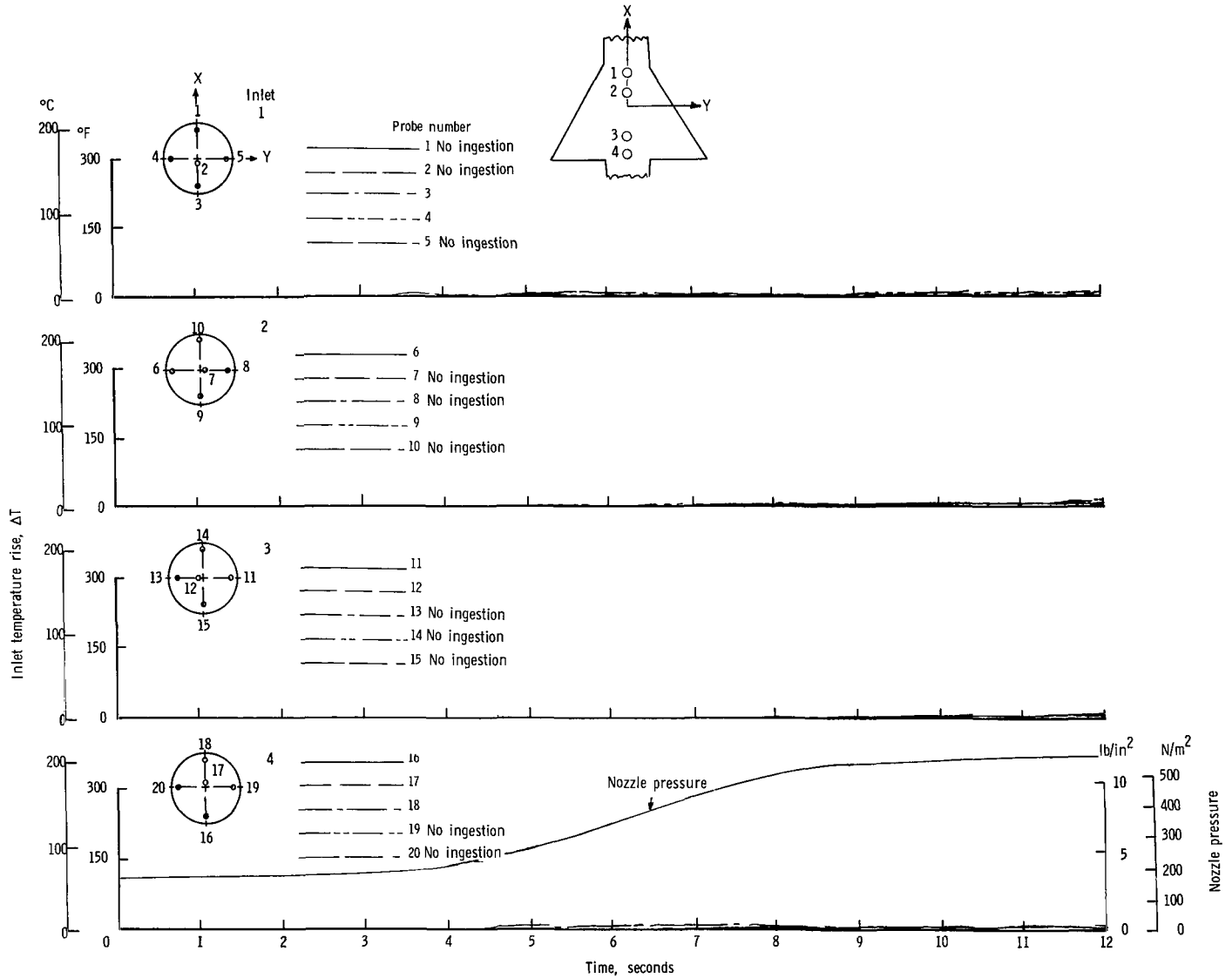

(a) $\psi = 0^0$; V = 0 knots.

Figure 24.- Variation of inlet air temperature rise with time for the in-line nozzle arrangement with top inlets and low delta wing. $h/D_e = 1.17$.

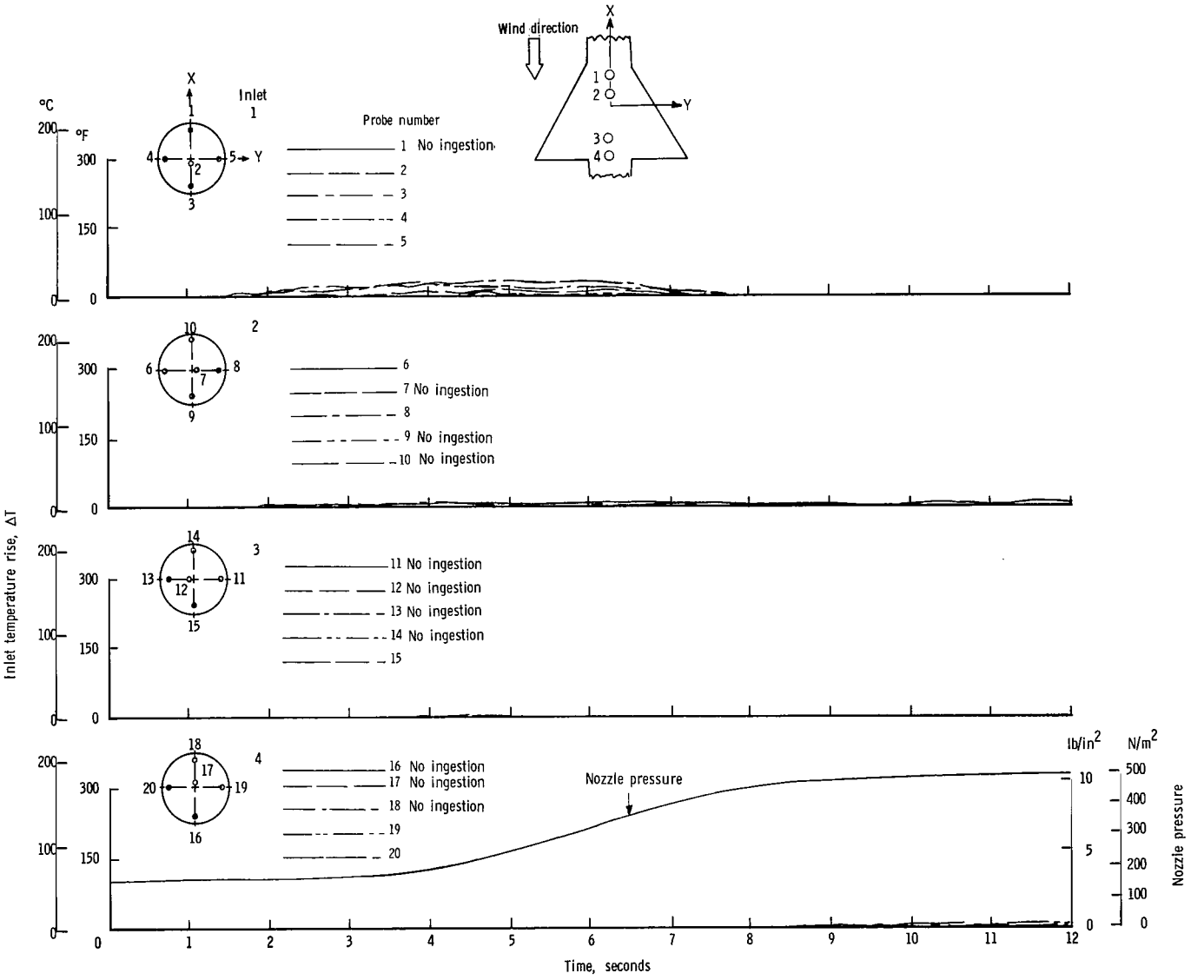

(b) $\psi = 0^0$; V = 5.92 knots.

Figure 24.- Continued.

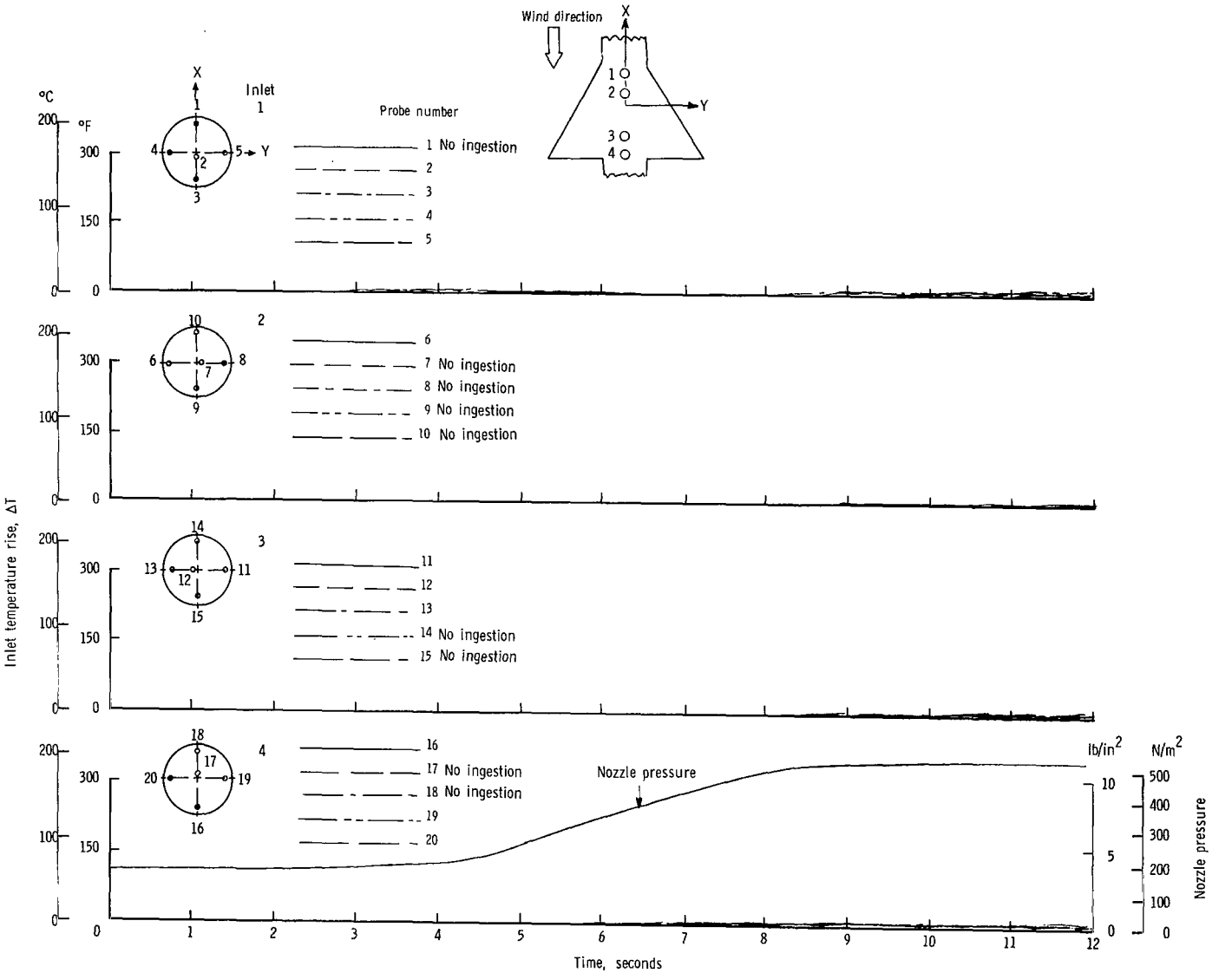

(c) $\psi = 0^0$; V = 11.85 knots.

Figure 24.- Continued.

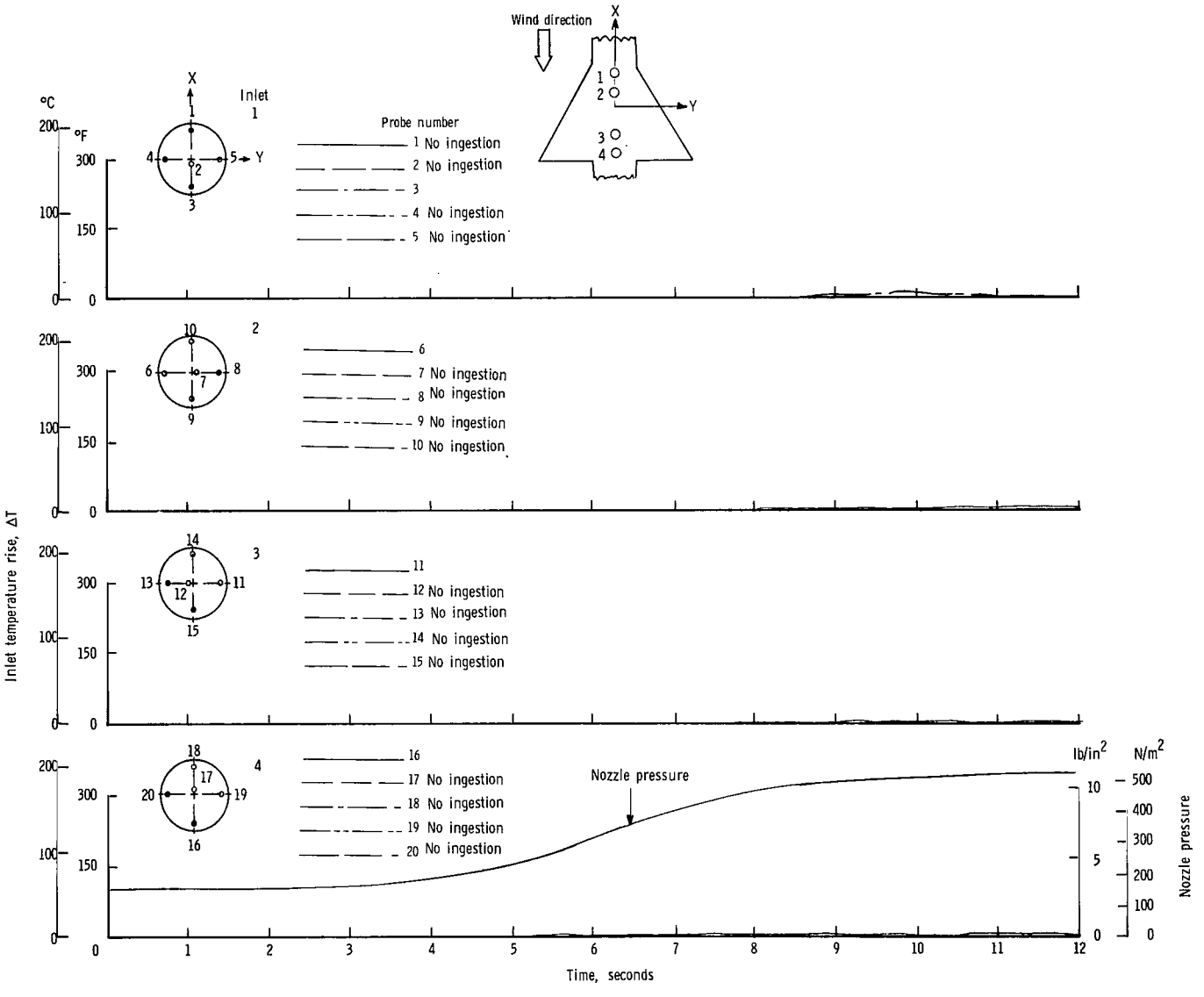

(d) $\psi = 0^{0}$; V = 17.78 knots.

Figure 24.- Continued.

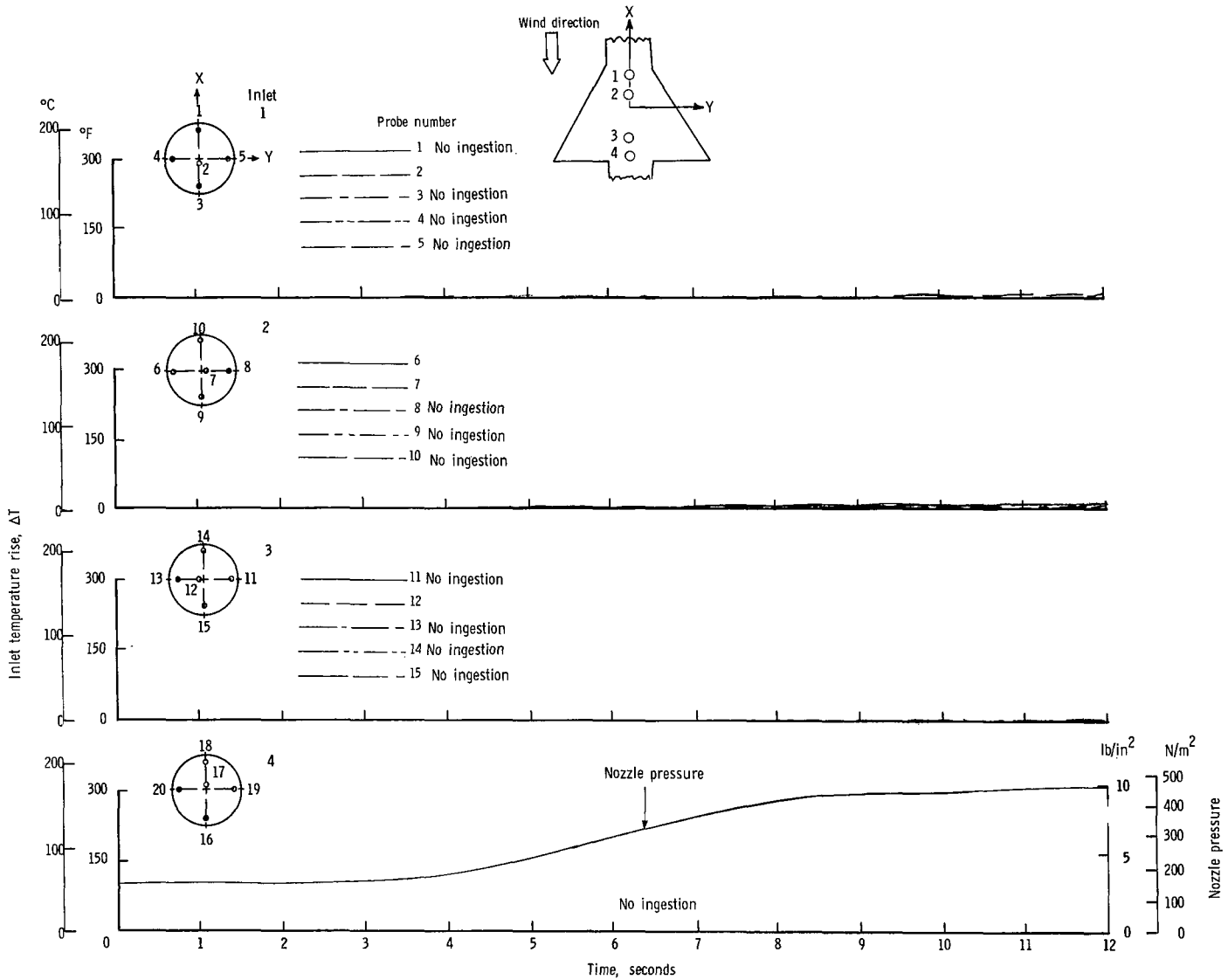

(e) $\psi = 0^0$; V = 23.70 knots.

Figure 24.- Continued.

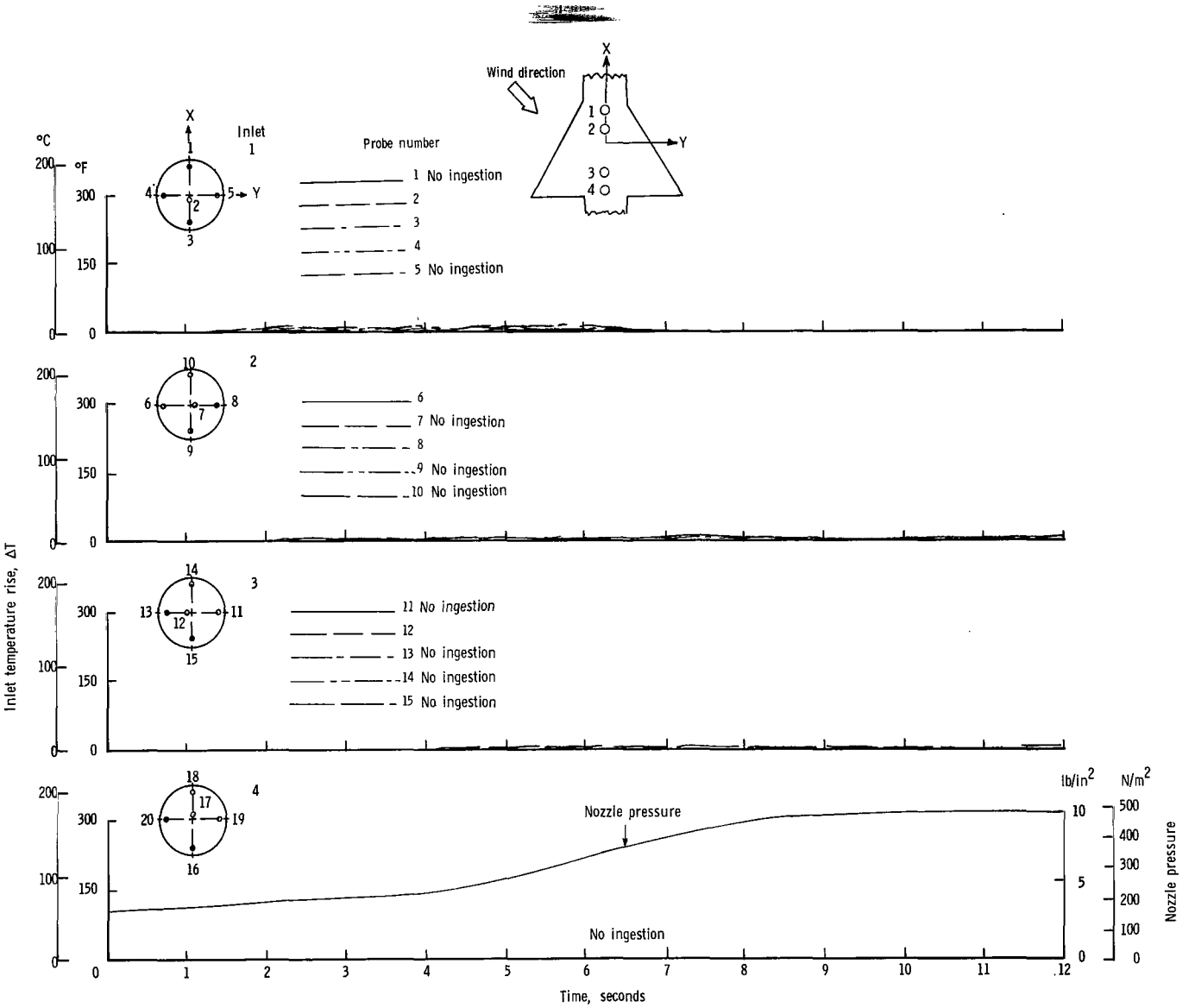

(f) $\psi = 45^0$; V = 5.92 knots.

Figure 24.- Continued.

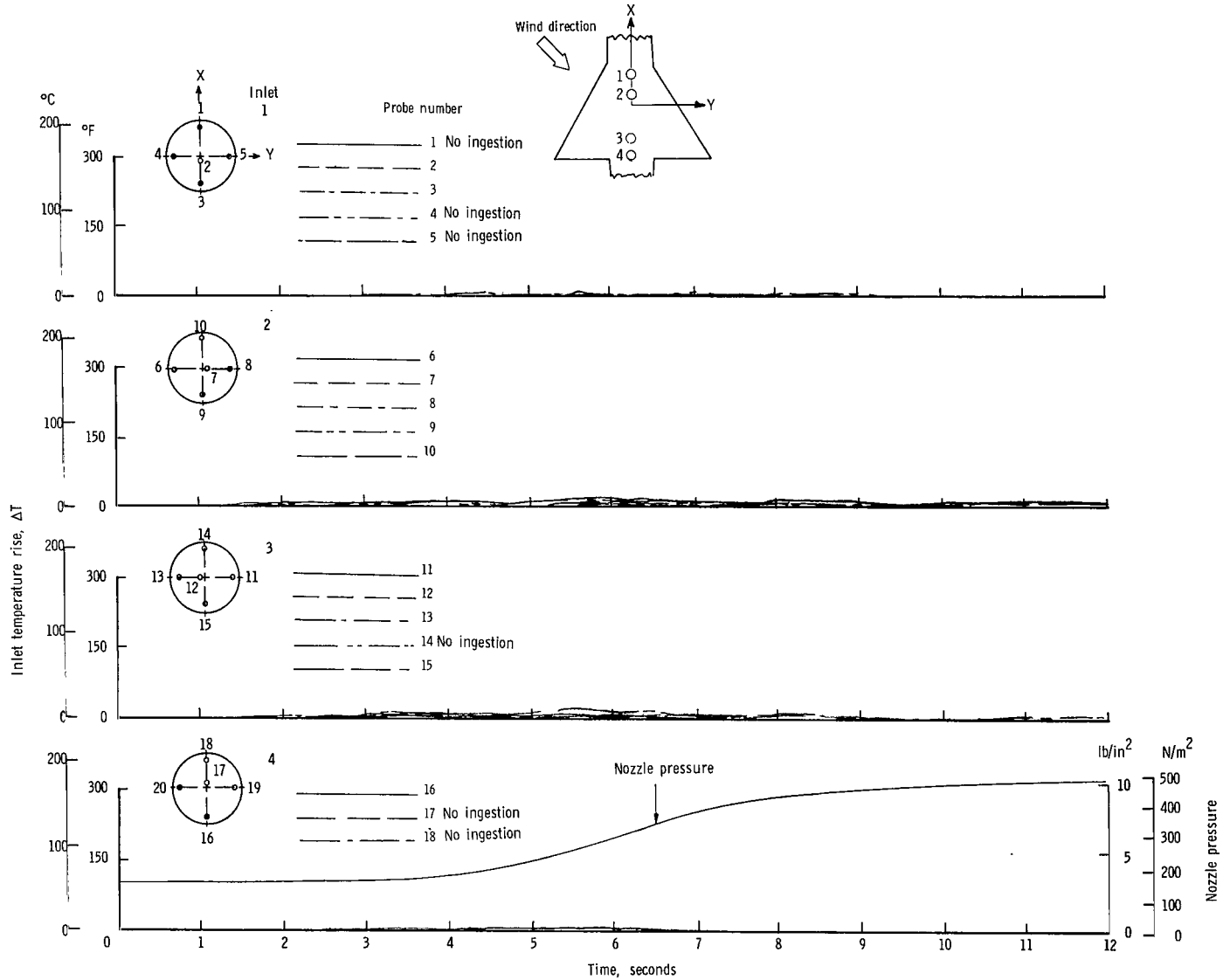

(g) $\psi = 45^{0}$; V = 11.85 knots.

Figure 24.- Continued.

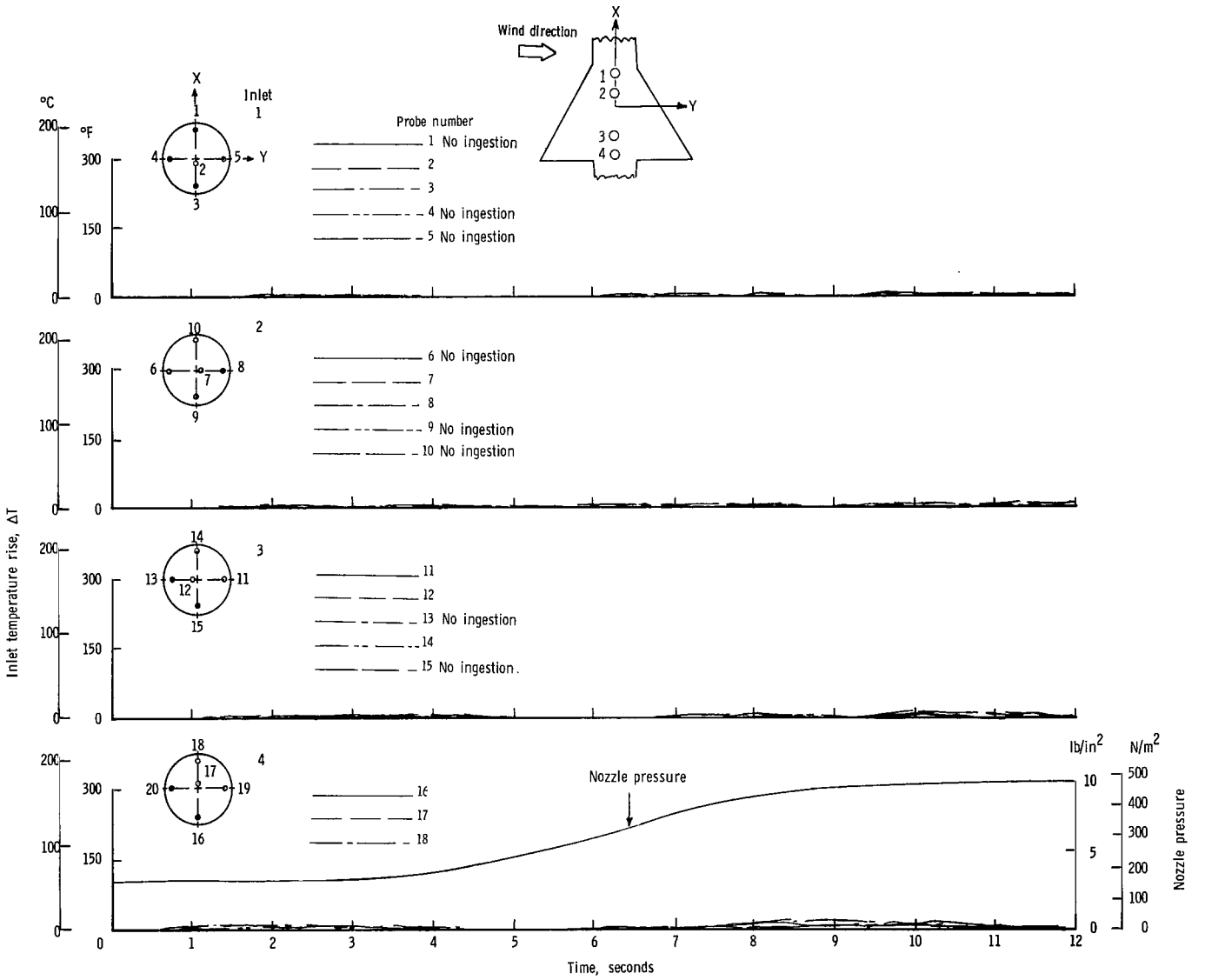

(h) $\psi = 90^0$; V = 5.92 knots.

Figure 24.- Continued.

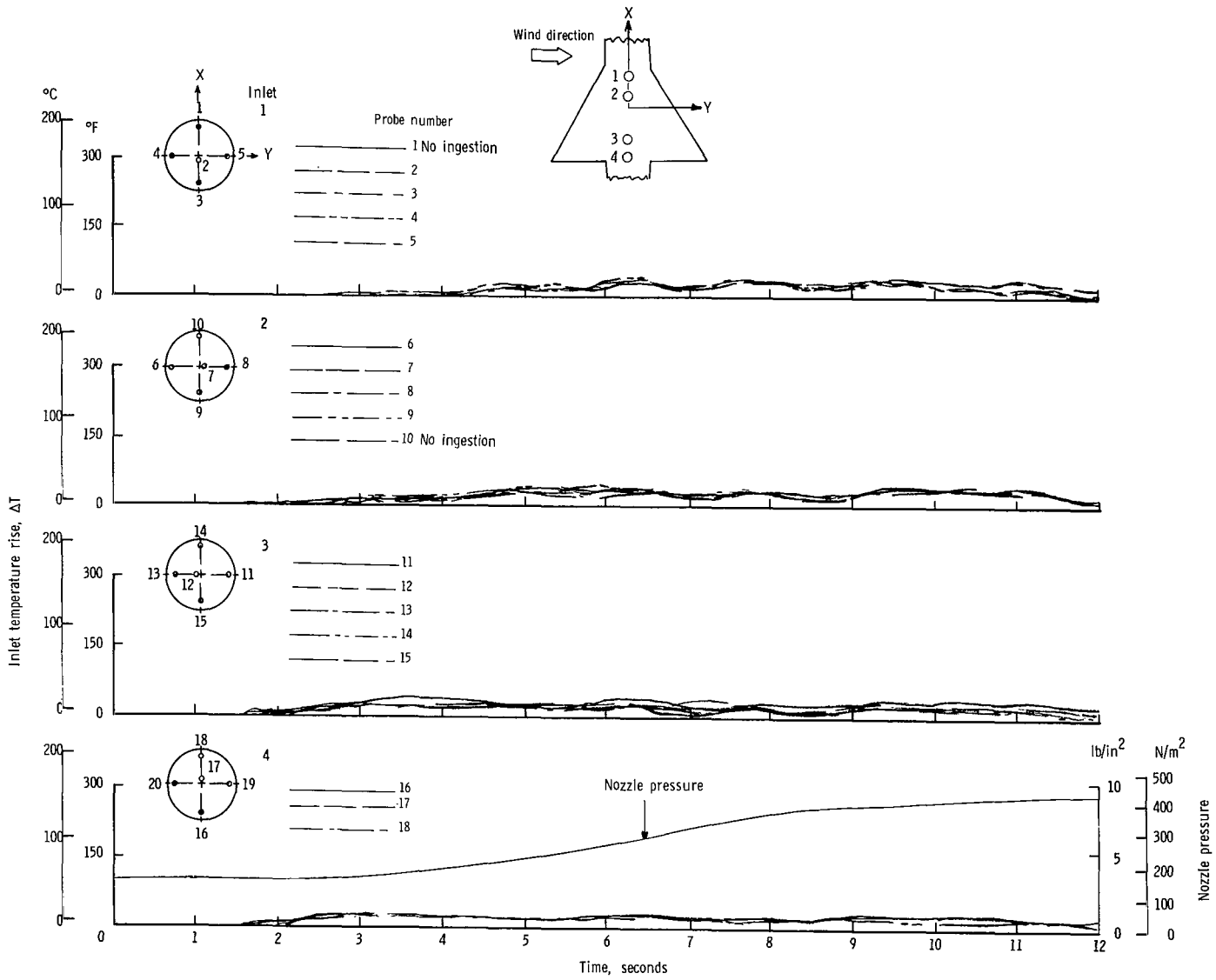

(i) $\psi = 90^{0}$; V = 11.85 knots.

Figure 24.- Concluded.

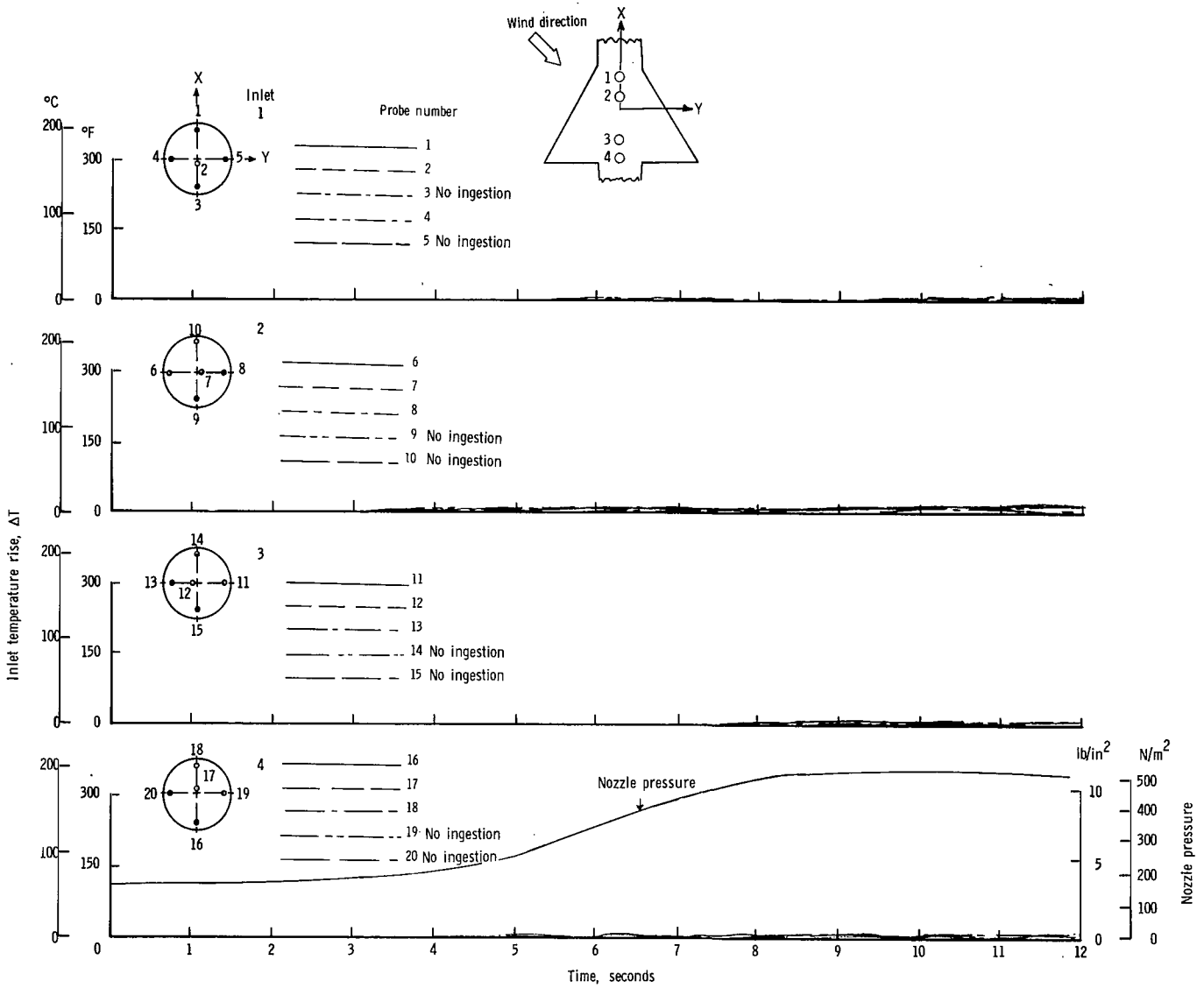

(a) $\psi = 45^{0}$; V = 5.92 knots.

Figure 25.- Variation of inlet air temperature rise with time for the in-line nozzle arrangement with top inlets and low delta wing. $h/D_e = 3.0$.

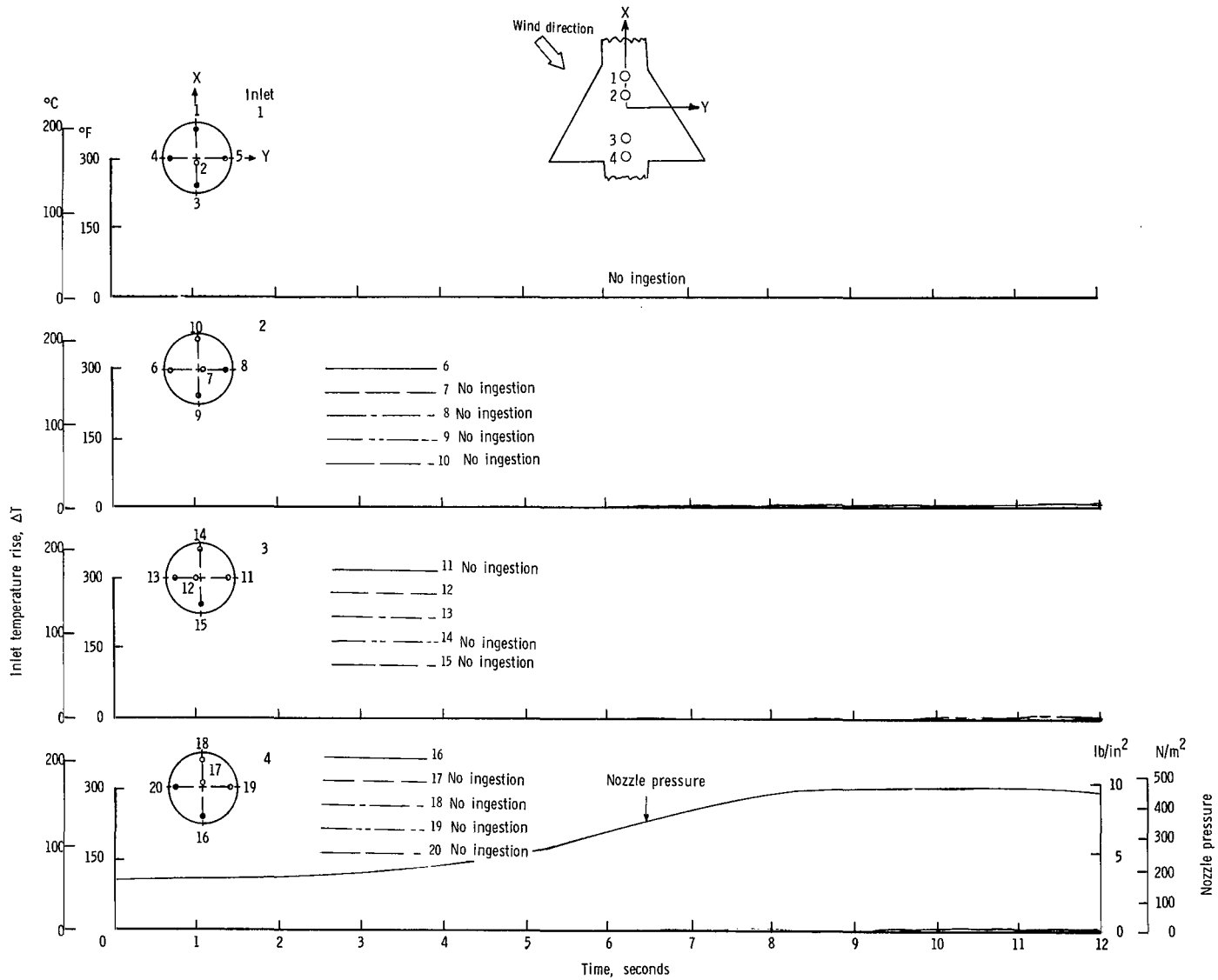

(b) $\psi = 45^{0}$; V = 11.85 knots.

Figure 25.- Continued.

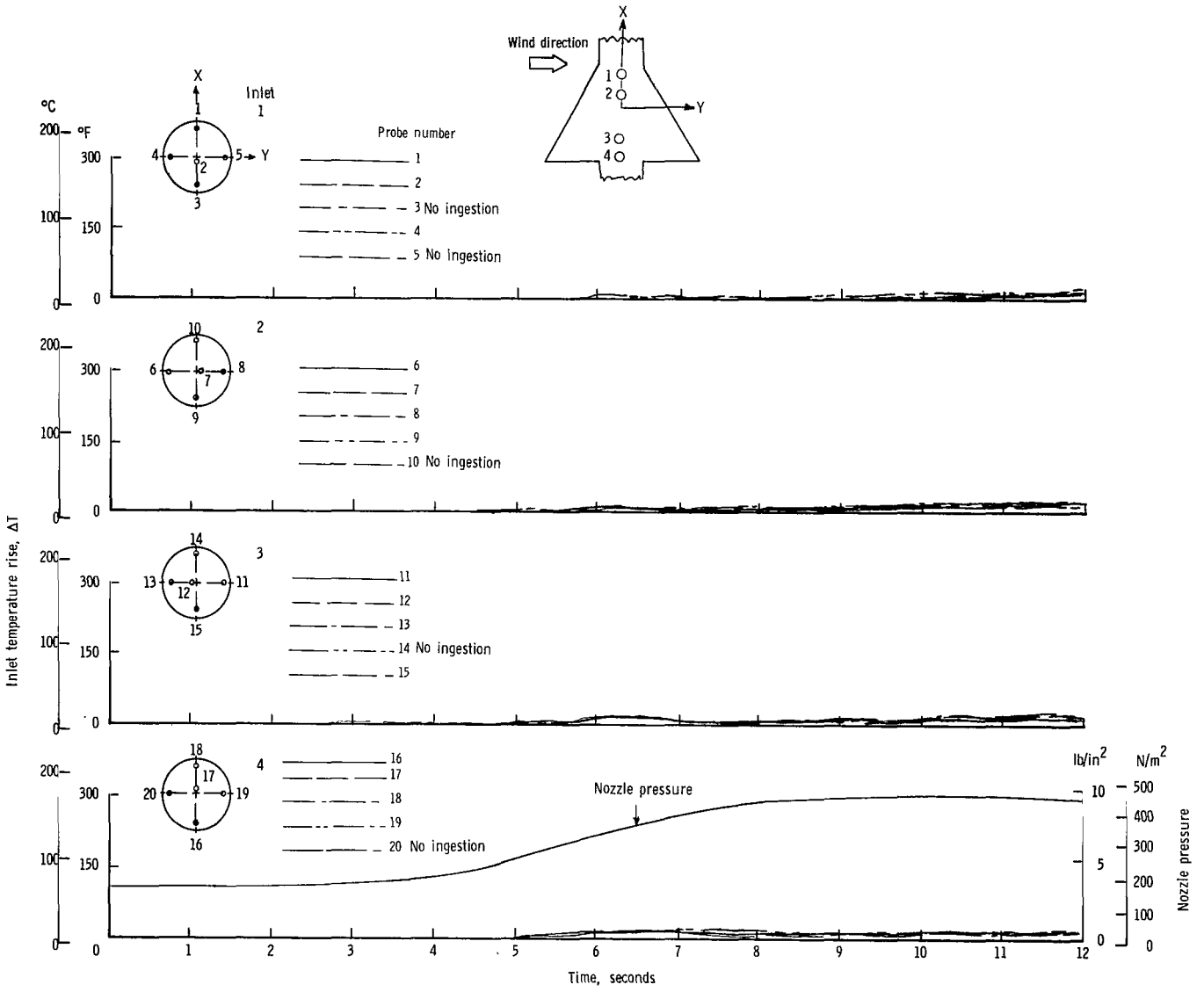

(c) $\psi = 90^{0}$; V = 5.92 knots.

Figure 25.- Continued.

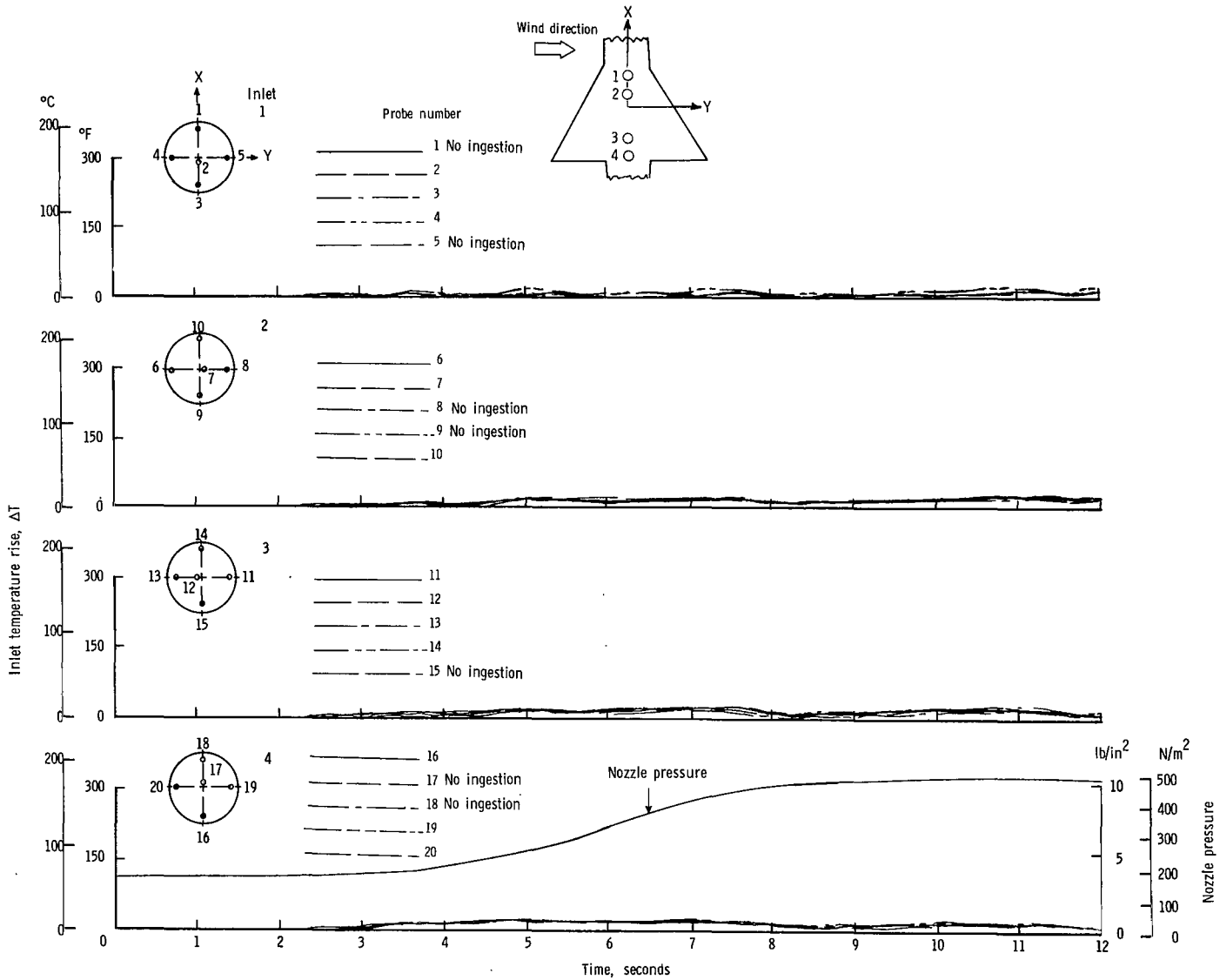

(d) $\psi = 90^0$; V = 11.85 knots.

Figure 25.- Concluded.

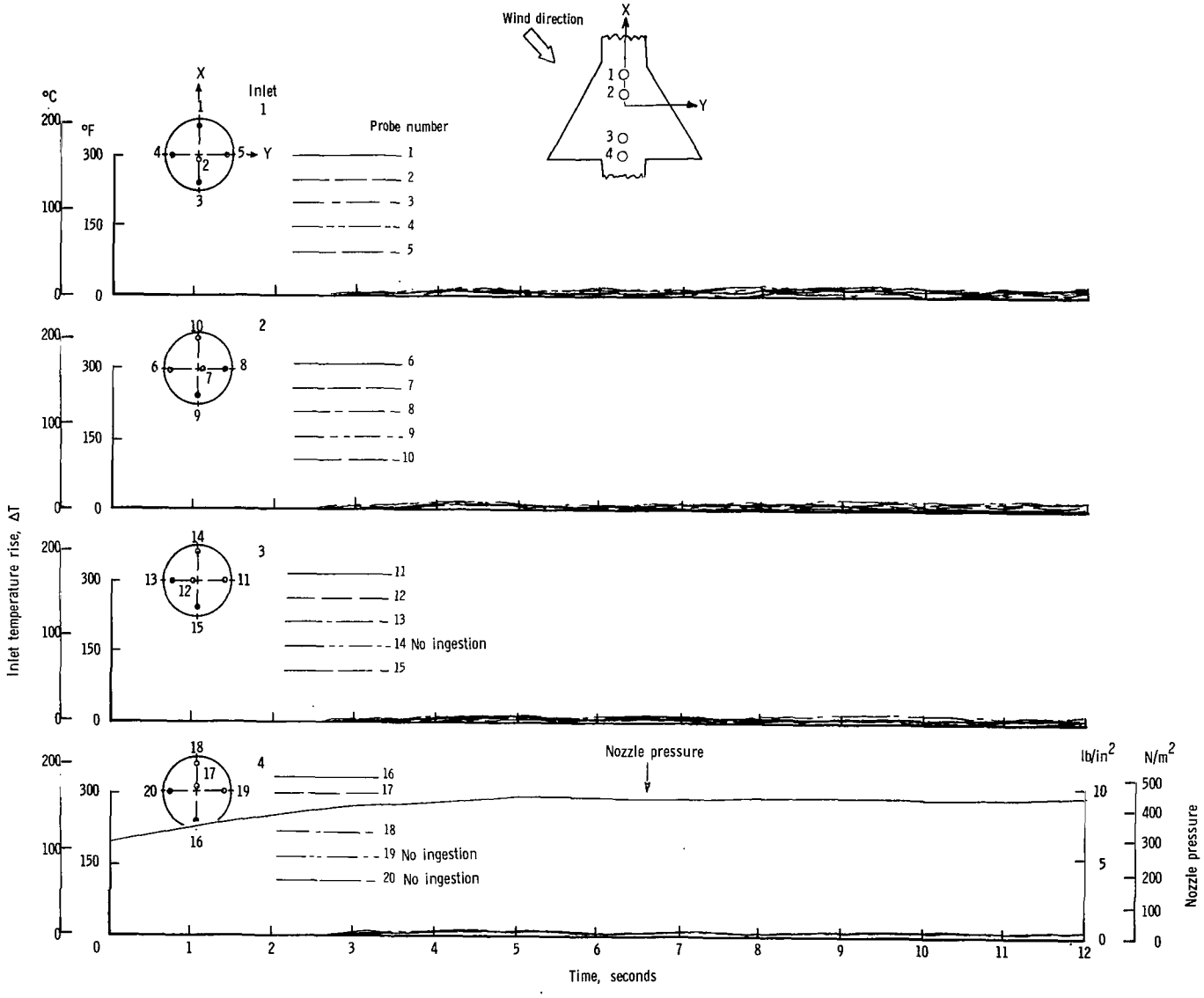

(a) $\psi = 45^0$; V = 5.92 knots.

Figure 26.- Variation of inlet air temperature rise with time for the in-line nozzle arrangement with top inlets and low delta wing. $h/D_e = 5.0$.

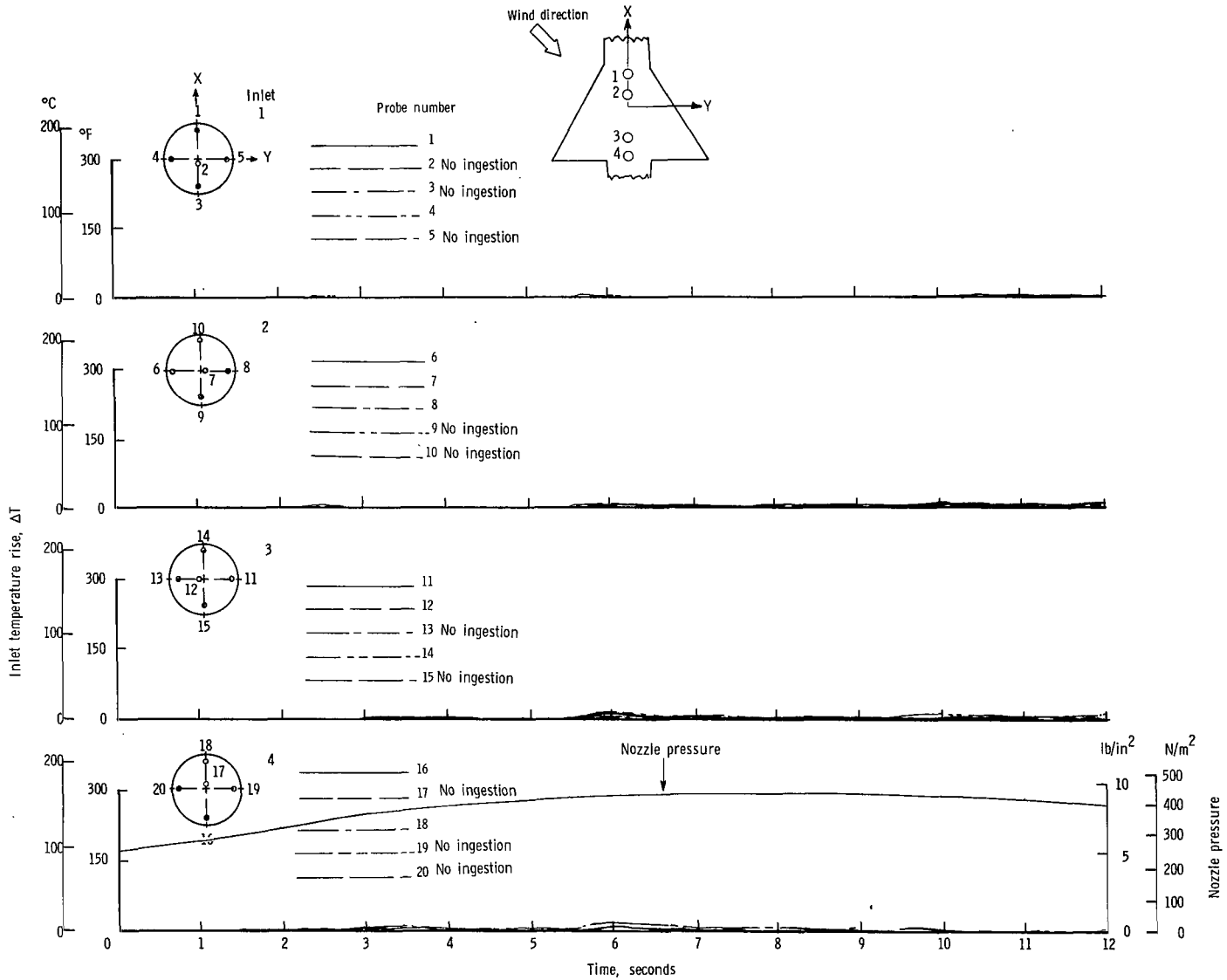

(b) $\psi = 45^0$; V = 11.85 knots.

Figure 26.- Continued.

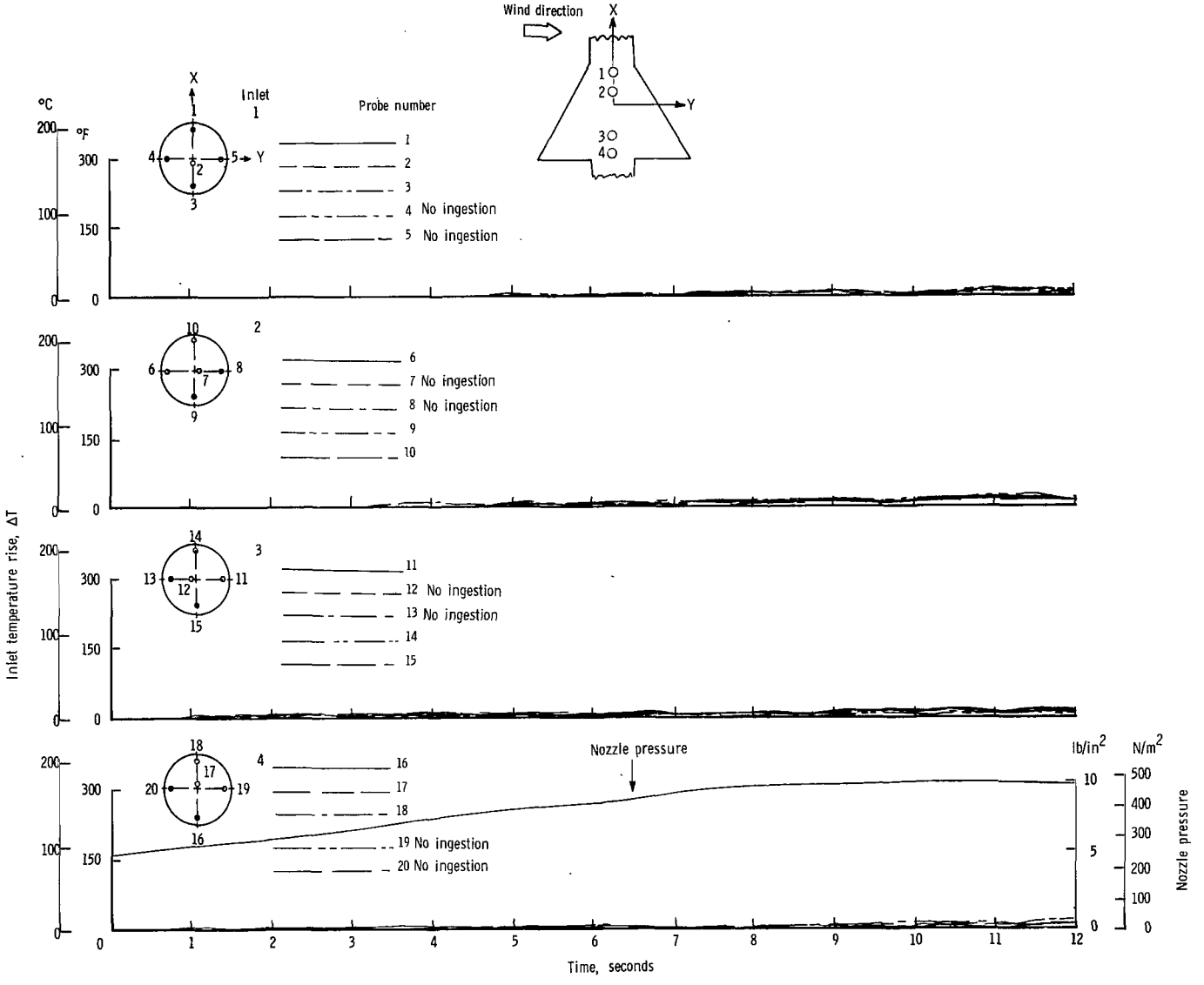

(c) $\psi = 90^0$; V = 5.92 knots.

Figure 26.- Concluded.

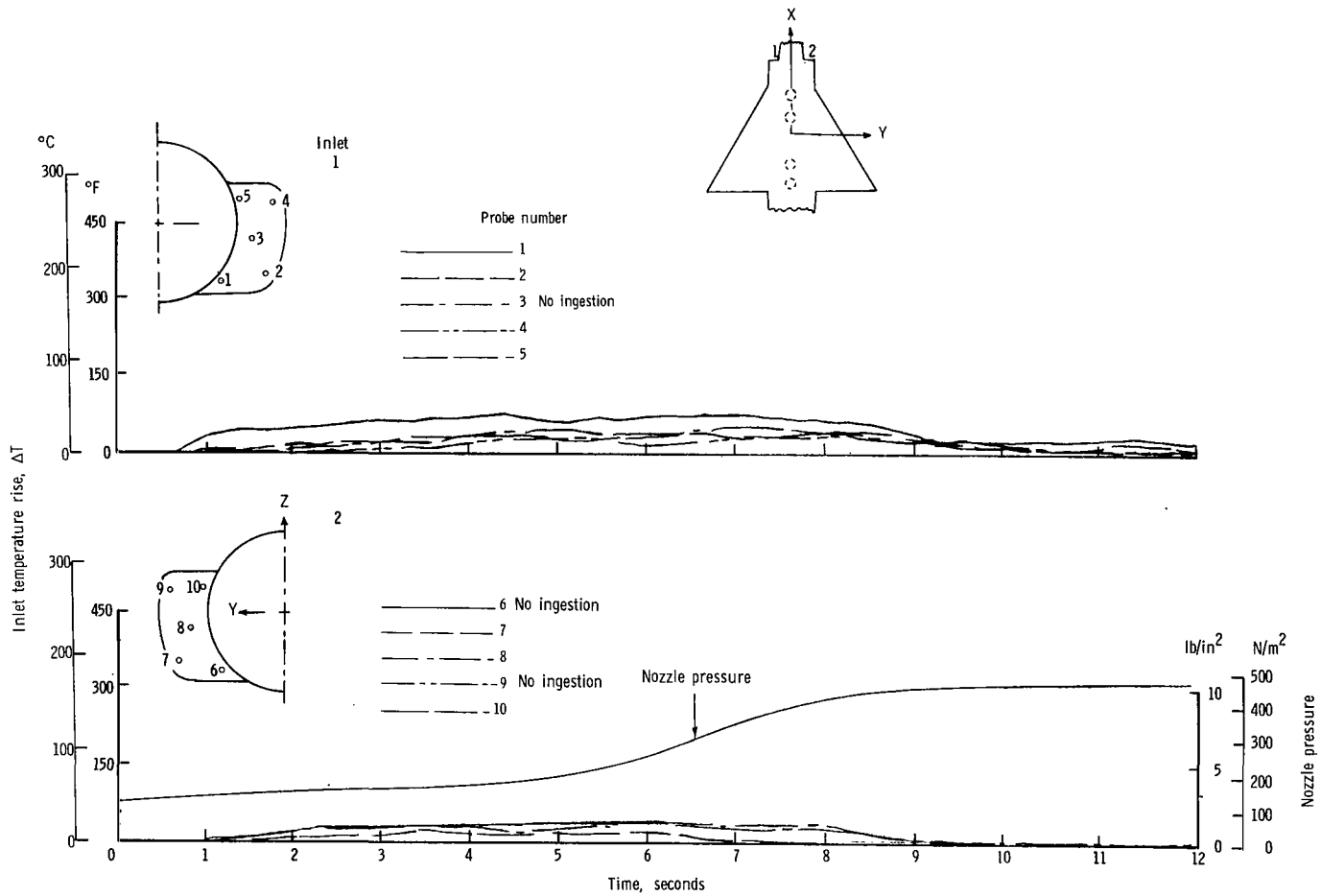

(a) $\psi = 0^0$; V = 0 knots.

Figure 27.- Variation of inlet air temperature rise with time for the in-line nozzle arrangement with side inlets and high delta wing. $h/D_e = 1.17$.

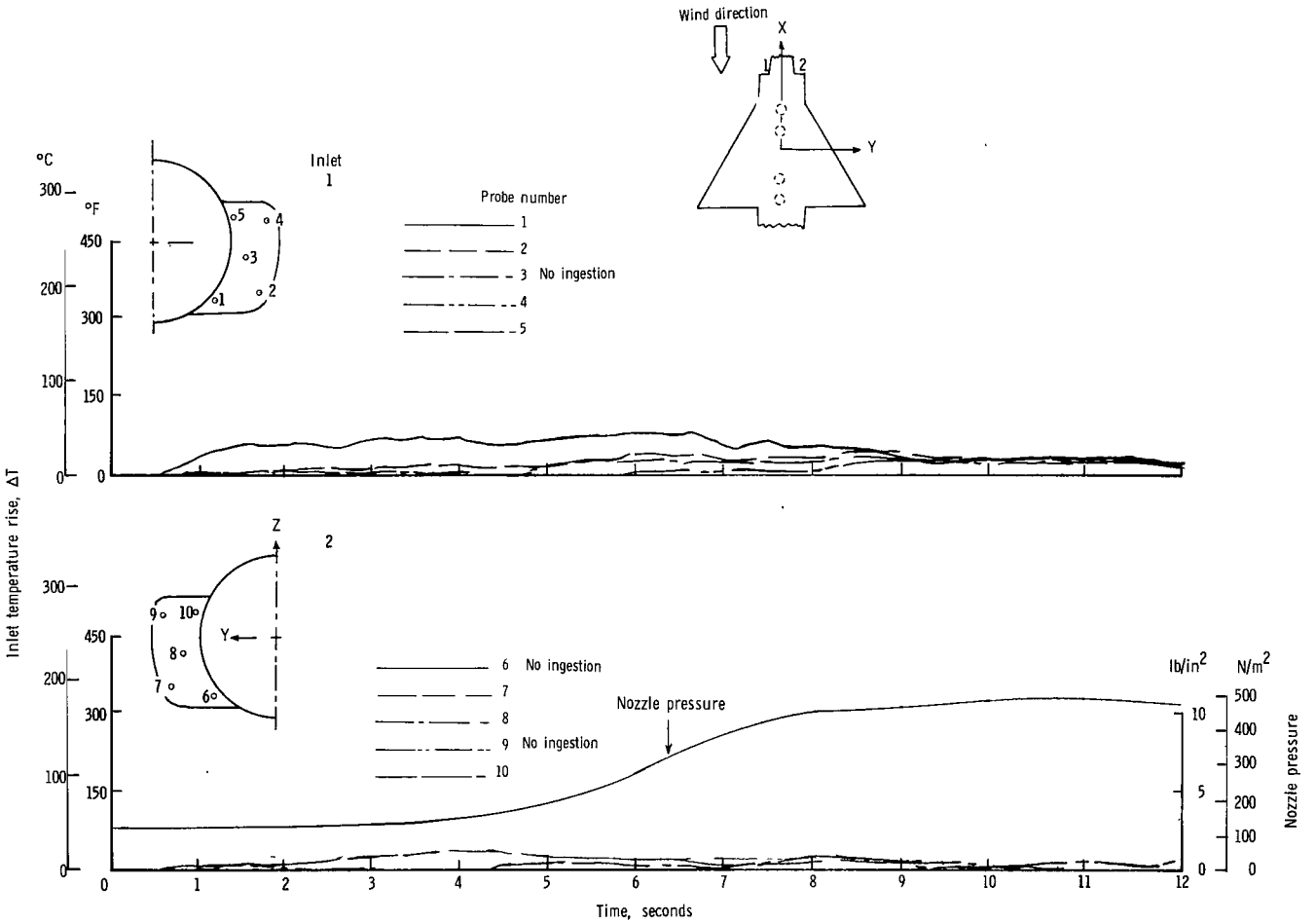

(b) $\psi = 0^0$; V = 5.92 knots.

Figure 27.- Continued.

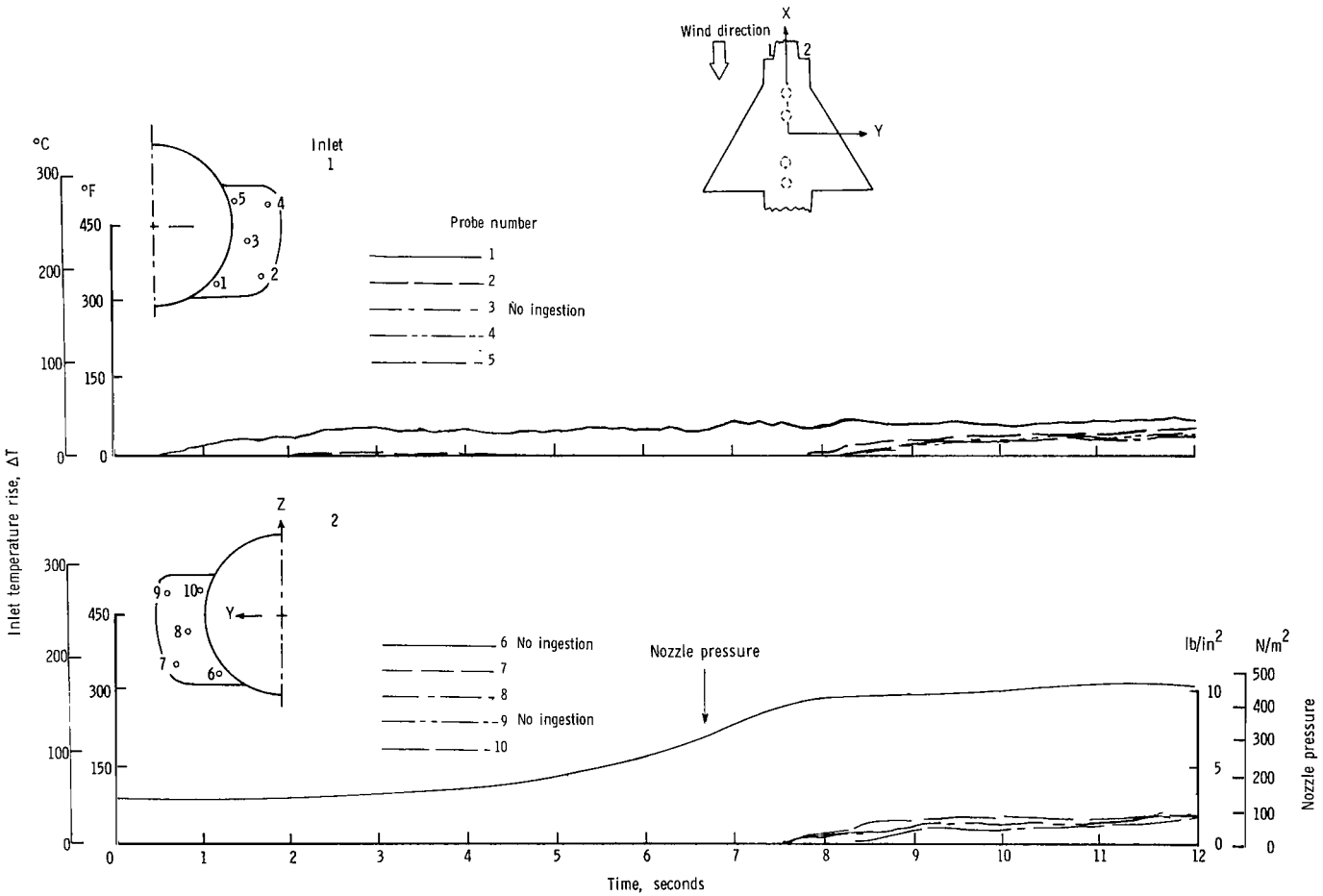

(c) $\psi = 0^0$; V = 11.85 knots.

Figure 27.- Continued.

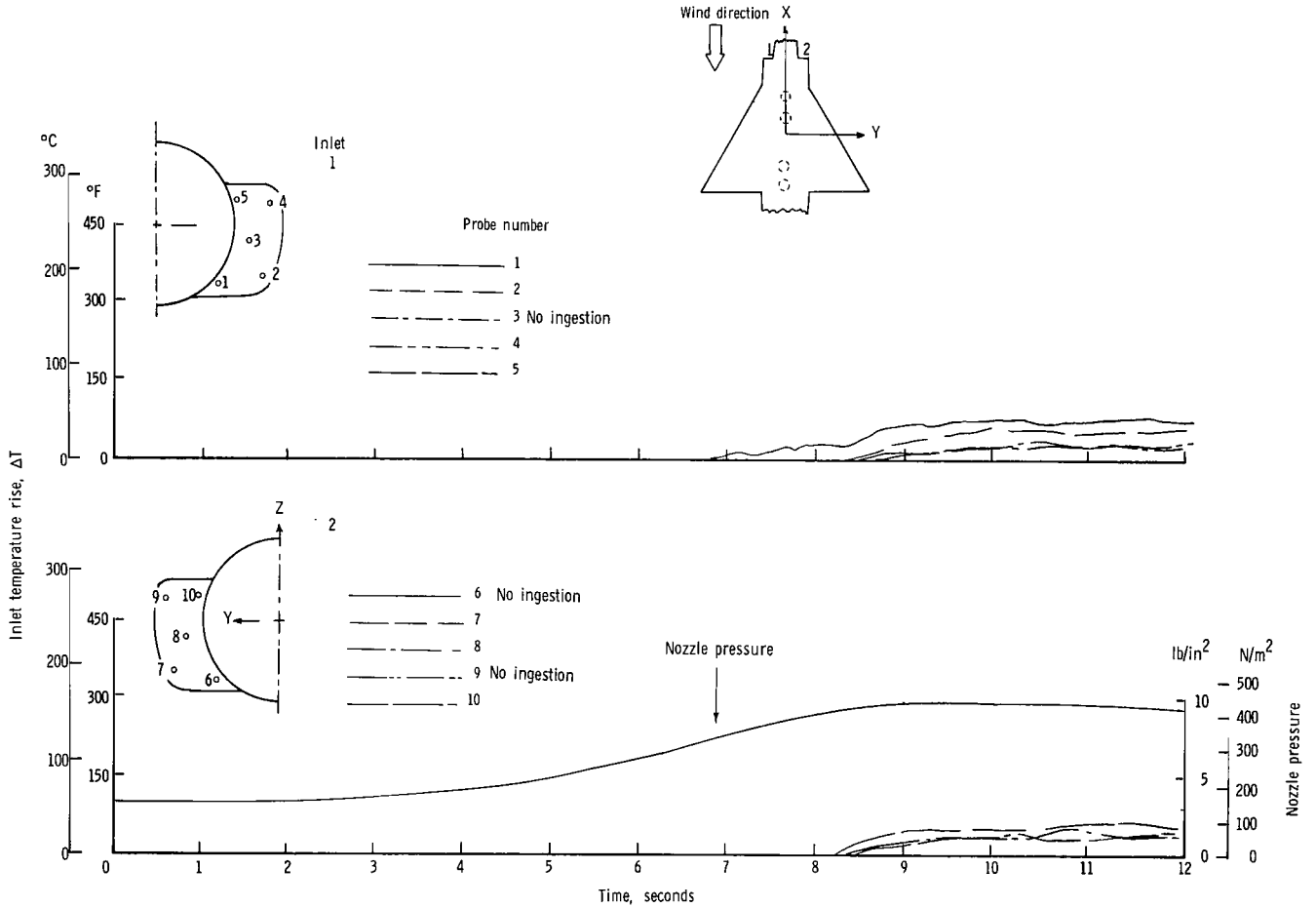

(d) $\psi = 0^0$; V = 17.78 knots.

Figure 27.- Continued.

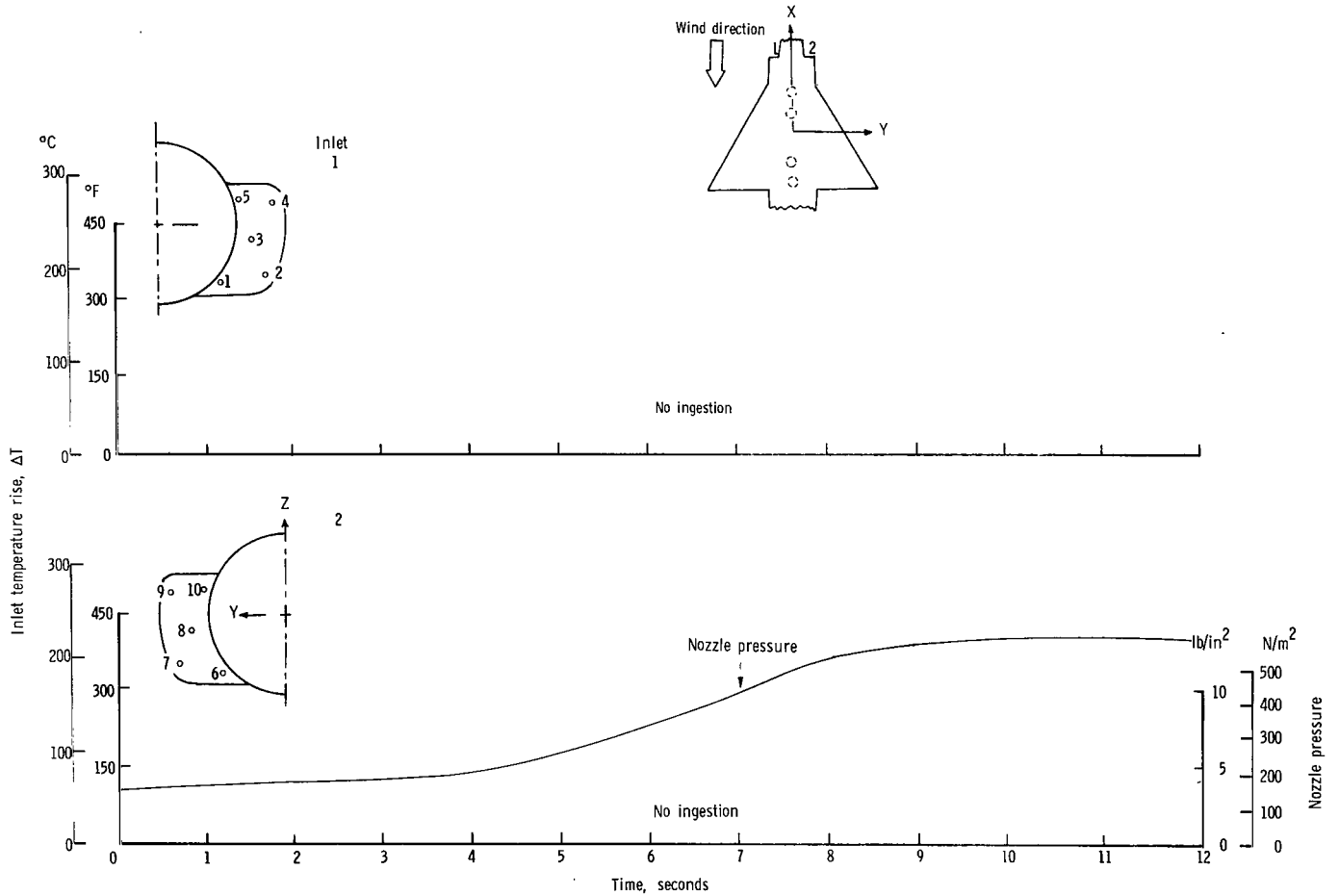

(e) $\psi = 0^0$; V = 29.70 knots.

Figure 27.- Continued.

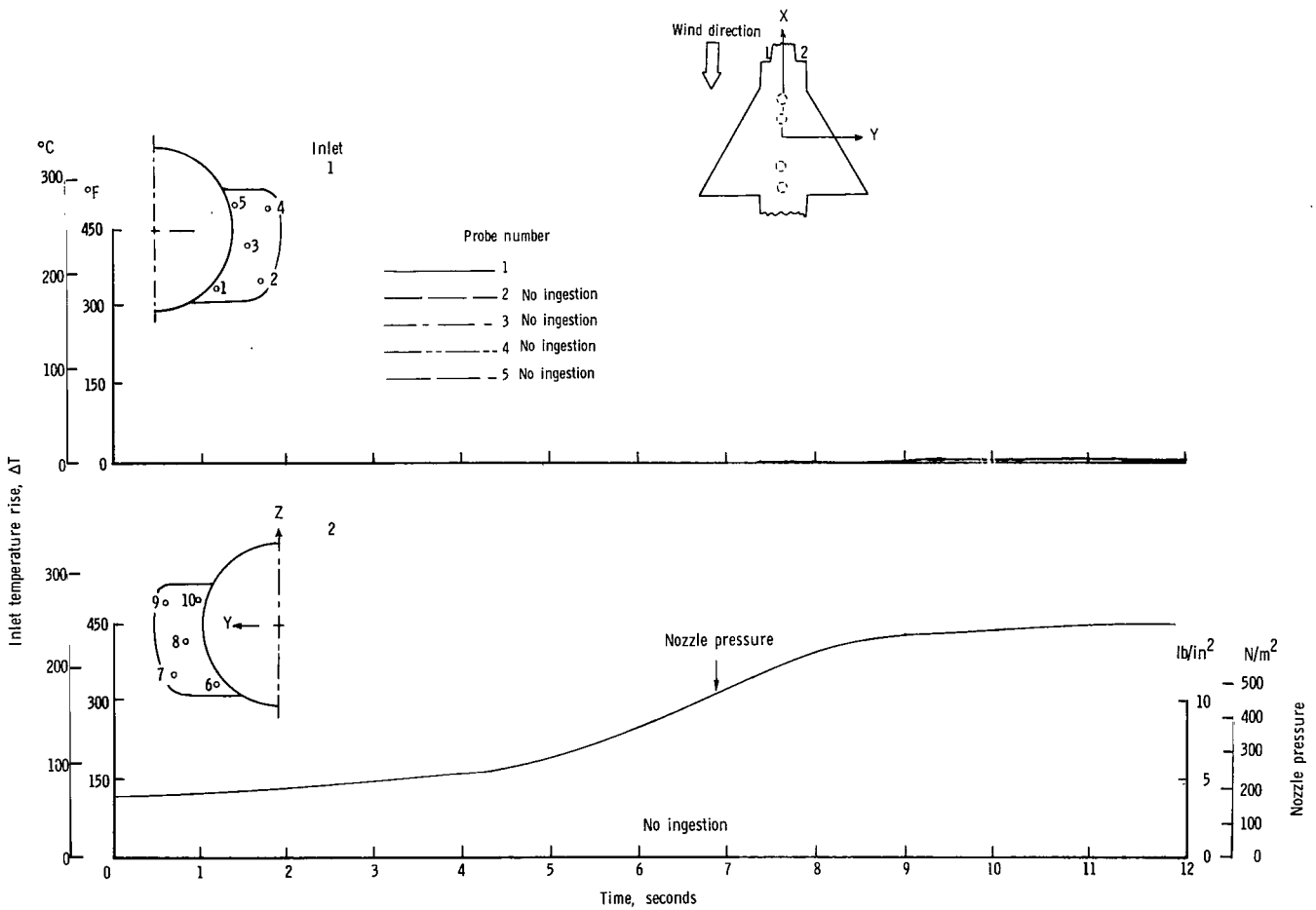

(f) $\psi = 0^{o}$; V = 35.55 knots.

Figure 27.- Continued.

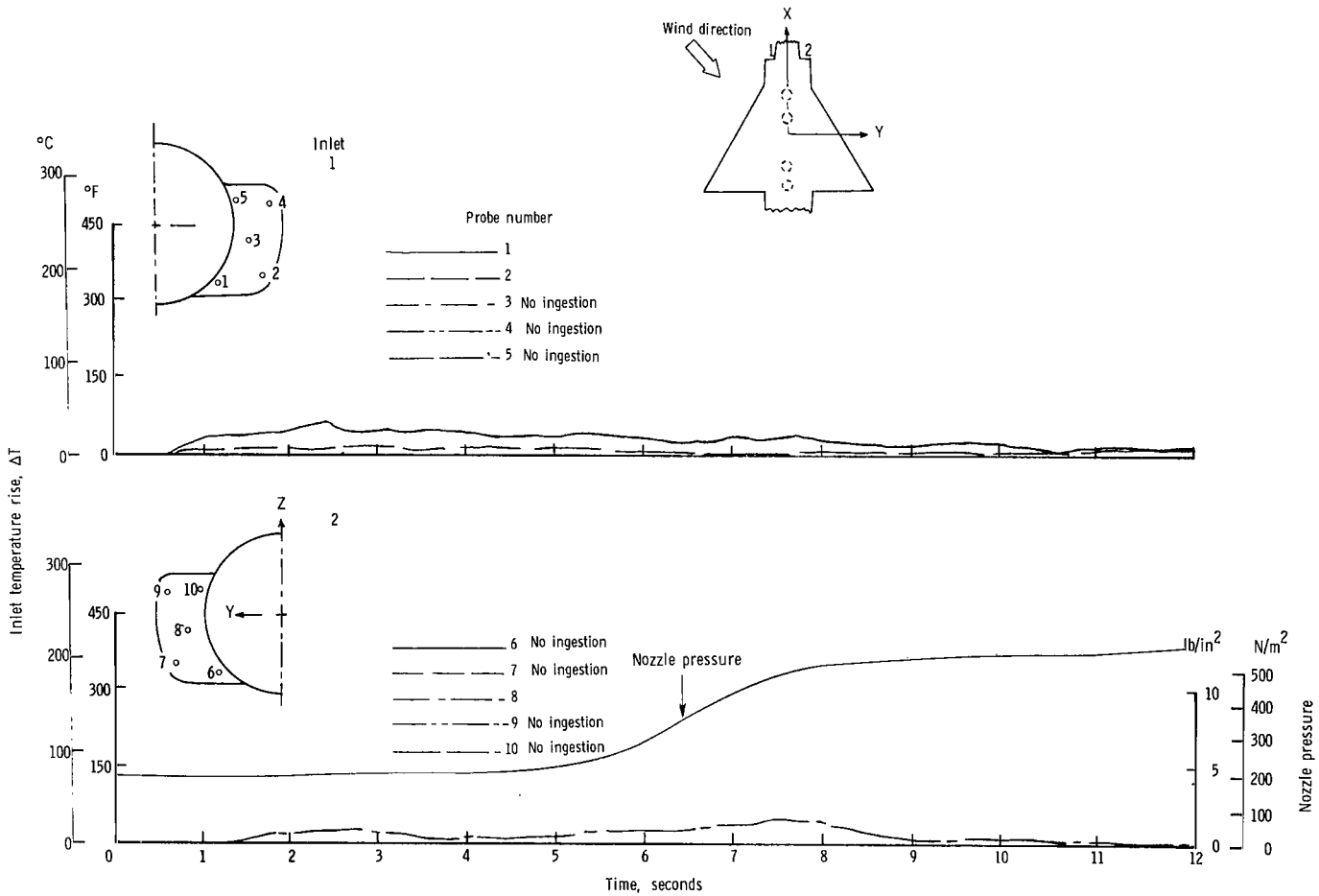

(g) $\psi = 45^{0}$; V = 5.92 knots.

Figure 27.- Continued.

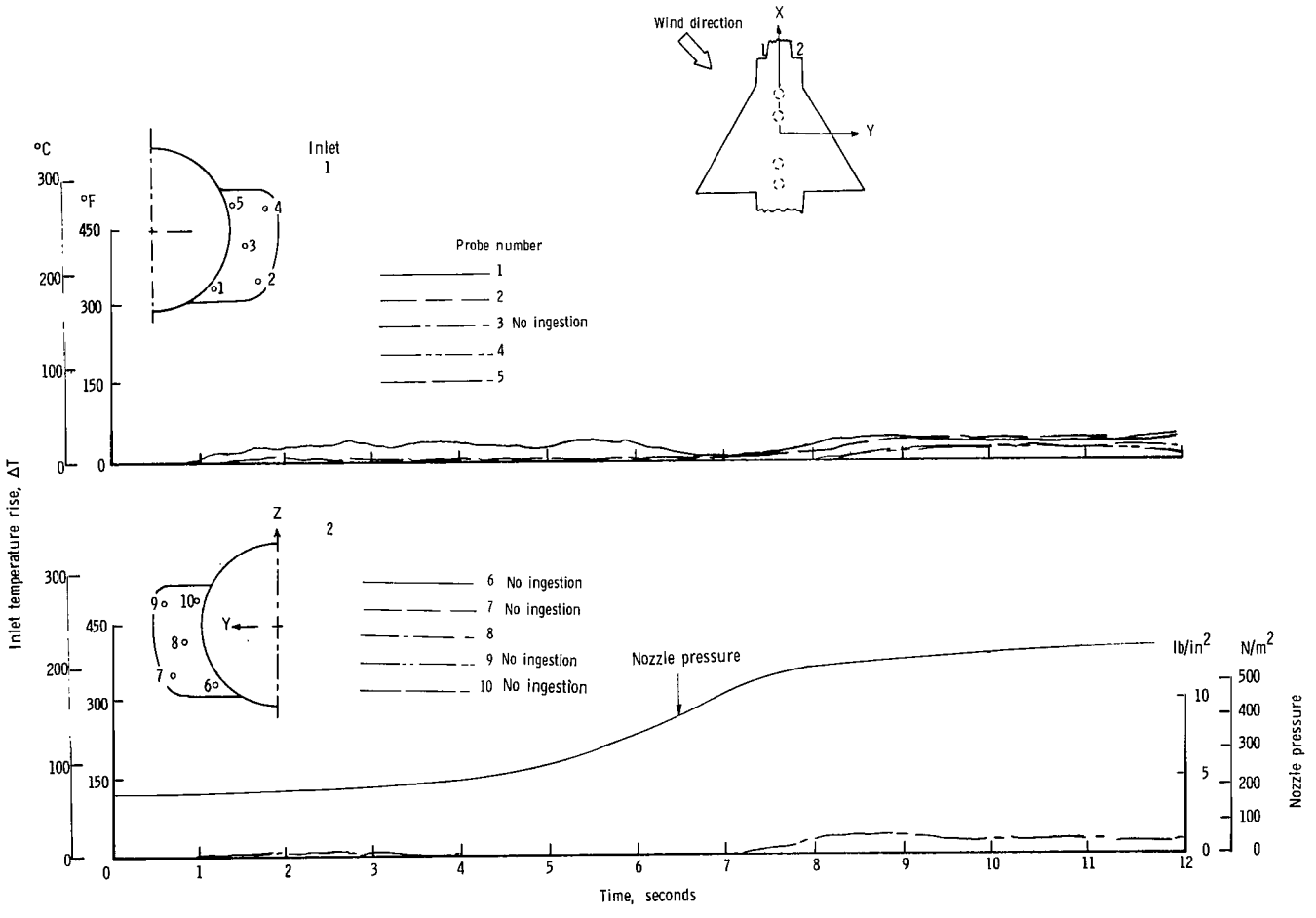

(h) $\psi = 45^0$; V = 11.85 knots.

Figure 27.- Continued.

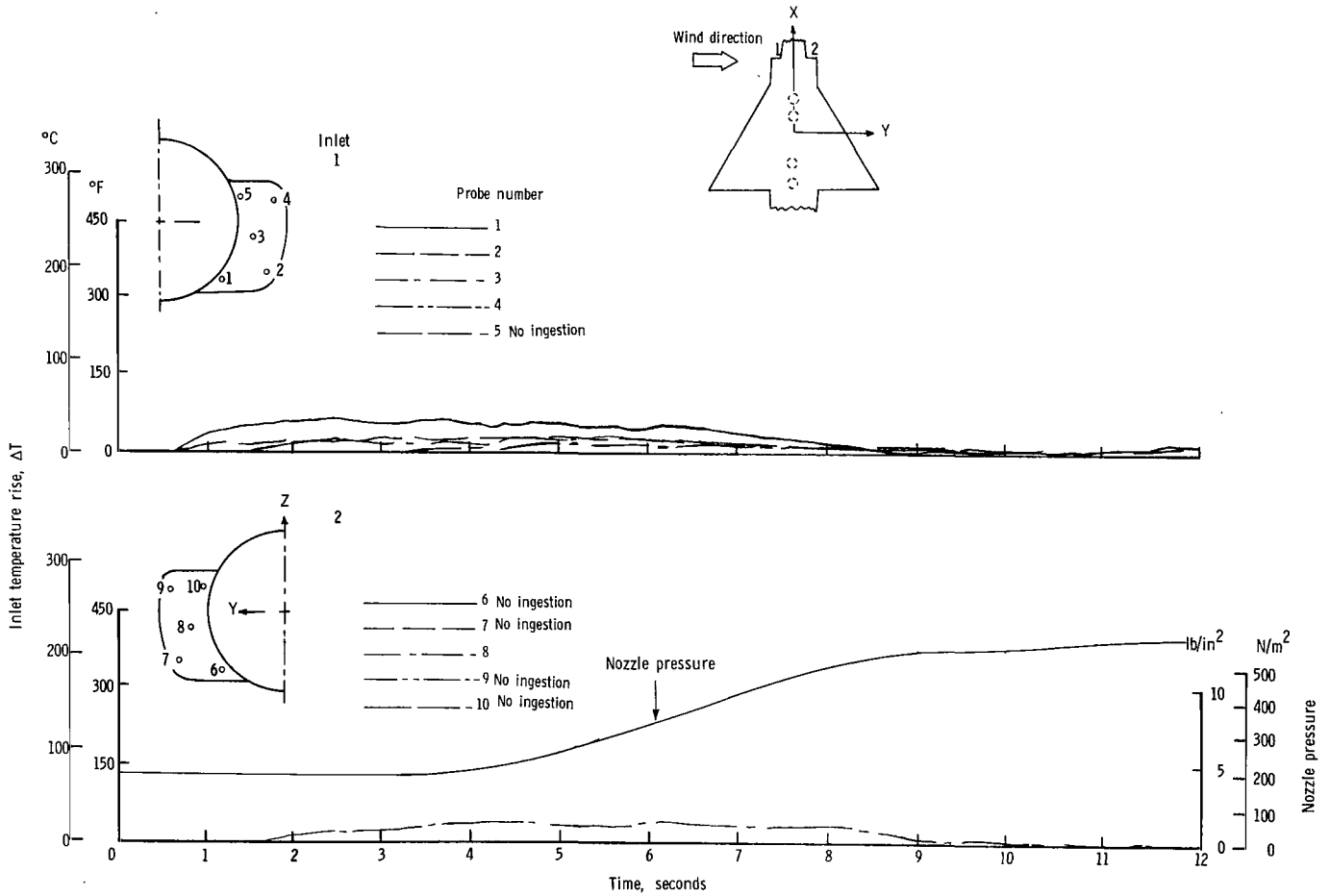

(i) $\psi = 90^{o}$; V = 5.92 knots.

Figure 27.- Continued.

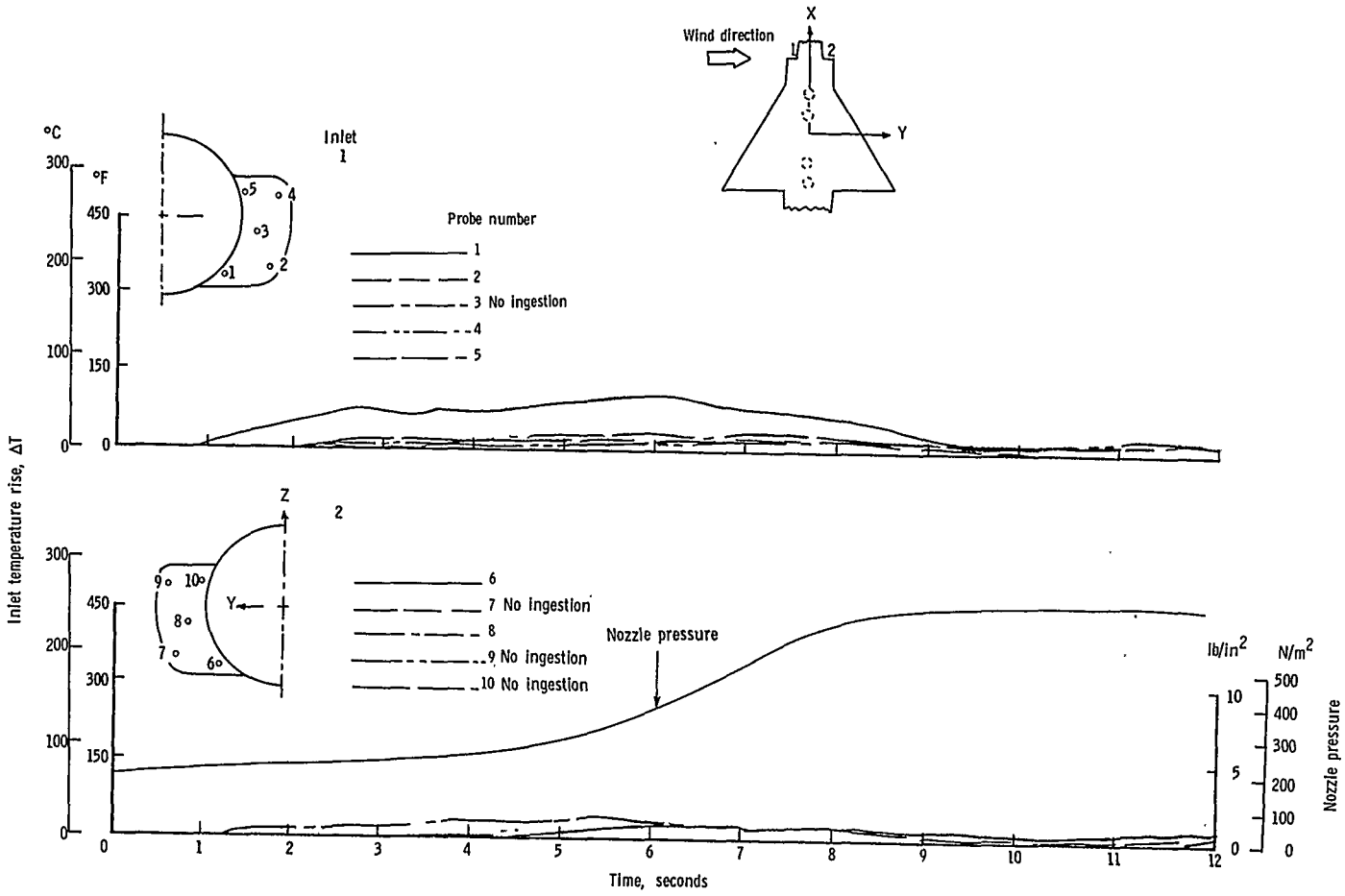

(j) $\psi = 90^0$; V = 11.85 knots.

Figure 27.- Concluded.

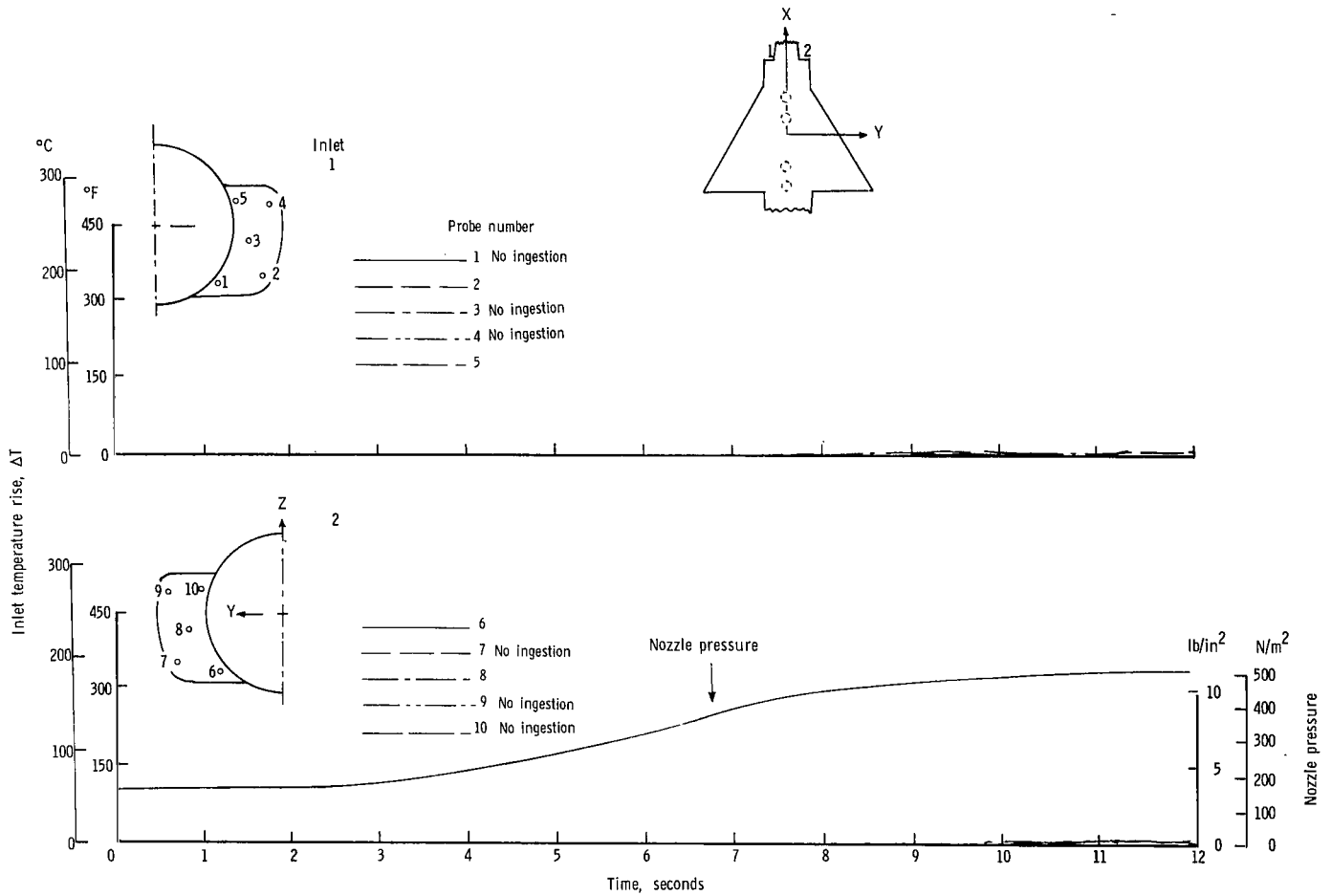

(a) $\psi = 0^0$; V = 0 knots.

Figure 28.- Variation of inlet air temperature rise with time for the in-line nozzle arrangement with side inlets and high delta wing. $h/D_e = 3.0$.

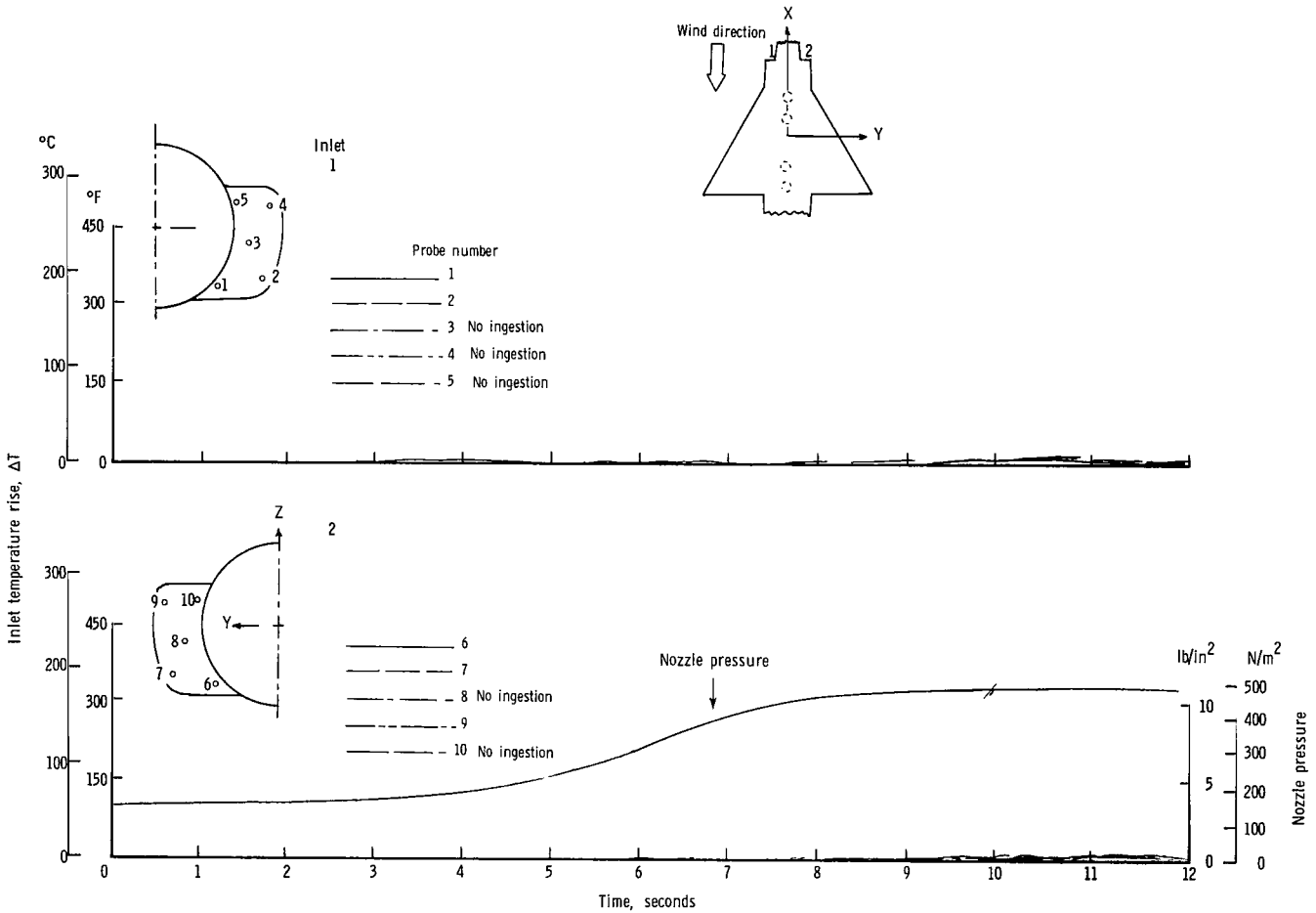

(b) $\psi = 0^{o}$; V = 5.92 knots.

Figure 28.- Continued.

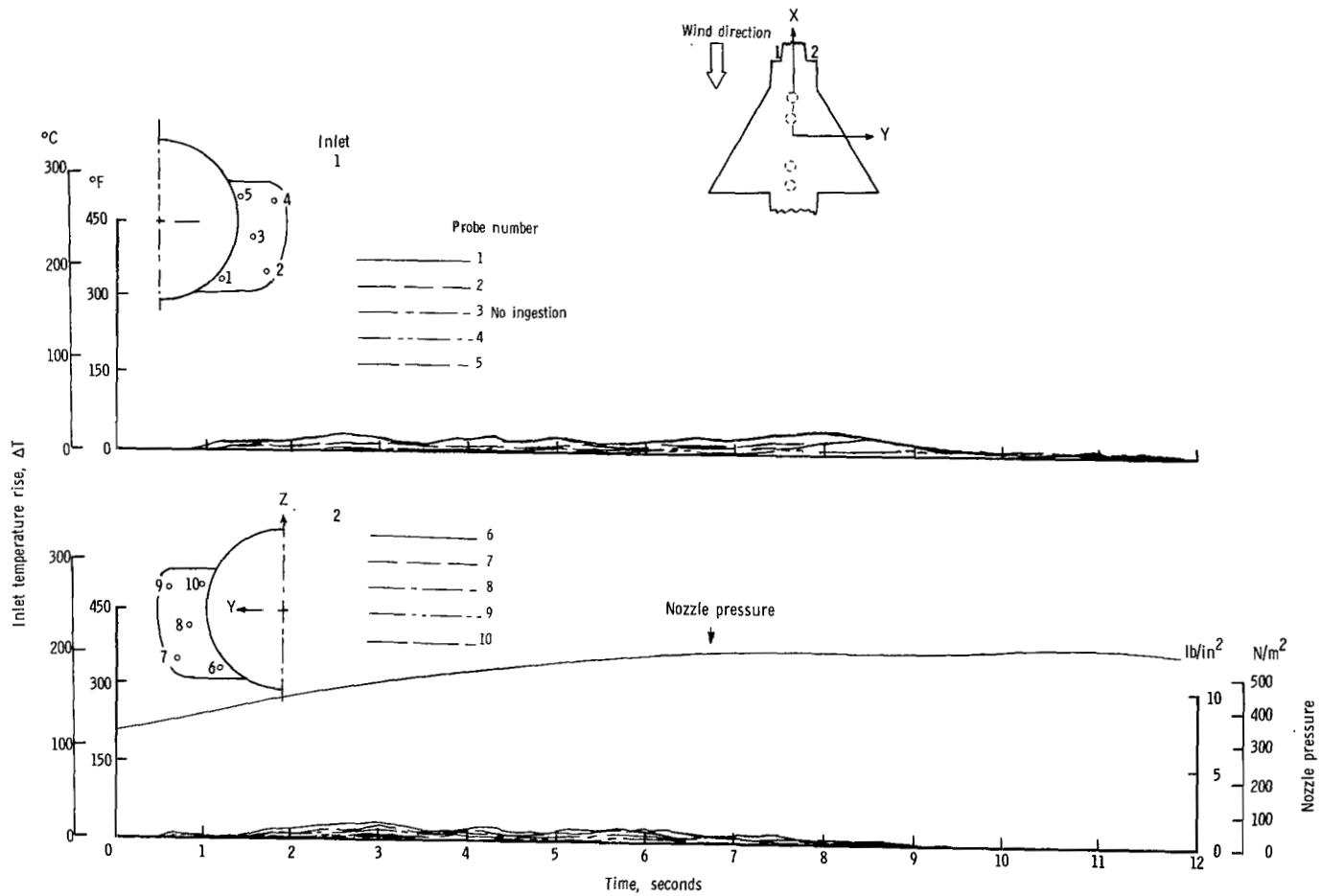

(c) $\psi = 0^0$; V = 11.85 knots.

Figure 28.- Continued.

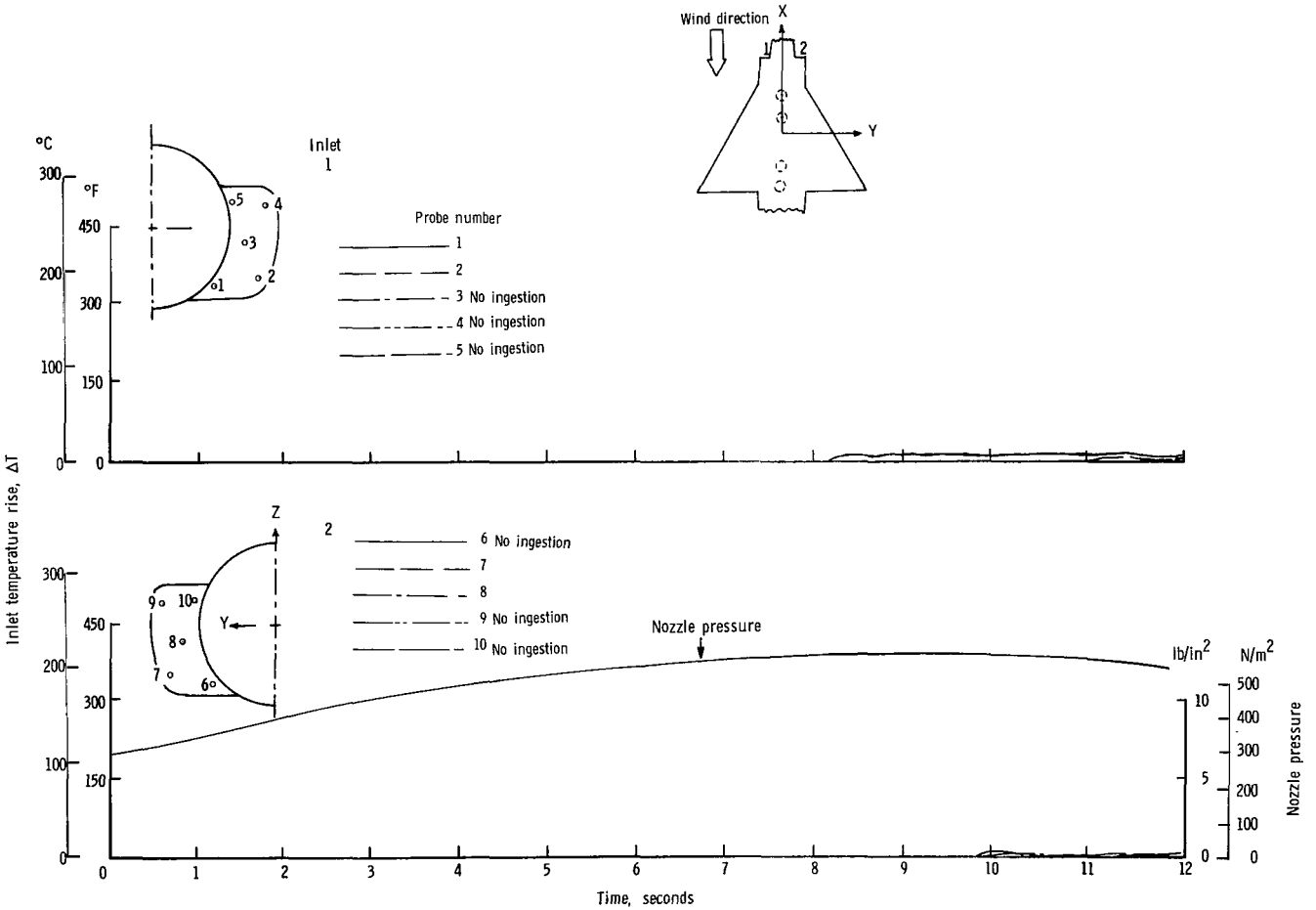

(d) $\psi = 0^{o}$; V = 17.78 knots.

Figure 28.- Continued.

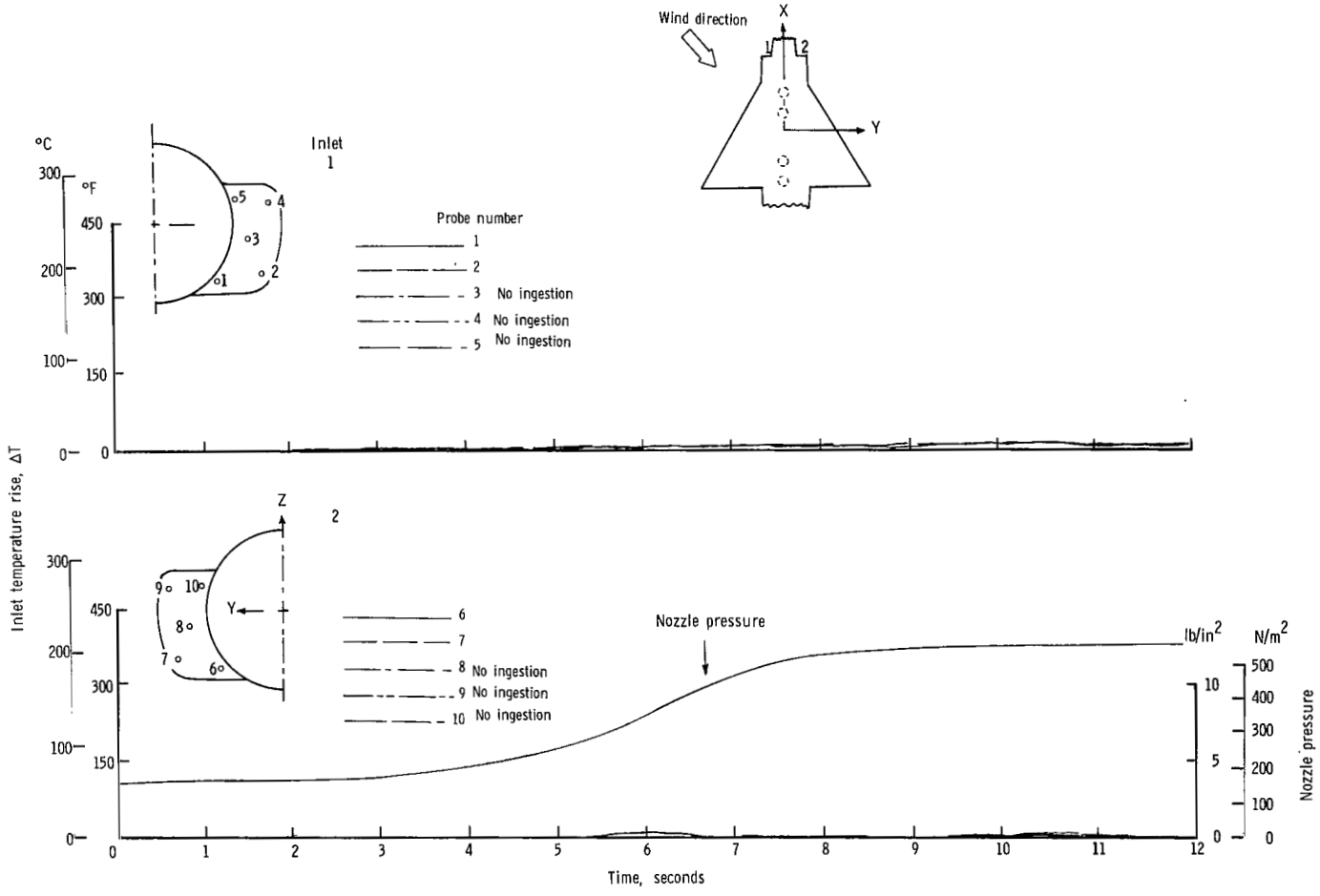

(e) $\psi = 45^{0}$; V = 5.92 knots.

Figure 28.- Continued.

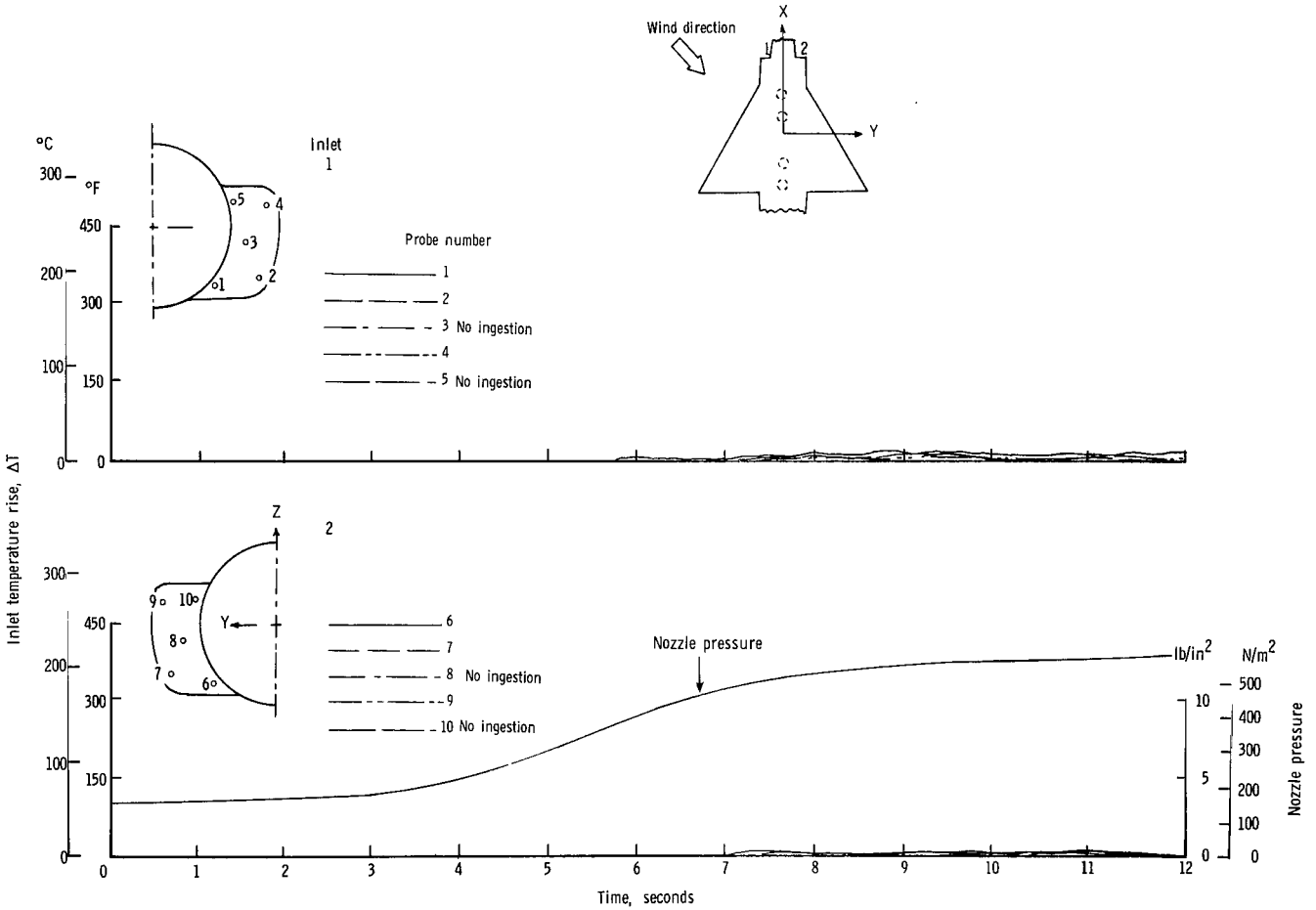

(f) $\psi = 45^0$; V = 11.85 knots.

Figure 28.- Continued.

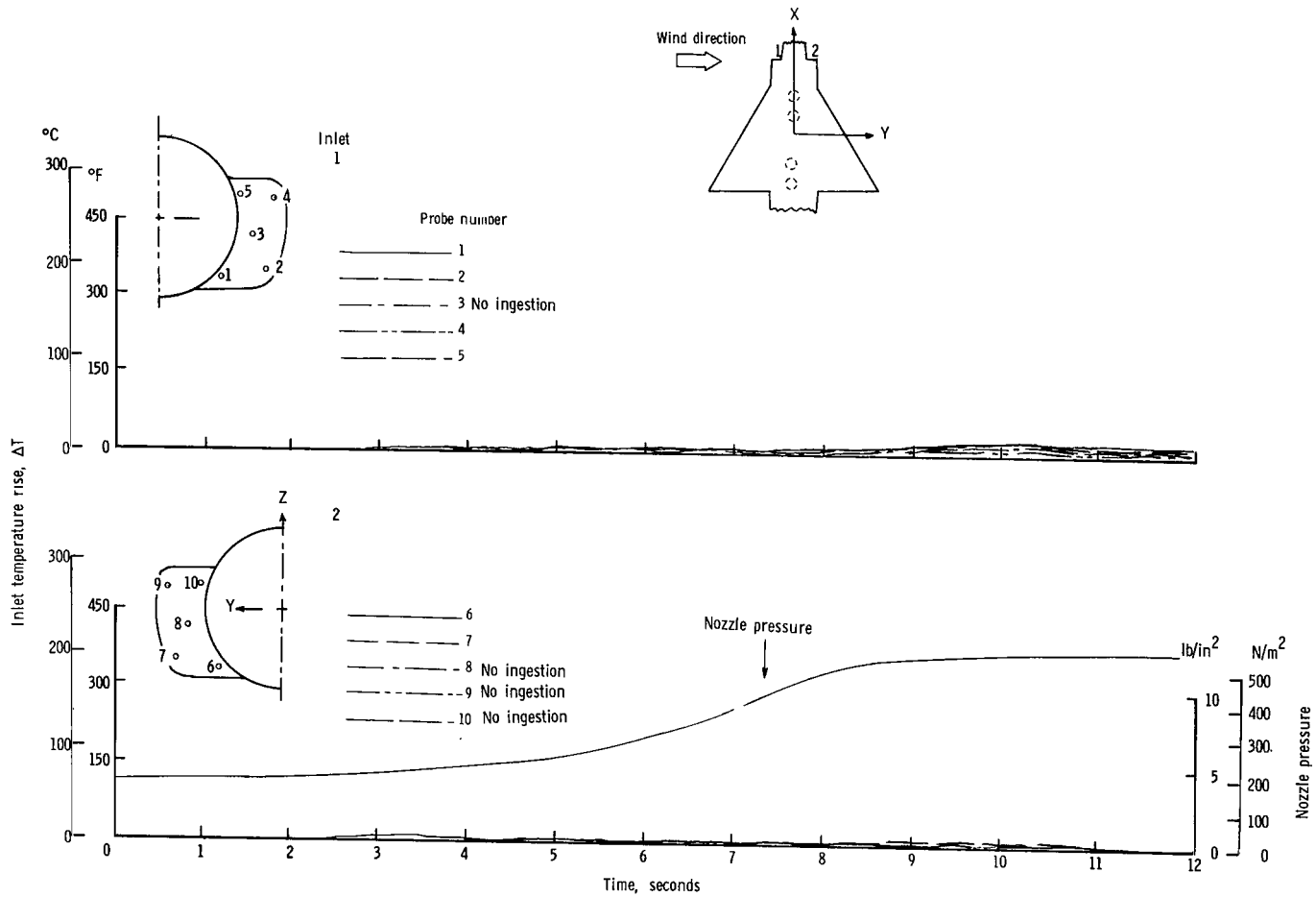

(g) $\psi = 90^0$; V = 5.92 knots.

Figure 28.- Continued.

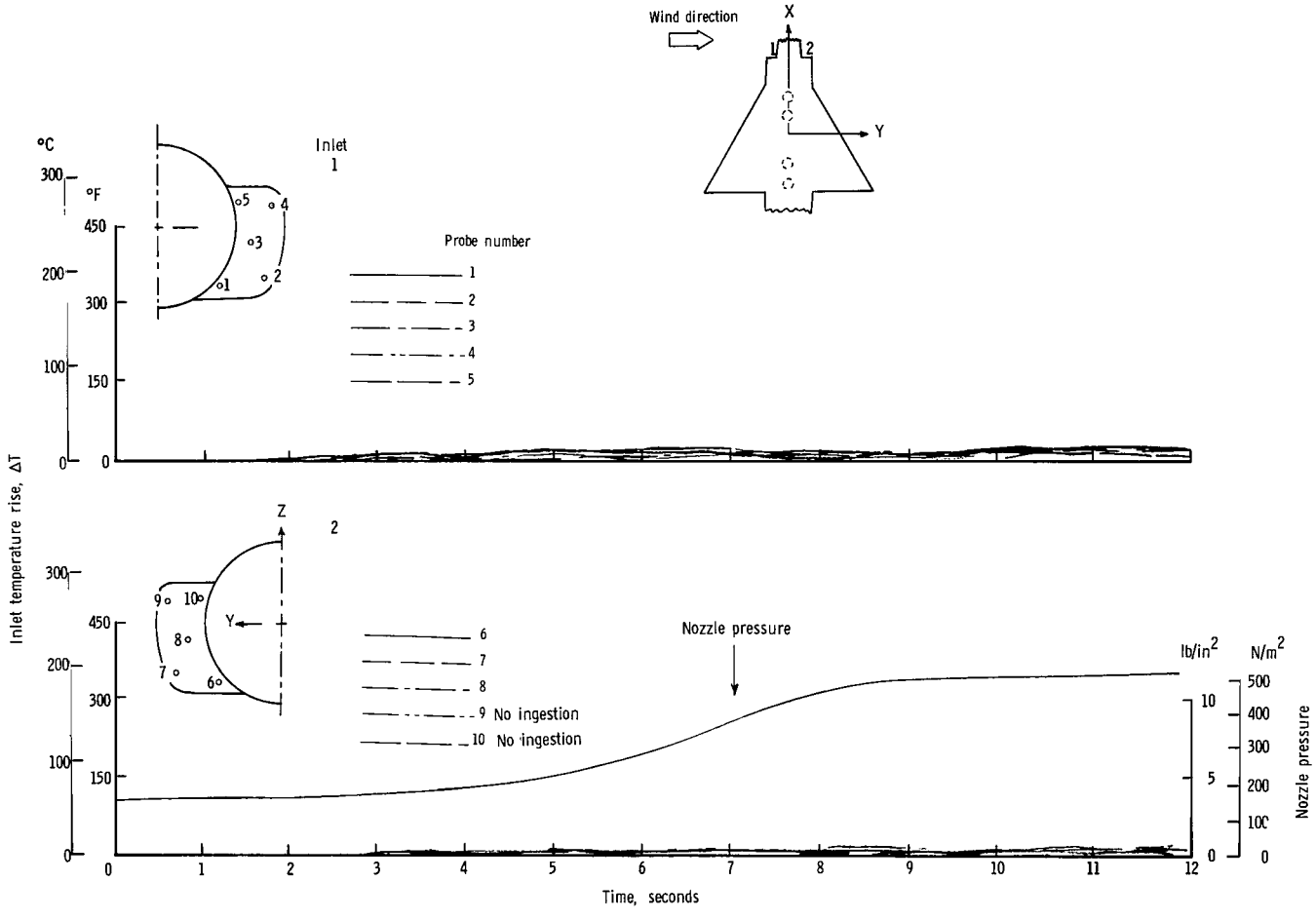

(h) $\psi = 90^0$; V = 11.85 knots.

Figure 28.- Concluded.

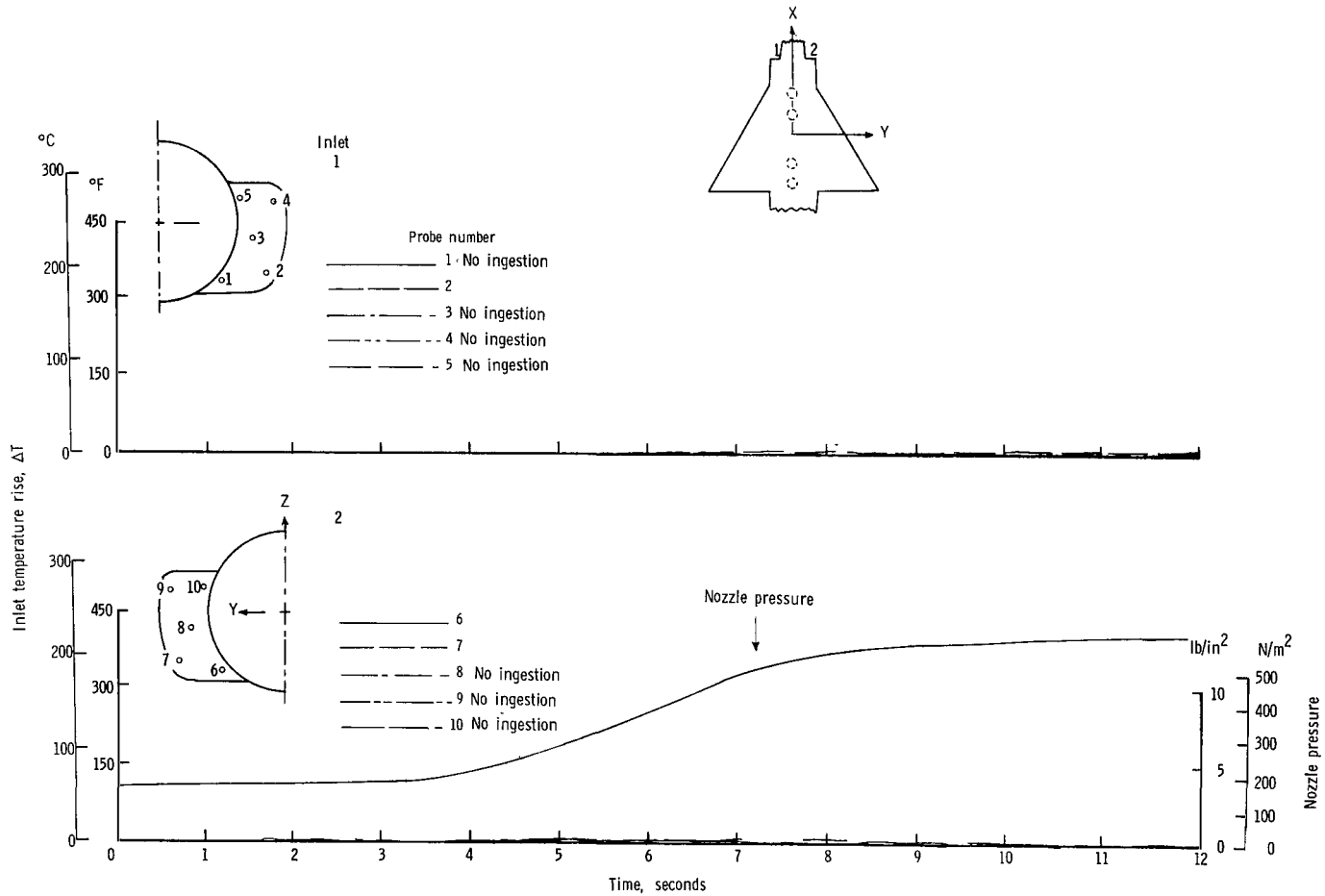

(a) $\psi = 0^0$; V = 0 knots.

Figure 29.- Variation of inlet air temperature rise with time for the in-line nozzle arrangement with side inlets and high delta wing. $h/D_e = 5.0$.

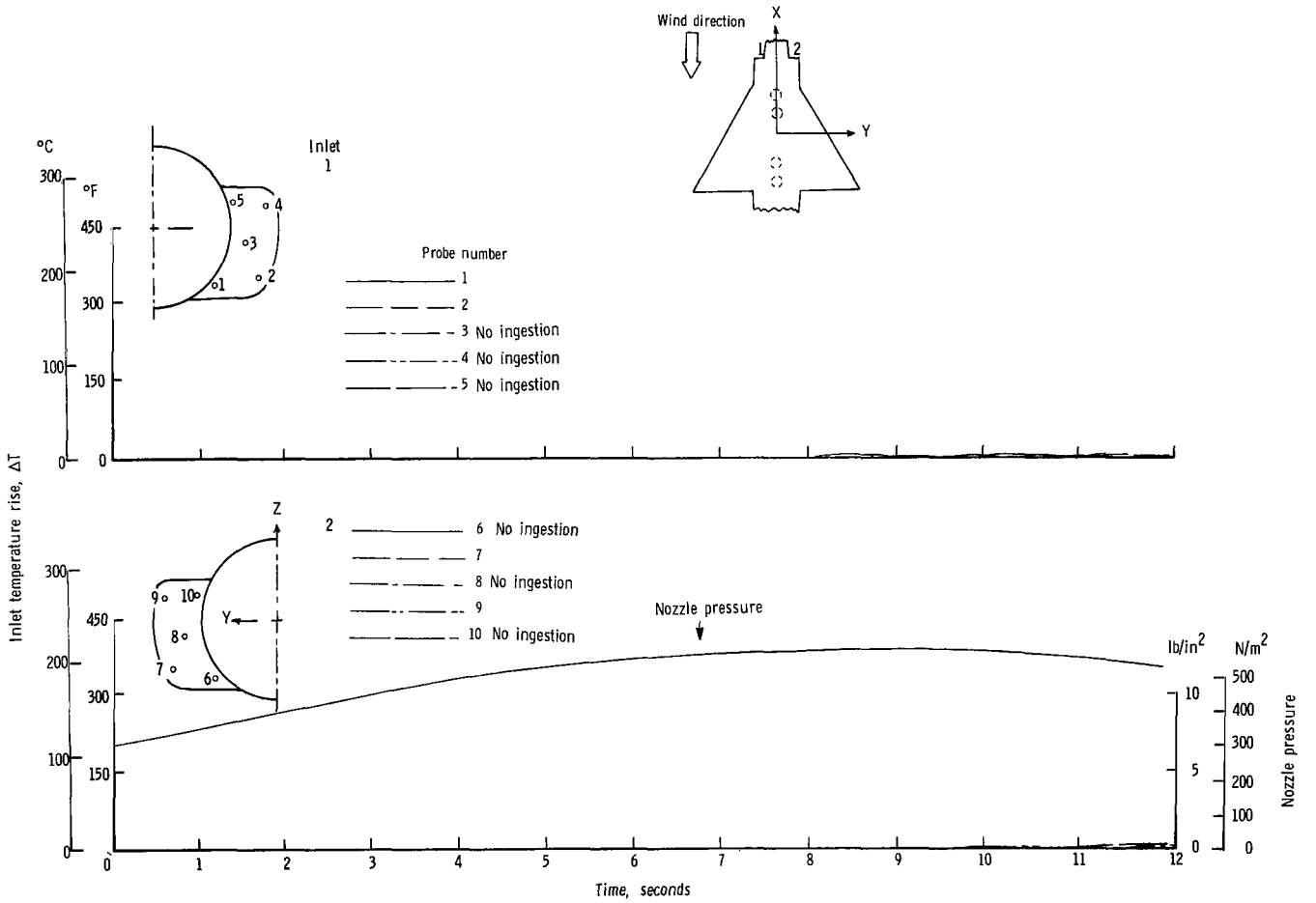

(b) $\psi = 0^{o}$; V = 5.92 knots.

Figure 29.- Continued.

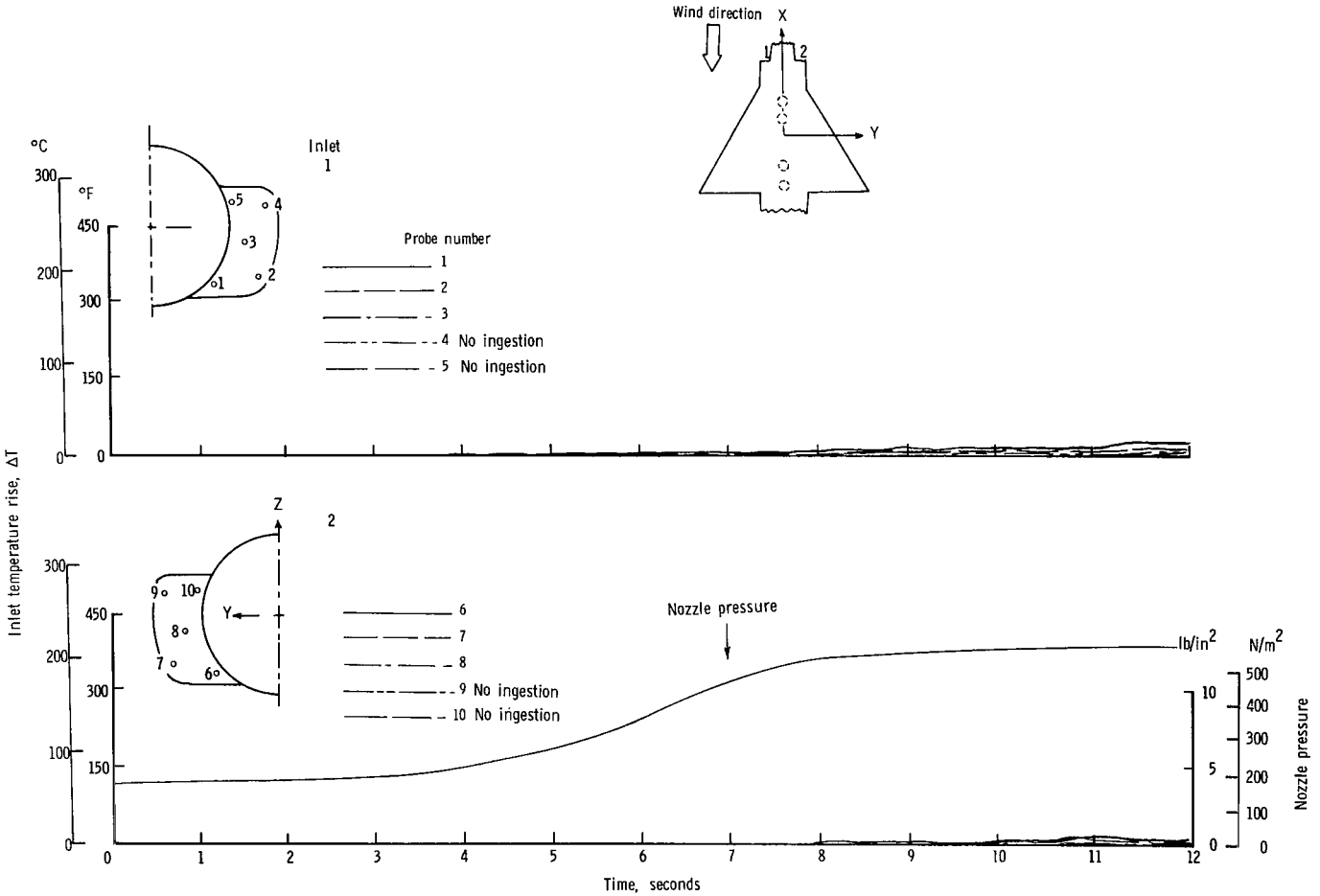

(c) $\psi = 0^0$; V = 11.85 knots.

Figure 29.- Continued.

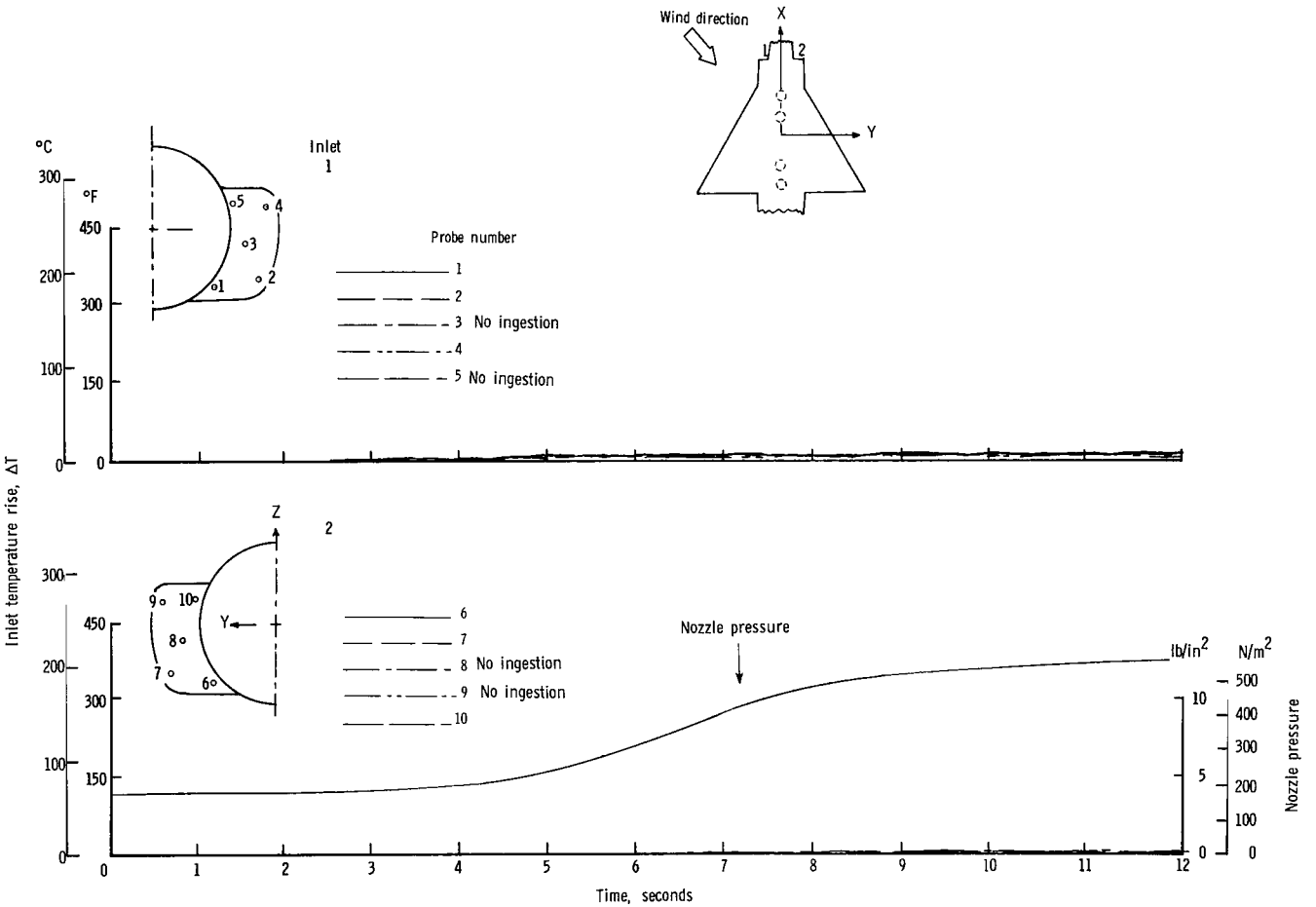

(d) $\psi = 45^{0}$; V = 5.92 knots.

Figure 29.- Continued.

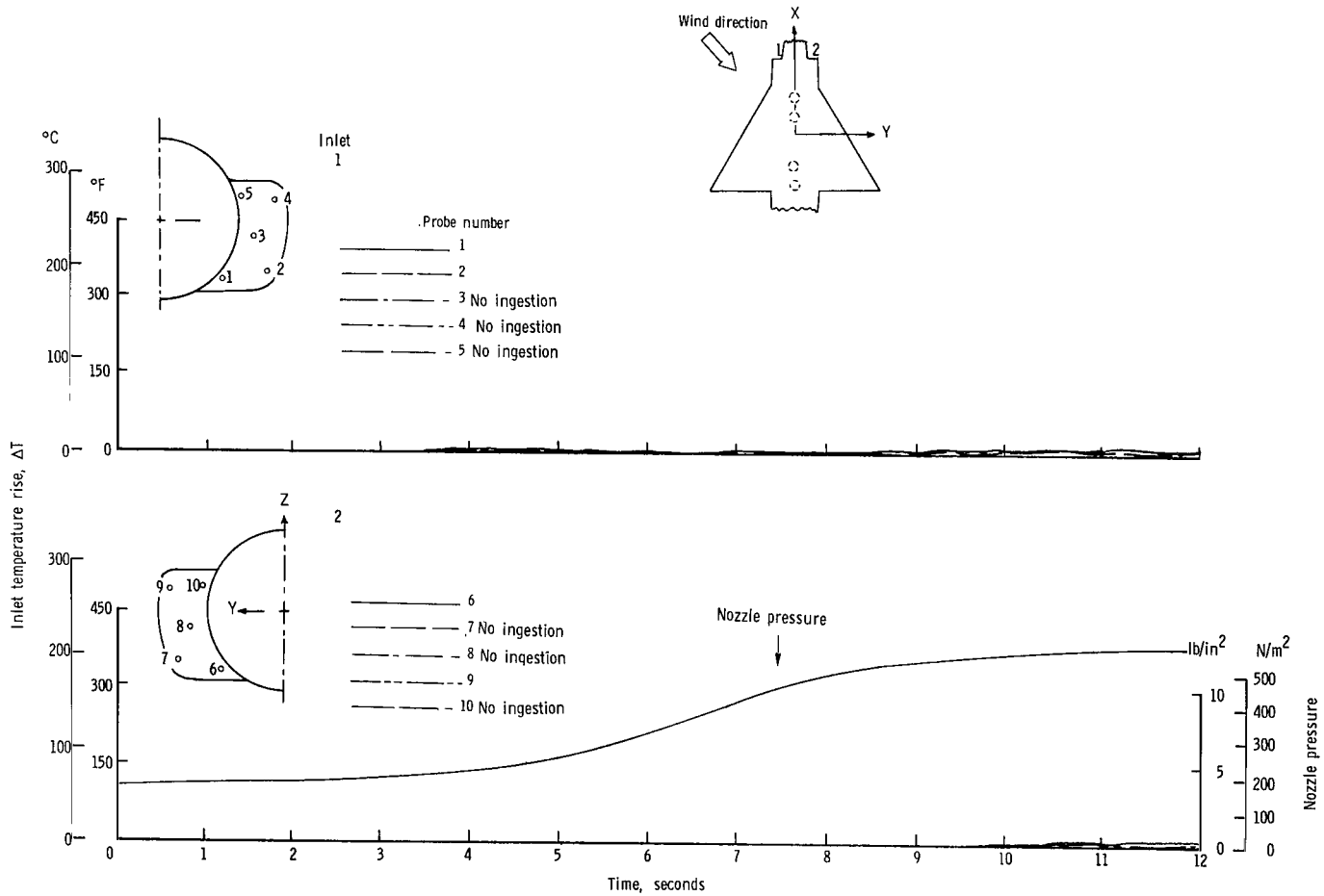

(e) $\psi = 45^0$; V = 11.85 knots.

Figure 29.- Continued.

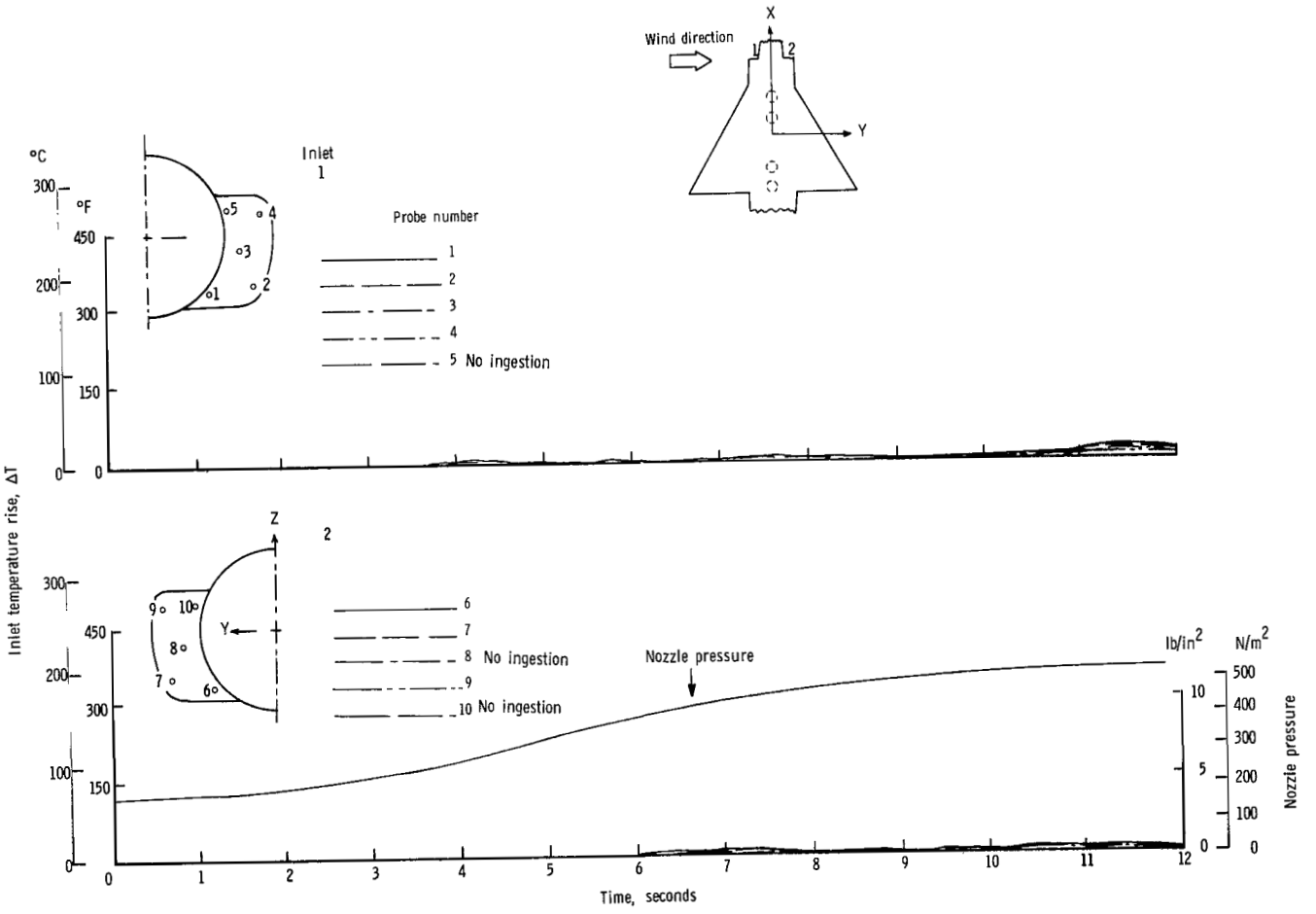

(f) $\psi = 90^{o}$; V = 5.92 knots.

Figure 29.- Continued.

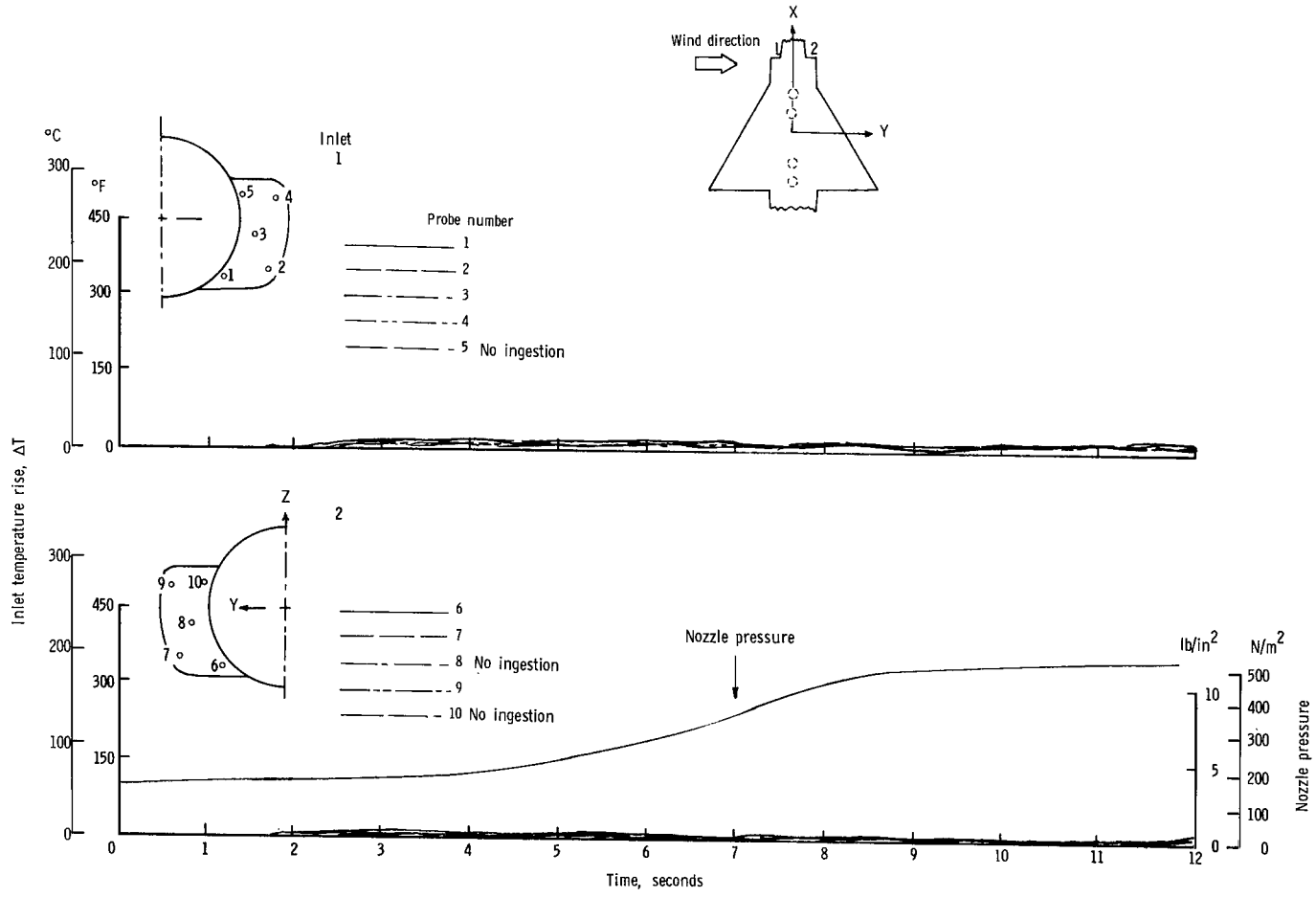

(g) $\psi = 90^0$; V = 11.85 knots.

Figure 29.- Concluded.

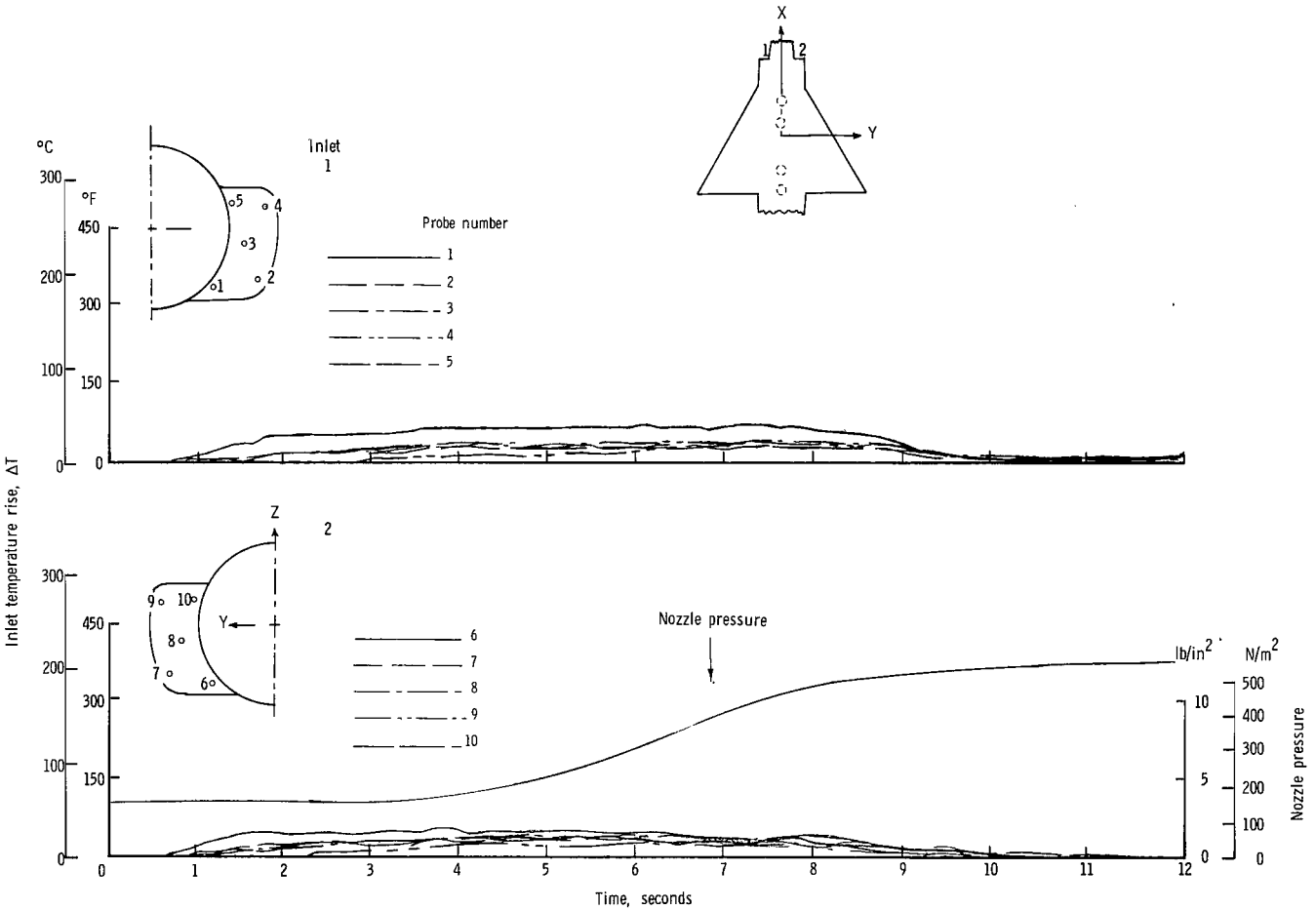

(a) $\psi = 0^{o}$; V = 0 knots.

Figure 30.- Variation of inlet air temperature rise with time for the in-line nozzle arrangement with side inlets and low delta wing. $h/D_e = 1.17$.

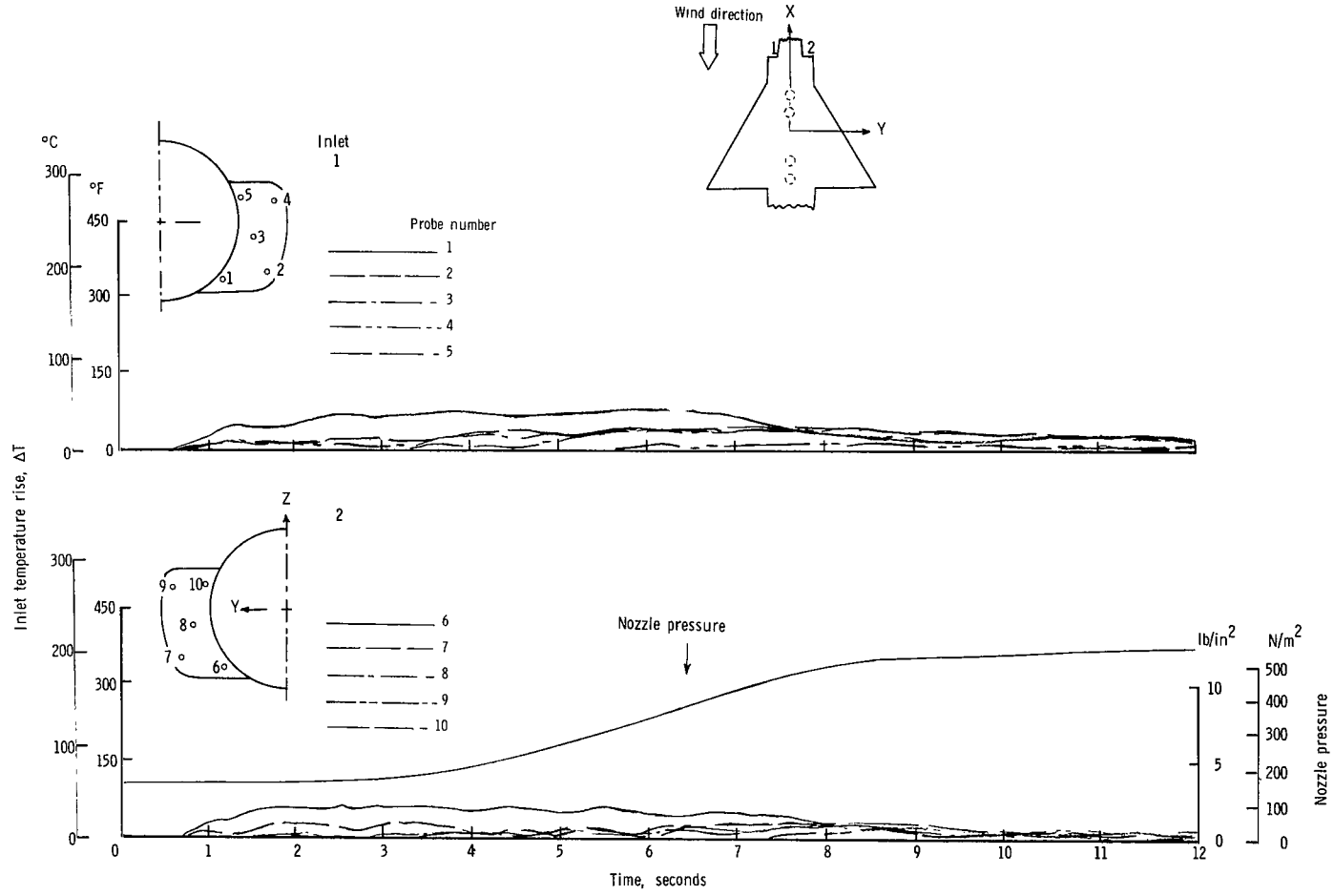

(b) $\psi = 0^0$; V = 5.92 knots.

Figure 30.- Continued.

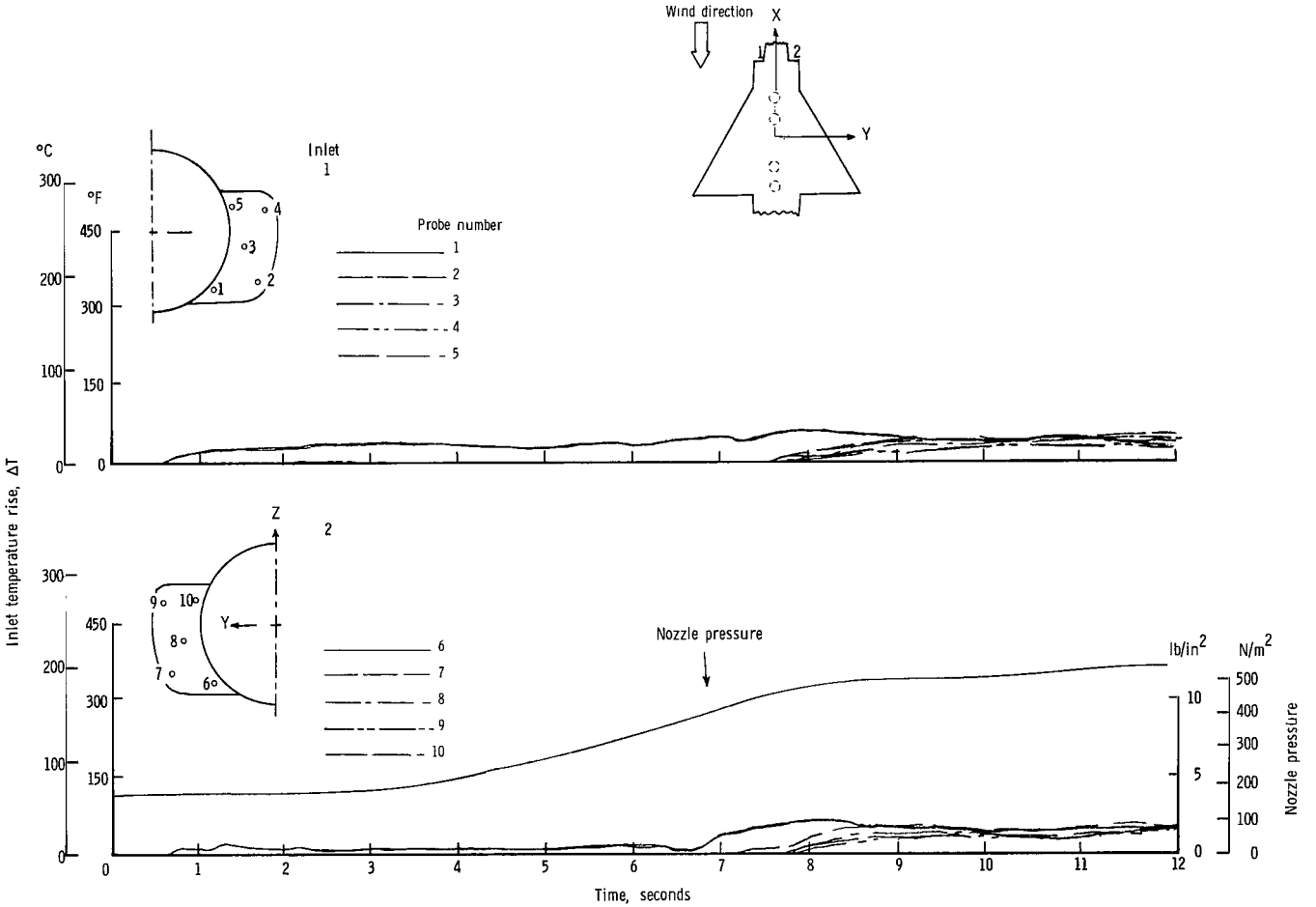

(c) $\psi = 0^0$; V = 11.85 knots.

Figure 30.- Continued.

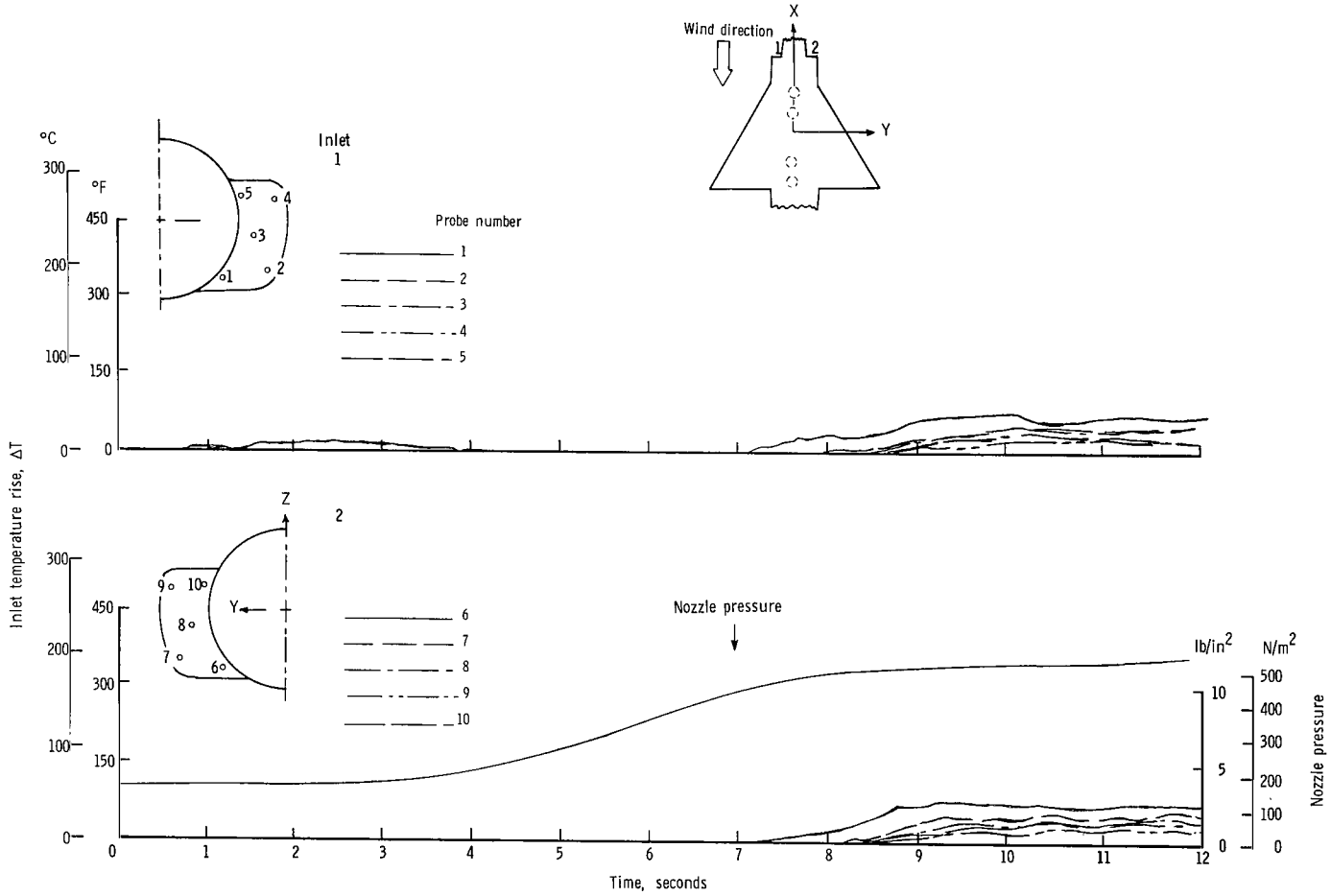

(d) $\psi = 0^{o}$; V = 17.78 knots.

Figure 30.- Continued.

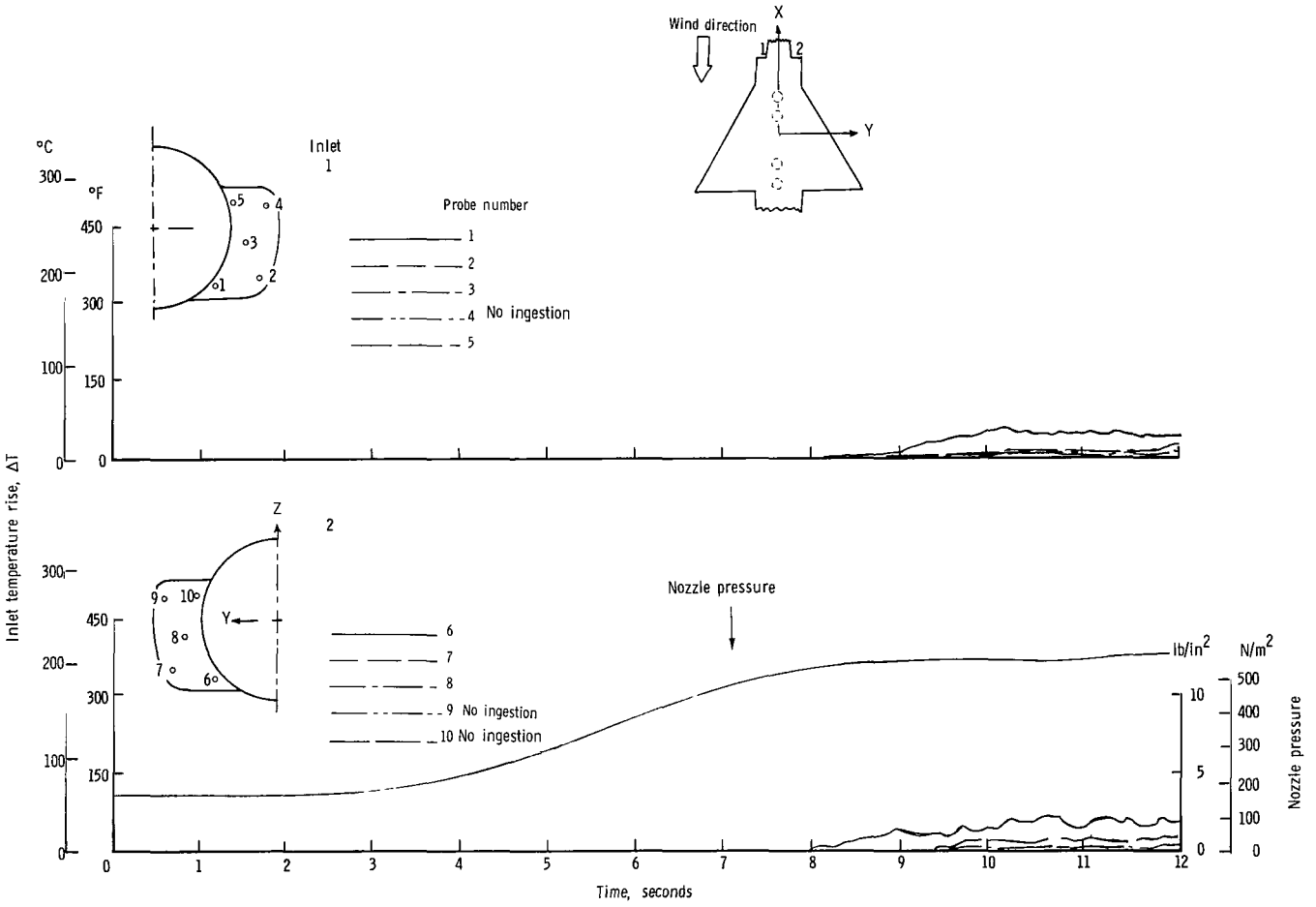

(e) $\psi = 0^0$; V = 23.70 knots.

Figure 30.- Continued.

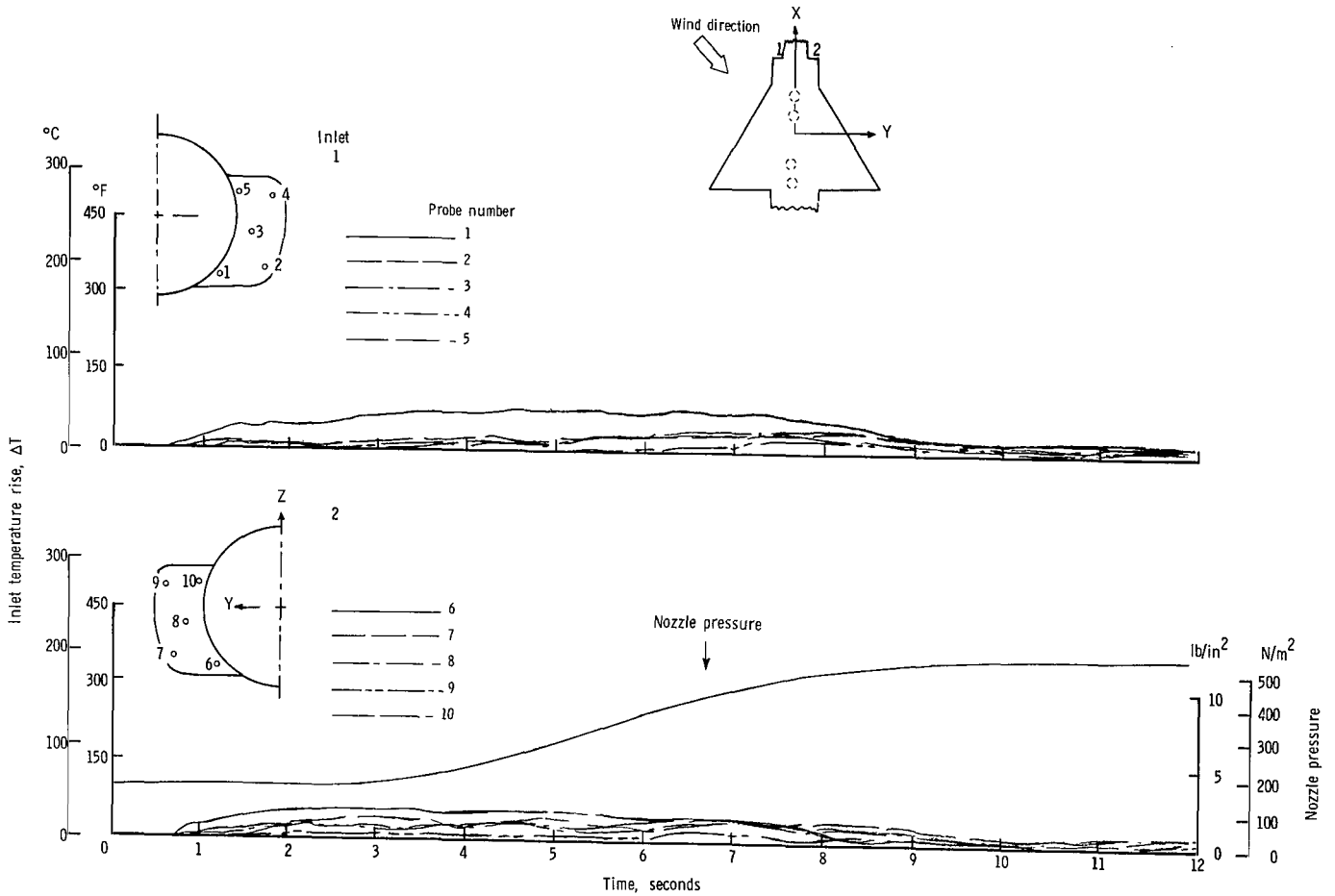

(f) $\psi = 45^0$; V = 5.92 knots.

Figure 30.- Continued.

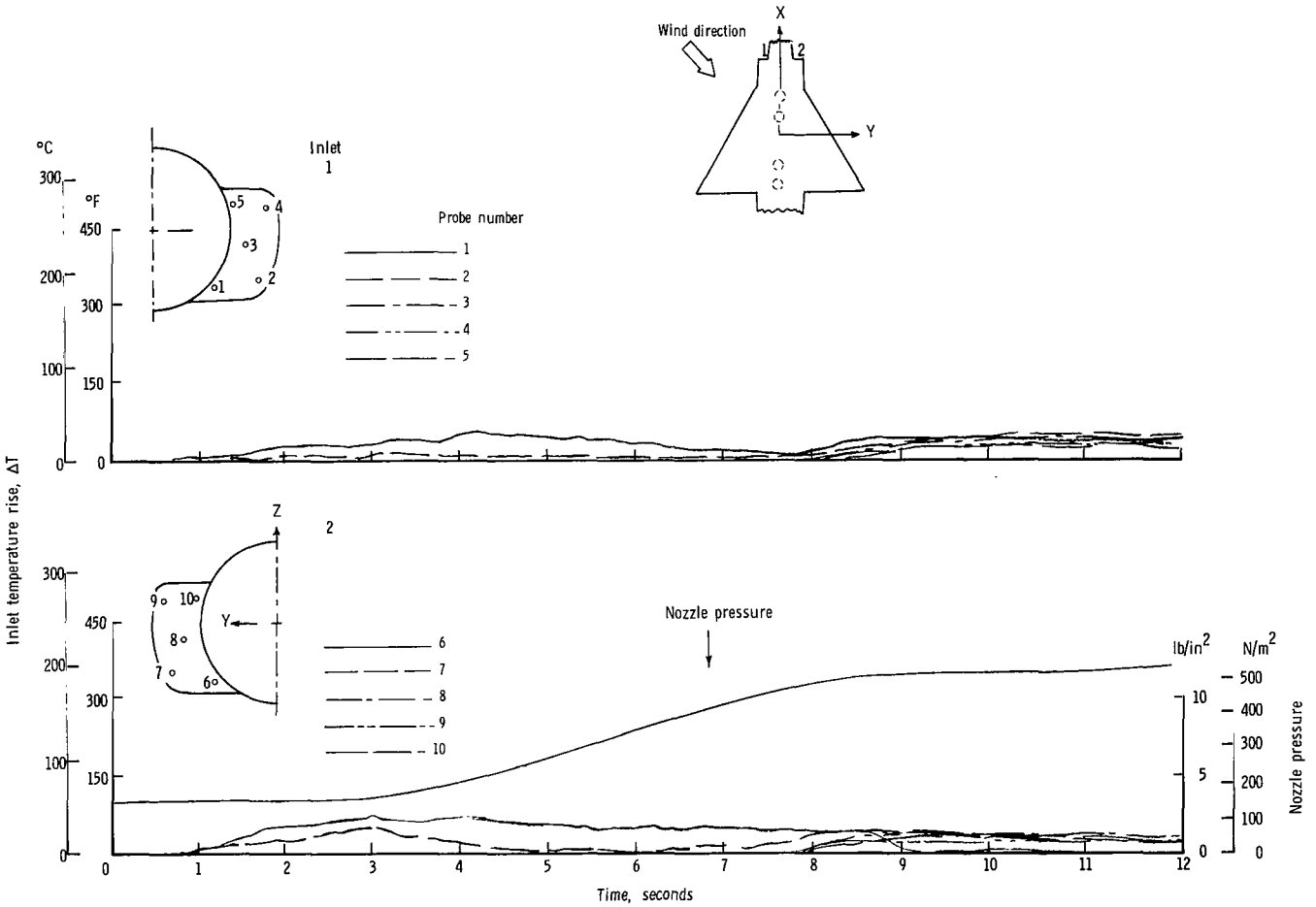

(g) $\psi = 45^0$; V = 11.85 knots.

Figure 30.- Continued.

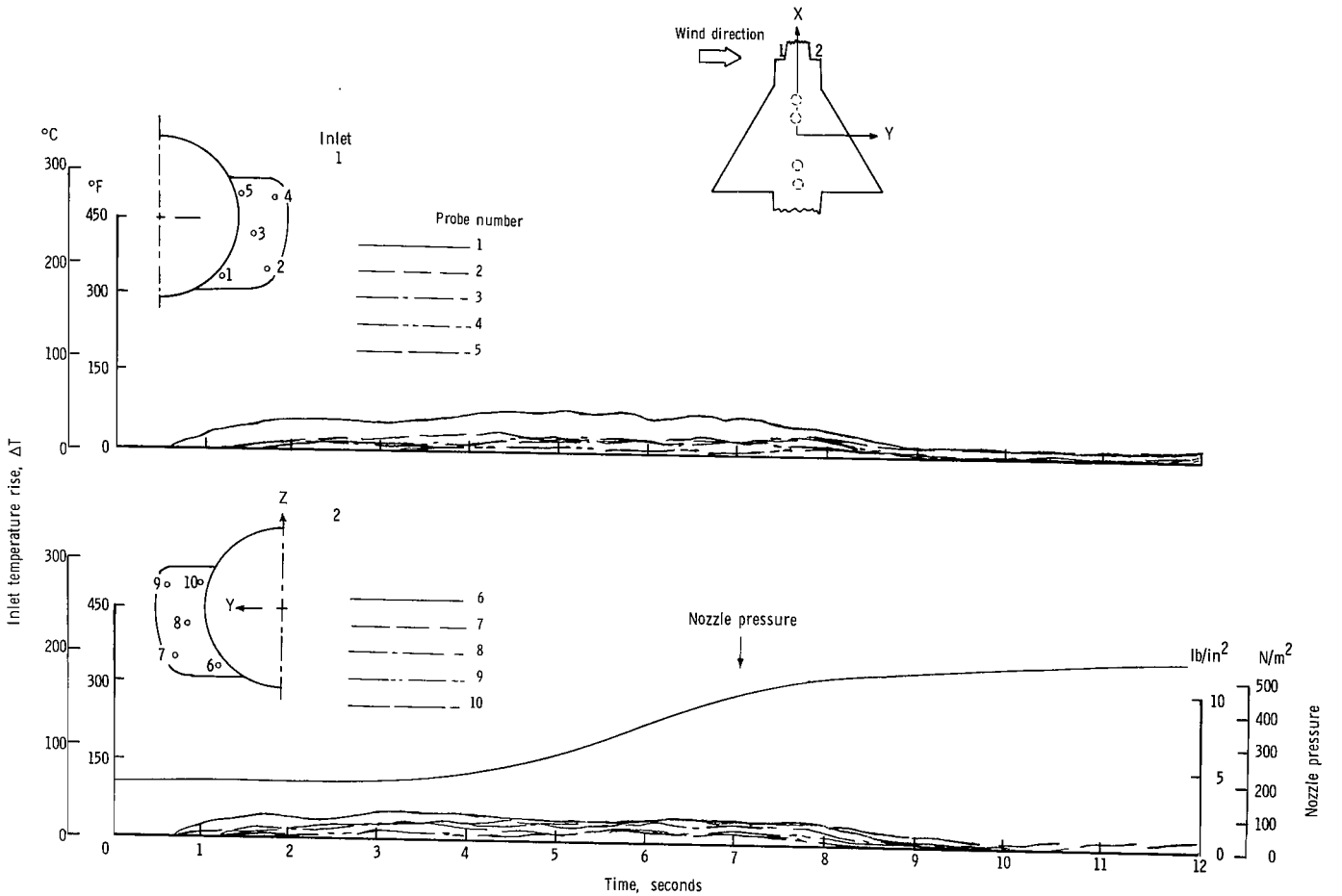

(h) $\psi = 90^0$; V = 5.92 knots.

Figure 30.- Continued.

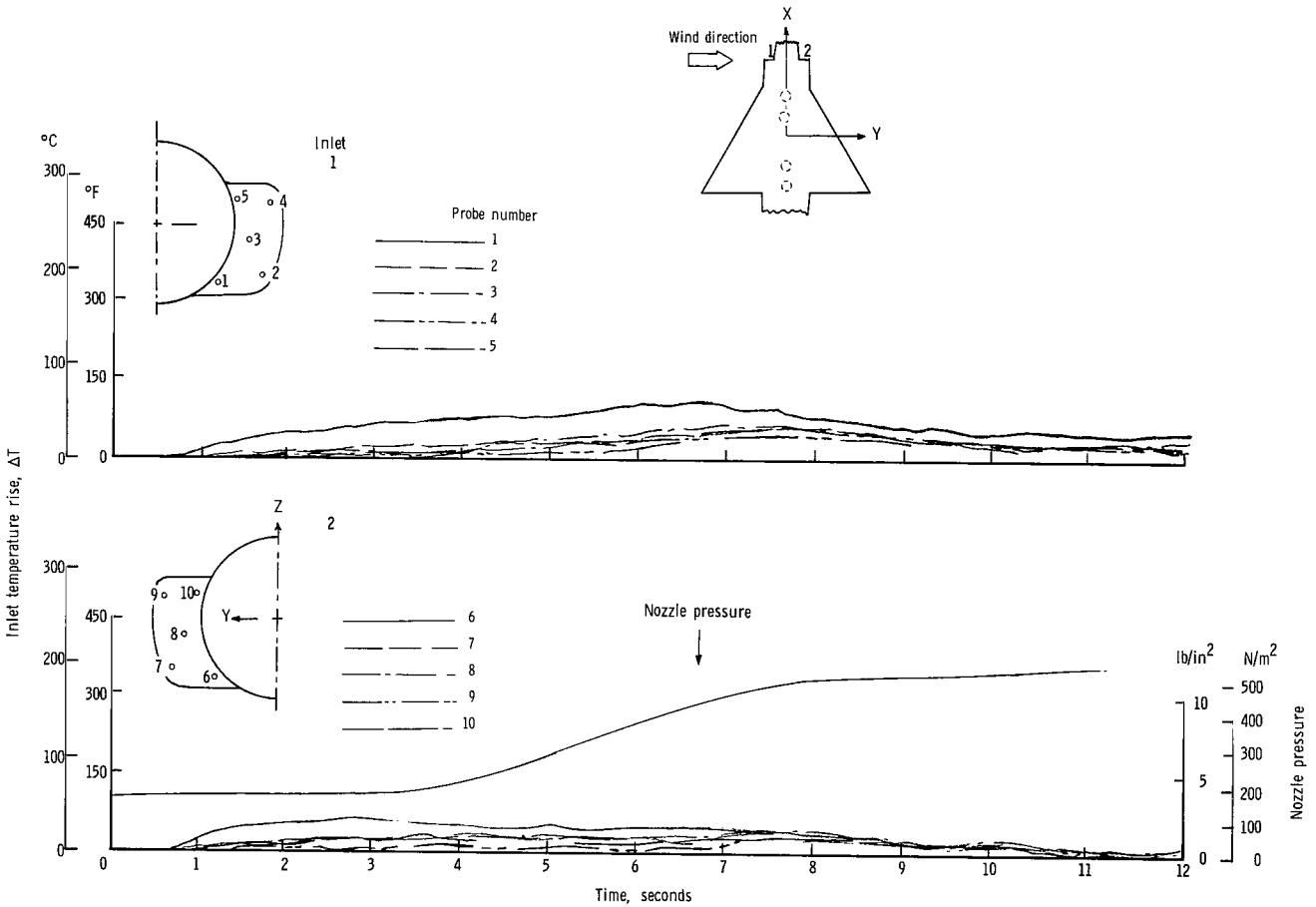

(i) $\psi = 90^0$; V = 11.85 knots.

Figure 30.- Concluded.

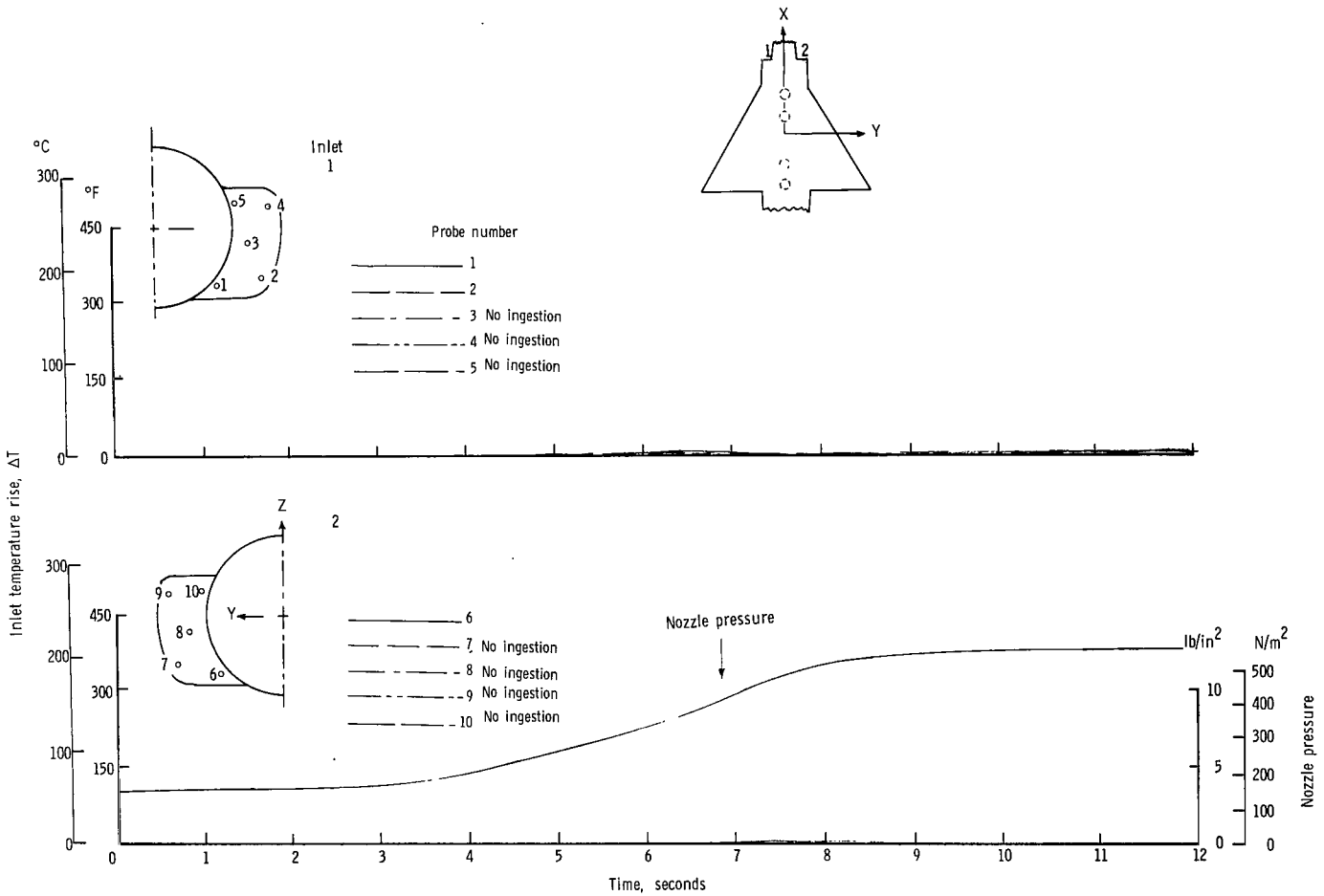

(a) $\psi = 0^0$; V = 0 knots.

Figure 31.- Variation of inlet air temperature rise with time for the in-line nozzle arrangement with side inlets and low delta wing. $h/D_e = 3.0$.

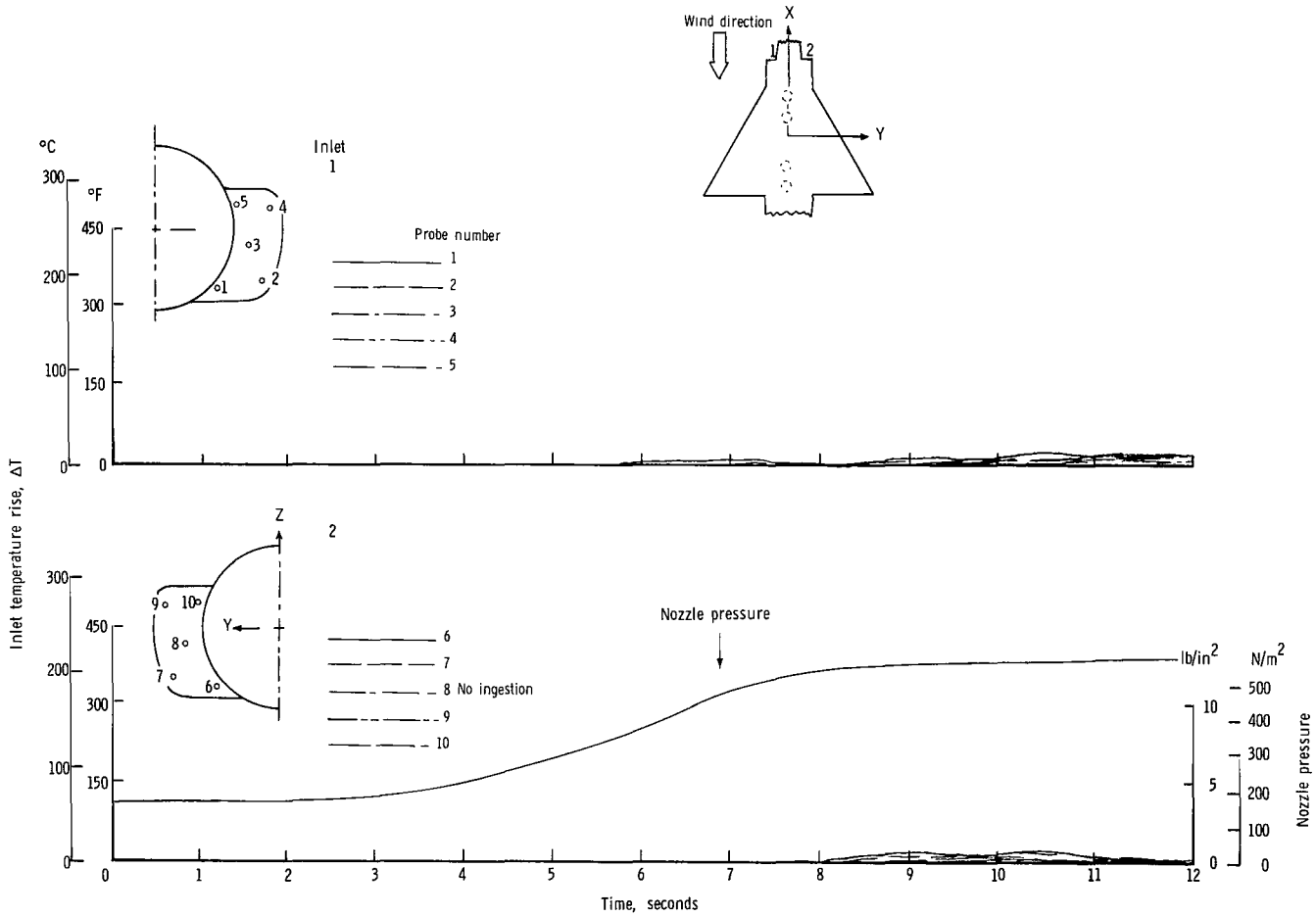

(b) $\psi = 0^{o}$; V = 5.92 knots.

Figure 31.- Continued.

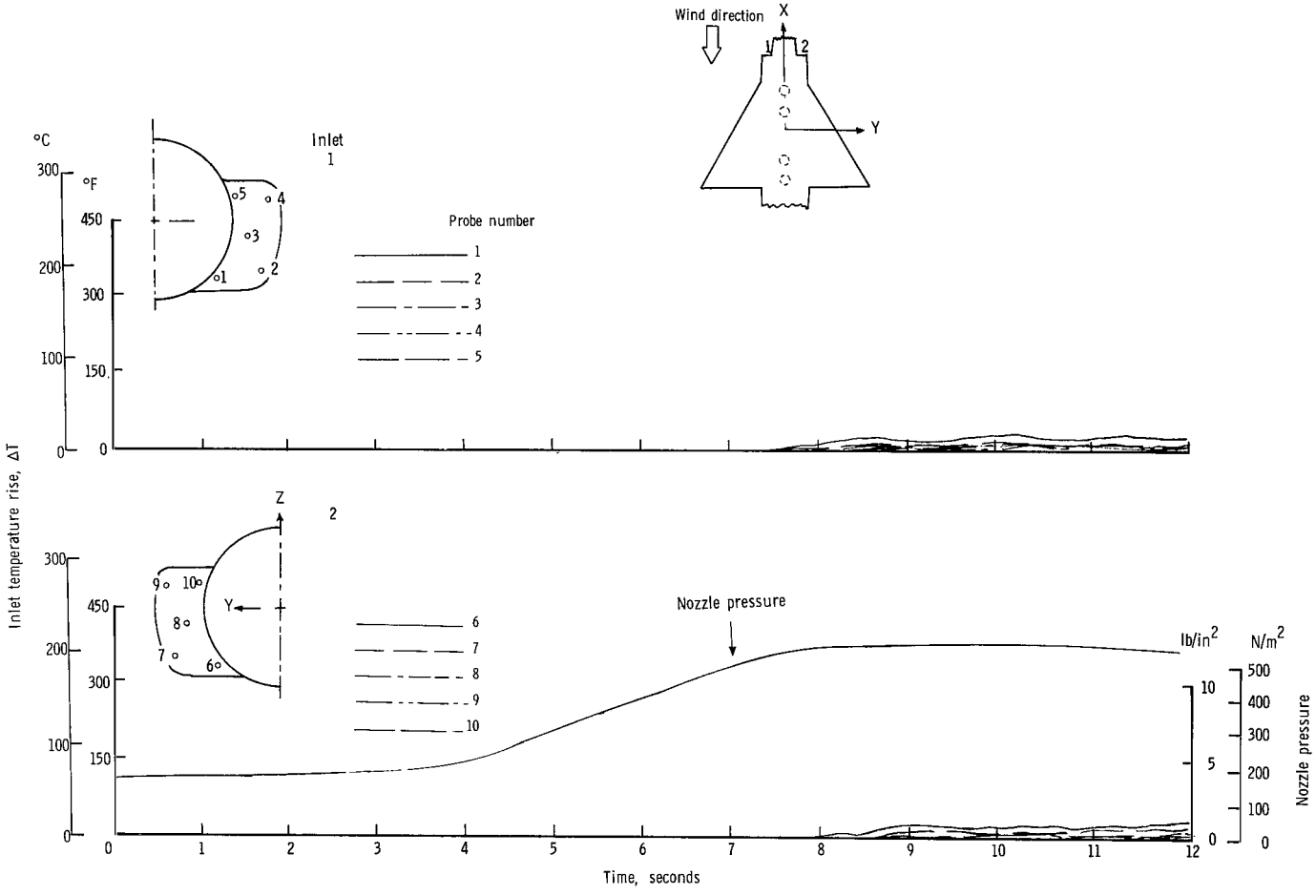

(c) $\psi = 0^{o}$; V = 11.85 knots.

Figure 31.- Continued.

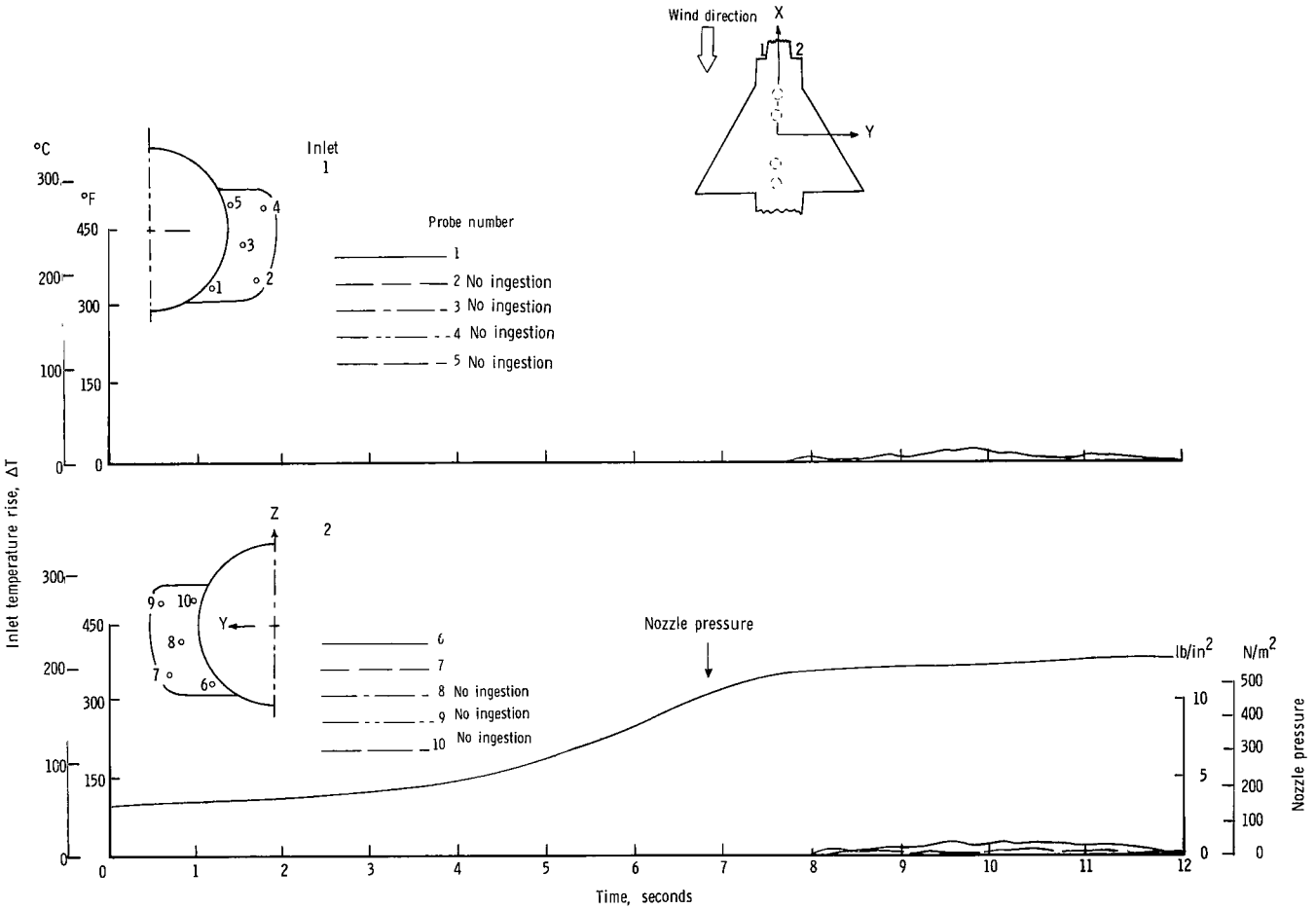

(d) $\psi = 0^0$; V = 17.78 knots.

Figure 31.- Continued.

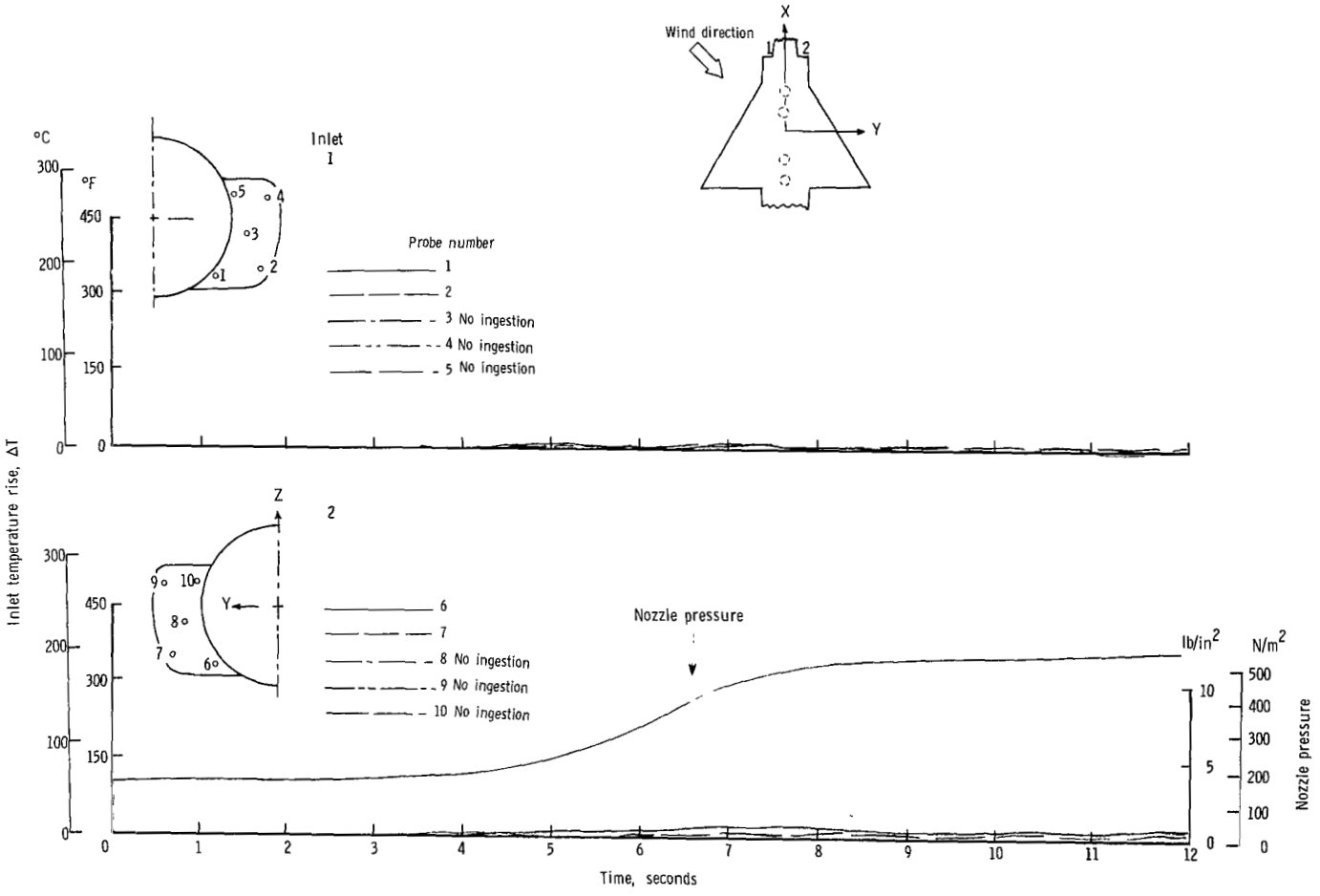

(e) $\psi = 45^0$; V = 5.92 knots.

Figure 31.- Continued.

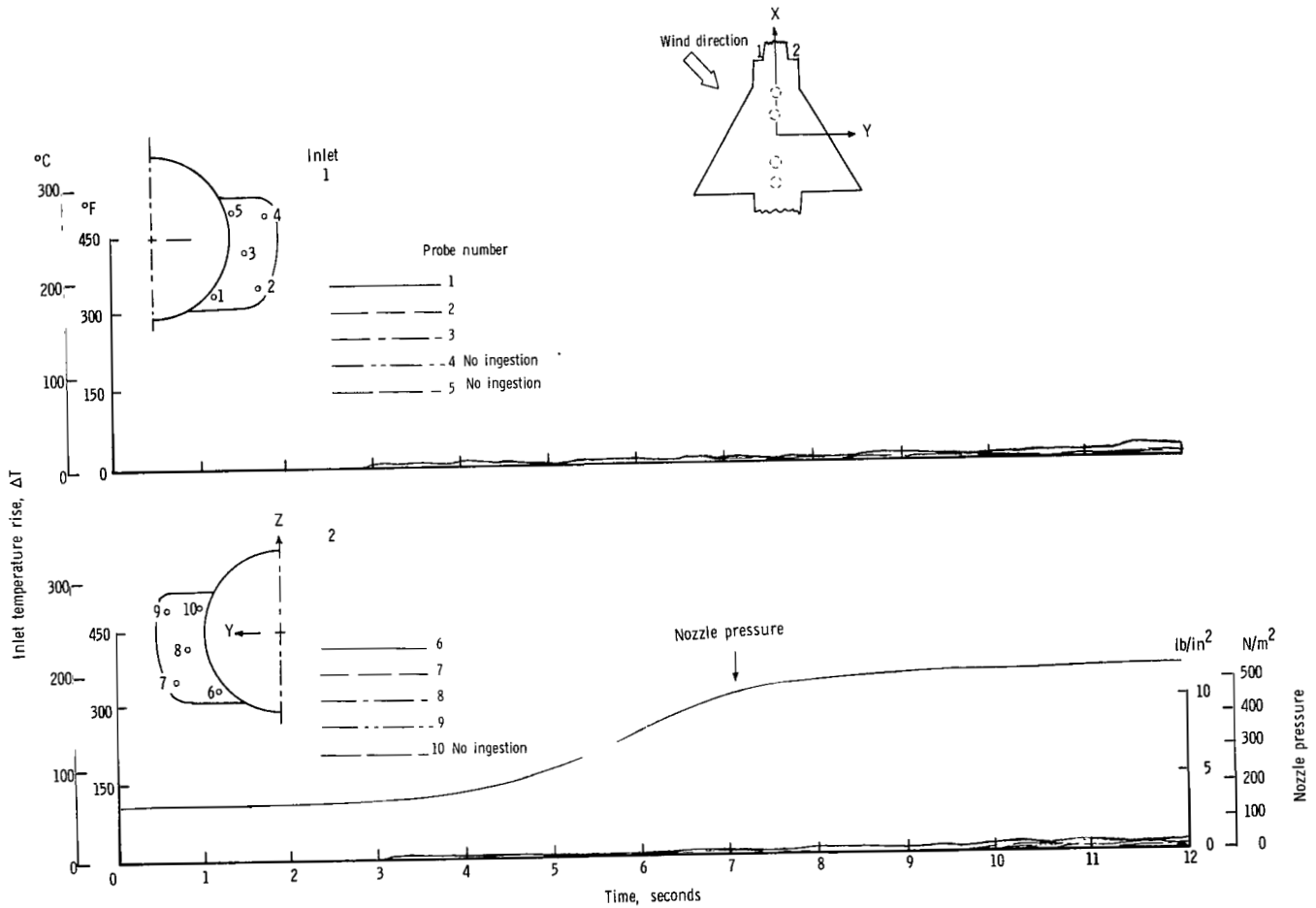

(f) $\psi = 45^{o}$; V = 11.85 knots.

Figure 31.- Continued.

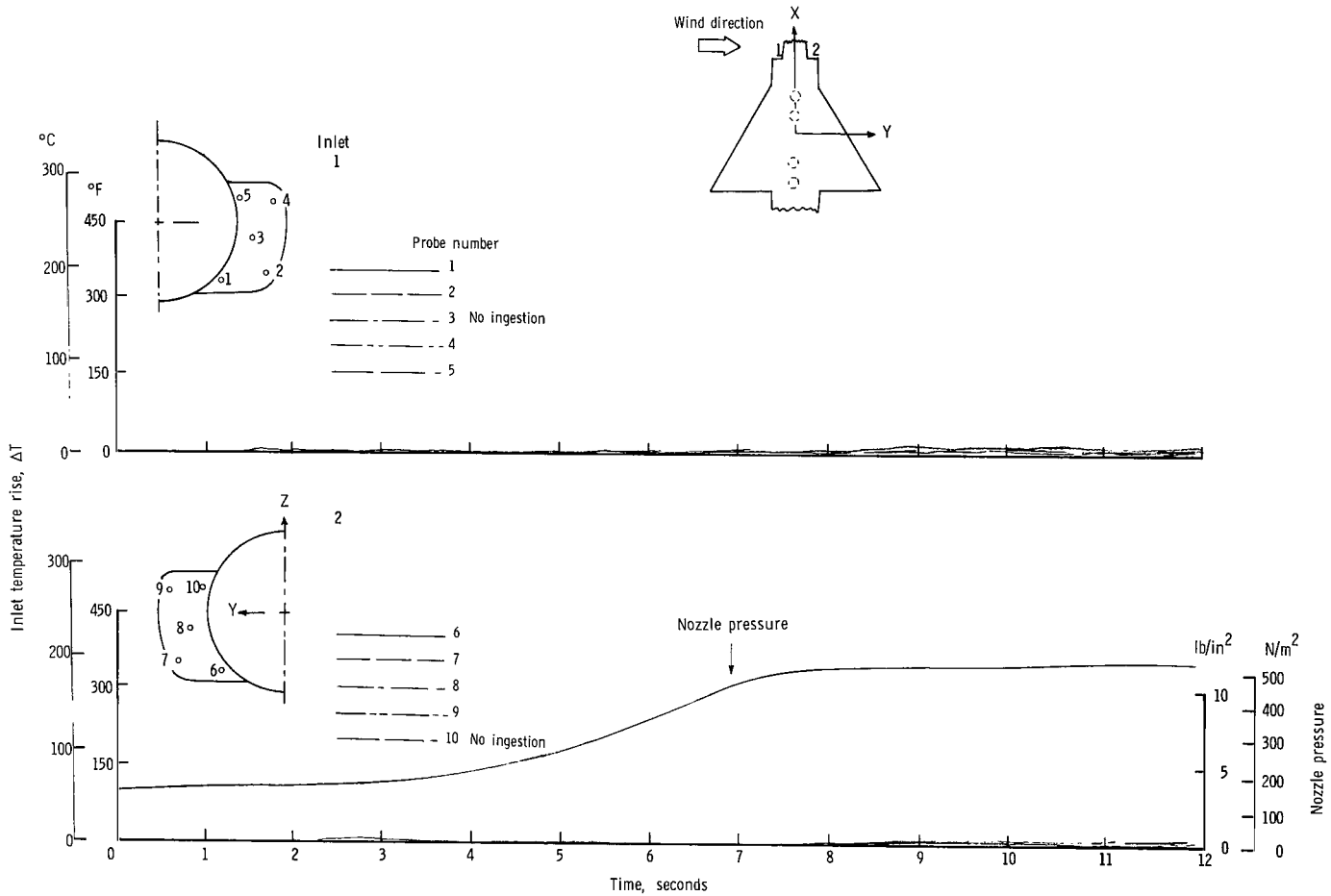

(g) $\psi = 90^0$; V = 5.92 knots.

Figure 31.- Continued.

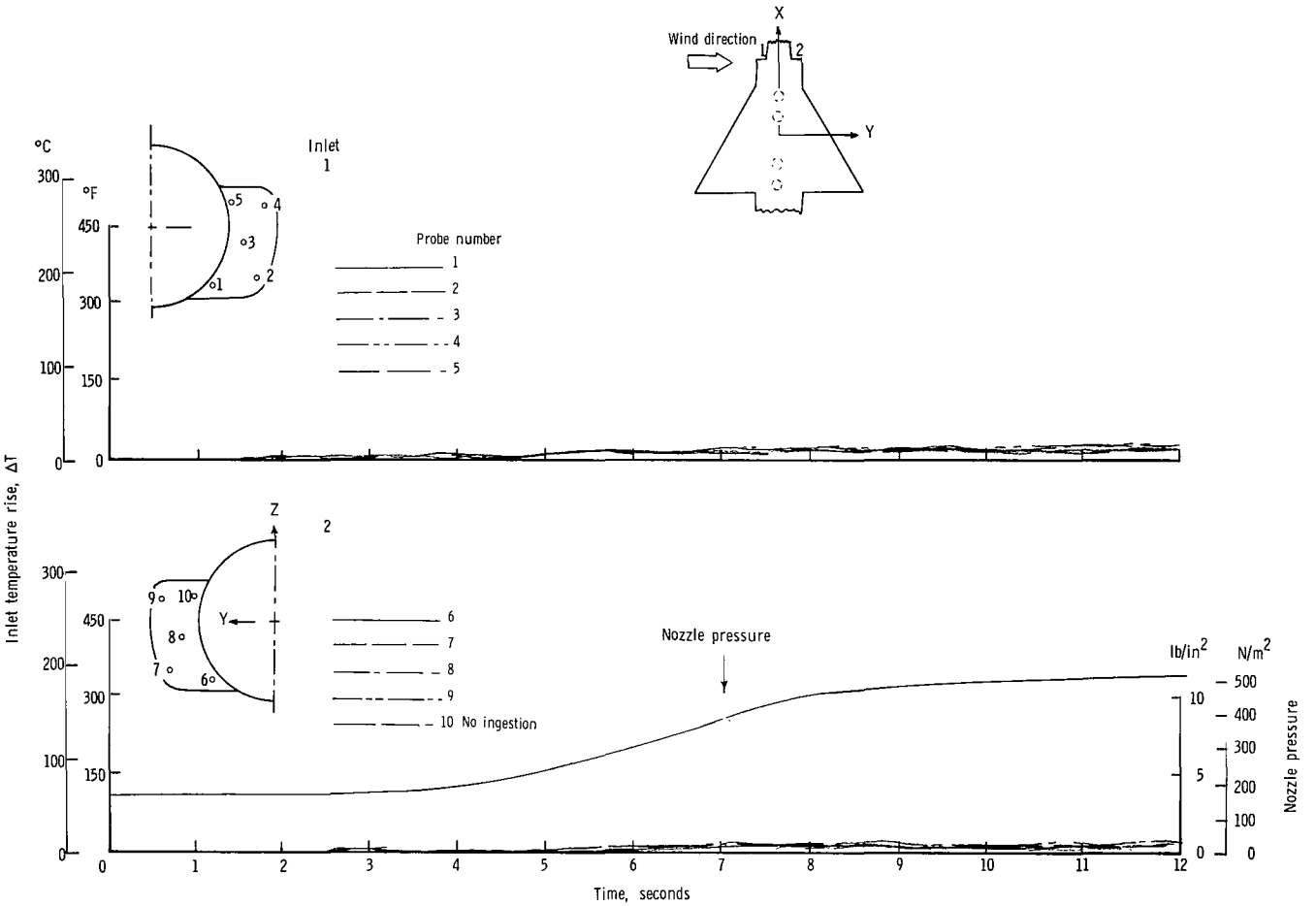

(h) $\psi = 90^0$; V = 11.85 knots.

Figure 31.- Concluded.

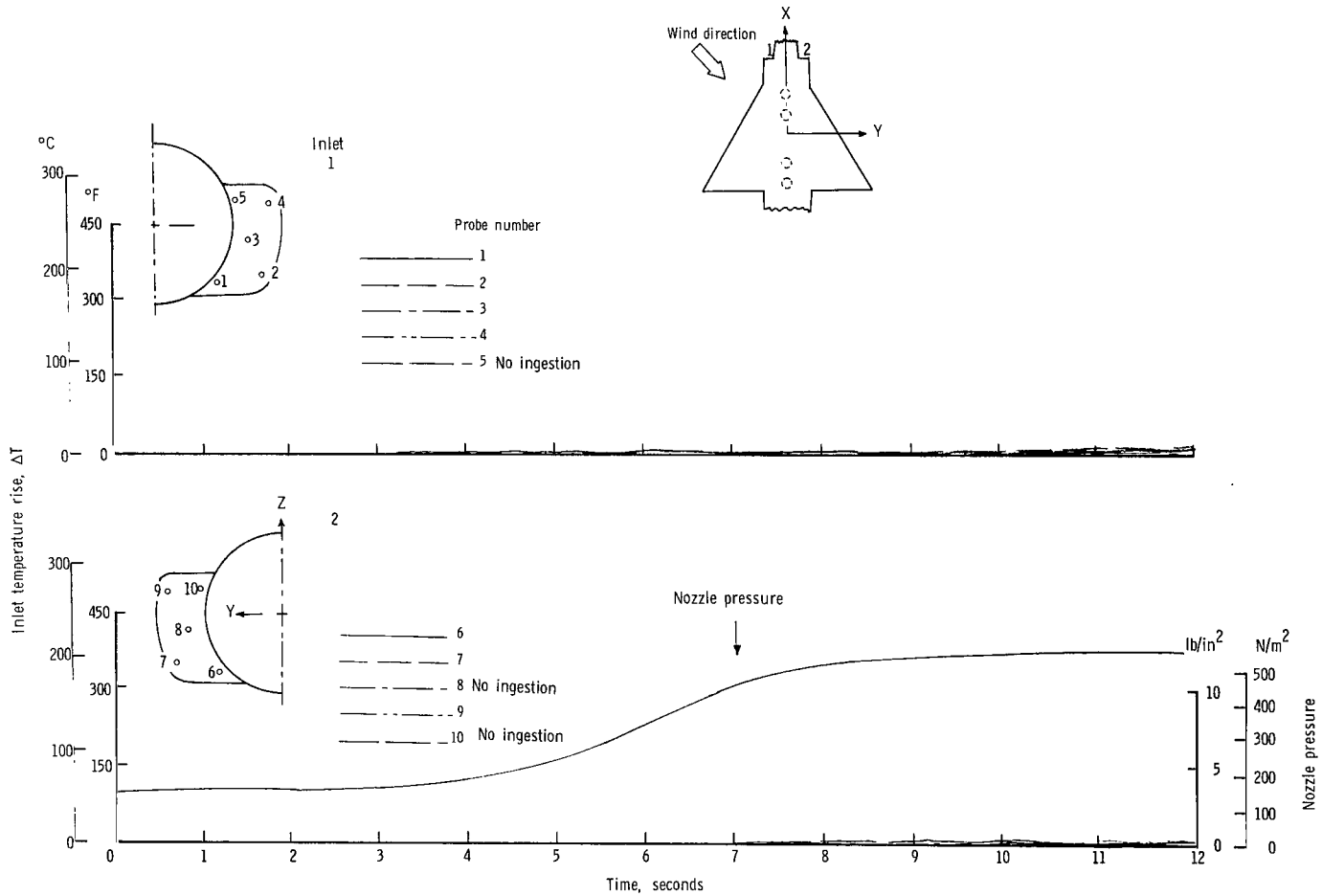

(a) $\psi = 45^0$; V = 5.92 knots.

Figure 32.- Variation of inlet air temperature rise with time for the in-line nozzle arrangement with side inlets and low delta wing. $h/D_e = 5.0$.

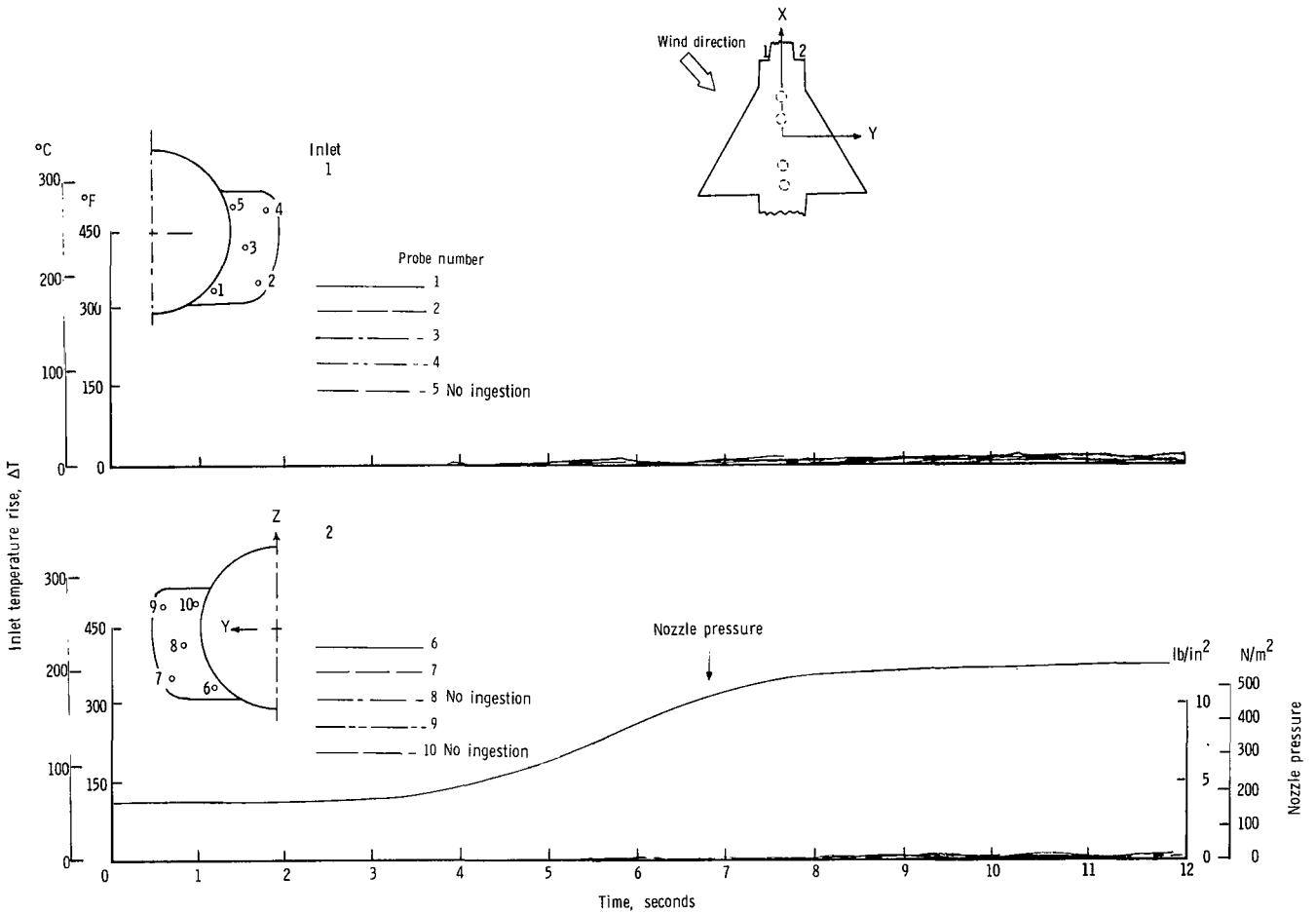

(b) $\psi = 45^0$; V = 11.85 knots.

Figure 32.- Continued.

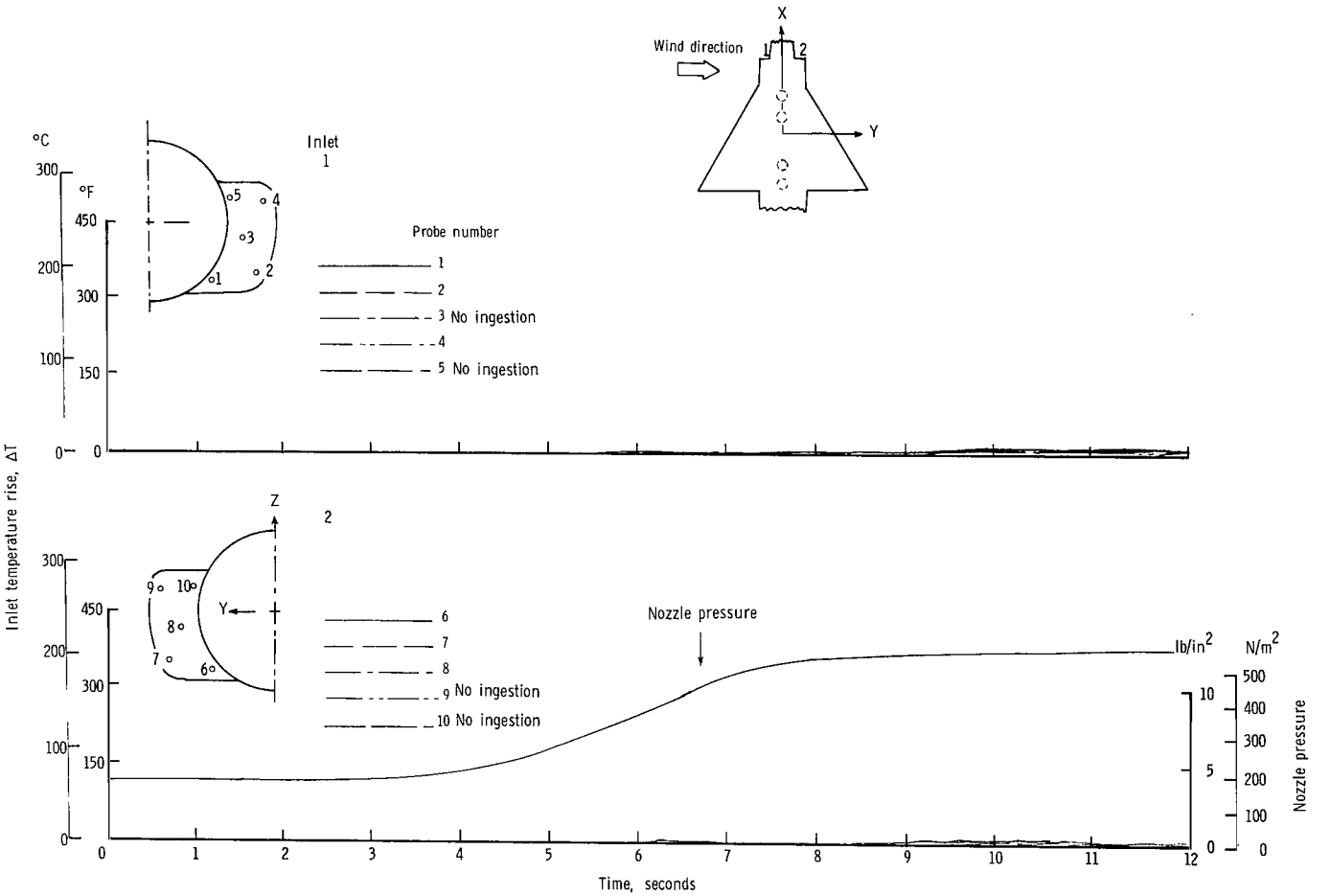

(c) $\psi = 90^0$; V = 5.92 knots.

Figure 32.- Continued.

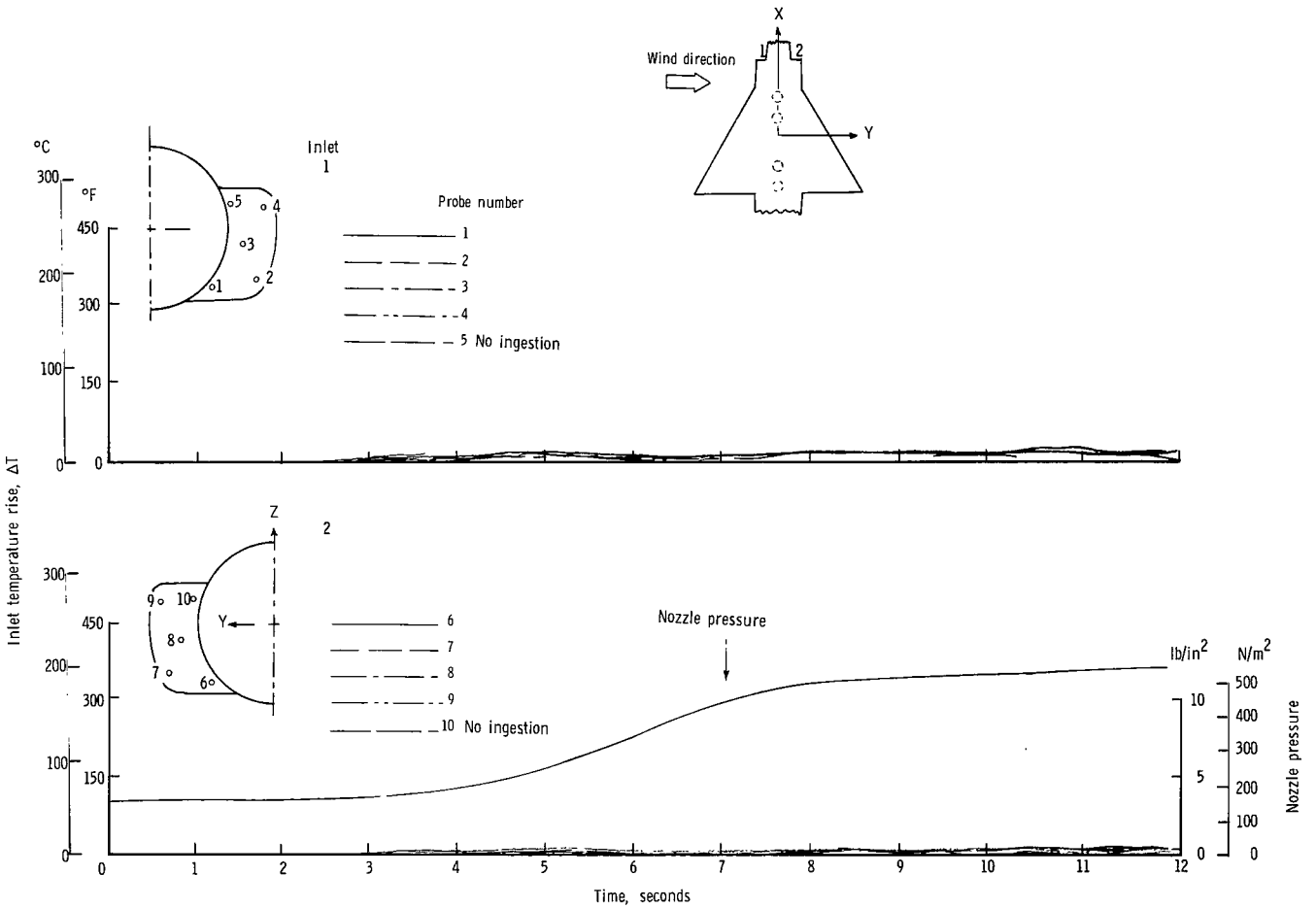

(d) $\psi = 90^{o}$; V = 11.85 knots.

Figure 32.- Concluded.

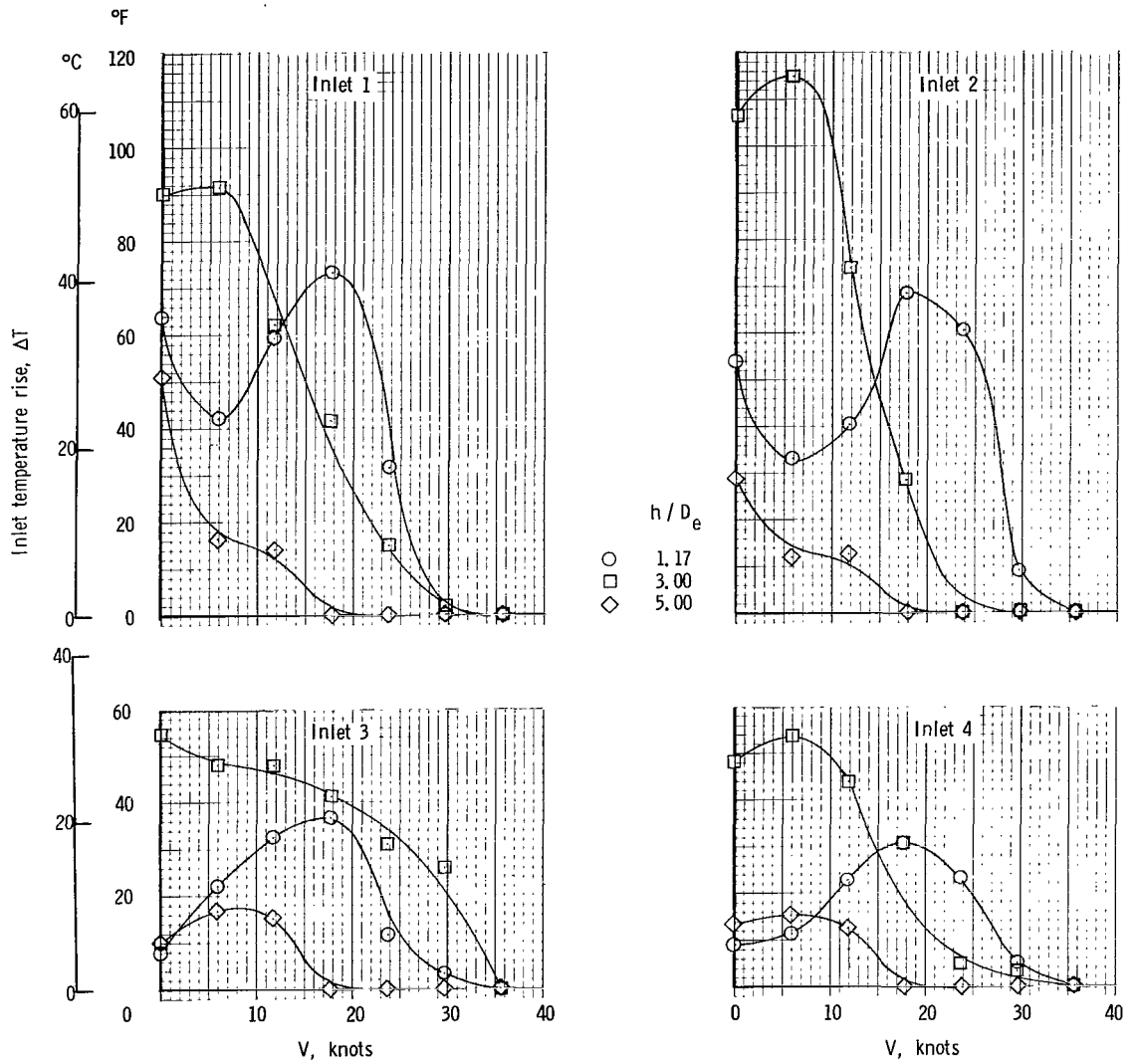

(a) $\psi = 0^{o}$.

Figure 33.- Variation of average inlet air temperature rise with windspeed for the rectangular nozzle arrangement with top inlets. High delta wing.

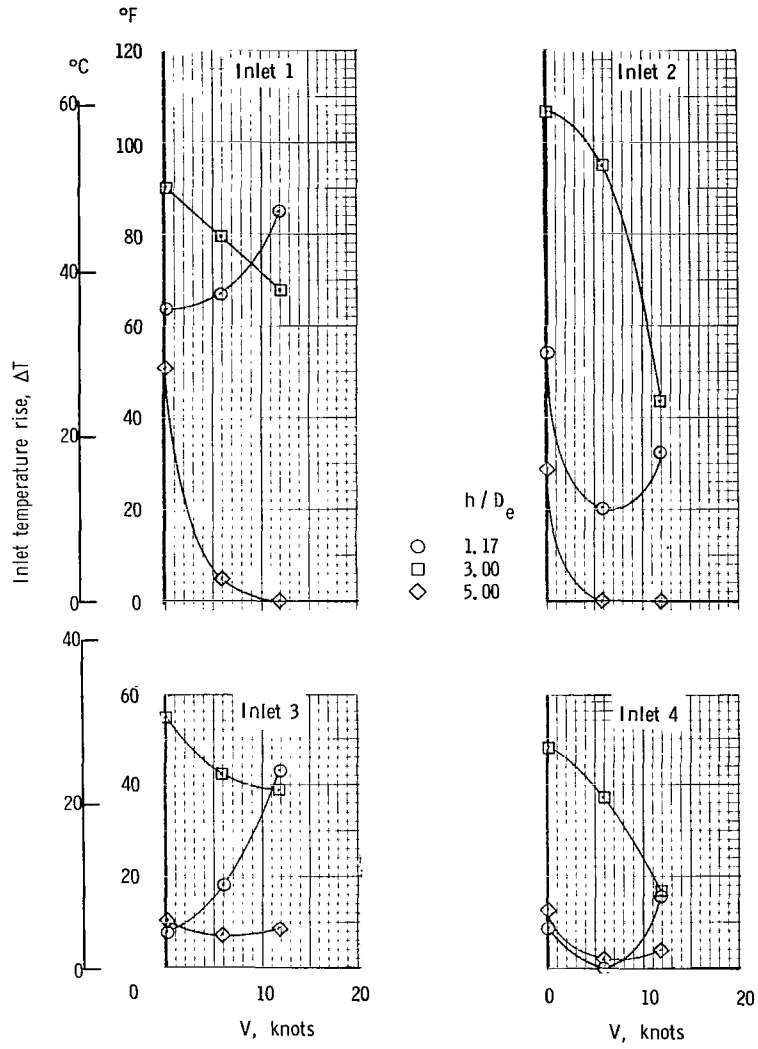

(b) $\psi = 45^{\circ}$.

Figure 33.- Continued.

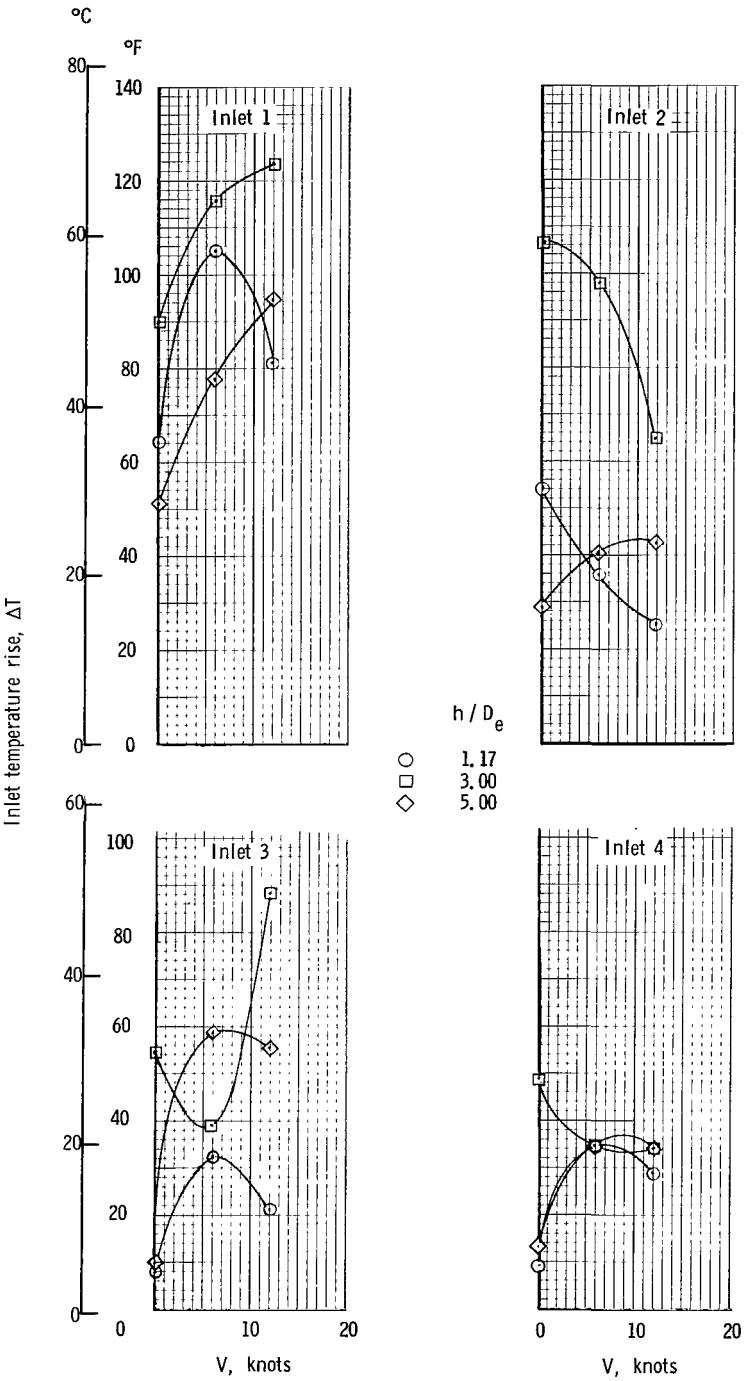

(c) $\psi = 90^{0}$.

Figure 33.- Concluded.

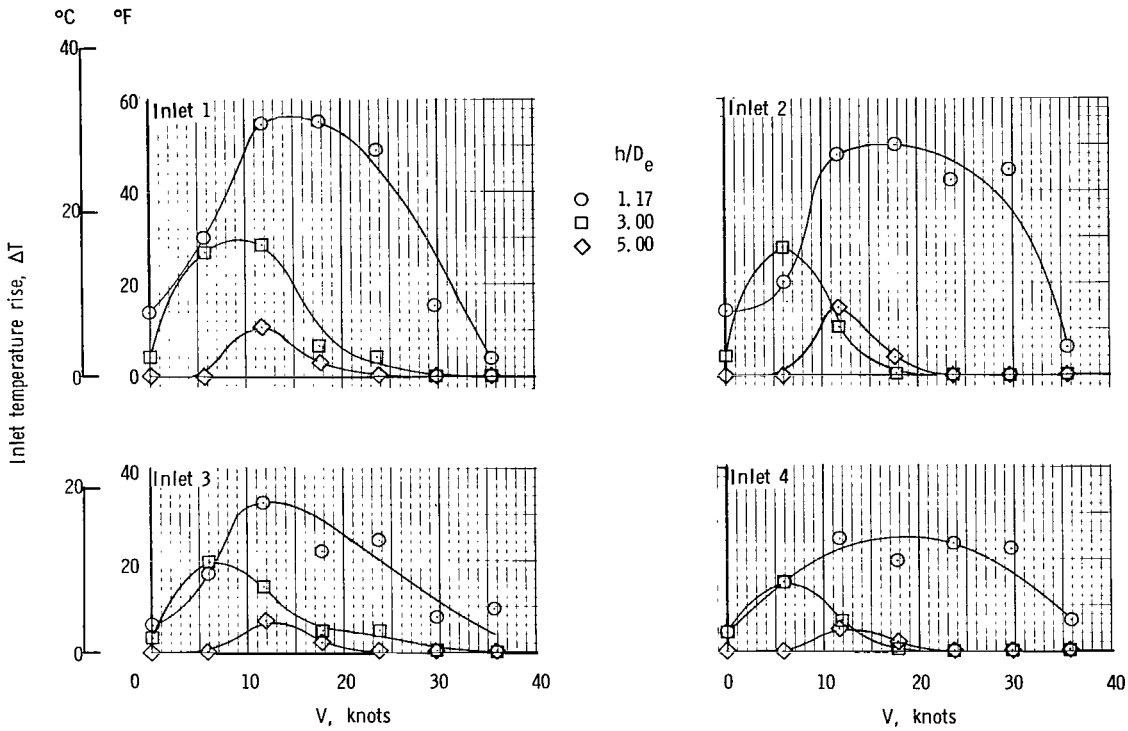

(a) $\psi = 0^{o}$.

Figure 34.- Variation of average inlet air temperature rise with windspeed for the rectangular nozzle arrangement with top inlets. Low delta wing.

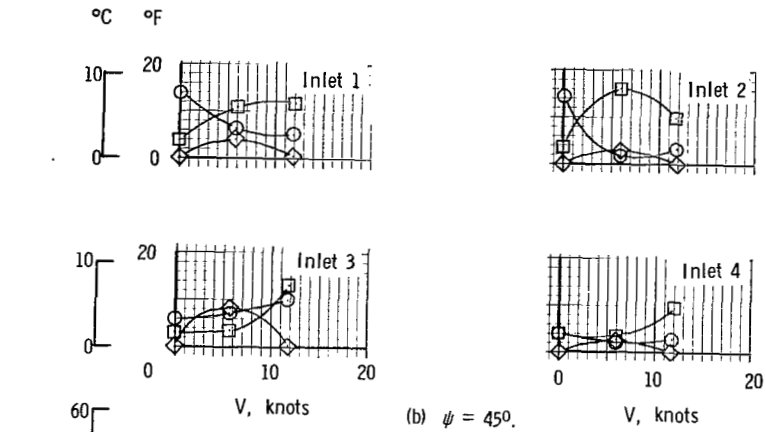

(b) $\psi = 45^{\circ}$.

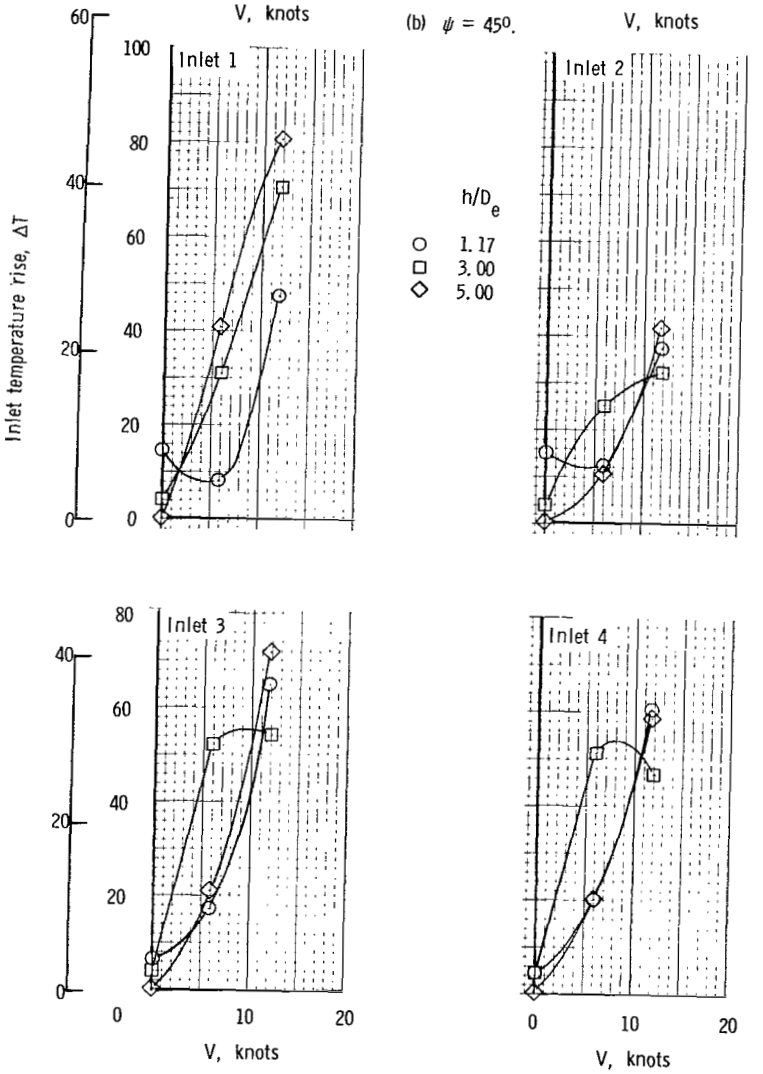

(c) $\psi = 90^{\circ}$.

Figure 34.- Concluded.

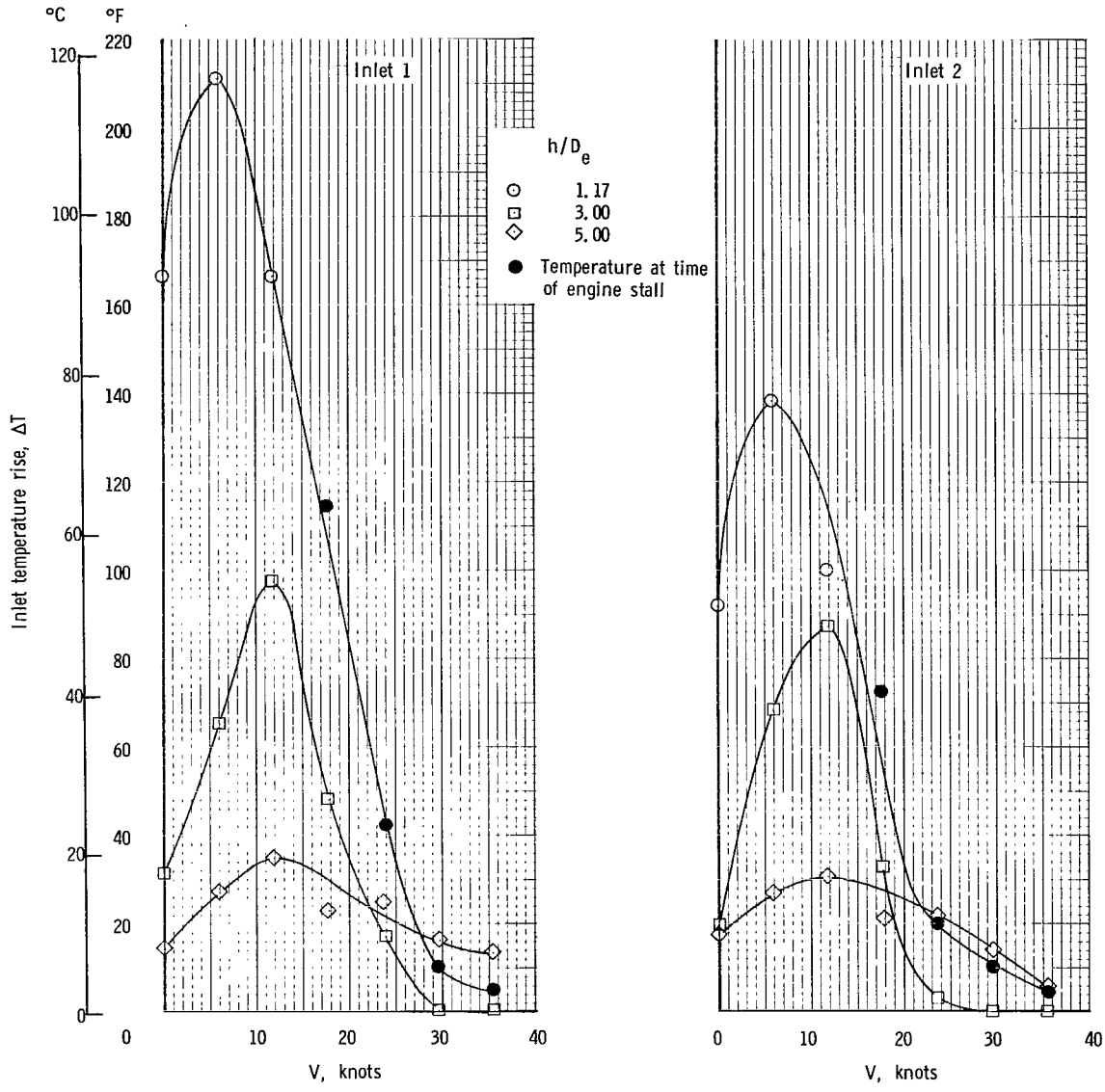

(a) $\psi = 0^{o}$.

Figure 35.- Variation of average inlet air temperature rise with windspeed for the rectangular nozzle arrangement with side inlets. High delta wing.

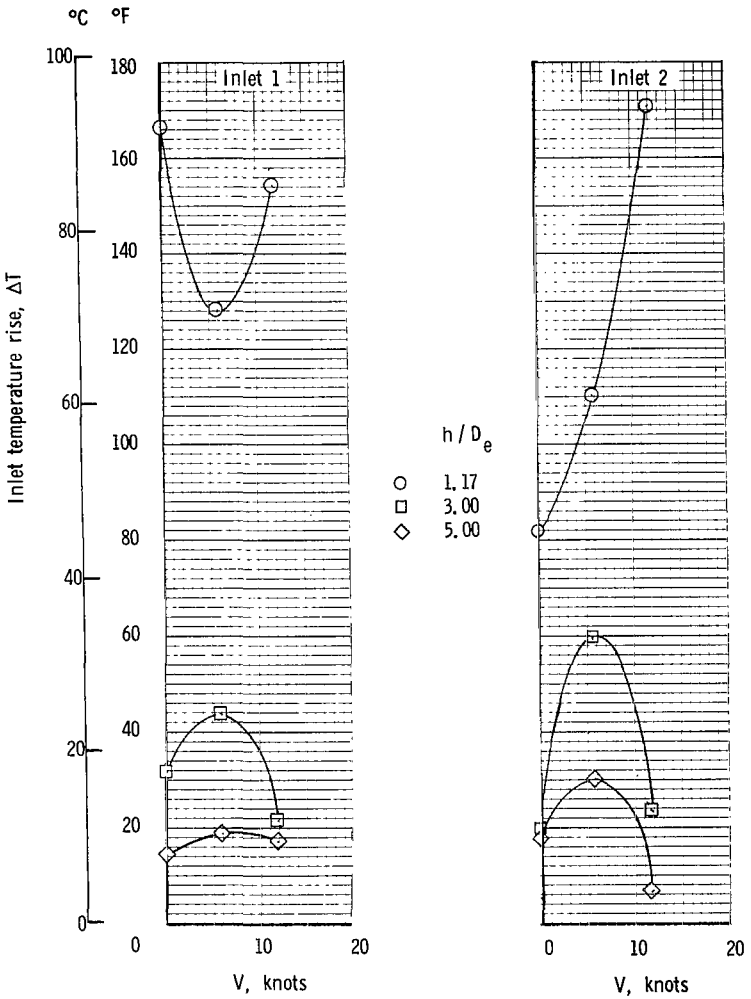

(b) $\psi = 45^{o}$.

Figure 35.- Continued.

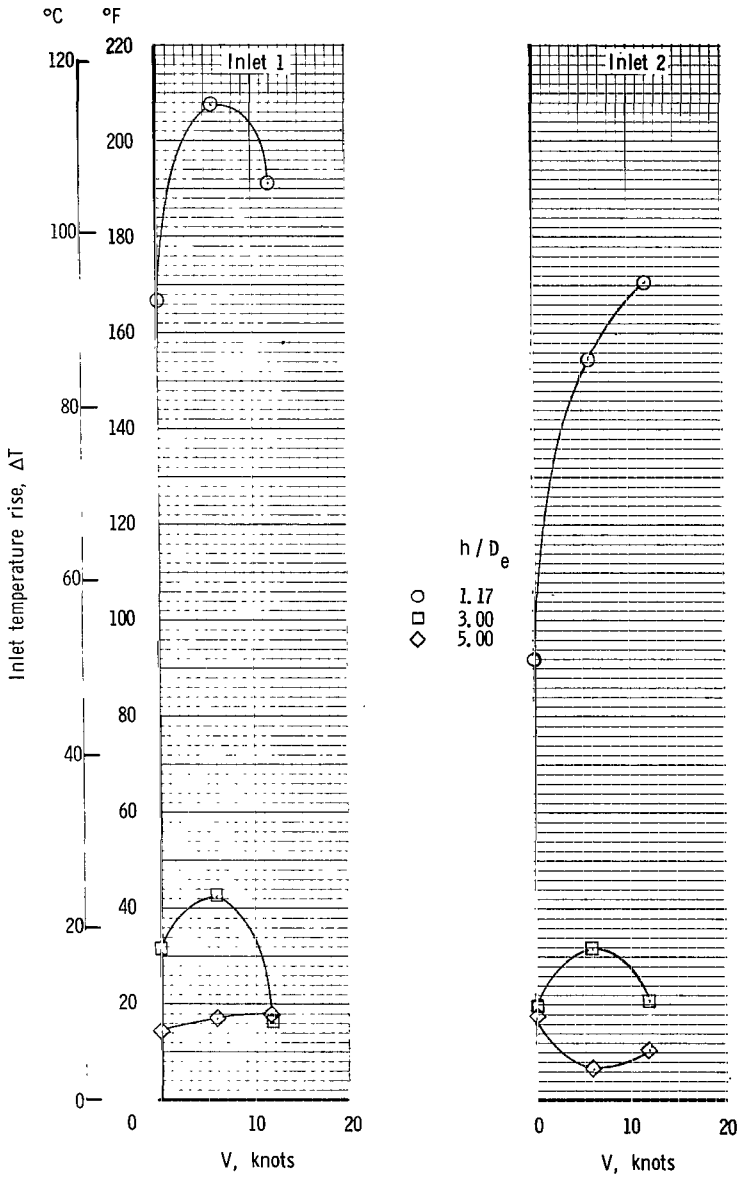

(c) $\psi = 90^{o}$.

Figure 35.- Concluded.

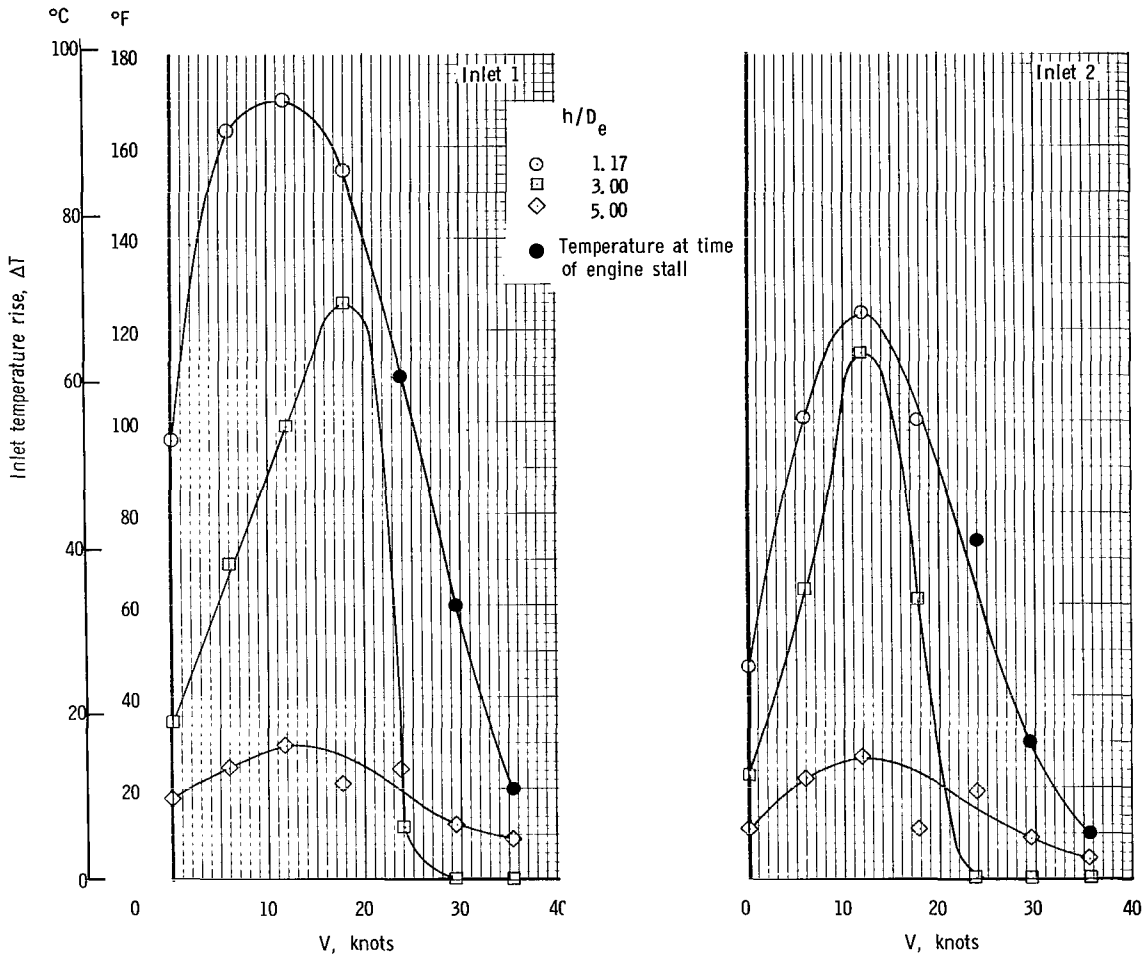

(a) $\psi = 0^{o}$.

Figure 36.- Variation of average inlet air temperature rise with windspeed for the rectangular nozzle arrangement with side inlets. Low delta wing.

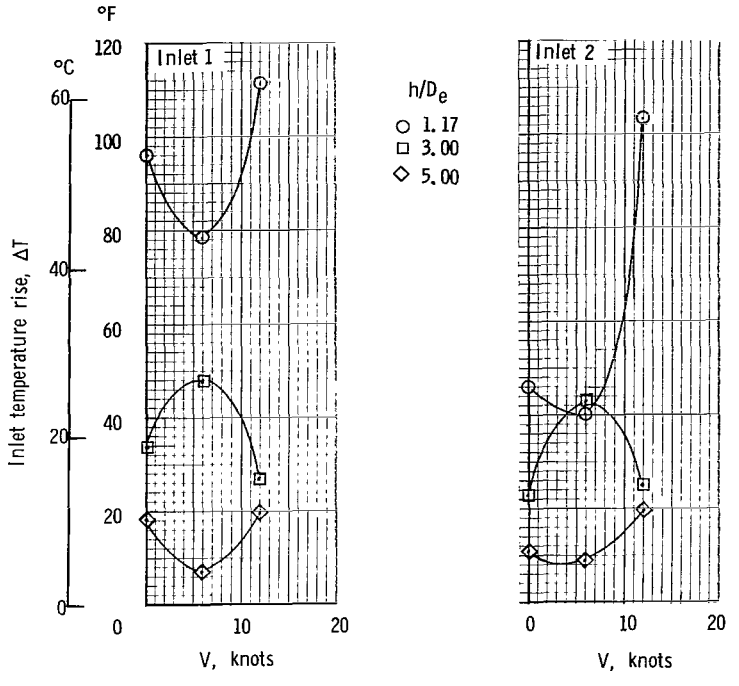

(b) $\psi = 45^{o}$.

Figure 36.- Continued.

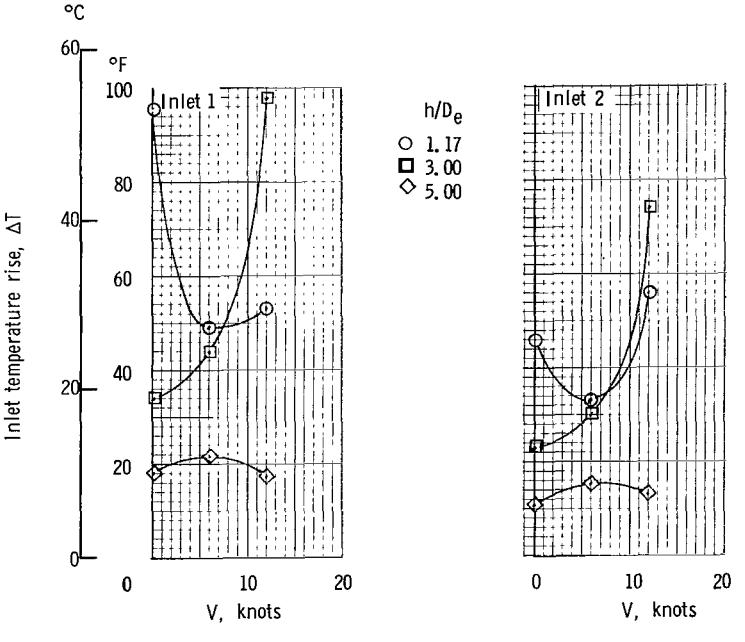

(c) $\psi = 90^{o}$.

Figure 36.- Concluded.

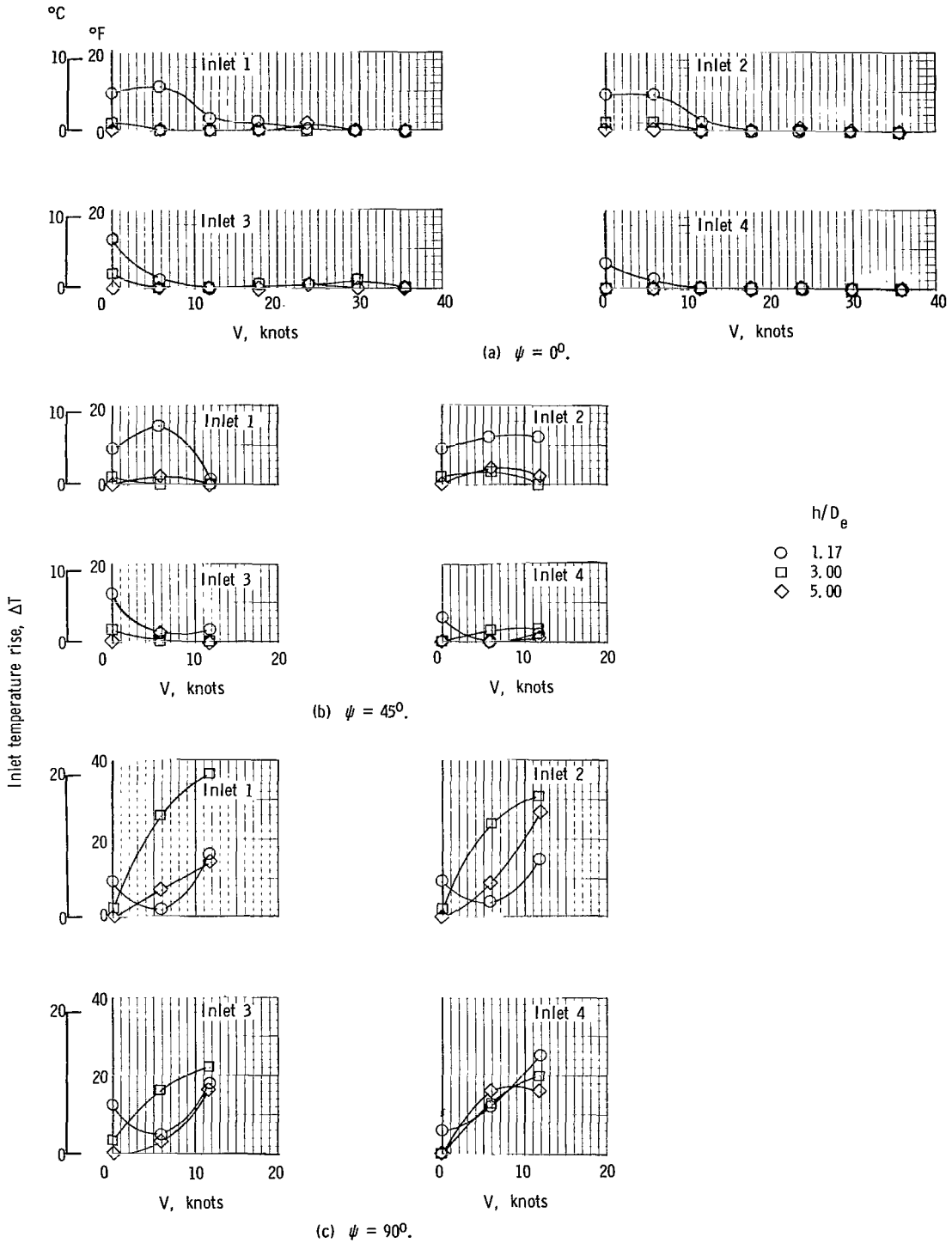

Figure 37.- Variation of average inlet air temperature rise with windspeed for the in-line nozzle arrangement with top inlets. High delta wing.

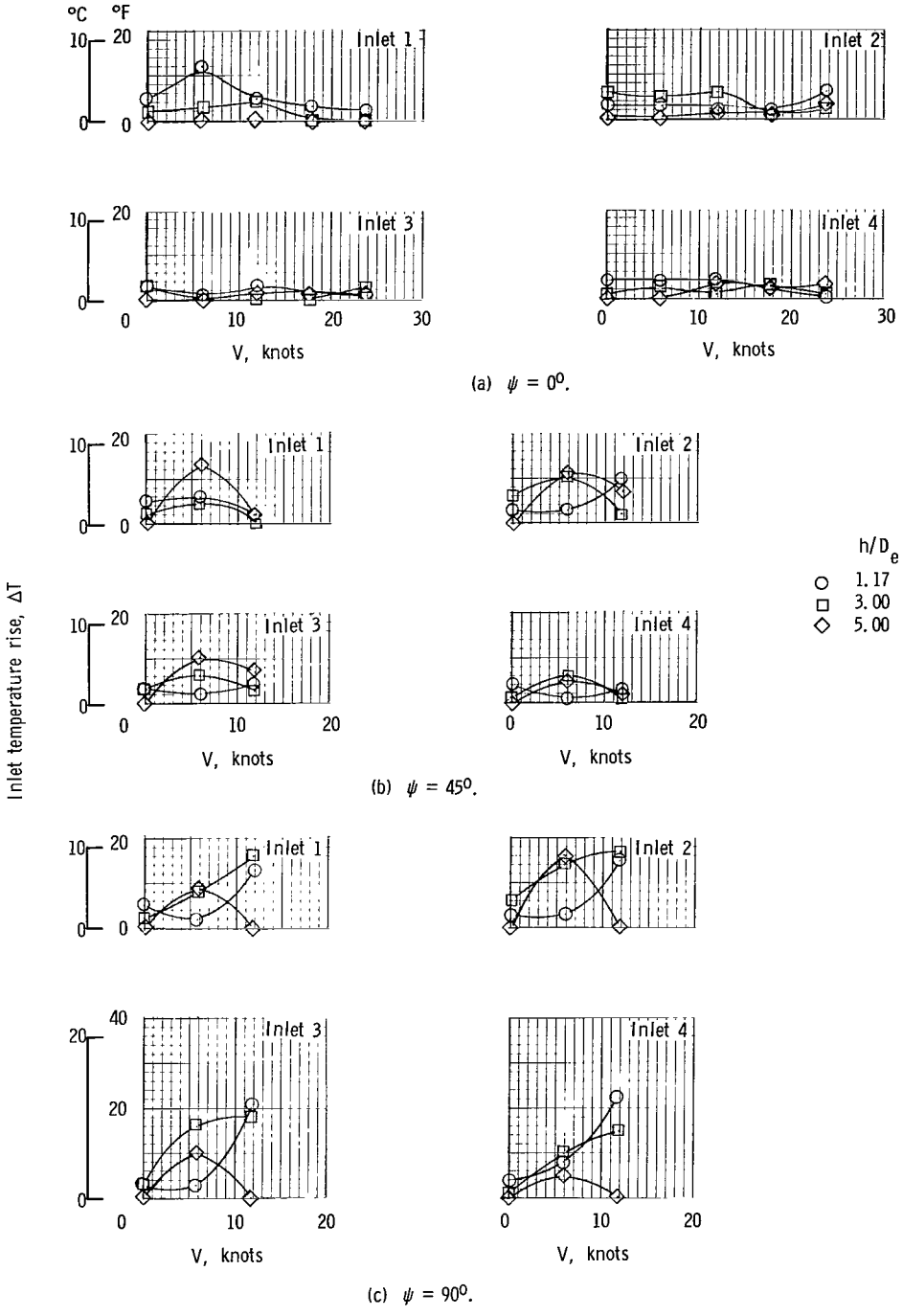

Figure 38.- Variation of average inlet air temperature rise with windspeed for the in-line nozzle arrangement with top inlets. Low delta wing.

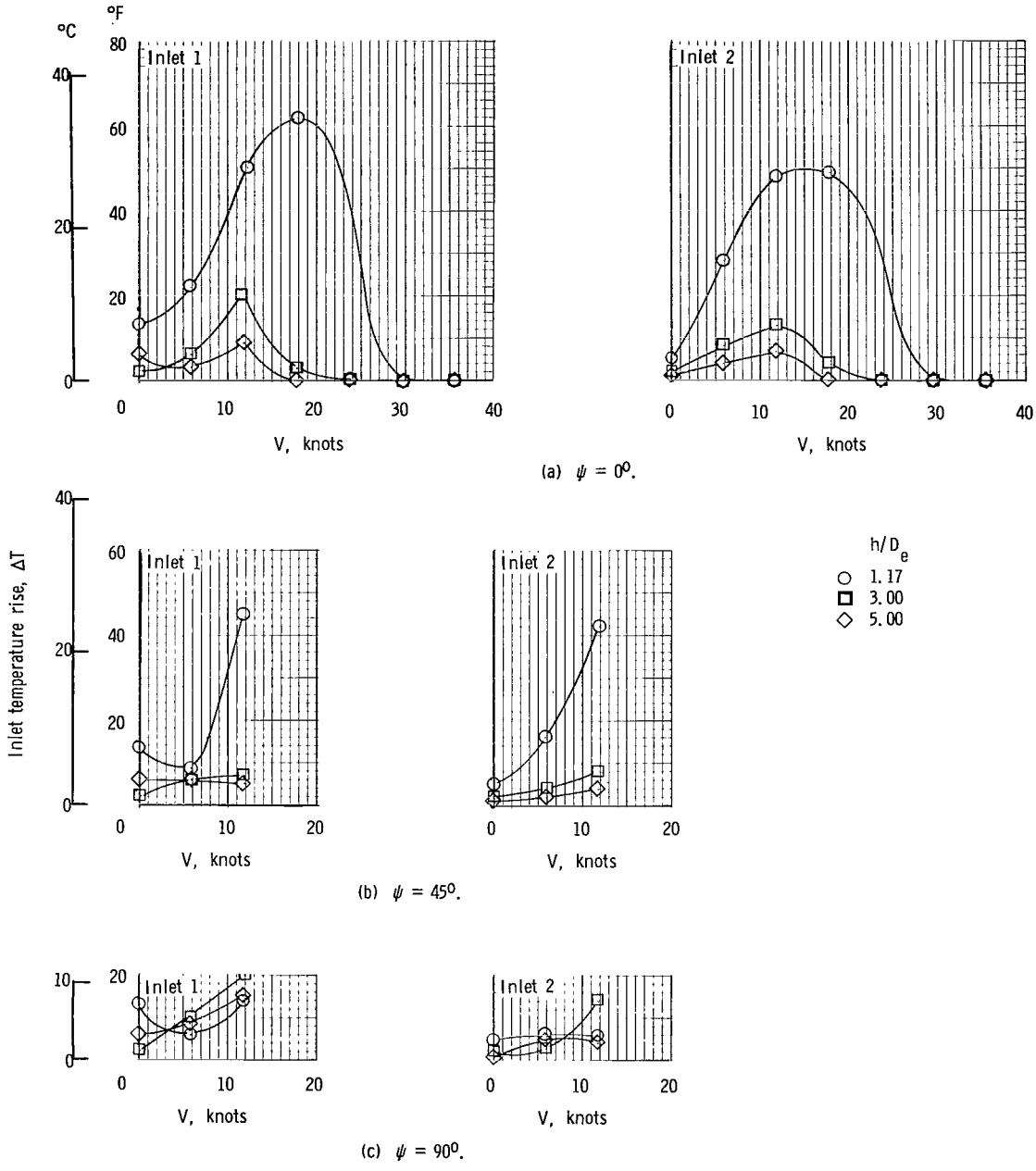

Figure 39.- Variation of average inlet air temperature rise with windspeed for the in-line nozzle arrangement with side inlets. High delta wing.

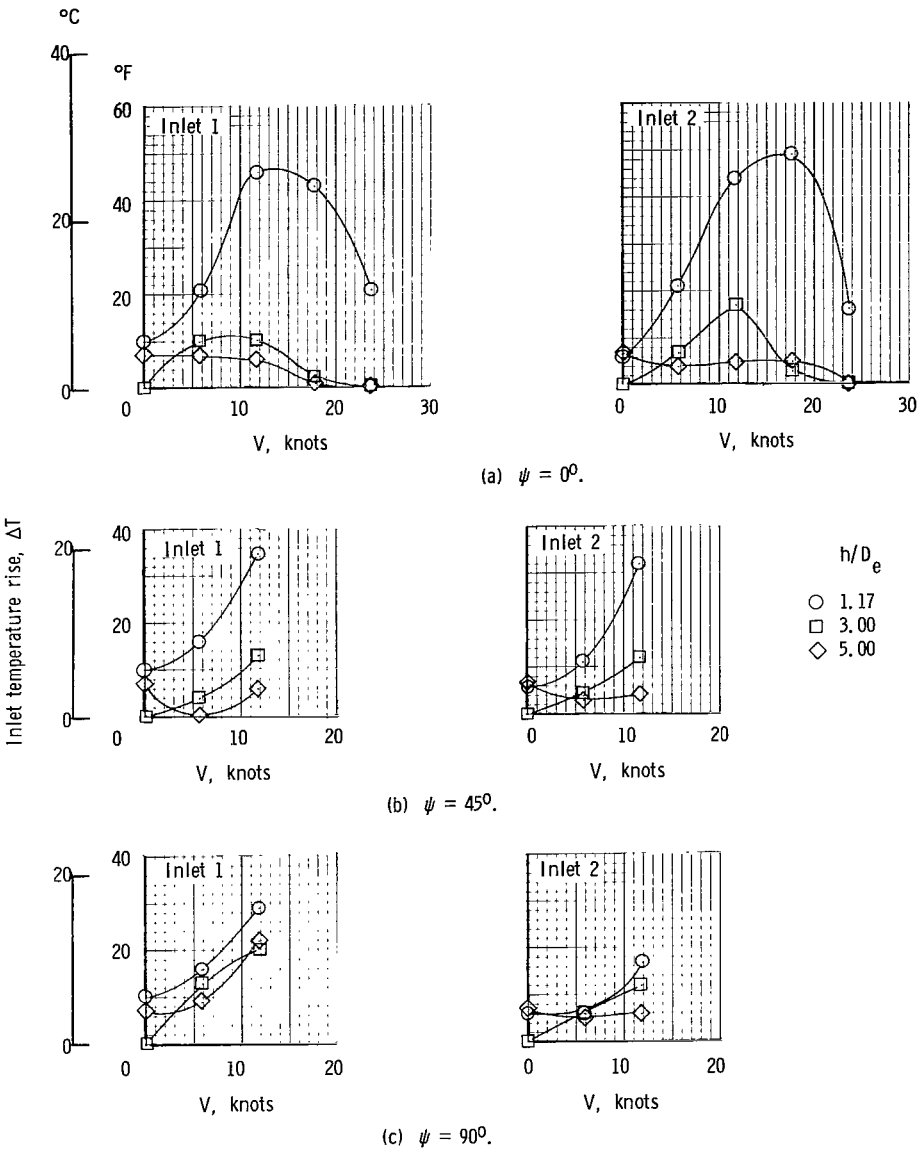

Figure 40.- Variation of average inlet air temperature rise with windspeed for the in-line nozzle arrangement with side inlets. Low delta wing.

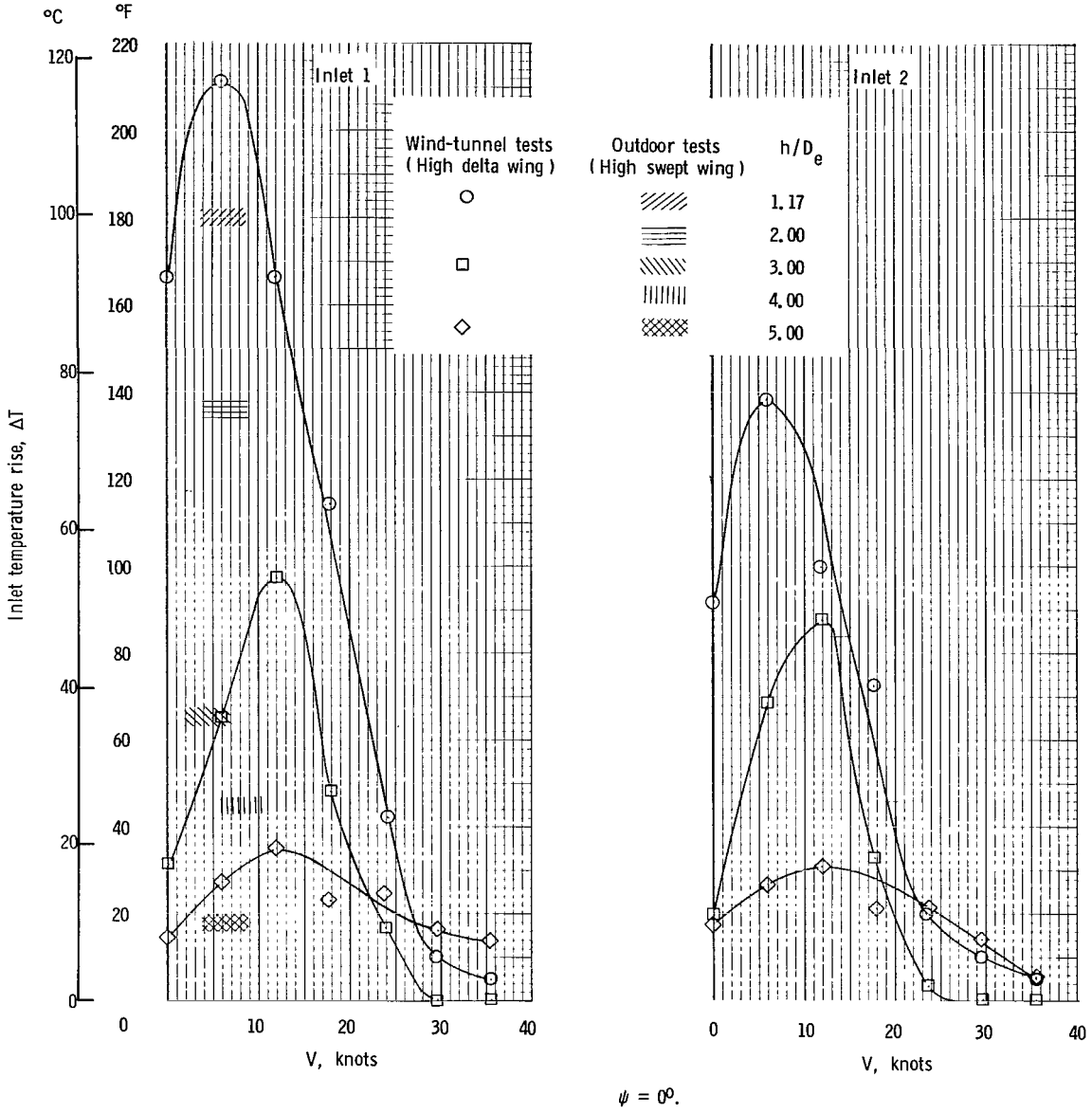

Figure 41.- Comparison of outdoor and wind-tunnel tests for the rectangular nozzle arrangement with side inlets. (For these outdoor tests, the temperature acquisition system for inlet 2 malfunctioned.)

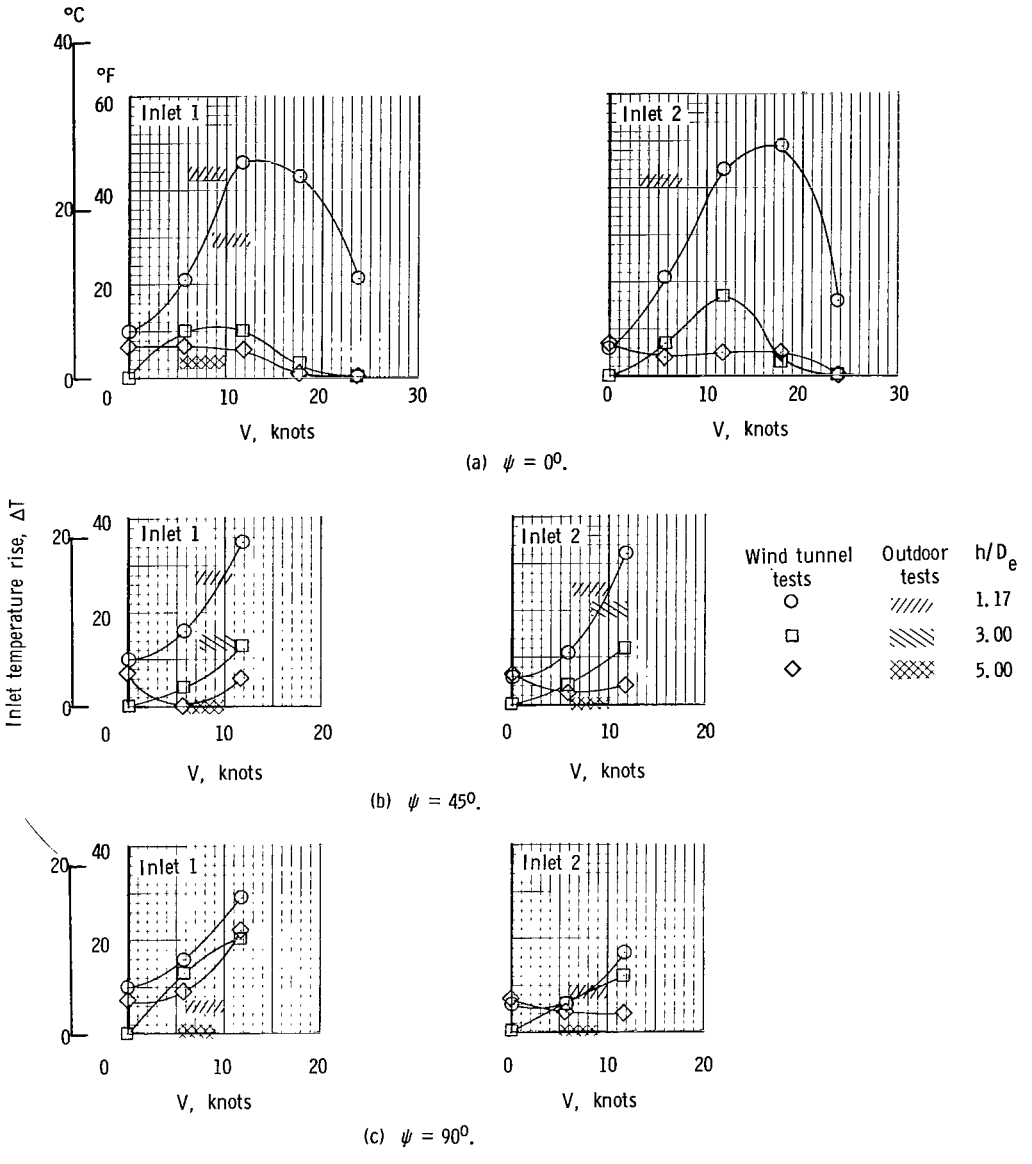

Figure 42.- Comparison of outdoor and wind-tunnel tests for the in-line nozzle arrangement with side inlets and low delta wing.

"The aeronautical and space activities of the United States shall be conducted so as to contribute . . . to the expansion of human knowledge of phenomena in the atmosphere and space. The Administration shall provide for the widest practicable and appropriate dissemination of information concerning its activities and the results thereof."

—NATIONAL AERONAUTICS AND SPACE ACT OF 1958

NASA SCIENTIFIC AND TECHNICAL PUBLICATIONS

TECHNICAL REPORTS: Scientific and technical information considered important, complete, and a lasting contribution to existing knowledge.

TECHNICAL NOTES: Information less broad in scope but nevertheless of importance as a contribution to existing knowledge.

TECHNICAL MEMORANDUMS: Information receiving limited distribution because of preliminary data, security classification, or other reasons.

CONTRACTOR REPORTS: Scientific and technical information generated under a NASA contract or grant and considered an important contribution to existing knowledge.

TECHNICAL TRANSLATIONS: Information published in a foreign language considered to merit NASA distribution in English.

SPECIAL PUBLICATIONS: Information derived from or of value to NASA activities. Publications include conference proceedings, monographs, data compilations, handbooks, sourcebooks, and special bibliographies.

TECHNOLOGY UTILIZATION PUBLICATIONS: Information on technology used by NASA that may be of particular interest in commercial and other non-aerospace applications. Publications include Tech Briefs, Technology Utilization Reports and Notes, and Technology Surveys.

Details on the availability of these publications may be obtained from:

SCIENTIFIC AND TECHNICAL INFORMATION DIVISION

NATIONAL AERONAUTICS AND SPACE ADMINISTRATION

Washington, D.C. 20546